

Università degli Studi di Napoli “Federico II”
Scuola Politecnica e delle Scienze di Base



PhD School in Earth, Environment and Resources Sciences

-XXX Cycle-

PhD Thesis

**Integrated analysis of building vulnerability in urban areas
affected by slow-moving, intermittent landslides
using SAR Interferometry**

Donato Infante

Advisor:

Prof. Domenico Calcaterra

Co-Advisors:

Prof. Massimo Ramondini

Prof. Roberto Tomás

PhD Coordinator

Prof. Maurizio Fedi

Academic Year 2016-2017

Contents

Abstract	vi
List of Figures	vii
List of Tables	xix
CHAPTER 1: Introduction	1
1.1 Structure of the thesis.....	3
1.2 Objectives of the research.....	4
CHAPTER 2: Landslides	6
Introduction.....	6
2.1 Landslide definition and classifications.....	7
2.2 Landslide features.....	15
2.3 Landslide causes.....	18
2.4 Landslides in Italy.....	20
2.5 Slow-moving landslides and impacts on existing facilities.....	24
CHAPTER 3: Slow-moving landslide risk assessment	27
Introduction.....	27
3.1 Landslide risk definition: literature review.....	29
3.2 Landslide risk management.....	31
3.3 Landslide risk assessment.....	35
3.3.1 Data collection for landslide risk assessment.....	37
3.3.2 Landslide hazard assessment.....	38
3.3.3 Landslide vulnerability assessment.....	41
3.3.4 Landslide risk assessment methods.....	43

CHAPTER 4: Vulnerability assessment in a landslide risk analysis.....	48
Introduction.....	48
4.1 Landslide vulnerability assessment: literature overview and issues.....	49
4.2 Elements at risk a different scale of analysis.....	53
4.3 Physical building vulnerability: the concept of damage.....	55
4.4 Approaches for physical vulnerability assessment.....	59
4.4.1 Vulnerability matrices and indices-based approaches.....	62
4.4.2 Vulnerability curves approach.....	64
4.4.3 Fragility curves approach.....	66
CHAPTER 5: Landslide investigation and monitoring techniques.....	69
Introduction.....	69
5.1 The process of landslide investigation.....	70
5.2 Landslide monitoring.....	72
5.3 Ground monitoring.....	74
5.3.1 Conventional in-situ techniques.....	75
5.3.2 Remote sensing detection.....	80
5.3.2.1 Topographic methods.....	82
5.3.2.2 Geodesic methods.....	84
5.3.2.3 Photogrammetric methods.....	85
5.3.2.4 Laser scanner technique.....	87
5.3.2.5 Radar remote sensing techniques.....	88
5.4 Synthetic Aperture Radar (SAR): introduction.....	92
5.4.1 SAR: acquisition geometry and images characteristics.....	94
5.4.2 SAR limitations affecting radar backscatter and distortions.....	98
5.4.3 Spaceborne SAR missions.....	100
5.4.4 SAR Interferometry.....	103

5.4.4.1	Baseline.....	106
5.4.4.2	Interferometric phase.....	107
5.4.5	Differential Interferometry SAR (DInSAR).....	108
5.4.5.1	Differential Interferometry SAR algorithms.....	111
5.4.5.2	DInSAR applications.....	116
CHAPTER 6: Characterization and survey of buildings in a landslide -affected area.....		118
Introduction.....		118
6.1	Vulnerability factors influencing performance of building affected by slow-moving landslide.....	120
6.2	Assessment of deformations on building-foundation system: definitions and symbols.....	132
6.3	Building damage induced by landslide displacements	134
6.4	Existing approaches to damage assessment	140
6.4.1	Burland (1977) approach	143
6.4.2	Alexander (1986) approach	144
6.4.3	Iovine & Parise (2002) approach	145
6.4.4	DPC (2009) approach	147
6.5	Conventional instruments to the cracks monitoring.....	151
CHAPTER 7: A procedure for building vulnerability assessment at different scales of analysis.....		154
7.1	The proposed approach for building vulnerability assessment.....	154
7.2	Procedure for building vulnerability analysis at small scale.....	158
7.3	Procedure for building vulnerability analysis at medium scale.....	165
7.4	Procedure for building vulnerability analysis at detailed scale.....	173

CHAPTER 8: Case study: multi-level vulnerability analysis of Moio della Civitella (SA) urban settlement.....	181
8.1 Geographical setting.....	181
8.2 Geological setting.....	183
8.3 Geomorphological setting.....	186
8.4 Landslide inventory map of Moio della Civitella	188
8.5 Vulnerability assessment at small scale.....	194
8.5.1 Assessment of landslide kinematics by DInSAR technique.....	194
8.5.2 Characterization of exposed elements.....	200
8.5.3 Identifying stable/unstable areas, stable/unstable buildings and prevalent direction of movement.....	207
8.5.4 Assessment of possible scenarios of building behavior.....	212
8.5.5 Updating of available landslide inventory map.....	220
8.5.6 Preliminary zoning of buildings vulnerability.....	227
8.6 Vulnerability assessment at medium scale.....	228
8.6.1 Detection of landslide kinematics by integrated analysis of DInSAR and conventional monitoring data.....	228
8.6.2 Characterization of exposed elements.....	236
8.6.3 Identifying areas with different degree of vulnerability at more detailed level.....	239
8.6.4 Assessment of relationship between landslide intensity and worsening of damage level.....	243
8.6.5 Analysis of influence of vulnerability factors on building performance.....	263
8.6.6 Forecasting of future damage conditions of whole urban settlement.....	270
8.7 Vulnerability assessment at a detailed scale.....	271
8.7.1 Characterization of landslide kinematics affecting each building.....	272
8.7.2 Detailed survey of exposed elements.....	275
8.7.3 Analytical approach: equivalent beam model and building 3D fragility curves.....	279

8.7.4 Numerical approach: 3D computational model and building vulnerability domains.....	287
8.7.5 Assessment of building behavior through DInSAR and structural analysis.....	294
CHAPTER 9: Conclusion.....	304
9.1 Future perspectives.....	309
References	310
Acknowledgments.....	329

Abstract

Slow-moving landslides are a natural hazard which affects wide areas in the world causing relevant economic damage to structures and infrastructures. To this reason, the analysis of landslide-induced consequences plays a key role in risk prevention and mitigation activities. The thesis shows a general methodology which can be used to forecast spatial and temporal evolution of building vulnerability in urban settlements affected by slow-moving and intermittent landslides. Multi-level and integrated analysis of landslide kinematics and exposed elements allows to assess at different scales of representation and at different levels of accuracy, future conditions of damage of existing facilities.

Satellite Radar Interferometry and in particular the Differential SAR Interferometry (DInSAR) technique has been successfully applied as a remote-sensing tool to provide information both on spatial and temporal landslide evolution and on interaction with structures in urban areas. Integration of C and X-band SAR data (acquired between 2002 and 2016) with conventional monitoring techniques allows to reach a thorough knowledge of landslide kinematics; subsequently, structural analyses to detect the relationship between slope movements and building damage have been performed, by using qualitative, semi-quantitative and quantitative approaches.

Such methodology has been tested in Moio della Civitella urban settlement, Salerno Province, whose territory is affected by several slow-moving landslides. At small scale of representation, preliminary cause-effect relationship and the updating of landslide inventory map have been provided; at medium scale of analysis, vulnerability zoning map through matrix-approach and influence of vulnerability factors on performance of structures through fragility curves approach, have been defined. Finally, at a detailed scale, structural behavior of buildings has been investigated by means of analytical or numerical analyses.

The proposed methodology could be applied to other scenarios affected by similar phenomena and once validated, can be valuably used for damage analysis and forecasting.

Keywords

Slow-moving landslides, building vulnerability, damage, Differential SAR Interferometry, risk mitigation, displacements monitoring.

List of Figures

Figure 2.1	Spatial distribution of fatal landslides.....	6
Figure 2.2	Classification of landslide movement types.....	8
Figure 2.3	Classification of landslide typologies.....	9
Figure 2.4	Classification of landslides typologies.....	10
Figure 2.5	Scheme of the state of activity of a landslide.....	11
Figure 2.6	Scheme of the distribution of activity of a landslide: 1) Advancing landslide; 2) Retrogressive landslide; 3) Enlarging landslide; 4) Diminishing landslide; 5) Confined landslide; 6) Moving landslide; 7) Widening landslide.....	12
Figure 2.7	Scheme of the style of activity of a landslide, modified from WP/WLI: 1) Complex landslide; 2) Composite landslide; 3) Successive landslide; 4) Single landslide; 5) Multiple landslide.....	13
Figure 2.8	Landslide velocity scale according to Cruden and Varnes classification.....	14
Figure 2.9	Block diagram of typical landslide features.....	15
Figure 2.10	Features of a landslide.....	17
Figure 2.11	Checklist of landslide causes.....	19
Figure 2.12	Map of urban centers affected by landslide phenomena.....	21
Figure 2.13	Map of the landslide events with “victims” between 1965 and 2014.....	23
Figure 2.14	Examples of building damages within landslides affected areas: (a) San Fratello (province of Messina), Verbicaro (province of Cosenza) and (c) Gorga (province of Salerno) urban area.....	24
Figure 2.15	Interaction between slow-moving landslide and man-made works and expected damage.....	25
Figure 3.1	Graphical representation of landslide risk.....	30
Figure 3.2	Conceptual framework for landslide risk management.....	32
Figure 3.3	Flow chart for landslide risk management.....	33
Figure 3.4	Simplified scheme for the landslide risk assessment.....	35
Figure 3.5	Methodological framework for spatial landslide risk assessment.....	36
Figure 3.6	Flow diagram illustrating vulnerability components.....	42
Figure 4.1	Overview of types of loss resulting from landslide hazard: structural and non-structural damage to buildings are highlighted.....	51
Figure 4.2	Flow diagram illustrating vulnerability components.....	52

Figure 4.3	Logical framework for vulnerability assessment and different scale of analysis.....	53
Figure 4.4	Exposed elements at different scales of analysis.....	55
Figure 4.5	Examples of damage detected on buildings in Gorga urban settlement, Salerno Province (Italy): aesthetic (a), functional (b), structural (c).....	57
Figure 4.6	Vulnerability of various elements at risk according to damage level.....	62
Figure 4.7	Vulnerability matrix from Dai et al. (2002)	63
Figure 4.8	Relationship between ground distortions and damage category: (a) after Boscardin and Cording (1989) and (b) after Burland (1997)	65
Figure 4.9	Fragility curves developed by empirical data (a) and by numerical analysis (b).....	67
Figure 5.1	Differential extensometer.....	77
Figure 5.2	(a) Inclinomometer configuration, (b) scheme of inclinometer installation, (c) and (d) inclinometric readings.....	78
Figure 5.3	Piezometers: “Casagrande” (a), open pipe (b), scheme of “Casagrande” piezometer (c) and (d).....	79
Figure 5.4	Examples of pluviometer stations.....	80
Figure 5.5	Electromagnetic spectrum.....	81
Figure 5.6	Examples of theodolite (a) and total station (b).....	83
Figure 5.7	Differential Global Positioning System scheme (a) and GPS sensor (b).....	85
Figure 5.8	Examples of terrestrial (a) and aerial (b) photogrammetry.....	86
Figure 5.9	Examples of Laser scanner applications to landslides monitoring.....	88
Figure 5.10	GB-SAR observations of landslide phenomena.....	89
Figure 5.11	Temporal schedule of the most important SAR missions.....	91
Figure 5.12	Radar acquisition geometry.....	92
Figure 5.13	SAR acquisition modes by TerraSAR-X satellite.....	93
Figure 5.14	Geometric model of SAR system.....	94
Figure 5.15	Synthetic Aperture Radar scheme.....	96
Figure 5.16	Scattering mechanisms on different surfaces.....	96
Figure 5.17	Examples of corner reflector installations.....	97
Figure 5.18	Geometric distortion effects: foreshortening (a), layover (b) and shadowing (c).....	99
Figure 5.19	Representative scheme of PSInSAR, on the left, of SBAS, on the right...	115

Figure 6.1	Distribution of damage severity according to building location on landslide: for reinforced concrete (a) and masonry (b) buildings.....	120
Figure 6.2	Possible stress concentration and torsion effects on a L-shaped building configuration.....	123
Figure 6.3	Different floor height of adjacent buildings and potential point of damage.....	123
Figure 6.4	Example of differential settlement of adjacent buildings with different height.....	124
Figure 6.5	Sections 1 and 2 of DPC classification scheme: identification of building location (1) and description of geometrical and urbanistic parameters (2)	126
Figure 6.5	Sections 3, 4, 5, 6, 7 of DPC classification scheme: identification of building typology (3); survey of damage and adopted mitigation measures to structural (4) and non-structural (5) elements; potential damages induced by adjacent buildings (6); damage consequences surveyed on ground (7)...	127
Figure 6.5	Sections 8 and 9 of DPC classification scheme: judgment of conformity to standards and suggested early warning measures (8) and further observations (9)	128
Figure 6.6	Definitions of ground and foundations movements.....	133
Figure 6.7	Types of foundation settlements induced by ground movements.....	135
Figure 6.8	Cracks induced on partition walls of reinforced concrete building by differential settlements: lateral settlement (a) and central settlement (b)..	136
Figure 6.9	Cracks induced above the openings by a central settlement of foundation..	136
Figure 6.10	Classification of vertical settlements for masonry buildings.....	137
Figure 6.11	Example of “central” settlement of a masonry wall.....	137
Figure 6.12	Schemes of cracks in masonry walls induced by “central” settlements: shear stress (a, b) and bending stress (c, d).....	138
Figure 6.13	Examples of “arc-shape” cracks induced by “central” settlements of masonry wall.....	138
Figure 6.14	Schemes of cracks in masonry walls induced by “lateral” settlements: bending stress (a) and shear stress (b, c)	139
Figure 6.15	Examples of damages induced by “lateral” settlement on masonry buildings.....	139
Figure 6.16	Examples of damage in masonry buildings induced by relative horizontal displacement (a) and by rotational movement of foundation (b)	140
Figure 6.17	Burland & Wroth (1974) method: equivalent beam model of a real building.....	142

Figure 6.18	Glass crack monitoring system.....	151
Figure 6.19	Example of “Tell Tale” crack monitoring.....	152
Figure 6.20	Example of crack-meter to monitoring movement of crack.....	153
Figure 7.1	General framework for vulnerability assessment at different scales of analysis.....	154
Figure 7.2	Building vulnerability assessment: approaches, input and output data at different scales of analysis.....	157
Figure 7.3	Flow chart of the analyses to be carried out at small scale of representation.....	160
Figure 7.4	Possible scenarios and related building behavior resulting from comparison between stable and unstable targets data located on top of buildings and on surrounding area/roads.....	162
Figure 7.5	“DInSAR data-building damage” matrices for vulnerability assessment at small scale analysis: for masonry building (a) and reinforced concrete building (b).....	164
Figure 7.6	Flow chart of analyses to be carried out at medium scale of representation.....	166
Figure 7.7	“DInSAR data-building damage” matrix for vulnerability assessment of masonry building at medium scale analysis.....	168
Figure 7.8	“DInSAR data-building damage” matrix for vulnerability assessment of reinforced concrete building at medium scale analysis.....	169
Figure 7.9	Threshold values (red circles) of proposed vulnerability matrices, obtained by Boscardin & Cording (1989) approach.....	167
Figure 7.10	Flow chart of analyses to be carried out at detailed scale of representation.....	174
Figure 7.11	The equivalent beam approach.....	175
Figure 8.1	Location of Moio della Civitella, Salerno Province, southern Campania region.....	181
Figure 8.2	Panoramic view of Moio della Civitella urban centre: optical image (a) and 3d model (b).....	182
Figure 8.3	Tectonic map of the Southern Apennines of Italian peninsula.....	183
Figure 8.4	Complex structurally formations.....	184
Figure 8.5	Geological sketch map of the Moio della Civitella area: a1a, a1b: old and recent landslide deposits; b, b2, bn2: alluvial deposits; f2: debris; CET: Centola Conglomerates; MAU: San Mauro Formation; PLL: Pollica Sandstones; SCE, SCE1: Saraceno Formation; CRN: Crete Nere Formation; PNL: Pianelli Sandstones.....	185

Figure 8.6	Arenaceous and conglomeratic blocks belonging to the Quaternary cover cropping out within the urban centre of Moio della Civitella.....	186
Figure 8.7	Slope map of Moio della Civitella territory.....	187
Figure 8.8	Landslide inventory map at Moio della Civitella.....	188
Figure 8.9	Landslide inventory map at Moio della Civitella.....	189
Figure 8.10	Landslides inventory map at Moio della Civitella.....	190
Figure 8.11	Landslides state of activity at Moio della Civitella.....	190
Figure 8.12	Landslides inventory map at Moio della Civitella.....	191
Figure 8.13	Typologies of landslide at Moio della Civitella.....	191
Figure 8.14	Landslides state of activity at Moio della Civitella.....	192
Figure 8.15	Distribution of landslides state of activity at Moio della Civitella.....	192
Figure 8.16	Distribution of landslides which change state of activity from 2012 to 2016.....	193
Figure 8.17	Phase standard deviation vs. TSC for ascending (a) and descending (b) processing. Red points indicate the TSC threshold selected.....	195
Figure 8.18	Stable points identified at Moio della Civitella: 1 and 3 correspond to master points of GPS network installed in situ.....	196
Figure 8.19	Displacement rate maps obtained by ENVISAT images in time span 2002-2010: along ascending (a) and descending (b) tracks.....	197
Figure 8.20	Displacement rate maps obtained by COSMO-SkyMed images in time span 2011-2016: along ascending (a) and descending (b) tracks.....	198
Figure 8.21	Number of targets identified in the study area by ENVISAT medium-resolution and COSMO-SkyMed high resolution images.....	199
Figure 8.22	High resolution SAR image of Moio della Civitella acquired by COSMO-SkyMed constellation.....	200
Figure 8.23	Exposed elements identified by topographic map.....	200
Figure 8.24	Map of exposed elements identified by field survey and example of buildings aggregate obtained by topographic map (a) and by <i>in situ</i> campaign (b)...	201
Figure 8.25	Map of building typology surveyed in Moio della Civitella municipality..	202
Figure 8.26	Map of building age of construction in Moio della Civitella municipality: Moio (a) and Pellare (b) urban settlements.....	202
Figure 8.27	Map of building state of maintenance in February 2015 at Moio della Civitella municipality: Moio (a) and Pellare (b) urban settlements.....	203
Figure 8.28	Building damage map according to Burland (1977) classification.....	203
Figure 8.29	Building damage map according to Alexander (1986) classification.....	204

Figure 8.30	Building damage map according to Iovine & Parise classification.....	204
Figure 8.31	Building damage map according to Italian DPC (2009) classification...	205
Figure 8.32	Example of building characterized by different damage severity level according to: Burland (a), Alexander (b), Iovine & Parise (c) and Italian DPC (d) approaches.....	206
Figure 8.33	Examples of buffer created around buildings at Moio della Civitella.....	207
Figure 8.34	Differentiation of targets identified by COSMO-SkyMed images on the top of a building and in the surrounding area at ground level obtained by ascending (a) and descending (b) tracks.....	207
Figure 8.35	Targets identified on ground level (a) and on the top of buildings (b) in ascending track.....	208
Figure 8.36	Targets identified on ground level (a) and on top of buildings (b) in descending track.....	208
Figure 8.37	Maximum vertical and horizontal displacement rate of buildings in Moio della Civitella.....	209
Figure 8.38	Prevalent direction of movement of buildings in Moio della Civitella urban settlement.....	209
Figure 8.39	Ratio between horizontal and vertical components of movement for each building in Moio della Civitella urban settlement.....	210
Figure 8.40	Map of stable/unstable areas surrounding the buildings at Moio della Civitella.....	210
Figure 8.41	Map of stable/unstable buildings at Moio della Civitella.....	211
Figure 8.42	Example of buildings representative of the first possible scenario in Moio urban settlement (a): its identification in stable/unstable areas map (b) and in stable/unstable buildings map (c).....	212
Figure 8.43	Targets identified on a building and on the surrounding area by COSMO-SkyMed products obtained by ascending (a) and descending (b) tracks...	213
Figure 8.44	Example of buildings representative of the second possible scenario in Moio urban settlement (a): its identification in stable/unstable areas map (b) and in stable/unstable buildings map (c).....	213
Figure 8.45	Targets identified on a building and on the surrounding area by COSMO-SkyMed products obtained by ascending (a) and descending (b) tracks...	214
Figure 8.46	Example of buildings representative of the fifth possible scenario in Moio urban settlement (a): its identification in stable/unstable areas map (b) and in stable/unstable buildings map (c).....	215
Figure 8.47	Targets identified on a building and on the surrounding area by COSMO-SkyMed products obtained by ascending (a) and descending (b) tracks...	215

Figure 8.48	Example of buildings representative of the sixth possible scenario in Moio urban settlement (a): its identification in stable/unstable areas map (b) and in stable/unstable buildings map (c).....	216
Figure 8.49	Targets identified on a building and on the surrounding area by COSMO-SkyMed products obtained by ascending (a) and descending (b) tracks...	216
Figure 8.50	“LoS” cumulated displacement map of targets identified in Moio della Civitella urban settlement in “ascending” track in time span 2011-2016.....	217
Figure 8.51	“LoS” cumulated displacement map of targets identified in Moio della Civitella urban settlement in “descending” track in time span 2011-2016.....	218
Figure 8.52	Ratio between displacement of buildings and of surrounding areas along horizontal and vertical directions of movement for reinforced concrete (on the left) and masonry (on the right) buildings.....	219
Figure 8.53	Building damage map of Moio della Civitella urban settlement in February 2015, according to Iovine & Parise classification (2002)	220
Figure 8.54	Displacement velocity maps obtained by COSMO-SkyMed images in 2014: along ascending (a) and descending (b) tracks.....	221
Figure 8.55	Integrated map of landslide typologies and building damage in Moio della Civitella urban settlement.....	221
Figure 8.56	Distribution of building damage level for different landslide typologies in Moio della Civitella urban settlement.....	222
Figure 8.57	Combined use of DInSAR data (a, b) and results of <i>in situ</i> survey (c, d) for updating of landslide boundary (e).....	223
Figure 8.58	Combined use of DInSAR data (a, b) and results of <i>in situ</i> survey (c, d, e, f, g) to identify a new landslide (e).....	224
Figure 8.59	Distribution of building damage for different landslide state of activity recorded in Moio della Civitella urban settlement: map (a) and pie-chart (b).....	225
Figure 8.60	Examples of damage occurred to buildings within dormant landslide affected areas.....	225
Figure 8.61	Integrated map of landslides state of activity and targets identified by ascending (a) and descending (b) SAR images in Moio della Civitella urban settlement.....	226
Figure 8.62	Landslide state of activity map in Moio della Civitella urban settlement: as mapped by Hydro-geomorphological Setting Plan in 2012 (a) and updated in 2015 (b).....	226
Figure 8.63	Vulnerability map of Moio della Civitella in February 2015 according to proposed matrices.....	227

Figure 8.64	Conventional monitoring network installed at Moio della Civitella.....	229
Figure 8.65	Location of boreholes at Moio della Civitella and identification of inclinometers investigated.....	230
Figure 8.66	Inclinometer readings and stratigraphic column related to borehole I2....	231
Figure 8.67	Inclinometer readings and stratigraphic column related to borehole I3....	231
Figure 8.68	Inclinometer readings and stratigraphic column related to borehole I10....	232
Figure 8.69	Inclinometer readings and stratigraphic column related to borehole I4bis....	232
Figure 8.70	Inclinometer readings and stratigraphic column related to borehole I9....	233
Figure 8.71	Inclinometer readings and stratigraphic column related to borehole I8....	233
Figure 8.72	Location of targets identified for comparison with measurements of inclinometer boreholes: in ascending (on the left) and descending (on the right) tracks.....	234
Figure 8.73	Cumulated “LoS” displacement maps in time-span 2010-2014 acquired by “ascending” (a) and “descending” images.....	236
Figure 8.74	Cumulated displacement maps in time-span 2010-2014 along vertical (a) and horizontal E-W (b) directions: in the latter, also movement directions in horizontal plane recorded by inclinometers are indicated.....	236
Figure 8.75	Map of number building of storeys at Moio della Civitella.....	237
Figure 8.76	Isolated and aggregated buildings: possible configurations.....	237
Figure 8.77	Building damage maps of Moio della Civitella, performed in 2009 (on the left) and in 2015 (on the right), according to Iovine and Parise (2002) classification.....	238
Figure 8.78	Example of decomposition of E-W horizontal displacement obtained by DInSAR data in two components along building façades.....	239
Figure 8.79	Map of maximum angular distortions measured on each building in period 2010-2014.....	240
Figure 8.80	Map of maximum horizontal strains measured on each building in period 2010-2014.....	240
Figure 8.81	Vulnerability zoning map of buildings in Moio della Civitella.....	241
Figure 8.82	Buildings with different vulnerability level in Moio della Civitella urban center.....	242
Figure 8.83	Pie-charts of distribution of damage levels surveyed in 2009 and in 2015.....	243
Figure 8.84	Map of increase of damage level surveyed from 2009 to 2015 in Moio della Civitella.....	244

Figure 8.85	Examples of buildings that showed an increase of damage level in Moio urban center.....	245
Figure 8.86	Examples of buildings that showed an increase of damage level in Pellare urban center.....	245
Figure 8.87	Displacement velocity-damage level relationship for buildings surveyed in 2009.....	246
Figure 8.88	Displacement velocity-damage level relationship for buildings surveyed in 2015.....	246
Figure 8.89	Empirical fragility curves for masonry and reinforced concrete buildings in 2009.....	247
Figure 8.90	Empirical fragility curves for masonry and reinforced concrete buildings in 2015.....	247
Figure 8.91	Comparison of fragility curves of masonry and reinforced concrete buildings in 2009 and in 2015.....	247
Figure 8.92	Comparison of fragility curves in 2009 and in 2015, for masonry (on the left) and reinforced concrete (on the right) buildings.....	248
Figure 8.93	Increase of displacement velocity ΔV and related increase of damage level for masonry and reinforced concrete buildings.....	248
Figure 8.94	Empirical fragility curves for masonry (a) and reinforced concrete (b) buildings, and their comparison (c).....	249
Figure 8.95	Empirical fragility curves for isolated reinforced concrete buildings with none existing damage level (D0)	250
Figure 8.96	Empirical fragility curves for isolated reinforced concrete buildings with negligible existing damage level (D1)	251
Figure 8.97	Comparison of empirical fragility curves of isolated reinforced concrete buildings with different initial damage level.....	252
Figure 8.98	Empirical fragility curves for masonry buildings with none existing damage level (D0)	253
Figure 8.99	Empirical fragility curves for masonry buildings with negligible existing damage level (D1)	254
Figure 8.100	Comparison of empirical fragility curves of isolated masonry buildings with different initial damage level.....	255
Figure 8.101	Comparison of empirical fragility curves of masonry and reinforced concrete buildings.....	255
Figure 8.102	Empirical fragility curves for reinforced concrete buildings in a position of “extremity 1” of the aggregate with none existing damage level (D0).....	256

Figure 8.103	Empirical fragility curves for reinforced concrete buildings in a position of “extremity 2” of the aggregate with none existing damage level (D0)	257
Figure 8.104	Empirical fragility curves for reinforced concrete buildings in a central position of the aggregate with none existing damage level (D0)	258
Figure 8.105	Comparison of empirical fragility curves for reinforced concrete buildings in different positions of the aggregate.....	258
Figure 8.106	Empirical fragility curves for masonry buildings at “extremity 1” of the aggregate with different existing damage levels.....	259
Figure 8.107	Empirical fragility curves for masonry buildings at “extremity 2” of the aggregate with different existing damage levels.....	260
Figure 8.108	Empirical fragility curves for masonry buildings in a central position of the aggregate with different existing damage levels.....	261
Figure 8.109	Empirical fragility curves for masonry buildings in a corner position of the aggregate with different existing damage levels.....	262
Figure 8.110	Comparison of empirical fragility curves for masonry buildings in different positions of the aggregate with different existing damage levels.....	263
Figure 8.111	Comparison of fragility curves of buildings with different existing damage levels.....	264
Figure 8.112	Empirical fragility curves for reinforced concrete buildings with different number of stories.....	265
Figure 8.113	Empirical fragility curves for masonry buildings with different number of stories.....	265
Figure 8.114	Example of damage occurred in adjacent buildings with different height of stories.....	266
Figure 8.115	Ratio between displacement of building and displacement of the surrounding area for structures with $L/B = 1$ and $L/B \neq 1$	267
Figure 8.116	Distribution of damage levels occurred to reinforced concrete and masonry buildings with $L/B = 1$ and $L/B \neq 1$	268
Figure 8.117	Building alignment in comparison with landslide direction.....	268
Figure 8.118	Ratio between displacement of building and displacement of surrounding area for buildings with different orientation.....	269
Figure 8.119	Distribution of damage levels occurred to reinforced concrete and masonry buildings with different orientation.....	269
Figure 8.120	Map of probability to obtain an increase of one damage level in 2020 according to first scenario.....	270
Figure 8.121	Map of probability to obtain an increase of one damage level in 2020 according to second scenario.....	271

Figure 8.122 Cumulated displacement maps in 2011 along vertical (a) and horizontal E-W (b) directions.....	272
Figure 8.123 Cumulated displacement maps in period 2011-2012 along vertical (a) and horizontal E-W (b) directions.....	272
Figure 8.124 Cumulated displacement maps in period 2011- 2013 along vertical (a) and horizontal E-W (b) directions.....	273
Figure 8.125 Cumulated displacement maps in period 2011- 2014 along vertical (a) and horizontal E-W (b) directions.....	273
Figure 8.126 Cumulated displacement maps in period 2011- 2015 along vertical (a) and horizontal E-W (b) directions.....	274
Figure 8.127 Example of building surveyed according to the scheme proposed by Italian DPC.....	275
Figure 8.128 Sections 1 and 2 of DPC classification scheme for considered building..	276
Figure 8.129 Sections 3,4,5,6,7 of DPC classification scheme for considered building.	277
Figure 8.130 Sections 8 and 9 of DPC classification scheme for considered building...	278
Figure 8.131 Location of considered building and results of inclinometer measurements in the period November 2015-May 2017 in I3 borehole.....	279
Figure 8.132 Vertical displacement profiles measured along building façades in period 2011-2015.....	280
Figure 8.133 Horizontal displacement (E-W) profiles measured along building façades in period 2011-2015.....	280
Figure 8.134 Equivalent laminated beam model of considered building.....	281
Figure 8.135 Building damage level surveyed in 2009 and in 2015.....	284
Figure 8.136 Relationship between maximum tensile strain and distortions to building foundations (deflection ratio Δ/L and horizontal strain ε_h)	285
Figure 8.137 3D fragility curves obtained by equivalent beam model: axonometric views n. 1.....	286
Figure 8.138 3D fragility curves obtained by equivalent beam model: axonometric views n. 2.....	286
Figure 8.139 3D fragility curves obtained by equivalent beam model: axonometric views n. 3.....	287
Figure 8.140 The basic macro-element for masonry: (a) un-deformed configuration; (b) deformed configuration.....	288
Figure 8.141 Modelling of infilled frame with central door opening. (a) the geometrical layout; (b) model corresponding to the basic mesh; (c) model corresponding to a more refined mesh resolution.....	288

Figure 8.142 Three-dimensional finite-macro-element global model: axonometric views.....	289
Figure 8.143 Example of displacement profiles applied to building foundations along each façade according to DInSAR data recorded in period 2011-2015....	290
Figure 8.144 Damage distribution on masonry walls induced by displacement profiles shown in Figure 8.143.....	291
Figure 8.145 Comparison between damage surveyed by <i>in situ</i> campaign (on the left) and damage provided by analysis on computational model (on the right) on building façade named “b”	291
Figure 8.146 Distribution of damage levels obtained on computational model for each pair of distortions applied to building foundations.....	292
Figure 8.147 Vulnerability domains obtained by interpolating points with same damage level.....	292
Figure 8.148 Comparison between vulnerability domains obtained by numerical analysis on computational model and empirical domains provided by Boscardin & Cording (1989)	293
Figure 8.149 Location of building aggregate within an area affected by slow deformation/movements.....	294
Figure 8.150 Arenaceous and conglomeratic blocks outcrops on which building has been founded.....	295
Figure 8.151 Schematic geometrical view of building aggregate plan in original (pre-intervention) and current (post-intervention) configurations.....	296
Figure 8.152 “LoS” displacement velocity map of targets identified on building aggregate by ascending ENVISAT and COSMO-SkyMed data.....	297
Figure 8.153 “LoS” displacement time series measured on part of aggregate not subject to restoration works (on the left) and on the repaired part (on the right)...	298
Figure 8.154 Computational models of building aggregate corresponding to configurations pre- (a) and post- (b) restoration works: axonometric views.....	298
Figure 8.155 Vertical displacement profiles measured along building façades in period 2011-2015.....	300
Figure 8.156 Horizontal displacement profiles measured along building façades in period 2011-2015.....	300
Figure 8.157 Distribution of cracks surveyed on building aggregate (a) and on façade along South direction (b).....	301
Figure 8.158 Comparison between damage distribution obtained by computational model (on the top) and surveyed by <i>in situ</i> campaign in February 2015 (on the bottom) on building façade more damaged.....	302

Figure 8.159 Comparison of results obtained by numerical analyses performed on computational models corresponding to pre- and post-restoration works.....	303
---	-----

List of Tables

Table 3.1 Definitions for landslide hazard and risk assessment.....	30
Table 3.2 Definitions for landslide risk management.....	31
Table 3.3 Landslide hazard assessment methods.....	39
Table 3.4 Landslide risk assessment methods with some references.....	43
Table 3.5 Qualitative measures of likelihood.....	44
Table 3.6 Qualitative measures of consequences to property.....	44
Table 3.7 Qualitative risk level implications.....	44
Table 3.8 Quantitative landslide risk assessment methods.....	46
Table 4.1 Values of physical vulnerability.....	63
Table 5.1 Checklist for planning a landslide investigation.....	73
Table 5.2 Microwave bands (Frequency and Wavelength) commonly used in radar remote sensing.....	90
Table 5.3 Main features of the main SAR satellite missions.....	103
Table 5.4 Main DInSAR approaches.....	113
Table 6.1 Values of vulnerabilities depending on different foundation depths and landslide depths.....	121
Table 6.2 Relationship between category of damage and limiting tensile strain.....	142
Table 6.3 Classification of damage according to Burland (1977)	143
Table 6.4 Classification of damage according to Alexander (1986)	144
Table 6.5 Classification of damage according to Chiocchio et al. (1997)	145
Table 6.6 Classification of damage according to Iovine & Parise (2002)	146
Table 6.7 Classification of damage severity according to the ‘DPC’.....	147
Table 6.8 Scheme to compile for damage assessment according to the ‘DPC’	150
Table 7.1 Level of damage and limit tensile strain.....	176
Table 7.2 Damage state definitions and drift limit according to RISK-UE project....	178

Table 7.3	Thresholds values of ISDR of damage limits states for reinforced concrete buildings.....	179
Table 7.4	Thresholds values of ISDR of damage limits states for masonry buildings...	179
Table 7.5	Proposed approach to assess damage degree in a computational model of masonry buildings.....	180
Table 8.1	Scheme to evaluate ratio between displacements of building and surrounding area.....	218
Table 8.2	Summary of inclinometers features at Moio della Civitella.....	229
Table 8.3	Comparison between displacement obtained by DInSAR data and by inclinometer borehole.....	235
Table 8.4	Mechanical parameters E, G and n of masonry material considered in the analysis.....	282
Table 8.5	Annual distortions and corresponding average values measured in period 2011-2015.....	283
Table 8.6	Cumulated angular and horizontal distortions projected from 2011 to 2025.....	283
Table 8.7	Maximum tensile strain obtained by equivalent beam model in period 2011-2025.....	284
Table 8.8	Damage level corresponding to maximum tensile strain reached every year.....	285
Table 8.9	Mechanical characteristics of the masonry.....	289
Table 8.10	Mechanical characteristics of irregular masonry elements.....	299
Table 8.11	Mechanical characteristics of masonry elements roughly worked.....	299

CHAPTER 1

INTRODUCTION

Slow-moving landslides are widespread in different geological settings all over the world and they often cause extensive damage to buildings and infrastructures in urban and rural areas. Urbanized areas affected by landslides show ruptures and cracks on man-made facilities.

For this reason, periodic vulnerability assessment in a landslide risk analysis plays a key role in risk prevention and mitigation activities. In the last decade, a considerable interest towards approaches useful to provide information on spatial and temporal landslide evolution and on their interaction with existing facilities has grown among the scientific community and land management institutions: assessment, monitoring and prediction of building damage allow to avoid or to minimize the derived effects.

Landslide vulnerability analysis is still considered a difficult process since it depends on several factors. At present no standard methodologies exist to detect the relationship between slope movements and building damage: different approaches to assess building vulnerability have been described in literature, each one characterized by its own peculiarity, obviously with differences and discrepancy in the final results.

The present work provides a general methodology to assess current and future conditions of damage and local failures of buildings within landslide affected areas, through an integrated analysis which takes into account the vulnerability key factors, the landslide kinematics and the structural characterization of the exposed elements.

At different scales of representation, the two above mentioned datasets have been separately analyzed, and subsequently merged in order to detect landslide-induced damage to buildings. Generally, from low-resolution analysis, to medium and to detailed scale, the parameters useful for the landslide intensity definition and for the exposed elements characterization change.

Among the recent technological advancements, Remote Sensing techniques have demonstrated to be powerful investigation tools as a monitoring system for various phenomena, such as volcanic eruptions, earthquakes, landslides, subsidence, sinkholes, and nowadays also for deformation measurements of structures and infrastructures affected by ground instability.

In particular, the Differential SAR Interferometry (DInSAR) has been successfully applied as a remote-sensing tool in several analyses aimed to monitoring the impacts of ground movements in urban areas (Tomás et al., 2012; Cascini et al., 2013; Bianchini et al., 2014; 2015; Infante et al., 2016; Peduto et al., 2017), thanks to its accuracy, high spatial and multi-temporal coverage, fast data acquisition, and overall reasonable costs.

The processing results, however, could not be conveniently used without their validation: the integration of satellite data with “conventional” methods, such as inclinometers, piezometers and geomorphological *in situ* surveys, provides more detailed information about the nature and causes of ground deformation.

Subsequently, characterization of exposed elements requires to define the building structural properties accomplished with an accuracy level dependent on the building vulnerability diagnosis criteria.

Empirical, analytical and numerical analyses of above mentioned datasets, developed according to qualitative, semi-qualitative and quantitative approaches respectively, allow to detect, at different levels of detail, vulnerability of existing buildings within a landslide-affected area. In particular, such methodology allows to:

- detect the preliminary cause-effect relationship between landslide features and consequences to existing facilities;
- assess spatial and temporal damage evolution of buildings, investigating also the vulnerability factors influencing the performance of structures to slow-moving landslides;
- investigate the structural behavior of each building and forecast damage severity degree future condition.

The proposed methodology has been applied to Moio della Civitella urban settlement, located in the Cilento, Vallo di Diano and Alburni National Park, in Salerno Province, Italy, whose territory is widely affected by erosional and gravitational phenomena, causing severe damage on existing buildings. In such case, available *in situ* data have been sufficient to implement an integrated monitoring system with radar data. Moio della Civitella urban center, in fact, has been thoroughly investigated by means of conventional monitoring techniques such as boreholes, topographic measure points, inclinometers, GPS network and pluviometer station.

1.1 Structure of the thesis

The thesis is structured in nine sections.

The first chapter includes the thesis objectives and methods, providing information about the role of this research as a support in landslide mitigation activities.

The second chapter gives an illustration concerning landslides, starting from their description and classification, to the landslide diffusion in Italy and their interaction with existing facilities.

In the third chapter, an overview on landslide risk assessment methodologies has been taken into account, highlighting main goals, approaches and steps to define it.

Afterwards, in the fourth chapter, a general review on the role of vulnerability in a landslide risk analysis, analyzing issues and approaches for physical vulnerability assessment, is given.

Subsequently, the fifth and sixth chapters respectively, take into account the key factors to define building vulnerability, the landslide kinematics and the structural characterization of the exposed elements. In the fifth chapter, a general overview of different landslide monitoring systems is presented: in particular, SAR technique is described, illustrating the various SAR missions performed in the last 20 years, and the development of some algorithms available in the scientific community. In the sixth chapter, a particular focus is given on the characterization of exposed elements, showing vulnerability factors and existing approaches to building damage assessment.

The seventh chapter describes the proposed methodology for building vulnerability assessment at different scales of representation and with different levels of detail.

The following chapter, the eighth, deals with the study area: building vulnerability of Moio della Civitella urban settlement (Salerno Province, Italy) has been investigated through a multi-level analysis.

Finally, the last chapter deals with the discussions and the conclusions of this research, critically analyzing the role of such work in the general panorama of the scientific community, and illustrating the possible future perspectives.

1.2 Objectives of the research

The main objective of this work is to provide an innovative methodology which can be used to forecast the spatial and temporal evolution of building structural vulnerability in urban settlements affected by slow-moving, intermittent landslides.

Structure vulnerability analysis, meant as a detection of current and future damage conditions, represents a helpful tool that can be mostly aimed to support the decision-making process in the initial design of risk mitigation measures.

One of the most significant aims of this thesis is to apply SAR technique to the analysis of damage recorded to buildings located in slow-moving landslide-affected areas.

Widely used among scientific community to monitor deformation of ground surface on wide areas (kilometer-size extension), the intention is to show the potential of such technique also to assess behavior of structures affected by landslide phenomena.

The combination of DInSAR data and the results of structural analyses allowed the investigation of a cause-effect relationship at different levels of detail.

With reference to Moio della Civitella urban settlement, whose territory is affected by several slow-moving landslides, a multi-level and integrated analysis of landslide's kinematics and of exposed elements has been addressed to detect, at different levels of accuracy, vulnerability of existing facilities.

The main highlights of this thesis are discussed in the following.

At **small scale** of representation, the combined use of available landslide inventory and geomorphological maps, and medium-high resolution DInSAR data, integrated with building damage recorded by a field survey, allows to:

- identify stable/unstable areas, stable/unstable buildings and analyze their behavior;
- update the landslide inventory map (boundary and state of activity);
- provide a preliminary analysis about building damage susceptibility to ground movements, depending on the relationship between landslide intensity and recorded building damage;
- identify, through a qualitative analysis, areas with different level of vulnerability, combining landslide velocity and building damage severity in a vulnerability matrix.

Medium scale analysis, added to information of the previous level, requires to define geo-lithological settings and the stratigraphy of the study area, building characteristics such as geometrical data, number of stories, typology of construction.

This level of analysis allows to:

- define a vulnerability zoning map, useful for cause-effect qualitative correspondence identification, more detailed than in the previous scale;
- provide an empirical relationship between the changes in landslide intensity and the worsening of damage severity level;
- assess influence of vulnerability factors on performance of the structure to slow-moving landslide-induced movements;
- predict, at an intermediate level of detail, spatial and temporal evolution of buildings damage with reference to the whole territory of the study area.

Finally, analysis at a **detail scale**, carried out on a single building, has the following main goals:

- assess structural behavior of buildings to landslide-induced movements;
- define, for each building, by analytical or numerical analysis, the relationship between landslide intensity and expected damage class.
- forecast future conditions of damage and local failures of buildings.

Such methodology could represent a useful tool to assess building vulnerability complementary to the forensic analysis of structures. It allows, also, to define influence of constructive characteristics on building behavior to ground movements: empirical data and numerical analyses highlight structural parameters that can increase building vulnerability.

Furthermore, the same approach could be tested in different areas to demonstrate the possibility of their application to the risk mitigation in other test sites affected by similar phenomena. Once validated, can be suitable to evaluate how the elements at risk in a landslide affected area may change with time, contributing to the risk assessment, which is a very important task for decision making by Civil Protection Authorities, especially during the landslide post-event phase, in particular to forecast possible monetary losses induced by building damage.

CHAPTER 2

LANDSLIDES

Introduction

Ground deformation and instability globally represent one of the most remarkable and widespread natural hazards. Landslides, in particular, are recognized as one of the most damaging geological hazards all over the world, for extent, impact on man-made infrastructures and facilities and number of casualties, accounting every year severe damage, in terms of direct and indirect costs.

Landslides are natural phenomena of the Earth's dynamic but their activity is expected to increase, together with often catastrophic effects, as a consequence of human activities, such as rapid urbanization, deforestation and climate changes, that have severely modified the natural environment, making it extremely vulnerable.

Moreover, as urban and infrastructures development has expanded to hillside areas, the landslides exposed population counts approximately 300 million individuals (4-5% of world population), with 66 million people living in high risk zones (Nadim et al., 2006).

Individual slope failures are generally not so “spectacular” or so costly as earthquakes, major floods, hurricanes or some other natural catastrophes, being usually small scale events: however, over the years they may cause more damage to properties than any other hazards. The spatial distribution of fatal landslides (events with loss of lives reported) presents a strongly heterogeneous pattern, as shown in Petley et al. (2012), being located in all the continents (Fig. 2.1).

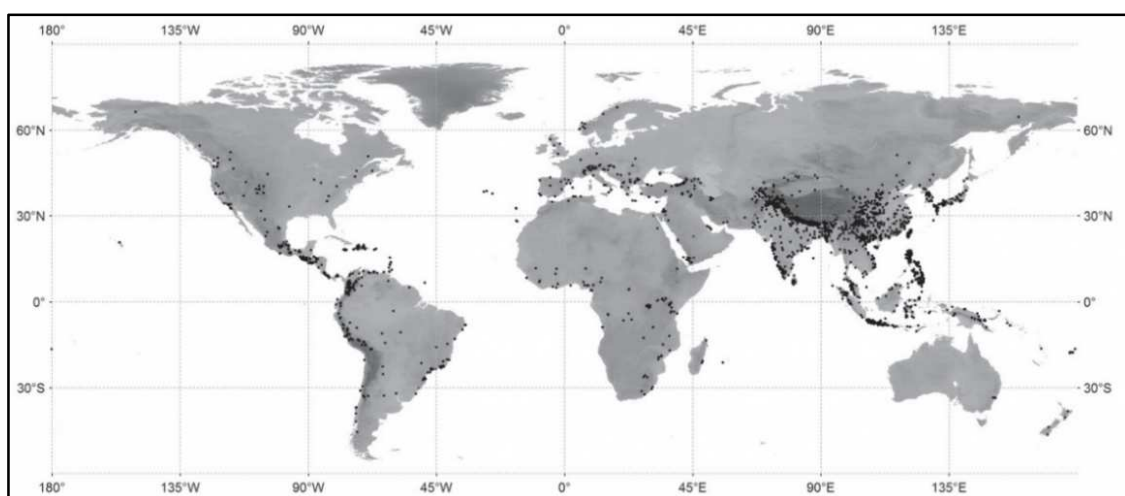


Figure 2.1 Spatial distribution of fatal landslides (modified from Petley et al., 2012).

Currently, many researches focus on the prediction, prevention and mitigation of the risk associated to landslides, because their direct and indirect costs are unsustainable for the affected communities. Schuster (1996), Guzzetti et al., (1999), reported a detailed analysis of landslide costs in several countries: in Europe, in particular, the landslide costs are significant, particularly in Austria, France, Switzerland and Italy. In this latter, mass movements cause annual losses significantly high considering the country's size.

Historically, Italy is one of the European countries most affected by this kind of events. In such a complex geological setting, where mass movements of different typologies are widespread, the increase of landslide occurrences is due also to the continuous urban expansion that brought to presence of buildings and infrastructures also in landslide-prone areas.

In the following, a general overview of the main topics related to landslides is presented, with particular reference to classification, kinematics, causes and triggering factors.

2.1 Landslide definition and classifications

A definition given by Varnes (1978) and Cruden (1991) describes the term landslide as “the movement of a mass of rock, debris or earth down a slope”, thus excluding natural phenomena, such as ground subsidence and sinkholes. Accordingly, landslides can be classified on the base of the two main components highlighted in the above definition: the type of material involved and the type of movement.

Five different materials have been included (Varnes, 1978):

- **Rock:** is “a hard or firm mass that was intact and in its natural place before the initiation of movement”.
- **Soil:** is “an aggregate of solid particles, generally of minerals and rocks, which either was transported or was formed by the weathering of rock in place. Gases or liquids filling the pores of the soil form part of the soil”.
- **Earth:** “describes material in which 80% or more of the particles are smaller than 2 mm, the upper limit of sand sized particles”.
- **Mud:** “describes material in which 80% or more of the particles are smaller than 0.06 mm, the lower limit of silt sized particles”.
- **Debris:** “contains a significant proportion of coarse material; 20% to 80% of the particles are larger than 2 mm, and the remainder are less than 2 mm”.

As regards the movements, the different types have been classified (Fig. 2.2):

- **Falls:** movements composed by masses detached from steep slopes or cliffs, with little or no shear displacement, and going downward through air (free fall) or bouncing and rolling;
- **Topples:** movements of masses of different materials made of a forward rotation about a fulcrum point;
- **Rotational slides:** in this case the masses slide downwards and outwards on one or more concave surfaces, sinking at the back and heaving at the toe;
- **Translational slides:** in this case the movements occur along a planar failure surface and it may continue parallel to the slope;
- **Spreads:** involve the fracturing and the lateral extension of coherent rocks or soils, after the liquefaction of the subjacent materials;
- **Flows:** they can be a slow to rapid movement of saturated or dry material, advancing like a viscous fluid;
- **Complex landslides:** they consist in the composition of one or more types of movements, one following the others (Varnes, 1978).

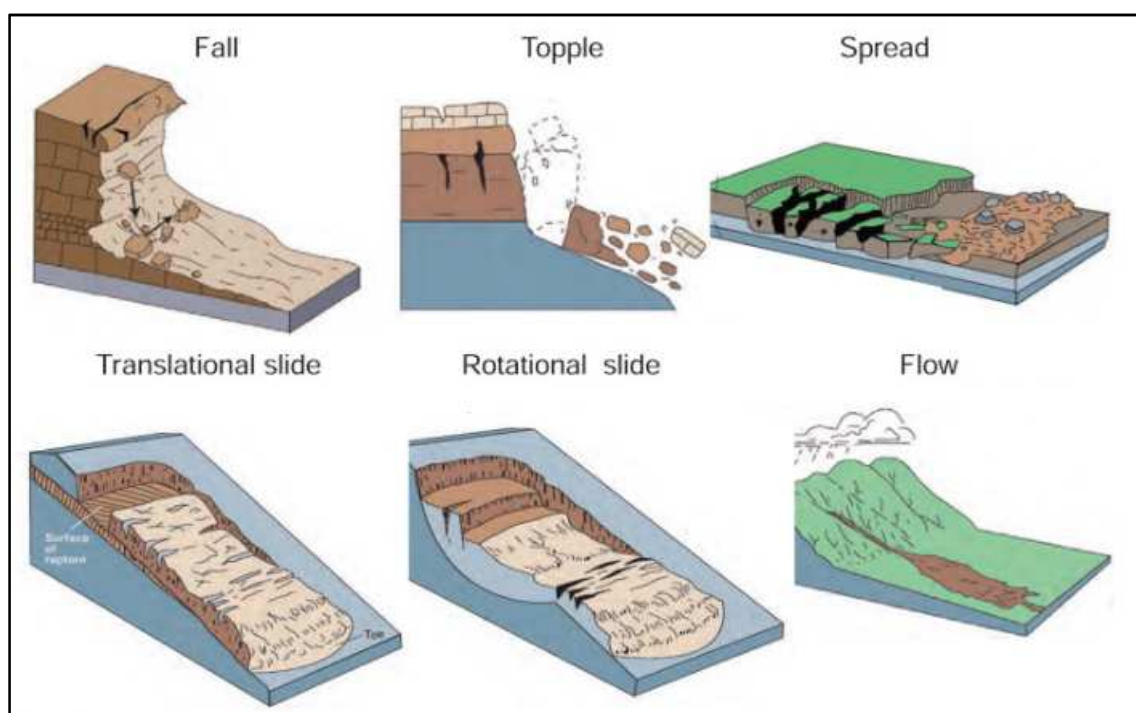


Figure 2.2 Classification of landslide movement types (modified from Cruden and Varnes, 1996).

By combining the types of movements and the material involved in a landslide, the following categories indicated in Figure 2.3 can be defined.

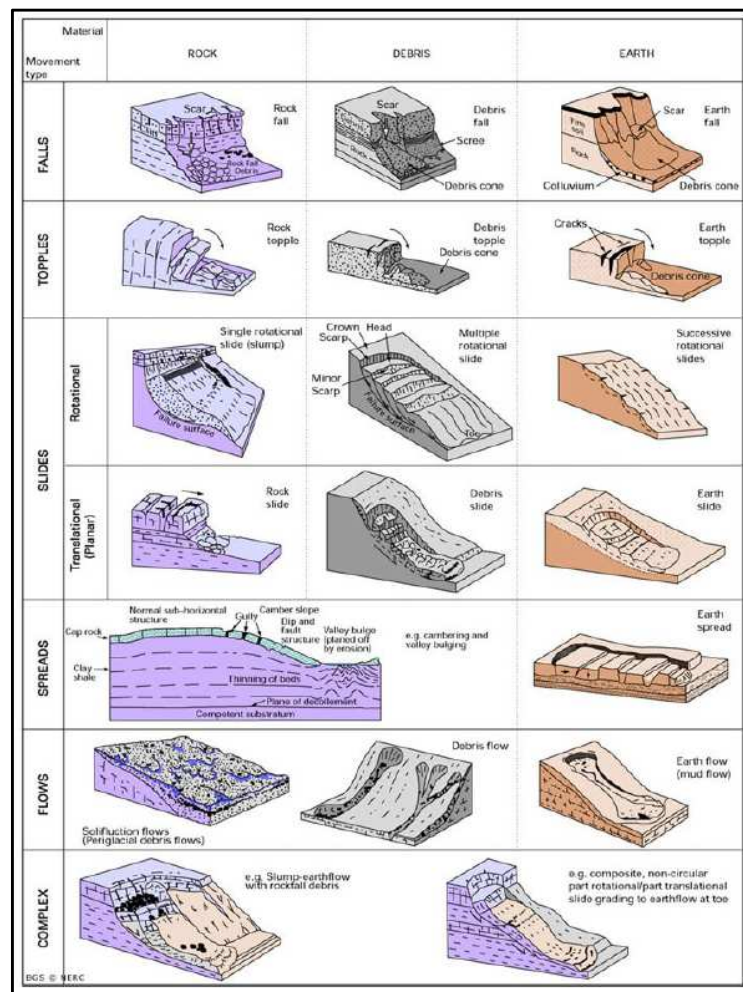


Figure 2.3 Classification of landslide typologies (modified from Cruden and Varnes, 1996).

It is worth to mention that other classifications have been proposed in engineering geological studies, starting from Balzer (1875) onward, but Varnes (1978), ideating a classification based on type of material involved and type of movement, has given a first modern approach. Successively, Pierson and Costa (1987) focused their attention to classify the flow type landslide, based on velocity and sediment concentration. Hutchinson (1988) proposed a geomorphological and geotechnical approach, shown in Figure 2.4, and then the European Programme On Climate and Natural Hazards, (EPOCH, 1993) focused its efforts on classifying landslides on the base of the European experiences and conditions. Dikau et al. (1996) suggested a classification of landslide mechanisms compatible with Hutchinson (1988) and EPOCH (1993), and finally, Hungr et al. (2001) analyzed and reorganized the flow-type landslides, based on the genetic and

the morphological aspects, and in the year 2014 attempted to revise several aspects of the well-known classification of Varnes (1978), modifying the definition of landslide-forming materials and providing compatibility with accepted geotechnical and geological terminology of rocks and soils, and in conclusion individuating 32 landslide types.

A	Rebound	
	1	Movements associated with man-made excavations
	2	Movements associated with naturally eroded valleys
B	Creep	
	1	Superficial, predominantly seasonal creep; mantle creep
	2	Deep-seated, continuous creep; mass creep
	3	Pre-failure creep; progressive creep
	4	Post-failure creep
C	Sagging of mountain slopes	
	1	Single-sided sagging associated with the initial stages of landsliding
	2	Double-sided sagging, associated with the initial stages of double landsliding, leading to ridge spreading
	3	Sagging associated with multiple toppling
D	Landslides	
	1	Confined failures
	2	Rotational slips
	3	Compound failures (markedly non-circular, with listric or bi-planar slip)
	4	Translational slides
E	Debris movements of flow-like form	
	1	Mudslides (non-periglacial)
	2	Periglacial mudslides (gelifluction of clays)
	3	Flow slides
	4	Debris flows, very to extremely rapid flows of wet debris
	5	Sturzstroms, extremely rapid flows of dry debris
F	Topples	
	1	Topples bounded by pre-existing discontinuities
	2	Topples released by tension failure at rear of mass
G	Falls	
	1	Primary, involving fresh detachment of material; rock and soil falls
	2	Secondary, involving loose material, detached earlier; stone falls
H	Complex slope movements	
	1	Cambering and valley-bulging
	2	Block-type slope movements
	3	Abandoned clay cliffs
	4	Landslides breaking down into mudslides or flows at the toe
	5	Slides caused by seepage erosion
	6	Multi-tiered slides
	7	Multi-storeyed slides

Figure 2.4 Classification of landslides typologies (modified Hutchinson, 1988).

In this thesis the Cruden and Varnes (1996) classification has been followed.

Moreover, the state of activity, which describes, through geomorphological information, the temporal evolution characteristics of a landslide, has been defined, selecting eight different types (Fig. 2.5):

- **Active:** landslides are active when are actually moving;
- **Suspended:** when landslides moved within the last seasonal cycle, but they are not currently active;

- **Reactivated:** landslides are reactivated when they are again active after being inactive;
- **Inactive:** when landslides moved for the last time before the last seasonal cycle.

Besides the inactive landslides can be further divided in the following states:

- **Dormant:** inactive landslide which could be reactivated following instability;
- **Stabilized:** inactive landslides protected after human intervention;
- **Abandoned:** inactive landslides protected from their original causes;
- **Relict:** inactive landslide developed in a geomorphological and climatic condition completely different from the actual situation.

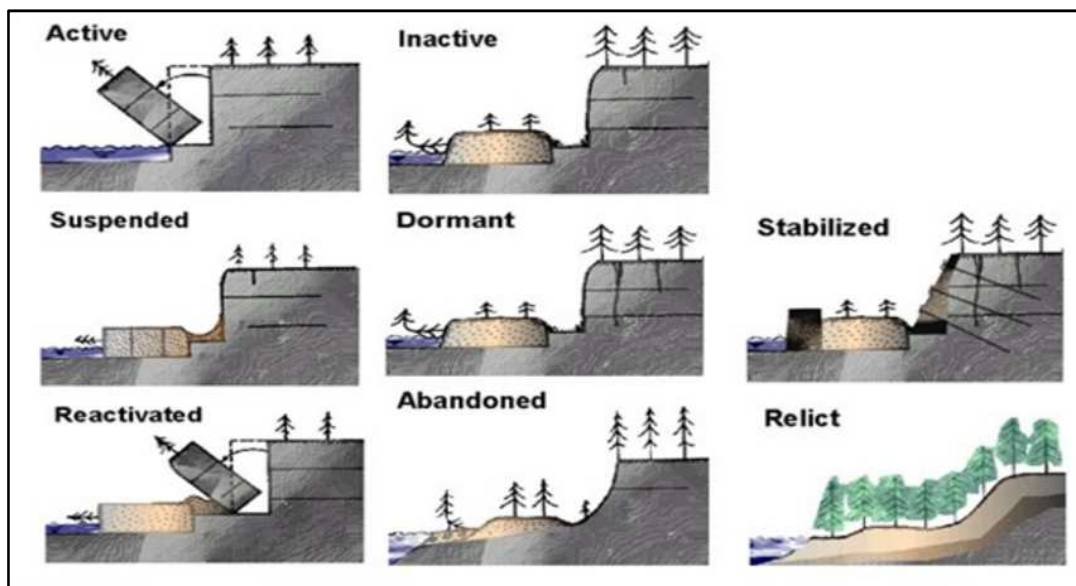


Figure 2.5 Scheme of the state of activity of a landslide, modified from WP/WLI (1993).

Another important task which has been defined by the WP/WLI (1993) is the delineation of the distribution of activity, which refers to how and where the landslide is moving. It can be (Fig. 2.6):

- **Advancing:** the rupture surface of a landslide extends towards the direction of the movement;
- **Retrogressive:** the rupture surface is extending in the opposite direction respect to the movement direction;
- **Enlarging:** the rupture surface is extending in two or more directions;
- **Diminishing:** the volume of mobilized material decreases;
- **Confined:** there is the presence of a scarp, but no rupture surface is clearly visible;

- **Moving:** the mobilized material continues to move without any visible change in the rupture surface and in the volume;
- **Widening:** in this case the rupture surface extends into one or both flanks of the landslide.

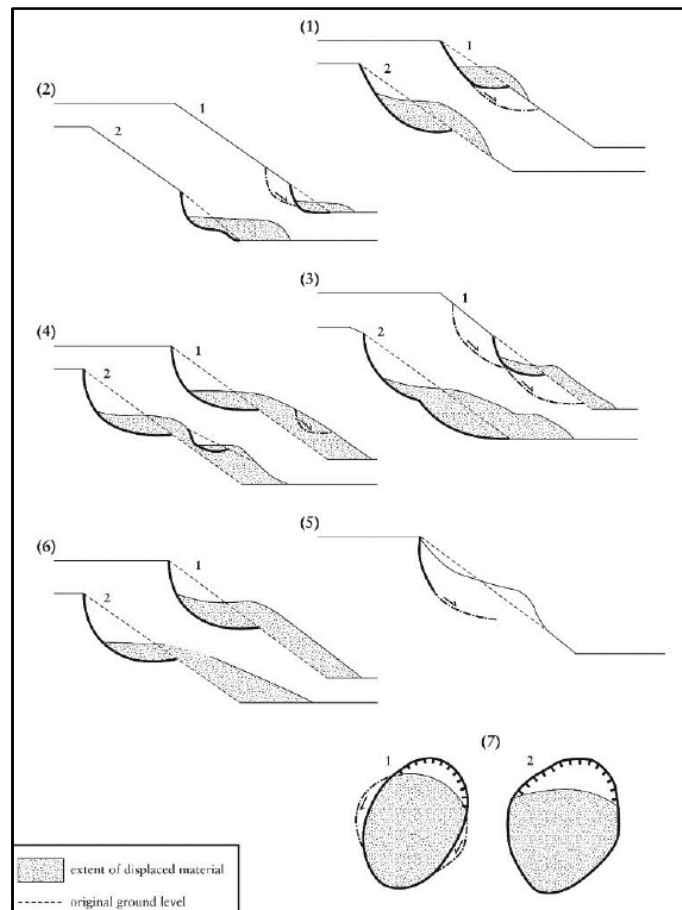


Figure 2.6 Scheme of the distribution of activity of a landslide, modified from WP/WLI (1993).

- 1) Advancing landslide; 2) Retrogressive landslide; 3) Enlarging landslide; 4) Diminishing landslide;
5) Confined landslide; 6) Moving landslide; 7) Widening landslide.

Furthermore, also the style of a landslide activity has been defined and described, consisting in the contribution of different movements within a single landslide and their relationship. Several styles have been identified (Fig. 2.7):

- **Complex:** a complex landslide is made of at least two different types of movement (e.g., sliding and flowing) in sequence;
- **Composite:** a composite landslide shows at least two types of simultaneous types of movements, but located in different parts of the landslide;
- **Successive:** it is a similar type as a nearby, earlier landslide, but not sharing mobilized material or a rupture surface with it;

- **Single:** a single landslide is a single movement of displaced material;
- **Multiple:** a multiple landslide shows repeated movements of the same kind.

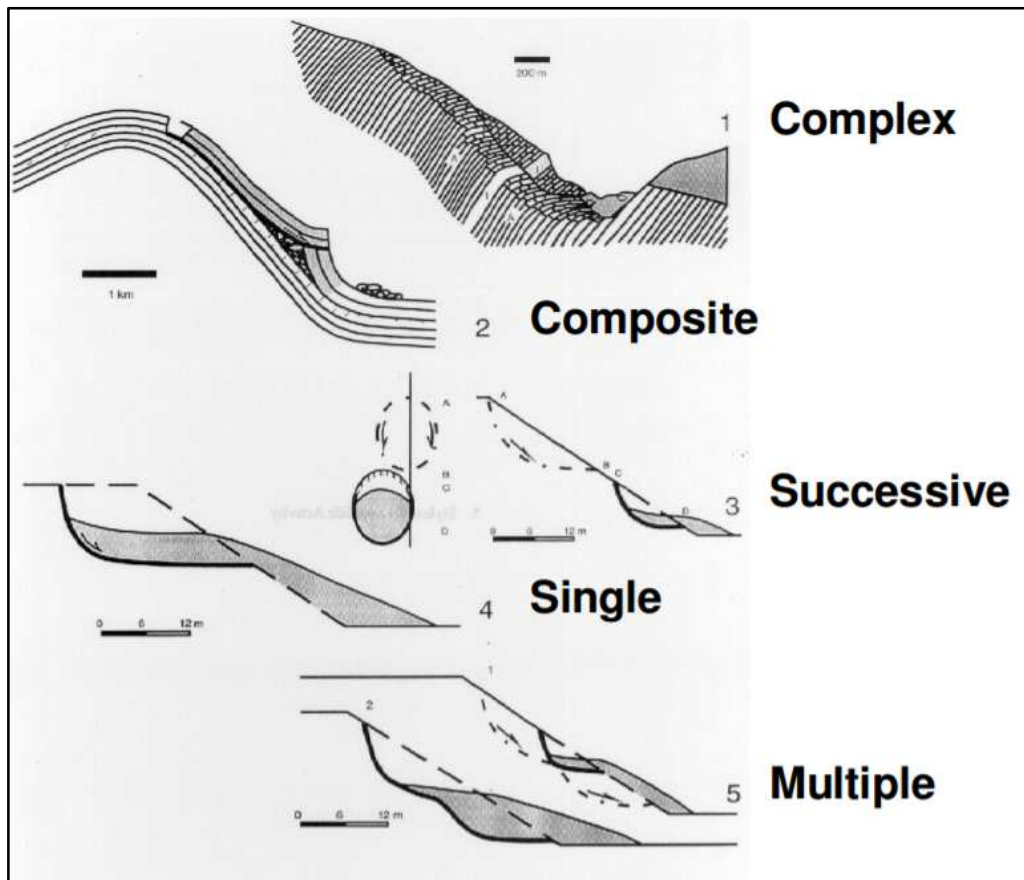


Figure 2.7 Scheme of the style of activity of a landslide, modified from WP/WLI (1993). 1) Complex landslide; 2) Composite landslide; 3) Successive landslide; 4) Single landslide; 5) Multiple landslide.

Finally, the assessment of landslide effects on structures and infrastructures, requires a deep understanding of the phenomenon, including the investigation of its intensity.

Landslide intensity can be defined through different categories of parameters (Leone et al., 1996):

- **geometrical** parameters (volume, boundary, area, depth);
- **kinematic** parameters (velocity, absolute displacement, differential displacement);
- **others** (density, viscosity, etc.).

The most common classification of landslide intensity is introduced by Cruden & Varnes (1996) which proposed a velocity scale (Fig. 2.8): for a landslide, velocity is intended as the highest speed achieved after the slope failure. It represents a very important parameter for the risk assessment in hazardous areas.

Seven classes of velocity have been identified, from extremely rapid movements, whose rate can exceed the speed of a person running (5 m/sec), to extremely slow movements (below 16 mm/year) that are imperceptible without appropriate instruments.

Velocity Class	Description	Velocity (mm/sec)	Typical Velocity	Probable Destructive Significance
7	Extremely Rapid	5×10^3	5 m/sec	Catastrophe of major violence; buildings destroyed by impact of displaced material; many deaths; escape unlikely
6	Very Rapid	5×10^1	3 m/min	Some lives lost; velocity too great to permit all persons to escape
5	Rapid	5×10^{-1}	1.8 m/hr	Escape evacuation possible; structures, possessions, and equipment destroyed
4	Moderate	5×10^{-3}	13 m/month	Some temporary and insensitive structures can be temporarily maintained
3	Slow	5×10^{-5}	1.6 m/year	Remedial construction can be undertaken during movement; insensitive structures can be maintained with frequent maintenance work if total movement is not large during a particular acceleration phase
2	Very Slow	5×10^{-7}	15 mm/year	Some permanent structures undamaged by movement
	Extremely SLOW			Imperceptible without instruments; construction POSSIBLE WITH PRECAUTIONS

Figure 2.8 Landslide velocity scale according to Cruden and Varnes classification (1996).

From what stated above, it appears that velocity of a landslide should be considered as one of the most significant factor for evaluation of the hazard and risk related to slope movements. It is demonstrated that the vulnerability of a territory may greatly increase with the landslide velocity: small but rapid phenomena might bring to catastrophic effects, in terms of damage and loss of life, when compared to larger but slow phenomena. Thus, each one of the seven classes of velocity above specified can be associated to a probable destructive power, as shown in Figure 2.8.

2.2 Landslide features

A more complete knowledge about landslides passes compulsorily through the individuation and the definition of the main features that characterize landslides in their totality. The following terminology is based on Cruden & Varnes (1996) (Fig. 2.9) and modified by the WP/WLI (1993) (Fig. 2.10).

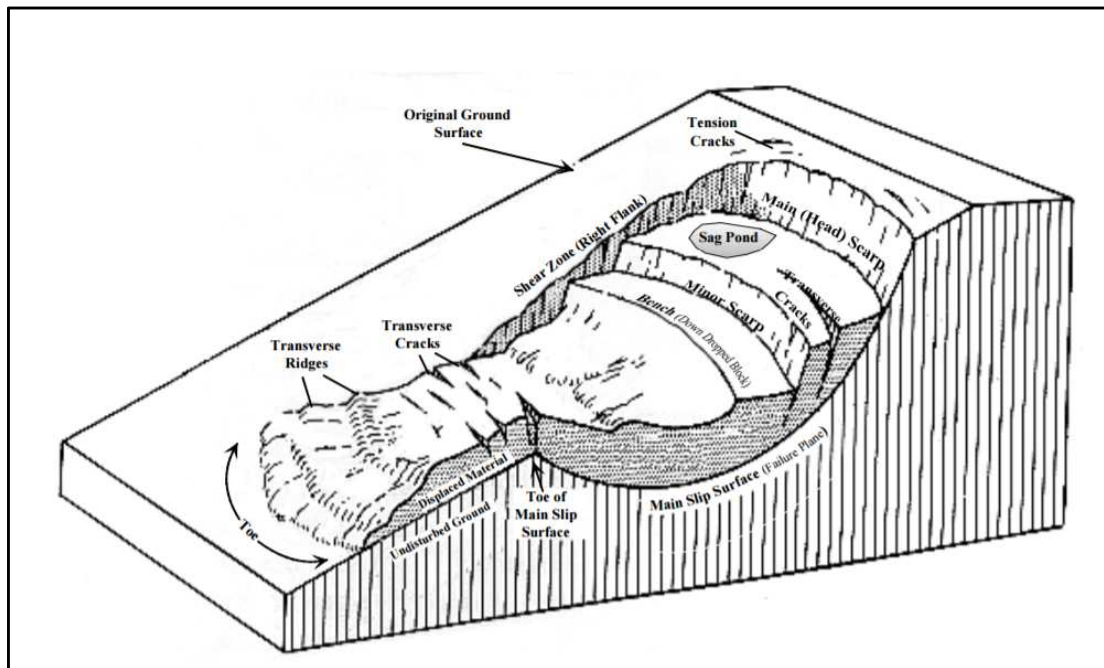


Figure 2.9 Block diagram of typical landslide features (from Cruden and Varnes, 1996).

1. **Crown:** The non-mobilized material still in place and adjacent to the highest parts of the main scarp.
2. **Main Scarp:** A steep surface on the undisturbed ground at the upper edge of the landslide, caused by movement of the displaced material away from the undisturbed ground.
3. **Top:** The highest point of contact between the displaced material and the main scarp.
4. **Head:** The upper parts of the landslide along the contact between the displaced material and the main scarp.
5. **Minor Scarp:** A steep surface on the displaced material of the landslide produced by differential movements within the displaced material.
6. **Main Body:** The part of the displaced material of the landslide that overlies the surface of rupture between the main scarp and the toe of the surface of rupture.

- 7. Foot:** The portion of the landslide that has moved beyond the toe of the surface of rupture and overlaid the original ground surface.
- 8. Tip:** The point of the toe farthest from the top of the landslide.
- 9. Toe:** The lower, usually curved margin of the displaced material of a landslide, it is the most distant from the main scarp.
- 10. Surface of Rupture:** The surface which forms (or which has formed) the lower boundary of the displaced material below the original ground surface.
- 11. Toe of the Surface of Rupture:** The intersection (usually buried) between the lower part of the surface of rupture of a landslide and the original ground surface.
- 12. Surface of Separation:** The part of the original ground surface overlain by the foot of the landslide.
- 13. Displaced Material:** Material displaced from its original position on the slope by movement in the landslide. It forms both the depleted mass and the accumulation.
- 14. Zone of Depletion:** The area of the landslide within which the displaced material lies below the original ground surface.
- 15. Zone of Accumulation:** The area of the landslide within which the displaced material lies above the original ground surface.
- 16. Depletion:** The volume bounded by the main scarp, the depleted mass and the original ground surface.
- 17. Depleted Mass:** The volume of the displaced material, which overlies the rupture surface but underlies the original ground surface.
- 18. Accumulation:** The volume of the displaced material, which lies above the original ground surface.
- 19. Flank:** The undisplaced material adjacent to the sides of the rupture surface. Compass directions are preferable in describing the flanks but if left and right are used, they refer to the flanks as viewed from the crown.
- 20. Original Ground Surface:** The surface of the slope that existed before the landslide took place.

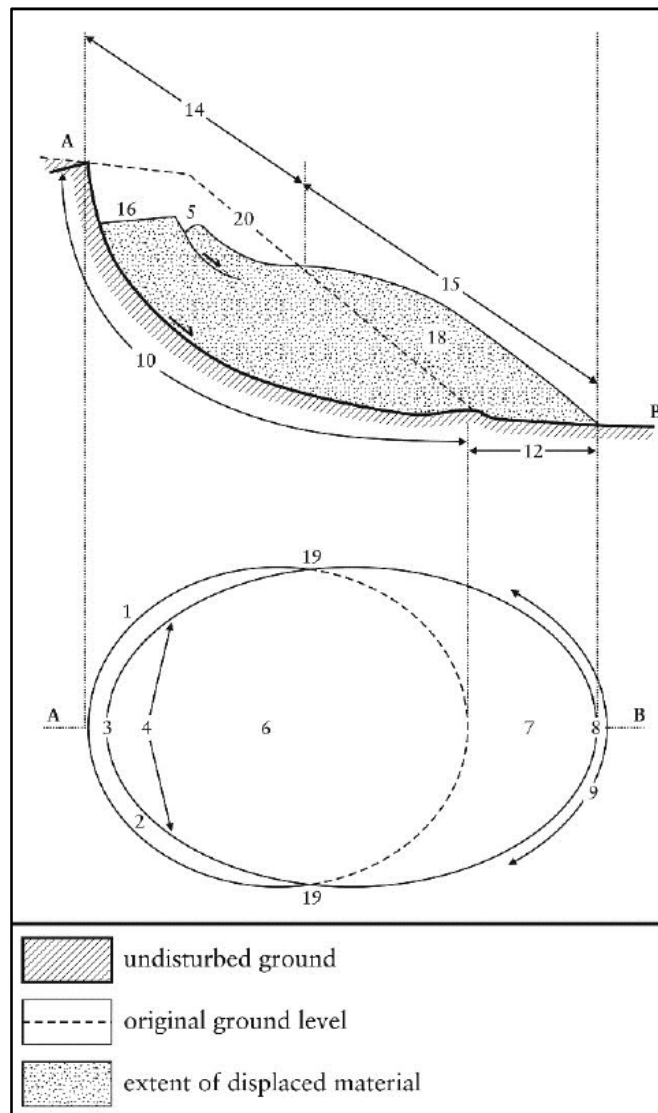


Figure 2.10 Features of a landslide (modified from WP/WLI, 1993).

Landslide features, as defined and illustrated above, change with time and represent, with geometrical dimensional characteristics (width, length, depth), the basis for developing a model aimed to define the causes of landslides and the factors for a possible reactivation in a prone area.

2.3 Landslide causes

The project of effective and efficient remedial measures requires a deep understanding of the phenomenon under investigation, namely of its type, rate of movements and of the other factors above mentioned and, not less important, of the possible processes that cause the landslide.

The great variety of slope movements reflects the diversity of conditions that cause the slope to become unstable and the many processes that trigger the movement: generally, they can be due to one or more of the following actions (Cruden & Varnes, 1996):

- **increasing the shear stress**, through the removal of support at the lateral margins of the landslide or at the toe of the slope, for instance by excavations for quarries and infrastructures or by river erosion; material can be removed also from below the landslide by piping or karst processes. Moreover, the application of surcharges and the occurrence of transitory stress can result in an increase of the shear stresses: in the first case, surcharges include rain and snow, growth of vegetation, volcanic activity, anthropogenic features such as waste dumps or irrigation systems, aqueducts and sewages leaking water. Transitory stresses, instead, can derive by explosions (of human and natural origin), earthquakes, storms and even by the passage of heavy vehicles;

- **contributing to low strength**: the low strength can be an intrinsic characteristic of the material involved by a landslide, as in the case of organic soils or clays that are naturally weak materials, or it may result by natural processes, such as water saturation and weathering; moreover, discontinuities, such as faults, fissures, bedding surfaces, foliations, etc., can lead to the weakness of the whole unstable mass;

- **reducing the shear strength**, including processes as softening of fissured clays (Picarelli et al., 2006), slaking due to cycles of freezing/thawing or wetting/drying (Botts, 1998), chemical weathering, progressive failure, seepage erosion.

However, it has to be highlighted that assessing the cause of a landslide is a complex task: often it is the combination of some of the above causes that makes a slope susceptible to failure. In fact, it is more correct to consider three stages of slopes' stability (Crozier, 1986):

- **stable**, in which stability forces are sufficiently strong and higher than the destabilizing ones;

- **marginally stable**, in which destabilizing forces reach a certain level of activity and prevail some time on stability forces;

- **actively unstable**, finally, in which destabilizing forces produce continuous or intermittent movement.

The transition from one stage to another is the result of two causal factors categories:

- **Preparatory causal factors** which make the slope susceptible to movement without actually initiating it and thereby tending to place the slope in a marginally stable state;

- **Triggering causal factors** which initiate movement. The causal factors shift the slope from a marginally stable to an actively unstable state.

According to the effects classification above mentioned (preparatory or triggering), landslide causal factors can be discretized in four practical groups, based on their origin (Fig. 2.11).

<p>Geological causes</p> <ol style="list-style-type: none">1. Weak materials2. Sensitive materials3. Weathered materials4. Sheared materials5. Jointed or fissured materials6. Adversely oriented mass discontinuity (bedding, schistosity, etc)7. Adversely oriented structural discontinuity (fault, unconformity, contact, etc)8. Contrast in permeability9. Contrast in stiffness (stiff, dense material over plastic materials)
<p>Morphological causes</p> <ol style="list-style-type: none">1. Tectonic or volcanic uplift2. Glacial rebound3. Fluvial erosion of slope toe4. Wave erosion of slope toe5. Glacial erosion of slope toe6. Erosion of lateral margins7. Subterranean erosion (solution, piping)8. Deposition loading slope or its crest9. Vegetation removal (by forest fire, drought)
<p>Physical causes</p> <ol style="list-style-type: none">1. Intense rainfall2. Rapid snow melt3. Prolonged exceptional precipitation4. Rapid drawdown (of floods and tides)5. Earthquakes6. Volcanic eruption7. Thawing8. Freeze-and-thaw weathering9. Shrink-and-swell weathering
<p>Human causes</p> <ol style="list-style-type: none">1. Excavation of slope or its toe2. Loading of slope or its crest3. Drawdown (of reservoirs)4. Deforestation5. Irrigation6. Mining7. Artificial vibration8. Water leakage from utilities

Figure 2.11 Checklist of landslide causes (after Cruden & Varnes, 1996).

In the following, we will focus on the most important triggering factor: the precipitations.

Water surely represents the main trigger for landslide activation; in particular, the slope saturation by water is the primary reason (Iverson et al., 1997). Many cases of landslides around the world (Larsen & Sánchez, 1998; Jakob & Weatherly, 2003) have been related to intense rainfall lasted for hours as well as to less intense rainfall but lasted for several days. Loose or weak soils are particularly susceptible to be triggered by rainfall: this is also the case, for example, of burned areas where often, due to the presence of a water-repellent (hydrophobic) soil layer produced by the wildfire, small debris flows can occur (DeBano, 2000). To this purpose, several researches have long attempted to determine the amount of precipitation needed to trigger slope failures, a problem of scientific and societal interest. Rainfall thresholds can be defined on physical (process-based, conceptual) or empirical (historical, statistical) basis. In particular, statistical techniques are often used for analyzing the relation between rainfall and landslides over regional areas and, as result, if a large amount of precipitation data and information on the temporal occurrence of landslides are available, critical triggering thresholds can be identified (Caine, 1980; Cannon & Ellen, 1985; Guzzetti et al., 2007).

However, it is worth to note that these threshold values can be considered reliable if the analyzed context is homogeneous. In the real cases, we deal with settings characterized by a complexity of landslide types and involved materials, and thus, in order to obtain reliable results, we need to carry out very detailed analysis at local scale.

For examples of landslides triggered by other factors, see Wieczorek (1996), Boschi et al., (1997), Bozzano et al., (2004), Larsen (2008) and Meusburger & Alewell (2008).

2.4 Landslides in Italy

Historically, Italy has always been a country severely affected by landslide events: to this purpose the role of the Italian nature scientists has been to acquire the right knowledge and awareness of such phenomena.

A first attempt to conduct a census of the landslides was done by the geographer Roberto Almagià (1910), on behalf of the Italian Geological Society. The final result was a complete knowledge of the landslides occurred between the 19th and 20th century on the whole national territory (excluding the Alps and the islands), carried on after several field surveys.

Successively, another census has been done by the Minister of Public Works during the 60's, publishing in 1965 a volume with all the inventory collected between 1957 and 1963.

More recently a more complete survey on areas hit by landslides and floods between 1918 and 1994 has been carried out by the National Group for the Hydro-geological Catastrophes Defense (GNDCI) in 1998 (Fig. 2.12).

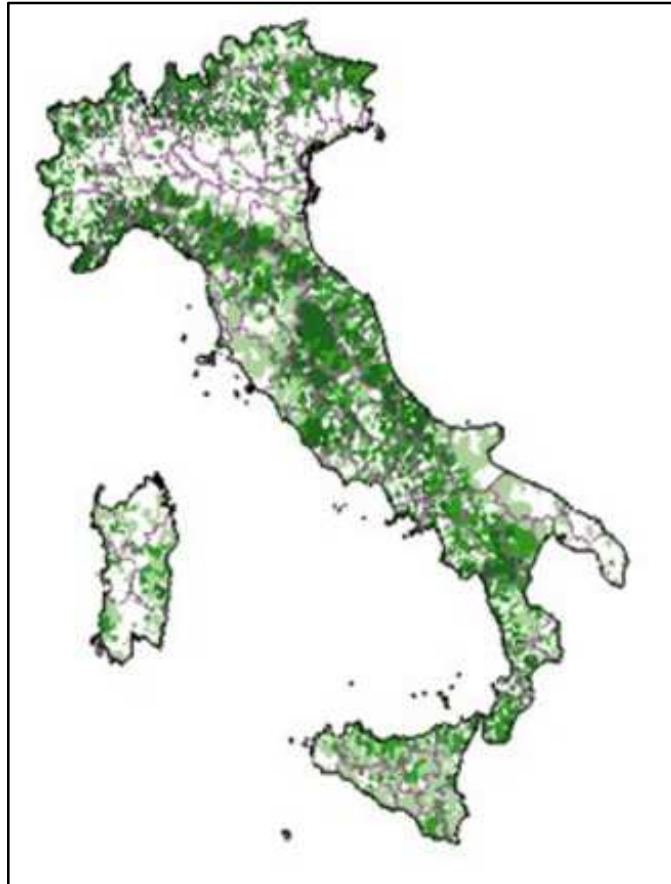


Figure 2.12 Map of urban centers affected by landslide phenomena (GNDCI, 1998).

It is only after the disaster of Sarno (1998), involving also the municipality of Siano, Quindici, Bracigliano and S.Felice a Canello in Campania Region, that the Government felt the need of a complete and homogeneous analysis of the distribution of landslides on the national territory.

Hereafter started the IFFI project, providing for an accurate landslide inventory on the Italian territory, based on photointerpretation and geological field surveys. The IFFI project represents the first homogeneous and updated landslide inventory of the Italian territory. More than 300 among geologists and bureaucrats collaborated for the realization of this project.

The archive is published on the Web, in order to promote the accessibility of information to as much people as possible (<http://www.progettoiffi.isprambiente.it>).

The archive, up to the end of 2014, counted 614.799 landslide phenomena involving an area of about 23.000 km², equal to 7,5% of the national territory.

The two main products of the IFFI project are the online cartography service, allowing to visualize the landslides and the main parameters associated, and the Report on landslides in Italy (ISPRA), published each year, and summarizing the information on the national and regional situation.

In parallel, the Law 183/1989 on the soil defense established the “Basin plan” as a cognitive, normative and technical instrument for the planning of the actions and the rules for the conservation, the defense and the development of the soil and the correct use of the water, on the base of the physical and environmental characteristics of the area of interest (Law 183/1989).

Accordingly, the new-established Basin’s Authorities are the agencies predisposed for such aims. The Hydro-geomorphological Setting Plan (HSP) is the tool which the Basin’s Authorities use to understand and determine a territorial setting capable to ensure a balance between the hydrogeological dynamics and the growing urbanization. One of the tasks of the Basin’s Authorities deal with the slope instabilities, starting from a census of the landslides present on the given territory, in order to identify landslide hazard and risk and eventually define, in some cases, the proper interventions.

Generally, the growing number of landslide phenomena is related with an increase of national population, associated with an intensive – and locally excessive – exploitation of the land including development of new settlements, and construction of roads, railways, and other infrastructures. In many areas of Italy, due to the local physiographical setting, expansion of new settlements and infrastructure occurred in dangerous or potentially hazardous areas.

The Research Institute for Geo-Hydrological Protection (CNR-IRPI), collected and organized an archive of the events between 1965-2014, arranged in a map, and calculating 1279 deaths, 1702 casualties and 158.923 evacuees (Fig. 2.13).

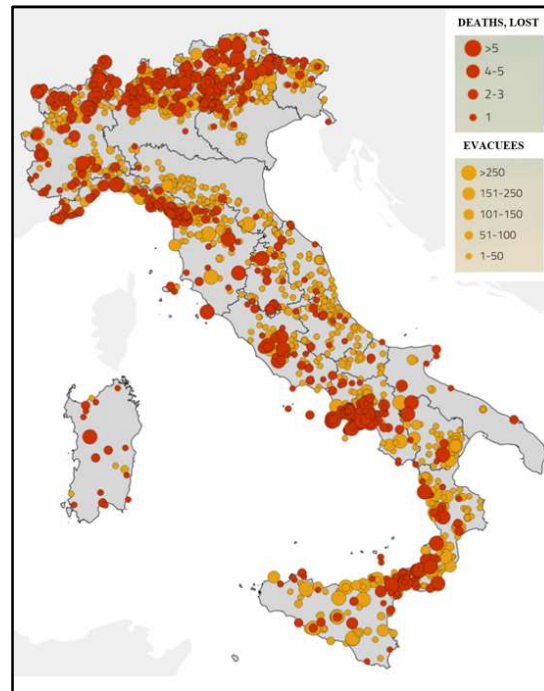


Figure 2.13 Map of the landslide events with “victims” between 1965 and 2014 (CNR IRPI, 2015).

Among the main events in the last 60 years with catastrophic consequences, it is possible to cite Genova (1970), Ancona (1982) (Coltorti et al., 1985; Cotecchia, 2006), Stava (1985) (Chandler et al., 1995; Sammarco, 2004), Sarno (1998) (Del Prete et al., 1998; Calcaterra et al., 2000; Zanchetta et al., 2004), Nocera Inferiore (2005) (Revellino et al., 2013).

It is necessary to highlight that the Southern Apennine of Italy are one of the most multi-hazard active areas in the world, due to the frequency and intensity of earthquakes, to the severity of erosion processes and to the diffusion of landslides (Del Prete, 1993).

In particular, the Campania Region, characterized by different geomorphologic settings, is affected by different types of natural hazards, from landslides to volcanic eruptions, to severe coastal erosion and seismic events.

As regards the slope instability phenomena, the different lithologic, structural, hydrogeologic and geomorphologic settings of the Campania territory make it prone to different types of mass movements. For instance, in the volcanic sectors the most frequent type of landslide is represented by falls and topples involving the lithoid portions of lava and tuffs and, after intense rainfall, by flows in the pyroclastic deposits; along the calcareous – dolomitic slopes of the Sorrentina Peninsula and the Picentini Mountains, on the other hand, translational slides and topples as well as complex landslides (slides-flows) involving the pyroclastic cover on carbonate ridges, occur.

Finally, a predominance of flows, followed by rotational slides and complex phenomena, mainly rotational slides grading into flows, is observed where highly tectonized clayey and flysch formations crop out.

2.5 Slow-moving landslides and impacts on existing facilities

Slow-moving landslides generally do not cause human loss of life but often generate significant damage to existing structures and infrastructures. Urbanized areas affected by landslide displacements show ruptures and cracks on man-made facilities (Fig. 2.14).

For this reason, scientific community study these events and their consequences: prevention, prediction and monitoring of these phenomena play a key-role to avoid or to minimize the derived effects.



Figure 2.14 Examples of building damages within landslides affected areas: (a) San Fratello (province of Messina) (from Bianchini et al., 2015), (b) Verbicaro (province of Cosenza) (from Nicodemo et al., 2014) and (c) Gorga (province of Salerno) urban area (from Infante et al., 2016).

When buildings are located within landslide, the interaction is of “static” type, generating rigid rotations or angular distortions as a result of differential displacements (Fig. 2.15). These effects occur when the ground movements affecting buildings are greater than the tensions which structures are capable to absorb without showing deformations.

The survey of the damage eventually affecting buildings and infrastructures, on one side, and the analysis of slope movements distribution and activity, on the other, can help in better understanding the interaction between landslides and anthropogenic features: combining the results of the two activities can be an useful tool in the assessment of vulnerability and risk associated to landslides.

Class	Description	Types of man-made works interacting with landslides	Mode of interaction	Expected damage and population reaction (modified, after Cruden and Varnes, 1996)
1	Extremely rapid	Structures, infrastructures and lifelines located along the landslide path or at the foot of the slope (I)	Impact, invasion of open spaces and filling of basements	Catastrophic event. Buildings and structures destroyed by the impact. Many victims. Evacuation is impossible
2	Very rapid			As above; some victims. Evacuation is impossible
3	Rapid	(I) + (II)	Invasion of open spaces and infrastructures (roads, railways), increase of thrust against retaining structures	Buildings and other structures are destroyed or severely damaged; infrastructures out of action; lifelines damaged. Evacuation is possible
4	Moderate			
5	Slow	Structures, infrastructures and lifelines located on the landslide body (II)	Invasion of open spaces and infrastructures, increase in thrust against retaining structures. Deformation of buildings and of other structures	Stabilization works can be carried out even during landslide movement. Some structures can be working by means of frequent maintenance works
6	Very slow			
7	Extremely slow		Increase in thrust on retaining structures. Deformation of buildings and of other structures	Damage is not destructive. Structures can be kept working, despite secondary damage. Movements cannot be detected without instrumentation. Buildings and structures are not seriously damaged

Figure 2.15 Interaction between slow-moving landslide and man-made works and expected damage (from Picarelli & Urciuoli, 2008).

It is important to point up that urban damage depends on typology and velocity of landslides, involved lithologies, slope gradient, the main component of movement prevailing where the building is located (i.e. different kind of cracks are associated to rotational or translational deformations; Capecchi & Focardi, 1988), as well as on age, typology and material of the buildings. About this latter, for example, in the case of many urban contexts in Southern Italy, a distinction between buildings in masonry and in reinforced concrete is important, because the same damage can have different effects on their stability.

At present no standard methodologies exist to evaluate the relationship between slope movements and building damages: different approaches to assess building vulnerability have been described in literature, each one characterized by its own peculiarity, obviously with differences and discrepancy in the final results (Alexander 1989, 2005, Cardinali et al., 2002, Cascini et al., 2005, Glade 2004, Del Soldato et al., 2013).

The most significant recent cases in Italy which caused damage to urban settlements and communication infrastructures are in Parma and Reggio Emilia province in 2013, Cinque Terre and Lunigiana in October 2011 (Cevasco et al., 2013), Massa (province of Massa) in October 2010, Montaguto (province of Avellino) in March 2010 (Giordan et al., 2013; Guerriero et al., 2013), Maierato (province of Vibo Valentia) in February 2010

(Gattinoni et al., 2012), San Fratello (province of Messina) in February 2010 (Bardi et al., 2014; Bianchini et al., 2014), Giampilieri (province of Messina) in October 2009 (Aronica et al., 2012), Borca di Cadore (province of Belluno) in July 2009 and Altilia (province of Cosenza) in January 2009, Volterra (province of Pisa) (Bianchini et al., 2015), Moio della Civitella (province of Salerno) (Infante et al., 2016), Verbicaro (province of Cosenza) (Ferlisi et al., 2015).

The large amount of urban settings in unstable areas has developed, among the scientific community and land management institutions, a growing interest towards innovative approaches useful to provide information on temporal and spatial evolution about their interaction with existing buildings. To this purpose, the present work would provide a general methodology to define future conditions of damage and local failures of buildings within landslide affected area, through a deep knowledge of relevant factors related to both landslides (type, intensity, etc.) and exposed facilities (materials, state of maintenance, foundation type, etc.).

CHAPTER 3

SLOW-MOVING LANDSLIDE RISK ASSESSMENT

Introduction

In everyday life human beings are in constant contact and continuously compare themselves with the natural environment; as a consequence, human life conditions are strictly related to the environmental conditions. Moreover, due to the increase of large scale disasters in recent years, society is becoming more vulnerable.

Risk assessment is the final goal of many landslide studies, that have the aim to protect population, economy and the environment against potential damage caused by landslides. In this context, risk is defined as the damage and losses that could happen in the future due to landslide action. According to this relationship, it is evident that an accurate assessment model is of the utmost importance as it may under- or over- estimate the occurrence of future events.

However, at present there is not yet a common agreement on risk assessment at least for landslide phenomena and no standard methodologies exist. To this purpose, taking into account the importance of risk mitigation activities, investigations on this topic have increased enormously in the last decade.

Assessing landslide risk is a complex and uncertain operation that requires the combination of different techniques, methods and tools, and the interplay of various expertises pertaining – among the others – to geology and geomorphology, engineering and environmental sciences, meteorology, climatology, mathematics, information technology, economics, social sciences and history. Despite the indisputable importance of landslide risk evaluation for decision making, comparatively little efforts have been made to establish and systematically test methods for landslide risk assessment, and to determine their advantages and limitations.

The World Conference on Disaster Reduction (United Nations, 2005), defined the strategy goals and priorities actions to “identify, assess and monitor disaster risks and enhance early warning” with the following key activities:

- a) develop, update periodically and widely disseminate risk maps and information related to decision-makers, general public and communities at risk in an appropriate format;
- b) develop system of indicators of disaster risk and vulnerability at national and sub-national scales that will enable decision-makers to assess the impact of disasters on social, economic and environmental conditions and disseminate the results to decision makers, the public and populations at risk;
- c) record, analyze, summarize and disseminate statistical information on disaster occurrence, impacts and losses, on a regular basis through international, national regional, and local mechanisms.

As above mentioned, landslide risk analysis is a complex and time-consuming task but recently scientists, practitioners and decision-makers demonstrated an important interest on this topic. This topic, used to estimate the risk of landslide hazard to individuals, populations, properties, or the environment (Fell et al., 2008; Corominas et al., 2014) generally contains five main steps:

1. hazard identification;
2. hazard assessment;
3. inventory of elements at risk and exposure;
4. vulnerability assessment;
5. risk estimation.

It is important to highlight that, at present, the expression “management of landslide risk” denotes a complex and multidisciplinary process focused more on the prevention and reduction of the risk associated to landslides than on the rehabilitation and reconstruction phases provided after disasters occurred, as in the past. To this aim, four strategies can be adopted, whose details can be found in Schuster & Kockelman (1996):

1. restriction of development in landslide-prone areas, through an effective territory planning based on appropriate land use zoning and law restrictions;
2. development of codes for excavations, grading and constructions, in order to ensure that they will not impact on slope stability;
3. protection by means of physical measures, such as drainage, modification of the slope geometry, retaining walls, anchors, caissons, and other methods that can be useful to prevent/control landslides;

4. development of warning systems, including monitoring instruments that can also provide real-time data in order to protect properties and population living in the area potentially affected.

In this chapter, after a brief review of the relevant literature, concepts and definitions useful for landslide risk assessment are shown, including a discussion on the differences between quantitative (probabilistic) and qualitative (heuristic) approaches.

Furthermore, a particular attention is focused on conceptual frameworks for vulnerability detection of exposed elements that will be in detail explained in the subsequent chapter and represents the principal topic of this work.

3.1 Landslide risk definition: literature review

The trend during the last three decades shows an increase both in the number of natural hazard events and in the number of affected people. Disasters not only affect poor and characteristically more vulnerable countries but also those thought to be well protected. In their well-known report, Varnes and the IAEG Commission (1984) established that *“landslide risk evaluation aims to determine the expected degree of loss due to a landslide (specific risk) and the expected number of lives lost, people injured, damage to property and disruption of economic activity (total risk)”*.

It is important to highlight that the aim of the risk evaluation is substantially different from that of landslide susceptibility or hazard assessment. When assessing landslide susceptibility or hazard, the interest is on the single slope or the mapping unit where landslides can occur, posing a threat and eventually causing damage. When attempting to establish landslide risk, the focus is on the element at risk that may suffer damage from a harmful landslide.

This apparently insignificant difference has serious consequences. The first, to determine landslide risk information on slope failures and their expected evolution is necessary, but insufficient. Estimation of landslide risk requires information on the type, abundance, distribution, vulnerability and value of the facilities in the study area. The second, if it is possible to zone an area for landslide susceptibility or hazards, it is generally unfeasible to zone an area for landslide risk. Risk is an attribute of an element and not of the area where the element is located. For example, in the same area many elements may be present, each with a different type or degree of vulnerability. Further, the distribution and abundance of the elements at risk in an area may change with time.

According to Varnes and IAEG (1984), the most common set of definitions regarding hazard and risk, widely accepted, is shown in Table 3.1.

Term	Definition
Natural hazard (H)	Probability of occurrence within a specified period of time and within a given area of a potentially damaging phenomenon.
Vulnerability (V)	Degree of loss to a given element at risk (see below) resulting from the occurrence of a natural phenomenon of a given magnitude. It is expressed on a scale from 0 (no damage) to 1 (total loss).
Specific risk (R_s)	Expected degree of loss due to a particular natural phenomenon. It may be expressed by the product of H times V.
Elements at risk (E)	Population, properties, economic activities, including public services, etc. at risk in a given area.
Total risk (R_t)	Expected number of lives lost, persons injured, damage to property, or disruption of economic activity due to a particular natural phenomenon, and is therefore the product of specific risk (R_s) and elements at risk (E). Thus: $R_t = (E) (R_s) = (E) (H \times V)$

Table 3.1 Definitions for landslide hazard and risk assessment (Varnes and IAEG, 1984).

A graphical representation of landslide risk, from Alexander (2002), is shown in Figure 3.1. From this perspective, risk is the zone where both vulnerability and hazard meet. The level of risk thus results from the intersection of hazard with the value of the elements at risk by the way of their vulnerability. This intersection zone tends to grow due to climate change (for the hazard part) and due to further development and population growth (for the vulnerability part). Finally, many definitions and approaches have been implemented and published (Einstein, 1988; Fell, 1994; Cruden and Fell, 1997; Glade et al., 2005), allowing one to conclude that nowadays definitions regarding landslides risk assessment are generally accepted.

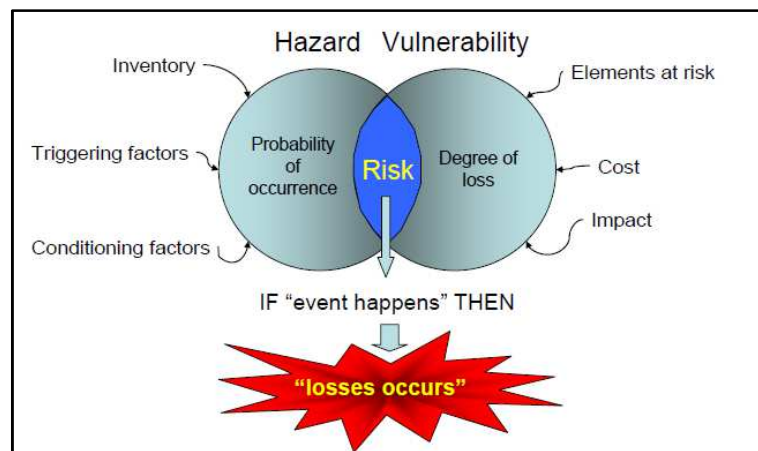


Figure 3.1 Graphical representation of landslide risk (after Alexander, 2002).

3.2 Landslide risk management

Disasters caused by landslides have continued to increase during the last decades. For this reason, some countries have already progressed in the development of procedures for managing urban and population growth as well as for minimizing the associated risks.

Risk management is defined as the systematic application of management policies, procedures and practices to the tasks of identifying, analyzing, mitigating and monitoring risk. The definitions of the different parts for the framework are shown in Table 3.2.

Term	Definition
Risk estimation	the process used to produce a measure of the level of health, property, or environmental risks being analysed. Risk estimation contains the followings steps: frequency analysis, consequence analysis and their integration.
Risk analysis	the use of available information to estimate the risk to individuals or populations, property, or the environment, from hazards. Risk analysis generally contains the following steps: scope definition, hazard identification, and risk estimation.
Risk evaluation	the stage at which values and judgements enter the decision process, explicitly or implicitly, by including consideration of the importance of the estimated risks and the associated social, environmental, and economic consequences, in order to identify a range of alternatives for managing the risks.
Risk assessment	the process of risk analysis and risks evaluation
Risk control or risk treatment	the process of decision making for managing risks, and the implementation, or enforcement of risk mitigation measures and the re-evaluation of its effectiveness from time to time, using the results of risk assessment as one input.
Risk management	the complete process of risk assessment and risk control (or risk treatment).
Individual risk	the risk of fatality or injury to any identifiable (named) individual who live in the zone impacted by the landslide; or follows a particular pattern of life that might subject him or her to the consequences of the landslide.
Societal risk	the risk of multiple fatalities or injuries in society as a whole: one where society would have to carry the burden of a landslide causing a number of deaths, injury, financial, environmental, and other losses.
Acceptable risk	a risk for which, for the purpose of life or work, we are prepared to accept as it is with no regard to its management. Society does not generally consider expenditure in further reducing such risks justifiable.
Tolerable risk	a risk that society is willing to live with so as to secure certain net benefits in the confidence that it is being properly controlled, kept under review and further reduced as and when possible.

Table 3.2 Definitions for landslide risk management (IUGS, 1997).

Although this terminology used for landslide often does not match the terminology used in other types of disasters, it seems to have been generally accepted by the landslide scientific community (Cruden and Fell, 1997; AGS, 2000; ICG, 2003).

Figures 3.2 and 3.3 describe the methodological framework and flow-chart for landslide risk management.

The components necessary for risk control and mitigation (risk management), include hazard and risk identification, hazard and consequence analysis, risk calculation (risk analysis) and finally risk evaluation (risk assessment).

In particular:

- **risk analysis** includes scope definition, hazard and risk identification and risk estimation (hazard analysis and consequence analyses). Hazard analysis involves characterizing the landslide (classification, size, velocity, mechanics, location, travel distance), and the corresponding frequency (annual probability) of occurrence. Consequence analysis includes identifying and quantifying the elements at risk (property, persons), their temporal spatial probability, their vulnerability either as conditional probability of damage to conditional probability of damage to property, or conditional probability of loss of life or injury;
- **risk assessment** takes the output from risk analysis and assesses them against values judgements, and risk acceptance criteria;
- **risk management** takes the output from the risk assessment, and considers risk mitigation, including accepting the risk, reducing the likelihood, reducing consequences, develops a risk mitigation plan and possibly implements regulatory controls.

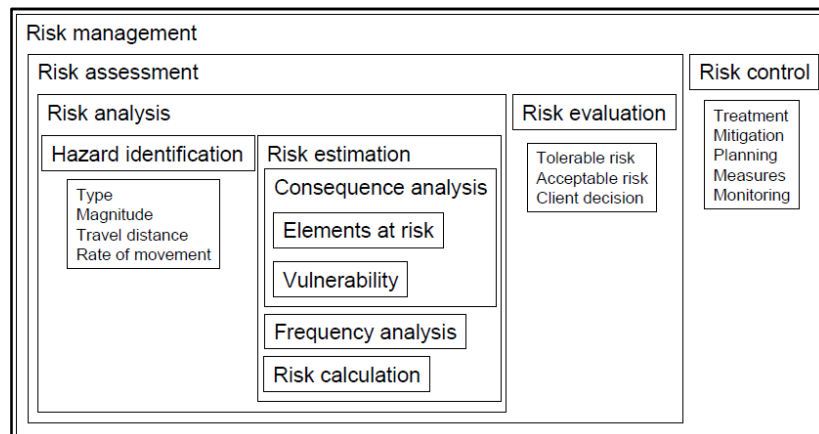


Figure 3.2 Conceptual framework for landslide risk management (from IUGS, 1997).

The risk management process evaluates also the consideration of the risk mitigation options and the results of the implementation of the mitigation measures and of the monitoring. To this purpose the outputs of the risk assessment could be either:

- risks are tolerable or at least acceptable, then no mitigation options need to be considered;

- risks are intolerable, then risk mitigation options need to be considered, such as reducing the frequency and probability of landslides and spatial probability of the element a risk.

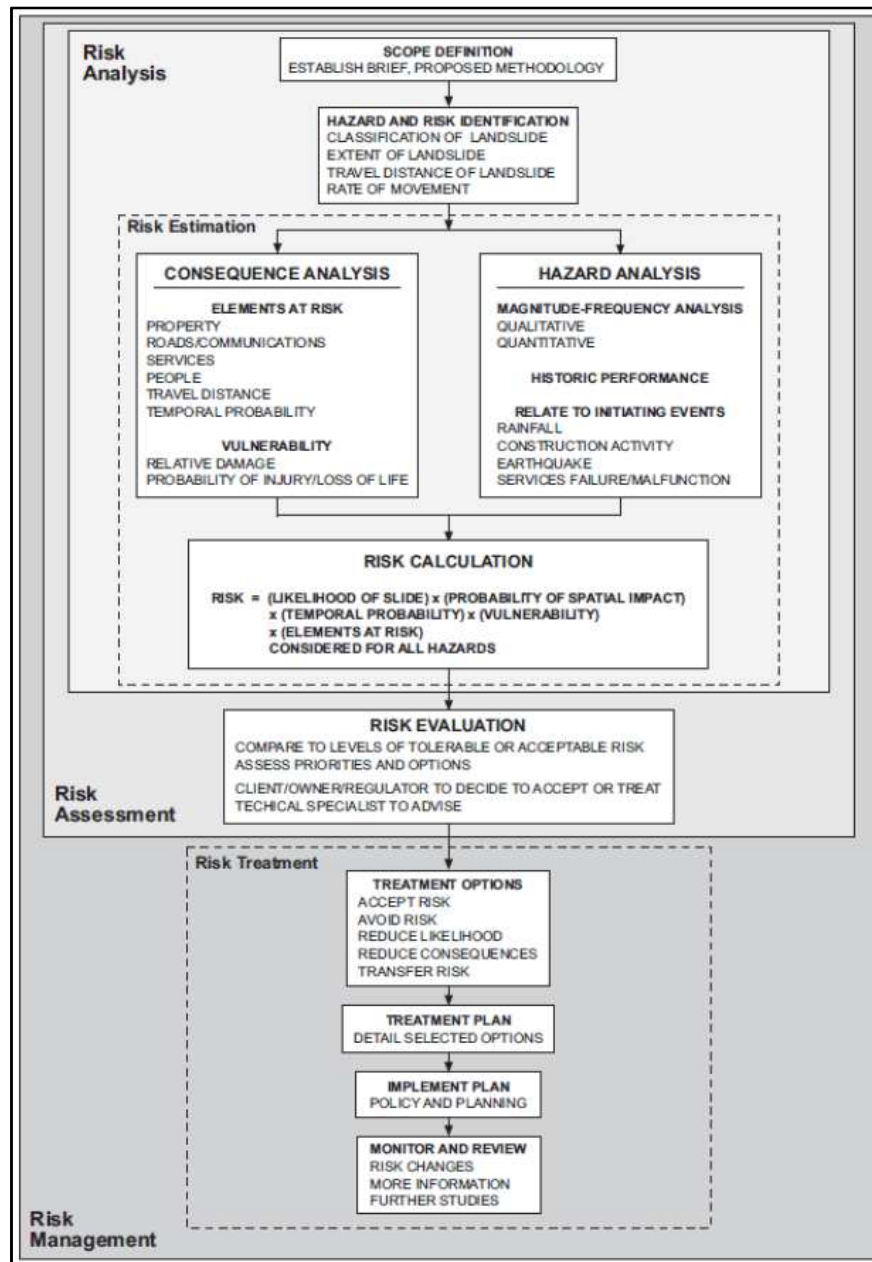


Figure 3.3 Flow chart for landslide risk management (Crozier and Glade, 2005).

Risk mitigation can use structural and non-structural solutions (as public education campaigns, public information services to address the issue of risk tolerance by the general public). Several options for risk mitigation can be identified. The most common are (AGS, 2000):

-accept the risk: this usually requires the risk is considered to be within the acceptable or tolerable range;

-avoid the risk: this would require abandonment of the project, seeking an alternative site or form of development such that the revised risk would be acceptable or tolerable;

-reduce the likelihood: this would require stabilization measures to control the initiating circumstances, such as reprofiling the surface geometry, groundwater drainage, anchors, stabilizing structures or protective structures etc. After implementation, risk should be acceptable or tolerable.

-reduce the consequences: this would require provision of defensive stabilization measures, or relocation of the development to a more favorable location to achieve an acceptable or tolerable risk.

-monitoring and warning systems: in some cases monitoring and the establishment of warning systems may be used to manage the risk on an interim or permanent basis.

-transfer the risk: by requiring another authority to accept the risk or to compensate for the risk such as by insurance;

-postpone the decision: where there is sufficient uncertainty resulting from the available data, additional investigations or monitoring are required to enable a better risk assessment.

It is necessary to highlight that the landslide risk management process is not the same method used in each country; indeed, numerous factors lead to modification of the tools used, the approach followed and the objectives to be reached.

Wherever possible, the above recommended options should be engineered in order to reduce the uncertainties, but natural assets, cultural or social issues concerning the entire area will have to be taken into account.

In the following sections of this chapter, general guidelines on landslide risk assessment step are shown, with particular reference to hazard and vulnerability aspects.

3.3 Landslide risk assessment

It is evident that the management of the risk associated to landslides supposes, as first step, its assessment through several techniques according to specific guidelines, as shown in Figure 3.4.

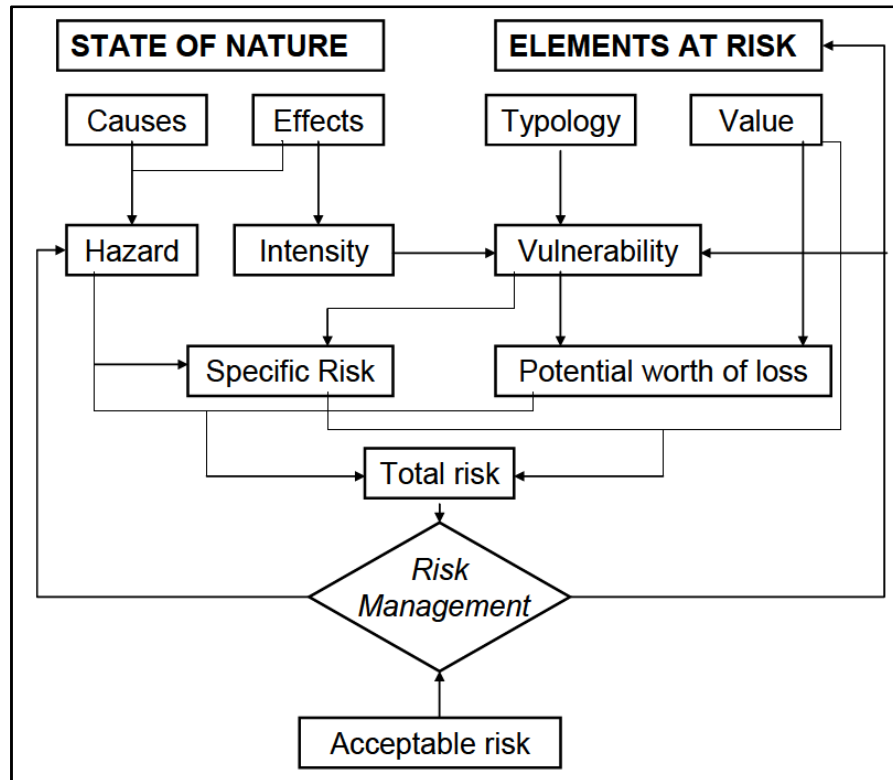


Figure 3.4 Simplified scheme for the landslide risk assessment (after Calcaterra et al., 2003).

Conceptual flowchart for landslides risk assessment includes four major phases (Fig. 3.5):

- 1) **data collection for landslide risk assessment** consists of collecting all available information and data on the study area. The importance of accurate collection and storage of information in the database is widely acknowledged and generally its reliability and accuracy should subsequently be reviewed from time to time.
- 2) **landslide hazard assessment** is, probably, the best-known part for landslide studies since much research has been undertaken on this topic for the last twenty years;

- 3) **landslide vulnerability assessment** is probably the weakest part in the whole process since relatively little work has been made on the quantification of physical vulnerability due to landslides;
- 4) **landslide risk assessment methods:** the classification, based on the level of quantification, divides landslide risk assessment methods in qualitative, semi-quantitative and quantitative (AGS, 2000).

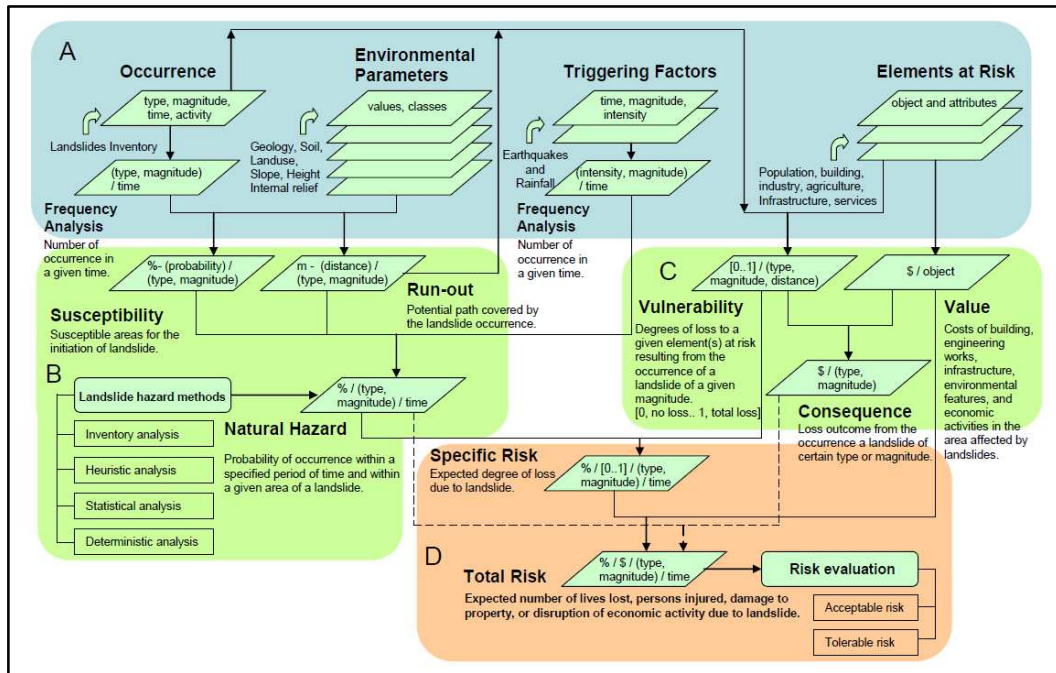


Figure 3.5 Methodological framework for spatial landslide risk assessment (Dai et al., 2002).

Preliminary to risk assessment, an important step is represented by the choice of the work-scale adopted for investigation: generally, it is based on three factors:

- 1) the purpose of the assessment: in land use, for example, planning on a regional scale could be adopted (1:100.000 – 1:500.000), whereas for more specific problems such as the implementation of large engineering structures or the definition of a plane of priority measures, the scale should be more detailed (medium scale: 1:25.000 – 1:50.000). Frequently, these analyses are preliminary to more specific studies to be conducted on perhaps a single slope or small areas where an even larger scale would be appropriate;
- 2) the extent of the studied area;
- 3) data availability.

The following paragraphs provide a more detailed overview on the four steps above mentioned for landslide risk assessment.

3.3.1 Data collection for landslide risk assessment

It is the first step in every assessment and generally research in landslide risk involves many different types of data. Many factors need to be considered for landslide risk assessment in an inter-disciplinary context.

Landslide-related data could be grouped into four sets: landslide occurrence, environmental parameters, triggering factors and elements at risk (Soeters and van Westen, 1996). The selection of data that could or should be taken into account for the assessment of a given area depends essentially on the size of the study area, the work-scale, the technique adopted and the type of landslide.

Landslide occurrence data are sometimes called landslide danger data (Einstein, 1997). Indeed, it is a landslide inventory database that can be compiled for a certain area, a whole nation or even, the whole world. Nationally, many countries like Italy (Guzzetti, 2000; Guzzetti and Tonelli, 2004), France (Faure, 2004), Colombia (Gonzalez, 1989) have developed their own national landslide inventory database, which helps the authorities to assume decisions. A landslide inventory is considered as “indispensable” when attempting to produce any kind of probabilistic forecasting. Without a landslide map it is not possible to predict the future behavior of these events.

For the analysis of the landslide causal factors it is required to study different environmental parameters which could be affecting the areas with landslide problems. Depending on the level of detail and the conditions of the area, a number of parameters are essential to the study.

The most frequently used parameters that should be surveyed are: terrain map units, geomorphological units, lithologies, Digital Elevation Model (DEM), slope map, aspect map, soils and material sequences, structural geological map, land-use map.

Landslide causal factors could be divided into “preparatory” and “triggering”. However, there are generally two main causes that have been recognized: rainfalls and earthquakes. In particular, there are several papers dealing with the relationship between rainfall and landslides (e.g. Wasowski, 1998; Crozier, 1999; Dai and Lee, 2001; Crosta, 2003; Guzzetti et al., 2007). While some of them deal with specific cases, others are more concerned with the statistical relationship for creating correlation models and even produce forecasting models based on rainfall threshold values.

Finally, to evaluate landslide risk it is necessary to survey and analyze the elements at risk that could be potentially affected by the occurrence of these phenomena. Still there is no worldwide understanding on how to classify elements at risk, but one general proposal (UNDRO, 1991) has subdivided them into infrastructure, housing, economic activities and community services. However, other publications classify the elements at risk differently, such as physical, economical, societal and environmental, with a more detailed sublevel classification (IADB, 2005). Generally, elements at risk should be classified by their typologies, since each type of element requires a structural or engineering characterization, as well as a monetary evaluation. Thus, the structural analysis is used to determine the vulnerability to landslide occurrence, whereas monetary valuation is used for the loss estimation needed in the risk assessment. The study of the “population at risk” requires a particular type of analysis, since its risk is expressed in terms of human loss or people injured.

It is important to highlight that particularly useful in the data collection activity is the use of Geographical Information Systems (GIS): generally, as indicated by Leroi (1996), two fundamental rules must be observed when creating a database:

- 1) information must be homogeneous, i.e. they must have the same work-scale and the same geographic projection system;
- 2) the database must be organized into basic monothematic layers, each of which contains homogeneous data.

3.3.2 Landslide hazard assessment

The assessment of “hazard” is a obviously very important step of landslide risk assessment. Hazard is defined as the probability of occurrence of a potentially damaging phenomenon within a specified period of time and within a given area.

Hazard may be expressed as the frequency of a particular type of landslide of a certain volume, or landslides of a particular volume and velocity, or in some cases as the frequency of landslides with a particular intensity, where intensity may be measures in kinetic energy terms (van Westen, 1993).

The most precise way to assess landslide hazard is by deterministic methods based on the modelling of safety factors from the physical/mechanical material properties, slope and triggering factors information.

Landslide hazard assessment methods have been divided into four groups (Table 3.3); the selection of one method over another depends on several factors such as: the data costs and availability, the scale of analysis, the output requirements, the geological and geomorphological conditions and the morphogenetic behavior of the landslides.

Term	Definition
Inventory analysis	Analysis the spatial and temporal distribution of landslide attributes.
Heuristic analysis	Based on expert criteria with different assessment methods.
Statistical analysis	Several parameter maps are surveyed to apply bivariate and multivariate analysis
Deterministic analysis	Apply hydrological and slope instability models to evaluate the safety factor

Table 3.3 Landslide hazard assessment methods (van Westen, 1993).

By analyzing data certain conclusions could be reached about landslide hazard. Three types of analysis have been recognized as the most useful (van Westen, 1993):

- 1) **distribution analysis**: the objective is to know the spatial distribution of the landslides classified by types, activity, distribution of activity, among other properties that may be surveyed;
- 2) **activity analysis**: also known as temporal analysis, as it allows for the recognition of temporal changes in the landslide activities and to correlate these changes with other like land use changes;
- 3) **density analysis**: visualizes the landslide abundance per area or terrain units or classes of other type of maps like geological or geomorphological maps.

These analyses are related to the tree hazard component which are probability within specified period (temporal probability), probability within certain areas (spatial probability) and intensity (magnitude).

Landslide spatial probability methods are classified as direct and indirect methods (Chakraborty, 2008). The direct method uses geomorphological mapping deal with past and present landslide events and the zonation is created in areas in which failure frequently occur. Otherwise, indirect methods can be divided in two methods, namely heuristic method and statistic method.

Heuristic method considers landslide influencing factors, such as slope, rock type, land-form and land-use and then is ranked or weighted based on their influence on causing mass movements.

In a statistical method, spatial probability is determined by defining the relationship with the past/present landslide distribution.

Temporal probability can be derived from several methods. Jaiswal et al. (2009) distinguished temporal probability methods, based on physical threshold and empirical methods, based rainfall threshold.

In physical threshold based model, certain features of the local terrain (e.g. slope, gradient, soil depth, lithology) are used,

based on a dynamic hydrological model where the most important variable is rainfall.

Otherwise, an empirical rainfall threshold method measures temporal probability based on the calculation of rainfall threshold causing landslides.

Landslides magnitude is the most important element in assessing landslide risk, determining the amount of damage on each element. Magnitude can be determined by several methods (Guzzetti et al., 2002; Malamud et al., 2004; Jaiswal et al., 2010). The magnitude class can be classified based on volume, type and characteristics of landslides (location, potential damages, field investigations).

The results of the hazard assessment are commonly expressed in the form of maps showing the spatial distribution of hazard classes, namely their zonation, that plays a significant role in establishing programs aimed at reducing landslide disasters.

Generally, hazard zoning may be quantitative or qualitative. It is preferable to determine the frequency of landslides in quantitative terms so the hazard from different sites can be compared, and the risk estimated consequently also in quantitative terms. However, in some situations it may not be practical to assess frequencies sufficiently accurately to use quantitative hazard zoning and a qualitative system of describing hazard classes may be adopted (Fell et al., 2008).

3.3.3 Landslide vulnerability assessment

Landslide vulnerability assessment is still considered a difficult process since it depends on several factors. Different definitions for vulnerability have been developed, thus confirming that vulnerability could be interpreted from many points of view.

In the literature, a first definition of vulnerability is given by Westgate and O'Keefe (1976): it is the degree to which a community is at risk from the occurrence of extreme physical or natural phenomena; risk refers to the probability of occurrence and the degree to which socio-economic and socio-political factors affect the community's capacity to absorb and recover from extreme phenomena.

Recent researches include into vulnerability definition also the characteristics and circumstances of a community, generated by social, economic and environmental factors, that influence a person or a group of people and their capacity to anticipate, cope with, resist and recover from the impact of a natural hazard (Leone et al., 1996; Van Westen, 2004; UNISDR, 2009).

The main factors, that may influence the degree of vulnerability, can be summarized as follow:

- political-institutional factors (such as lean legislation, inadequate personnel and financial resources, underdeveloped democratic institutions, lacking or inadequate mechanisms and instruments for spreading financial risk, culture of prevention obstructed or insufficiently promoted);
- economic factors (like governmental financial resources insufficient for disaster risk management, poverty, low level of economic diversification, influence of economic activities on disaster risk);
- socio-cultural factors (such as poor education, the tradition of slash-and-burn clearance or the application of out-data method in the natural environment, population not prepared to engage in mutual support schemes or to search for greater levels of general welfare).

As suggested by Leone et al. (1996) in a general framework considering the vulnerability components (Fig. 3.6), it depends on damage functions or vulnerability functions where the characteristics of the landslide and their impact on the exposed elements are modelled.

Generally, this could be carried out by historical data or theoretical information: to this, the availability of historical data provides several advantages from detailed landslide risk analysis.

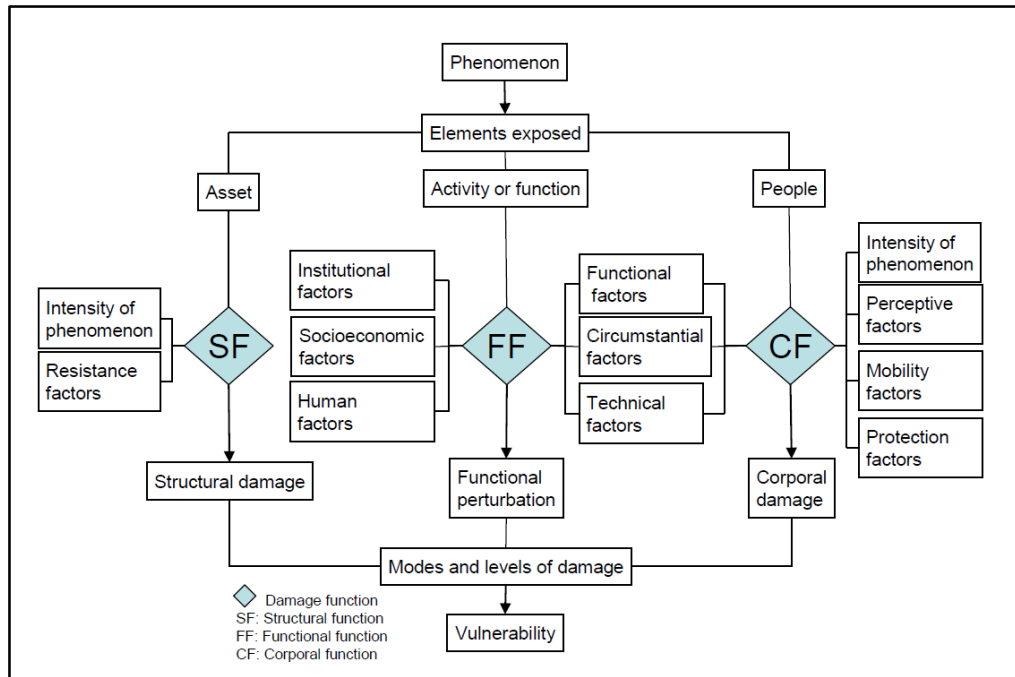


Figure 3.6 Flow diagram illustrating vulnerability components (Leone et al., 1996).

Commonly, the results of the vulnerability assessment is expressed in the form of maps showing the spatial zonation of vulnerability classes, that plays a significant role in establishing programs aimed at reducing landslide disasters; the maps are expressed with values between 0 and 1, where 0 means no damage and 1 means total loss.

Landslide vulnerability maps could be made through the integrated analysis of landslide parameters and elements at risk. In fact, evaluation of vulnerability requires an analysis of the structural consequences for each element. Thus, it is possible to develop a vulnerability function in order to identify the relationship between landslide characteristics (volume, area, intensity) and the stability of structure.

This is one of the most important starting points for reducing risk by diminishing the structural vulnerability using effective mitigation plans. By collecting and processing historical damage, landslide vulnerability assessment could be more precise when similar conditions occur.

Among the attributes of elements at risk surveyed are the costs related to each element, such as total value, recovering costs and service interruption costs. These costs are classified as direct or indirect depending on their relation to the disaster (Barbat, 2003),

but generally their assessment in case of landslides is very difficult, due to the detailed economic information needed.

Once vulnerability assessment is made, the consequence analysis, defined as the potential outcomes arising from landslide occurrence (damage, injury, loss of life or any other loss) can be carried out.

The vulnerability assessment of structures located within landslide areas, in term of current and future structural instability likelihood due to the ground movements, represents the principal topic of this work. In Chapter 4 a detailed analysis on vulnerability assessment approaches present in literature has been developed.

3.3.4 Landslide risk assessment methods

Generally, to illustrate difficulties in landslide risk assessment, different typical approaches can be considered. The classification defines qualitative, semi-quantitative and quantitative methods (Table 3.4), as presented in the following of this section. Most of them are based on a large amount of assumptions and simplifications mostly due to scarcely available data.

Method	Principle	References
Qualitative	Based on risk classes categorized by expert judgment. Risk classes: High, Moderate and Low	(Lateltin, 1997; AGS, 2000; Budetta, 2004; Cascini, 2004; Ko Ko et al., 2004; Mossa, 2004; IADB, 2005; Nadim et al., 2006)
Semi-quantitative	Based on ranking and weights assignments by a given criteria. Risk index: ranked values (0-1, 0-10 or 0-100). (dimensionless)	(Brand, 1988; Koirala and Watkins, 1988; Chowdhury and Flentje, 2003; Blochl and Braun, 2005; Castellanos Abella and Van Westen, 2005; Saldivar-Sali and Einstein, 2007)
Quantitative	Based on probabilities or percentage of losses expected. Risk value: probabilistic values (0-1) over certain amount of monetary or human loss.	(Einstein, 1988; Morgan et al., 1992; Fell, 1994; Leroi, 1996; Ragozin, 1996; Cruden and Fell, 1997; Einstein, 1997; Fell and Hartford, 1997; Leroi, 1997; Ragozin and Tikhvinsky, 2000; Kong, 2002; Bell and Glade, 2004; Decaulne, 2005; Fell et al., 2005; Karimi and Hullermeier, 2007; Roberts, 2007)

Table 3.4 Landslide risk assessment methods with some references (from Castellanos Abella, 2008)

The *qualitative approach* is based on the experience of experts and risk areas are categorized generally with terms as “very high”, “high”, “moderate”, “low” and “very low” risk, which have a direct line with practical indications on strategy of action.

Fell (1994) proposed terminology definitions for qualitative risk assessment considering classes for magnitude, probability, hazard, vulnerability and specific risk.

A terminology proposal guideline for assessing risk to property was developed by the Australian Geomechanics Society (AGS, 2000), considering a combination of landslide likelihood and the possible consequences (Tables 3.5, 3.6, 3.7).

Following this criterion, likelihood incorporates frequency of landslide, probability of the landslide reaching the element at risk, and temporal spatial probability. Consequences incorporate the vulnerability and the value of the element at risk.

Level	descriptor	Description	Indicative annual probability
A	Almost certain	The event is expected to occur	$\geq 10^{-1}$
B	Likely	The event will probably occur under adverse conditions	$= 10^{-2}$
C	Possible	The event could occur under adverse conditions	$= 10^{-3}$
D	Unlikely	The event might occur under very adverse circumstances	$= 10^{-4}$
E	Rare	The event is conceivable but only under very exceptional circumstances	$= 10^{-5}$
F	Not credible	The event is inconceivable or fanciful	$\leq 10^{-6}$

Table 3.5 Qualitative measures of likelihood (Australian Geomechanics Society, 2000).

Level	Descriptor	Description
1	Catastrophic	Structure completely destroyed or large scale damage requiring major works for stabilisation
2	Major	Extensive damage to most of the structure, or extending beyond site boundaries requiring significant stabilisation works.
3	Medium	Moderate damage to some structure, or significant part of the site requiring large stabilisation works
4	Minor	Limited damage to part of structure, or part of sit requiring some reinstatement/ stabilisation works
5	Insignificant	Little damage

Table 3.6 Qualitative measures of consequences to property (AGS, 2000).

Risk level	General guide to implications
Very High risk	Extensive detailed investigation and research planning and implementation of treatment options essential to reduce risk to acceptable levels: may be too expensive and not practicable
High risk	Detailed investigation, planning and implementation of treatment options required to reduce risk to acceptable levels.
Moderate risk	Tolerable provided implementation plan is implemented to maintain or reduce risks. May be accepted. May require investigation and planning of treatment options
Low risk	Usually accepted. Treatment requirements and responsibility to be defined to maintain or reduce risk
Very low risk	Acceptable. Manage by normal slope maintenance procedures.

Table 3.7 Qualitative risk level implications (AGS, 2000).

Usually, qualitative methods can be used in the analyses:

- as an initial screening process to identify hazards and risks which require more detailed consideration and analysis;

-when the level of risk does not justify the time and effort required for more detailed analyses;

-where the possibility to obtain numerical data is limited so that a quantitative analysis is unlikely to be meaningful or may be misleading.

Qualitative risk assessment is subject to limitations, which include potentially imprecise and subjective description of the likelihood term, and hence are liable to result in wide differences in the estimated risks, together with lack of risk acceptance criteria.

Semi-quantitative methods may be a combination of qualitative and quantitative methods. The main difference between qualitative and semi-quantitative approaches is the assignment of weights under certain criteria which provide numbers as outcome instead of qualitative classes.

The semi-quantitative estimation is useful in the following situations (AGS, 2000):

- as an initial screening process to identify hazards and risks;
- when the level of risk does not justify the time and effort;
- where the possibility to obtain numerical data is limited.

The final risk values can also be categorized and ranked with qualitative implications and the risk estimation should be done separately for loss of life and economic loss.

Besides the limitations found, this semi-quantitative approach could be adapted from the “slope” based to cover larger areas, but, in any case, there will be the dilemma of adapting the scoring system to each particular region where the analysis will be made, since landslide instability and consequences estimations depend very much on the particular conditions of the study area. Nowadays, such a semi-quantitative approach can efficiently use spatial multi-criteria techniques implemented in GIS that facilitate standardization, weighting and data integration in a single set of tools.

Finally, *quantitative approaches* for landslide risk assessment have been used for specific slopes or very small areas using probabilistic methods. Quantitative risk analysis is carried out by expressing hazard frequency and consequences in measured, numerical terms and determining their product.

Table 3.8 shows some methods for calculating landslide total risk.

Total risk equation in quantitative approaches uses the same combination of hazard and consequences, but differs in practice on many details. In the calculation factors as risk to property or/and loss of life, annual probability of the hazardous event, probability of spatial impact by the hazard, vulnerability, element at risk are taken into account.

Reference	Equation, Risk =
<ul style="list-style-type: none"> (Morgan, 1992) 	$P(H) \times P(S H) \times V(P S) \times E$ <ul style="list-style-type: none"> - P(H): annual probability of landslide event - P(S H): probability of spatial impact given the event - V(P S): vulnerability of the property (proportion of property value lost) - E: element at risk (the value of the property)
<ul style="list-style-type: none"> (Einstein, 1988; 1997) 	$P[\text{Danger}] \times u(x)$ <ul style="list-style-type: none"> - P[Danger]: danger probability - u(x): vector of attributes, which are consequences
<ul style="list-style-type: none"> (Fell, 1994; Fell et al., 2005) 	$\sum (E \times P \times V)$ <ul style="list-style-type: none"> - E: element at risk (value) - P: probability of hazard - V: vulnerability
<ul style="list-style-type: none"> (Anderson et al., 1996) 	$P(P_i) \times P(L O) \times P(C L) \times L_e$ <ul style="list-style-type: none"> - P(P_i): probability of ith pathway - P(L O): conditional probability of the exposure of property to the outcome - P(C L): conditional probability of property damage given this exposure - L_e: resulting economic consequences
<ul style="list-style-type: none"> (Ragozin, 1996; Ragozin and Tikhvinsky, 2000) 	$P^l(L) \times V_m(L) \times V_e(L) \times D_e$ <ul style="list-style-type: none"> - P^l(L): landslide probability occurrence - V_m(L): landslide vulnerability degree - V_e(L): vulnerability degree of object under the event (L) - D_e: full cost of objects with definite damage degree
<ul style="list-style-type: none"> (Leroi, 1996; Leroi, 1997) 	$\sum A_i \times (\sum V_{ji} \times C_j)$ <ul style="list-style-type: none"> - A_i: hazard i - V_{ji}: vulnerability of object j exposed to hazard i - C_j: "cost" or value of the object j
<ul style="list-style-type: none"> (Bell and Glade, 2004) 	$H \times C \times E$ <ul style="list-style-type: none"> - H: Hazard - C: Consequence - E: Element at risk
<ul style="list-style-type: none"> (Lee and Jones, 2004) 	$P(H_i) \times \sum (E \times V \times E_x)$ <ul style="list-style-type: none"> - P(H_i): probability of particular magnitude of landslide - E: value of element at risk - V: vulnerability of proportion of E - E_x: exposure of element at risk
<ul style="list-style-type: none"> (AGS, 2000) 	$P_{(H)} \times P_{(S:H)} \times V_{(prop:S)} \times E$ or $P_{(H)} \times P_{(S:H)} \times P_{(T:S)} \times V$ <ul style="list-style-type: none"> - P_(H): annual probability of landslide - P_(S:H): probability of spatial impact according to the travel distance - V_(prop:S): vulnerability of the property - E: element at risk - P_(T:S): temporal probability of the building of being occupied - V: vulnerability of the individual

Table 3.8 Quantitative landslide risk assessment methods (from Castellanos, 2008).

The results of the risk assessment are commonly expressed in the form of maps showing the spatial distribution of risk classes, namely their zonation, that plays a significant role in establishing programs aimed at reducing landslide disasters. However, it has to be pointed out that these types of maps are not diffused in the scientific literature, mainly due to the difficulty, especially for large areas, in determining the probability of occurrence of the landslides within a certain period, that requires the collection of many information and complex analyses (Soeters & Van Westen, 1996).

As a consequence, in most of the cases it should be more correct to consider the produced maps as susceptibility maps, whose main difference is therefore the absence in the latter of the temporal factor: as before outlined, in fact, susceptibility is the likelihood that a landslide will occur in an area on the basis of local terrain conditions (Soeters & van Westen, 1996).

CHAPTER 4

VULNERABILITY ASSESSMENT IN A LANDSLIDE RISK ANALYSIS

Introduction

Landslide vulnerability assessment is still considered a difficult process since it depends on several factors. Different definitions for vulnerability have been developed, thus confirming that vulnerability could be interpreted from many points of view.

Generally, the methodologies available for the analytical quantification of the vulnerability of buildings which are subject to actions resulting from slope instabilities and landslides are relatively limited in comparison with other components of quantitative landslide risk assessment.

Most of the definitions of vulnerability to natural disasters agree to state that the vulnerability is multi-dimensional (vulnerability has several facets: e.g. physical, social, economic, environmental, institutional), dynamic (vulnerability changes over time), scale-dependent (vulnerability can be expressed at different scales from human or household to country resolution) and site-specific (each study area might need its own approach) (Thywissen, 2006).

For the United Nations, the term "vulnerability" refers to the conditions which make a community susceptible to the impact of hazards, the conditions being determined by physical, social, economic and environmental factors or processes (UNISDR, 2009). This makes it a term with different facets, which should be all considered to make a complete vulnerability assessment.

Not only the built environment factors are important in terms of natural disaster outcome, but also the social factors (Zahran et al., 2008); social vulnerability is linked to the inherent characteristics of social systems that create potential for harm. It exists before the occurrence of a disaster and is function of the exposure of the element at risk and sensitivity of system (Cutter, 1996; Cutter et al., 2008). To assess the social vulnerability of a population, social scientists collect and explore a set of socioeconomic factors in order to know which part of the population would have more difficulty to recover from a natural disaster, and which part would be less vulnerable and more able to cope with stress or change (Fuchs, 2009).

Several studies have been more often interested to physical vulnerability assessment (also called structural vulnerability) of the buildings. Physical vulnerability can be estimated by considering different scenarios and by calculating the likelihood of occurrence of specific process scenarios (Fuchs, 2009), that indicates the interaction between the intensity of the hazard and the type of element at risk (Corominas et al., 2014). In detail, physical vulnerability of buildings to landslides is a term used to describe their potential for physical loss when they are affected by any type of action induced by unstable terrains. Economists focus on the economic vulnerability. Guillaumont (2009) developed an Economic Vulnerability Index (EVI) which measures the likelihood that a country's economic development process is hindered by the occurrence of exogenous unforeseen events, often called external shocks, and which come from the occurrence of a natural disaster.

In this work, vulnerability assessment of structures located within landslide areas, meant as a prediction of current and future structural instability likelihood due to the ground movements, is developed: to this aim, in the following chapters, through qualitative and quantitative analyses, the degree of loss of a given element or set of elements at risk, in term of probability to reach a certain damage level, resulting from landslide occurrence of a given magnitude, has been defined.

4.1 Landslide vulnerability assessment: literature overview and issues

Nowadays, different approaches to assess building vulnerability have been described in literature, each one characterized by its own peculiarity, obviously with differences in the final results. Indeed, at present no vulnerability assessment standard methodologies exists. A literature review demonstrates a lack of vulnerability studies in landslide risk research with regard to both social and natural science approaches. Existing approaches to vulnerability assessment determine risk associated with landslide processes of a given magnitude as a function of landslide hazard, elements at risk with attributed damage potentials and vulnerabilities of each of these elements at risk.

This concept has been applied to landslide issues by various authors (Westgate and O'Keefe, 1976; Einstein, 1988; Fell 1994; Leone et al., 1996; Leroi, 1996; Dai et al., 2002; Amatruda et al., 2004; Van Westen, 2004; Negulescu et al., 2010; Pitilakis et al., 2013; Mavrouli et al., 2014; Ferlisi et al., 2015, Peduto et al., 2016).

A first definition of vulnerability is given by Westgate and O’Keefe (1976): it is the degree to which a community is at risk from the occurrence of extreme physical or natural phenomena; the risk refers to the probability of occurrence and the degree to which socio-economic and socio-political factors affect the community’s capacity to absorb and recover from extreme phenomena.

Recent researches consider into vulnerability definition also the characteristics and circumstances of a community, generated by social, economic and environmental factors, that influence a person or a group of people and their capacity to anticipate, cope with, resist and recover from the impact of a natural hazard (Leone et al., 1996; Van Westen, 2004; UNISDR, 2009).

The main factors, that may influence the degree of vulnerability, can be summarized as follow:

- political-institutional factors (such as lean legislation, inadequate personnel and financial resources, underdeveloped democratic institutions, lacking or inadequate mechanisms and instruments for spreading financial risk, culture of prevention obstructed or insufficiently promoted);
- economic factors (like governmental financial resources insufficient for disaster risk management, poverty, low level of economic diversification, influence of economic activities on disaster risk);
- socio-cultural factors (such as poor education, the tradition of slash-and-burn clearance or the application of out-data method in the natural environment, population not prepared to engage in mutual support schemes or to search for greater levels of general welfare).

In contrast to other natural processes such as earthquakes, it is very difficult to evaluate landslides vulnerability due to the complexity and the wide range of variety of this process (Leroi, 1996). Diverse effects have to be considered:

- *vulnerability of different elements at risk varies for similar processes*: “a house may have similar vulnerability to a slow- and a fast- moving landslide, but persons living in the house may have a low vulnerability to slow-moving landslide but a higher vulnerability to fast- moving landslide” (Fell, 1994);
- *different groups of humans have different potential vulnerability*: in contrast to adults, children or handicapped people might not be able to react to endangering processes (Liu et al., 2002);

- *temporal conditions of an exposed element change during the landslide event:* depending by the instant of the day, less people are into building, less severe are the potential consequences; similar to this, the different building structural property or the worsening of damage level during landslide evolution, can modify vulnerability;
- *spatial and temporal evolution of landslide occurrence changes:* for example, although a landslide occurs in a zone, intensity and boundary could change during the time, producing a variation of vulnerability level.

Some authors, as Roberds (2005) and Fuchs (2007) distinguish the potential losses or consequences of a natural disaster in *direct* and *indirect* (Fig. 4.1):

- *direct losses* belonging to social and physical vulnerabilities are more frequently evaluated: correspond to loss of life, interruption of facilities (infrastructures), damage to buildings, collapse and destruction;
- *indirect losses* are a consequence of direct losses: related to business and service interruption, job losses, loss of property, psychological impacts, represent a socioeconomic vulnerability indicator on the degree of preparedness, effectiveness of the response and capacity to recover from the damage caused by landslides. Nevertheless, indirect losses are more difficult to assess than direct losses, and are therefore less considered than direct losses.

	Human - social	Physical	Economic	Cultural Environmental
Direct losses	<ul style="list-style-type: none"> • Fatalities • Injuries • Loss of income or employment • Homelessness 	<ul style="list-style-type: none"> • Structural damage or collapse to buildings • Non-structural damage and damage to contents • Structural damage infrastructure 	<ul style="list-style-type: none"> • Interruption of business due to damage to buildings and infrastructure • Loss of productive workforce through fatalities, injuries and relief efforts • Capital costs of response and relief 	<ul style="list-style-type: none"> • Sedimentation • Pollution • Endangered species • Destruction of ecological zones • Destruction of cultural heritage
Indirect losses	<ul style="list-style-type: none"> • Diseases • Permanent disability • Psychological impact • Loss of social cohesion due to disruption of community • Political unrest 	<ul style="list-style-type: none"> • Progressive deterioration of damaged buildings and infrastructure which are not repaired 	<ul style="list-style-type: none"> • Economic losses due to short term disruption of activities • Long term economic losses • Insurance losses weaken-ing the insurance market • Less investments • Capital costs of repair • Reduction in tourism 	<ul style="list-style-type: none"> • Loss of biodiversity • Loss of cultural diversity

Figure 4.1 Overview of types of loss resulting from landslide hazard: structural and non-structural damage to buildings are highlighted (from van Westen, 2009).

In this work, we have focused on buildings physical vulnerability, meant as the assessment of structure damage degree, present and future, due to slope movements.

As suggested by Leone et al. (1996) in a general framework considering the vulnerability components (Fig. 4.2), it depends on damage functions or vulnerability functions where the characteristics of the landslide and their impact on the exposed elements are modelled.

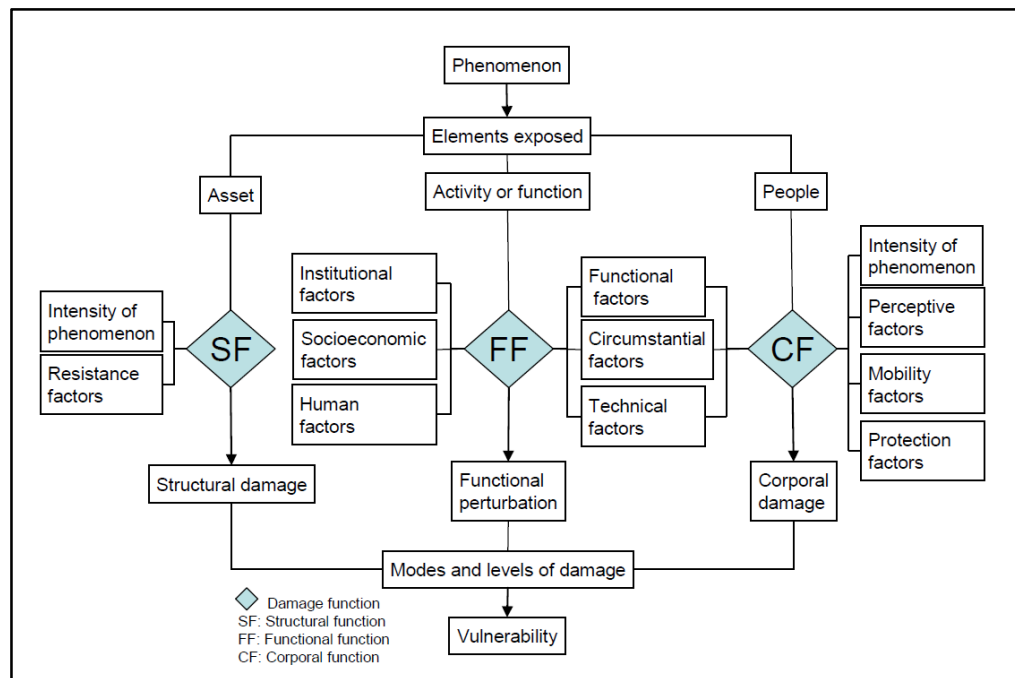


Figure 4.2 Flow diagram illustrating vulnerability components (Leone et al., 1996).

As reported in detail in the following paragraphs, vulnerability is related to the fragility of physical structures and is defined as the expected degree of loss resulting from the impact of a certain event on the elements at risk. Its assessment requires the evaluation of different parameters and factors such as landslide type, boundary, state of activity and intensity, lithological and geomorphological characteristics of soil, building typology, constructive characteristics, state of maintenance, structural properties of materials.

4.2 Elements at risk a different scale of analysis

As above mentioned, landslide vulnerability assessment requires an integrated analysis of landslide parameters and elements at risk, as indicated in several logical frameworks regarded by literature (Cruden & Fell, 1997; Cascini et al., 2005, Infante et al., 2016) (Fig. 4.3).

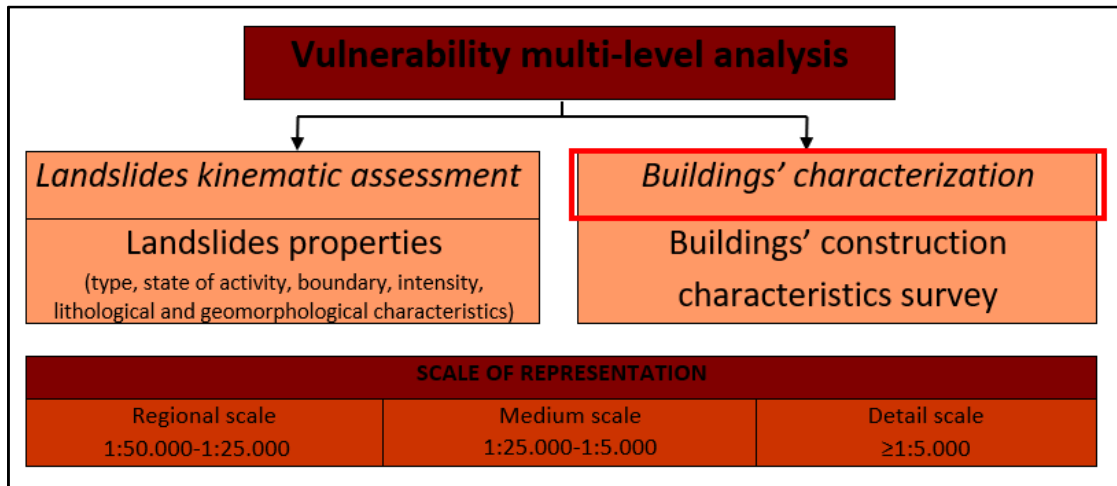


Figure 4.3 Logical framework for vulnerability assessment and different scale of analysis.

To this purpose, the identification of elements at risk is an essential part in landslide risk assessment: an updated database with information about elements exposed to such hazards is fundamental to support crisis preparedness and response activities.

Physical vulnerability evaluation is very important in the risk assessment: buildings are the most common type of elements at risk, firstly for people safety and also because they represent the main content in economic losses.

Fell (2005) considered that building vulnerability is the product of spatial probability, temporal probability and probable damage degree. These elements are the key for quantitative vulnerability analysis of buildings.

At present, no uniform approach exists to identify elements at risk, and no well-established methods are generally available.

The characterization of buildings interacting with slow-moving landslide bodies is a difficult task because it requires a deep knowledge of relevant factors related to exposed facilities (structural typology, age of construction materials, state of maintenance, foundation type, etc.) as well as information on their relative location within the landslide affected area (Fell et al., 2008).

However, the inventory of elements at risk is acquired in time-consuming procedures through integrated collection of data, through official government data sources, land cover databases and individually gathered data.

It is necessary to highlight that such methodologies are accomplished with an accuracy level depending on the scales of analysis and on the applied building vulnerability diagnosis criteria. From regional to medium and detailed scale, in fact, the parameters useful for the landslide intensity definition and for the exposed elements characterization change (Fig. 4.4).

In particular, with reference to Regional scale analysis (1:100.000-1:50.000), homogeneous building aggregations within landslide affected area can be identified through the available digital topographic database map, aerial and satellite photos, considering that, at small scale, the identification of a single building (van Westen, 2004) is impracticable and not significant.

At medium scale analysis (1:25.000), several difficulties in single building characterization are involved. To this aim, a preliminary in-situ survey to define construction (isolated or aggregate) and structural (masonry, reinforced concrete, other buildings) typology, in order to distinguish buildings in terms of homogeneous units, is required.

Futhermore, to this level of detail, geometrical characteristics of each building (length of facades and spatial orientation with respect to landslide movement) should be assessed.

Finally, at large scale representation (1:5.000), where a numerical analysis is performed, the characterization of buildings model requires a very detailed geometrical and structural survey, in order to define construction and structural typology, state of preservation, foundation structures, constructive parameters (number of floors, aggregate typology), type of structural instability, damage degree and distribution, mechanical properties of structural materials. The vulnerability varies significantly according to the structural typology and whether the loadbearing system is reinforced concrete, masonry, steel, timber or a mixed structure.

Different load-bearing systems have in fact different responses and resistances to the static actions of a slow-moving landslide, and present differences in their failure mechanisms. The global vulnerability level of a building is affected by the hierarchical resistance and dissipation capacity of the structural frame, the infill panels and the openings on the face of the building.

To this purpose, potential sources of uncertainties for buildings vulnerability assessment are the properties of the structures from, their geometries, the resistances of structural sections and their supports, the number of floors, the typology of foundation, the quality of masonry units, in terms of materials and construction characteristics.

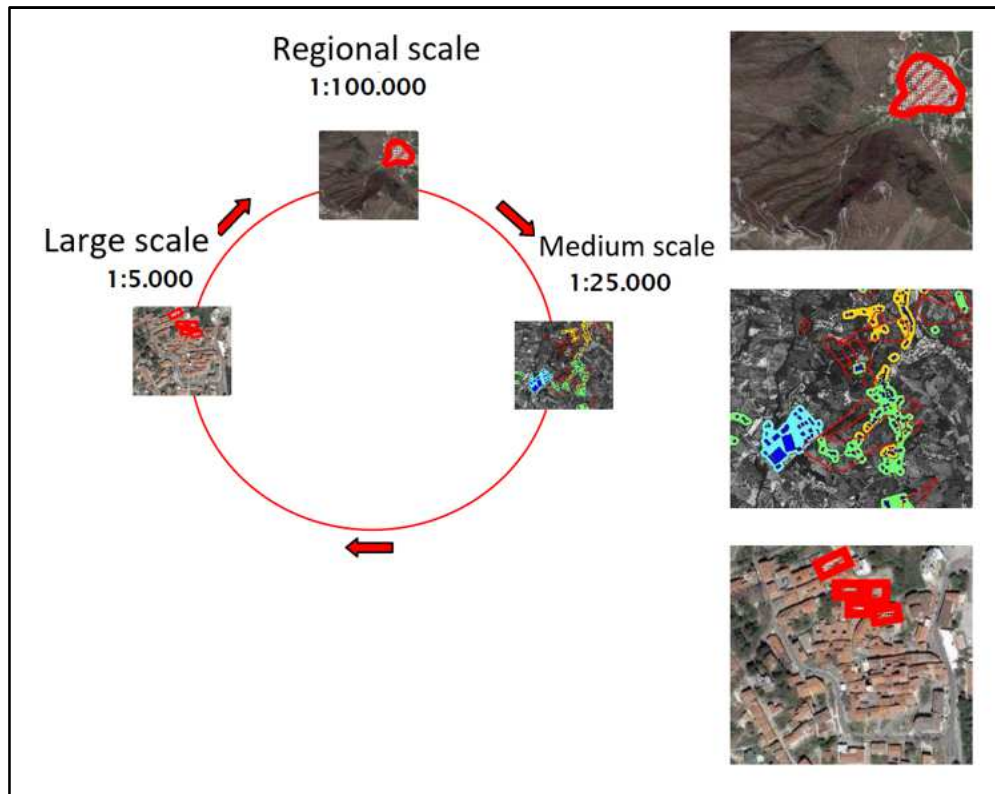


Figure 4.4 Exposed elements at different scales of analysis (from Pisciotta, 2008).

4.3 Physical building vulnerability: the concept of damage

Most of the disasters have a natural origin; however, some disasters are man-made as well. On this basis, disasters can be broadly classified into two groups:

- *natural causes*: occur when damages are due to natural events, over which man has hardly any control. Some common natural disasters are earthquakes, landslides, floods, hurricanes, cyclones, tsunamis, volcanic eruptions, etc.;
- *man-made causes*: are the result of carelessness or human errors during construction and use phases. The disasters are in the form of accidents, which occur all of a sudden and take a huge toll on life and property. Mostly such disasters cause injuries, diseases and casualties where they occur.

It is important to highlight that most damages due to natural events are aggravated by anthropogenic activities. Thus, hazards, which are part of nature, often turn into disasters due to human actions or inactions. Several natural events are aggravated by urbanization, deforestation, negligence or errors in the design, execution and maintenance phases.

The accurate evaluation of landslide-induced damage is a necessity for planning of proper and effective mitigation measures. The analysis and forecasting of structural failures, usually requires a huge amount of data, dealing with the kinematical features of the unstable slopes as well as the damage to affected facilities.

A comprehensive approach for the surveying and classification of landslide-induced damage plays a key role in the strategy to better delineate mass-movement boundary and state of activity, by categorizing its detectable impacts both on the ground and on the buildings, as well as to improve knowledge of the instability, to avoid repeated occurrences and to plan mitigation measures.

As related in Chapter 6, a considerable amount of damage classifications is available in scientific literature (Skempton and MacDonald, 1956; Burland, 1977; Alexander, 1986; Boscardin and Cording, 1989; Chiochio et al., 1997; Grunthal, 1998; Iovine and Parise, 2002; Cooper, 2008; Baggio et al., 2009; Mansour et al., 2011; Del Soldado et al., 2017), each one characterized by particular benefits and constraints.

The existing methods, in fact, demonstrate several advantages and drawbacks depending on the parameters considered, as lack of some important features and difficulties in applicability.

Generally, damage to structures is classified as:

- *Aesthetic* (or minor) damage, where the functionality of buildings is not compromised and the damage can be repaired rapidly at low cost (Fig. 4.5a);
- *Functional* (moderate or medium) damage, where the functionality of structures is compromised, and the damage takes time and large resources to be fixed (Fig. 4.5b);
- *Structural* (severe or total) damage, where buildings are severely or completely damaged, and extensive work may be required to be fixed or demolition and reconstruction (Fig. 4.5c).

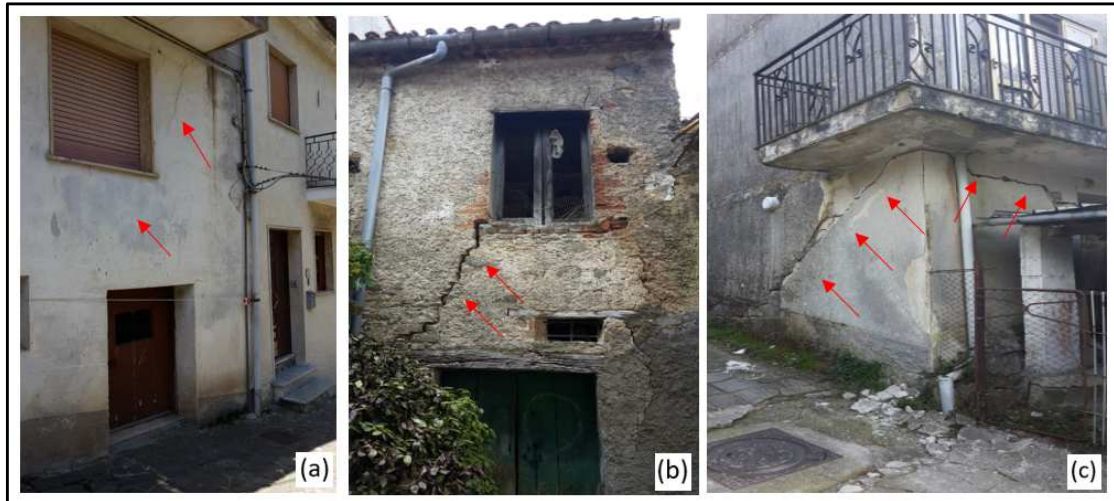


Figure 4.5 Examples of damage detected on buildings in Gorga urban settlement, Salerno Province, (Italy): aesthetic (a), functional (b), structural (c).

Usually, building failures occur when the building loses its ability to perform its function. Hence, building failures can be categorized into the two broad groups of physical (structural) failures which result in the loss of certain characteristics, e.g., strength and performance failures, which means a reduction in function below an established acceptable limit (Douglas and Ransom, 2007).

Structural failures correspond to the exceedance of ultimate limit state in many of the load-carrying elements, which compromise the structural stability of the building. In practice, this corresponds to extensive damage, partial or total collapse of the building, resulting in repair costs that are high relative to the replacement value of the building.

Failure of a structure can occur from many types of causes, when the overstressed construction reaches a critical stress level.

Temporal and spatial evolution of cracks occurred on a building should be studied and monitored, in order to identify the cause of damage through comprehensive damage assessment. A rigorous analysis and the correlation between cause and effect is not always easy: building damage can be caused by numerous mechanisms and every crack is not generated by a single external factor, since “perturbing” causes can be not isolated but combined with other effects.

Indeed, the response of buildings is dependant on the type and condition of the structure: buildings instability and external forces-induced damage degree depends also on geometry, materials, or structural properties, causing cracks to slowly form and then progress through cyclic loading conditions.

Most of the structural failures are associated with materials and are the consequence of human blunders involving a lack of know-how about materials or the combination of contrary materials.

Ruptures and cracks on man-made facilities occur when the tensional strains affecting building elements are greater than the tensions which structures are capable to absorb without showing deformations. The weakest constructive elements of the structure are the first that show suffering injuries, e.g. walls and façades and joints, respectively (Bru et al., 2013). Cracks and fractures represent, in general, the worsening of tension states in the structure. They do not always identify alarm conditions, but simply achieving one new building balance configuration that could be equally stable respect to that previous.

The occurrence of cracks provides information on a probable instability event, investing part of the construction: however, there is not an univocal correlation between building damage and static condition, since it can not be assessed with certainty that a building with damage signs is in a instability condition, while that without damage is in a safe condition.

The accurate evaluation of induced damage is a necessity for planning of proper and effective mitigation measures. In particular, the investigation of landslide-induced damage can be motivated by a wide range of user purposes, as administrative (to declare restrictive rules such as the evacuation for no safe constructions), planning (to estimate direct and indirect costs and assess the needed restoration, reconstruction or relocation of structures), scientific (to study the phenomena, its extension and possible evolution) and engineering design (to arrange a reconstruction plan) (Alexander, 1986).

A literature review of common approaches to detect building damage level induced by ground movements will be discuss in Chapter 6.

4.4 Approaches for physical vulnerability assessment

The vulnerability assessment process allows to quantify vulnerability of buildings to landslides, meant as the potential physical losses when they are affected by distortions induced by ground movements.

Commonly, results of vulnerability assessment are expressed through “zoning” maps showing the spatial zonation of vulnerability classes: these maps could be expressed by “quantitative” methods, using values between 0 and 1, where 0 means no damage and 1 means total loss, or by “qualitative” analyses, using definitions like “low, medium, high” or “acceptable, tollerable”.

Various studies have investigated the vulnerability of buildings to landslides in more detail, suggesting different approaches, each one characterized by advantages, drawbacks and differences in results achievable. Indeed, at present no vulnerability assessment standard methodologies exists.

Existing methods to quantify the probability of expected future damage occurrence, commonly used up to now, can be classified into four groups:

- empirical;
- judgmental (or heuristic);
- analytical;
- hybrid.

Empirical methods (e.g. Fuchs et al., 2007; Blahut et al., 2010; Peduto et al., 2017) may provide more reliable assessments although they are often based on generic assumptions: are mainly based on data derived from well-documented case studies and require available statistical damage data recorded during in situ-surveys from previous slow-moving landslide events. The observational method, when available, is the most realistic, allowing to take into account all practical details of the exposed elements, as construction properties, mechanical parameters, soil-structure interaction effects, etc. The most common problem when applying a purely empirical approach is the unavailability of sufficient and reliable statistical data. An usual but sometimes misleading approach of adopting data from different areas with similar conditions should be treated with caution.

The concept of *judgement-based methods* (Bell and Glade, 2004; Gonçalves et al., 2016) involves use of the opinions of experts with experience in landslide damage assessment. Although the reliability of such methods can be questionable due to the subjectivity of each expert, these methods are used as the predominant means for the

generation of damage probability matrices and vulnerability curves. The final outcome of these approaches is typically a vulnerability index: judgmental methods usually provide discrete values rather than continuous ones, possibly for a range of landslide intensities.

Analytical procedures for vulnerability assessment (Negulescu et al., 2014; Zuccaro et al., 2014; Tessari et al., 2016) adopt damage functions obtained from the analyses of structural models under increasing landslides movements and induced distortions.

Depending from different level of details, the analytical procedure generally take into account different simplified assumptions that might underestimate or overestimate building vulnerability and consequently future damage conditions: to this aim, they should be supported by experimental results in order to increase their reliability.

Finally, *hybrid approaches* attempt to overcome the lack of observational data, subjectivity of judgemental data and modelling assumptions of analytical procedures, by combining data from different sources. These methods, starting from available statistical data (appropriate for the considered area and building typology), estimate future damage conditions, for different values of landslide intensity, by performing numerical analyses on a building computational model.

Another classification of vulnerability assessment methods, found in literature, distinguishes the following approaches (Viscardi, 2009):

- “*direct*” *approach*: it allows to forecast landslide induced consequences basing on the experience and the judgment of an expert;
- “*tree*” *approach*: based on a logical and inductive assessment aimed to identify a range of possible solutions;
- “*consequences*” *model*: based on a logical structure which takes into account historical data of vulnerability key factors, such as landslide characteristics and exposed elements properties, is the most widely used for assessing building future conditions in a landslide affected area.

Through these approaches, it is possible to develop a vulnerability function in order to identify the relationship between landslide induced ground movements (volume, area, intensity) and the likelihood of occurrence of building damage scenarios.

Based on the scale of analysis and the availability and quality of input data, the consequence analysis, defined as the potential outcomes arising from landslide phenomena (damage, injury, loss of life or any other loss) can be carried out and expressed using the following methods:

- vulnerability matrices and indices-based approach;
- vulnerability curves or domains;
- fragility curves.

Vulnerability matrices and indices-based approaches can estimate the expected degree of loss to a given building, by using a qualitative measures of likelihood and consequences or a numeric rating scale ranging from 0 (no loss) to 1 (total loss).

The matrix approach is often the most practical one as a basis for spatial planning, where the effect of vulnerability mitigation methods can be seen as changes in the classes within the matrix. Matrices, using numerical indices, provide only qualitative information on vulnerability based on descriptions of damage patterns and landslide phenomenon, but results may not be translated into monetary loss.

Vulnerability functions and fragility curves approaches, instead, are used to provide quantitative assessment of building physical vulnerability.

Vulnerability curves, generally, show the relationship between the damage severity degree of a given building and a parameter representative of landslide kinematic (intensity, volume, area).

Fragility curves are an useful tool to assess the conditional probability of reaching or exceeding a certain level of damage severity as a function of the landslide characteristics; thus, they express the vulnerability of buildings in probabilistic terms, incorporating also uncertainties related. To this purpose, a large number of affected buildings are required.

Vulnerability and fragility curves cannot be used to assess buildings vulnerability in urban areas with different housing types. Last but not least, results are not expressed in monetary losses.

In the following paragraphs a review of existing physical vulnerability assessment methods through examples from the literature, with corresponding benefits and drawbacks, are described.

4.4.1 Vulnerability matrices and indices-based approaches

Vulnerability matrices are a qualitative method which presents the possible damage on elements at risk along with the corresponding intensity of the process.

Very often matrices are based on real events to guide risk analysis or more detailed vulnerability assessment approaches. The popularity of vulnerability matrices is based on the qualitative nature of results and the use of expert judgement to evaluate empirical data. Buildings that have not been damaged by the event will be given a vulnerability of 0, while the ones that are totally damaged a vulnerability of 1. All the other buildings will be organised within inbetween categories by an expert.

They contribute to the understanding of the interaction between the process and the elements at risk and in some cases they are used to determine thresholds for buildings damage classes. In particular, landslide intensity may be expressed in different ways (velocity, area, volume) usually as a range of values.

Several examples of vulnerability matrices are developed in the literature.

Leone et al. (1996) suggest one of the first vulnerability matrices, based on various damage states, resulting to a vulnerability value from 0 to 1 (Fig. 4.6).

Element at risk	Damage intensity	Type of damage	Vulnerability (0-1)
Building	I	Slight non-structural damage, stability not affected, furnishing or fitting damaged	0.01 - 0.1
	II	Cracks in the wall, stability not affected, reparation not urgent	0.2 - 0.3
	III	Strong deformations, huge holes in wall, cracks in supporting structures, stability affected, doors and windows unusable, evacuation necessary	0.4 - 0.6
	IV	Structural breaks, partly destructed, evacuation necessary, reconstruction of destructed parts	0.7 - 0.8
	V	Partly or totally destructed, evacuation necessary, complete reconstruction	0.9 - 1
Road	I	Slight damage of road	0.05 - 0.3
	II	Damage of roadway, reparation using 10 th m ³ material	0.3 - 0.6
	II	Damage of roadway, reparation using 100 th m ³ material	0.5 - 0.8
	IV	Destruction of roadway	0.8 - 1
Person	I	Moral disadvantage	0.001
	II	Psychological problems	0.002
	II	Slight physical injury	0.003 - 0.005
	IV	Severe physical injury. Invalidity	0.04 - 0.1
	V	Death	1

Figure 4.6 Vulnerability of various elements at risk according to damage level (from Leone et al., 1996).

Further examples are provided by Dai et al., (2002), Amatruda et al., (2004), Wong, (2005), Galli e Guzzetti, (2007), Li et al., (2010), Corominas et al. (2014), Infante et al., (2016).

Dai et al. (2002), have merged into a vulnerability matrix location, typology and other properties of elements at risk and characteristics of landslides phenomena (Fig. 4.7).

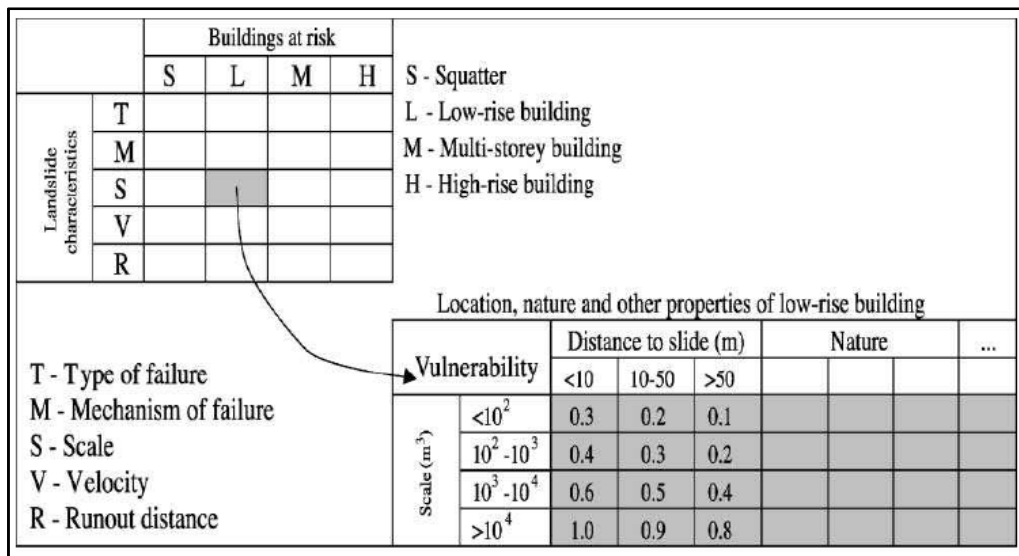


Figure 4.7 Vulnerability matrix from Dai et al. (2002).

Amatruda et al. (2004) suggested physical vulnerability values and corresponding indices of losses, basing on induced consequences of elements at risk (Table 4.1).

Damage level	Range of losses	Index
No damage	0	0
Local damage	1-25%	0,25
Severe damage	26-50%	0,50
Partial collapse	51-75%	0,75
Total collapse	76-100%	100

Table 4.1 Values of physical vulnerability (modified from Amatruda et al., 2004).

Vulnerability matrices represent an useful tool in cases of limited data for the identification of the most critical areas where more detailed analysis is required.

This approach has several advantages since it allows to investigate preliminary cause - effect relationship, as building vulnerability indicator by slow-moving landslides affected. Information regarding financial value or costs of damage are not required for the development of matrices. However, subjectivity of the method is very high: the assessment of damage severity degree, in fact, may be different among experts. For this reason, transferability and comparison possibilities of results in different urban settings are limited.

4.4.2 Vulnerability curves approach

Vulnerability functions (or curves) are used for assessing physical vulnerability in a quantitative way. Several authors (Skempton and MacDonald, 1956; Burland and Wroth, 1975; Boscardin and Cording, 1989; Burland, 1997; Infante et al., 2016; Peduto et al., 2017) defined analytical and empirical vulnerability functions as “continuous curves associating the intensity of ground movement (X-axis) to the damage response of a building (Y-axis)”.

The overcoming of these domains entails a progressive worsening of damage degree.

When landslides affect a large amount of buildings, empirical data are often sufficient.

Empirical methods, based on functional connection phenomenon intensity-damage degree, do not take into account any structural and architectonic building characteristics, nor the mechanical properties of the soil.

The empirical vulnerability domains suffer from the major drawback of being used directly by risk assessment practitioners without having to repeat the analysis for each building, given the expected range of landslide intensity and for similar building typologies and ranges of structural characteristics. Consequently, not taking into account uncertainties which may relate to the landslide attributes, to the inherent characteristics of the buildings or to their interaction with the landslide, the same ground displacement can generate a similar damage degree in structures which are really different from each other.

Additionally, a significant disadvantage of the vulnerability curves is that their reliability depends on the quality and the quantity of the available empirical data and specifically, on the survey method for the data collection, as well as, on the statistical method used for the analysis of the data.

To overcome this gap, an analytical approach can be used: totally different from empirical curves obtained by recorded building damage data from real case histories, it requires a detailed geometrical and structural survey. In particular, it is essential to define construction typology, state of preservation, properties foundation structures, type of structural instability, damage degree and distribution, mechanical properties of structural materials, soil geotechnical properties.

In both cases, a significant source of uncertainty in the development of vulnerability curves derives from curve fitting. The comparison between analytical curves and the empirical ones found in literature (Boscardin & Cording, 1989) shows some inconsistencies, related to the threshold values, mostly because the empirical methods, based on functional connection phenomenon intensity – damage degree, do not take into account any structural and architectonic building characteristic, nor the mechanical properties of the soil. Moreover, the numerical analysis, even if detailed, is characterized by simplified assumptions, concerning building modeling and damage degree assessment correspondent to each value of ground movement (Infante et al., 2016).

However, the main reason of their popularity is that they provide a quantitative representation of physical vulnerability. Loss may be described also in monetary terms and may be compared to the costs of protection measures for a cost-benefit analysis.

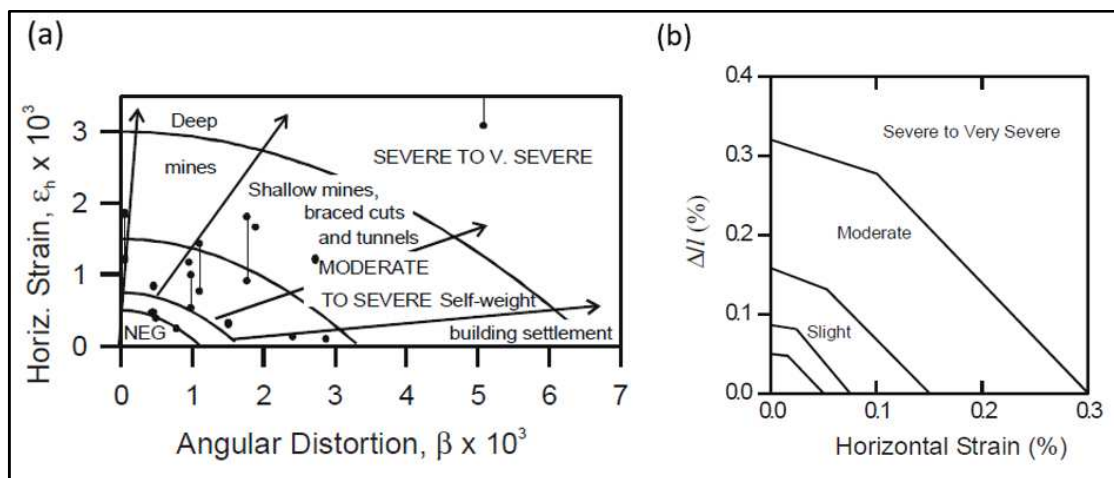


Figure 4.8 Relationship between ground distortions and damage category: (a) after Boscardin and Cording (1989) and (b) after Burland (1997).

4.4.3 Fragility curves approach

Fragility curves, unlike to vulnerability curves, express the relationship between the intensity of landslide phenomena and damage probability of occurrence. Thus, these functions provide information on probability of reaching or exceeding a particular damage severity level for a given value of landslide parameter, whose choice depends on the scale of analysis.

According to Shinozuka et al. (2000) this probability is calculated using a two-parameter cumulative log-normal distribution function:

$$F(\text{MFD}) = \Phi \left[\frac{1}{\beta} \ln \left(\frac{\text{MFD}}{\overline{\text{MFD}}} \right) \right] \quad (\text{eq. 4.1})$$

where MFD is the adopted landslide parameter, $\Phi[\]$ is the standard normal cumulative distribution function, $\overline{\text{MFD}}$ is the median value of MFD at which the building reaches each damage level, and β is the standard deviation of the natural logarithm of MFD for each damage degree.

As above mentioned, cumulative log-normal distribution function depends on the median value and on the standard deviation of the natural logarithm of considered landslide intensity parameter at which the building reaches each damage level D_i . These parameters describe the variability associated with each fragility curve.

The median values of MFD that correspond to each state of damage are those that give a 50 % probability of exceeding damage level. The standard deviation β describes the total variability associated with each fragility curve.

Fragility curves can be obtained according to the following procedures:

- statistical analysis of empirical data;
- analytical or numerical methodologies;
- combination of these methodologies.

Empirical approaches represented for many years, the only reasonable and possible means of developing empirical fragility curves at small scale of representation, based on the treatment of post-landslide damage observation data.

The main drawbacks of this approach lies precisely in the subjectivity on evaluating damage state of each building or in the lack of accuracy in the determination of the ground motion affecting the urban settlement.

Analytical approaches are commonly used for the construction of fragility curves above all in detailed analysis, at large scale of representation, defining a direct relationship between landslide ground movements and building structural response in terms of damage effects.

At this level of detail, vulnerability assessment can focus on the identification of variables that influence the vulnerability of an element at risk (vulnerability indicators).

Tarbotton et al. (2015) suggest, in fact, that accuracy and reliability of the results of empirical vulnerability curves depend on a series of factors including the accuracy of the data regarding the building damage as well as the building characteristics.

For this reason, vulnerability of buildings to slow-moving landslides is determined considering different attributes such as building typology, type of foundation, number of floors and structural properties of material.

In recent years several examples (e.g. Mavrouli et al., 2014; Negulescu et al., 2014; Peduto et al., 2017) of fragility functions to assess building vulnerability within landslide affected area have been proposed (Fig. 4.9).

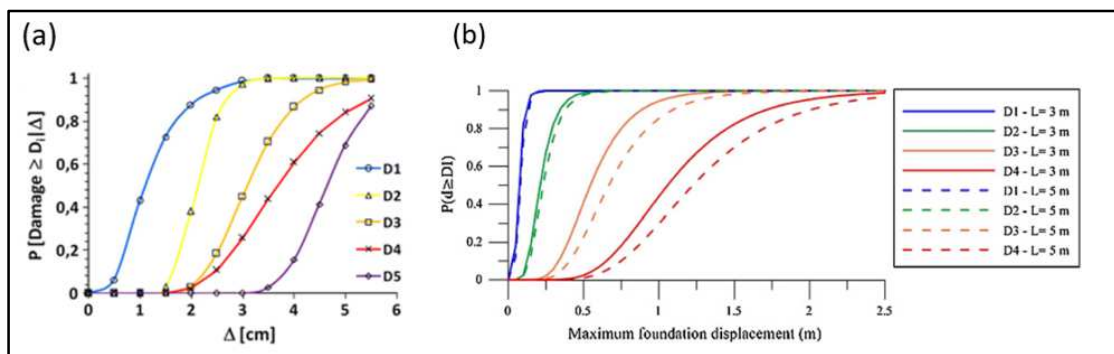


Figure 4.9 Fragility curves developed by empirical data (a) (after Peduto et al., 2017) and by numerical analysis (b) (after Mavrouli et al., 2014).

These curves, once further validated, can be valuably used as tools for consequence forecasting purposes and, more in general, for planning the most suitable slow-moving landslide risk mitigation strategies.

The applicability/exportability of the obtained results, although site-specific, could be significant in urban settlement with similar structural typology.

In particular, widening the sample of analyzed buildings in similar geological contexts would allow better calibrating and also validating the generated curves.

Fragility curves represent an useful tool so popular among practitioners since they connect directly the intensity of a process with the corresponding probability of degree of loss, providing concrete quantitative results and translating potential events into monetary damage (Mazzorana et al., 2009).

CHAPTER 5

LANDSLIDE INVESTIGATION AND MONITORING TECHNIQUES

Introduction

As indicated in the previous Chapter, landslide vulnerability assessment is still considered a difficult process since it depends on several factors. In this work, the proposed approach is based on a logical structure which takes into account the vulnerability key factors, landslide intensity and the characterization of the exposed elements.

Many examples of interaction between landslides and man-made constructions (Cascini et al., 2013; Ciampalini et al., 2014; Zuccaro et al., 2014) point out that damage caused by slope movements, depend on several factors, either natural, such as types, size and velocity of the phenomenon, or anthropogenic, such as typology and location of buildings respect to the landslide boundary; overall, such factors determine the degree of vulnerability of the elements at risk (Iovine & Parise, 2002).

To this reason, it is evident that in cases of slow-moving or intermittent landslide, investigations of the areas affected by slope instabilities aim at controlling the evolution of the displacements and at preventing or mitigating the damage that could derive by possible re-activations of the phenomena.

Landslide mapping and monitoring are essential for the investigation on causes and effects of such phenomena. Landslide mapping is a fundamental tool to identify, locate and define landslides in a given area; after mapping, regular observation and recording of the landslides evolution, especially for events characterized by slow and intermittent kinematic, assume a paramount role, in order to prevent eventually damage to structures and to preserve buildings.

For this reason, it is essential to develop methods based on the collection of survey data and monitoring as to define scenarios and to implement warning system and/or civil protection plans. The selection of adequate instruments depends on several factors, such as time to install and get results, site accessibility, weather conditions.

Generally, conventional methods include the installation of tools directly in the area and provide information on the punctual measured variables. This includes exposure to environmentally hazardous conditions, long periods for the installation of equipments and high costs for their management and maintenance. Many of the limitations can be overcome through the use of advanced technologies for the information acquisition. Geo-information science and Earth Observation consist of a combination of tools and methods for the collection, storage and processing of geo-spatial data and for the dissemination and use of these data and of services based on these data.

In this Chapter, after a brief introduction on the process of landslide investigation, a summary review and a classification of the main approaches of investigation and monitoring, advantages and disadvantages of different methods, relationship between type of approach and scale of work are discussed.

Finally, particular attention is given to the landslide monitoring method used in this research, Remote Sensing technique and, in general, how an integrated field-Earth Observation systems approach can support the analysis of slope instabilities.

5.1 The process of landslide investigation

The role of investigations has been recognized as central and decisive in a landslide study: they should be addressed to analysis, and classification, of occurred phenomena as well as to the recognition of potential slope failures (Hutchinson, 1988).

Landslide mapping is a fundamental tool for the assessment of landslide hazard, even with the differences that characterize their generation, due to variability of scale and procedure existing, the requirements of the end user and the purpose of the investigation (Varnes, 1974, 1978; Rockaway, 1976; Cotecchia, 1978). Landslide inventory is an essential part of any landslide zoning and understanding of the evolution of landscapes. It involves location, classification, volume, travel distance, state of activity and date of occurrence of landsliding in an area (Fell et al., 2008).

Landslide mapping is essential for the investigation on causes and effects of such phenomena, but landslide monitoring is fundamental, too. After mapping, regular observation and recording of the evolution of landslides, especially for the events characterized by slow and intermittent kinematics assume a paramount role, in order to prevent possible damage to structures and to preserve buildings.

An investigation process should essentially include five broad steps, from its planning to implementation and analysis of the results (Johnson & DeGraff, 1988):

- *formulation of the investigation*
- *data collection*
- *data interpretation*
- *application of the analysis techniques*
- *communication of the results.*

It has to be pointed out that, considering the complexity of the landslide phenomena, each step does not represent an isolated activity, but should rather be part of an iterative process, thanks to the feedback coming after the data interpretation: new information generates new questions and, thus, more data for their resolution.

This Chapter describes the steps needed to build an effective monitoring system. Ideally, the best monitoring system for a given phenomenon is identified on the basis of the answers to the following questions:

- What has to be monitored?
- Which is the magnitude of the event?
- How to monitor?
- Which scale has to be used?
- What is the monitoring frequency?
- How long does the monitoring campaign have to last?
- What are the costs?
- What are the expected results and advantages?

The working phases can be outlined as follows:

- a) Phenomenon description
- b) Action planning
- c) Monitoring network development

The first phase (phenomenon description) is carried out by archive research of thematic maps, aerial photographs, photographic documentation, historical data, cause and type of event, previous studies, etc.

In the action planning a critical analysis of what was found out in the first phase is carried out, the first data are taken in the site of interest, as well as a functional enhancement of the monitoring planning.

The result would be to suggest possible investigations or peculiar measures to be done preliminarily. In this phase some kinds of monitoring (i.e. of superficial movements) are frequently activated to better understand the real activity of the phenomena and their extension. This allows to determine whether additional surveys and investigations are needed.

The monitoring network development entails the installation and maintenance of a true monitoring network. To do so, it is required to conduct those investigations (preliminary, detailed), specified in the previous phases. It is a matter of direct surveys and geological and geotechnical investigations whose results allow to define:

- Which are the parameters to measure;
- Where, when and how to measure them.

Ideally, investigations should last a very long period in order to detect changes in landslides behavior and to relate them to possible environmental factors. Furthermore, the formulation of aims, mainly consists in the identification of the objectives, namely of the questions that it should address, and of some technical aspects that are not easy to be defined in advance, including area and depth to be investigated, both factors depending on the type of landslide, and the duration of the monitoring campaigns.

5.2 Landslide monitoring

The monitoring of natural phenomena has acquired relevance also due to the improvement in technology, allowing more detailed analyses and interpretations. A correct monitoring is achieved through the observation of kinematics, hydrological and climatic parameters in order to (Angeli et al., 2000):

- identify movements before important morphological changes at the surface have taken place;
- define the geometry of the moving mass with precision;
- quantify the principal kinematic parameters (velocity, acceleration, etc.) and their possible correlation with hydrological and climatic characteristics;
- carry out constant surveillance for events that put inhabited areas at risk;
- propose reasonable plans to help people in risk areas.

An exhaustive checklist of features that should ideally be investigated is reported in Sowers & Royster (1978), as shown in Table 5.1.

Topography
1. Contour map
2. Surface drainage
3. Slope profiles
4. Topographic changes
Geology
1. Formations at site
2. Structure: three-dimensional geometry
3. Weathering
Groundwater
1. Piezometric level within slope
2. Variations in piezometric level
3. Ground surface indications of subsurface water
4. Effect of human activity on groundwater
5. Groundwater chemistry
Weather
1. Precipitation
2. Temperature
3. Barometric changes
Vibration
1. Seismicity
2. Human induced vibration
History of slope changes
1. Natural process
2. Human activity
3. Rate of movement
4. Correlations of movements

Table 5.1 Checklist for planning a landslide investigation (simplified after Sowers & Royster, 1978).

For what concerns the monitoring applied to the phenomena of instability of the considered test-site is to be understood as a source of measures to understand their extension and magnitude and then estimate the risk associated. More generally, the understanding of the phenomenon must provide for the acquisition of information on:

- the system of sub-superficial displacements, in terms of direction, modulus, and rate of velocity;
- scheme of deep displacements, with definition of the position of the sliding surface;
- the aquifer system regimen;
- rainfall regimen.

Obviously, a correct monitoring makes the implementation of appropriate instrumentations mandatory: specific instruments installed within landslides can provide useful information regarding possible landslide movements and the potential for increased hazards.

It has to be pointed out that landslide investigations include many activities for collecting data. In this work we will focus on the parameters inherent to the landslide under investigation (surface and deep displacements) and on the external factors that can infer on the slope stability (climate conditions like the precipitation and the pore-water pressures).

5.3 Ground monitoring

Surface observation, intended as identification of surface features related to slope movements, plays an important role in interpreting the phenomenon and assessing the relative causes (Parise, 2003). It can be carried out through several techniques, e.g. from field surveys to the use of geologic maps and aerial photographs, and, eventually, results can be reported on thematic maps. In addition, surface displacements can be computed by means of ad hoc instrumentation, such as Electronic Distance Measurement (EDM), total stations, tiltmeters, Global Positioning System (GPS), Radar Interferometry.

McGuffey et al. (1996) reported that subsurface investigation methods can be summarized as in the following:

- reconnaissance methods, mainly involving quick and low-cost techniques in order to define the general characteristics of the materials, through the use e.g. of portable hand tools, soundings and penetration tests;
- surface geophysical methods, providing relatively inexpensive information on large areas and in short time, related to the distribution of physical properties of the soils, by means e.g. of electrical/electromagnetic and seismic methods, or Ground-Penetrating Radar (GPR);
- test and core borings, allowing to obtain direct data on the stratigraphy, the geotechnical properties of the materials (e.g. shear strength, plasticity, moisture content, etc.) through laboratory and in situ tests and the hydrogeologic characteristics (e.g. free water levels, artesian pressures, etc.) by converting the exploratory holes in wells for the monitoring of groundwater;
- borehole logging, giving information on different properties of the materials as a function of the depth, by means of several logging devices, such as electric, nuclear and seismic (i.e. up-hole, down-hole and cross-hole surveys) logs;

- field tests, more expensive than those carried out in laboratory, but that provide more reliable information on the strength properties of the materials, overcoming the limitations due to the recovery of “not representative” samples; they can be carried out through e.g. dilatometer tests, vane shear tests and shafts.

Considering the peculiarities of each of these techniques, it is often useful to proceed to their simultaneous use, so as to obtain the same information that can then be added to a better and more objective interpretation of the data. To this end it is necessary to have in mind what are the potentials and limitations of each technique.

The principal methods to the displacements monitoring (*extensometers, inclinometers, topographic levels, GPS, total stations, laser systems, radar interferometry, ...*) can be classified into two principal categories: “*in situ*” techniques and “*Remote sensing detection*”.

Different factors affect the selection of these methods and their applicability, internal factors, typical of the instrument used, and external factors, independent of the instrumentation. In the evaluation of ground surveys methods, each system has been described about internal parameters and, also, external considering the same arguments for each one. These factors are: time available, studied area and its accessibility, exposure to hazardous condition and representation scale.

5.3.1 Conventional in-situ techniques

Generally, landslide investigation and monitoring requires a preliminary analysis of geological and geomorphological conditions. Traditional surveys include different products: geological, geomorphological, topographic survey. These methods consist in analysis directly on the field in order to provide information on the characteristics and to identify the most dangerous local situations.

The identification of features and elements at risk will be done through the comparison of the characteristics local with situations type derived from experiences and studies in the field. Furthermore, the collection of geological, geomorphological and geotechnical available data in the study area is significant for the reconstruction of the preliminary model and the subsequent recognition of the geo-mechanical parameters of the rock types outcrops.

The geological survey should lead to the definition of the geological model of the study area, in particular must be identified and mapped all rock types and the features considered significant for the reconstruction of the stratigraphic and structural area. Indeed, geological map must contain all the formations outcropping and primary and secondary discontinuities (directions layer, faults, etc.).

The geomorphologic survey is capable to identify and mapping the forms and processes associated with the action of gravity, surface water and groundwater, human activity, as well as those affected by the geological structure. The geomorphologic map it must identify the geomorphologic processes current and past.

The lithological survey is derived from all the formations in the geological map in order to group the lithostratigraphic units in terms of mechanics-technical features. The map must be accompanied by profiles oriented so that they are significant for the reconstruction of dip and dip direction and relations between the litho-units, also in relation to the morphological aspect.

Traditional in-situ survey must be accompanied by quantitative measurements aimed to provide a detailed assessment of landslide phenomena.

Generally, instrumental methods include all the techniques to measure “*in situ*” surficial or deep displacements. Measurements can be linear or angular and can be managed in one, two or three perpendicular directions.

The most used instruments are extensometers, inclinometers and piezometers.

The *Extensometers* (Fig. 5.1) are enable to evaluate axial deformation with respect to reference points placed along the same axis; even in this case they can be installed inside boreholes. The most widespread extensometers are characterized by a measurement accuracy of the order of ± 0.3 mm for every 30 m. Among the main factors influencing the measurement gauge there are temperature and correct installation of the equipment. Further limitations lie in the fact that the measurement is one-dimensional, then only useful in case the direction of the displacement vector is already known.

Various typologies exist and the most common are:

- rod extensometers, used to monitor the movements of “measuring points”, permanently installed in the borehole at selected depths. The absolute deformation profiles are so determined by knowing the extensometer position respect to a fixed reference;

- differential extensometer, constituted by two deep anchored reference bases to control the movements.

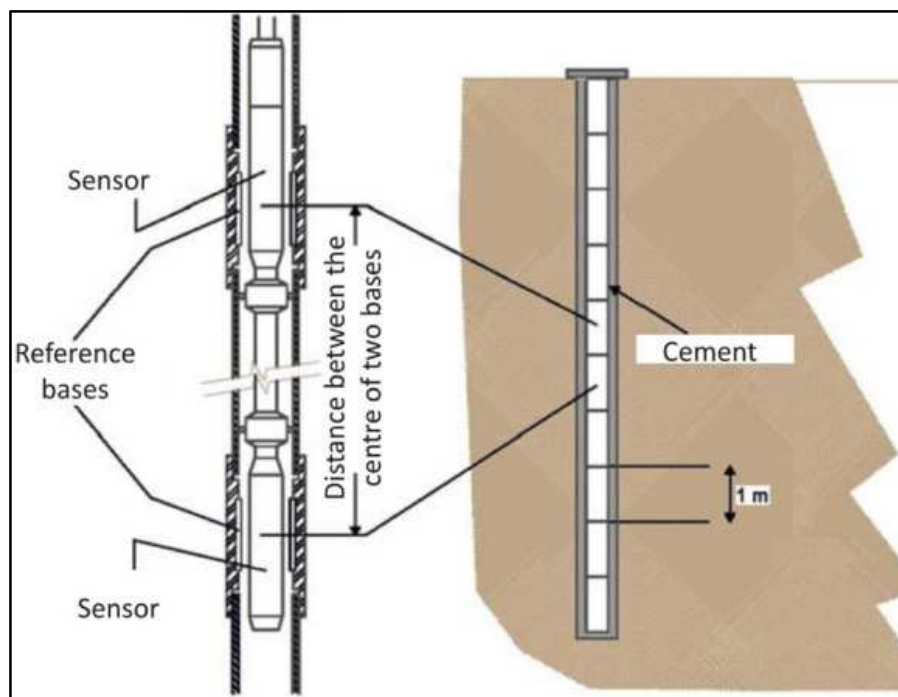


Figure 5.1 Differential extensometer (Mulas et al., 2010).

For the study of deep deformations of the mass and for the individuation of the slip surface, one of the best-suited instruments is the *inclinometer*. In many cases, inclinometers are used to determine subsurface movement of landslides (Borgatti et al., 2006; Bonnard et al., 2008; Bressani et al., 2008); they are devices installed in boreholes located within the landslide (Fig. 5.2).

They consist of a hollow metal tube, which is installed within a drilled hole. Such installation registers the deformation of the terrain, determining the variation of the original inclination of the tube. The inclinometer monitors deformation normal to the axis of the casing and the depth detected for the shear movement is the depth of the failure surface. The acquisition of the deformation is executed periodically using an inclinometric probe, the inclinometer indeed, even if nowadays real-time transmission of measurement data to data loggers is much more widespread.

They allow to evaluate the depth of the sliding surfaces, by measuring at the same time the displacements along the vertical and the direction of displacement (azimuth). The accuracy of the measurement is of the order of ± 0.02 mm for every 3 m of depth. The major limitation lies in the fact that for the shape of the instrumentation it is possible to estimate the displacements only in 2D without obtaining three-dimensional repositioning.

The inclination of the probe body is measured by two force-balanced servo-accelerometers (which are inside the probe). One accelerometer measures the tilt in the inclinometer wheels plane, which tracks the longitudinal grooves of the casing. The other accelerometer measures the inclination in the plane perpendicular to the wheels. Inclination measurements are converted to lateral deviations. The obtained measurements are related to the initial reading (called “zero reading”), which consists of four cycles of measures in which the probe is rotated of 90° to minimize the systematic errors.

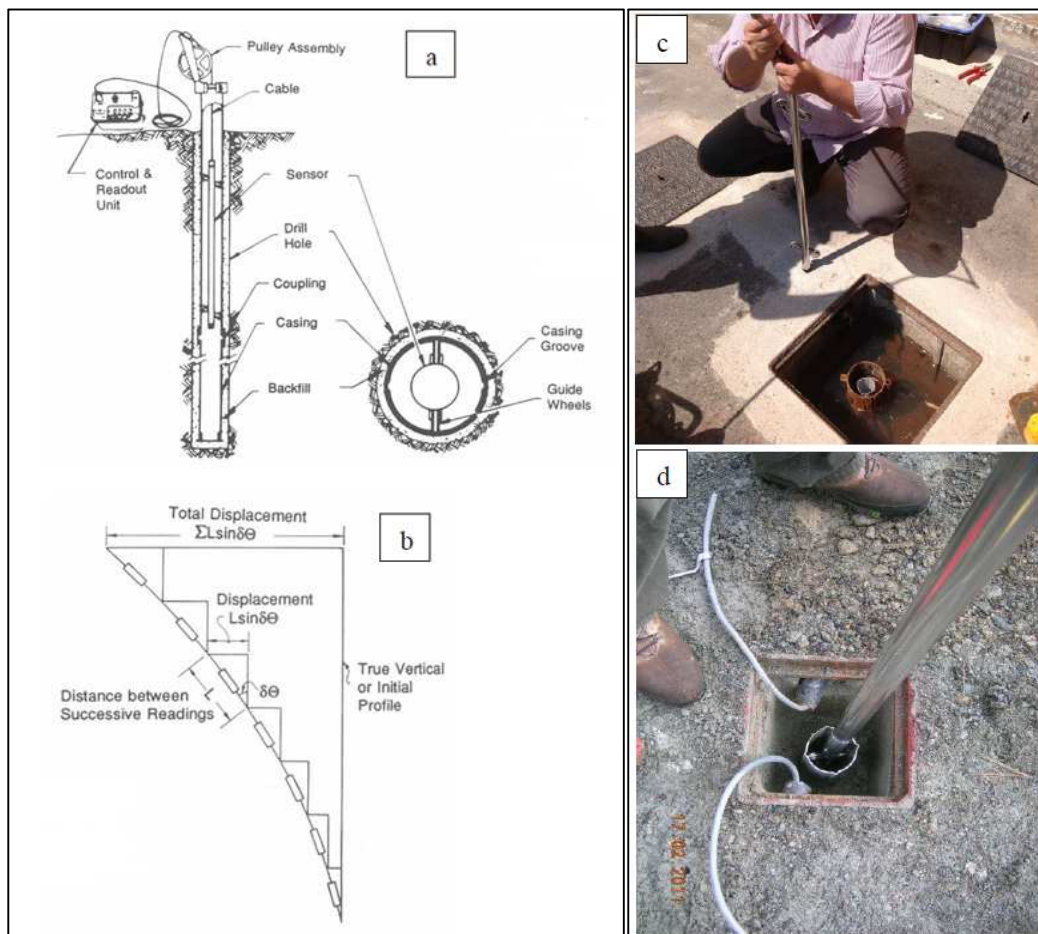


Figure 5.2 (a) Inclinometer configuration, (b) scheme of inclinometer installation, (c) and (d) inclinometric readings (Confuorto, 2016).

Connected to ground displacements control, also the assessment of triggering factors has to be taken into account. In particular, one of the most significant triggering factors is the pressure of groundwater, related, very often, to precipitations.

To this purpose, *piezometers* are installation of instruments, within a drill hole, for detecting first the depth of water, but also the groundwater fluctuation and the pressure of groundwater levels at specific depths and the pore pressure (Fig. 5.3).

The latter parameter in particular can provide information on the stresses and the strains in a rock or terrain mass.

Typically, these instruments are used for understanding initial site condition, determining safe rates for placement of fill, predicting slope stability, designing for lateral earth pressure and finally for evaluating the effectiveness of drainage schemes.

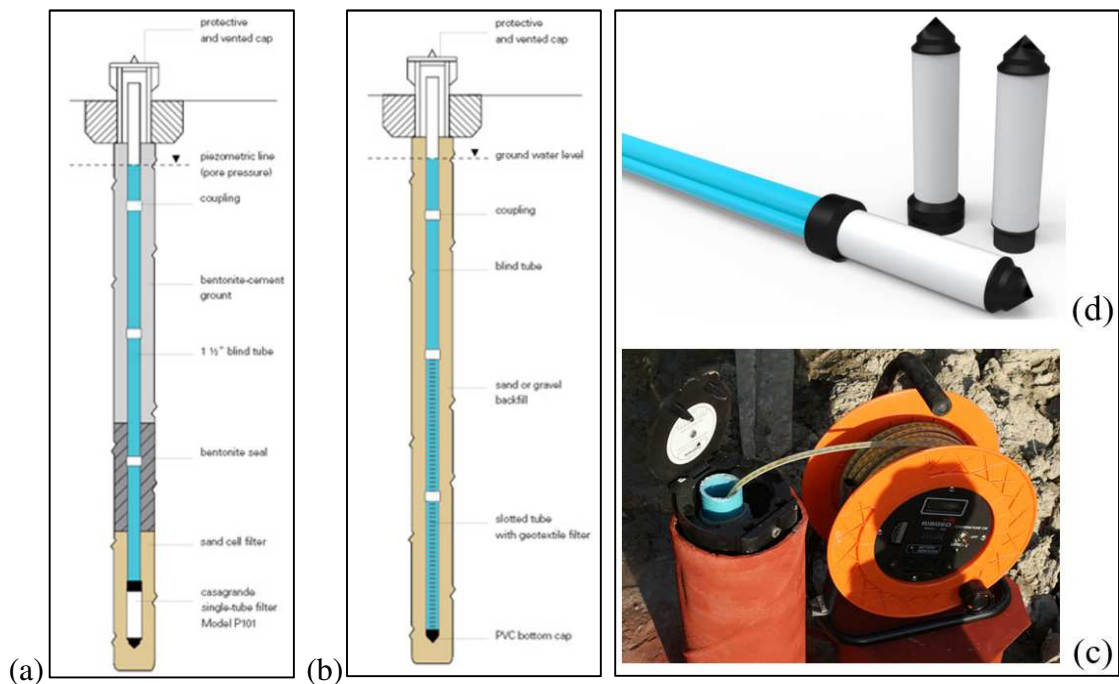


Figure 5.3 Piezometers: “Casagrande” (a), open pipe (b), scheme of “Casagrande” piezometer (c) and (d).

Several types of piezometers have been invented in the last 80 years, according to the type of terrain to investigate or to the parameters to obtain. Generally, they can be distinguished among different types (vibrating string, tires, Casagrande, open pipe, hydraulic piezometer) according to the filtration speed of the water inside the soil, which in turn will affect the accuracy and response times of the piezometric measurements.

Furthermore, the critical evaluation of rainfall represents an useful tool aimed to assess the occurrence of landslides. In fact, rainfall-triggered landslides are, from a quantitative point of view, very significant. In particular, landslides with a slow and intermittent kinematics present acceleration and deceleration according to the intensity of precipitation, especially for the shallow deformations (Caine, 1980).

High-resolution temporal rainfall data can be acquired by using specific instruments, like automatic tipping bucket rain gauges, weighing rain gauge, acoustic rain gauge,

optical rain gauge, etc., all known as pluviometers (De Luca, 2014). These are instruments to gather and measure the precipitation occurring in a given period of time (Fig. 5.4).

A special weighing rain gauge features a rotating drum, a pen, and a storage bin. The storage drum collects any form of precipitation while the pen positioned below the drum records its weight.



Figure 5.4 Examples of pluviometer stations.

5.3.2 Remote sensing detection

Various definitions have been provided since the origin of the appropriate instruments for the Earth observation; one of the most interesting and concise was given by Barrett and Curtis (1976) which defined Remote Sensing as “the observation of a target by a device separated from it by some distance”. Generally, this term refers to all the techniques that allow to investigate a phenomenon through the use of sensors that work with different wavelengths placed at a considerable distance from the considered object. The distance of the observer from the information collected can range from a few meters (Proximal Sensing) to thousands of kilometers (Remote Sensing). Forty years of progresses in the sensors technology and in developing an always higher number of tools, able to observe the environment in different spectral bands, have considerably improved the effectiveness of the Earth observation through these techniques.

The origin of the remote sensing obviously derives from the beginning of the practice of photography. Nowadays, the monitoring of deformations occurring on the Earth surface works also by means of electromagnetic radiations: all the objects emit electromagnetic radiations, and can also reflect radiations emitted by other objects.

The most familiar form of electromagnetic radiation is visible light, which is a part of the complete electromagnetic spectrum.

In fact, in addition to the passive sensors, which measure the energy emitted by an external source and reflected by the observed target, there are the active ones which generate electromagnetic waves, illuminate the scene and detect the backscattered signal. The first ones allow a qualitative observation of an area, exploiting mainly optical data; in this case the electromagnetic energy is characterized by wavelengths belonging to the visible up to the infrared in the electromagnetic spectrum (Fig. 5.5).

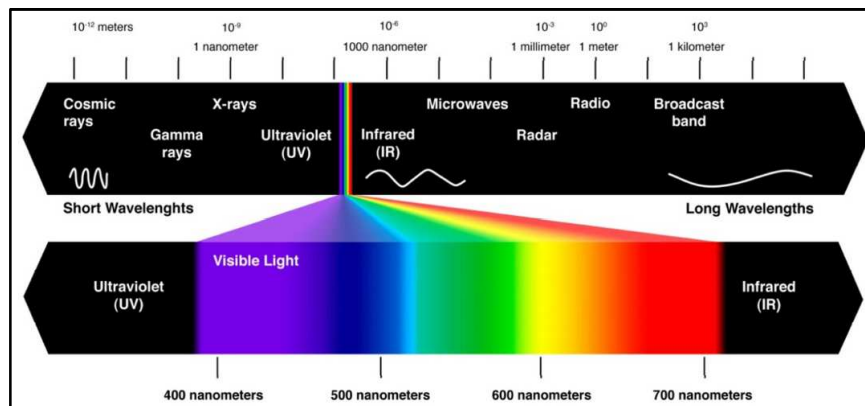


Figure 5.5 Electromagnetic spectrum.

For remote sensing applications, every wavelength has a very important application: ultraviolet spectrum can be useful to induce fluorescence in some materials, but it is not generally used for remote sensing. The visible spectrum is obviously significant for Earth observation, being the spectrum for optical imagery meanwhile the infrared, also used for optical sensors, in particular the far infrared radiation, consists of heat or thermal energy.

Microwave spectrum is the spectrum for RADAR (RADio Detection And Ranging) applications.

In particular, it is possible to distinguish “non-imaging passive sensors” which are microwaves radiometers or magnetic sensors from “imaging” ones which are cameras, optical mechanical scanners, spectrometers, microwave radiometers.

On the other hand, active sensors yield to quantitative information of an observed phenomenon, working especially with L, C or X bands. Moreover, radars are active sensors which use electromagnetic waves in the radio wavelengths and determine the distance of an object (registering the two-way travel time of the pulse) and its physical properties, measuring its backscattered intensity.

On account of this, among the remote sensing techniques there are the topographic levelling, the photogrammetric, the laser and radar techniques.

Each technique can be classified respect to the platform where the instrumentation is located. Photogrammetry, for example, can be distinguished in terrestrial, aerial and satellite. In the same way, among the laser techniques, they can be found the Terrestrial Laser Scanner, if it is on a terrestrial platform, or LIDAR, ALS and ALTM, if on an aerial platform can be found. To the radar techniques belong the Ground Based Synthetic Aperture Radar, (GB-SAR), which is a terrestrial radar, the Airborne Radar (on aerial platform) and Spaceborne Radar (satellite platform).

5.3.2.1 Topographic methods

The term “topography” includes all the techniques of earth cartography, traditionally used by surveyors to monitor and quantify land surface deformations.

Starting from topographic base, which are points having known coordinates, those ones for the monitoring points (called “control points”) at the beginning of the monitored period (x_0, y_0, z_0) have to be achieved.

After that, reference system variation components are performed, measuring the control points x, y and z changes [$dx(t_i), dy(t_i), dz(t_i)$] in different times (t_i).

Topographic methods can be divided in altimetric and planimetric.

The first ones allow to obtain the control points height variations respect to a reference horizontal surface (usually the sea surface). In particular, optical levelling is a traditional surveying technique for determining the elevations of points on the Earth’s surface relative to some starting point or height datum. Surveyors place points or monuments, referred to as “benchmarks”, in or on the ground, and make repeated measurements over a certain period of time to measure changes in height. The used instrument is the optical level. Generally mounted on a tripod, the optical level enables the observer to sight along a horizontal line, perpendicular to the local gravity vector. By reading the height of benchmarks below this horizontal line, using a precise ruler commonly known as a “staff”, the relative heights of different benchmarks can be determined. By repeating this process in a leapfrog manner and adding up all the differences in height, the total difference in height between two distant points can be calculated.

If the first point is a tide gauge or a benchmark where Mean Sea Level height has been previously established, then all the points measured in the survey will have known heights above Mean Sea Level.

Applying the planimetric topographic method results in obtaining the horizontal projection of the control points which are defined through their cartographic coordinates (x, y). The most important are the intersection methods which consist in the determination of the coordinates of the vertex of a triangle, knowing the other two vertices coordinates and the geometric characteristics.

Depending on the topographic used technique, the height measures accuracy can vary between ± 0.1 mm/Km (achievable with the precision geometric levelling) and 20 mm of the trigonometric levelling. However, they are labour-intensive and best suited to small regions only.

Using a Total Station (Fig. 5.6), measurements of distance are accomplished with a modulated microwave or infrared carrier signal, generated by a small solid-state emitter within the instrument's optical path, and reflected by a prism reflector or the object under survey. The modulation pattern in the returning signal is read and interpreted by the computer in the total station. The distance is determined by emitting and receiving multiple frequencies, and determining the integer number of wavelengths to the target for each frequency. This technique reaches to very accurate results, the angles are measured with a precision of 1", while distances with a standard mode have a precision of 1 mm + 1.5 ppm. Depending on weather conditions (temperature, humidity and pressure) that influence the resulted accuracy, this instrument allows measurements on very long distances, up to 3 km.



Figure 5.6 Examples of theodolite (a) and total station (b).

5.3.2.2 Geodesic methods

Geodesy is the scientific discipline that deals with the measurement and representation of the Earth, including its gravitational field, in a three-dimensional time-varying space. It reconstructs the Earth shape through points distributed on its surface, called geodesics; furthermore, it permits to know the coordinates of their projection on the Earth reconstructed surface, as the same as their height upon sea level (geoid).

In the last century, a new branch of this discipline, called Spatial Geodesy, revolutionized the Earth observation systems.

Among the various techniques of the Spatial Geodesy, the principal are GPS (Global Positioning Systems) and DGPS (Differential Global Positioning Systems). They consist in a radio-location system that, through connections established with some satellite constellations, yield to the three-dimensional coordinates of the points.

GPS systems allow to perform both occasional, repeated over time, and real-time measurements, allowing studies both in small and large scale.

The main advantages, with respect to the terrestrial instrumentation, are the possibility to work under any condition of visibility and weather. It is nevertheless required a certain satellite "visibility" from the monitored points.

As referred by Di Martire (2013), several experiments conducted in the field of monitoring of surface deformation estimated an error of about ± 5 mm for ranges of 50 km in diameter in the absolute positioning of the point. While, as far as the evaluation of displacements is concerned, they are characterized by a standard deviation of about 3 mm for the horizontal component and 1.5 times the horizontal to the vertical.

To achieve the measure, the minimum number of satellites to which the system has to be connected is 4, with a maximum of 12 above the horizon.

Differential Global Positioning System (Fig. 5.7) provides an increment in the precision achievable through the classic GPS, based on a reference station located on the Earth having a known position (B2). In this way, systematic errors in B1 movement computation are corrected.

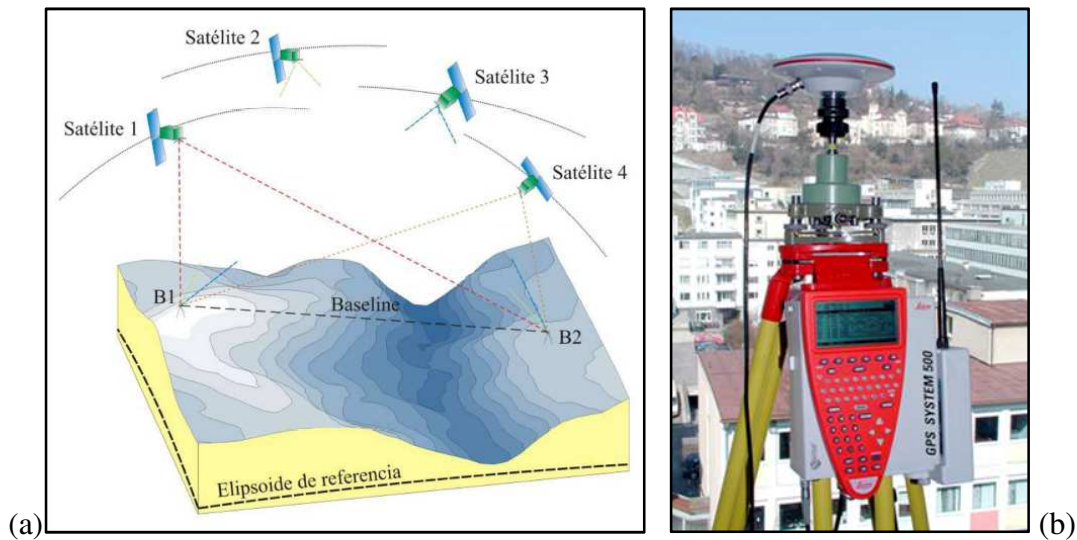


Figure 5.7 Differential Global Positioning System scheme (a) (from Tomàs, 2009) and GPS sensor (b).

5.3.2.3 Photogrammetric methods

Photogrammetry is a technique employed to obtain a three-dimensional scene through its acquisition by couples of photos, having a different capture angle, called photograms.

Photogrammetry has been defined by the American Society for Photogrammetry and Remote Sensing (ASPRS, 2009) as the science and technology of obtaining reliable information about physical objects and the environment through processes of recording, measuring and interpreting photographic images and patterns of recorded radiant electromagnetic energy and other phenomena.

Photogrammetry uses methods from many disciplines, including optics and projective geometry. Digital image capturing and photogrammetric processing includes several well-defined stages, which allow to generate 2D or 3D digital models of the object as an end product.

Aerial and terrestrial are two major types of photogrammetry (Fig. 5.8).

With reference to aerial photogrammetry, cameras fit to a machine that flies take pictures, and with the system: such pictures are used to generate measurements. The camera is mounted on an aircraft and is usually pointed vertically towards the ground. In this case, at least two photos of the same object or surface have to be taken for statistical comparison. Specially designed planes are used for this kind of photography.

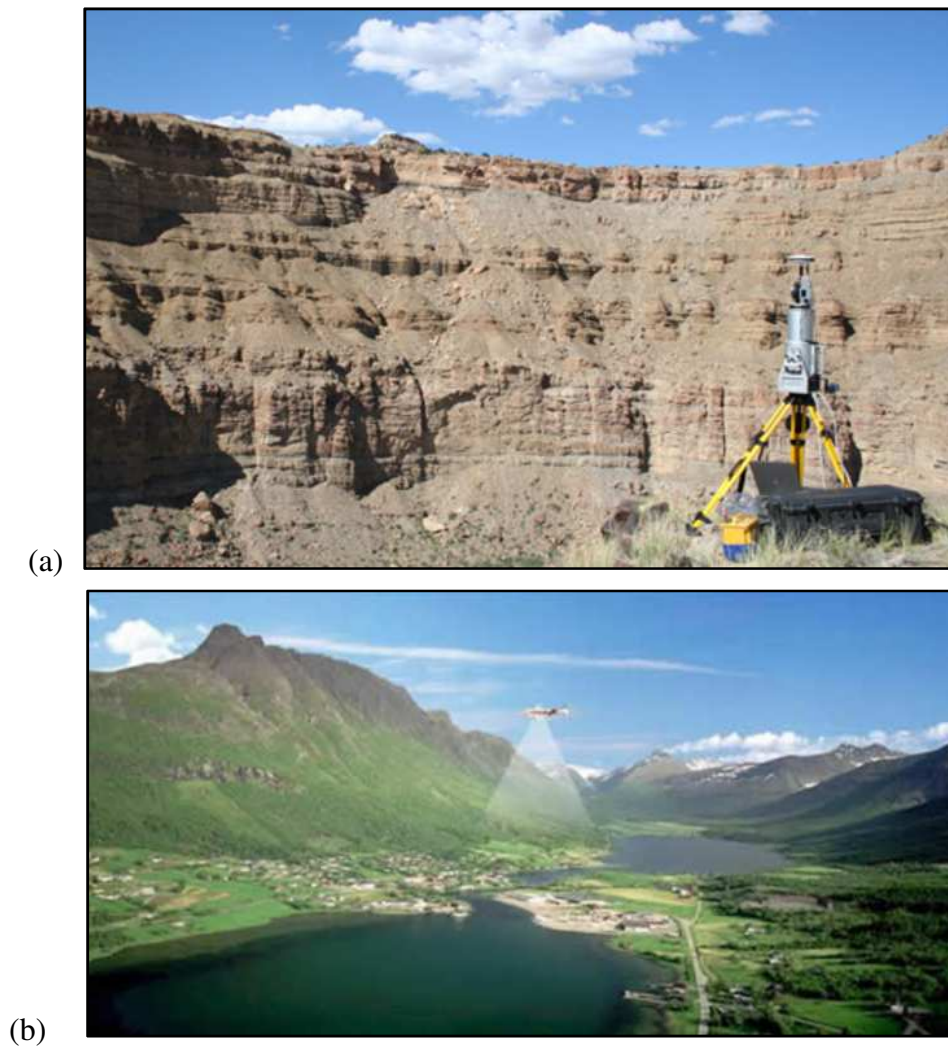


Figure 5.8 Examples of terrestrial (a) and aerial (b) photogrammetry.

Planes are made to fly over predetermined pieces of land, pointed with specific landmark edifices. Camera speed is regulated according to the speed of the plane; also, the height of the aircraft from the land is known. Stereo-plotters are used to create the base contour of the surface being photographed.

Multiple overlapping images (in the visible spectrum) of the ground are taken as the aircraft flies along a flight path.

In the kind of terrestrial photogrammetry, a camera is used in a stationary position. The camera is positioned on an elevated level. Tilt and other specifications of the camera are all controlled.

In both cases, these photos are processed by an instrument that lets an operator see two photos at once in a stereo-viewer called stereo-plotter.

Both aerial and terrestrial photogrammetry are used for issues related to mapping and also in automated processing for Digital Elevation Model (DEM) creation.

Comparing DEMs obtained for the same study area in different times, it is possible to obtain the occurred changes but with a low resolution (± 100 mm). However, methods are different, thus giving different results when at work.

The aerial kind of photogrammetry is suitable when a large piece of land has to be mapped, while terrestrial photogrammetry is a preferred method when designers and planners aim to monitor and map bridges, pipeline networks, transport network, etc..

Urban planning takes advantage of both methods. An aerial view of the proposed project along with its surroundings helps to generate a clear idea about the right perspective. Terrestrial photogrammetry, on the other hand, helps to see the interrelation between urban constructions, security issues, disaster management and many other issues benefit from this kind of analysis.

5.3.2.4 Laser scanner technique

Laser scanning technology plays an important role in the science and engineering arena. The aim of the scanning is usually to create a digital version of the object surface. Multiple scanning is sometimes performed via multiple cameras to obtain all slides of the scene under study. Laser Scanning is a non-contact, non-destructive technology that digitally captures the shape of physical objects using a line of laser light.

3D laser scanner creates “point clouds” of data from the surface of an object. In other words, 3D laser scanning is a way to capture a physical object’s exact size and shape into the computer world as a digital 3-dimensional representation. It measures fine details and capture free-form shapes to quickly generate highly accurate point clouds. 3D laser scanning is ideally suited to the measurement and inspection of contoured surfaces and complex geometries which require massive amounts of data for their accurate description and where doing this is impractical with the use of traditional measurement methods or a touch probe.

Within a very short time, thanks to the overall performance improvement, especially in the capacity (range) and accuracy in angular displacement of rotating mirrors, the laser scanner has been used for applications in different fields, as geomorphology (e.g. landslide slopes and caves).

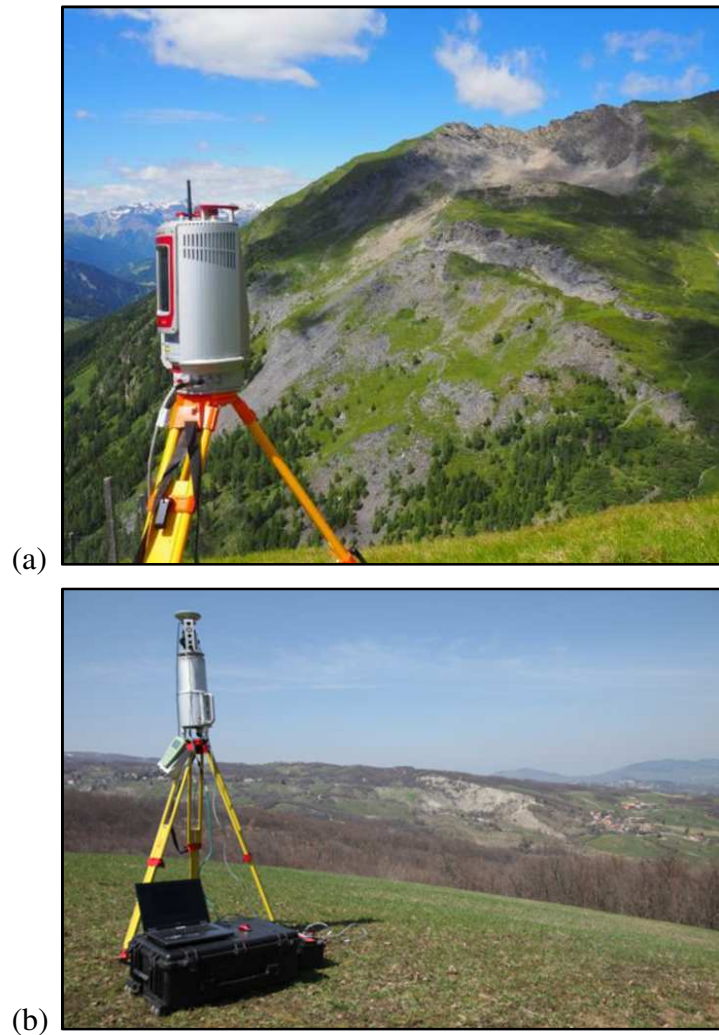


Figure 5.9 Examples of Laser scanner applications to landslides monitoring.

5.3.2.5 Radar remote sensing techniques

Radar (RADio Detection And Ranging) is an active remote sensing system operating at the microwave wavelength. The sensor transmits a microwave (radio) signal, (specifically in the frequency interval from 40.000 to 300 megahertz -MHz- of the electromagnetic spectrum) towards a target and detects the backscattered radiation. The strength of the backscattered signal is measured to discriminate between different targets and the time delay between transmitted and reflected signals determines the distance (or range) to the target. The latter frequency extends into the higher frequencies of the broadcast-radio region. Among the radar remote sensing techniques, there are the Ground Based Synthetic Aperture Radar, GB-SAR (terrestrial radar), the Airborne Radar (aerial radar) and the Space-borne Radar.

Ground based radar (GB-SAR) (Fig. 5.10) with synthetic aperture and interferometric technique (GBInSAR) is an innovative type of remote detection that furnishes a very accurate movement measurement of the ground over large areas. It employs a combination of devices and methods that can generate raster maps of two-dimensional deformations (and/or velocity) of a slope irradiated, from a remote location, with electromagnetic waves covering an area of several square kilometers and obtaining a sub-millimetric precision (equivalent to or even better than conventional topographic and geotechnical instrumentation). The output maps are made up of thousands or tens of thousands of pixels, each one with its own time series of displacement.



Figure 5.10 GB-SAR observations of landslide phenomena.

Various reasons make GB-SAR an attractive device: it provides displacement measurements with sub-millimetric precision on areas large up to a few square kilometers; it acquires images with "high" frequency; it has a ground resolution of a few meters and it is able to monitor also relatively fast movements. This large amount of information and the spatial distribution of data are typically useful for understanding the phenomena, for real time monitoring, and, finally, for the decision-making process.

Periodic monitoring of landslides phenomena with GB-SAR represents a promising approach for the long-term evaluation of instability conditions, especially in those areas where property and infrastructure are exposed to risk (Del Ventisette et al., 2011; Nolesini et al., 2013; Pratesi et al., 2014).

Airborne radar is constituted by an active radar and is mounted on a plane. The problems related to this technique are due to the difficulty in eliminating the error phase contribution due to atmospheric turbulence.

The backscattered signal time, in fact, provides the target position, function of that of the plane which is not stable like the satellite ones. In the last years, the research development also in this field, has permitted to focus SAR images acquired on planes, which, thanks to the smaller distance from the target respect to that of satellite platforms, corresponds to an high pixel resolution.

A *Space-borne radar* illuminates the Earth's surface in a side-looking style. The sensor moves along a path and transmits microwave pulses, receiving then the echoes of each pulse scattered back from the Earth surface. The SAR receiver detects the stream of echoes coherently and separates it into individual echoes, each corresponding to a transmitted pulse (Bamler & Hartl, 1998). Wavelengths of the pulse or signal characterize the bands of the electromagnetic spectrum.

The most used frequency bands in civilian space-borne SAR missions are the L-band, C-band and X-band (Table 5.2) (Barbieri & Lichtenegger, 2005). Higher frequency sensors, such as C- and X-band enable higher spatial resolutions, while lower frequencies (L-Band), are less influenced by vegetation.

Band	Frequency (GHz)	Wavelength (cm)
P-band	0.225 - 0.39	140 - 76.90
L-band	0.39 - 1.55	76.90 - 19.30
S-band	1.55 - 4.00	19.30 - 7.50
C-band	4.00 - 8.00	7.50 - 3.75
X-band	8.00 - 10.90	3.75 - 2.75

Table 5.2 Microwave bands (Frequency and Wavelength) commonly used in radar remote sensing.

The advantages respect to optical remote sensing can be synthetized in the following points:

- all weather capability (small sensitivity of clouds, light rain)
- day and night operation (independence of sun illumination)
- no effects of atmospheric constituents (multitemporal analysis)
- sensitivity to dielectric properties (water content, biomass, ice)
- sensitivity to surface roughness (ocean wind speed)
- accurate measurements of distance (interferometry)
- sensitivity to man-made objects

- sensitivity to target structure (use of polarimetry)
- subsurface penetration

In the development of the radar technology, a considerable limitation was represented by the achievable resolution of the pixels that did not allow the applicability of simple radar sensors on satellite platforms to the displacement measurements. This limitation was overcome through a Synthetic Aperture Radar, in which signal processing is used to improve the resolution beyond the limitation of physical antenna aperture. This innovation changed the possibilities in the remote sensing applications, because these instruments, using microwaves, are not affected by the presence of clouds and could achieve measures 24 hours a day obtaining radar images of wide areas.

Furthermore, during the last twenty years many satellite constellations have been launched. Among them, ERS1/2 and ENVISAT ASAR (European Space Agency), JERS-1 SAR (Japanese Aerospace Exploration Agency), RADARSAT-1/2 (Canadian Space Agency), TerraSAR-X and TanDEM-X [Infoterra (Germany)], and COSMO-SKYMed (Italian Space Agency) can be mentioned (Fig. 5.11).

In recent years, the great amount of SAR images has guaranteed the improvement of research studies in algorithms implementation for their processing, reaching a quite high precision in the natural hazard assessment.

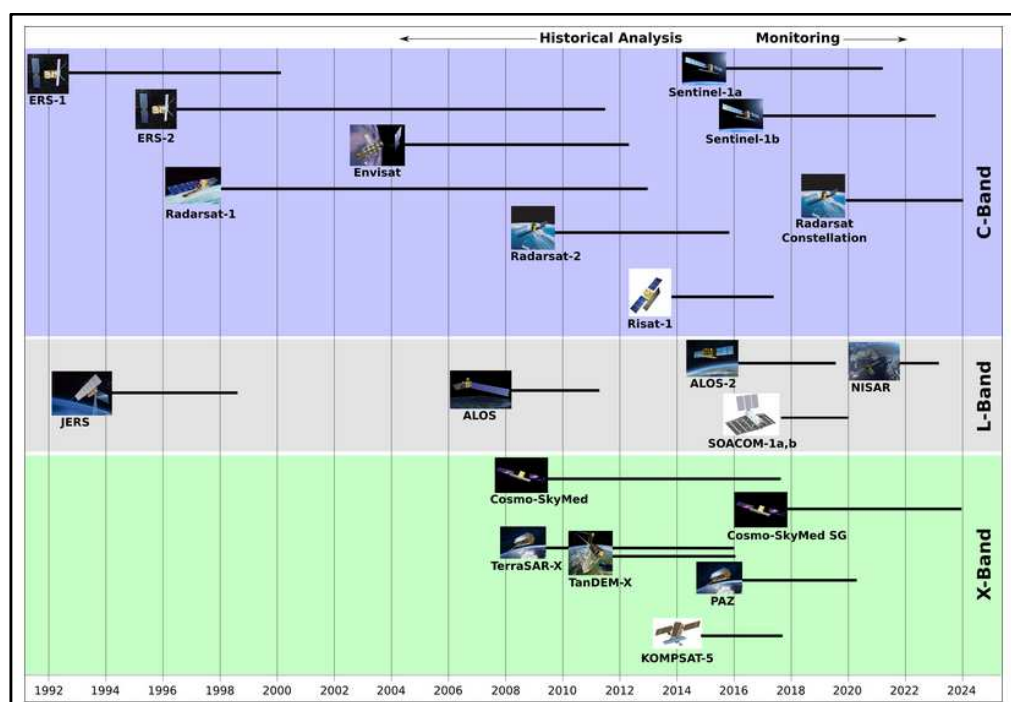


Figure 5.11 Temporal schedule of the most important SAR missions (from Tessitore, 2014).

5.4 Synthetic Aperture Radar (SAR): introduction

As introduced in paragraph 5.3.2.5, radars are active sensors which use electromagnetic waves in the radio wavelengths. Radar acquisition geometry is represented in Figure 5.12.

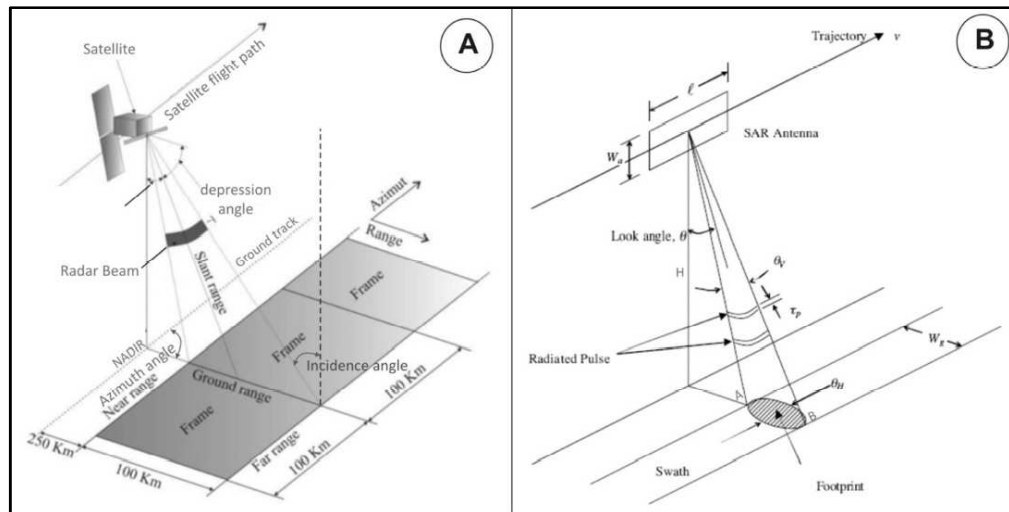


Figure 5.12 Radar acquisition geometry (image credit: NASA/JPL).

A space-borne or airborne SAR illuminates the Earth's surface in a side-looking style. The sensor moves along a path at an altitude H over a reference point and transmits microwave pulses, receiving then the echoes of each pulse scattered back from the Earth surface. The SAR receiver detects the stream of echoes coherently and separates it into individual echoes, each corresponding to a transmitted pulse (Bamler & Hartl, 1998). The wavelengths of the pulse or signal characterize the bands of the electromagnetic spectrum.

In particular, the returning echoes of the energy pulses providing information on:

- target distance (time interval between pulse emission and return from the object);
- phase;
- magnitude;
- polarization;
- doppler frequency.

Radar images are pixels matrices where, to each of them, is associated a value of the phase and the amplitude relative to the wave emitted by the antenna and backscattered from the targets. The targets detected information are projected in the sensor's acquisition plane, namely in the slant-range plane.

SAR imagery can be acquired in different geometries (Fig. 5.13), according to the system configuration:

- Stripmap: Antenna pointing is fixed relative to the flight line (perpendicular to the flight line). In this case, the result of the acquisition is a moving antenna footprint sweeping along a terrain strip parallel to path motion. The stripmap mode is usually applied for the mapping of large areas (however, characterized by coarser resolution of the image);

- ScanSAR: The sensor drives the antenna beam to illuminate a strip of terrain at any angle to path of platform motion. Basically, the assumption is that with the ScanSAR mode, it is possible to share the radar operation time between two or more separate sub-swaths in order to obtain full image coverage of each of them;

- Spotlight: The sensor steers its antenna beam to illuminate continuously a specific spot or terrain patch being imaged while the platform flies by in a straight line. The spotlight mode is very recommended for fine-resolution data from very specific areas. Thanks to the spotlight acquisition, it is possible to have finer azimuth resolution than in the other ways, even using the same physical antenna; moreover, spotlight imagery provides the possibility of imaging a scene at multiple viewing angles during one single pass.

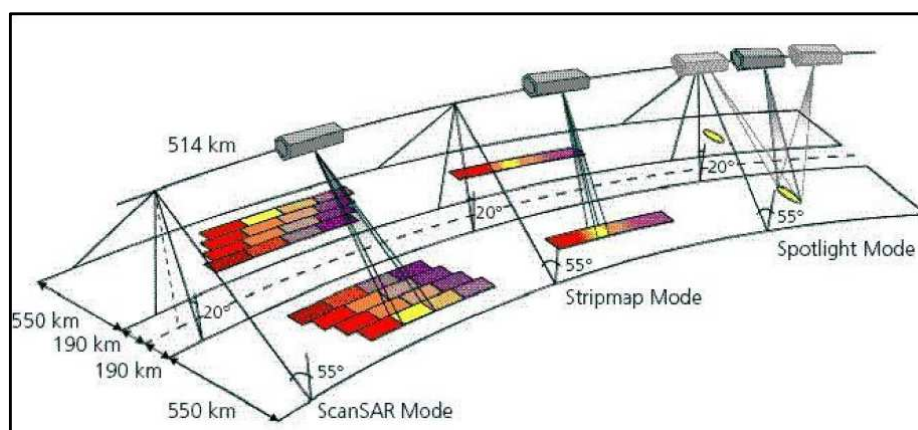


Figure 5.13 SAR acquisition modes by TerraSAR-X satellite (credit: DLR).

More recently, with the development of the Sentinel-1 mission, a new acquisition mode has been proposed, the TOPSAR mode. With the TOPSAR technique, in addition to steering the beam in range as in ScanSAR, the beam is also electronically steered from backward to forward in the azimuth direction for each burst, avoiding scalloping and resulting in a homogeneous image quality throughout the swath (De Zan & Guarnieri, 2006).

5.4.1 Synthetic Aperture Radar (SAR): acquisition geometry and images characteristics

A SAR antenna (Fig. 5.14) is mounted on a platform moving with velocity V at an altitude H , acquiring images through the emission of electromagnetic radiations. The direction of travel is the azimuth direction, while the distance from the radar track represents the range direction.

The range (or across track) is the measure of the “line of sight” distance from the radar to the target; the azimuth direction (or along track) is perpendicular to range and parallel to the flight path of the antenna. The angle between the radar beam and a line perpendicular to the surface is referred to as the off-nadir, or look angle, or incidence angle (θ), and it changes from near-range, the value at the shortest path of radar beam, to far-range, the value at the longest path of radar beam.

The distance between antenna and objects on the Earth’s surface is defined as slant range, while the horizontal distance along the ground is called ground range. The closest sector of the image to the radar track is the so-called near range, while the furthest one is the far range.

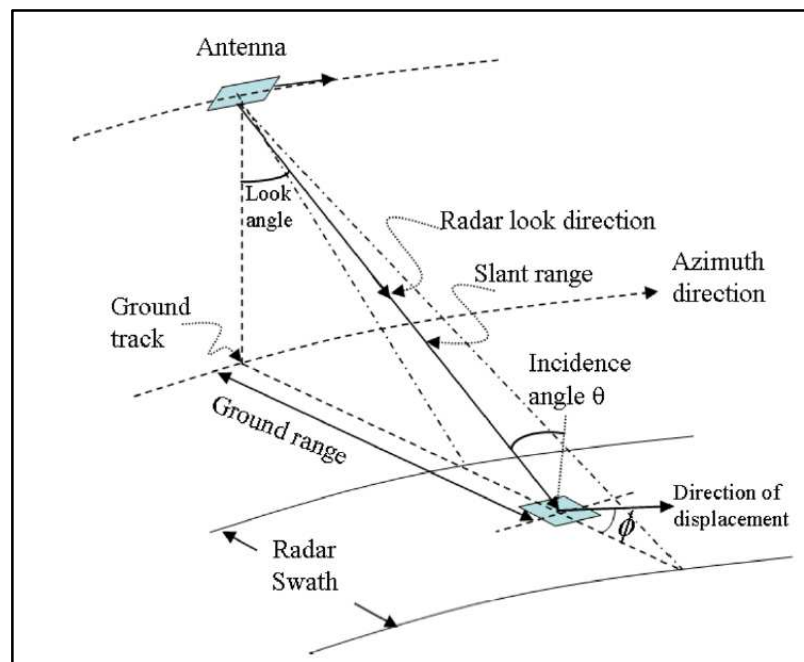


Figure 5.14 Geometric model of SAR system (modified from Zhou et al., 2009).

The two types of imaging radars most commonly used are the Real Aperture Radar (RAR) and the Synthetic Aperture Radar (SAR), different in the resolution along the direction of the satellite's movement.

Real Aperture Radars have an azimuth resolution determined by the antenna beam-width, so that it is proportional to the distance between the radar and the target (slant-range).

Ground range resolution (R_g) is defined as the capability of the sensor to detect two targets on the ground. It is function of the pulse duration of the transmitter (t_p) and of the incidence angle (also called “look angle”, θ), but it is independent from the carrier height (eq. 5.1).

To improve range resolution, radar pulses should be as short as possible, but, at the same time, their amplitude has to be increased; in fact, they have to transmit enough energy to allow the detection of the backscattered signals.

The building of a similar equipment, which transmits a very short, high-energy pulse, is very difficult.

In practice, chirp signals are used as they are long in time but also long in frequency (bandwidth, B). They can be compressed during the data processing step and thus provide a resolution which depends on the transmitted bandwidth.

Therefore, R_g can also be expressed as a function of B :

$$R_g = \frac{c \cdot t_p}{2 \sin \theta} = \frac{c}{2B \sin \theta} \quad (\text{eq. 5.1})$$

The Incidence angle represents the angle between the vertical to the terrain and the line going from the antenna to the object.

The azimuth resolution is the minimum distance on the ground in the direction parallel to the flight path of the platform by which two targets (at the same range) must be separated in azimuth to be distinguished by a radar set. It is equal to:

$$R_a = \frac{H \cdot \lambda}{l \cdot \cos \theta} \quad (\text{eq. 5.2})$$

where λ is the wavelength of the transmitted pulses, H is the height of the antenna, l is the geometric length of the antenna and θ is the look angle.

This equation states that the azimuthal resolution decreases with the altitude (H) increase. Only to have an order of magnitude of the azimuthal resolution achieving through a RAR system, considering the following values: $\lambda = 1$ cm, $l = 3$ m, $H = 700$ km, $\theta = 23^\circ$, the dimension of the pixel on Earth results to be of about 2.5 km along the satellite orbit direction.

For this reason, RAR systems cannot be used on satellite platform for the displacements assessment because, to obtain a good resolution from a satellite, a very long antenna would be required. In the development of the radar technology, *Synthetic Aperture Radar* (SAR) represented the innovative solution to this limit (Fig. 5.15).

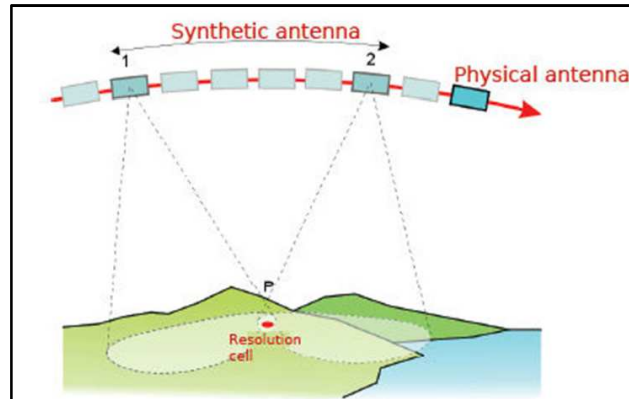


Figure 5.15 Synthetic Aperture Radar scheme (from Di Martire, 2013).

In other words, SAR “synthesizes” a very long antenna playing on the forward motion of the physical antenna, in particular, by operating on a sequence of signals recorded in the system memory.

It is important to describe how SAR data are recorded. Radar pulses, sent out by the radar, are scattered upon contact with the Earth's surface. The way in which the energy contained in the pulse is distributed is known as scattering mechanism. A radar can only measure the energy scattered back towards it, which will depend on the scattered surfaces characteristics, the pulse incidence angle and the frequency band used.

It is possible to introduce three principal scattering mechanism (Fig. 5.16) as a function of three surfaces:

- Smooth surface
- Rough surface
- Double-bounce and triple-bounce.

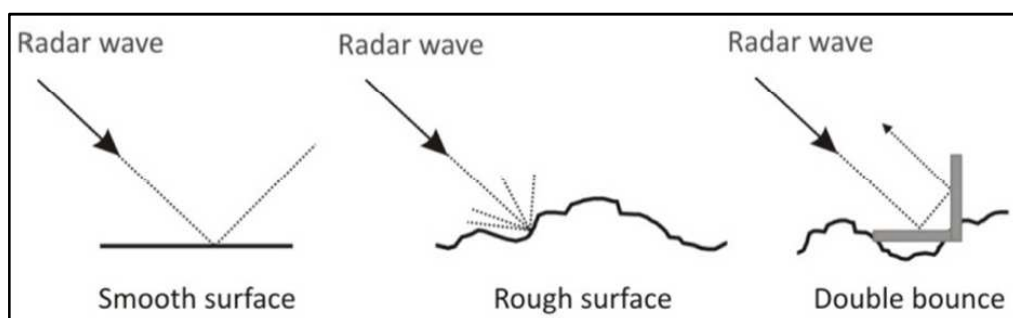


Figure 5.16 Scattering mechanisms on different surfaces (from Tessitore, 2014).

The rough surface mechanism differs from the smooth surface one because its scatter occurs in all the directions. Some fraction of the energy of the transmitted pulse is reflected back towards the radar. In the smooth case, backscattered energy can be very high if the surface is almost orthogonal to the beam, but it can also occur that a very small fraction of the energy in the transmitted pulse is reflected back towards the radar.

As it possible to note in Figure 5.16, a smooth surface generates a dark pixel in the SAR image since all the power is reflected in the specular direction.

The third type of scatter is the so-called double-bounce. In this case, most of the power is backscattered towards the sensor.

The double-bounce backscatter will tend to be fairly high and will appear bright in the radar image. Double-bounce scattering occurs commonly in urban areas, where there are plenty of vertical surfaces (the sides of buildings) and horizontal surfaces (sidewalks, streets). It represents also the mechanism on which the “Corner Reflectors” are based (double or triple bounce) (Fig. 5.17); they represent artificial reflectors, very cheap and simple to install, which influence the scattering mechanism, the radar geometry acquisition (incidence angle) and the slope geometry (local incidence angle, or local slope).

Several studies on their effectiveness are reported in literature (Sarabandi et al., 1995; Xia et al., 2004; Ferretti et al, 2007; Doerry 2008; Di Martire et al., 2013).



Figure 5.17 Examples of corner reflector installations.

5.4.2 SAR limitations affecting radar backscatter and distortions

In this paragraph are described the factors that influence the radar backscattering and contribute to the distortion of the images. These factors include:

- changes in the attitude, velocity and altitude of the sensing platform;
- the forward motion of the platform which causes scan skew;
- the radar oblique viewing geometry;
- the geometry of the images, affected by the Earth's rotation, its curvature and atmospheric refraction;
- sensor “noises”, due to poor calibration between detectors, to the atmosphere (e.g. presence of aerosols and scattering effect) and to the scene itself (e.g. effect of relief on reflection and type of reflection of the object).

All these parameters have to be taken into account for a preliminary analysis that is necessary to choose the best system to use; in fact, it has to be chosen in function of the phenomena to observe. In particular, it is very important to analyze the geomorphological settings of the study area, the presence of vegetation, the scene aspect respect to the satellite line of sight (LOS), the presence of buildings, etc..

SAR images differ from the optical ones mainly because of the acquisition geometry. The acquisition of SAR images is done in slant range coordinates, corresponding to the radar coordinate system. As a consequence, ground elevation will cause geometric distortions in the imagery, as a function of the incidence angle respect to the surface morphology. The result is the compression of features in the near-range relative to features in the far range.

However, knowing the height of the sensor and assuming a flat area, it is possible to approximate the real positions of the radar return. Such operation is called slant-to-ground projection. The geometric distortions (Fig. 5.18) can be subdivided in three types:

- *shadowing*: it occurs when the signal is not able to illuminate the ground surface, or certain areas are not reached by the radar pulse. Shadowing occurs at slopes oriented averse to the SAR antenna, hence when the slope angle α is greater than 90 minus the incidence angle θ . The consequence of shadowing on the final image is the darkness on objects on the surface not backscattered;
- *foreshortening*: it is caused by the shorter travel time of the radar pulse, as the slant range distance to an object on the inclined slope is shorter than to an object

on flat areas. The fore-shortened areas appear brighter in the SAR image, due to the compression into a smaller image part of the backscattered slope;

- *layover*: it is an extreme form of foreshortening, occurring when the slope angle α is greater of the incidence angle θ . For instance, layover can be observed when, in very steep slopes, the radar pulse first hits the top of a mountain and then its foot. Consequently, the top is imaged in front of the mountain's foot, leading to great geometric distortions in the radar image. Layover areas are usually characterized by very high intensity values.

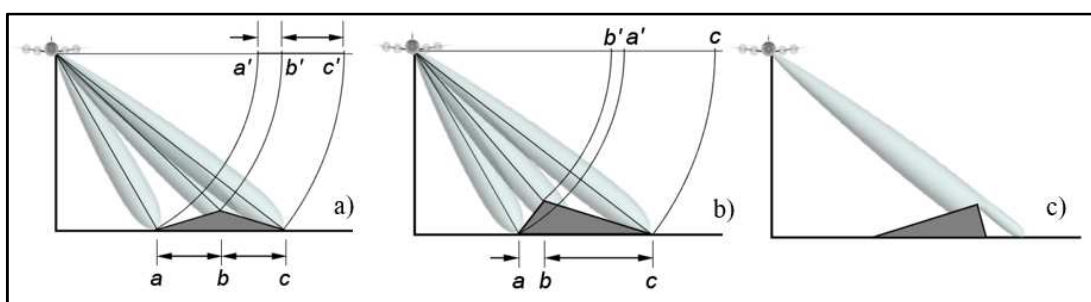


Figure 5.18 Geometric distortion effects: foreshortening (a), layover (b) and shadowing (c) (from Di Martire, 2013).

In order to estimate these effects, various techniques have been developed, which are based on the use of several images aimed to have different view angles and digital elevation models (DEM), such as shown in Notti et al. (2010; 2014) or in Plank et al. (2013).

Radiometric distortions, instead, have an influence on the energy received by the sensor. These are due to the:

- System characteristics and illumination geometry;
- Interactions between radar signal and atmosphere;
- Sensor failures or system noise;
- Terrain which influences radiance;
- Seasonal changes (which affect radiometric values).

Speckle noise is the principal cause of radiometric distortions, due to the casual interference among different back-scatterer signals in every cell. This is caused by random constructive and destructive interference from the multiple scattering returns that will occur within each resolution cell.

However, reflections from the individual blades of grass within each resolution cell results in some image pixels being brighter and some being darker than the average tone, so that the field appears speckled. Speckle is basically the product of the interference among waves coming from different objects inside the pixel. This means that the energy registered by the sensor can come from several objects whose backscattering energies are combined together.

Speckle reduces the quality of the image and its interpretation becomes more complicated. The reduction of the speckle can be done through a multi-look process and spatial filtering. The multi-look processing is a procedure for the re-projection of the image to a geometry comparable to the reality, having a ground range resolution with a square pixel. This operation, however, reduces the spatial resolution.

Speckle can be reduced also applying different filters to the image, like the Frost filter (Frost et al., 1982), the Gamma filter (Lopes et al., 1993), the Lee filter (Lee et al., 1994), and others (Hanssen, 2001). Filters must preserve the average scattering value, maintain sharp edges between adjacent objects and preserve spatial variability of the scene.

5.4.3 Spaceborne SAR missions

The first satellite designed for the observation and the study of oceans implemented with SAR instruments was SeaSat-1, launched in 1978. SIR-C/X-SAR, in 1994 and SRTM/X-SAR, in 2000, were successive experiences of modern spaceborne SAR systems: The first, covering 230 test sites acquired into two periods of the vegetation growing season, and the latter, producing topographic products, such as DEM in a mosaic format, generated from C- and X-band radar frequencies (Eineder et al., 2000; Werner, 2000). The main spaceborne missions started with the **ERS 1/2** experience, carried out by ESA (European Space Agency). ESA launched ERS-1 in July 1991 and ERS-2 in April 1995. These satellites represented the first ESA Earth observation missions, and they were characterized by a Synthetic Aperture Radar (SAR), a radar altimeter and ocean surface temperature and sea winds instruments. Both of them acquired images in C-band, with an incidence angle of 23° and a resolution of 30m x 26m. ERS-1 was deactivated in March 2000, while ERS-2, which had an additional ozone sensor, was deactivated in 2011. The **JERS-1** mission, instead, started in February 1992, led by the National Space Development Agency of Japan (NASDA).

It was an Earth observation satellite whose task was to cover the global land area for national land survey, agriculture, forestry and fishery, and also for the environmental and disaster protection. It acquired images in L-band with a westward repeat cycle of 44 days. The JERS-1 mission ended in 1998 due to a malfunction. The **RADARSAT-1** satellite was launched in November 1995 and it provided imagery for operational monitoring services on a global basis ever since. It was equipped with a C-band SAR. It was the Canada's first commercial Earth observation satellite. Its peculiarity was the ability to shape and steer its radar beam over a 500-km range, having the possibility to image swaths from 45 to 500 km in width and a resolution from 8 to 100 m. Afterwards, the RADARSAT-2 mission was launched, on December 14, 2007. New features of such mission were higher resolution imaging, flexibility in selection of polarization, left and right-looking imaging options, shortened programming, processing and delivery timelines, superior data storage and more precise measurements of spacecraft position and attitude. On May 9, 2013, the Canadian Space Agency (CSA) reported the end of the RADARSAT-1 mission due to technical issues. RADARSAT-2 is then continuing the Canada's RADARSAT program. **EnviSAT**, acronym for Environmental Satellite, was an Earth Observation mission of ESA. Its objectives were: studying and monitoring the Earth's environments on various scales, from local to global, the management of Earth's resources, continuation and improvement of the services provided to the worldwide operational meteorological community, contribution to the understanding of the structure and dynamics of the Earth's crust and interior. It was ESA's successor to the ERS missions, and it was launched in 2002 with 10 instruments aboard, such as radar altimeter, temperature-measuring radiometer instruments, medium-resolution spectrometer, two atmospheric sensors for the monitoring of gases traces, etc.. On May 9, 2012 ESA declared the end for the EnviSAT mission, due to a loss of contact with the satellite. The Advanced Land Observing Satellite (**ALOS**) was a Japanese satellite launched in 2006. It followed the JERS-1 mission and was launched in January 2006. The satellite carried three sensors used for cartography and disaster monitoring of Asia and the Pacific. On 12, May 2011, JAXA (Japan Aerospace eXploration Agency) sent a command to the satellite to power down its batteries, and declared it dead in orbit, due to technical problems. In May 2014, the ALOS-2 mission started: it is the successor of the previous mission, with a more advanced radar sensor and with 2 optical cameras in addition.

The **TerraSAR-X** mission started on June 15, 2007; it is a German SAR satellite mission for scientific and commercial applications. The project is supported by BMBF (German ministry of Education and Science) and managed by DLR (German Aerospace Center). The science objectives were to make multi-mode and high-resolution X-band data available for a wide spectrum of scientific applications in fields as hydrology, geology, climatology, oceanography, environmental and disaster monitoring, and cartography (DEM generation). Its main features are: resolution up to 0.25 m (in-staring spotlight mode), an excellent radiometric accuracy, unique agility (rapid switches between imaging modes and polarizations). On June 21, 2010, the twin mission TanDEM-X started, and since then they fly in a close formation at distances of only few hundred meters and record data synchronously. This peculiar configuration allows the generation of WorldDEM, which is a DEM of the Earth's land surface with a vertical accuracy of 2 m (relative) and 10 m (absolute).

COSMO-SkyMed (COntellation of small Satellites for Mediterranean basin Observation) is a satellite mission ran by the ASI (Italian Space Agency) and the Italian Ministry of Defense. The CSK system is made up of four satellites and it is equipped with High-Resolution SAR, in sun-synchronous polar orbits, phased in the same orbital plane. This results in varied intervals between the satellites along the same ground track of between 1 and 15 days. The first two satellites were launched in 2007, the remaining two in 2008 and 2010, respectively. Its main goal is to provide imagery for environmental monitoring and surveillance applications for the management of exogenous, endogenous and anthropogenic risks, but also commercial products.

Finally, **Sentinel** satellites are the last generation of Earth observation satellites of the ESA and the Copernicus group (program of the European Commission). Sentinel-1A satellite was launched on April 3, 2014 and provides all-weather, day and night radar imaging for land and ocean services, such as: monitoring of Arctic sea-ice extent, routine sea-ice mapping, surveillance of the marine environment, including oil-spill monitoring, monitoring land-surface for motion risks, mapping of forests, water and soil management and to support humanitarian aid and crisis situations.

The Sentinel-2 satellite has been launched on June 23, 2015, and it is providing high-resolution optical imaging for land services (i.e. vegetation, soil and eater cover, etc.).

Sentinel-3 will provide ocean and global land monitoring services, Sentinel-4 and Sentinel-5 will be responsible for data for atmospheric composition monitoring and Sentinel-6 will be implemented for the observation of the topography of the global ocean. The main features of each satellite mission are shown in Table 5.3.

	ERS-1 and ERS-2		JERS-1 SAR		RADARSAT-1/2		ENVISAT
Agency	European Space Agency	Agency	Japanese Aerospace eXploration Agency	Agency	Canadian Space Agency	Agency	European Space Agency
Frequency	C-Band	Frequency	L-Band	Frequency	C-Band	Frequency	C-Band
Ground Resolution	25 m	Ground Resolution	20 m	Ground Resolution	10-100 m (Radarsat-1); 3100 m (Radarsat-2)	Ground Resolution	15-1000 m
Acquisition Mode	Stripmap	Acquisition Mode	Stripmap	Acquisition Mode	Stripmap and ScanSAR	Acquisition Mode	Stripmap and ScanSAR
Swath	100 km	Swath	70 km	Swath	50-500 km	Swath	100-405 km
Repeat Cycle	35 days	Repeat Cycle	44 days	Repeat Cycle	24 days	Repeat Cycle	35 days
Year of Start	1991-2000 (ERS-1); 1995-2011 (ERS-2)	Year of Start	1992-1998	Year of Start	1995-2013 (Radarsat-1); 2007 - (Radarsat-2)	Year of Start	2001-2012
	ALOS-PALSAR		TerraSAR-X		COSMO-SkyMed		Sentinel-1
Agency	Japanese Aerospace eXploration Agency	Agency	German Aerospace Center (DLR)	Agency	Italian Space Agency (ASI)	Agency	European Spatial Agency (ESA)
Frequency	L-Band	Frequency	X-Band	Frequency	X-Band	Frequency	C-Band
Ground Resolution	7-1000 m	Ground Resolution	1-16 m	Ground Resolution	1-100 m	Ground Resolution	15-1000 m
Acquisition Mode	Stripmap and ScanSAR	Acquisition Mode	Stripmap, ScanSAR, Spotlight, HR Spotlight, Staring Spotlight and Wide ScanSAR	Acquisition Mode	Stripmap, ScanSAR and Spotlight	Acquisition Mode	StripMap, Interferometric Wide Swath, Extra Wide Swath
Swath	120-350 km	Swath	15-60 km	Swath	20-400 km	Swath	100-405 km
Repeat Cycle	44 days	Repeat Cycle	11 days	Repeat Cycle	4/8/16 days	Repeat Cycle	12 days (6 with upcoming S1B)
Year of Start	2006-2011 (ALOS-1) 2014 - (ALOS-2)	Year of Start	2007 - ongoing	Year of Start	2007 - ongoing	Year of Start	2014 - ongoing

Table 5.3 Main features of the main SAR satellite missions (from Confuorto, 2016).

5.4.4 SAR Interferometry

As firstly described by Gabriel et al. (1989), Interferometry SAR (InSAR) is the study of the phase and amplitude difference of the back-scattered signal of two SAR images, observing the same scenes from different points of view (Gabriel et al., 1989; Massonet & Feigl, 1998). The first applications of SAR Interferometry can be dated back to the early 1970s, based on the analysis of single or few interferences, allowing to provide information about the topography of the Earth surface (Zebker & Goldstein, 1986; Li & Goldstein, 1987; Gabriel et al., 1989; Prati et al., 1989) or for the generation of DEMs (Digital Elevation Models) of the Earth surface (Franceschetti & Lanari, 1999; Rosen et al., 2000).

In fact, InSAR technique is based upon the analysis of phase differences between two SAR images acquired in different spatial positions. This phase difference conveniently processed, is compared to the ground topography, determining two kinds of results:

- Digital Elevation Model with high resolution (DEMs);
- Deformation maps characterized by millimeters resolution.

For the comprehension of the interferometry operation and of its generation, in the follow the main features, parameters and steps are briefly described.

SAR interferometric data have a different content from the simple optical data: the connection extent between two SAR images is, actually, very susceptible to the changes in the nature of the scatters inside the resolution cells (ground pixel). A satellite can observe the same area from slightly different look angles. This operation can be made with the help of two sensors applied on the same platform or in different periods with the aid of images captured on different satellite orbits. Satellites cover ascending and descending orbits: due to Earth rotation and to the fact that SAR antenna is pointed on the same side with respect to the velocity vector in the orbit trajectory, an area can be enlightened from East during descending orbits (from North to South) or from West during ascending ones. The perpendicular line to the trajectory orbit and the look line form an angle called look angle.

If we succeed in combining two acquisitions coming from East and West, we are able to eliminate the many spatial distortions previously described. However, it is difficult to acquire two SAR images from ascending and descending orbits at the same time identifying the same targets.

When this happens, it is possible to decompose the velocity vector. This operation can be better understood by considering a x, y, z Cartesian coordinate system, in which the three directions coincide with the horizontal E-W and N-S and vertical, respectively.

In such reference system, the velocity vector V can be calculated as:

$$\bar{V} = V_x \cdot \bar{s}_x + V_y \cdot \bar{s}_y + V_z \cdot \bar{s}_z \quad (\text{eq. 5.3})$$

where V_x , V_y e V_z are the velocity vector components along the horizontal (E-W and N-S) and vertical directions, and s_x , s_y , s_z the unit vectors of the three coordinate axes of the Cartesian system.

Thus, using mean velocity values V_a and V_d , obtained from the PS database, the following system is obtained:

$$\begin{cases} V_a = V_x \cdot s_{xasce} + V_y \cdot s_{yasce} + V_z \cdot s_{zasce} \\ V_d = V_x \cdot s_{xdesce} + V_y \cdot s_{ydesce} + V_z \cdot s_{zdesce} \end{cases} \quad (\text{eq. 5.4})$$

where s_{xasce} , s_{yasce} , s_{zasce} , s_{xdesce} , s_{ydesce} , and s_{zdesce} represent the direction cosines of the respective velocity vectors V_a and V_d .

In this reference system the number of unknown variables (V_x , V_y and V_z) is higher than that of the equations and therefore it cannot be solved. However, due to the geometrical characteristics of the acquisition, the component on N-S direction appears to be negligible.

Velocity in this direction is acceptably approximated to zero, thus allowing to solve the previous system and to assess motion components in E-W and vertical directions (corresponding to x and z directions):

$$\begin{cases} V_a = V_V \cos \theta_{asce} + V_E \sin \theta_{asce} \\ V_d = V_V \cos \theta_{desce} + V_E \sin \theta_{desce} \end{cases} \quad (\text{eq. 5.5})$$

where V_a and V_d are respectively the velocity values in ascending and descending geometry and ϑ_{asce} and ϑ_{desce} are the incidence angles in the two geometries.

Actually, this technique employs the phase measures to infer the differential range (difference between distances perceived by the radar sensor to the same target on two different points of view) and the range change (difference between two couples of images, proving that a target transfer took place between the two acquisitions) in the SAR acquisitions concerning the earth surface, while the amplitude is crucial for the co-registration of the images.

At computational level, the interferogram is obtained by multiplying one image by the complex conjugate of the other and contains, on a pixel by pixel basis, the phase difference between the two acquisitions. One of the images is taken as a reference (usually the first according to a chronological order) and will be called master, while the other one will be called slave. This product is performed on the complex value typical of the single pixel $A_1 e^{i \phi_1}$ for the complex combined of the second $A_2 e^{i \phi_2}$:

$$\Delta A e^{i \Delta \phi} = A_1 e^{i \Delta \phi_1} \cdot A_2 e^{i \Delta \phi_2} = A_1 A_2 e^{i(\phi_1 - \phi_2)} \quad (\text{eq. 5.6})$$

The deriving result will have amplitude ΔA equal to the one of the first image multiplied for the second, while the phase will be the difference between the two.

5.4.4.1 Baseline

The acquisition of SAR images for interferometric purposes can be done in two different ways, single pass or dual pass. The first is characterized by the simultaneous acquisition with a slight difference in the geometry of acquisition; in the latter, instead, images are acquired in dissimilar time intervals (e.g. the same antenna passing on the area of interest two times). In this last case, very peculiar for the spaceborne SAR, the distance between the two-acquisition orbits can vary of several meters. The distance between the two acquisitions on the perpendicular plan to the orbit direction is the interferometer baseline (B_r), while the component projected on the normal direction to the image acquired in the second-time interval is called perpendicular baseline (B_n). The time interval between two succeeding is called temporal baseline (B_t).

If the two images of the same area are detected at the same time, the phase difference allows to obtain the three-dimensional position of the pixel and, therefore, to achieve a Digital Elevation Model of the area.

If the satellite acquires two images passing on the same area in two different times (temporal baseline) and in different orbit positions (spatial baseline), the phase difference contains various contributions among which the topography of the observed scene, and the possible soil deformation occurred in the interval of time between the two acquisitions. Subtracting the topographic component is possible to estimate the component due to the displacement.

Once a reference point on the surface has been identified, the path difference between the two satellites in the slant-range direction, defined as Δr , is equal to the equation (5.7):

$$\Delta r = -2 \frac{B_n q_s}{R} \quad (\text{eq. 5.7})$$

where: B_n is the perpendicular baseline, R is the distance in slant range between target and sensor and q_s is the distance between two points in perpendicular direction to the slant range. The interferometric phase difference ($\Delta\phi$) (Equation 5.8) between the two observations, corresponding to the path difference Δr between two acquisitions, is proportional to the relationship between a complete phase cycle in radians (equal to 2π) and the wavelength λ , which is the distance between the two following peaks, all multiplied for Δr .

$$\Delta\varphi = \frac{2\pi\Delta r}{\lambda} = \frac{4\pi}{\lambda} * \frac{B_n q_s}{R} \quad (\text{eq. 5.8})$$

Due to the periodicity of the signal, path differences Δr , differing among them of a multiple integer of the wavelength, introduce the same phase difference (Ferretti et al., 2007), for instance equal to 2π , 4π and so on, basically a path difference equal to a phase cycle. Hence, the SAR phase signal is the measurement of the fractions of Δr , which is smaller than the wavelength of the signal (Ferretti et al., 2007).

Considering a phase difference equal to a 2π cycle (Equation 5.9),

$$r = \frac{\Delta\varphi * \lambda}{4\pi} = \frac{2\pi * \lambda}{4\pi} = \frac{\lambda}{2} \quad (\text{eq. 5.9})$$

so that an interferometric fringe corresponds to a deformation variation of half of the wavelength (Casu et al., 2011).

5.4.4.2 Interferometric phase

The interferometric phase (φ_{int}) is the difference between two SAR images acquired from different angles of view. It is equal to the sum of several contributions (Equation 5.10), such as:

$$\varphi_{int} = \varphi_{geom} + \varphi_{topo} + \varphi_{displ} + \varphi_{atm} + \varphi_{err} \quad (\text{eq. 5.10})$$

where;

- φ_{geom} is the contribution due the slight difference of the geometry of acquisition of two images;

- φ_{topo} is the phase concerning the topographic information: topographic distortions arising from slightly different viewing angles of the two satellite passes. This factor contains the information relative to the scene topography (Δh) and is function of the perpendicular baseline (B_n);

- φ_{displ} is the contribution due to the eventual displacements occurring between the two acquisitions;

$-\varphi_{atm}$ is the part of the interferometric phase caused by atmospheric patterns such as humidity, temperature, etc.; this factor generates phase patterns in the interferograms and is due to the changes in the atmospheric conditions existing during the images acquisition; $-\varphi_{err}$ is the contribution due to errors in different procedures or due to radiometric distortions.

For the calculation of one single contribution, the latter must be isolated from the other ones. This is the base for the calculation, for instance, of the displacements occurring on the Earth surface.

The phase can be influenced by different factors, due to the interferometry or by instrumental sources. Geometrical decorrelation and temporal decorrelation belong to the first category, while in the second group instability of radar frequency and thermic instrumental noises can be mentioned.

Geometrical decorrelation is caused by the angular variation of the scene acquisition of the two SAR images which form the interferometric couple. Temporal decorrelations are caused by the modification of the electromagnetic signal due to atmospheric patterns (such as humidity, temperature, pressure), or to human modifications, or to vegetation growth. Coherence is the value of the variation of backscattering property of the target on the surface between two or more satellite passages. It is a parameter which better expresses the quality of the information within an interferogram. It can vary between 0 and 1: lower values of coherence are due to severe modifications of the area observed; on the contrary, higher values means that the target has not changed.

5.4.5 Differential Interferometry SAR (DInSAR)

As mentioned before, the interferometric processing, besides providing elevation maps, can also be exploited for the measurement of the deformation of different genesis occurring on the Earth surface. The interferometric phase is represented by different contributions; in order to get the displacement contribution (or the topographic one) the other contribution must be removed (or reduced). The exploitation of DInSAR methods, using multi-temporal stacks of SAR images, allows to remove all these other contributions and to isolate the phase related to the displacement. Moreover, analyzing a great number of SAR images acquired in a large time interval, it is also possible to follow long-duration deformation phenomena (with millimeter accuracy).

The first differential interferometry applications have been developed at the end of the 1990s and at the beginning of the 2000s (Wegmuller et al., 1998; Costantini et al., 2000; Ferretti et al., 2000, 2001; Berardino et al., 2002; Mora et al., 2003), with several applications and algorithms, which will be further discussed in the next paragraphs.

The interferometric phase model equation (eq. 5.11) can be written as follows (Hanssen, 2001; Mora, 2004):

$$\Delta\varphi_{\text{int}} = 4\pi \cdot \frac{r_1 - r_2}{\lambda} = \Delta\varphi_{\text{flat}} + \Delta\varphi_{\text{topography}} + \Delta\varphi_{\text{moving}} + \Delta\varphi_{\text{atmosphere}} + \Delta\varphi_{\text{noise}} \quad (\text{eq. 5.11})$$

It is usually possible to classify DInSAR techniques in Conventional and Advanced. To the first group belong the “two-pass method” (with two images and an external DEM), “three-pass method” (with three images) and the “short baseline method” (Mora, 2004).

In these three cases, a simulation of the topographic contribution (considering B_n known from orbital data) allows the estimation of the total deformation ($\Delta\rho$) projected along the slant range direction (or line of sight, LOS); the topographic contribution can be simulated using an external DEM or obtaining the DEM from an independent interferogram. If a DEM with an adequate precision is available, the contribution of the known topography can be almost completely removed from the interferometric phase. Using an external DEM, the topographic contribution is equal to:

$$\Delta\varphi_{\text{topo_est}} = \frac{4\pi}{\lambda \cdot r_1} \cdot \frac{B_n \cdot \Delta h_{\text{DEM}}}{\sin \theta} \quad (\text{eq. 5.12})$$

When an external DTM is not available, it is possible to use a third independent image to generate a second interferogram (called “topographic interferogram”). It has to have a short temporal baseline and a high spatial baseline to achieve a good precision of the topographic component.

Besides the factor ($\Delta\varphi_{\text{topo}}$), which represents the contribution of the topography and the deformation one ($\Delta\varphi_{\text{mov}}$), other three factors contribute to the definition of the interferometric phase for a given scatter:

$-\Delta\varphi_{\text{flat}}$: the parameters which identify the satellite position during the acquisition of the image on the ground are called “orbital parameters”, and they are made up of a series of points on the satellite orbit path, whose position and speed are known.

This information is usually given by the service supplier. In order to minimize the error, more accurate state vectors (position and speed) are needed. These data were obtained from the European Space Agency and from other institutions and universities, several months after the satellite acquisition. The flat term will be the phase pattern generated by a flat terrain. The separation from the topographic term is just from the mathematical point of view as both depend on the spatial baseline. The former can be mathematically calculated with the orbital information and the latter if a DEM is available;

$-\Delta\varphi_{\text{atm}}$: when two SAR images are acquired in different dates, the travelling speeds of the electromagnetic waves are different due to the atmosphere variations. This signal disturbance can take place due to variations in humidity, temperature and pressure in the air. This effect usually arouses a phase shift included inside a single cycle 2π , with a gradual variation inside the image. Usually, the images at one's own disposal have very different conditions of acquisition; for this reason, to eliminate a part of this disturbance it is possible to relate every one of them to only one master image, following the APS pattern (Atmospheric Phase Screen) for the spreading in atmosphere. Another possibility can be to use atmosphere patterns specifically realized for the area of interest, which are also able to determine a phase shift contribution due to the tropospheric refractivity when the signal passes through.

$-\Delta\varphi_{\text{noise}}$: atmospheric effect is not usually predominant in the phase noise, but the latter is the sum of several distributed factors, which can vary considerably through time between two acquisitions. As we said before, the elements which create a phase interference of phase speckle are mainly:

- variation of the scatters, mainly for densely lush reservoirs and areas densely lush, which change in few milliseconds, the response on earth of the signal will hardly supply comparable values, even if it is acquired in a short time. This factor can be defined temporal decorrelation;
- variation of the incidence angle, which has as a main consequence the variation of the critic baseline, beyond which the response is only noise. This factor depends on the dimensions of the pixel on earth, and the ground formation, on the radar frequency and the distance from the sensor – target. In order to reveal this special contribution to the noise we can use the term spatial decorrelation;
- volume scattering, when there is a volumetric distribution of scatters on the resolution cell, the incident signal can carry out different paths inside it, with a different number of

rebounds, return time, and so on. As the previous, this decorrelation source depends on the critical baseline too.

$-\Delta\varphi_{\text{mov}}$ represents the earth surface motion and is constituted by a linear and a non-linear part.

$$\Delta\varphi_{\text{mov}} = \Delta\varphi_{\text{lin}} + \Delta\varphi_{\text{non-lin}} \quad (\text{eq. 5.13})$$

Non-linear deformation can be assumed to present a narrower correlation window in space (or at least much narrower than atmospheric artefacts) and a low pass behavior in time.

5.4.5.1 Differential Interferometry SAR algorithms

The development of DInSAR techniques has permitted to pass from the methods that allow to calculate displacements occurred between two images acquisition dates, to multi-pass methods which take into account all the SAR images available for an area. In this way, it is possible to obtain information on the historical time evolution of an instability phenomenon, whose detail is function of the time elapsed between observations of the same point (revisit time).

Interferometric processing is composed of various stages.

Coregistration is a fundamental step, necessary for making two SAR images comparable and in the same slant range geometry. The procedure consists in a precise superimposition of two or more images in the same area, removing scale differences and correcting rotations and translations. A “master” image must be selected, which is the reference image, on which all the “slave” images will be overlapped. Coregistration is also significant for the coherence estimation of a stack of images. Co-registration accuracy must be in sub-pixel scale, because InSAR processing requires sub-pixel accuracy.

The *interferogram generation* is the basic step of SAR interferometry. Interferograms are generated from the complex product between the single values of the pixels.

The final result is the phase difference, the interferometric phase, between the master and the slave images.

The *filtering step* is useful for reducing potential noises in the interferograms.

There are several filtering methods, such as the adaptive windows (Lopes et al., 1993), the Goldstein method (Goldstein & Werner, 1998), the boxcar, etc..

The adaptive windows filter the interferogram in a window based on the frequency and the homogeneity of the area, the boxcar are low-pass filters that eliminate noises exploiting small windows, in order to preserve the interferometric features. The Goldstein filter is coherence-based, filtering more the low-coherence areas respect to the high-coherence areas.

During the *flattening phase*, DEM is removed, hence is removed the contribution of the topography in the interferometric phase. Also the “flat earth” phase is removed (i.e. fringes due to the range). The result is a levelled interferogram, where the width of the fringes is due to the altimetry residuals and to possible displacements. Every color of an interferogram corresponds to a phase cycle equal to 2π , so to a variation in altitude or to the movement of a target. Because of the unwrapping, the phase, explaining the multiple 2π , obtains a value in meters. Several algorithms for the *phase unwrapping* have been developed, such as the minimum least square (Fried, 1977), the minimum cost flow (Costantini, 1998), the region growing (Xu et al., 1999), etc.. The basic assumption of all these algorithms is that adjacent pixels show a not unwrapped phase difference between $-\pi$ and π .

After the unwrapping, another necessary operation before obtaining the height or the displacement is the *orbital refinement*, which is an improvement of the orbital parameters available. In order to further refine the geometry of acquisition, the generation of so-called Ground Control Points (GCPs) can be also useful. They must be located in easy-to-observe areas, such as bridges, crossroads, or peculiar buildings, to get a good correspondence between SAR and geographical coordinates.

Moreover, it is necessary that they are located in high coherence areas and outside from the area of the displacement (if known).

In the step of *height/displacement conversion*, the value Δr , the difference between the slant-range vectors, is determined and expressed as topographic measurement (InSAR) or as a displacement velocity (DInSAR).

Geocoding phase is the conversion from slant range coordinates to a reference cartographic system (e.g. WGS 84).

As regards the displacement information, SAR processing is able to calculate it only in slant range coordinates, and the results is then geocoded.

However, deformation is given in Line-of-Sight (LoS) geometry. In the last twenty years many DInSAR algorithms have been developed and the capability of the DInSAR has been extensively documented.

The first attempts to develop advanced DInSAR (A-DInSAR) methods able to reduce atmospheric artefacts and uncertainties in the sensor orbit information (orbital artefacts) were made by Peltzer et al. (2001), who created the so-called InSAR stacked approach.

In this way, the deformation velocity is calculated as a weighted average computed from the single interferograms, allowing then to retrieve the mean deformation rate of the investigated area. By means of developments of more advanced techniques, aimed at the computation of time series of deformation calculated over several SAR images analysis, a step forward has been done toward an improved Earth observation.

Usually such techniques require at least 15-20 SAR images for a reliable analysis (Hanssen, 2001; Colesanti et al., 2003; Crosetto et al., 2008) and can be grouped into two main categories:

-techniques exploiting localized targets, the so called Persistent Scatterers (PS) (Ferretti et al., 2000) approaches;

-techniques which exploit distributed targets, the so-called Small Baselines Subset (SBAS) (Berardino et al., 2002) methods. Moreover, more recently approaches combining PS and SBAS methods have been proposed (Hooper, 2008).

In Table 5.4 the main algorithms belonging to the three approaches are resumed.

PS Approaches	SBAS approaches	Mixed approaches
<ul style="list-style-type: none"> • Permanent Scatterers (PSInSAR, Ferretti et al. 2001) • Point Target Analysis (IPTA, Wemer et al., 2003) • GENESIS-PSI (Adam et al. 2003) • Spatio-Temporal Unwrapping Network (STUN, Kampes, 2006) • DePSI (Kampes, 2006) • Stable Point Network (SPN, Crosetto et al., 2008) • Persistent Scatterers Pairs - Differential InSAR method (PSP-DIFSAR, Costantini et al., 2000) 	<ul style="list-style-type: none"> • Small Baseline Subset (Berardino et al., 2002) • Coherent Pixel Technique (CPT, Mora et al., 2003) • Enhanced Spatial Differences (ESD, Fornaro et al., 2007) • Multidimensional SBAS (MSAS, Samsonov & d'Oreye, 2012) • Intermittent SBAS (ISBAS, Sowter et al. 2013) 	<ul style="list-style-type: none"> • Stanford Method for PS (StaMPS, Hooper, 2006) • SqueeSAR (Ferretti et al., 2011)

Table 5.4 Main DInSAR approaches (from Confuorto, 2016).

The **Permanent Scatterers Interferometry SAR** (PSInSAR, Ferretti et al., 2001) is one of the basic algorithms belonging to the PS category. It is an algorithm successfully used for long series of SAR data, in order to estimate and remove the atmospheric effects (Ferretti et al., 2000, 2001). Phase and amplitude are the main parameters exploited by the PSInSAR method: amplitude gives information about the reflectivity of the target, while the phase indicate the sensor-target distance; therefore, amplitude allows to individuate the PS and phase to estimate the movement of the PS. Persistent Scatterers (PS) are targets which keep stable the electromagnetic signal (hence, their reflectivity property) during the time span of acquisition of the image. Usually PSs correspond to man-made structures (i.e. buildings, dams, infrastructures, etc.) or to rocky outcrops, while vegetated areas, due to the frequent variation of their electromagnetic properties, cannot be considered as good scatterers.

The main concepts of the PS detection are based on the amplitude dispersion D_a (Ferretti et al., 2001) (Equation 5.14), which is calculated by dividing the temporal standard deviation of the amplitude by the temporal mean of the amplitude of a certain pixel in a stack of SAR images.

$$D_a = \frac{\sigma_a}{\mu_a} = \sigma_\phi \quad (\text{eq. 5.14})$$

where D_a is the dispersion index, σ_a is the temporal standard deviation of the amplitude, μ_a is the temporal mean of the amplitude and σ_ϕ is the estimated phase standard deviation. The basic idea of this concept is that a pixel characterized by a high and more or less constant amplitude value is assumed to show a low phase dispersion.

The final PS candidates are selected if the value D_a is below a given threshold (Kampes, 2006). The final result of the PSInSAR is an accurate measurement of the movements along the SAR Line of Sight (LoS velocities) of each PS, respect to an assumed reference point (considered as stable), in the time interval considered. Deformation and velocity maps and time series of the displacements are the main final products.

The **Small Baseline Subset** approach (SBAS, Berardino et al., 2002) is a DInSAR algorithm able to retrieve temporal series of deformation exploiting interferograms characterized by small temporal and spatial baseline. This algorithm aims to limit the spatial decorrelation taking into account the spatial and the temporal information from the SAR data (Berardino et al., 2002). By reducing the spatial separation between SAR

images, it is possible to reduce the decorrelation especially due to the large baseline separation and to obtain correlated interferograms. These interferograms are used as inputs to calculate the unwrapping stage, from which the estimation of the topographic contribution and the extraction of the Low Pass (LP) temporal deformation, which will be subtracted from the wrapped interferogram module 2π , is done. Hence, the interferograms will be considered as residual phase and be unwrapped. Therefore, the spatial and temporal filters are applied to the unwrapping residual file which contains the temporal deformation and the topographic phase residual. Finally, the inversion of the stack of interferograms is guaranteed using the singular value decomposition (SVD) method. The advantage of the SBAS technique is represented by the high coherence and the high spatial density of the final product, and the reduction of the errors due to the redundancy of the information (more interferograms for every image), although disadvantages are due to the high computational requests.

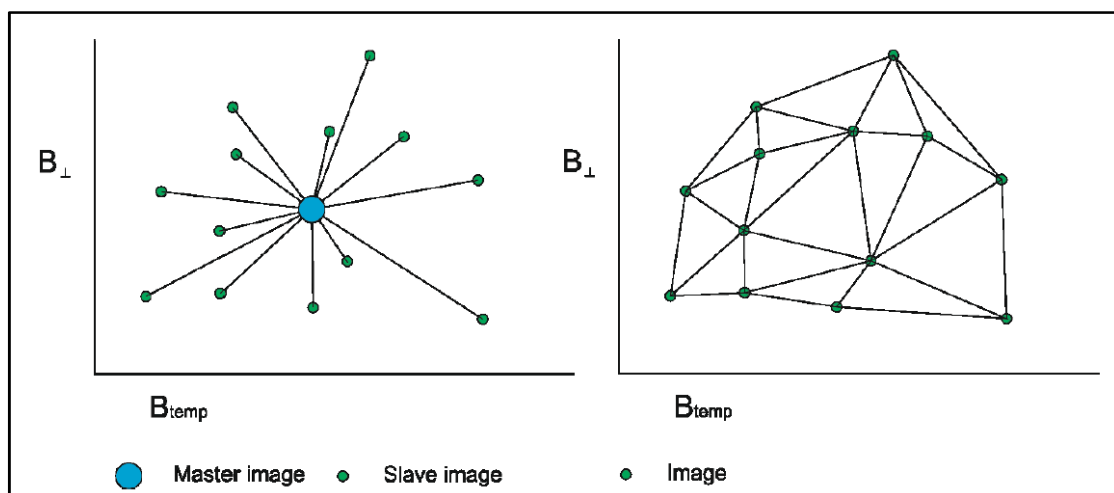


Figure 5.19 Representative scheme of PSInSAR, on the left, of SBAS, on the right (from Confuorto, 2016).

The **Coherent Pixels Techniques** (CPT, Mora et al., 2003), developed at the Remote Sensing Laboratory (RSLab) of Universitat Politècnica de Catalunya (UPC), is an algorithm able to extract from a stack of differential interferograms the deformation evolution during long time spans.

The main steps of its processing are: 1) the generation of the best interferogram set among all the available images, 2) the selection of the pixels with reliable phase within the employed interferograms and 3) the phase analysis of the interferograms in order to calculate deformation time series of the period of observation.

The selection of the best set of interferograms is done selecting the temporal baseline, the spatial baseline and the Doppler frequency. The interferogram selection is then achieved using the Delaunay method for the triangulation of the available images.

The pixel selection is an important step in order to obtain reliable results. Only pixels characterized by a considerable phase quality are selected. There are several criteria for selecting pixels, one based on the coherence stability (Berardino et al., 2002), the other one based on the amplitude dispersion (Ferretti et al., 2001).

More recently, also the Temporal Sublook Coherence method (TSC, Iglesias et al., 2015) has been produced. The first one is based on the spatial coherence estimator (Seymour et al., 1994) and the pixel will be selected if it shows a coherence higher than an assigned threshold; the second one, as a PS-like method, exploits the dispersion index, where all the pixels characterized by a Da value below a certain threshold are selected; the latter is a selection method able to detect point-like scatterer analyzing the spectral properties of the scattered signal.

The advantage with respect to the PS selection based on the amplitude dispersion is that there is no need of applying a radiometric calibration. Hence, in this case, pixel selection is carried out exploiting the spectral properties of point-like scatterers.

The last step consists in the phase analysis, to calculate their linear deformation time series within the observation period. In this case, the Delaunay triangulation allows to connect neighboring pixels, and, after that, it is possible to evaluate the phase increment between two neighboring pixels.

Finally, an integration process is necessary to obtain the velocity values for each pixel: it is necessary to identify a control point (named seed) characterized by linear velocity and height well known.

5.4.5.2 DInSAR applications

In the last twenty years many applications have been carried out exploiting DInSAR methods, which proved to be an efficient tool in the monitoring and the investigation of several types of natural hazards and deeply contributed to the development of several geosciences. Among the most significant DInSAR applications, the following can be mentioned:

-*earthquakes*: seismology is one of the geoscience branches in which interferometry has been most widely implemented. In particular DInSAR approaches have been carried out in the co-seismic phase (Zebker et al., 1994; Peltzer & Rosen, 1995; Tobita et al., 1998; Stramondo et al., 1999; Klinger et al., 2000), post-seismic deformation (Peltzer et al., 1996; Massonet et al., 1996) and inter-seismic tectonic events (Wright et al., 2001; Colesanti et al., 2003);

- *volcanology*: the study of deformations due to volcanic deflation and uplift has been widely analyzed by means of DInSAR techniques (e.g. in Rosen et al., 1996; Lanari et al., 1998; Lu et al., 2000; Lundgren et al., 2003; Hooper et al., 2004);

- *glaciology*: the study of glaciers through DInSAR has been led by several authors, whose aim was to detect ice topography measurements (Kwok & Fahnestock, 1996) and ice velocity estimation (Goldstein et al., 1993; Fatland & Lingle, 1998; Strozzi et al., 2002);

- *subsidence*: subsidence due to natural or anthropic causes can be monitored and investigated by DInSAR, being able to follow the long duration of the deformation (Galloway et al., 1998; Ferretti et al., 2000; Mora et al., 2001; Strozzi et al., 2001; Crosetto et al., 2002; Tomás et al., 2010; 2011; 2012; 2013; Fiaschi et al., 2015; Tessitore et al., 2016);

- *landslides*: landslide monitoring with DInSAR methods gained a lot of attention in recent years by the scientific community, even though the detection of gravitational phenomena is limited to slow and very slow movements. Some of the most relevant results are described in Fruneau et al. (1996), Squarzoni et al. (2003), Tarchi et al. (2003), Strozzi et al. (2005), Colesanti & Wasowski (2006), Calò et al. (2012), Meisina et al. (2008), Cascini et al. (2010), Herrera et al. (2011), Novellino et al. (2015) and Di Martire et al. (2016);

- *structures and infrastructures*: the monitoring of man-made infrastructure can be also conducted by means of DInSAR methods, for the estimation of the deformation and settlements of dams, buildings, highways, bridges, etc., as for instance in Perissin et al. (2009), Stabile et al. (2012), Cascini et al. (2013), Sousa & Bastos (2013), Bianchini et al. (2014), Di Martire et al. (2014), Milillo et al. (2014), Del Soldato et al. (2016), Milillo et al. (2016-a), Milillo et al. (2016-b), Peduto et al. (2017), Infante et al. (2016);

- *heritage sites*: the preservation of archaeological and cultural sites can be also monitored by DInSAR methods, as done by Tapete et al. (2011, 2012) or by Zeni et al. (2011).

CHAPTER 6

CHARACTERIZATION AND SURVEY OF BUILDINGS IN A LANDSLIDE-AFFECTED AREA

Introduction

In the last decade, several complementary approaches to conventional techniques have been developed in order to provide integrated systems to better understand structural instabilities due to ground displacements.

A vulnerability analysis addressed to landslide emergency management and protection strategies planning, requires a multi-level and integrated evaluation of landslide's kinematics and the exposed elements.

The vulnerability analysis of buildings interacting with slow-moving landslide bodies is a difficult task because it requires a deep knowledge of relevant factors related to both landslides (type, intensity, etc.) and exposed facilities (building materials, state of maintenance, foundation type, etc.).

In this work, an innovative approach combining the results of landslide movements analysis with survey of facilities characteristics, accomplished with an accuracy level dependent on the vulnerability diagnosis criteria, has been developed.

Existing buildings in landslide-affected areas are often characterized by specific vulnerabilities, mainly due to both intrinsic properties and to the concomitance with several modifications occurring over time. They can be summarized as follows:

- position of building on landslides body;
- use of different constitutive materials;
- behavior of different structural typologies (isolated or buildings aggregate);
- different behavior depending on intrinsic constructive parameters (foundation typology, number of floors, geometry, position in a buildings aggregate);
- presence of irregularities and possible alterations occurred (both geometrical and of mass or stiffness distribution);
- current state of maintenance;
- the presence of existing damage level.

In such cases, the adequate characterization of the building properties is often fundamental for a reliable vulnerability assessment.

These data can be recorded via surveys carried out by experts.

In this work, in order to identify an objective technique of building survey, a classification scheme (Baggio et al., 2009), provided by the Italian Department of Civil Protection (in Italian, DPC) for a preliminary building analysis in the post-seismic events, has been adopted. The latter can be used for building characterization when landslide events occur, because also in slope movements damage is due to the effects of shear stress.

The investigation of landslide-induced damage, in particular, can be motivated by a wide range of user purposes, as administrative (to declare restrictive rules such as the evacuation for no safe constructions), planning (to estimate direct and indirect costs and assess the needed restoration, reconstruction or relocation of structures) and scientific (to study the phenomena, its extension and possible evolution).

To the latter purpose, landslide-induced damage – whether known – can be considered as movement indicators to assess the spatial and temporal evolution of the buildings' structural vulnerability in urban settlements affected by slow-moving intermittent landslides. Movements of the building foundations induced by ground instability over time are cause of cracks occurrence on structural and non-structural elements.

A detailed approach for the surveying and classification of landslide-induced damage plays a key role in the strategy to better delineate mass-movement boundaries and state of activity, by categorizing its detectable impacts on the ground, as well as to improve knowledge of the instability, to avoid repeated occurrences and to plan mitigation measures.

A considerable amount of scientific literature has been conducted with regard to a damage assessment of areas prone to and affected by slow-moving landslides: in this thesis, Burland (1977), Alexander (1986), Iovine and Parise (2002) and DPC (2009) approaches have been used. Each classification presents particular benefits and constraints, i.e. the choice of the relevant parameters to use into assessment model.

6.1 Vulnerability factors influencing performance of building affected by slow-moving landslide

The main topic of this work is the assessment of physical vulnerability of buildings, meant as an evaluation of direct structural losses to construction induced by ground instability.

As indicated in the previous chapters, structural vulnerability pertains to the structural elements of the buildings, e.g., load bearing walls in masonry structures, columns and beams in reinforced concrete, floor and roof.

For a systematic understanding, it is necessary to identify the basic constructive factors influencing the performance of building affected by ground movements.

Generally, causative factors of building behavior can be summarized as follows:

- **location of the structure:** location determines the type and extent of the expected hazard: intensity and characteristics of movements along the slope can change depending on the zone on landslide boundary (Fig. 6.1);

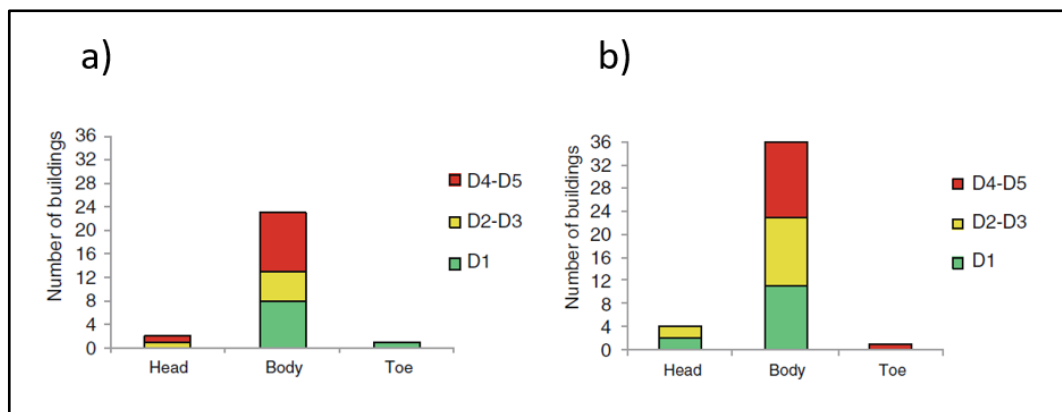


Figure 6.1 Distribution of damage severity according to building location on landslide: for reinforced concrete (a) and masonry (b) buildings (from Ferlisi et al., 2015).

Building orientation, in comparison with the landslide direction, plays a key role in vulnerability assessment activity, influencing damage severity and distribution.

Buildings with the long axis parallel to the landslide direction suffer less loss in comparison with the ones experiencing frontal impact (Hu et al., 2012). According to Du et al., (2013) the angle between the direction of the building and the landslide determines the severity of the damage with the latter being lower for 0° and higher for 45° .

- **construction typology:** masonry (brick-masonry, stone masonry, cement-block masonry) and reinforced concrete buildings are the principal types of construction in the Italian building stock. Other typologies (steel, timber and mixed construction) represent only a small percentage, diffused in recent years with modern constructive techniques.

Most of the load-bearing masonry structures are un-reinforced: the material lacks ductility, tensile- or shear strength. Reinforced concrete frame construction type has become prevalent in the past century, and it has introduced a myth that the buildings of this type are infinitely strong and can be constructed as high as needed.

Depending on the constitutive model of materials and structural behavior to static actions, masonry and reinforced concrete buildings have a different response to the occurrence of foundation displacements. In particular, reinforced concrete buildings are seriously damaged by differential settlements occurring to their foundation; masonry buildings, on the contrary, characterized by very low ratios between tensile and compression strengths, show higher damage susceptibility to horizontal movements;

- **foundation type:** assessment of physical vulnerability to slow-moving landslide requires to identify also the structural parameter such as foundation type.

Information regarding the structural foundation typology (e.g. direct foundations or bearing piles), dimensions and materials, allows to take into account also the interaction soil-structure.

Ragozin and Tikhvinsky (2000) considered that vulnerability of structures is related with the foundation depth. Table 6.1 summarizes the vulnerability values for the structures with different foundation depths depending on the depth of predicted landslide.

Depth of foundation (including piles), m	Landslide debris depth	Vulnerability
≤2	<2	1.0
>2	<2	0
Less than a landslide depth	2–10	1.0
10–13	2–10	0.5–1.0
>13	2–10	0.0–0.5
Any	>10	1.0

Table 6.1 Values of vulnerabilities depending on different foundation depths and landslide depths (from Ragozin and Tikhvinsky, 2000).

The range of vulnerability depending on different landslide depths. In fact, depth of phenomena reflects the intensity, while foundation depth reflects the resistance ability of a structure. Generally, structure on a deeper foundation often has higher resistance ability;

- **state of maintenance:** a poorly maintained building becomes gradually vulnerable as the unattended weak element accelerates deterioration causing the whole structure to become weaker.

Deteriorated structural materials may reduce the capacity of the vertical- and lateral-force resisting systems. The most common type of deterioration is caused by the intrusion of water.

Poor-quality masonry elements can result in significant reduction in the strength of structural elements. Deteriorated concrete and reinforcing steel can significantly reduce the strength of concrete elements. This statement is concerned with deterioration such as spalled concrete associated with rebar corrosion and water intrusion;

- **geometry:** configuration of buildings is related to dimensions, building form, geometric proportions and the location of structural components. The configuration of a building will influence its performance to ground movements, particularly regarding the distribution of stress.

Typical building configuration deficiencies include an irregular geometry, a weakness in a given story, a concentration of mass, or a discontinuity in the distribution of forces. Complex configurations (e.g., L-shape, Y-shape, H-shape, etc.) increase the building's vulnerability to damage and destruction during a landslide action, generating an excessive concentration of stresses during the movement. Structural joints (separation) should be provided if such overall configuration cannot be avoided due to any constraint.

Structural regularity can also be achieved by distributing lateral elements in the building in such a way that they do not cause excessive torsion (Fig. 6.2).

During a landslide, a building that is regular in plan (both directions) performs much better than an asymmetrical building. Symmetry is measured with respect to the distribution of the lateral resisting elements of the building in plan;

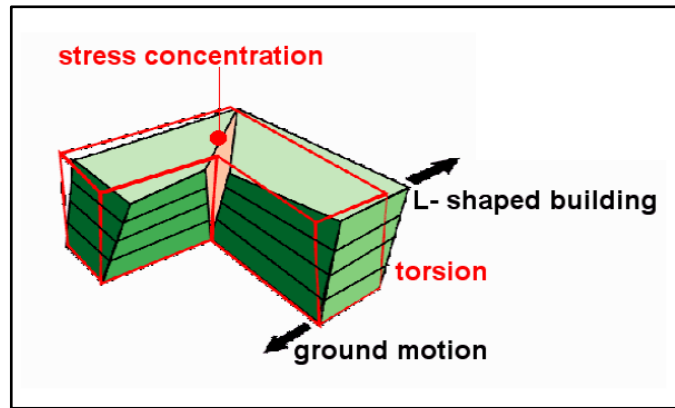


Figure 6.2 Possible stress concentration and torsion effects on a L-shaped building configuration (from Guragain et al., 2004) .

- **number of stories:** this factor directly influences the degree of loss, but generally the behavior of reinforced concrete and masonry buildings is different, depending on strength and stiffness which change with the height of the structure.

Additionally, vertical irregularities in a building aggregate increase vulnerability of involved structures. If the building is abutting against each other, the behavior of one during landslide movement will influence that of the other one.

Adjacent buildings can alter the response of both buildings and impart additional loads on both structures.

Buildings of the same height with matching floors will exhibit similar behavior to ground movement, while, when the floors of adjacent buildings are at different elevations, there is a potential for structural damage on the connection of walls and at the corners of building depending on an increase of stresses (Figures 6.3 and 6.4);

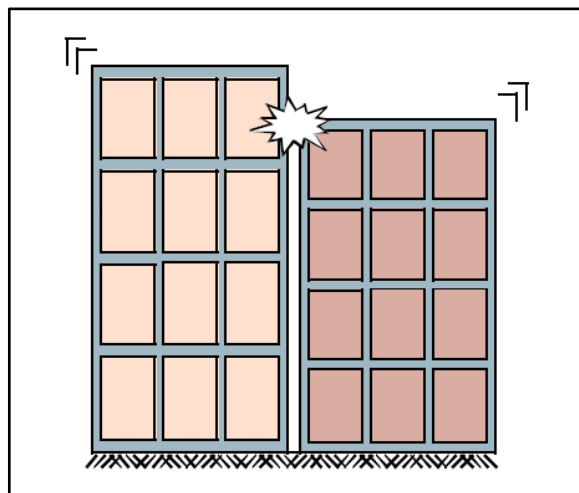


Figure 6.3 Different floor height of adjacent buildings and potential point of damage (from Guragain et al., 2004) .

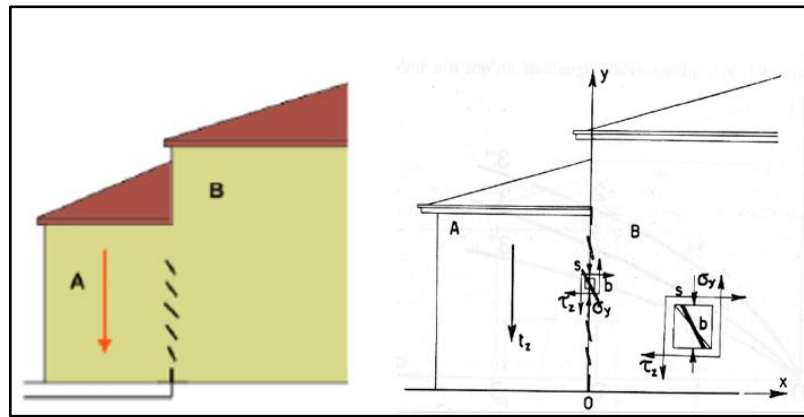


Figure 6.4 Example of differential settlement of adjacent buildings with different height (from Menditto G., 2010).

- **alteration:** alterations are frequently due to the changes in the requirements with time. Unfortunately, not all of the alterations are done at the advice of cognizant technical personnel. This practice leads to increased vulnerability of buildings. One important form of alteration is “adding stories” to the existing building to gain additional floor space, generating mass irregularities with respect to original weights. Another example of alteration is represented by creation of new openings in existing buildings. Several, large and unsymmetrical openings, especially for masonry buildings, generate an irregular configuration with a local weakness in the wall, a concentration of stress and a discontinuity in the force resisting system. The consequences of these actions are weaker structural walls which could result in a failure or partial collapse of building increasing, absolute or differential landslide displacements;
- **existing damage:** the presence of existing cracks may indicate distress in the structural elements from past events. Crack width is commonly used as a convenient indicator of damage, but it should be noted that other factors, such as location, orientation, number, distribution and pattern of the cracks could be equally important in measuring the extent of damage affecting in the walls. All these factors should be considered when evaluating the reduced capacity of a cracked element. In a masonry joints, especially diagonal cracks, may affect the interaction of the masonry units leading to a reduction of strength and stiffness. In reinforced concrete buildings, small cracks have little effect on the strength. A significant reduction in strength is usually the result of large displacements or crushing of concrete.

Only when the cracks are large enough to prevent aggregate interlock or have the potential for buckling of the reinforcing steel does the adequacy of the concrete element capacity become a concern. Extensive cracking in the columns, in particular, may indicate locations of possible weakness. Such columns may not be able to function in conjunction with the infill panel as expected.

According with all above mentioned, the characterization of buildings requires a detailed geometrical and structural survey: in particular, it is essential to define construction typology, geometrical characteristics, state of preservation, properties foundation structures, type of structural instability, damage degree and distribution, mechanical properties of structural materials.

In order to identify an objective technique of building survey, the Italian Department of Civil Protection (DPC) has provided a preliminary classification scheme (Baggio et al., 2009) to be used in the post-seismic events, which can be adopted for building survey when landslide events occur, because also in these cases damage are due to effects of the shear stress (Fig. 6.5 a,b,c).

The ‘DPC’ approach was devised for quick surveys and to classify the damage magnitude, even if the requested field analysis on the structure has been conducted with care. It is composed of several tables and schemes to be followed during the post-seismic events survey: the form of ‘DPC’ classification requires to compile nine sections during the field campaign:

- three tables dedicated to the identification and description of the examined building (section 1 provides building identification and localization, section 2 provides building description, section 3 building structural type);
- two sections (4 and 5) refer to the structural and non-structural damage assessment and existing emergency measures; the novelty of this method is the evaluation of damage severity degree for structural and non-structural components, which could modify the behaviour of buildings affected by ground movements, in particular for reinforced concrete structures;
- one part (section 6) including the evaluation of the induced hazard for surrounding constructions;
- one section (7) about movement effects on ground and foundations;
- last sections (8 and 9) conceived for the judgment of conformity to standards and to note down further assessments.

(a)

SEZIONE 1 Identificazione edificio				IDENTIFICATIVO SOPRALLUOGO						
Provincia: _____		Comune: _____		Squadra Scheda n. Data		giorno mese anno				
Frazione/Località: _____ (denominazione Istat)		Cod. di Località Istat		Istat Reg. Istat Prov. Istat Comune		N° aggregato N° edificio				
1 <input type="radio"/> via		Num. Civico		Sez. di censimento Istat		N° carta				
2 <input type="radio"/> corso				Tipo carta _____						
3 <input type="radio"/> vicolo				Foglio		Allegato				
4 <input type="radio"/> piazza				Particelle						
5 <input type="radio"/> altro	(Indicare: contrada, località, traversa, salita, etc.)			Dati Catastali						
Coordinate geografiche (ED50 - UTM fuso 32-33)		E		Fuso		Posizione edificio 1 <input type="radio"/> Isolato 2 <input type="radio"/> Interno 3 <input type="radio"/> D'estremità 4 <input type="radio"/> D'angolo				
Denominazione edificio o proprietario							Codice Uso S			
Fotocopia dell'aggregato strutturale con identificazione dell'edificio										
SEZIONE 2 Descrizione edificio										
Dati metrici			Età	Uso - esposizione						
N° Piani totali con interrati	Altezza media di piano [m]	Superficie media di piano [m ²]		Costruzione e ristrutturaz. [max 2]	Uso	N° unità d'uso	Utilizzazione	Occupanti		
<input type="radio"/> 1 <input type="radio"/> 9	1 <input type="radio"/> ≤ 2.50	A <input type="radio"/> ≤ 50	I <input type="radio"/> 400 ÷ 500	1 <input type="checkbox"/> ≤ 1919	A <input type="checkbox"/> Abitativo		A <input type="radio"/> > 65%	100	10	1
<input type="radio"/> 2 <input type="radio"/> 10	2 <input type="radio"/> 2.50 ÷ 3.50	B <input type="radio"/> 50 ÷ 70	L <input type="radio"/> 500 ÷ 650	2 <input type="checkbox"/> 19 ÷ 45	B <input type="checkbox"/> Produttivo			B <input type="radio"/> 30 ÷ 65%	0	0
<input type="radio"/> 3 <input type="radio"/> 11	3 <input type="radio"/> 3.50 ÷ 5.0	C <input type="radio"/> 70 ÷ 100	M <input type="radio"/> 650 ÷ 900	3 <input type="checkbox"/> 46 ÷ 61	C <input type="checkbox"/> Commercio		C <input type="radio"/> < 30%	1	1	1
<input type="radio"/> 4 <input type="radio"/> 12	4 <input type="radio"/> > 5.0	D <input type="radio"/> 100 ÷ 130	N <input type="radio"/> 900 ÷ 1200	4 <input type="checkbox"/> 62 ÷ 71	D <input type="checkbox"/> Uffici		D <input type="radio"/> Non utilizz.	2	2	2
<input type="radio"/> 5 <input type="radio"/> > 12	Piani interrati	E <input type="radio"/> 130 ÷ 170	O <input type="radio"/> 1200 ÷ 1600	5 <input type="checkbox"/> 72 ÷ 81	E <input type="checkbox"/> Serv. Pub.		E <input type="radio"/> In costruz.	3	3	3
<input type="radio"/> 6		A <input type="radio"/> 0 C <input type="radio"/> 2	F <input type="radio"/> 170 ÷ 230	P <input type="radio"/> 1600 ÷ 2200	6 <input type="checkbox"/> 82 ÷ 91	F <input type="checkbox"/> Deposito		F <input type="radio"/> Non finito	4	4
<input type="radio"/> 7	B <input type="radio"/> 1 D <input type="radio"/> ≥ 3	G <input type="radio"/> 230 ÷ 300	Q <input type="radio"/> 2200 ÷ 3000	7 <input type="checkbox"/> 92 ÷ 01	G <input type="checkbox"/> Strategico		G <input type="radio"/> Abbandon.	5	5	5
<input type="radio"/> 8		H <input type="radio"/> 300 ÷ 400	R <input type="radio"/> > 3000	8 <input type="checkbox"/> ≥ 2002	H <input type="checkbox"/> Turis-ricet.			6	6	6
					Proprietà		A <input type="radio"/> Pubblica	B <input type="radio"/> Privata		

Figure 6.5 (a) Sections 1 and 2 of DPC classification scheme: identification of building location (1) and description of geometrical and urbanistic parameters (2), (Baggio et al., 2009).

(b)

SEZIONE 3 Tipologia (multiscelta; per gli edifici in muratura indicare al massimo 2 tipi di combinazioni strutture verticali-solai)

Strutture verticali / Strutture orizzontali		Strutture in muratura								Altre strutture			
		Non identificate	A tessitura irregolare e di cattiva qualità (Pietrame non squadrato, ciottoli,...)				A tessitura regolare e di buona qualità (Blocchi; mattoni; pietra squadrata,...)				Telai in c.a.	Regolare	
			Senza catene o cordoli	Con catene o cordoli	Senza catene o cordoli	Con catene o cordoli	Piastri isolati	Mista	Rinforzata	Pareti in c. a.	Non regolare	Regolare	
A	B	C	D	E	F	G	H	Telai in acciaio	A	B			
1	Non identificate	<input type="radio"/>	<input type="checkbox"/>	<input type="checkbox"/>	<input type="checkbox"/>	<input type="checkbox"/>	<input type="checkbox"/>	<input type="checkbox"/>	SI	<input type="checkbox"/>	<input type="checkbox"/>		
2	Volte senza catene	<input type="checkbox"/>	<input type="checkbox"/>	<input type="checkbox"/>	<input type="checkbox"/>	<input type="checkbox"/>	<input type="checkbox"/>	<input type="checkbox"/>	<input type="checkbox"/>	G1	H1		
3	Volte con catene	<input type="checkbox"/>	<input type="checkbox"/>	<input type="checkbox"/>	<input type="checkbox"/>	<input type="checkbox"/>	<input type="checkbox"/>	<input type="checkbox"/>	<input type="checkbox"/>	<input type="checkbox"/>	<input type="checkbox"/>		
4	Travi con soletta deformabile (travi in legno con semplice tavolato, travi e voltre,...)	<input type="checkbox"/>	<input type="checkbox"/>	<input type="checkbox"/>	<input type="checkbox"/>	<input type="checkbox"/>	<input type="checkbox"/>	<input type="checkbox"/>	NO	G2	H2		
5	Travi con soletta semirigida (travi in legno con doppio tavolato, travi e tavelloni,...)	<input type="checkbox"/>	<input type="checkbox"/>	<input type="checkbox"/>	<input type="checkbox"/>	<input type="checkbox"/>	<input type="checkbox"/>	<input type="checkbox"/>	<input type="checkbox"/>	<input type="checkbox"/>	<input type="checkbox"/>		
6	Travi con soletta rigida (solai di c.a., travi ben collegate a solette di c.a.,...)	<input type="checkbox"/>	<input type="checkbox"/>	<input type="checkbox"/>	<input type="checkbox"/>	<input type="checkbox"/>	<input type="checkbox"/>	<input type="checkbox"/>	<input type="checkbox"/>	G3	H3		

SEZIONE 4 **Danni ad ELEMENTI STRUTTURALI e provvedimenti di pronto intervento (P.I.) eseguiti**

Livello - estensione / Componente strutturale - Danno preesistente	DANNO (1)									PROVEDIMENTI DI P.I. ESEGUITI						
	D4-D5 Gravissimo			D2-D3 Medio grave			D1 Leggero			Nullo	Nessuno	Demolizioni	Cercchiature e/o tiranti	Riparazione	Puntelli	Trasenne e protezione passaggi
	> 2/3	1/3 - 2/3	< 1/3	> 2/3	1/3 - 2/3	< 1/3	> 2/3	1/3 - 2/3	< 1/3							
	A	B	C	D	E	F	G	H	I	L	A	B	C	D	E	F
1	Strutture verticali	<input type="checkbox"/>	<input type="checkbox"/>	<input type="checkbox"/>	<input type="checkbox"/>	<input type="checkbox"/>	<input type="checkbox"/>	<input type="checkbox"/>	<input type="checkbox"/>	<input type="checkbox"/>	<input type="checkbox"/>	<input type="checkbox"/>	<input type="checkbox"/>	<input type="checkbox"/>	<input type="checkbox"/>	<input type="checkbox"/>
2	Solai	<input type="checkbox"/>	<input type="checkbox"/>	<input type="checkbox"/>	<input type="checkbox"/>	<input type="checkbox"/>	<input type="checkbox"/>	<input type="checkbox"/>	<input type="checkbox"/>	<input type="checkbox"/>	<input type="checkbox"/>	<input type="checkbox"/>	<input type="checkbox"/>	<input type="checkbox"/>	<input type="checkbox"/>	<input type="checkbox"/>
3	Scale	<input type="checkbox"/>	<input type="checkbox"/>	<input type="checkbox"/>	<input type="checkbox"/>	<input type="checkbox"/>	<input type="checkbox"/>	<input type="checkbox"/>	<input type="checkbox"/>	<input type="checkbox"/>	<input type="checkbox"/>	<input type="checkbox"/>	<input type="checkbox"/>	<input type="checkbox"/>	<input type="checkbox"/>	<input type="checkbox"/>
4	Copertura	<input type="checkbox"/>	<input type="checkbox"/>	<input type="checkbox"/>	<input type="checkbox"/>	<input type="checkbox"/>	<input type="checkbox"/>	<input type="checkbox"/>	<input type="checkbox"/>	<input type="checkbox"/>	<input type="checkbox"/>	<input type="checkbox"/>	<input type="checkbox"/>	<input type="checkbox"/>	<input type="checkbox"/>	<input type="checkbox"/>
5	Tamponature-tramezzi	<input type="checkbox"/>	<input type="checkbox"/>	<input type="checkbox"/>	<input type="checkbox"/>	<input type="checkbox"/>	<input type="checkbox"/>	<input type="checkbox"/>	<input type="checkbox"/>	<input type="checkbox"/>	<input type="checkbox"/>	<input type="checkbox"/>	<input type="checkbox"/>	<input type="checkbox"/>	<input type="checkbox"/>	<input type="checkbox"/>
6	Danno preesistente	<input type="checkbox"/>	<input type="checkbox"/>	<input type="checkbox"/>	<input type="checkbox"/>	<input type="checkbox"/>	<input type="checkbox"/>	<input type="checkbox"/>	<input type="checkbox"/>	<input type="checkbox"/>	<input type="checkbox"/>	<input type="checkbox"/>	<input type="checkbox"/>	<input type="checkbox"/>	<input type="checkbox"/>	<input type="checkbox"/>

(1) - Di ogni livello di danno indicare l'estensione solo se esso è presente. Se l'oggetto indicato nella riga non è danneggiato compilare Nullo.

SEZIONE 5 **Danni ad ELEMENTI NON STRUTTURALI e provvedimenti di pronto intervento eseguiti**

Tipo di danno	PRESENZA DANNO	PROVEDIMENTI DI P.I. ESEGUITI					
		Nessuno	Rimozione	Puntelli	Riparazione	Divieto di accesso	Trasenne e protezione passaggi
	A	B	C	D	E	F	G
1	Distacco intonaci, rivestimenti, controsoffitti...	<input type="checkbox"/>	<input type="checkbox"/>	<input type="checkbox"/>	<input type="checkbox"/>	<input type="checkbox"/>	<input type="checkbox"/>
2	Caduta tegole, cornicioni...	<input type="checkbox"/>	<input type="checkbox"/>	<input type="checkbox"/>	<input type="checkbox"/>	<input type="checkbox"/>	<input type="checkbox"/>
3	Caduta cornicioni, parapetti...	<input type="checkbox"/>	<input type="checkbox"/>	<input type="checkbox"/>	<input type="checkbox"/>	<input type="checkbox"/>	<input type="checkbox"/>
4	Caduta altri oggetti interni o esterni	<input type="checkbox"/>	<input type="checkbox"/>	<input type="checkbox"/>	<input type="checkbox"/>	<input type="checkbox"/>	<input type="checkbox"/>
5	Danno alla rete idrica, fognaria o termoidraulica	<input type="checkbox"/>	<input type="checkbox"/>	<input type="checkbox"/>	<input type="checkbox"/>	<input type="checkbox"/>	<input type="checkbox"/>
6	Danno alla rete elettrica o del gas	<input type="checkbox"/>	<input type="checkbox"/>	<input type="checkbox"/>	<input type="checkbox"/>	<input type="checkbox"/>	<input type="checkbox"/>

SEZIONE 6 **Pericolo ESTERNO indotto da altre costruzioni e provvedimenti di p.i. eseguiti**

Causa potenziale	PERICOLO SU			PROVEDIM. DI P.I. ESEGUITI	
	Edificio	Via d'accesso	Vie interne	Divieto di accesso	Trasenne e protez. passaggi
	A	B	C	D	E
1	Crolli o cadute da altre costruzioni	<input type="checkbox"/>	<input type="checkbox"/>	<input type="checkbox"/>	<input type="checkbox"/>
2	Rottura di reti di distribuzione	<input type="checkbox"/>	<input type="checkbox"/>	<input type="checkbox"/>	<input type="checkbox"/>

SEZIONE 7 **Terreno e fondazioni**

MORFOLOGIA DEL SITO				DISSESTI (in atto o temibili): <input type="checkbox"/> Versanti incombenti <input type="checkbox"/> Terreno di fondazione			
1	<input type="radio"/> Cresta	2	<input type="radio"/> Pendio forte	3	<input type="radio"/> Pendio leggero	4	<input type="radio"/> Pianura
A	<input type="radio"/> Assenti	B	<input type="radio"/> Generati dal sisma	C	<input type="radio"/> Acuti dal sisma	D	<input type="radio"/> Preesistenti

Figure 6.5 (b) Sections 3, 4, 5, 6, 7 of DPC classification scheme: identification of building typology (3); survey of damage and adopted mitigation measures to structural (4) and non-structural (5) elements; potential damages induced by adjacent buildings (6); damage consequences surveyed on ground (7), (Baggio et al., 2009).

(c)

SEZIONE 8 Giudizio di agibilità

Valutazione del rischio

RISCHIO	STRUTTURALE (Sez. 3 e 4)	NON STRUTTURALE (Sez. 5)	ESTERNO (sez. 6)	GEOTECNICO (sez. 7)
	BASSO	<input type="checkbox"/>	<input type="checkbox"/>	<input type="checkbox"/>
BASSO CON PROVVEDIMENTI	<input type="checkbox"/>	<input type="checkbox"/>	<input type="checkbox"/>	<input type="checkbox"/>
ALTO	<input type="checkbox"/>	<input type="checkbox"/>	<input type="checkbox"/>	<input type="checkbox"/>

Esito di agibilità

A	Edificio AGIBILE	<input type="checkbox"/>
B	Edificio TEMPORANEAMENTE INAGIBILE (tutto o parte) ma AGIBILE con provvedimenti di pronto intervento (1)	<input type="checkbox"/>
C	Edificio PARZIALMENTE INAGIBILE (1)	<input type="checkbox"/>
D	Edificio TEMPORANEAMENTE INAGIBILE da rivedere con approfondimento	<input type="checkbox"/>
E	Edificio INAGIBILE	<input type="checkbox"/>
F	Edificio INAGIBILE per rischio esterno (1)	<input type="checkbox"/>

(1) riportare nella colonna argomento della Sez. 9 l'esito e nelle annotazioni le parti di edificio inagibili (esiti B, C) e le cause di rischio esterno (esito F)

Sull'accuratezza della visita

1 Solo dall'esterno 4 Non eseguito per: a Sopralluogo rifiutato (SR) b Rudere (RU) c Demolito (DM)

2 Parziale d Proprietario non trovato (NT) e Altro (AL)

3 Completa (> 2/3)

Provvedimenti di pronto intervento di rapida realizzazione, limitati (*) o estesi ()**

*	**	PROVVEDIMENTI DI P.I. SUGGERITI	*	**	PROVVEDIMENTI DI P.I. SUGGERITI
1	<input type="checkbox"/>	Messa in opera di cerchiate o tiranti	7	<input type="checkbox"/>	Rimozione di cornicioni, parapetti, aggetti
2	<input type="checkbox"/>	Riparazione danni leggeri alle tamponature e tramezzi	8	<input type="checkbox"/>	Rimozione di altri oggetti interni o esterni
3	<input type="checkbox"/>	Riparazione copertura	9	<input type="checkbox"/>	Transennature e protezione passaggi
4	<input type="checkbox"/>	Puntellatura di scale	10	<input type="checkbox"/>	Riparazioni delle reti degli impianti
5	<input type="checkbox"/>	Rimozione di intonaci, rivestimenti, controsoffittature	11	<input type="checkbox"/>	
6	<input type="checkbox"/>	Rimozione di tegole, comignoli, parapetti	12	<input type="checkbox"/>	

Unità immobiliari inagibili, famiglie e persone evacuate

Unità immobiliari inagibili Nuclei familiari evacuati N° persone evacuate

SEZIONE 9 Altre osservazioni

Sul danno, sui provvedimenti di pronto intervento, l'agibilità o altro

Argomento	Annotazioni	Foto d'insieme dell'edificio	spilla

Il compilatore (in stampatello)

Firma

Figure 6.5 (c) Sections 8 and 9 of DPC classification scheme: judgment of conformity to standards and suggested early warning measures (8) and further observations (9), (Baggio et al., 2009).

In detail, 'DPC' scheme is aimed at surveying the typological, damage and usability characteristics of residential buildings, in the emergency phase following an earthquake.

The form is composed of the following nine sections:

Section 1 - Building identification;

Section 2 - Building description;

Section 3 – Typology;

Section 4 - Damage to structural elements and countermeasures carried out;

Section 5 - Damage to non-structural elements and countermeasures carried out;

Section 6 - External damage due to other constructions and countermeasures carried out;

Section 7 - Soil and foundations;

Section 8 - Usability judgment;

Section 9 - Other observations.

Section 1 of the form contains information concerning the identification of both the building and its survey.

On the cartography, it is necessary to indicate the single structural aggregates, to be intended as a set of non-homogeneous buildings (structural elements), in contact or connected in a more or less effective way, which can interact in case of earthquake or, more in general, in case of any dynamic action. A structural aggregate may hence be constituted by a single building (as is often the case for reinforced concrete buildings) or by more buildings joined together, generally with different structural characteristics.

Inside the structural aggregates, it is possible to identify buildings, defined as homogeneous units and generally distinguishable from adjacent buildings for structural typology, different height, age of construction, different storeys height, etc..

The identification of buildings is not always easy and unambiguous, especially in case of masonry buildings aggregates, which are typical of historical settlements. In particular, a masonry building can be defined as a building with structural continuity, delimited by vertical bearing walls extending for the entire height of its structure.

Section 2 collects information concerning metrical data, age, with indication of the period of construction and eventually of renovation of the building, as well as type of use and exposure. Metrical data must include the total number of storeys including basements, the number of basements, the average storey height and the average storey surface.

The total number of storeys refers to those which can be counted starting from the foundation level, including the eventual attic, but only when practicable.

The values of average storey height and average storey surface are listed in ranges and the rule to be followed, in case of significant variation among different storeys, is to consider the average value better representing the total volume.

In the column concerning age, it must be highlighted the period of construction of the building and, eventually, the period relative to the renovation.

As regards use, all types of use eventually coexistent in the building and the relative number of units have to be indicated. In the column concerning utilization (which refers in any case to the pre-event conditions), it should be indicated the approximate percentage of utilization of the building in spatial and/or temporal terms, according to three levels.

In the number of occupants, the average number of people usually present should be indicated, while the last information of this section concerns the type of property, distinguishing between public or private.

Section 3 of the form has its main aim to provide a deep knowledge of building typology. Masonry is subdivided in two types, based on the quality (materials, mortar, construction quality); for each type, it is possible to identify also the presence of tie beams or tie rods, when significantly widespread. Floors are subdivided into flexible, semi-rigid and rigid, in their plane. Usually, reinforced concrete floors are considered as rigid.

Buildings should be considered as having reinforced concrete or steel frame structures when the entire bearing structure is in reinforced concrete or steel. Mixed vertical bearing structures (masonry – frames) should be indicated in the column of the masonry section.

For frame structures, infill panels are irregular when they are not symmetric in plan and/or in elevation or when they are practically missing at one floor in at least one direction. In the following, some additional information concerning the previously described fields refer to building regularity in plan and in elevation, infill panels distribution and roofs, which may influence the static behavior of building under landslide movements in a positive or negative way.

The damage assessment, defined by *section 4 and 5*, is aimed to estimate the structural and non-structural risk (section 8) in terms of modification of the building bearing capacity with respect to a reference original state.

In order to allow a better understanding and to provide a common basis, some quantitative measures of damage are associated to the description of the different damage grades.

The damage reported in section 4 is the apparent damage, i.e. what can be observed on the structural components during the survey, being it pre-existent or related to landslide effects. The first 4 rows are relative to structural components; row 5 refers to non-structural components of particular relevance (infills and partitions), which may modify the resistance and/or the response of the structure, in particular for frame structures; row 6 records the pre-event damage to the whole building. A detailed definition of damage level according to ‘DPC’ classification will be showed into paragraph 6.4.4.

The damage to non-structural components, assessed in *section 5*, is important both for the usability classification and for the estimate of the repair costs. Typical damages to non-structural components are those concerning plasters, coatings, stuccos, false ceilings, infill panels, non-structural roof components, covering, eaves and parapets. Damages to the water, gas or electricity plants are also included.

Another factor of risk, which is important to ascertain during the safety inspection, is related to damage to components that are external to the building under survey. Danger may derive from instability of adjacent buildings (risk of collapses or objects falling), or from unsafe conditions of the distribution systems. In *section 6*, reference is made to these two situations. In addition, it has to be evaluated, whether the risk affects directly the building, the entry road or the lateral roads.

In *section 7*, qualitative information concerning the soil and the foundation, needed for the geotechnical risk evaluation, are collected. The information includes the description of the morphology of the site where the building is located and the possible presence of visible soil instabilities, with a distinction between unstable slopes and settlements affecting the building foundations.

Section 8 is devoted to the usability classification and to short term countermeasures. It is composed of four parts:

- risk evaluation: where the observations reported in the previous sections are summarized in terms of risk, with the aim of providing some guidance for the usability classification;
- usability classification: where five possible outcomes are reported;
- unusable building units, families and people to be evacuated: where the consequences of the delivered judgement are quantified in social terms;
- short term countermeasures are proposed.

Finally, *section 9* is devoted to the surveyor’s notes used to clarify the contents of the other sections of the form.

6.2 Assessment of deformations on building-foundation system: definitions and symbols

In recent years, the assessment of landslide impact on existing buildings has become a normal and required procedure. The question of allowable displacements and the influence of settlements on the performance and serviceability of structures has received great attention: to this aim, a standard terminology and sign conventions are widely required.

Generally, all the definitions adopted to assess building effects to slow-moving landslide action are carried out by theory on building response to tunneling (Burland & Wroth, 1974), considering that distortions and strains induced on foundations by ground movement have similar concepts.

Construction of tunnels and deep excavations is inevitably accompanied by ground movements. The ground response from tunnelling involves stress relief from excavation with resulting ground strains. At the ground surface, the latter are usually characterised by a settlement trough and the challenge is to estimate whether the ground movements will cause damage to overlying buildings and structures.

There are nowadays well-established approaches available for estimating ground movements and potential building damage from tunnelling (Burland, 1995).

Terzaghi (1935) pointed out that the complete description of the settlement of a structure requires a large number of observation points, so that detailed profiles of foundation movement can be plotted.

A study of the literature provides a wide variety of symbols and terminology describing foundation movements, much of it very confusing.

In order to overcome this problem, it is necessary to have a clear and consistent set of definitions describing the types of movements and deformations of building-foundation system. It is very important that the used terms do not relate to concepts about the behavior of the associated superstructure, since this depends on a large number of other additional factors, as mentioned in the previous paragraphs.

Burland & Wroth (1974) proposed a consistent set of definitions based on the displacements of a number of discrete points on the foundations of a building.

These definitions will be used subsequently as a measure of the ground deformation profile when evaluating damage predictions.

The definitions appear to have been widely accepted and are illustrated in Figure 6.6.

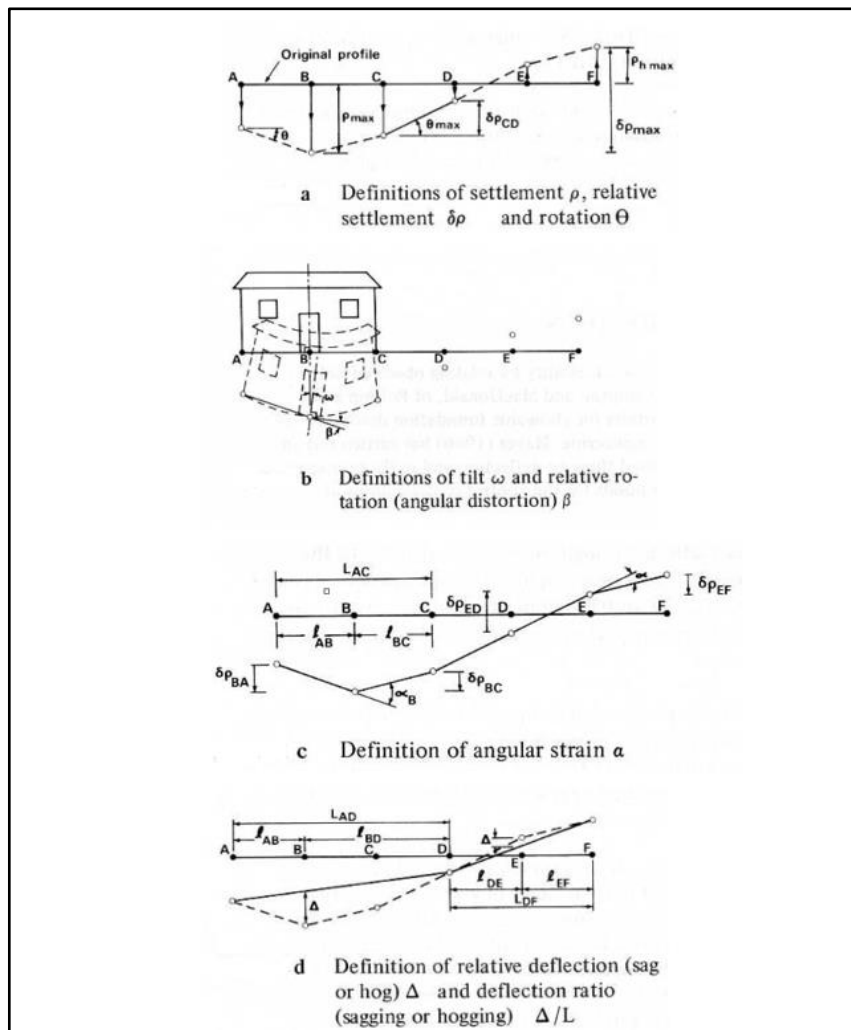


Figure 6.6 Definitions of ground and foundations movements (from Burland & Wroth, 1974).

The following are a few points to note:

- a **change of length** equal to δL over a length L gives rise to an average horizontal strain $\varepsilon = \delta L/L$; a shortening of $-\delta L$ over a length L gives rise to a compressive horizontal strain $\varepsilon = -\delta L/L$;
- **settlement** is indicated by the symbol ρ (Fig. 6.6a);
- **differential or relative settlement** is denoted by $\delta\rho$ (Fig. 6.6a);
- **rotation or slope** θ is the change in gradient of a line joining two reference points embedded in the foundation (Fig. 6.6a);
- **tilt**, denoted by ω , describes the rigid body rotation of the whole superstructure or of a well-defined part of it (Fig. 6.6b). Normally it is not possible to ascertain the tilt unless details of the superstructure and its behavior are known;

- **relative rotation or angular distortion** is denoted by β and describes the rotation of the line joining two points, relative to the tilt ω (Fig. 6.6b). It is not always straight forward to identify the tilt and the evaluation of β can sometimes be difficult. It is also very important not to confuse relative rotation β with angular strain α . For these reasons Burland & Wroth (1974) preferred the use of Δ/L as a measure of building distortion;
- the **angular strain** α is defined in Figure 6.6c. It is positive for upward concavity (sagging) and negative if it produces downward concavity (hogging);
- **relative deflection** Δ is the displacement of a point relative to the line connecting two reference points on either side (Fig. 6.6d). For upward concavity Δ is positive, while for downward concavity Δ is negative;
- **deflection ratio** (sagging ratio or hogging ratio) is denoted by Δ/L where L is the distance between the two reference points defining Δ (Fig. 6.6d).

The above definitions only apply to in-plane deformations and no attempt has been made to define three-dimensional behavior.

6.3 Building damage induced by landslide displacements

Movements of the building foundations, induced by slow-moving landslides over time, are cause of cracks occurrence on structural and non-structural elements. If the structure is unable to accommodate this movement, cracking is likely to occur. The appearance of distortions and cracks can be visually unattractive and disconcerting for occupants, and if left untreated they can affect the integrity, safety and stability of the structure.

Effective treatment requires first that the causes of cracking are understood. In the following we distinguish among vertical and horizontal displacement induced-effects, although in most cases landslide movement is composed of both components simultaneously. Furthermore, to take into account the different behaviour of buildings depending on structural typology, reinforced concrete and masonry buildings will be assessed separately.

- Cracks typology induced by vertical settlements:

As illustrated in Figure 6.7, slow-moving landslide movements can generate the types of settlements illustrated and discussed in more detail below:

- *uniform settlement*: an entire building moves up or down together, causing little or no foundation cracking or damage, though there could be important damage to mechanical connections to the building and even dangerous gas line leaks;
- *tipping settlement*: a part of foundation element or an entire building leans out of plane. Generally, this is considered a lateral or horizontal structural movement: in fact one end of a building can move substantially higher or lower than its opposite end, generating a total/partial rotation of the structure;
- *differential settlement*: we use the term "differential settlement" to describe a condition in which a part of a building foundation is moving down at a different rate from other portions of the foundation. Differential settlements often induce damage of elements of superstructure by producing usually vertical, possibly diagonal or stair-stepped cracks of walls.

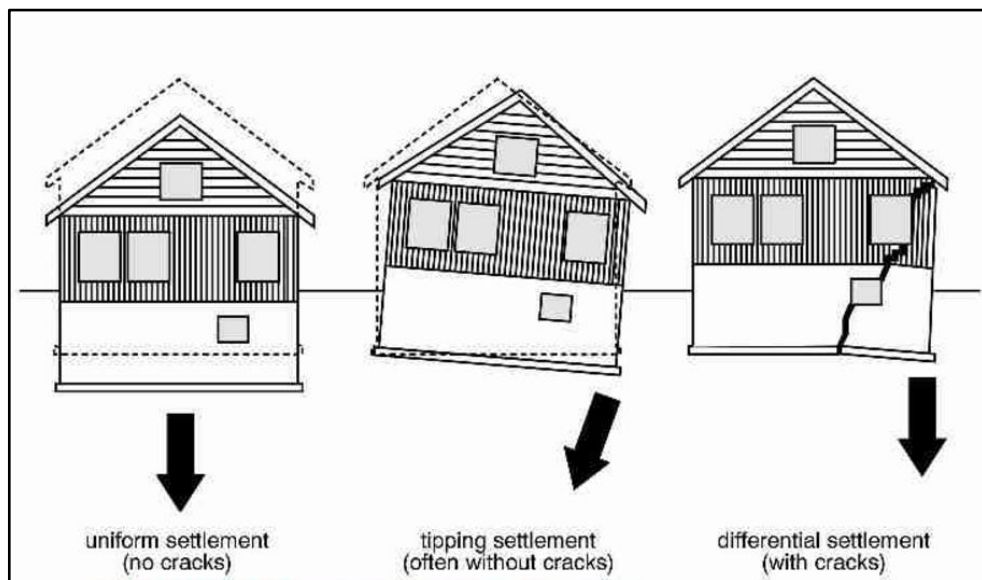


Figure 6.7 Types of foundation settlements induced by ground movements (Srivastava, 2016).

In order to assess the potential damages induced by landslide movements, the position of settlement have to be taken into account. “Central” settlements, in fact, are less dangerous than lateral ones, increasing the possibilities of collaboration between adjacent resistant parts of the involved structure (Antonucci, 2001) which allows to building to preserve its static stability.

For **reinforced concrete buildings**, foundation settlements, both *central* than *lateral*, can produce cracks tilted of angles in the range of 30° - 60° on partition walls (Fig. 6.8) and opening of superstructure (Fig. 6.9).

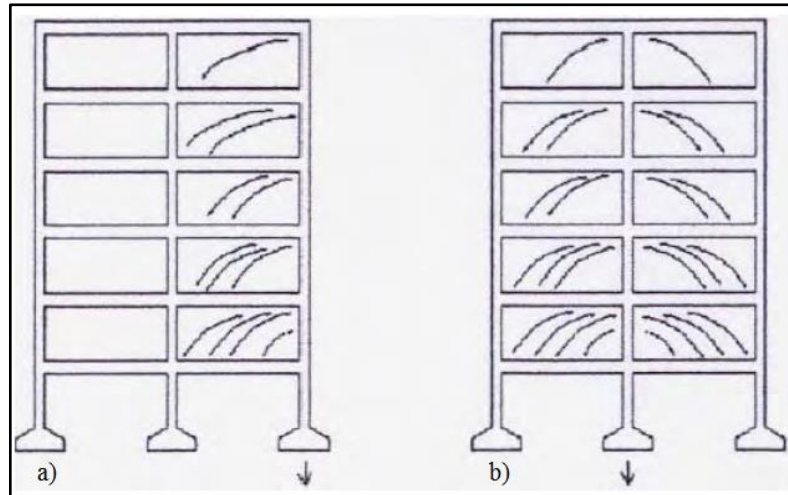


Figure 6.8 Cracks induced on partition walls of reinforced concrete building by differential settlements: lateral settlement (a) and central settlement (b) (from Menditto, 2010).

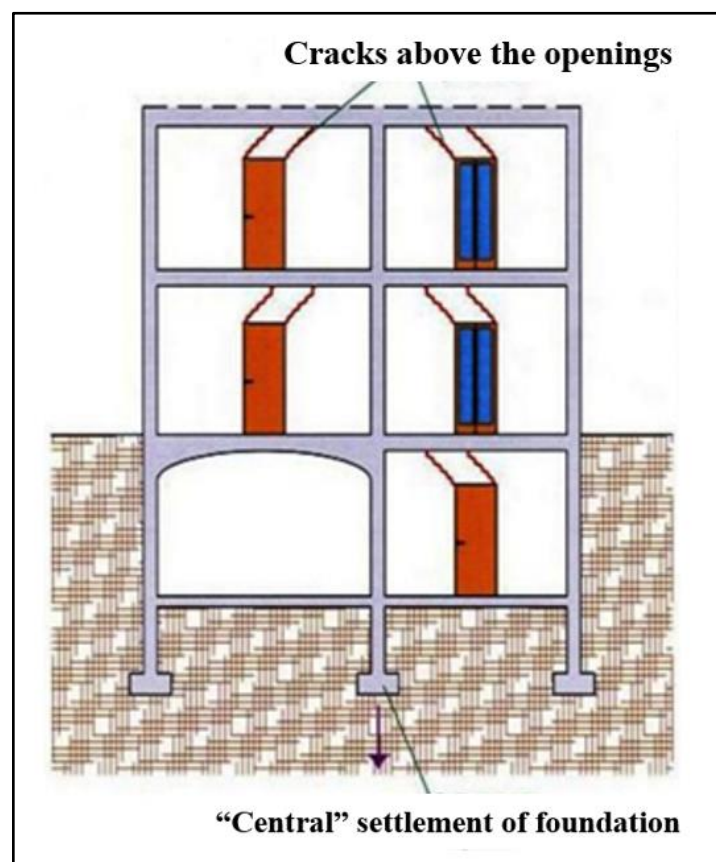


Figure 6.9 Cracks induced above the openings by a central settlement of foundation (Menditto, 2010).

Damage induced by foundation settlements on **masonry building**, such as for reinforced concrete structures, depend on position of settlement (central or lateral) and on presence and width of openings along building façade.

Generally, they are classified by considering their position (central and lateral), and ratio L/H between length L of settlement profile and height H of building.

In Figure 6.10 the potential typologies of settlement which may occur in masonry buildings are showed.

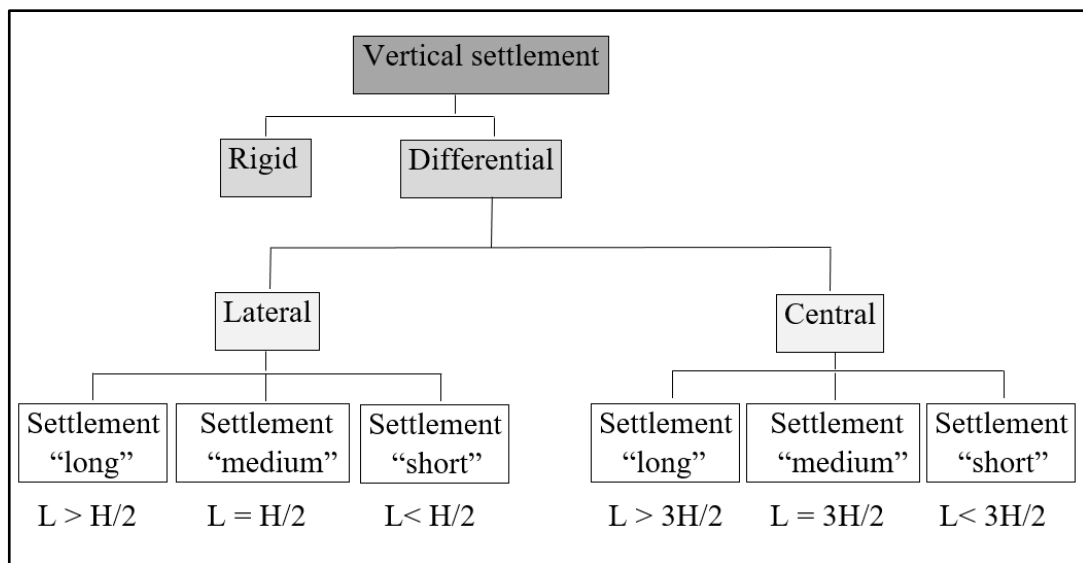


Figure 6.10 Classification of vertical settlements for masonry buildings (modified by Menditto, 2010).

The “*central*” settlement occurs in an intermediate area of interested load bearing wall (Fig. 6.11).

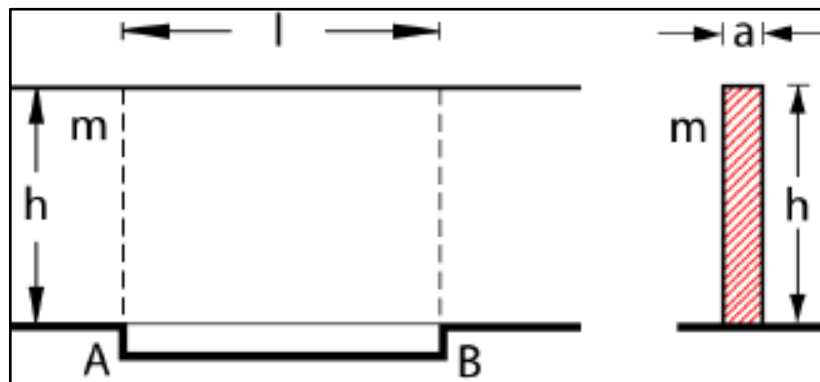


Figure 6.11 Example of “central” settlement of a masonry wall (modified by Anzani et al., 2008).

This profile of settlement can produce shear and bending cracks, depending on ratio L/H , between length L of wall affected by settlement and height H of building (Fig. 6.12).

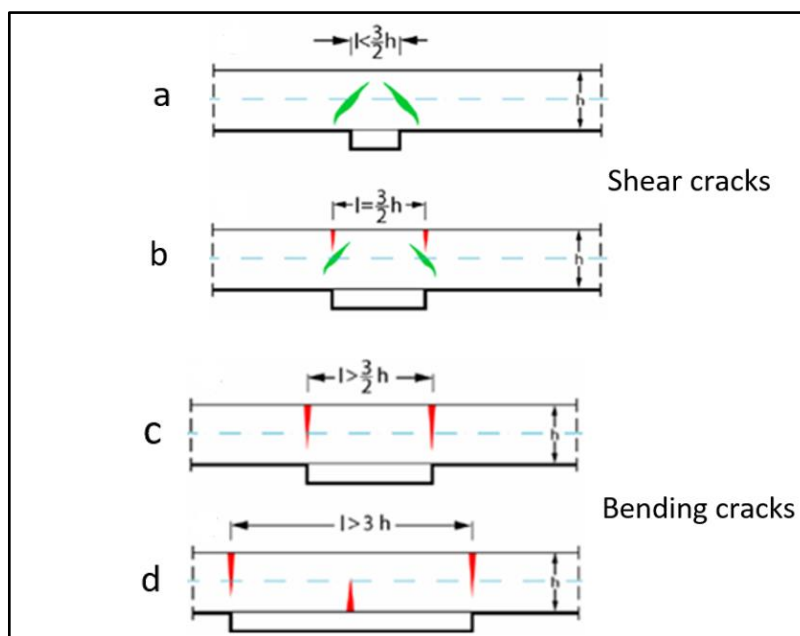


Figure 6.12 Schemes of cracks in masonry walls induced by “central” settlements: shear stress (a, b) and bending stress (c, d) (modified by Anzani et al., 2008).

Very often this kind of settlement produces cracks called “arc-shaped” on load bearing walls. As mentioned, this configuration can be more or less irregular, depending by presence and position of openings on building façade (Fig. 6.13).

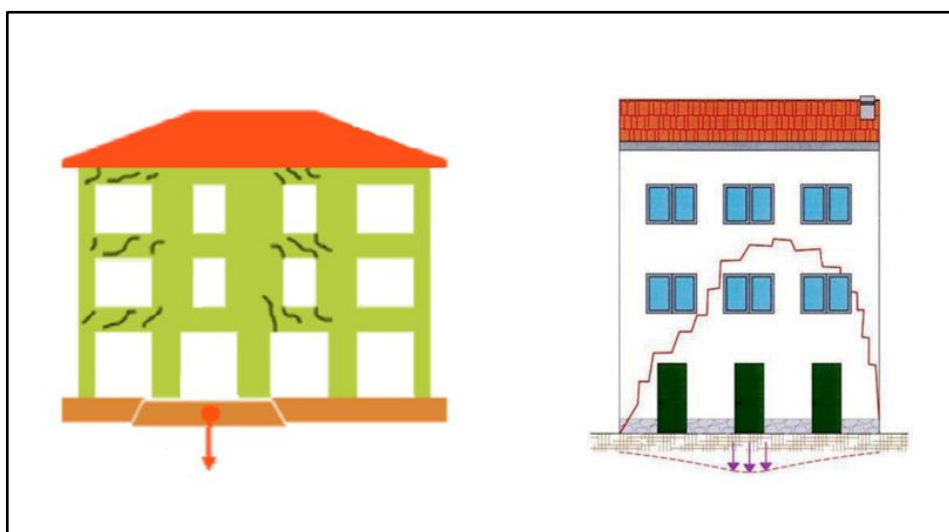


Figure 6.13 Examples of “arc-shape” cracks induced by “central” settlements of masonry wall (from Anzani et al., 2008).

The “lateral” settlement occurs at the end of the wall, close to the corner of building. Figure 6.14 shows potential cracks produced by this profile of displacement.

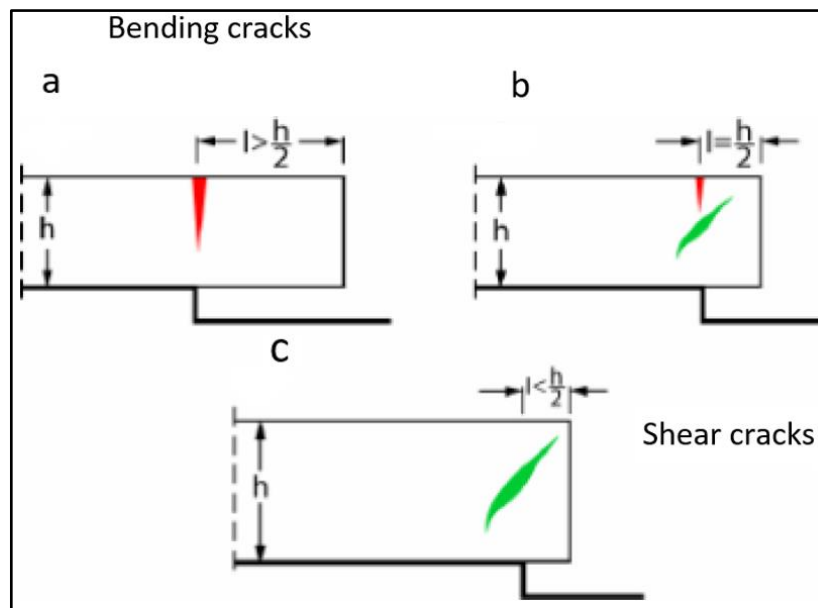


Figure 6.14 Schemes of cracks in masonry walls induced by “lateral” settlements: bending stress (a) and shear stress (b, c) (modified by Anzani et al., 2008).

Frequently, “lateral” settlement effects may produce parallel cracks on interested building zone, oriented along the same direction. Cracks orientation depends, also in this case, on more or less regular position of openings. Such damage level is due to the distortion of part of building interested by non-uniform local ground settlement (Fig. 6.15).

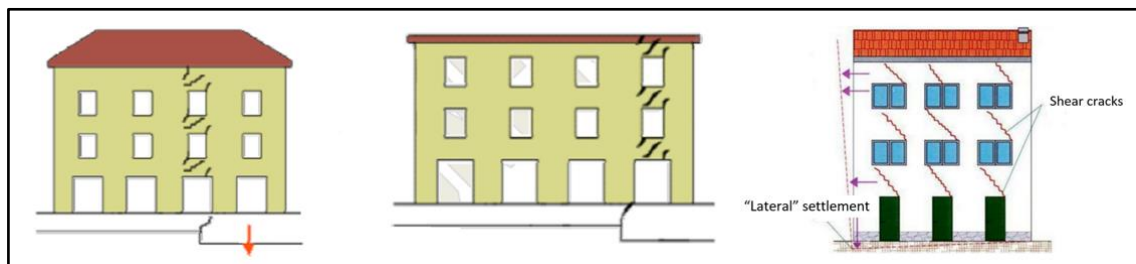


Figure 6.15 Examples of damages induced by “lateral” settlement on masonry buildings (from Anzani et al., 2008).

- Cracks typology induced by horizontal displacements:

Masonry buildings show damage susceptibility to horizontal displacements higher than reinforced concrete, since they are characterized by high critical values of vertical strain and very low critical values of horizontal extension strain.

A differential displacement along horizontal direction generates tensile stresses: the overcoming of masonry horizontal strength may induce vertical cracks on the building façade (Fig. 6.16a).

Furthermore, tensile cracks may be due to horizontal displacement generated by rotational movements of foundation (Fig. 6.16b).

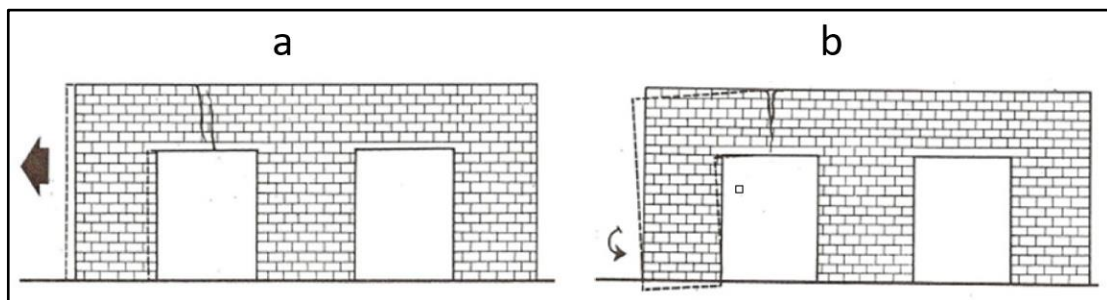


Figure 6.16 Examples of damage in masonry buildings induced by relative horizontal displacement (a) and by rotational movement of foundation (b) (from Menditto, 2010).

6.4 Existing approaches to damage assessment

During the second half of the last century the scientific community developed some specific damage classifications for areas affected by natural catastrophic phenomena as earthquakes (e.g. Wood & Neumann, 1931; Medvedev, 1965; Grünthal, 1998; Baggio et al., 2009), subsidence (e.g. Van Rooy, 1989; Freeman et al., 1994) and landslides (e.g. Burland, 1977; Alexander, 1986; Lee and Moore, 1991; Chiocchio et al., 1997; Iovine & Parise, 2002; Cooper, 2008; Del Soldato et al., 2017).

In particular, a considerable amount of scientific literature dealing with damage assessment in landslide-prone and -affected areas already exists (Skempton and MacDonald, 1956; Burland, 1977; Lee and Moore, 1991; Chiocchio, et al. 1997; Cooper, 2008; Mansour et al., 2011). Each classification presents some benefits and constraints, i.e. the choice of the relevant parameters to use, the lack of concern on some important features and the difficulty of applicability (Del Soldato et al., 2017).

Most of the existing damage classification methods, in fact, consider different conflicting parameters, do not allowing a simple and univocal application and result. In practice, damage affecting facilities are assessed performing field surveys highly conditioned by the criteria adopted and by the experience of the operators.

The first simple classification of building damage, based on the severity of the cracks affecting elements, even if without defining clear limits of evaluation, was employed by Skempton and MacDonald (1956), which examined 98 case histories to identify a basis on which to determine allowable total and differential foundation settlements. From their work, they suggested that "...the settlement characteristic causing cracking is probably the radius of curvature". No consideration was given to the relative length to height ratio of the affected parts of the structures.

Authors divided damage in three main categories: architectural, functional and structural damage.

Architectural damage is referred to the appearance on the construction, e.g. fine cracks in finishes, floor or panel walls (wider than 0.5 mm), in plaster (wider than 1 mm) and in rough concrete and masonry walls.

Functional damage involves the use of the structure producing extensive cracks, tilting of floors and walls, falling plaster, obstructed doors and windows and other non-structural damage.

Structural damage affects the stability of the construction manifesting ruptures and distortions in support elements (e.g. pillars, columns and load-bearing walls).

Subsequently, several approaches based on empirical data have been developed. The operator and its experience play an important role in damage assessment studies: the field campaign is the best criterion to assess the damage, although practical difficulties to reach places can arise during the development of the works. However, the main disadvantages of this method are the subjectivity of damage evaluation and the difficulty of assessing which factors influence possible defects.

Undoubtedly, the conclusions which may be drawn from a set of data must be formulated with great caution, due to the fact that the problem of the soil/structure interaction is extremely complex and influenced by a high number of parameters.

In order to overcome these difficulties, in recent years, analytical methods using detailed finite element calculations have been used.

Numerical analyses, developed at different level of detail, represent an important tool widely used to assess and predict present and future conditions of building damage due to ground movements.

An analytical method, given by Burland & Wroth (1974), is based on realistic simplifications to building system: it provides the relationship between the tensile strains caused by displacements and resulting damage degree.

The building is treated as a weightless, uniform, deep elastic beam of length L , and height H , with unit thickness (Fig. 6.17).

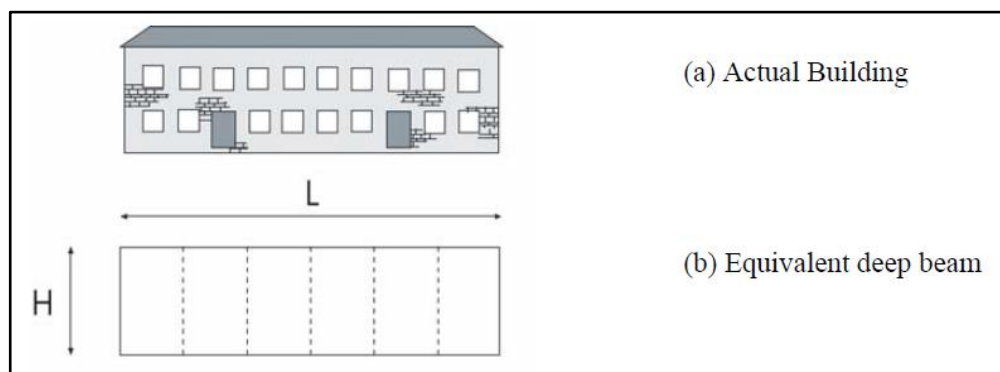


Figure 6.17 Burland & Wroth (1974) method: equivalent beam model of a real building.

Burland & Wroth (1974) and subsequently Boscardin & Cording (1989) used the concept of limiting tensile strain to study the onset of cracking in simple weightless elastic beams undergoing sagging and hogging modes of deformation. This simple approach gives considerable insight into the mechanisms controlling cracking.

The problem is to calculate the tensile strains in the beam for a given deflected shape of the building foundations and hence obtain the sagging or hogging ratio Δ/L at which cracking is initiated. The value for the maximum tensile strain obtained from this model allows to associate the building into a specific category of damage (Tab. 6.2).

Category of damage	Normal degree of severity	Limiting tensile strain (ϵ_{lim})(%)
0	Negligible	0 - 0.05
1	Very slight	0.05 - 0.075
2	Slight	0.075 - 0.15
3	Moderate*	0.15 - 0.3
4 to 5	Severe to very severe	> 0.3

Table 6.2 Relationship between category of damage and limiting tensile strain (Boscardin & Cording, 1989).

In the following, four approaches existing in literature, applied during the thesis to classify buildings damage level, are described.

6.4.1 Burland (1977) approach

Burland (1977) disseminated the first classification including a ranking scheme and some suggested values in order to limit the subjectivity of the operator.

The Author presented a simple system derived from the cumulated experience by three previous works:

- a study of the economic consequences of the heave of construction on swelling clays where a simple categorization of the damage based on their restoration was conceived (Jennings and Kerrich, 1962);
- a simple classification based on wide experiences of damage caused by subsidence (National Coal Board, 1975);
- a ranking proposed by the Coal Board's recommendations (MacLeod and Littlejohn, 1974).

The Burland (1977) classification (Table 6.3) consists of six classes of damage, including the width of cracks (measured in millimeters), the quantity of fractures, a description of the visible damage (e.g. the distortion of doors and windows or the sloping of floors) and their relationship with the facility of restoration.

The provided values are related only to visible damage, observed corrosion and cracks permitting the penetration or the lacking of liquids or gases. For reinforced concrete, the approach to adopt should be more severe (Nawy, 1968).

Subsequently, Boscardin and Cording (1989) slightly modified the classification maintaining the same structure and correcting some approximations based on their experience.

Grades	Damage level	Crack width (CW in mm)	Description of damage
0	Negligible	< 0.1	Hairline cracks
1	Very Slight	< 1	Fine cracks and isolated generally restricted to internal walls finishes
2	Slight	< 5	Several slight fractures inside building; exterior cracks visible; doors and windows may stick slightly
3	Moderate	5 < CW < 15 or several > 3 mm	Several cracks; doors and windows sticking. Utility service may be interrupted; weathertightness often impaired
4	Severe	15 < CW < 25 depending on number of cracks	Windows and door frames distorted; floor sloping noticeably; Walls lean or bulge noticeably, some loss of bearing in beams; utility service disrupted
5	Very severe	> 25	Beams lose bearing; walls lean badly and require shoring; windows broken with distortion; danger of instability.

Table 6.3 Classification of damage according to Burland (1977), as modified by Boscardin & Cording (1989).

Categories 0, 1 and 2 represent aesthetic damage, categories 3 and 4 serviceability damage and 5 stability damage.

The aesthetic damage level affects only the appearance of the property, serviceability is related to cracking and distortion which impairs other functions as fracturing of service pipes, jamming of doors and windows, while stability damage provides an unacceptable risk that some part of the structure will collapse unless preventative action is taken.

6.4.2 Alexander (1986) approach

In 1986, Alexander, after an important landslide event affecting Ancona (central Italy) in December 1982 (Alexander, 1983), presented an alternative intensity scale of damage.

This methodology is referred to landslide-induced damage observable on buildings and it was developed in order to compare visible damage on different structures involved in the same event. The ranking shows eight categories, two more than the previous one (Burland, 1977) to consider also the partial and total collapse as well as the possibility of the “no damage” condition: none, negligible, light, moderate, serious, very serious, partial collapse and total collapse (Table 6.4).

Alexander approach is based on the crack observation on walls, their position and extension, their distortion of the rigid elements and on the settlement affecting foundations. The classification of the building damage based on their description includes the visual description of the internal and external damage and few referring values in centimetres, for the differential settlement, and in grades, for the inclination of the floor.

Grade	Category of damage	Description of building damage
0	None	Building is intact
1	Negligible	Hairline cracks in walls or structural members, no distortion of structure or detachment of external architectural details
2	Light	Building continue to be habitable; repair not urgent. Settlement of foundation, distortion of structure and inclination of walls are not sufficient to compromise overall stability
3	Moderate	Walls out of perpendicular by 1°-2°, or substantial cracking has occurred to structural members, or foundations have settled during differential subsidence of at least 15 cm; building requires evacuation and rapid attention to ensure its continued life
4	Serious	Walls out of perpendicular by several degrees; open cracks in walls; fracture of structural members; fragmentation of masonry; differential settlement of at least 25 cm compromise foundations; floors inclined by up to 1°-2°, or ruined by soil heave; internal partition walls will need to be replaced; door and window frames too distorted to use; occupants must be evacuated and major repair carried out
5	Very serious	Walls out of plumb by 5°-6°; structure grossly distorted and differential settlement will have seriously cracked floors and walls or caused major rotation or swelling of the building (wooden buildings may have detached completely from their foundations). Partition walls and brick infill walls will have at least partly collapsed; occupants will need to be rehoused on a long-term basis and rehabilitation of the building will probably not be feasible
6	Partial collapse	Requires immediate evacuation of the occupants and cordoning of the site to prevent accidents with falling masonry
7	Total collapse	Requires clearance of the site

Table 6.4 Classification of damage according to Alexander (1986).

Some missing features were spotted applying this method (Crescenzi et al., 1994; Iovine & Parise, 1995), such as the lack of the distinction between the building materials of the structure in addition to the lacking of data about the opening and the number of the cracks. In spite of the very simple scheme, the author suggested a checklist of suitable information to better describe the structure affected (e.g. typology of construction, description of building and foundations, if available), the phenomenon occurred (e.g. type of ground movement and position of the structure respect to the landslide) and the specific damage (e.g. direction and magnitude of the movement, inclination of the elements and typology of cracking).

6.4.3 Iovine & Parise (2002) approach

In order to overcome the drawbacks of the aforementioned classifications arisen during some applications (Crescenzi et al. 1994), a new approach for structural damage assessment, involving interdisciplinary knowledges of geologists, geomorphologists and civil engineers, was implemented by Chiochio et al. (1997) (Table 6.5).

For the first time, the new classification provided the distinction of two different typologies of structures (i.e. masonry and reinforced concrete) and quantitative reference values for some parameters were suggested.

Grade	Damage level	Load-bearing structures	Rigid settlement	Cracking	Immediate measures
0	None	Masonry	0	None	None
		Reinforced concrete frame	0	None	None
1	Negligible	Masonry	0	Hairline cracks of the plaster	None
		Reinforced concrete frame	0	Hairline cracks of the plaster	None
2	Light	Masonry	2 - 3 cm	Small cracks through walls and partitions	None
		Reinforced concrete frame	2 - 3 cm	Small cracks through walls and partitions	None
3	Moderate	Masonry	10 - 15 cm	Open cracks in walls; walls disjunction; little deformation; badly working casings	Evacuation suggested
		Reinforced concrete frame	10 - 15 cm	Significant cracking in the beams; partition walls deformed and crumbling; badly working casing	Evacuation suggested
4	Serious	Masonry	15 - 20 cm	Considerable disjunction of walls; space deformation; partition walls collapsed; unusable casing	Evacuation & shoring
		Reinforced concrete frame	15 - 20 cm	Perimetric and partition walls partly collapsed; deformed structures; spread cracking	Evacuation
5	Very serious	Masonry	>25 cm	Open cracks in floor; partition walls totally collapsed; seriously ruined lintels	Evacuation & cordoning
		Reinforced concrete frame	>20 cm	u.d.	Evacuation & cordoning
6	Partial collapse	Masonry	u.d.	u.d.	Cordoning
		Reinforced concrete frame	u.d.	u.d.	Cordoning
7	Total collapse	Masonry	u.d.	u.d.	Cordoning
		Reinforced concrete frame	u.d.	u.d.	Cordoning

Table 6.5 Classification of damage according to Chiochio et al. (1997).

Starting from Alexander (1986) and Chiocchio (1997) schemes of classification of landslide damage to buildings in urban areas, a new proposal was performed by Iovine and Parise in 2002 (Table 6.6). The latter has 7 different levels of damage; it also provides suggestions regarding immediate and rehabilitation measures suitable to the different damage levels. Each level represents a state of the damage affecting the building: the first three levels correspond to negligible and weak damage; buildings affected by the fourth grade of damage exhibit some serious cracks and restoration strategies are suggested for them; the fifth grade is characterized by several failures affecting the construction and the surrounding area; the last two classes are for buildings in which the level of damage is so severe that the decision to renovate or relocate them has to be accurately evaluated.

Levels 1-2 of the classification scheme are characterized by small damage not requiring intervention of the Authorities. From level 3 upward, when more serious damage is to be found, it is necessary to evacuate the building, even if temporarily, in order to renovate it by rehabilitation measures. Level 4, defining a high risk of the building requires to adopt security measures such as cribs and cordoning. From level 5 on, damage is so severe that it should be accurately evaluated whether to renovate or pull down the building and rebuild it in a safer area.

Grade	Damage level	Building typology	Rigid settlement (cm)	Rigid Rotation (cm)	Differential settlement (cm)	Cracking	Suggested measures
0	None	Masonry	0	0	0	None	None
		Reinforced concrete	0	0	0	None	None
1	Negligible	Masonry	0	0	0	Hairline cracks of the plaster	None
		Reinforced concrete	0	0	0	Hairline cracks of the plaster	None
2	Light	Masonry	2-3	2,5‰* H	3‰* L	Small cracks through walls	None
		Reinforced concrete	2-3	2,5‰* H	3‰* L	Small cracks through partitions	None
3	Moderate	Masonry	10-15	4‰* H	4 - 5‰* L	Open cracks in walls; walls disjunction; little deformation; badly working casings	Evacuation suggested
		Reinforced concrete	10-15	4‰* H	4 - 5‰* L	Significant cracking in the beams; partition walls deformed and crumbling; badly working casing	Evacuation suggested
4	Serious	Masonry	15-20	8‰* H	7‰* L	Considerable disjunction of walls; space deformation; partition walls collapsed; unusable casing	Evacuation & shoring
		Reinforced concrete	15-20	8‰* H	7‰* L	Perimetric and partition walls partly collapsed; deformed structures; spread cracking	Evacuation
5	Very serious	Masonry	>25	>10‰*H	>10‰*L	Open cracks in floor; partition walls totally collapsed; seriously ruined lintels	Evacuation & cordoning
		Reinforced concrete	>20	>10‰*H	>10‰*L	Partition walls totally collapsed; deformed structures; cracks in floor	Evacuation & cordoning
6	Partial collapse	Masonry	u.d.	u.d.	u.d.	u.d.	Cordoning & demolition
		Reinforced concrete	u.d.	u.d.	u.d.	u.d.	Cordoning & demolition
7	Total collapse	Masonry	u.d.	u.d.	u.d.	u.d.	Cordoning & demolition
		Reinforced concrete	u.d.	u.d.	u.d.	u.d.	Cordoning & demolition

Table 6.6 Classification of damage according to Iovine & Parise (2002).

This scheme can be applied only to urban areas. These improvements were relevant to analyze the fractures, to distinguish the meaning of similar cracks in different materials and to minimize the subjectivity of the survey, providing quantitative reference values of several parameters, such as rigid settlement and rotation or differential displacement.

6.4.4 DPC (2009) approach

In Italy, a further approach to classify damage affecting civil constructions and to evaluate the reliability of buildings to host safely its inhabitants was presented by the Italian Department of Civil Protection (DPC hereafter) (Baggio et al., 2009).

This approach was conceived to survey damage after seismic events, in order to assess the fitting for human habitation of the buildings, but it is applicable also to landslides because, also in slope movements, damage is due to the effects of shear stress.

The assessment of damage magnitude was realized through six grades of severity, but divided in four classes in order to facilitate the classification: distinguishing masonry and reinforced concrete structures, nothing (no damage), weak (slight), moderate & serious, very serious & collapse levels are defined according to the European Macro-seismic Scale ‘Ems 98’ (Grüntal, 1998) (Table 6.7).

Grades	Damage level	Crack width (CW in mm)	General description of the damage
D0	Nothing	None	None
D1	Weak	≤ 1	Damage don't change significantly the resistance of the structure; slightly cracks (≤ 1mm) in walls; limited separation of elements and dislocation (≤ 1mm); limited distortion without separation or structural failure
D2/D3	Moderate & Serious	< 10 or 15	Damage that could change significantly the resistance of the structures without the collapse of elements; cracks with big entity than D1 with possible expulsion of material (≤ 1cm or more close to the opening); symptom of crushing crack; important disjunctions; possible small collapse
D4/D5	Very Serious & Collapse	> 15	Damage that evidently modify the resistance of the structures; possible partial and total collapse

Table 6.7 Classification of damage severity according to the ‘DPC’ (Baggio et al., 2009).

The damage classification (section 4 of DPC scheme) is simply done by checking the squares of the table relevant for the case under study, with the following considerations:

- each square corresponds to a given damage grade and to a given extension of that damage grade;
- the whole list of components must be explicitly considered (rows 1 – 5): if no damage is noticed for any one of them, the option ‘none’ must be checked and the other options in the row should not be checked. If some damage is observed, the corresponding squares should be checked;

- in the rows from 1 to 5, the total apparent damage to each component at the moment of the inspection is described, i.e. the visible changes with respect to an ideal original condition of the building, without any damage. In row 6 the pre-existing damage of the building, presumably existing before the occurred event is described.

A brief damage description of damage levels is reported in the following;

- Level D0: no damage

In masonry buildings, cracks in the plaster, repaired and not reactivated, may be associated to this damage grade, while in reinforced concrete buildings, cracks in structural components within the width limits reported by the code (in the range of 0.2–0.4 mm).

- Level D1: slight damage

It is a damage that does not affect significantly the capacity of the structure and does not jeopardise the occupants safety due to falling of non-structural elements; the damage is slight when the falling of objects can immediately be avoided.

In masonry, cracks of width ≤ 1 mm, no matter how distributed in masonry walls and in floors, without material expulsion, limited separations or slight dislocations (≤ 1 mm) between parts of structures, for example between walls and floors or between walls and stairs or between orthogonal walls. Falling of small portions of degraded plaster or stucco, not connected to the masonry.

In reinforced concrete buildings, slight cracks in the beams (up to 1 mm), widespread, but not vertical, cracks (< 0.5 mm) in columns or in partitions. Cracks up to 2 mm due to separation of the infill walls from the structures.

Level D2-D3: medium-severe damage

It is a damage that changes significantly the capacity of the structure, without getting close to the limit of partial collapse of the main structural components.

In masonry, more severe cracks with respect to D1, also with expulsion of material and few mm wide (up to approximately 1 cm) or wider, if close to the openings, symptoms of cracks due to crushing, significant separations between floors and/or stairs and walls and between orthogonal walls, some partial collapses in the secondary beams of the floors. Cracks of some mm in the vaults, and/or with symptoms of crushing. In wooden or steel roofs with tiles covering, damage in the secondary beams and falling of a significant portion of the tiles covering. Visible out of plumb but in any case not larger than approximately 1%.

In reinforced concrete buildings, flexural cracks in beams up to 4-5 mm, cracks in columns and in shear walls up to 2-3 mm, beginning of buckling of the compressed bars in the columns, with spalling of the concrete cover, just perceptible residual out of plumb.

Evident cracks (> 2 mm) in infill walls due to the separation from the structure, diagonal cracks up to few mm, evident crushing at the corners in contact with the bearing structures, sometimes with localised expulsion of material.

Level D4-D5: very heavy damage and/or collapse

It is a damage that significantly modifies the capacity of the structure, bringing it close to the limit of partial or total collapse of the main structural components. This state is characterised by damages heavier than the previous ones, including collapse.

In masonry, damage to structural components more severe than the previous grade (D2-D3), with expulsion of a significant amount of structural material and/or localised collapse of bearing walls and of wall corners.

In reinforced concrete buildings, damages more serious than those described for the grade D2-D3: cracks > 5 mm in beams and > 3 mm in columns and walls, total collapse of infill panels, partial collapse of the structural components.

The peculiarity of the proposed approach is the introduction of the evaluation of the damage extension. It has to be evaluated in percentage, separating the categories into three parts to be assessed separately and then reassembled. To this purpose, three levels of damage extension have been defined:

- few: not more than $1/3$ of the elements are damaged;
- many: more than $1/3$ and not more than $2/3$ of the elements are damaged;
- most: more than $2/3$ of the elements are damaged.

The damage extension has to be estimated for each component separately and with reference to the entire building. This means that, for each component, the surveyor has to:

- a) evaluate the percentage of the building affected by each of the damage grades. To this aim, it is necessary to appropriately combine the relative damage extension in each floor and the number of damaged storeys. It should be also noticed that if one of the three damage grades is not present for a given component, none of the corresponding extensions will be checked;
- b) estimate the relative extension to be assigned to each damage grade. For each component, the sum of the damaged relative extensions must not be larger than 1.

To assess damage affecting structures, section by section, the extension of the cracks and their magnitude have to be taken into account considering that the sum of the damage extension cannot exceed 1, representing the entire building (e.g. $2/3$ of D4-D5 + $1/3$ of D2/D3) (Table 6.8).

Level Extension Structural component	Damage level									
	D4-D5 Very serious			D2-D3 Moderate-serious			D1 Weak			None
	$>2/3$	$1/3-2/3$	$<1/3$	$>2/3$	$1/3-2/3$	$<1/3$	$>2/3$	$1/3-2/3$	$<1/3$	
	A	B	C	D	E	F	G	H	I	L
Structural vertical components										
Floor										
Stairs										
Roof										
Non-structural components (partition walls)										
Existing damage										

Table 6.8 Scheme to compile for damage assessment according to the ‘DPC’ (Baggio et al., 2009).

Finally, several possible combinations between percentage of the extension of damage level and the four classes of cracks size are taken into account using a matrix to evaluate a whole unit. For each level of damage, a value was assigned and, then, the values were grouped between 0 (negligible damage) and 7 (total collapse) to be comparable with the other above described classifications.

6.5 Conventional instruments to the cracks monitoring

The monitoring of cracks is one of the major sources of information for damage detection of buildings within a landslide-affected area. More frequent and rigorous monitoring of spatial and temporal evolution of cracks represents the main source of information on landslide activity, allowing also to assess the behaviour of involved buildings.

Monitoring the changes in crack width is an important diagnostic technique for determining the cause and specifying the remedial work. In particular, it is important to analyse crack geometry and propagation time, because they represent the consequence of an active phenomenon.

In case of presence of cracks on a building, their inclination and location can help to individuate, for example, a differential displacement as their cause. In this case, if they correspond to a structural failure, their monitoring and analysis allow to understand the risk level for the inhabitants.

The simplest crack monitoring system consists in a piece of glass which is fixed through lime across the crack (Fig. 6.18). If the glass is broken it is a proof that the crack moved. Nevertheless, this method allows only to visually understand where the cracks are increased but not to quantify their widening.



Figure 6.18 Glass crack monitoring system.

Another system for the structural crack monitoring is the so called “Tell Tale” (Fig. 6.19) which overcomes the above limit. It consists of two slips of overlapping plastic plates with a red cross on one and a marked grid on the other. Once this monitor is fixed in position, an initial reading is taken. Then, more readings are gotten at regular intervals to establish if the movement is occurring and if so, at what rate.

By comparing the different rates of movement for cracks at different locations in a building, the cause and location of the weakness can be established.



Figure 6.19 Example of “Tell Tale” crack monitoring.

This system is available for internal or external use, monitors the opening or closing of a crack to an accuracy of 1,00 mm, is capable of monitoring vertical as well as horizontal movements.

In order to monitor cracks in corners of a building, it is useful to use this system singly to evaluate two-dimensional movement, in pairs to analyse three-dimensional displacement.

The most common transducer is the linear variable displacement transformer (LVDT) that consists of a movable magnetic core passing through one primary and two secondary coils.

In recent years several advantages to monitor movements of joints and cracks of structures are obtained by using crack-meter, a displacement transducer.

Crack-meters are used to detect differential movement between two points. Anchors are typically installed on opposite sides of the crack (Fig. 6.20). It can incorporate a displacement transducer mounted across the anchors. A change in the distance across the crack causes a change in the frequency signal produced by the displacement transducer if excited by the readout or data logger. The initial reading is used as a datum. Subsequent readings are compared to the previous datum to calculate the magnitude, rate, and acceleration of movement across the crack.



Figure 6.20 Example of crack-meter to monitoring movement of crack.

The main advantages of crack-meters are:

- high accuracy: crack-meters provide a repeatability of 0.3 mm;
- temperature Measurement: crack-meters are equipped with a temperature sensor;
- manual or automatic readings: crack-meters may be read manually, or equipped with a vibrating wire transducer for automated monitoring.

Finally, cracks in masonry or reinforced concrete structures are evidence that the building has moved or is still moving: examine the nature and severity of the crack, what direction are the cracks going and where are they the widest, is aimed at monitoring potential ground movements and consequently to define strategy of mitigation measures.

CHAPTER 7

A PROCEDURE FOR BUILDING VULNERABILITY ASSESSMENT AT DIFFERENT SCALES OF ANALYSIS

7.1 The proposed approach for building vulnerability assessment

The main topic of this work is to provide an innovative methodology which can be used to forecast the spatial and temporal evolution of the buildings' structural vulnerability in urban settlements affected by slow-moving intermittent landslides.

A multi-level and integrated analysis (Fig. 7.1) of landslide's kinematics and the exposed elements is addressed to detect, at different levels of accuracy, vulnerability of existing facilities within a landslide-affected area. In detail, it allows to:

- investigate the preliminary cause-effect relationship between landslide features and consequences to existing facilities;
- assess spatial and temporal damage evolution of buildings, investigating also the vulnerability factors influencing the performance of structures to slow-moving landslides;
- investigate the structural behavior of each building and forecast damage severity degree future condition.

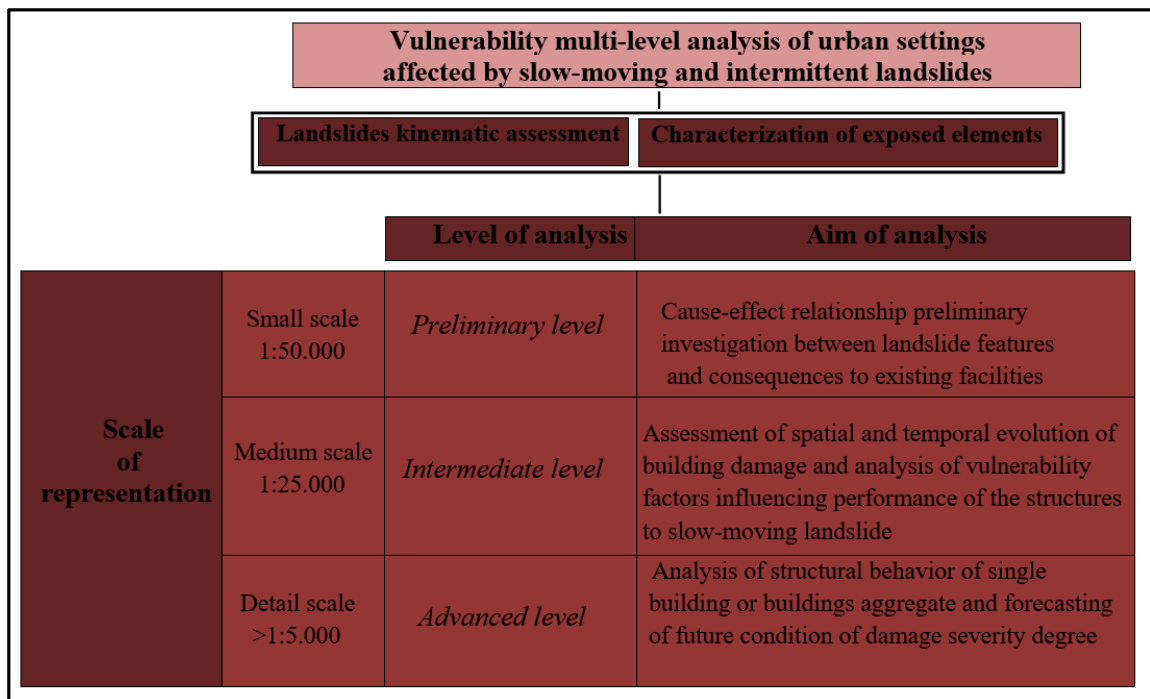


Figure 7.1 General framework for vulnerability assessment at different scales of analysis.

Different approaches to assess building vulnerability have been described in literature, each one characterized by its own peculiarity, obviously with differences in the final results. Indeed, at present no vulnerability assessment standard methodology exists.

The approach here proposed is based on a logical structure which takes into account vulnerability key factors, landslide kinematics and structural characterization of the exposed elements.

At different scales of representation, the two above mentioned datasets have been separately analyzed, and subsequently merged in order to detect landslide-induced damage to buildings. Generally, from low-resolution analysis, to medium and to detailed scale, the parameters useful for the landslide intensity definition and for the exposed elements characterization change.

Hereafter, aims, input and output data for vulnerability assessment at different level of detail are described (Fig. 7.2).

At **small scale** (1:50.000-1:25.000), analysis is aimed to investigate preliminary cause-effect relationship between landslide intensity and damage susceptibility, as indicator of building vulnerability within a landslides-affected area.

To this aim, with reference to the municipal territory of the study area, the combined use of available landslide inventory and geomorphological maps, and medium-high resolution DInSAR data, integrated with building damage recorded by a field survey, allows to:

- identify stable/unstable areas derived with reference to a fixed velocity threshold, buildings affected by landslide movements and analyze their behavior;
- update the landslide inventory map (boundary and state of activity);
- provide a preliminary and fast analysis about building damage susceptibility to ground movements, depending on the relationship between landslide intensity and recorded building damage;
- identify very quickly areas with different level of vulnerability, combining landslide intensity and building damage severity in a qualitative vulnerability matrix.

Physical vulnerability assessment at **medium scale** (1:25.000-1:5000) requires to define, added to information of the previous level, geo-lithological settings and the stratigraphy of the study area, building characteristics such as geometrical data, number of stories, typology of construction (isolated or aggregated and position of each structure in a building's aggregate).

This level of analysis allows to:

- define a vulnerability zoning map, useful for cause-effect qualitative correspondence identification, more detailed than in the previous scale;
- provide an empirical relationship between the changes in landslide intensity and the worsening of damage severity level;
- assess the behavior of buildings, analyzing vulnerability factors influencing performance of the structure to slow-moving landslide-induced movements;
- predict, at an intermediate level of detail, spatial and temporal evolution of buildings damage with reference to the whole territory of the study area.

Finally, the “**detail scale**” analysis ($\geq 1:5.000$), carried out on a single building or on building’s aggregate, follows a different methodological approach. Aim of the study is to:

- define, for each building, by analytical or numerical analysis, the relationship between landslide intensity and expected damage class.

The proposed approach is totally different from empirical methods adopted in a medium scale analysis, using recorded building data from real case histories.

Implementation of the building computational model in numerical software requires a detailed geometrical and structural survey: in particular, it is essential to define geometrical data, construction typology, types and materials of structures, state of maintenance, properties foundation structures, damage degree and distribution, mechanical properties of structural materials.

As mentioned in Chapter 6, the scheme provided by the Italian Department of Civil Protection (DPC), is a useful tool to obtain a detailed technique of building survey. Further, a complete characterization of landslide requires, together with information of previous level, the assessment of lithological stratigraphy, of geotechnical properties and mechanical parameters of soil under the considered building;

- forecast, based on the above mentioned methodology and under simplifying assumptions, future conditions of damage and local failures of a building.

Multi-scale vulnerability analysis			
Scale of analysis	INPUT DATA	APPROACH	OUTPUT DATA
Small scale (low resolution)	<ul style="list-style-type: none"> - Topographic map - Lithological and geo-morphological maps - Landslides inventory map - Medium-high resolution DInSAR data - Buildings typology and damage maps 	<ul style="list-style-type: none"> - Qualitative - Empirical - Matrices-based 	<ul style="list-style-type: none"> - Moving/not moving areas map - Moving/not moving buildings map - Updated landslide inventory map - Preliminary and very fast buildings vulnerability map
Medium scale (medium resolution)	<ul style="list-style-type: none"> - Information of the previous level - Geological settings maps - Stratigraphy of the study area - Buildings geometrical data and characteristics (number of stories, isolate/aggregate construction) 	<ul style="list-style-type: none"> -Semi-quantitative -Empirical -Matrices-based -Fragility curves 	<ul style="list-style-type: none"> - Buildings vulnerability map - Empirical fragility curves for different vulnerability factors - Predicted map of future buildings damage likelihood
Detailed scale (high resolution)	<ul style="list-style-type: none"> - Information of the previous level - Geotechnical properties and mechanical parameters of soil - Buildings structural characteristics (types and materials of structures, state of maintenance, properties foundation structures, mechanical properties of structural materials) 	<ul style="list-style-type: none"> - Quantitative - Analytical and numerical - Fragility curves - Vulnerability curves 	<ul style="list-style-type: none"> For each building: - 3D fragility curve and/or - Vulnerability domains - Forecasting spatial and temporal evolution of damage degree, local failure and collapse condition

Figure 7.2 Building vulnerability assessment: approaches, input and output data at different scales of analysis.

It is important to highlight that carrying out a detailed analysis for a whole urban settlement is a difficult task. It requires a deep knowledge on the characteristics of the exposed structures as well as on the stratigraphy and physical/mechanical properties of local soils.

To this purpose, gathering information on the spatial distribution and severity of damage suffered by existing buildings, associated with displacement rates as indicator of landslide intensity, is essential for developing reliable models, based on empirical data which, once validated, can be valuably used for damage analysis and forecasting.

In the following paragraphs, a detailed overview of the main topics related to procedures, input and output data used to building vulnerability assessment at different scales, will be discussed.

7.2 Procedure for building vulnerability analysis at small scale

As mentioned in the above paragraph, aim of small scale analysis is to assess preliminary cause-effect relationship between landslide kinematics and building damage susceptibility.

In order to characterize landslide kinematics, knowledge of landslide involved geological and geomorphological settings is required: further, it should be noted that effects induced on buildings by slope movements depend on several factors, for instance on slope gradient, typology and intensity of landslide, the prevalent component of movement where the building is located (i.e. different kinds of cracks are associated to rotational or translational deformations). To this purpose, a fundamental step in the landslide vulnerability analysis is represented by landslide inventory mapping, which usually includes location, classification, assessment of intensity, volume, state of activity, date of occurrence (if available) and other characteristics of landslides.

To this regard, remote sensing techniques can offer a valuable contribution, as it is testified by the rapidly growing number of scientific works dealing with landslide inventory mapping achieved by means of the analysis of the information gathered by either passive or active air- and space-borne sensors.

Synthetic Aperture Radar Differential Interferometry (DInSAR) technique, in particular, represents a useful tool to define landslide inventory map, providing information on temporal and spatial trends deformation both of ground surface and man-made structures within landslide-affected or -prone areas.

Generally, it is important to highlight that a thorough knowledge of landslide kinematic cannot be conveniently reached without an adequate *in situ* monitoring.

The integration of conventional and innovative monitoring techniques allows to, on one hand, obtain the most precise information on slope failures mechanisms, contributing to the definition of type, intensity, triggering factors and its temporal evolution; on the other hand, it provides for a reliable support to landslide mapping and to the update of the inventory, recognizing unstable areas in urban settlements.

At this scale of representation, to define slow-moving landslide intensity, mean velocity of displacement, obtained through DInSAR processing and confirmed by conventional *in situ* measurements, could be taken into account.

Additionally, the second step of vulnerability analysis requires the preliminary characterization of exposed elements: firstly, existing buildings on the basis of the available digital topographic map at this scale of representation (1:5000) are identified.

As mentioned in the previous chapter, the position of the structure with regard to the landslide body determines the type and extent of the expected damage: different interactions and, as a result, different levels of damage affect buildings located at the landslide boundaries, namely the scarps, flanks and toe, and buildings located within the landslide body: the latter usually move in a rigid way and, thus, the resulting damage is generally less severe than in the first case (Focardi, 1969).

Subsequently, homogeneous building aggregations, in terms of shape configuration and orientation respect to landslide movement direction are classified. Finally, building structural typology and damage severity level, via very fast field campaigns, are surveyed.

It is important to note that identification of a single building geometrical and structural characteristics is impracticable and not significant at this level of analysis.

According to the proposed approach, integrated use of following data:

- available lithological and landslide inventory maps;
- medium-high resolution DInSAR data;
- building structural typology map;
- building and facilities damage maps recorded by field survey,

allows to achieve the following main goals, as shown in Figure 7.3.

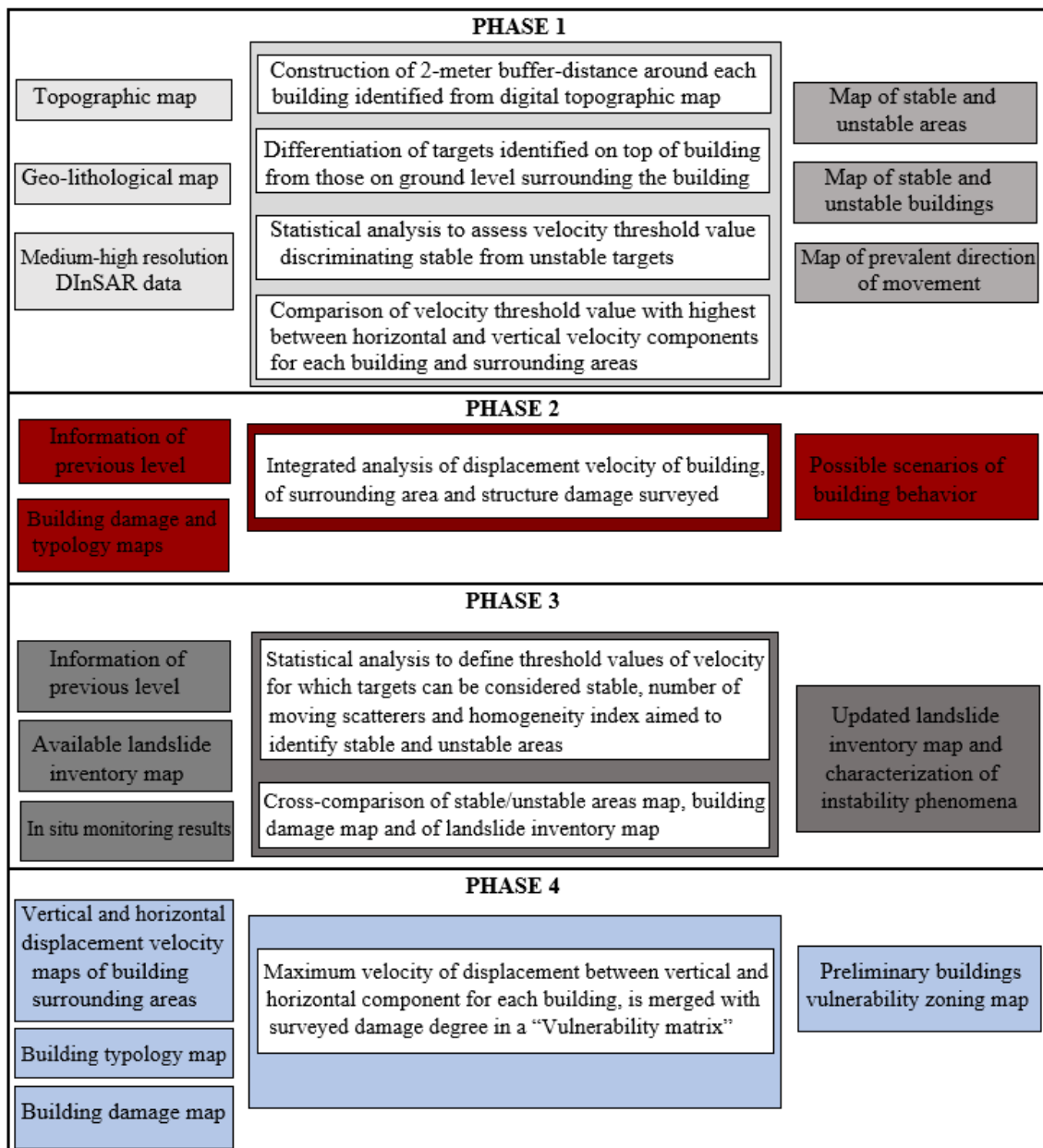


Figure 7.3 Flow chart of the analyses to be carried out at small scale of representation.

Identifying stable/unstable areas, stable/unstable buildings and prevalent direction of movement

As above mentioned, landslide intensity parameter can be defined by annual displacement rate of targets, the so called Persistent Scatterers (PS), identified through DInSAR technique on the whole urban settlement.

In order to identify the buildings affected by ground displacements and to analyze their behavior, DInSAR data at ground level and on top of buildings were preliminarily used to differentiate building aggregates and the areas/roads surrounding the buildings that are “moving” from those which are “not moving”.

To this aim, around each building identified from the available digital topographic map, a 2-m buffer-distance was considered in order to take into account spatial resolution of interferometric products and graphical error related to the working scale.

According to this assumption, it is possible to distinguish all scatterers identified on ground level near the building, from those on top of building: the first are representative of landslide intensity while the second refer to building deformation. They are differentiated by assuming that targets belonging to a building are affected by residual topographic phase (called DEM_Error) compared with Digital Elevation Model (DEM). In detail, all targets with $DEM_Error \geq 3$ m have been considered as belonging to structure.

Subsequently, a velocity threshold discriminating moving from not moving targets has been assessed: to such identification, a coefficient of variation, given by the ratio between the standard deviation and the velocity average module, for all selected scatterers, has been calculated. The threshold value determined is about 2 mm/year; it corresponds to a value for which standard deviation is higher than mean velocity value.


Moreover, the combination of interferometric data, acquired along “ascending” and “descending” tracks, allows to identify, for each building and surrounding ground, vertical and horizontal (East-West) components and prevalent direction on movement.

Finally, comparison of velocity threshold value with the highest among the horizontal or vertical velocity components, provides the distinction of “stable/unstable” building aggregates and surrounding areas and roads.

Assessment of possible scenarios of building behavior

Following to distinction between “moving/not moving” structures and surrounding areas near buildings, as indicator respectively of building response and ground movement, four possible scenarios can be identified, taking into account also building damage occurrence, as indicated in Figure 7.4.

CASES	DISPLACEMENT RATE OF BUILDING AND SURROUNDING AREA	POSSIBLE SCENARIO	BEHAVIOR OF BUILDING	
			DAMAGE OCCURRENCE	
			SI	NO
I	$V_{\text{building}} < 2 \text{ mm/yr}$ $V_{\text{ground}} < 2 \text{ mm/yr}$	Buildings and surrounding area are stable and no problems and deformation for structure	Structural problems are due to other causes	No problems to building
II	$V_{\text{building}} < 2 \text{ mm/yr}$ $V_{\text{ground}} > 2 \text{ mm/yr}$	Surrounding area is not stable with possible damage to roads and services, while buildings do not show deformations/distortions	Building damage is not induced by building deformation/distortions	Landslide induced movement do not cause damage and distortions to building
III	$V_{\text{building}} > 2 \text{ mm/yr}$ $V_{\text{ground}} < 2 \text{ mm/yr}$	Surrounding area is stable while building shows possible deformations/distortions	Building damage/deformation are due to other causes or structural problems	Building deformation are due to other causes No damage occurred
IV	$V_{\text{building}} > 2 \text{ mm/yr}$ $V_{\text{ground}} > 2 \text{ mm/yr}$	Building and surrounding area are unstable with possible damage to building, roads and services (sidewalks, sewers, etc.)	Landslide induced movement causes distortions and damage to building	Landslide induced movement causes building deformations No damage occurred



<p>$V_{\text{building}} < V_{\text{ground}}$ Foundation and building stiffness, building structural properties and geological local conditions induce a decrease of effects on superstructure</p>	<p>$V_{\text{building}} > V_{\text{ground}}$ Foundation and building stiffness, building structural properties and geological local conditions induce an increase of effects on structure (possible rotation of building)</p>
--	--

Figure 7.4 Possible scenarios and related building behavior resulting from comparison between stable and unstable targets data located on top of buildings and on surrounding area/roads.

Small scale analysis also allows to understand preliminary relationship between landslide evolution and effects on existing structures, providing a qualitative cross comparison of landslide intensity and building damage.

In detail, such procedure, through an integrated analysis of damage severity degree and landslide intensity, obtained by corresponding interferometric data in the time span preceding damage survey, can provide a cognitive basis helpful to establish empirical cause-effect relationships between ground displacement rate and damage level.

Updating of available landslide inventory map

Available landslide inventory maps need to be not only accurate but also updated on a regular basis. To this aim, DInSAR data, integrated with the information provided by geomorphological maps and with the results of an accurate damage survey to facilities, can provide an useful tool to update boundaries and state of activity of slow-moving landslides. Indeed, landslide induced damage – whether recorded – can be considered as movement indicators and, thus, can be used to validate DInSAR products: such point is more evident in urbanized areas, where the high density of identified scatterers allows to overcome any lacks of remote sensing data availability (e.g. over vegetated areas).

The proposed approach requires to carried out separately DInSAR and damage data: after, the two datasets are merged with available landslide inventory map to updated state of activity as output.

In order to compare more specifically DInSAR results with local failures and building damage, a cluster analysis of identified targets is required (Di Martire et al., 2016). Furthermore, to assess if a given cluster of scatterers can be defined as moving, following parameters for the extraction of the anomalous areas have to be assessed:

- *threshold values of velocity* define range of displacement rate for which targets can be considered stable; velocities higher or lower than a given threshold represent evidence of instability; as above mentioned, a value of ± 2 mm/yr, along vertical or horizontal direction, has been selected as threshold;
- *number of moving scatterers* within an area: more than one target showing velocities higher or lower than the threshold range is a necessary condition for the identification of anomalous area:
- *homogeneity index*, defined as the ratio between number of moving targets and total number of targets within considered area, is fixed equal to 0,2.

Once identified moving and not moving areas by DInSar data, the following step requires to integrate this result by means of field survey carrying out map of damage recorded both on buildings and on facilities.

Finally, thanks to the cross-comparison of surveyed damage and DInSAR radar-interpreted data, an updating of the existing landslide inventory map of the whole study area can be performed.

Identifying areas with different level of vulnerability

The adopted approach allows to obtain a preliminary zoning map with different vulnerability rates: firstly, for each building, maximum horizontal and vertical velocity components in the surrounding area are carried out from interferometric data, as indicator of landslide intensity. Separately, building damage survey is provided by *in situ* campaign, by using current damage classifications available in literature.

Subsequently, the two obtained datasets are merged in a qualitative vulnerability matrix, which, combining landslide intensity and building damage severity, provides information about current structural instability likelihood due to ground movements.

As mentioned by Infante et al. (2016), according to critical strength properties of masonry and reinforced concrete buildings, two matrices with different value threshold of vulnerability have been developed (Fig. 7.5).

(a)		VULNERABILITY				
		DAMAGE DEGREE OBSERVED ON MASONRY BUILDING				
LANDSLIDE INTENSITY	Maximum velocity of displacement between vertical and horizontal component for each building	NONE/ NEGLECTIBLE	LIGHT	MODERATE	SERIOUS	VERY SERIOUS/ PARTIAL COLLAPSE
		VERY LOW $V < 5$ mm/anno	VERY LOW	VERY LOW	LOW	MEDIUM
LOW $5 \text{ mm/anno} < V < 10 \text{ mm/anno}$	VERY LOW	LOW	MEDIUM	HIGH	HIGH	
MEDIUM $10 \text{ mm/anno} < V < 20 \text{ mm/anno}$	LOW	MEDIUM	MEDIUM	HIGH	VERY HIGH	
HIGH $20 \text{ mm/anno} < V < 40 \text{ mm/anno}$	MEDIUM	HIGH	HIGH	HIGH	VERY HIGH	
VERY HIGH $V > 40$ mm/anno	HIGH	HIGH	VERY HIGH	VERY HIGH	VERY HIGH	

(b)		VULNERABILITY				
		DAMAGE DEGREE OBSERVED ON REINFORCED CONCRETE BUILDING				
LANDSLIDE INTENSITY	Maximum velocity of displacement between vertical and horizontal component for each building	NONE/ NEGLECTIBLE	LIGHT	MODERATE	SERIOUS	VERY SERIOUS/ PARTIAL COLLAPSE
		VERY LOW $V < 5$ mm/anno	VERY LOW	VERY LOW	VERY LOW	LOW
LOW $5 \text{ mm/anno} < V < 10 \text{ mm/anno}$	VERY LOW	LOW	LOW	MEDIUM	MEDIUM	
MEDIUM $10 \text{ mm/anno} < V < 20 \text{ mm/anno}$	VERY LOW	LOW	MEDIUM	MEDIUM	HIGH	
HIGH $20 \text{ mm/anno} < V < 40 \text{ mm/anno}$	LOW	MEDIUM	MEDIUM	HIGH	HIGH	
VERY HIGH $V > 40$ mm/anno	MEDIUM	MEDIUM	HIGH	HIGH	VERY HIGH	

Figure 7.5 “DInSAR data- building damage” matrices for vulnerability assessment at small scale analysis: for masonry building (a) and reinforced concrete building (b) (from Infante et al., 2016).

Seven vulnerability levels, from very low to very high, have been defined, corresponding to a progressive worsening of structural conditions.

7.3 Procedure for building vulnerability analysis at medium scale

Physical vulnerability assessment at medium scale (1:25.000) provides information on spatial and temporal damage evolution of buildings, investigating also the vulnerability factors influencing performance of the structures to slow-moving landslides.

To this aim, such level of analysis requires to provide, added to information of previous level, more detailed parameters aimed to better characterize landslide phenomena and exposed elements.

At this scale of representation, in particular, stratigraphy of the study area, obtained through an integrated analysis of *in situ* monitoring data (boreholes and built-in inclinometers), allows to monitor selected slope movements identifying also the depth of slip surface. Furthermore, as to define slow-moving landslide intensity parameter, differential displacements and derivable parameters (angular distortion βw and horizontal strain βh) induced by ground movement to building foundations, have to be defined.

To this purpose, starting from Permanent Scatterers data, continuous displacement maps by geostatistical interpolation processing are generated.

Subsequently, also the parameters useful for characterization of the exposed elements have to be integrated. Such level of analysis requires to define, along with previous level data, further characteristics of buildings, such as geometrical properties (number of stories, typology of construction (isolated or aggregated and position of each structure in a buildings aggregate).

Below, the main goals of this analysis are discussed, as shown in Figure 7.6.

	Vulnerability analysis at medium scale	Approach Semi-Quantitative and empirical
Input	Procedure	Output
	PHASE 1	
<div style="border: 1px solid black; padding: 2px; margin-bottom: 5px;">Information used in the small scale analysis</div> <div style="border: 1px solid black; padding: 2px;">Building geometrical data</div>	<div style="border: 2px solid orange; padding: 5px;">Angular distortion and horizontal strain occurred to building foundation, and damage degree are merged in a “Vulnerability matrix” (Dealing with slow-moving landslides, distortions are assessed during a time span of 5 years)</div>	<div style="border: 1px solid black; padding: 2px; background-color: #f4a460;">Buildings vulnerability zoning map</div>
	PHASE 2	
<div style="border: 1px solid black; padding: 2px; background-color: #800000; color: white; margin-bottom: 5px;">Information of previous level</div> <div style="border: 1px solid black; padding: 2px; background-color: #800000; color: white; margin-bottom: 5px;">Building damage map in two different historical moments</div> <div style="border: 1px solid black; padding: 2px; background-color: #800000; color: white;">Building characteristics</div>	<div style="border: 2px solid darkred; padding: 5px; margin-bottom: 5px;">Relationship between the increase of building damage level obtained by two different historical surveys and distortions occurred in the time elapsed</div> <div style="border: 2px solid darkred; padding: 5px;">Possibility to take into account building construction characteristics (structural typology, building isolated or in aggregate, number of stories, foundation typology)</div>	<div style="border: 1px solid black; padding: 2px; background-color: #800000; color: white;">Empirical fragility curves for different building typologies and parameters</div>
	PHASE 3	
<div style="border: 1px solid black; padding: 2px; background-color: #808080; color: white; margin-bottom: 5px;">Information of previous level</div> <div style="border: 1px solid black; padding: 2px; background-color: #808080; color: white;">In situ monitoring results</div>	<div style="border: 2px solid gray; padding: 5px; margin-bottom: 5px;">Analysis of temporal evolution of landslides within affected area and forecasting of possible future scenarios of ground deformations</div> <div style="border: 2px solid gray; padding: 5px; background-color: #808080; color: white;">Assessment of building damage future condition by means of empirical fragility curves</div>	<div style="border: 1px solid black; padding: 2px; background-color: #808080; color: white;">Map of buildings future damage likelihood for different scenarios of landslide intensity</div>

Figure 7.6 Flow chart of analyses to be carried out at medium scale of representation.

Identifying areas with different degree of vulnerability at more detailed level

Such analysis, more detailed than in the previous scales of representation, allows to define a vulnerability zoning map, useful for cause-effect qualitative correspondence identification. In detail, building damage surveys provide information about the temporal and spatial evolution of building damage degree. Furthermore, analysis of corresponding differential displacements occurred for each building in the time span preceding each damage survey, allows to find a preliminary relationship between landslide intensity and damage severity level.

Dealing with slow-moving landslides which induce low annual distortion rates on building foundations, a time span of five years between each survey can be considered.

Anyway, a shorter period could be considered, if higher annual deformation rates, induced by landslide movement, occur.

Aimed to assess building vulnerability in a safety conditions, it is important to evaluate maximum angular distortion β_w and horizontal strain β_h , between distortions occurred along façades of each building within study area in the analyzed time span.

Angular distortion β_w can be evaluated as:

$$\beta_{w(i,j)} = |\delta_{w(i,j)}| / L_{(i,j)} \quad (\text{eq. 7.1})$$

where $\delta_{w(i,j)}$ is the differential settlement occurred between two corners of a façade and L is the façade length;

Horizontal strain β_h can be evaluated as:

$$\beta_{h(i,j)} = \delta_{h(i,j)} / L_{(i,j)} \quad (\text{eq. 7.2})$$

where $\delta_{h(i,j)}$ is the differential horizontal displacement occurred between two corners of a façade and L is the façade length.

Two “qualitative” vulnerability matrices, distinguishing buildings in terms of structural typology (masonry and reinforced concrete buildings), have been defined, as shown in Figures 7.7 and 7.8.

As is possible to note in Figure 7.9, threshold values of angular distortions and horizontal strain, as indicators of landslide intensity, are defined according to vulnerability domains based-approach proposed by Boscardin & Cording (1989), which provide damage categories as function of these parameters.

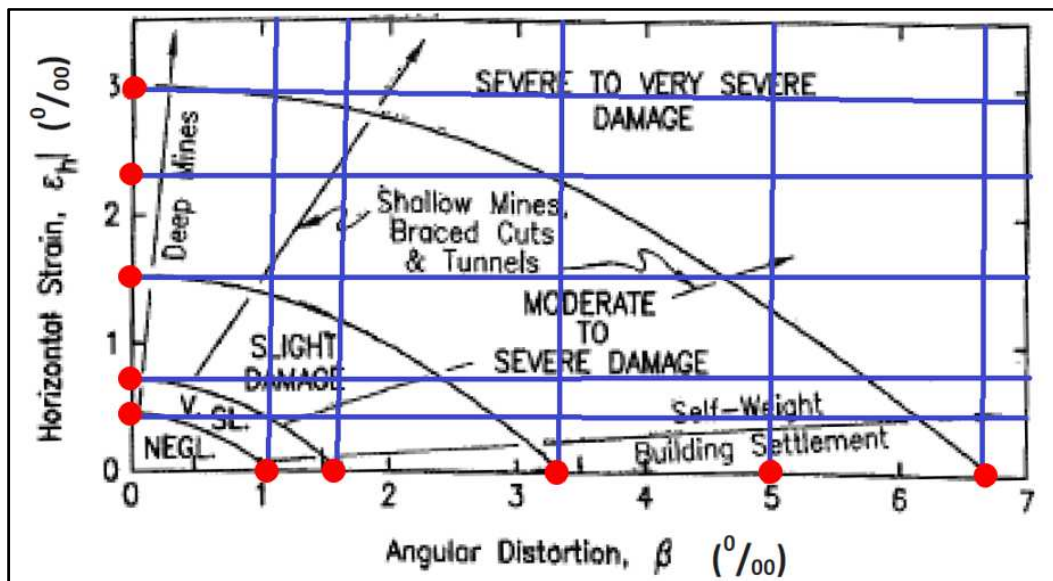


Figure 7.9 Threshold values (red circles) of proposed vulnerability matrices, obtained by Boscardin & Cording (1989) approach.

LANDSLIDE INTENSITY		VULNERABILITY					
		DAMAGE DEGREE OBSERVED ON MASONRY BUILDING					
β_h (‰)	β_w (‰)	None	Negligible	Light	Moderate	Serious	Very serious
< 0,45	<1	Very-low	Very-low	Low	Low	Medium	Medium
< 0,45	1 - 1,5	Very-low	Low	Low	Low	Medium	Medium
< 0,45	1,5 - 3,35	Low	Low	Medium	Medium	Medium	High
< 0,45	3,35 - 5	Low	Low	Medium	Medium	High	High
< 0,45	5 - 6,8	Medium	Medium	Medium	High	High	Very high
< 0,45	> 6,8	Medium	Medium	High	High	Very high	Very high
0,45 - 0,70	<1	Very-low	Low	Low	Low	Medium	Medium
0,45 - 0,70	1 - 1,5	Low	Low	Low	Medium	Medium	High
0,45 - 0,70	1,5 - 3,35	Low	Low	Medium	Medium	High	High
0,45 - 0,70	3,35 - 5	Low	Medium	Medium	High	High	Very high
0,45 - 0,70	5 - 6,8	Medium	Medium	High	High	Very high	Very high
0,45 - 0,70	> 6,8	Medium	High	High	Very high	Very high	Extreme
0,70 - 1,50	<1	Low	Low	Low	Medium	Medium	High
0,70 - 1,50	1 - 1,5	Low	Low	Medium	Medium	High	High
0,70 - 1,50	1,5 - 3,35	Low	Medium	Medium	High	High	Very high
0,70 - 1,50	3,35 - 5	Medium	Medium	High	High	Very high	Very high
0,70 - 1,50	5 - 6,8	Medium	High	High	Very high	Very high	Extreme
0,70 - 1,50	> 6,8	High	High	Very high	Very high	Extreme	Extreme
1,50 - 2,30	<1	Low	Low	Medium	Medium	High	High
1,50 - 2,30	1 - 1,5	Low	Medium	Medium	High	High	High
1,50 - 2,30	1,5 - 3,35	Medium	Medium	High	High	Very high	Very high
1,50 - 2,30	3,35 - 5	Medium	High	High	Very high	Very high	Very high
1,50 - 2,30	5 - 6,8	High	High	Very high	Very high	Extreme	Extreme
1,50 - 2,30	> 6,8	High	High	Very high	Very high	Extreme	Extreme
2,30 - 3,00	<1	Medium	Medium	Medium	High	High	Very high
2,30 - 3,00	1 - 1,5	Medium	Medium	High	High	Very high	Very high
2,30 - 3,00	1,5 - 3,35	Medium	High	High	Very high	Very high	Very high
2,30 - 3,00	3,35 - 5	High	High	Very high	Very high	Very high	Extreme
2,30 - 3,00	5 - 6,8	High	Very high	Very high	Very high	Extreme	Extreme
2,30 - 3,00	> 6,8	Very high	Very high	Very high	Extreme	Extreme	Extreme
> 3	<1	Medium	Medium	High	High	Very high	Very high
> 3	1 - 1,5	Medium	High	High	Very high	Very high	Very high
> 3	1,5 - 3,35	High	High	Very high	Very high	Very high	Extreme
> 3	3,35 - 5	High	Very high	Very high	Very high	Extreme	Extreme
> 3	5 - 6,8	Very high	Very high	Very high	Extreme	Extreme	Extreme
> 3	> 6,8	Very high	Very high	Extreme	Extreme	Extreme	Extreme

Figure 7.7 “DInSAR data- building damage” matrix for vulnerability assessment of masonry building at medium scale analysis.

LANDSLIDE INTENSITY		VULNERABILITY					
		DAMAGE DEGREE OBSERVED ON REINFORCED CONCRETE BUILDING					
β_h (%)	β_w (%)	None	Negligible	Light	Moderate	Serious	Very serious
< 0,45	<1	Very-low	Very-low	Low	Low	Medium	Medium
< 0,45	1 - 1,5	Very-low	Very-low	Low	Low	Medium	Medium
< 0,45	1,5 - 3,35	Low	Low	Low	Medium	Medium	High
< 0,45	3,35 - 5	Low	Low	Medium	Medium	High	High
< 0,45	5 - 6,8	Medium	Medium	Medium	High	High	High
< 0,45	> 6,8	Medium	Medium	High	High	High	Very high
0,45 - 0,70	<1	Very-low	Very-low	Low	Low	Medium	Medium
0,45 - 0,70	1 - 1,5	Very-low	Low	Low	Low	Medium	Medium
0,45 - 0,70	1,5 - 3,35	Low	Low	Medium	Medium	High	High
0,45 - 0,70	3,35 - 5	Low	Low	Medium	Medium	High	High
0,45 - 0,70	5 - 6,8	Medium	Medium	High	High	High	Very high
0,45 - 0,70	> 6,8	Medium	Medium	High	High	Very high	Very high
0,70 - 1,50	<1	Very-low	Low	Low	Low	Medium	Medium
0,70 - 1,50	1 - 1,5	Low	Low	Low	Medium	Medium	High
0,70 - 1,50	1,5 - 3,35	Low	Low	Medium	Medium	High	High
0,70 - 1,50	3,35 - 5	Low	Medium	Medium	High	High	Very high
0,70 - 1,50	5 - 6,8	Medium	Medium	High	High	Very high	Very high
0,70 - 1,50	> 6,8	Medium	High	High	Very high	Very high	Very high
1,50 - 2,30	<1	Low	Low	Low	Medium	Medium	High
1,50 - 2,30	1 - 1,5	Low	Low	Medium	Medium	High	High
1,50 - 2,30	1,5 - 3,35	Low	Medium	Medium	High	High	Very high
1,50 - 2,30	3,35 - 5	Medium	Medium	High	High	Very high	Very high
1,50 - 2,30	5 - 6,8	Medium	High	High	Very high	Very high	Very high
1,50 - 2,30	> 6,8	High	High	Very high	Very high	Very high	Extreme
2,30 - 3,00	<1	Low	Low	Medium	Medium	High	High
2,30 - 3,00	1 - 1,5	Low	Medium	Medium	High	High	Very high
2,30 - 3,00	1,5 - 3,35	Medium	Medium	High	High	Very high	Very high
2,30 - 3,00	3,35 - 5	Medium	High	High	Very high	Very high	Very high
2,30 - 3,00	5 - 6,8	High	High	Very high	Very high	Very high	Extreme
2,30 - 3,00	> 6,8	High	Very high	Very high	Very high	Extreme	Extreme
> 3	<1	Low	Medium	Medium	High	High	High
> 3	1 - 1,5	Medium	Medium	High	High	High	Very high
> 3	1,5 - 3,35	Medium	High	High	High	Very high	Very high
> 3	3,35 - 5	High	High	High	Very high	Very high	Extreme
> 3	5 - 6,8	High	High	Very high	Very high	Extreme	Extreme
> 3	> 6,8	High	Very high	Very high	Extreme	Extreme	Extreme

Figure 7.8 “DInSAR data- building damage” matrix for vulnerability assessment of reinforced concrete building at medium scale analysis.

Vulnerability levels are defined according to critical strength properties and foundation typology of masonry and reinforced concrete buildings.

As mentioned in the previous Chapter, building performance to static forces induced by ground movements depend also on foundation typology: with reference to local soil conditions and to age of construction, they are different in the two typologies of structures.

Reinforced concrete buildings have usually shallow foundations, such as individual footings, isolated or connected by beams, and raft foundation used when building loads have to be spread over a large area.

Load-bearing masonry building, instead, show strip footings, as a long masonry strip that supports the weight of an entire wall. These footings are used where the building loads are carried by entire walls rather than isolated columns, such as in older buildings made of masonry.

Furthermore, some buildings have pile foundations: when there is a layer of weak soil at the surface and it cannot support the weight of the building, or in a landslide-affected area, loads of building have to bypass this soil layer and to be transferred to stronger soil or rock that is below the weak layer.

Depending on stiffness foundation, masonry and reinforced concrete buildings can have different structural behavior: high stiffness of connected footings or raft in reinforced concrete buildings allows to decrease landslide-induced effects on superstructure more than masonry strip footing.

With reference to mechanical properties of material, for very low values of applied distortions both structure typologies show a similar structural behavior, while for higher differential displacements it is very different. Masonry buildings, in particular, are characterized by damage susceptibility to horizontal strains highest than angular distortions, depending on high critical values of vertical strain and very low critical values of horizontal extension strain.

Reinforced concrete buildings, instead, are more susceptible to high values of differential settlement.

Assessment of relationship between landslide intensity and worsening of damage level

Damage surveys carried out in different times allow to provide information about temporal and spatial evolution of building damage degree. Furthermore, analysis of corresponding differential displacements and derivable parameters occurred for each building in the time span elapsed between two damage surveys, allows to find a preliminary relationship between landslide intensity and the worsening of damage severity level.

In detail, such procedure is developed as follows:

- *in situ* surveys to assess the typology and damage severity degree for each building in different historical moments and evaluation of progressive worsening;
- analysis of corresponding interferometric data and assessment of maximum distortions (angular distortion and horizontal strain) occurred to each building in the time span between two surveys;
- generation of empirical fragility curves by combining the increase of damage level with the corresponding change of magnitudes intensity parameter exhibited by each building.

In detail, empirical fragility curves allow to obtain a preliminary analysis of the relationship between the worsening of damage degree and the distortions occurred to building foundation.

To this purpose, they provide the conditional probability for a given building of reaching or exceeding a certain increase of damage severity level as a function of landslide-induced distortions (Eq. 7.3).

$$P(\Delta D \geq \Delta Di | x) = \Phi \left[\frac{1}{\beta} \ln \left(\frac{x}{\bar{x}} \right) \right] \quad (\text{eq. 7.3})$$

where:

- x is the adopted landslide parameter (angular distortion βw or horizontal strain βh);
- $\Phi[\]$ is the standard normal cumulative distribution function;
- \bar{x} is the median value of x at which the building reaches each increase of damage level;
- β is the standard deviation of the natural logarithm of x for each damage degree.

Firstly, fragility curves can be obtained considering separately angular distortions and horizontal strain effects, and subsequently combined according to “Probability Theory” in order to take into account that they can occur together under building foundation.

Furthermore, the availability of building characteristics datasets got by *in situ* survey of the whole urban setting, allows to obtain empirical fragility curves distinguished for different vulnerability factors, so analyzing their influence on performance and behavior of structures to slow-moving landslide-induced movements.

Forecasting of future damage conditions of whole urban settlement

At medium scale of analysis, empirical fragility curves can be useful to forecast spatial and temporal evolution of buildings damage with reference to the whole territory of study area.

Under the assumption that building distortions are the representative landslide intensity parameter causing damage of different severity to single buildings, different future scenarios can be forecast. Dealing with very slow and slow-moving landslides, in turn characterized by low and almost constant values of annual distortion rate, it is possible to forecast future buildings deformation rates induced by ground instability, although a more detailed analysis to assess relationship between rainfall-triggering and landslide accelerations is required.

Starting from future scenarios of building distortions, empirical fragility curves provide, for each building, the probability to obtain an increase of one damage level compared with current degree.

As above mentioned, empirical fragility curves are obtained under the assumption that angular distortions and horizontal strain effects occur separately on each building; subsequently, theoretical elements of Probability Theory allow to combine them in order to take into account that vertical and horizontal distortions are concurrent under building foundations.

The overlap of two effects can be obtained by considering them as *mutually exclusive* events. Two events are mutually exclusive or disjointed if they cannot both occur and the occurrence of any one of them implies the non-occurrence of the remaining.

In detail, total probability for a given building of reaching an increase of one damage severity level, due to both angular and horizontal distortions, can be evaluated as follow:

$$P[\Delta D = 1, (\beta_w \text{ and } \beta_h)] = P_1 + P_2 \quad (\text{eq. 7.4})$$

where:

- P_1 is the probability that β_w causes an increase of one level of damage while the effect of β_h does not increase damage level;

$$P_1 = P[(\Delta D, \beta_w) = 1; (\Delta D, \beta_h) = 0] = P[(\Delta D, \beta_w) = 1] \times P[(\Delta D, \beta_h) = 0] \quad (\text{eq. 7.5})$$

- P_2 is the probability that β_h causes an increase of one level of damage while the effect of β_w does not increase damage level.

$$P_2 = P[(\Delta D, \beta_w) = 0; (\Delta D, \beta_h) = 1] = P[(\Delta D, \beta_w) = 0] \times P[(\Delta D, \beta_h) = 1] \quad (\text{eq. 7.6})$$

obtaining in conclusion:

$$P[\Delta D=1, (\beta_w, \beta_h)] = P[(\Delta D, \beta_w) = 1] \times P[(\Delta D, \beta_h) = 0] + P[(\Delta D, \beta_w) = 0] \times P[(\Delta D, \beta_h) = 1] \quad (\text{eq. 7.7})$$

As for the analysis at medium scale, the preliminary forecasting of different possible scenarios of exposed elements deformations allows to define for each building, through the above mentioned semi-quantitative fragility curves, the probability of reaching an increase of damage severity level starting from current condition, thus confirming that this approach can be helpful for authorities responsible of land management in order to focus their attention and mitigation activities on most susceptible buildings for what concerns movement-related consequences.

7.4 Procedure for building vulnerability analysis at a detailed scale

Vulnerability analysis at small and medium scale does not take into account structural properties of buildings, such as type of material and its mechanical parameters, typology of foundations and soil geotechnical properties. Such characteristics, in fact, are not significant at these levels of representation. Detail scale analyses, carried out on a single building or buildings aggregate, follow a different methodological approach. Aim of the study is to define, by analytical or numerical analyses, the relationship between landslide intensity and expected damage degree.

At this scale of representation, to define slow-moving landslide intensity parameter, annual cumulative displacement profile along façades of building can be taken into account. Subsequently, starting from such data maximum annual distortion rate is assessed.

Furthermore, the availability of *in situ* monitoring instruments, such as borehole, allows to define stratigraphic column of soil under each building, its geotechnical parameters and stiffness, useful to fully characterize soil condition.

Characterization of buildings computational model requires a detailed geometrical and structural survey. To this purpose, as mentioned in the Chapter 6, the scheme provided by the Italian Department of Civil Protection (DPC), can be a helpful tool to obtain an objective technique of building survey.

Two different approaches to forecast future conditions of damage and local failures of a building have been developed, each one characterized by its own peculiarity, assumptions, pros and cons, and obviously with differences in the final results, as shown in Figure 7.10.

Vulnerability analysis a detailed scale		Approach Quantitative Analytical or numerical
Input	Procedure	Output
	PHASE 1	
Information used in the medium scale analysis	Building is simplified as an elastic rectangular beam	3D fragility curve providing probability of exceeding a damage level as function of landslide intensity (angular distortion and horizontal strain)
Mechanical properties of building material	Angular distortions and horizontal strains applied to equivalent beam allow to assess the maximum between bending and shear strain	
	This value is compared with limit tensile strain to identify damage level corresponding to occurred distortions.	
	Future evolution of building distortions can be forecast by evaluating an average value of historical measured distortions	
	Interpolation in a numerical software of building distortions, occurred and future, and damage degree correspondent to obtained tensile strain	
	PHASE 2	
Information of previous level	Implementation of building computational model in a numerical software	Vulnerability domains as function of angular distortion β_w and horizontal strain β_h
Detailed building geometrical and structural parameters	Execution of non-linear static analyses, applying progressively horizontal strains and angular distortions to numerical model	
Geotechnical soil characteristics	Assessment of damage degree correspondent to each pair of applied damage distortions	
	Interpolation of points characterized by same damage degree	
	PHASE 3	
Information of previous level	Analysis of possible future scenarios of ground deformations and assessment, by structural analysis, temporal evolution of damage condition	Forecast of when total collapse will occur

Figure 7.10 Flow chart of analyses to be carried out at detailed scale of representation.

Analytical approach: the “Laminated Beam” Model

The laminated beam model by Burland & Wroth (1974) simplifies a structure by considering only its major features, adequately representing the response of ground movements. In this model, the building is represented by an elastic rectangular deep beam (Fig. 7.11), the foundation of which is assumed to follow a given displacements profile. Burland & Wroth considered two possible modes of deformation: bending and shear. In the first case, cracks are due to tensile strains ε_b close to the beam edge in tension, whereas in the second case the cracks are related to the tensile strain ε_d caused by shear deformations.

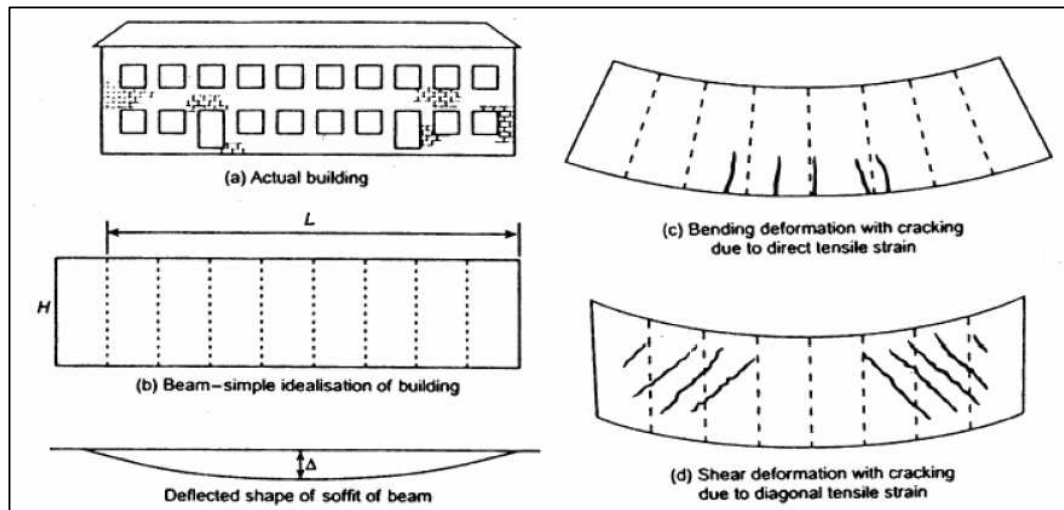


Figure 7.11 The equivalent beam approach (from Burland & Wroth, 1974).

The authors use results by Timoshenko theory (1955) and obtain expressions relating the deflection ratio Δ/L of a midpoint loaded beam with the maximum bending strain ε_{bmax} and the maximum shear strain ε_{dmax} ,

$$\frac{\Delta}{L} = \left(\frac{L}{12h} + \frac{3I}{2hLH} \frac{E}{G} \right) \varepsilon_{bmax} \tag{eq. 7.8}$$

$$\frac{\Delta}{L} = \left(1 + \frac{HL^2}{18I} \frac{G}{E} \right) \varepsilon_{dmax} \tag{eq. 7.9}$$

where h is the distance to the neutral axis from the edge of the beam in tension, which usually is chosen as $h = H$ for a building under hogging (neutral axis at the bottom edge) and $h = H/2$ for a building under sagging (neutral axis in the middle).

For a given deflection ratio, an estimation of the maximum tensile strain in the building can be obtained as the maximum of the values $\varepsilon_{d\max}$, $\varepsilon_{b\max}$ provided by Equations 7.8 and 7.9.

Later, Boscardin & Cording (1989) incorporated in their analysis the effect of the horizontal strains ε_h that can be induced in the foundations of the building. They directly superposed this effect to Burland & Wroth's (1974) bending and shear strains.

The incorporation of horizontal strains leads to the expressions:

$$\varepsilon_{br} = \varepsilon_{b\max} + \varepsilon_h \quad (\text{eq. 7.10})$$

$$\varepsilon_{dr} = \frac{1-\nu}{2} \varepsilon_h + \sqrt{\varepsilon_h^2 \left(\frac{1+\nu}{2} \right)^2 + \varepsilon_{d\max}^2} \quad (\text{eq. 7.11})$$

and in this case the maximum tensile strain in the building is given by the maximum between ε_{dr} and ε_{br} .

Application of this approach requires to assess constitutive properties of building, such as the length L , height H , Young modulus E , shear modulus G and Poisson's ratio ν of constructive material.

The value of the maximum tensile strain obtained from Equations (7.10) or (7.11) allows to identify damage level of building according to Table 7.1. Categories 0, 1 and 2 relate to aesthetic damage, categories 3 and 4 relate to serviceability damage and category 5 corresponds to damage affecting structural stability.

Category of damage	Degree of severity	Cracks	Limiting tensile strain, ε_{crit} (%)
0	Negligible	>0.1 mm	0 – 0.05
1	Very Slight	0.1 – 1 mm	0.05 – 0.075
2	Slight	1 – 5 mm	0.075 – 0.15
3	Moderate	5 – 15 mm or several > 3 mm	0.15 – 0.3
4 to 5	Severe	> 15 mm	> 0.3

Table 7.1 Level of damage and limit tensile strain (after Boscardin & Cording, 1989).

After schematizing each building as an equivalent elastic beam, the proposed approach, by using angular and horizontal occurred distortions recorded during every year by means of historical DInSAR data, provides temporal evolution of damage severity level.

Comparison of this result with real damage degree obtained by *in situ* survey allows to test and confirm the model.

Subsequently, an average value of historical measured distortions (angular and horizontal), is evaluated and under the assumption that future deformations occur following these rates, temporal evolution of building distortions can be forecasted.

Furthermore, according to above mentioned method, also temporal evolution of limit tensile strain and of damage degree can be assessed.

Finally, by considering the following datasets:

- damage severity degree corresponding to maximum tensile strain;
- building distortions,

their interpolation in a numerical software, such as MATLAB, allows to define a “3D Fragility Curve” which provides the probability of exceeding a damage level as function of the two intensity parameters (angular and horizontal strains).

The quantitative results of this approach should be carefully considered, being obtained for a specific structure with an analytical model able to partially recreate realistic building features; furthermore, numerical interpolation analysis of distortions, developed in MATLAB software, although requires time-consuming, is more detailed than theoretical probability concepts mentioned in the previous paragraph.

Numerical approach: a “3D Building Computational” Model

The laminated beam model simplifies a structure by considering only its major features, adequately representing the response of ground movements. The application of equations 7.10 and 7.11 in this model is based on a series of hypotheses. It is assumed that the maximum tensile strain is insensitive to the form of loading, so that the expressions for the deflection ratio of a centrally loaded beam can be used in general.

In addition, it is necessary to assume an independent decision about the position of the neutral axis in each part of the building; moreover, considering a building schematized as a linear beam along a single façade, it does not take into account three-dimensional behaviour of structures. For this reason, occurrence and location of cracks and local failures cannot be investigated.

The equivalent beam approach has been widely used, but, sometimes, the hypothesis and considerations just mentioned makes its application in practice somewhat uncertain.

Aimed to overcome these constraints, a soil-structure model of building is created using numerical software and subsequently structural analysis on buildings computational model has to be performed.

In detail, such approach is developed through following steps:

- characterization of building computational model through a detailed geometrical and structural building survey;
- implementation of building computational model in a numerical software;
- execution of non-linear static analyses applying progressively horizontal strains and angular distortions to the numerical model, in agreement with historical DInSAR data;
- assessment of damage degree corresponding to each pair of applied damage distortions βw and βh ;
- generation of vulnerability domains, as a function of the angular distortion βw and of the horizontal strain βh , interpolating the points derived from the analysis and characterized by the same damage degree.

The adopted procedure to correlate damage level to the above mentioned deformation parameters can be derived by several studies available in literature to assess earthquake induced-effects. Damage limit states were correlated to maximum inter-storey drift (ISDR): thresholds values were determined on the basis of the pushover curve according to the relations proposed by the RISK-UE project (Milutinovic and Trendafiloski, 2003). These relations provide a correlation between yield d_y and ultimate d_u displacement in the pushover curve and the EMS-98 (Grunthal, 1998) damage scale.

Damage state		Drift limit	Spectral displacement limit
DS1	No damage	$\Delta < 0.7\Delta_y$	$D < 0.7D_y$
DS2	Slight	$0.7\Delta_y < \Delta < 0.7\Delta_y + 0.05\Delta_{uy}$	$0.7D_y < D < D_y$
DS3	Moderate	$0.7\Delta_y + 0.05\Delta_{uy} < \Delta < 0.7\Delta_y + 0.2\Delta_{uy}$	$D_y < D < D_y + D_{uy}$
DS4	Extensive	$0.7\Delta_y + 0.2\Delta_{uy} < \Delta < 0.7\Delta_y + 0.5\Delta_{uy}$	$D_y + D_{uy} < D < D_u$
DS5	Very heavy	$0.7\Delta_y + 0.5\Delta_{uy} < \Delta < 0.7\Delta_y + \Delta_{uy}$	$D_u < D$
<i>With: $\Delta_{uy} = 0.9\Delta_u - 0.7\Delta_y$ and $D_{uy} = 0.25(D_u - D_y)$</i>			

Table 7.2 Damage state definitions and drift limit according to RISK-UE project (from Milutinovic and Trendafiloski, 2003).

According to some examples available in literature (Negulescu et al., 2014; Tan et al., 2014), inter-storey drift ratios threshold values for each damage state considered in this work are provided in the Tables 7.3 and 7.4, for reinforced concrete and masonry buildings, respectively.

Damage Limits State (DS)	ISDR (%)
No damage (DS1)	< 0,4
Slight (DS2)	0,4
Moderate (DS3)	0,64
Extensive (DS4)	1,6
Very heavy (DS5)	4,0

Table 7.3 Thresholds values of ISDR of damage limits states for reinforced concrete buildings.

Damage Limits State (LS)	ISDR (%)
No damage (DS1)	< 0,3
Slight (DS2)	0,3
Moderate (DS3)	0,4
Extensive (DS4)	0,6
Very heavy (DS5)	1,19

Table 7.4 Thresholds values of ISDR of damage limits states for masonry buildings.

Several numerical analyses performed on a test sample building allowed to provide a new approach to assess damage degree correspondent to each pair of distortions β_w - β_h on masonry buildings, as function of number of masonry walls which overall reach a breaking or plasticity final condition (Table 7.5) (modified after Infante et al., 2016).

The following threshold values have been obtained by cross-comparison with threshold values of ISDR indicated in Table 7.4.

Number of masonry walls which reach a breaking or plasticity condition [%]	Damage Limits State (assessed on building computational model)
< 20	Negligible
20-35	Light
35-60	Moderate
60-85	Extensive
>85	Very heavy

Table 7.5 Proposed approach to assess damage degree in a computational model of masonry buildings (modified after Infante et al., 2016).

Vulnerability domains, function of angular distortion β_w and horizontal strain β_h , provide the threshold values for which predetermined damage categories occur. The overcoming of these domains entails a progressive worsening of damage degree.

This procedure works perfectly for the intact structure, but should be adapted for previously damaged structures, since results are affected by a initial drift $(ISDR)_0$ due to ground displacement occurred in the past. To take into account existing damage level, the ISDR values (or number of walls broken and plasticized) obtained by numerical analysis on no-damaged structure, have to be added to $(ISDR)_0$ corresponding to current damage state surveyed by *in situ* campaign.

Finally, the availability of historical DInSAR data allows to forecast future displacement profiles to apply to building foundations, by considering an average value of annual distortion rate: their implementation in a computational model allows to provide information on future conditions of damage and local failures of buildings, also identifying when and for which displacements total collapse could occur.

In the following chapter, the proposed methodology has been applied in order to investigate, at different level of detail, buildings vulnerability of Moio della Civitella urban setting, in Salerno Province (Italy), whose territory is affected by several slow-moving intermittent landslides. Geological and geomorphological settings and available landslide inventory map have been preliminarily analyzed to understand the main factors predisposing instability phenomena at Moio della Civitella.

CHAPTER 8

CASE STUDY: MULTI-LEVEL VULNERABILITY ANALYSIS OF MOIO DELLA CIVITELLA (SA) URBAN SETTLEMENT

8.1 Geographical setting

Moio della Civitella, whose first settlement dates back to VI – IV century BC, is a small village, located in the Cilento, Vallo di Diano and Alburni National Park, in Salerno Province, southern Campania region (Fig. 8.1).

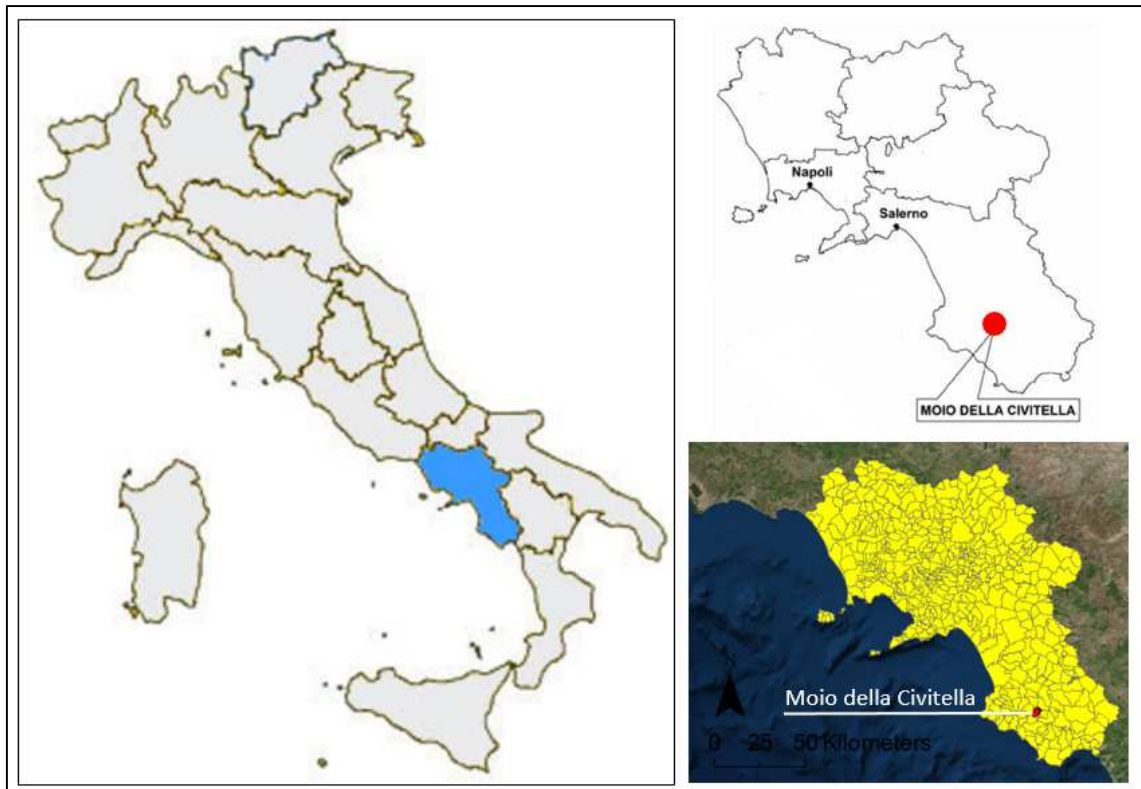


Figure 8.1 Location of Moio della Civitella, Salerno Province, southern Campania region.

Moio della Civitella, counting over 1.900 inhabitants and covering a surface of 17,19 km², is composed by two urban settings, Moio and Pellare situated on the slope of the Civitella mountain (818 m a.s.l.) (Fig. 8.2), and borders with the municipalities of Campora, Cannalonga, Gioi, and Vallo della Lucania.

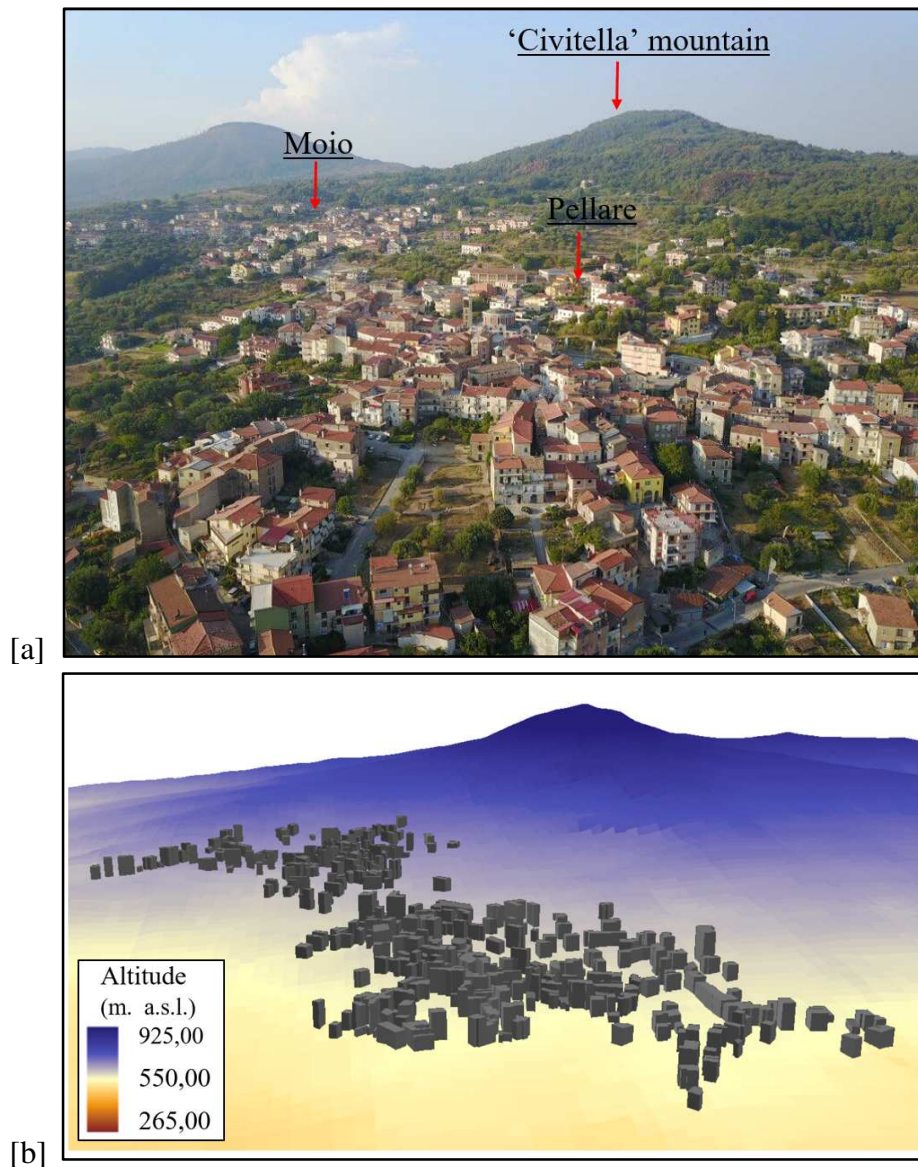


Figure 8.2 Panoramic view of Moio della Civitella urban centre: optical image (a) and 3d model (b).

The study area is one of the most interesting in the Campania region, combining peculiar geological characteristics with valuable natural resources and different lithologic, structural, hydrogeologic and geomorphologic settings.

Moio della Civitella urban settlement has been selected as case study according to the aims of the “TELLUS” (TELErilevamento Laboratori Unità di Supporto) regional project (2009), that was implemented in the framework of the “PODIS” (Progetto Operativo Difesa Suolo) project, funded by the European Union and aimed at providing technical support to the Department of Soil Defense – Campania Region, for landslide investigations at regional scale by means of satellite images and geological and geomorphological surveys.

8.2 Geological setting

The Southern Apennines constitute a sector of an East-verging thrust-fold system extending NW–SE along the Italian peninsula. The current tectonic setting of the area (Fig. 8.3) originated from two major deformation phases, the first one being a mainly compressive Miocene tectonics, resulting in crustal thickening and major uplift (Del Gaudio & Wasowski, 2004). Later on, the Quaternary extensional tectonics produced most of what is the present morpho-structural setting of the area, shaped mainly during the last lower Pliocene–Quaternary events (Aprile et al., 1979; Cinque et al., 1993).

The tectonic extension is still ongoing as demonstrated by the frequent earthquakes occurring along the Chain as well as by the intense volcanic activity of the Tyrrhenian Campania Region.

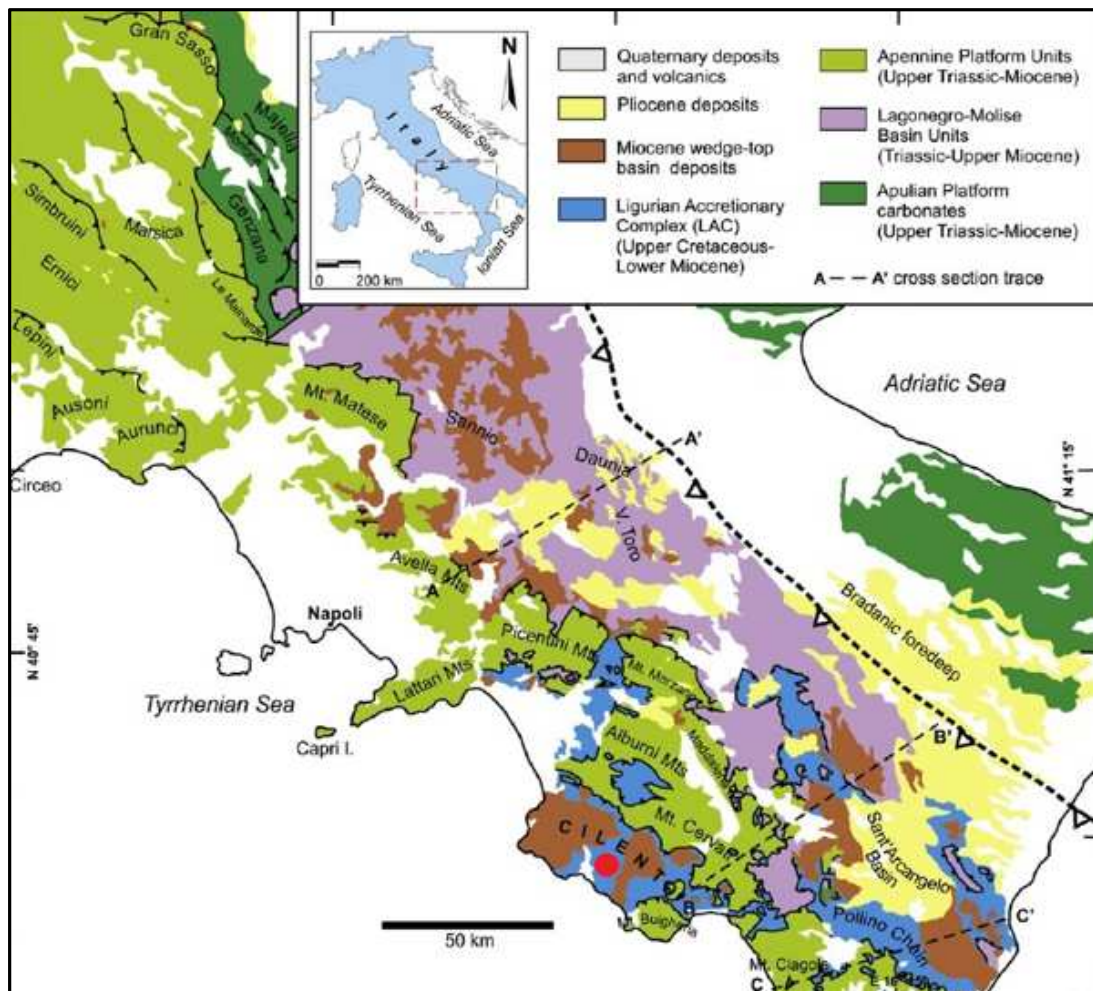


Figure 8.3 Tectonic map of the Southern Apennines of Italian peninsula (modified from Bonardi et al., 1988).

The main factors predisposing instability at Moio della Civitella are the local stratigraphy and morphology. The area is geologically characterized by the presence of the Crete Nere-Saraceno Formation (Bonardi et al., 1988), a structurally complex formation, Cenozoic in age, belonging to the North Calabrian Unit.

The formation is mainly made up of argillites with intercalated carbonate and silico-clastic arenites, often weathered at the outcrop. Upslope (near “La Civitella” hill) the Pollica Arenites formation crops out; it is made up by thin-bedded lithic and arenites and silty argillites with thick conglomerate layers. Downslope the Centola Conglomerates crop out formed by silty-sandy matrix-supported conglomerates.

These materials are defined in the literature as “Structurally Complex Formations” (Esu, 1977), and can be distinguished in three main groups (A, B and C): the first one is constituted by lithologically homogeneous materials, while the second one by heterogeneous material made up of at least two soils with different mechanical characteristics. Further, depending on the geologic structure, the following types of material can be identified in both the A and B groups (Fig. 7.4): a1) fissured and/or fractured clays (or argillites), and a2) scaly clays (or argillites); b1) regular alternance of rock and fissured and/or fractured clays (or argillites), b2) chaotic setting of rock strata and highly fissured/fractured or scaly clays (or argillites), and, eventually, b3) scaly clays (or argillites) produced as effect of tectonics, which include rocks.

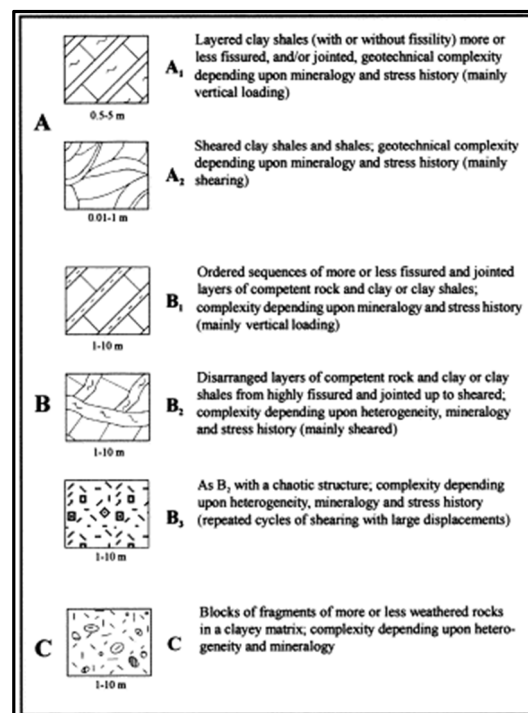


Figure 8.4 Complex structurally formations (after Esu, 1977).

The terrain in the study area, showing the typical features of the highly tectonized rocks of the southern Italian Apennines (diffuse and pervasive tectonic discontinuities, intense fracturing, extremely variable bedding, etc.), mainly consists of argillites, predominantly of grey colour, with intercalations of carbonate and silicoclastic arenites (Fig. 8.5) and often presents at the outcrop a weathered horizon whose thickness varies between 0.5 and 5 m (Calò, 2009). Further, the investigated area is almost continuously overlain by a heterogeneous Quaternary debris cover, about 3 to 25 m. thick, consisting of arenaceous and conglomeratic blocks of various dimensions, in a silty – clayey matrix (Fig. 8.6).

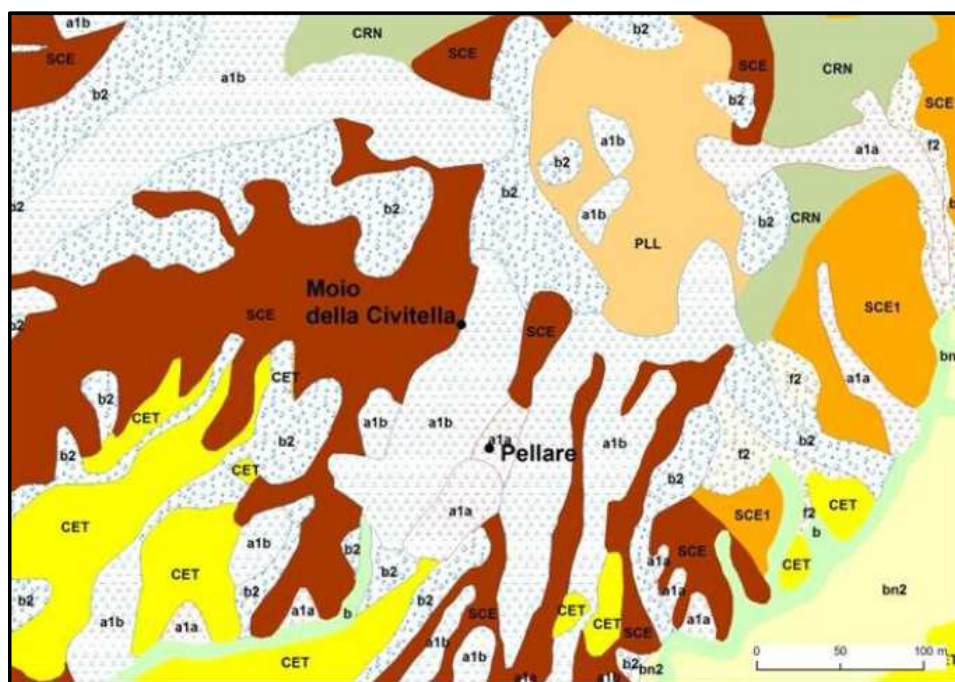


Figure 8.5 Geological sketch map of the Moio della Civitella area (redrawn from APAT, 2006): a1a, a1b: old and recent landslide deposits; b, b2, bn2: alluvial deposits; f2: debris; CET: Centola Conglomerates; MAU: San Mauro Formation; PLL: Pollica Sandstones; SCE, SCE1: Saraceno Formation; CRN: Crete Nere Formation; PNL: Pianelli Sandstones.

The differences in lithology and in the hydrogeological behavior of the terrains as well are among the main factors predisposing to instability at Moio della Civitella (Calcaterra et al., 2008). Furthermore, the geotechnical characteristics of the structurally complex formations depend partly on the relative sedimentary processes, and partly on the above mentioned tectonic phases that interested the Southern Apennines, significantly modifying the structure of the origin rock. Their lithologic and structural features result in a poor mechanical resistance and, thus, in a high ratio between the mobilized and the available shear resistance, even in the case of low-angle slopes (Calò, 2009).



Figure 8.6 Arenaceous and conglomeratic blocks belonging to the Quaternary cover cropping out within the urban centre of Moio della Civitella.

8.3 Geomorphological setting

The Southern Apennines of Italy are one of the most multi-hazard active areas in the world, due to the frequency and intensity of earthquakes, to the severity of erosion processes and to the diffusion of landslides (Del Prete, 1993).

The Campania region is characterized by different morphologic settings: an hilly and mountain sector, corresponding to the Apennines Chain, a coastal sector formed by large alluvial plains (Campanian Plain and Sele Plain) and, finally, several volcanic districts, namely the Vesuvius, the Roccamonfina and the Phlegrean Fields, the latter including the Ischia, Procida and Vivara Islands and more than sixty volcanic centres.

As a result, the region can be affected by different types of natural hazards, from landslides to volcanic eruptions, to severe coastal erosion and seismic events.

As regards the slope instability phenomena, the different lithologic, structural, hydrogeologic and geomorphologic settings of the Campania territory make it prone to different types of mass movements. For instance, in the volcanic sectors the most frequent type of landslide is represented by falls and topples involving the lithoid portions of lava and tuffs and, after intense rainfall, by flows in the pyroclastic deposits; along the calcareous – dolomitic slopes of the Sorrentina Peninsula and the Picentini Mountains, on the other hand, translational slides and topples as well as complex landslides (slides-flows) involving the pyroclastic cover on carbonate ridges, occur.

Finally, a predominance of flows, followed by rotational slides and complex phenomena, mainly rotational slides grading into flows, is observed where highly tectonized clayey and flysch formations crop out (Cilento sector).

Therefore, the complex geological setting of the region, together with an heavy development of the built-up environment, even in landslide-prone areas, make Campania one of the Italian areas with higher landslides costs, both direct and indirect (Schuster, 1996).

The landscape of Moio della Civitella, characterized by hilly morphologies with low-gradient slopes (Fig. 8.7) at altitudes between 600 and 200 m a.s.l., is widely affected by erosional and gravitational phenomena. Among them, landslides occupy a top-rank position.

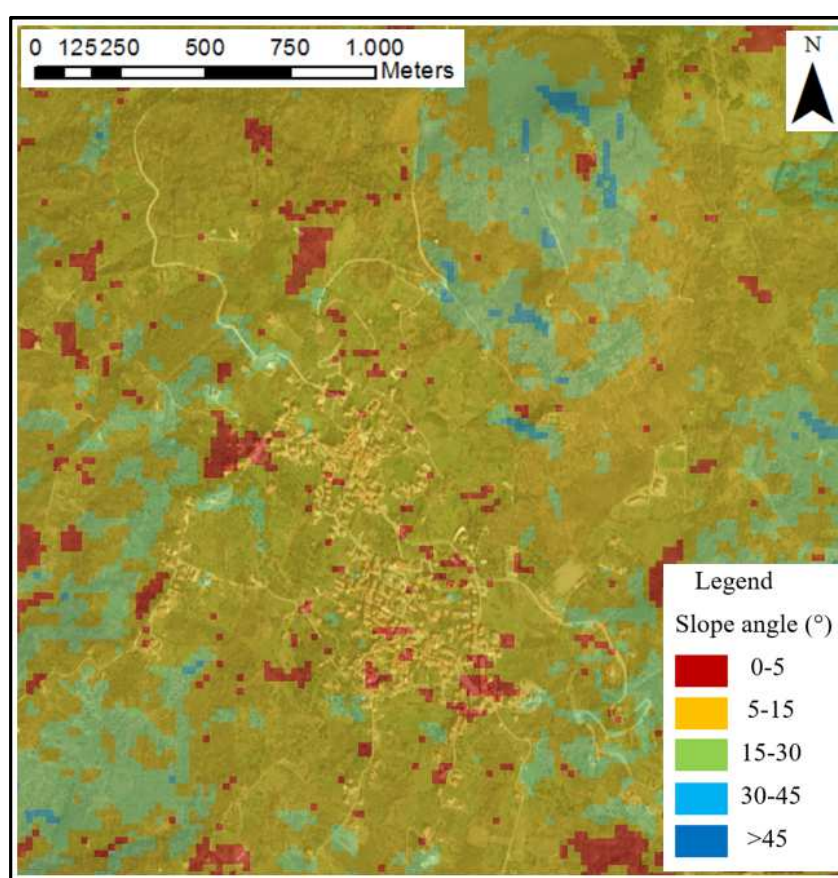


Figure 8.7 Slope map of Moio della Civitella territory.

The main slope movements derive from ancient phenomena which have involved large portions or the whole extension, 2-3 km in length, of the slopes and directly affect the urban setting, as shown in the following paragraphs.

8.4 Landslide inventory map of Moio della Civitella

As previously mentioned, landslide distribution in Moio della Civitella area is strictly related to the differences in lithology and in the hydrogeological behavior of the terrains.

The territory is widely affected by erosional and gravitational phenomena.

Over the years, several updates of landslide inventory map have been provided, by means of detailed geomorphologic analysis based on field surveys, air-photo interpretation, satellite -based data.

“IFFI” project (Amanti et al., 2001), dedicated to landslide inventory and mapping in Italy, in this area identified complex landslides such as rotational slides evolving to translational slides and flows (Servizio Geologico Nazionale, 2008), with multiple or superimposed phenomena (Fig. 8.8).

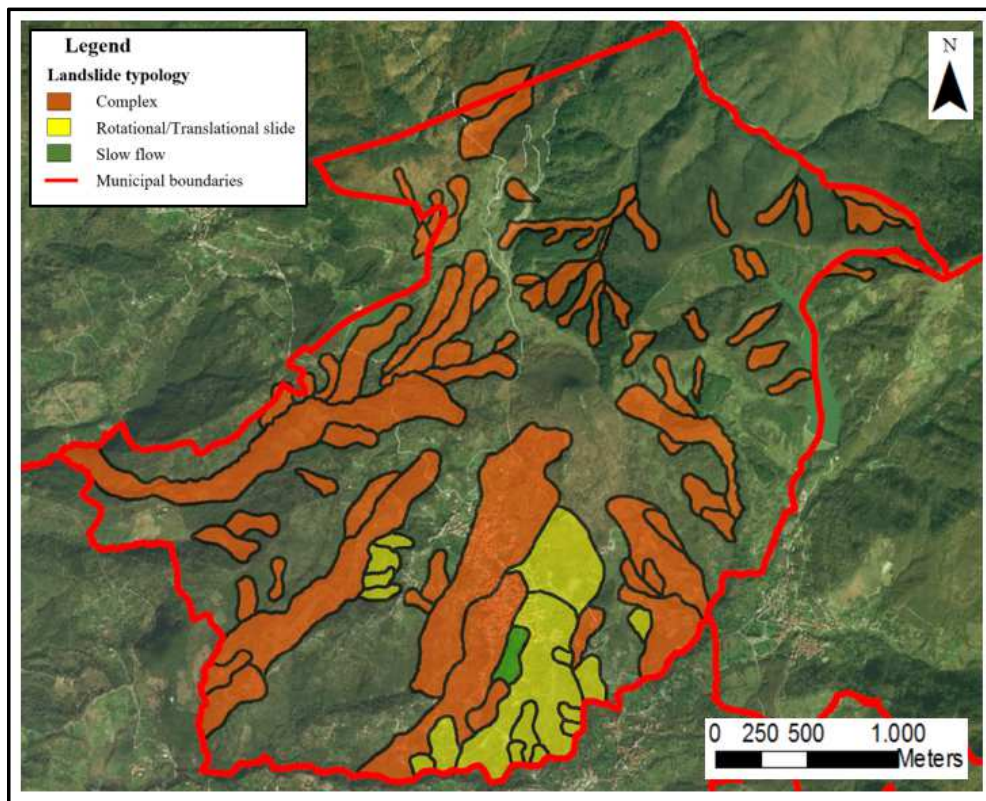


Figure 8.8 Landslide inventory map at Moio della Civitella (after IFFI project, available at <http://www.sinanet.apat.it/progettoiffi>, 2008).

As indicated by Calò F. (2009), landslides are generally dormant, whilst rainfall-triggered reactivations are common during the rainy seasons (the average value of annual precipitation is 1200 ÷ 1500 mm/year), generally involving limited parts of the landslides (Fig. 8.9).

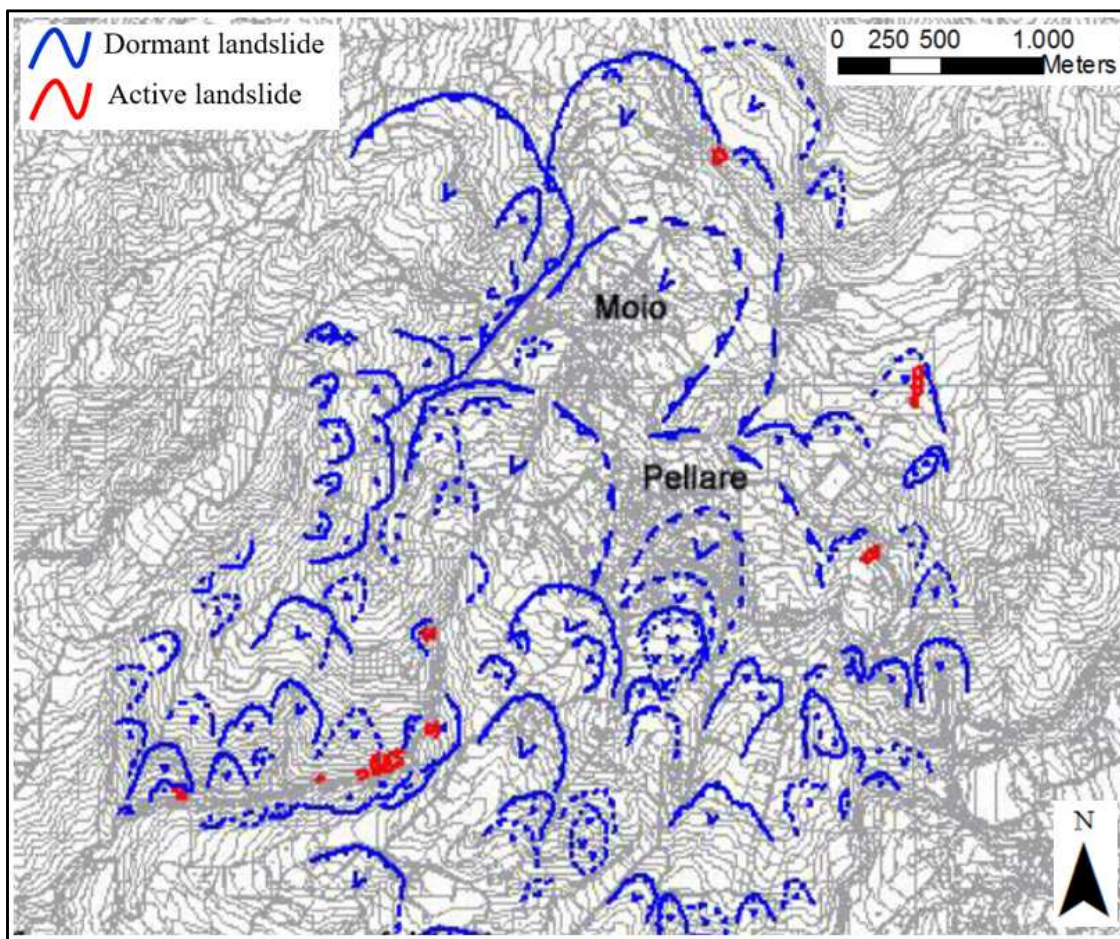


Figure 8.9 Landslide inventory map at Moio della Civitella (after Calò et al., 2009).

As shown in the landslide map (Fig. 8.10) provided by Hydro-geomorphological Setting Plan of South Campania River Basin Authority (2012), the largest slope movements, identified as flows, rotational/translational landslides and areas affected by diffuse slow movements, directly involve the inhabited areas, lifelines and the main communication routes, producing widespread damage to existing buildings, roads, sidewalks and walls.

In detail, rotational component of the complex slope movements is generally limited to the source areas, whilst most of the landslide body consists of the flow component, which may reach overall lengths on the order of several hundreds of meters.

Furthermore, as regards state of activity, also in 2012, most of landslides surveyed within municipal territory are classified as dormant, some of them as active and only seven are identified as inactive (Fig. 8.11). Due to the low seismicity of the area, reactivations are usually triggered by intense and continuous rainfall, as observed by local people and geologists and demonstrated by damage occurrence to buildings and infrastructures localized in the unstable areas.

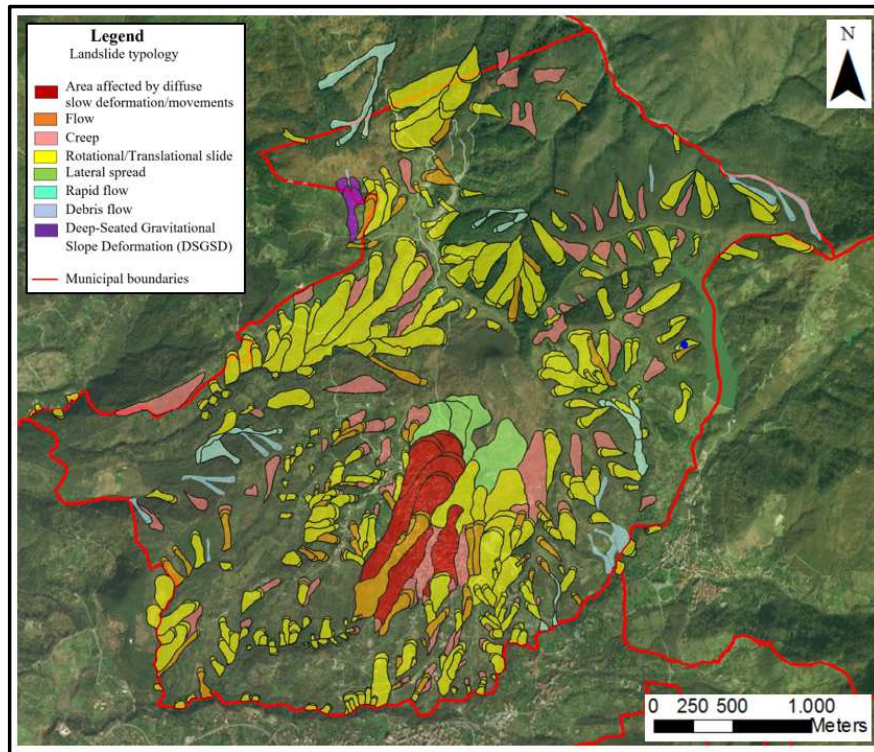


Figure 8.10 Landslides inventory map at Moio della Civitella (from Hydro-geomorphological Setting Plan of South Campania River Basin Authority, 2012).

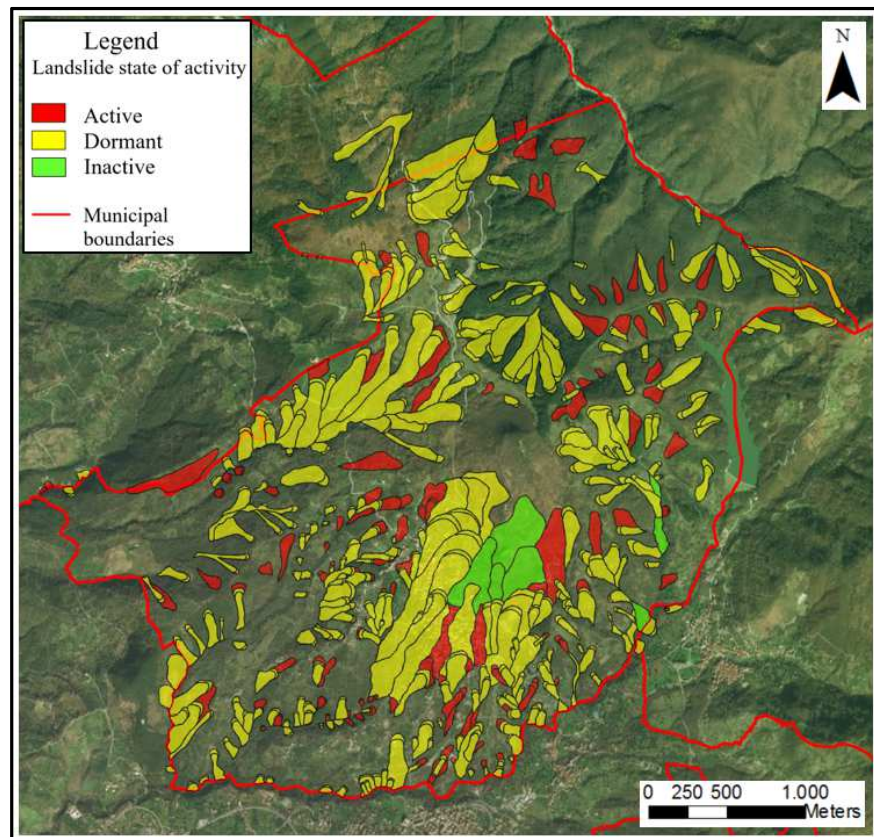


Figure 8.11 Landslides state of activity at Moio della Civitella (from Hydro-geomorphological Setting Plan of South Campania River Basin Authority, 2012).

In the last update (Fig. 8.12), provided in 2016 by Hydro-geomorphological Setting Plan of South Campania River Basin Authority, about 280 landslides are surveyed within municipal boundaries of Moio della Civitella, classified as shown in Figure 8.13.

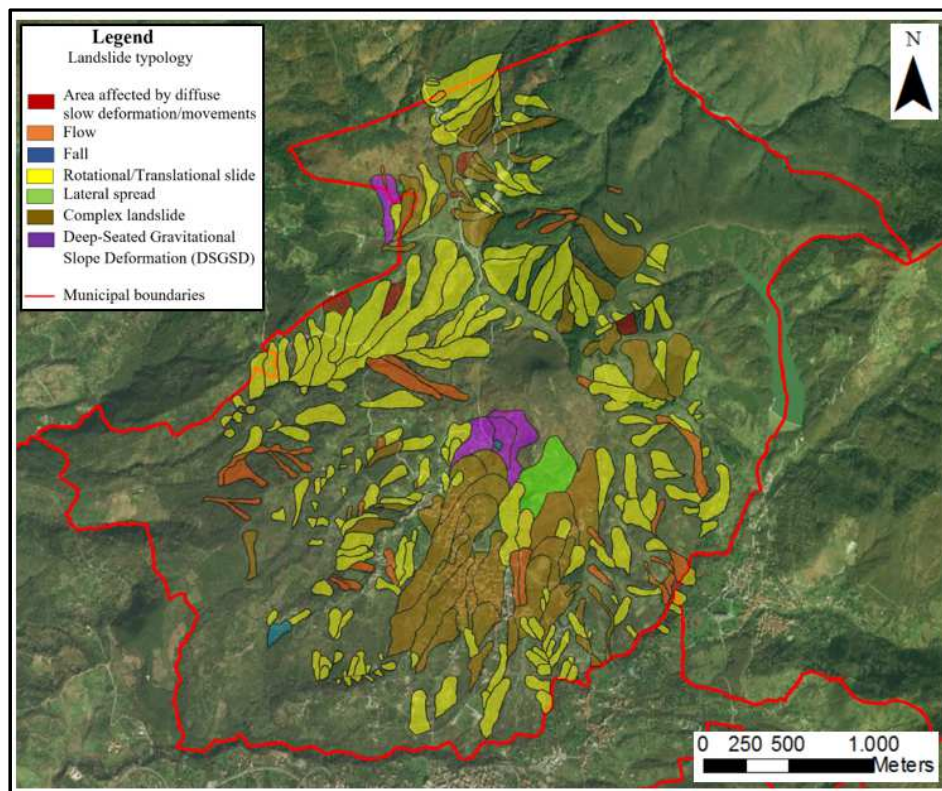


Figure 8.12 Landslides inventory map at Moio della Civitella (from Hydro-geomorphological Setting Plan of South Campania River Basin Authority, 2016).

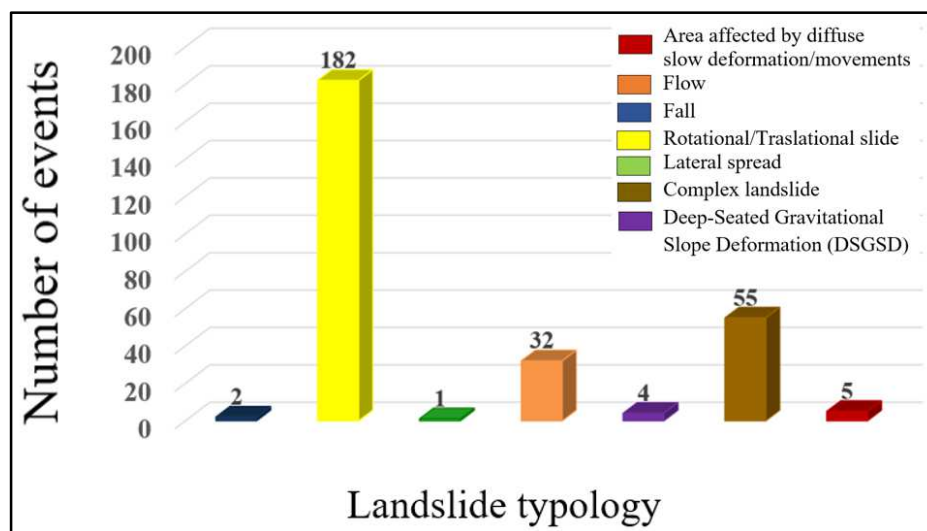


Figure 8.13 Typologies of landslide at Moio della Civitella (from Hydro-geomorphological Setting Plan of South Campania River Basin Authority, 2016).

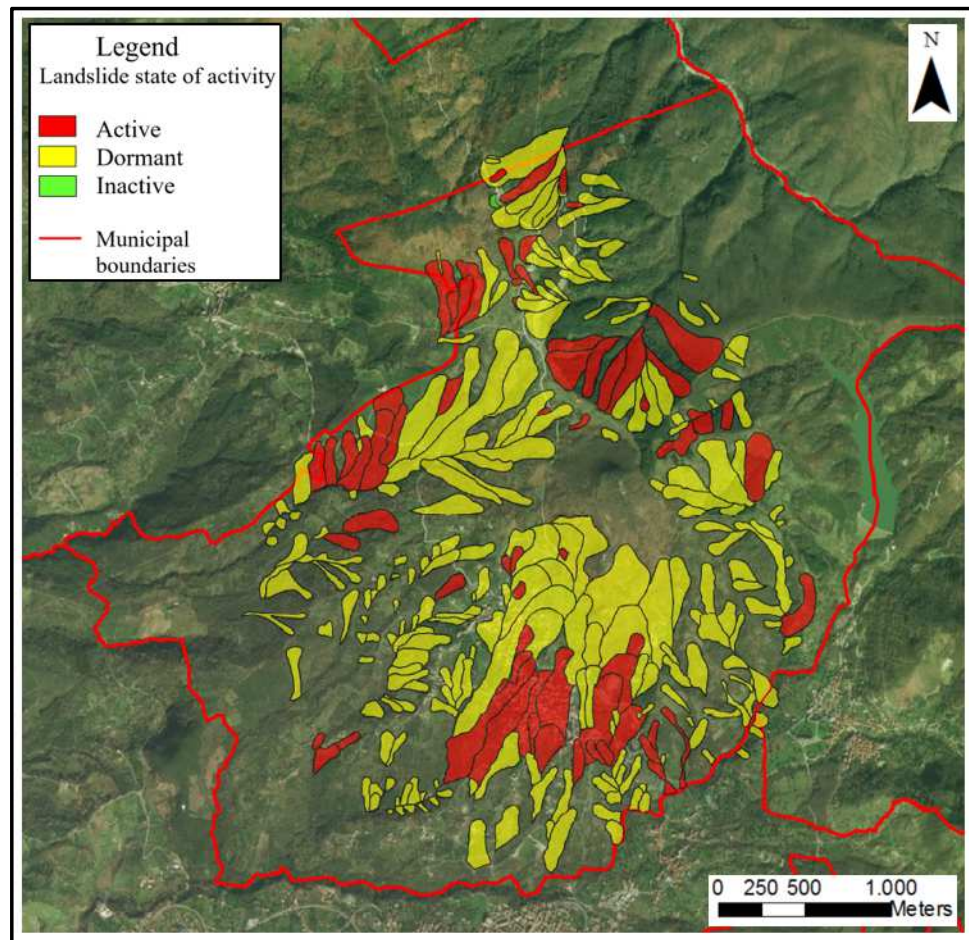


Figure 8.14 Landslides state of activity at Moio della Civitella
(from Hydro-geomorphological Setting Plan of South Campania River Basin Authority, 2016).

Moreover, as regards state of activity, in 2016, 68 events are classified as active, 212 as dormant and only 1 as inactive (Figures 8.14 and 8.15).

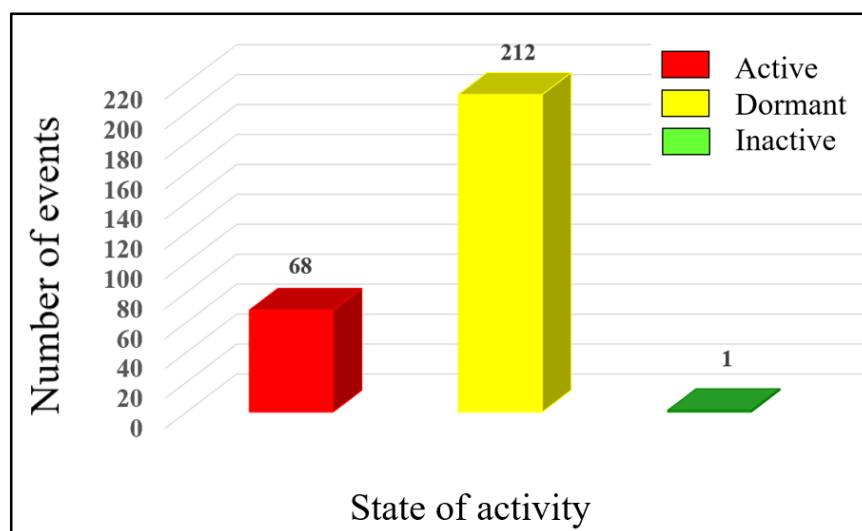


Figure 8.15 Distribution of landslides state of activity at Moio della Civitella
(from Hydro-geomorphological Setting Plan of South Campania River Basin Authority, 2016).

Finally, some landslides in Moio della Civitella territory have shown a change of state of activity between 2012 and 2016 inventory maps (Fig. 8.16). In detail, 35 landslides surveyed as dormant in 2012, were classified as active in 2016: most of them, showing local reactivations, affect above all the historical center of Moio della Civitella, inducing several damage to existing buildings, as discussed in following paragraphs.

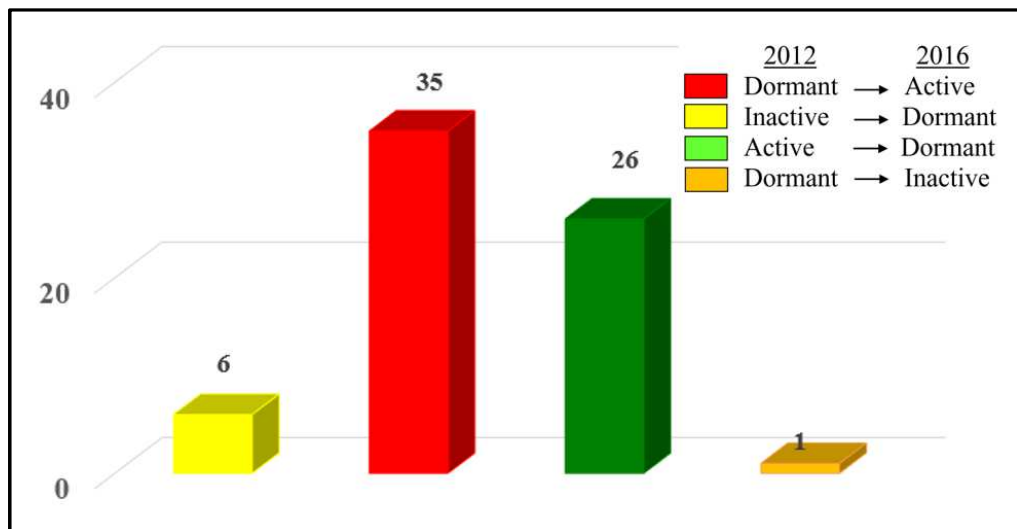


Figure 8.16 Distribution of landslides which change state of activity from 2012 to 2016.

8.5 Vulnerability assessment at small scale

As mentioned in the paragraph 7.2, aim of small scale analysis is to assess preliminary cause-effect relationship between landslide kinematics and building damage susceptibility.

In order to characterize landslide kinematics, starting from geological and geomorphological settings, and available landslide inventory maps, a knowledge of main landslide characteristics, such as intensity, boundaries and state of activity, is required.

To this purpose, an advanced DInSAR technique has been used to obtain from satellite radar images displacements both of ground and of structures/infrastructures in a landslide-affected area, providing information on their spatial and temporal evolution.

Furthermore, the second step of vulnerability analysis requires the preliminary characterization of exposed elements: existing buildings are identified on the basis of available digital topographic maps. Subsequently, building structural typology, state of maintenance, age of construction and damage severity level, and homogeneous construction in terms of orientation respect to landslide movement direction, are defined via field surveys.

In the following paragraphs, the above mentioned steps are developed separately and subsequently combined to achieve the main goals of a vulnerability analysis at small scale of representation.

8.5.1 Assessment of landslide kinematics by DInSAR technique

In order to assess ground displacements due to landslides, ENVISAT and COSMO-SkyMed (CSK) images have been processed by means of Coherent Pixels Technique (Mora et al., 2003).

In detail, the following datasets have been used:

- 51 “ENVISAT” images acquired along “ascending” track in the time span 2002-2010;
- 33 “ENVISAT” images acquired along “descending” track in the time span 2002-2010;
- 76 “CSK” images acquired along “ascending” track in the time span 2011-2016;
- 66 “CSK” images acquired along “descending” track in the time span 2011-2016;

The area of interest selected for the SAR analysis is about 9 km² wide. A DEM, extracted from the regional topographic cartography, with resolution cell of 10 x 10 m, has been used in order to remove the effect of topography on the interferometric phase.

The available satellite images have been processed through the SUBSIDENCE processor (Mora et al., 2003), developed at the Universitat Politècnica de Catalunya of Barcelona.

The processing consists of two sections:

- software PRISAR: which allows the SLC images crop, their coregistration, the differential interferograms and the coherence maps generation;
- software SUBSOFT: which allows the solution of the CPT algorithm, namely the decomposition of the differential phase in DEM error and estimated deformations.

The SUBSOFT analysis has been carried out, by exploiting the coherence stability approach and Temporal Sublook Coherence method (TSC) for pixel selection, respectively applied to ENVISAT and COSMO-SkyMed images.

Owing to the need to have a sufficient number of targets covering the entire study area, and to display, at the same time, a phase standard deviation of approximately 20° (which corresponds to a displacement standard deviation of 1,5 mm), the following threshold values have been fixed:

- for ascending ENVISAT images, two coherence value thresholds were set (0,40 and 0,35);
- for descending ENVISAT images, coherence value thresholds are 0.5 and 0.4;
- for ascending COSMO-SkyMed images, a threshold of TSC equal to 0.75 has been set;
- for descending COSMO-SkyMed images, the value of TSC is 0,70.

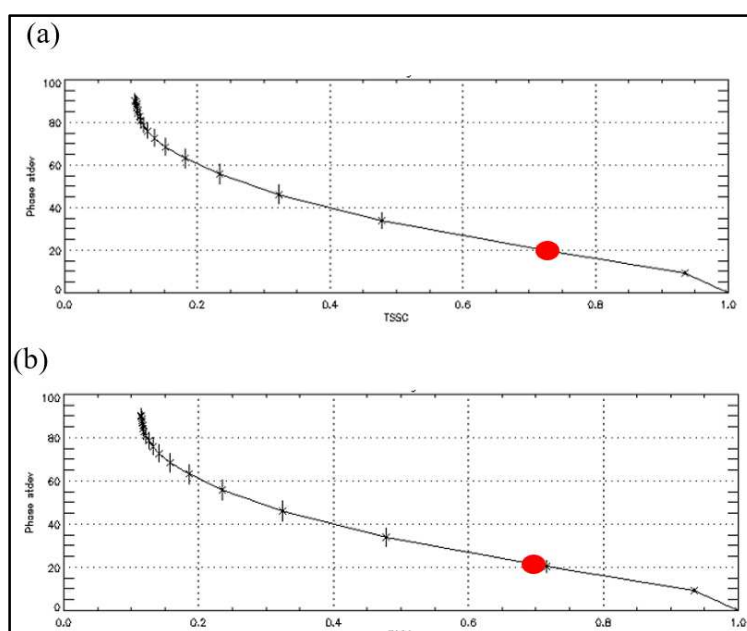


Figure 8.17 Phase standard deviation vs. TSC for ascending (a) and descending (b) processing. Red points indicate the TSC threshold selected.

In order to detect pixels with high phase quality, only the interferograms whose image pairs had spatial and temporal baselines lower than fixed values, have been selected.

In detail, for ENVISAT images 250 m and 210 days, respectively, while for COSMO-SkyMed images 250 m and 250 days, have been fixed.

Another important part of the interferometric chain was to identify a stable reference point; for this purpose, basing on available *in situ* monitoring data, three stable points were identified, as shown in Figure 8.18.

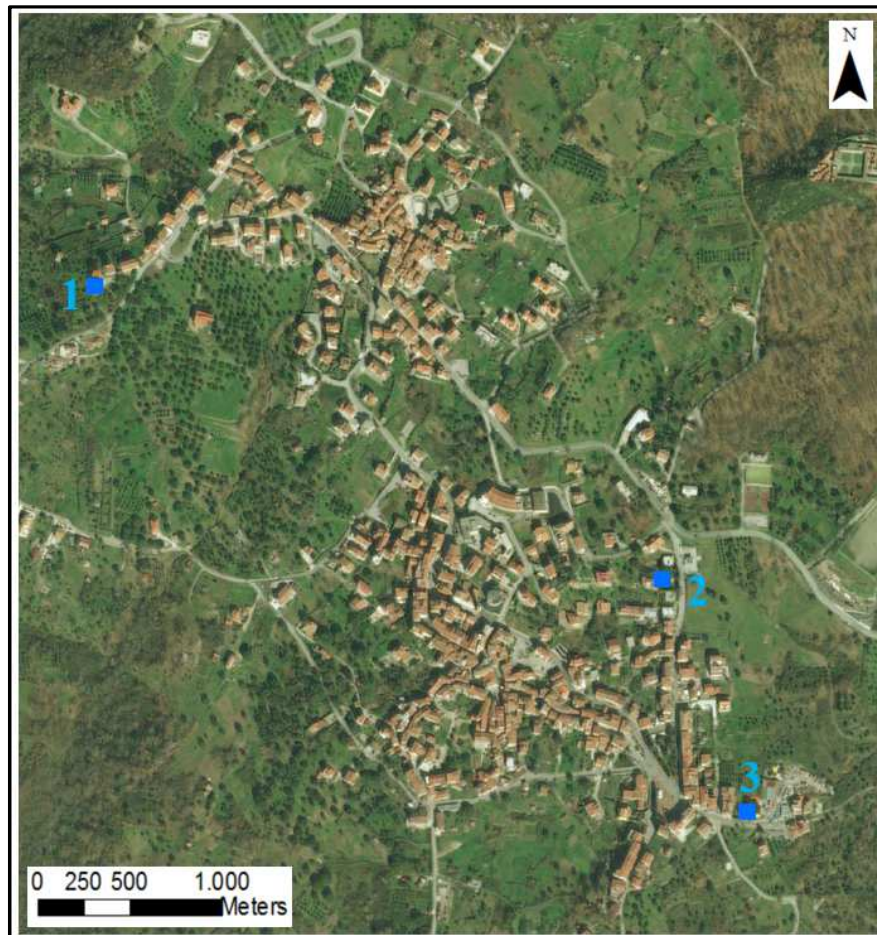


Figure 8.18 Stable points identified at Moio della Civitella: 1 and 3 correspond to master points of GPS network installed *in situ*.

As a result of this processing, for each dataset, displacement mean velocity maps measured along Line of Sight (LoS) have been obtained (Figs. 8.19 and 8.20); such parameter, in fact, can be considered very useful to define slow-moving landslide intensity, at this scale of representation.

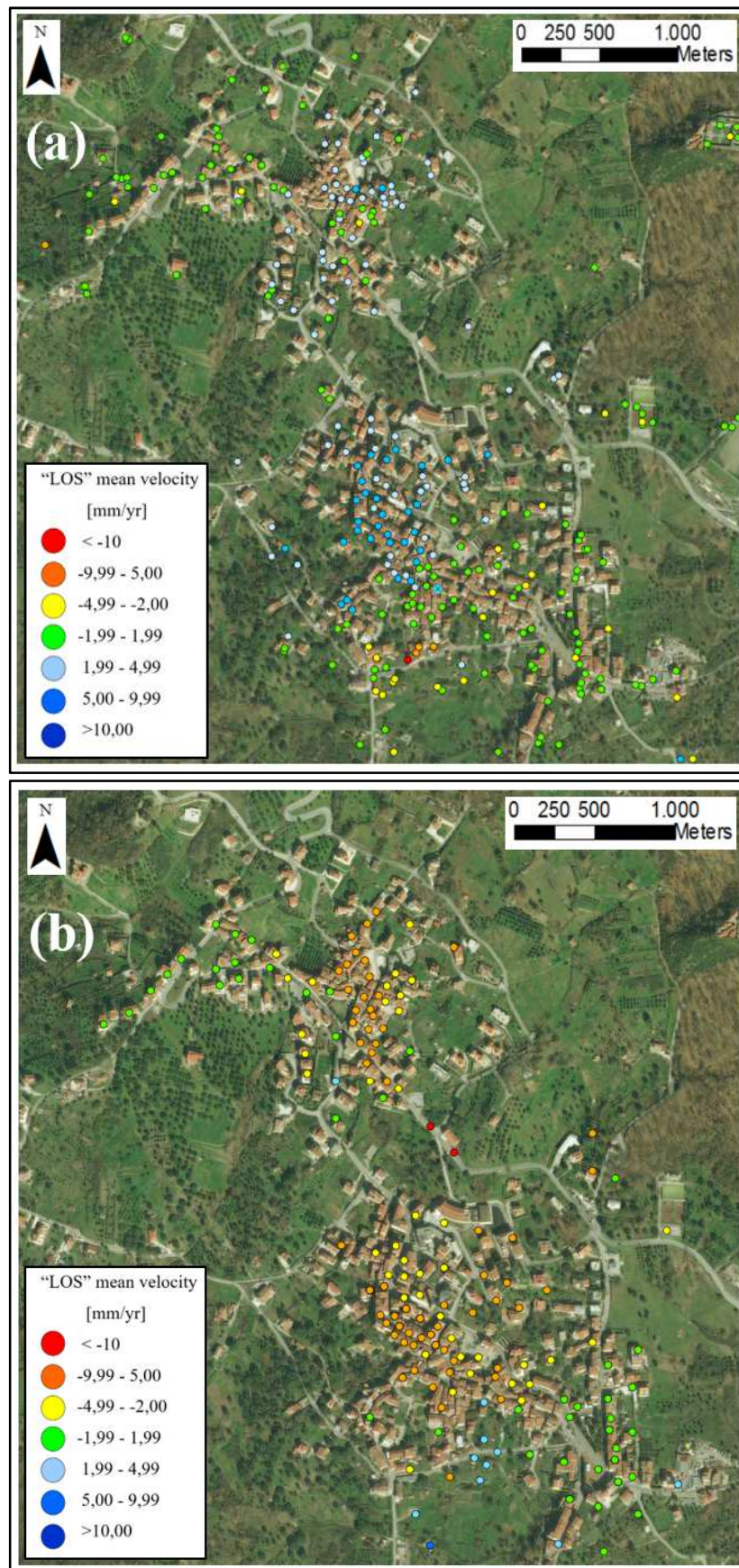


Figure 8.19 Displacement rate maps obtained by ENVISAT images in time span 2002-2010: along ascending (a) and descending (b) tracks.

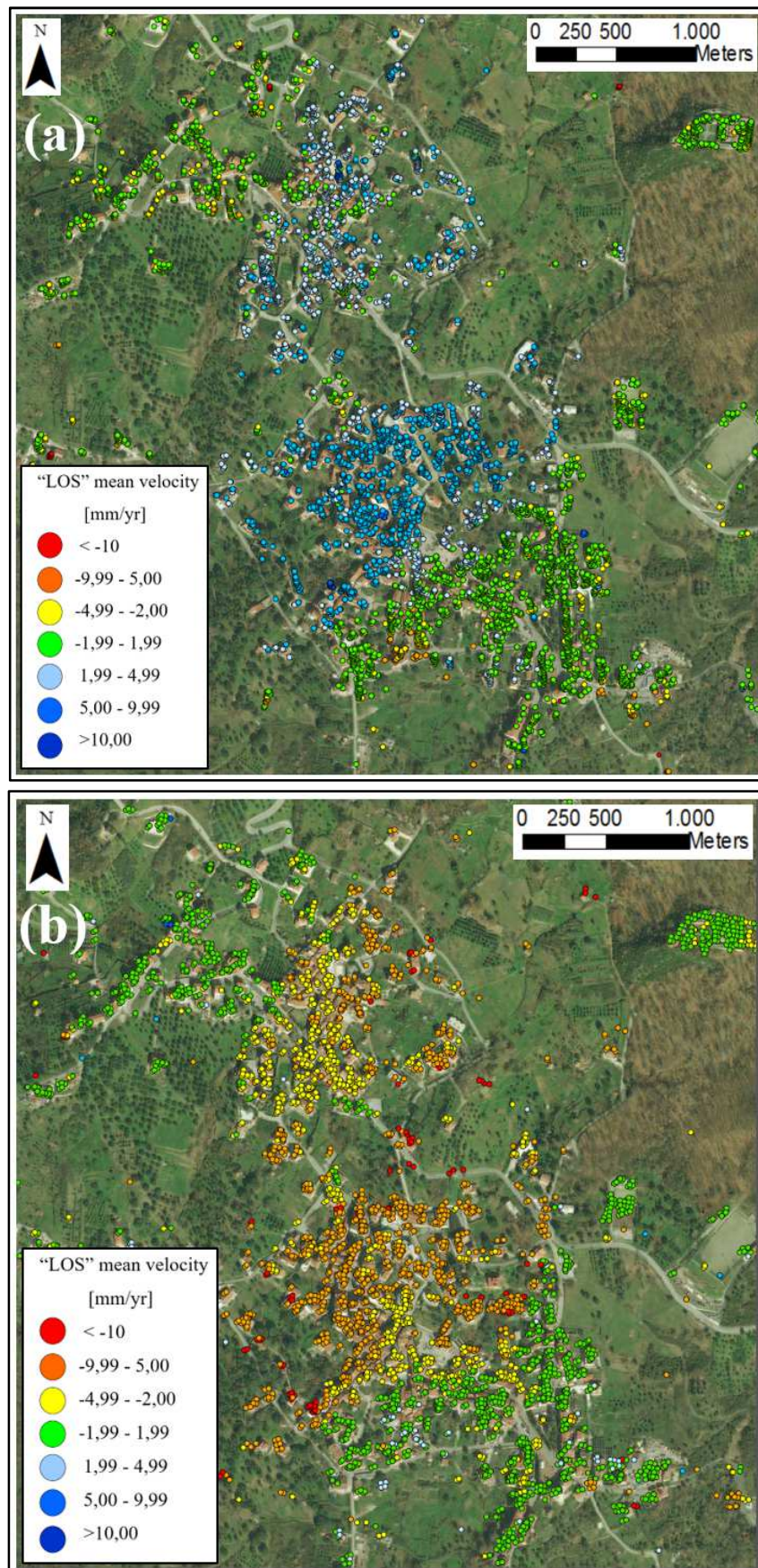


Figure 8.20 Displacement rate maps obtained by COSMO-SkyMed images in time span 2011-2016: along ascending (a) and descending (b) tracks.

Four different classes of velocities have been identified:

- Class 1, velocity of displacement higher than 10 mm/yr;
- Class 2, velocity of displacement between 5 and 10 mm/yr;
- Class 3, velocity of displacement between 2 and 5 mm/yr;
- Class 4, velocity of displacement lower than 2 mm/yr.

Targets localized in Moio della Civitella area mainly correspond to man-made features, such as buildings and roads. As it is possible to note, the use of COSMO-SkyMed images allows to obtain a number of targets higher than ENVISAT images (Fig. 8.21), depending on higher resolution of more recent satellite constellation (Fig. 8.22).

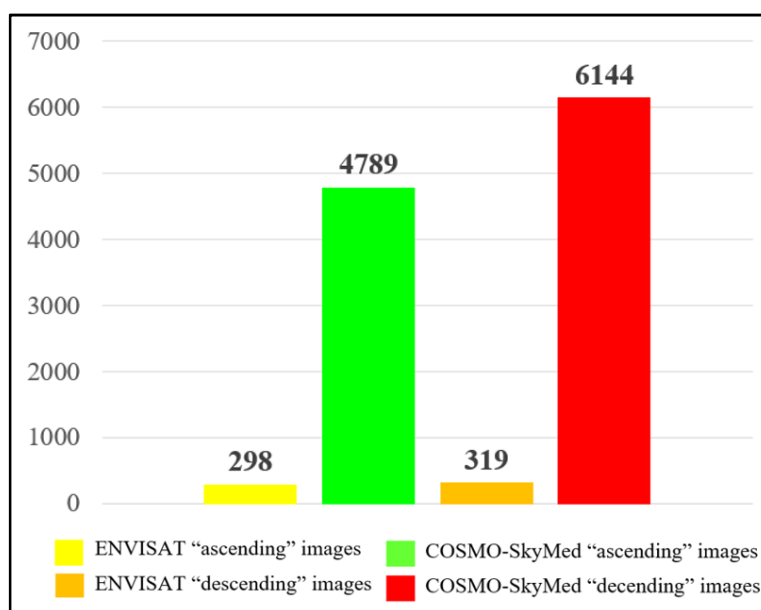


Figure 8.21 Number of targets identified in the study area by ENVISAT medium-resolution and COSMO-SkyMed high resolution images.

Maximum displacement rates detected by ENVISAT processing are + 9 mm/year and -16 mm/year, respectively acquired along ascending and descending tracks; higher values are obtained by COSMO-SkyMed images, equal to + 19 mm/year and -32 mm/year, along same geometry of acquisition.

Measured displacement rates show that the whole territory of Moio della Civitella urban settlement is interested by ground instability: in detail, according to Cruden & Varnes (1978) landslides classification, based on their velocity, interferometric products confirm the occurrence of very slow and slow-moving phenomena.

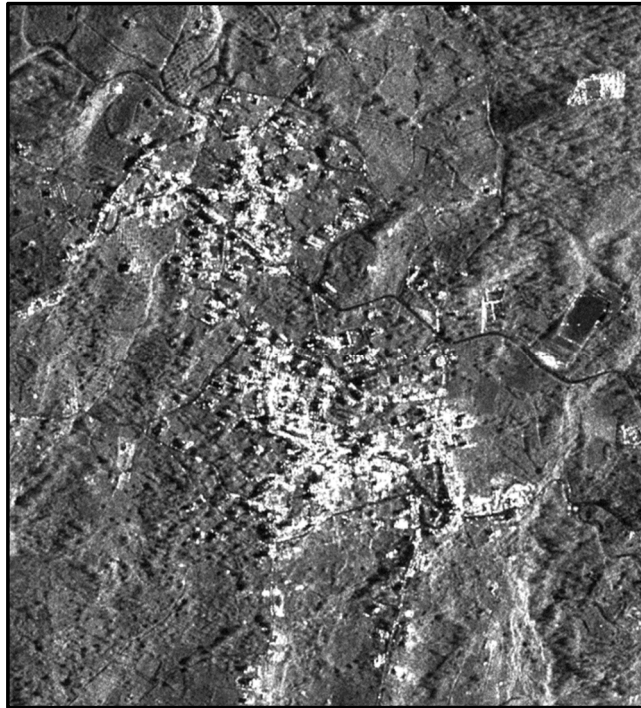


Figure 8.22 High resolution SAR image of Moio della Civitella acquired by COSMO-SkyMed constellation.

8.5.2 Characterization of exposed elements

At small scale analysis, existing buildings are identified from the available digital topographic map. In particular, buildings aggregation is preliminary sketched as a planar figure, without identifying single structures inside aggregate (Fig. 8.23).

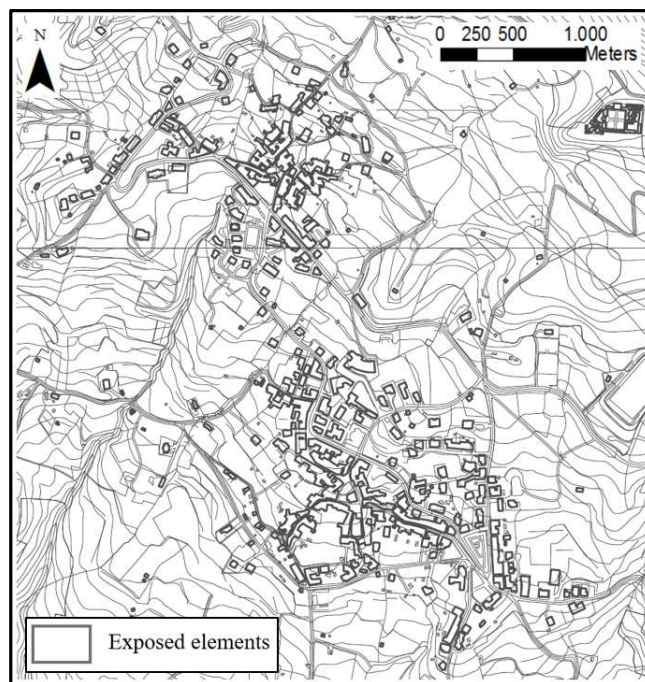


Figure 8.23 Exposed elements identified by topographic map.

Subsequently, a field campaign allows to identify different structures in a buildings aggregate (Fig. 8.24), surveying also their constructive typology (Fig. 8.25), age of construction (Fig. 8.26), state of maintenance (Fig. 8.27) and damage severity level.

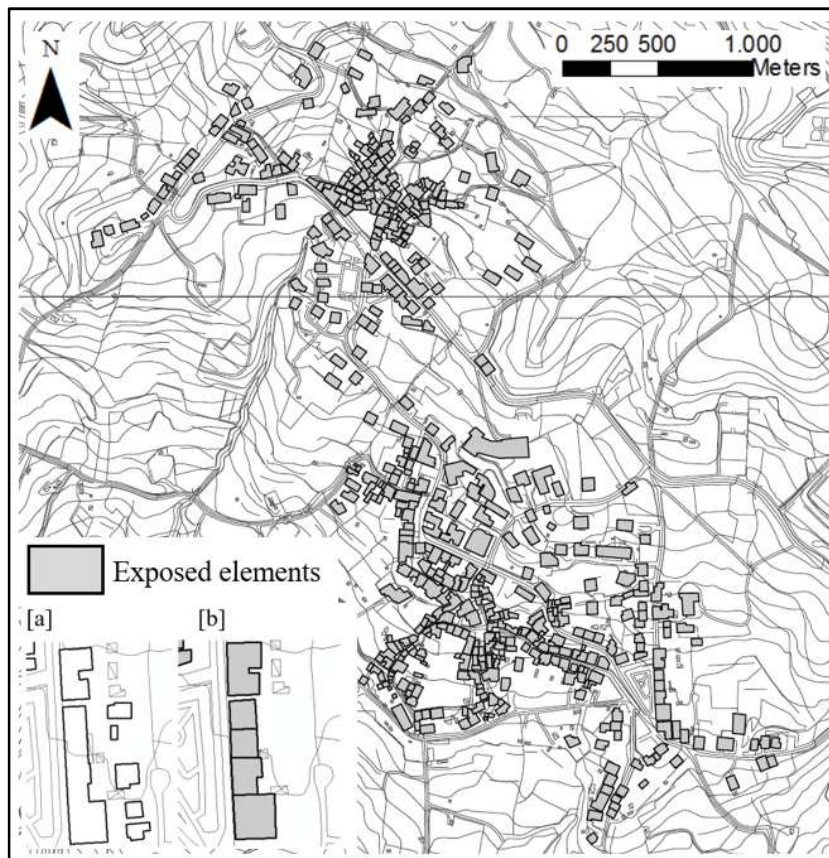


Figure 8.24 Map of exposed elements identified by field survey and example of buildings aggregate obtained by topographic map (a) and by *in situ* campaign (b).

Four different typologies of buildings have been surveyed in Moio della Civitella urban settlement, in terms of homogeneous structural types according to different critical strength properties: masonry and reinforced concrete buildings, constructions with mixed structure and other typologies (steel, wood, etc.).

About 504 different buildings have been identified: 352 masonry buildings, 143 in reinforced concrete, 7 buildings with mixed structure and 2 buildings with steel constructive typology.

Masonry buildings, built between 1850 and 1900, represent the most widespread constructive typology in historical urban centers both of Moio and of Pellare; reinforced concrete buildings instead were built after 1950, mostly in peripheral areas of the municipal territory.

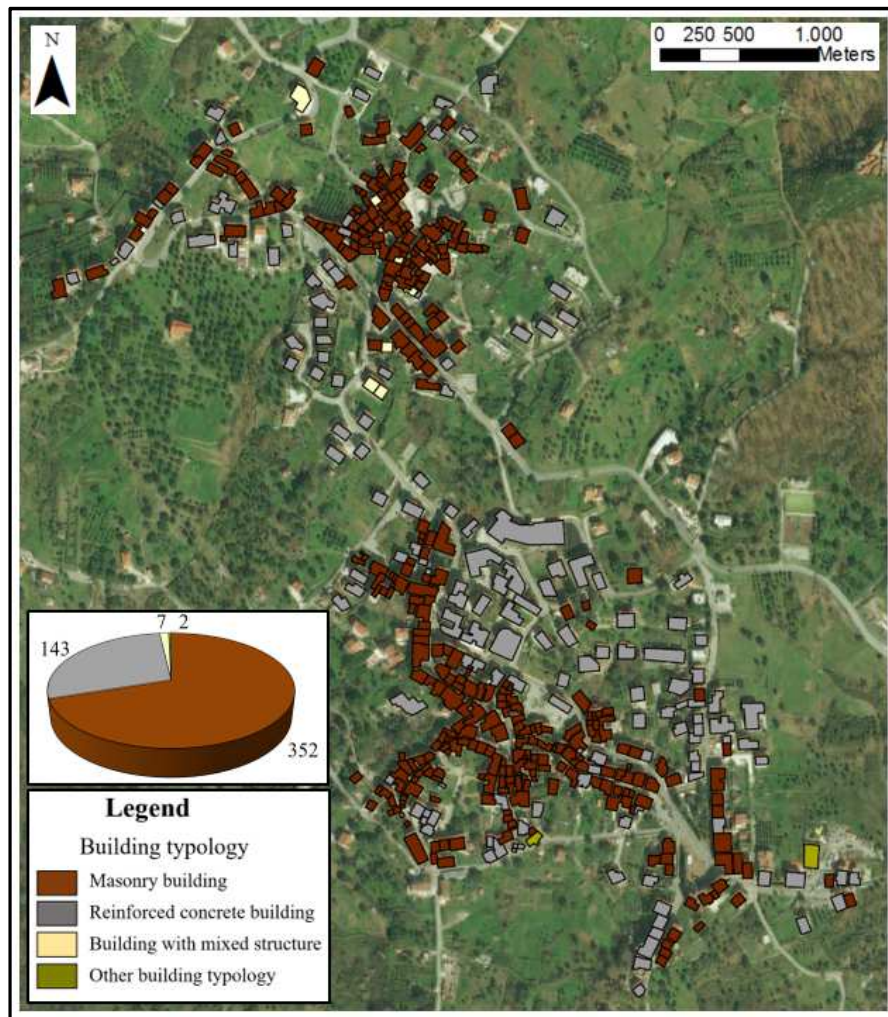


Figure 8.25 Map of building typology surveyed in Moio della Civitella municipality.

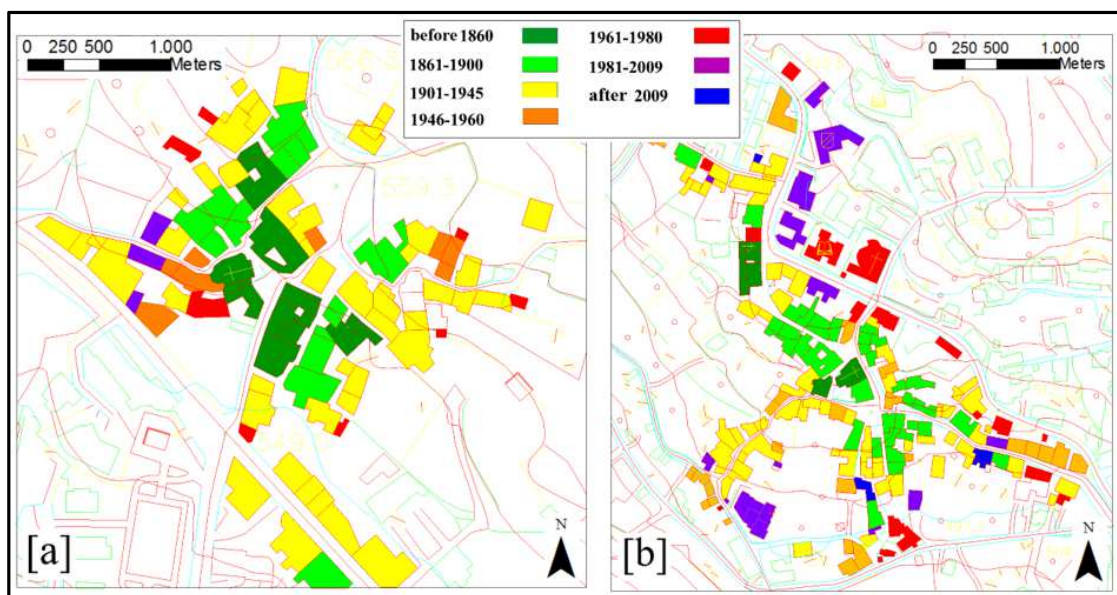


Figure 8.26 Map of building age of construction in Moio della Civitella municipality: Moio (a) and Pellare (b) urban settlements.

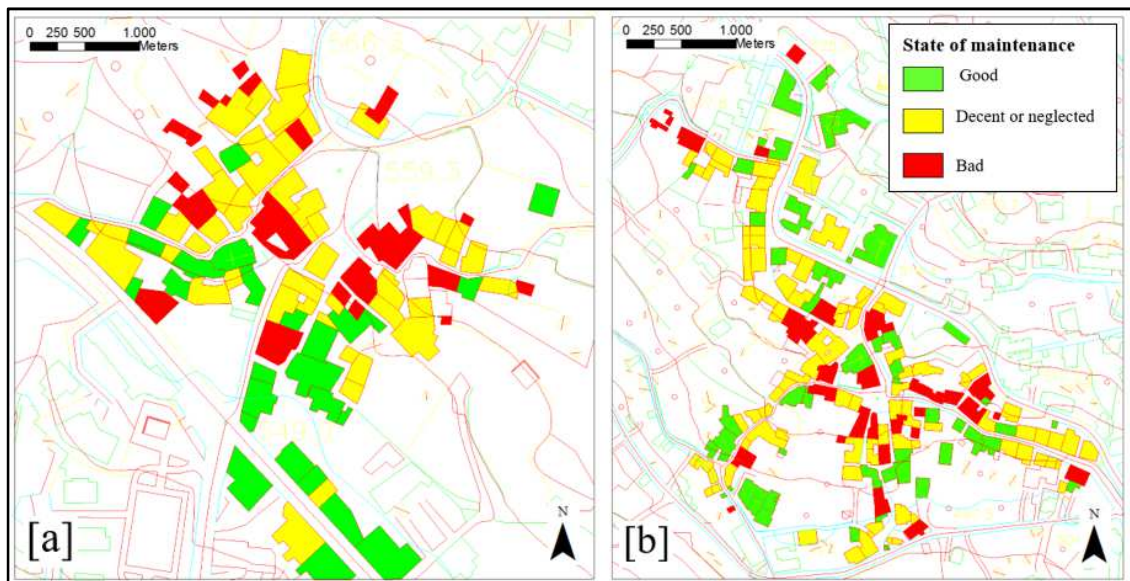


Figure 8.27 Map of building state of maintenance in February 2015 at Moio della Civitella municipality: Moio (a) and Pellare (b) urban settlements.

Furthermore, a structural survey of building damage degree has been performed in February 2015, using four classifications available in literature. In detail, as mentioned in Chapter 6, Burland (1977), Alexander (1986), Iovine & Parise (2002) and DPC (2009) approaches have been applied to the study area. Maps of building damage surveyed in Moio della Civitella municipality are shown in Figures 8.28, 8.29, 8.30 and 8.31.

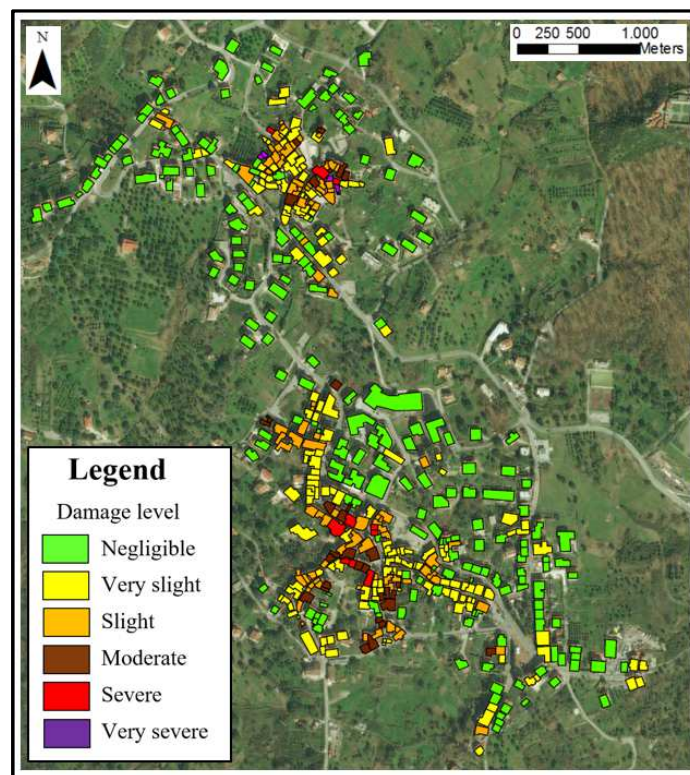


Figure 8.28 Building damage map according to Burland (1977) classification.

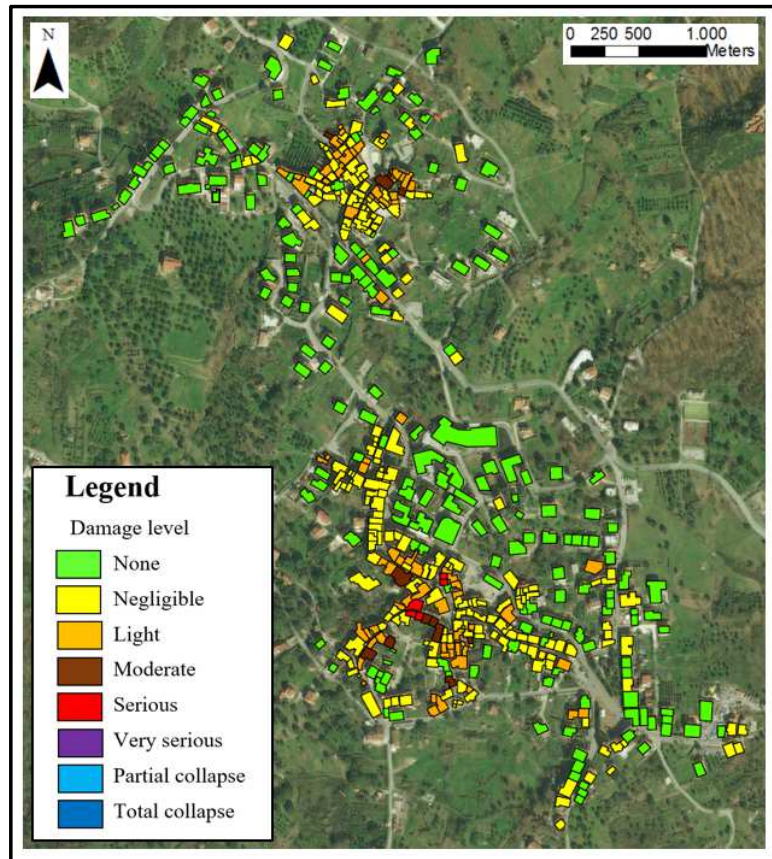


Figure 8.29 Building damage map according to Alexander (1986) classification.

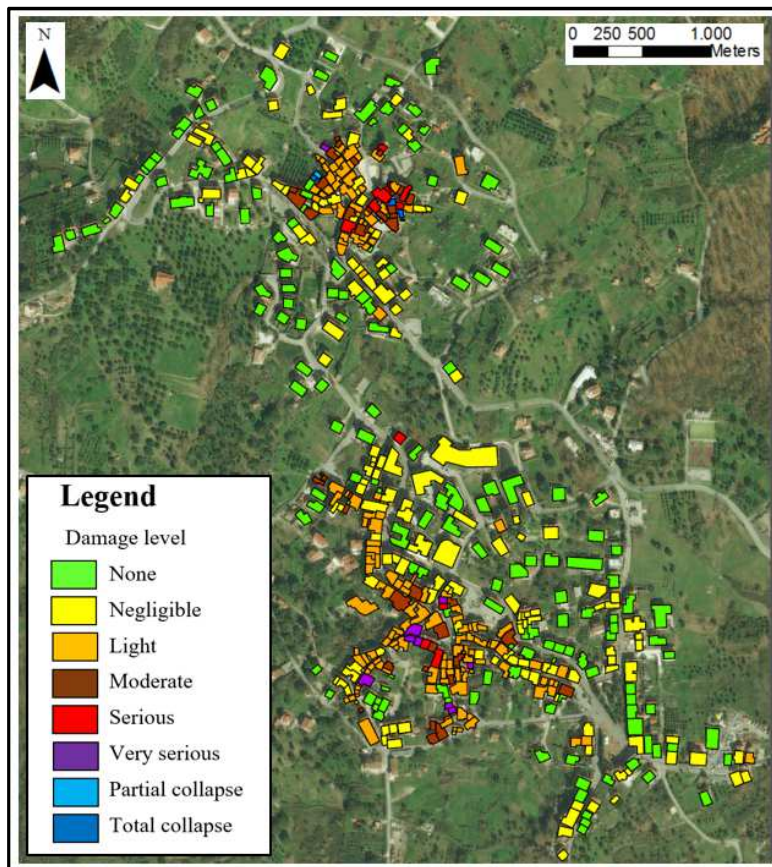


Figure 8.30 Building damage map according to Iovine & Parise (2002) classification.

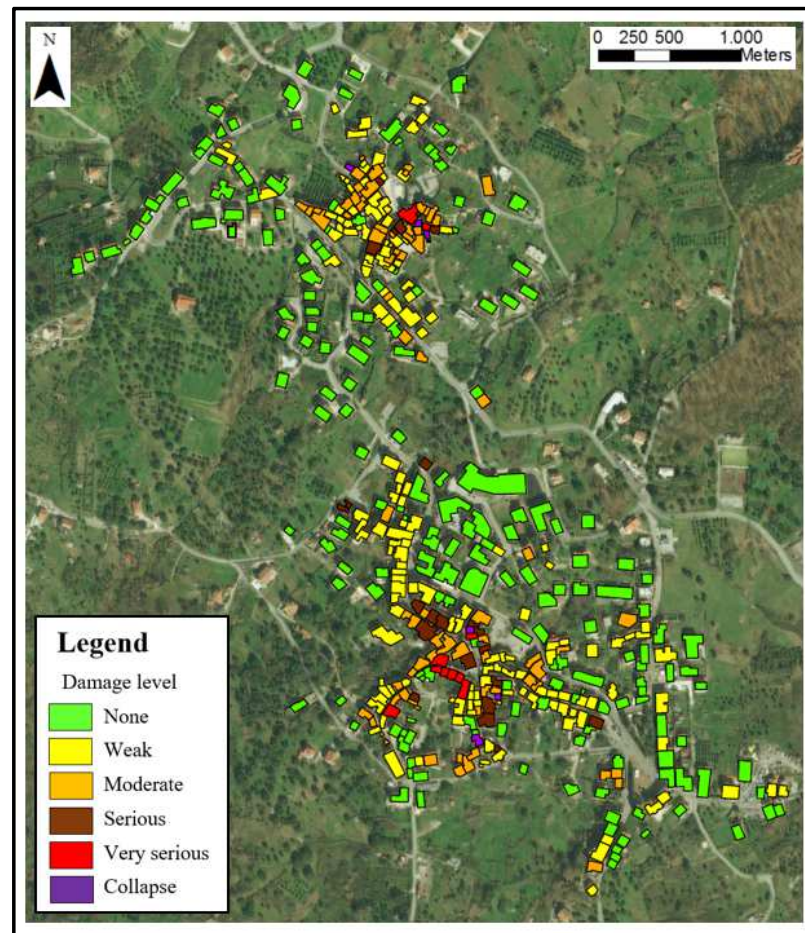


Figure 8.31 Building damage map according to Italian DPC (2009) classification.

As it is possible to note, the applied methodologies gave back different classifications of damage degree: in several cases, in fact, the same building is classified with different level of damage. This discrepancy is mainly due to the different parameters used to evaluate the state of cracks and also to the aims of use of such methodologies.

Figure 8.32 shows an example of building characterized by different damage severity degree according to the above mentioned classifications.

Such methods, in fact, consider different conflicting parameters (width of cracks, building distortion, foundation differential displacements, distortion of openings, etc.), not allowing a simple and univocal application and result.

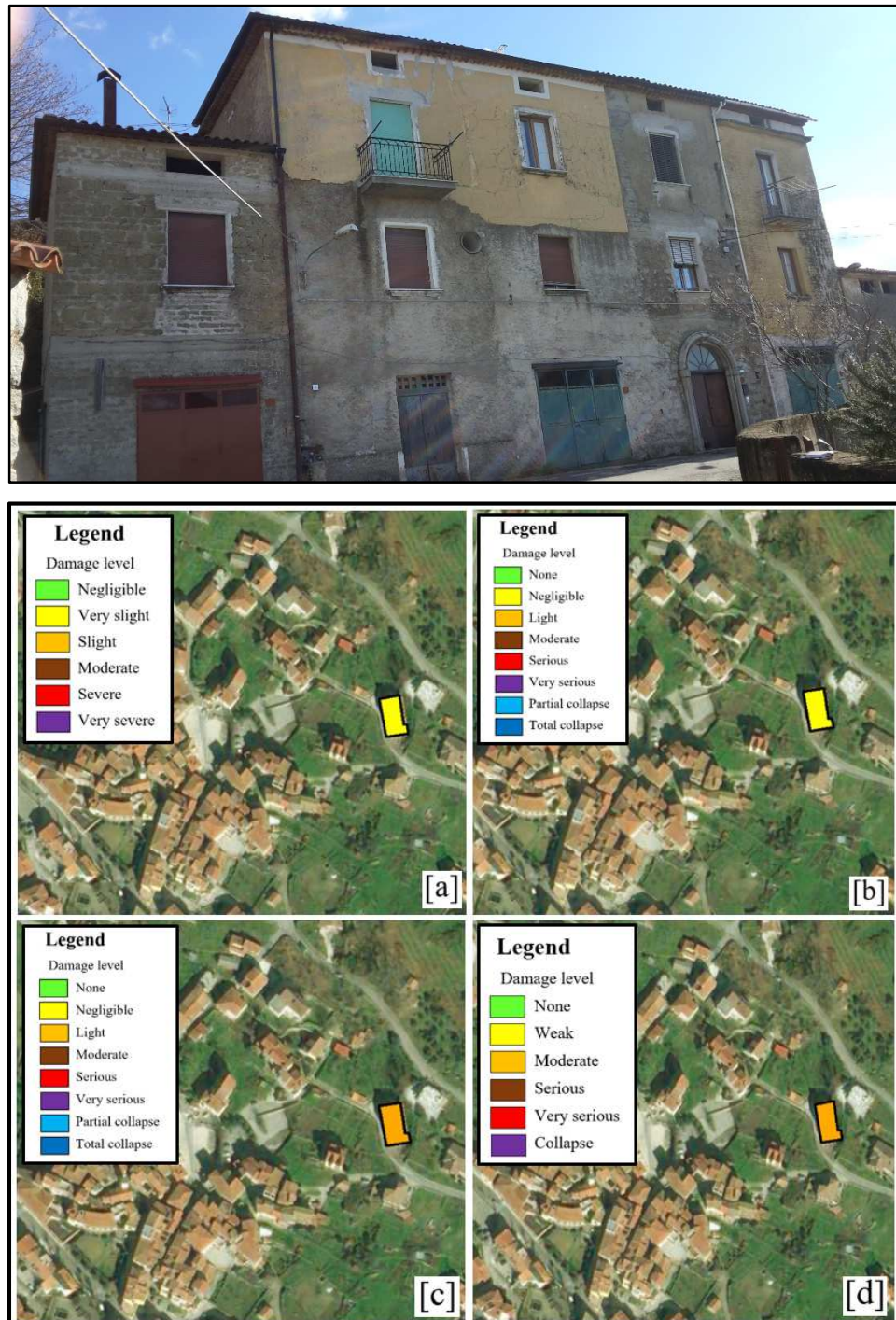


Figure 8.32 Example of building characterized by different damage severity level according to: Burland (a), Alexander (b), Iovine & Parise (c) and Italian DPC (d) approaches.

According to the approach proposed in paragraph 7.2 for building vulnerability assessment at small scale of representation, the following goals have been achieved.

8.5.3 Identifying stable/unstable areas, stable/unstable buildings and prevalent direction of movement

As previously mentioned, at this level of representation, landslide intensity can be defined by annual displacement rate of targets identified by DInSAR data.

In order to identify buildings affected by ground displacements and to analyze their behavior, scatterers at ground level and on top of buildings were preliminarily differentiated. To this aim, around each building identified from available digital topographic map, a 2-m buffer-distance is considered (Fig. 8.33).

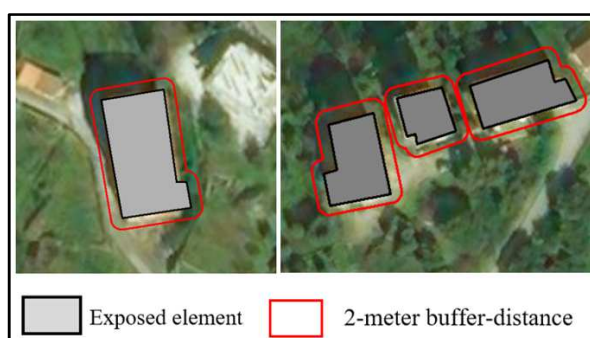


Figure 8.33 Examples of buffer created around buildings at Moio della Civitella.

Furthermore, to take into account spatial resolution of interferometric products and graphical error related to the working scale, targets on ground level have been distinguished from those on top of buildings, basing on DEM_Error processing output: such parameter defines a height of targets compared with Digital Elevation Model (DEM). In detail, aimed to identify targets belonging to buildings, only scatterers with $DEM_Error \geq 3$ m have been selected (Fig. 8.34).

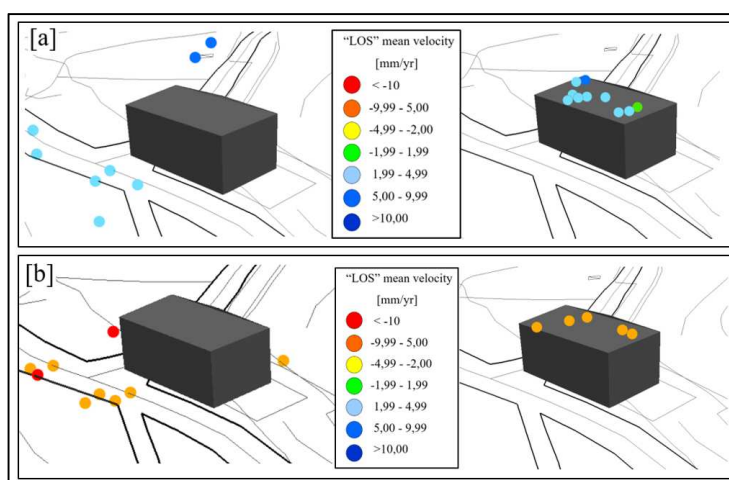


Figure 8.34 Differentiation of targets identified by COSMO-SkyMed images on the top of a building and in the surrounding area at ground level obtained by ascending (a) and descending (b) tracks.

Figures 8.35 and 8.36 show differentiation of targets identified both on ground level and on top of buildings in the whole territory of Moio della Civitella urban settlement, obtained respectively by COSMO-SkyMed ascending and descending orbits.

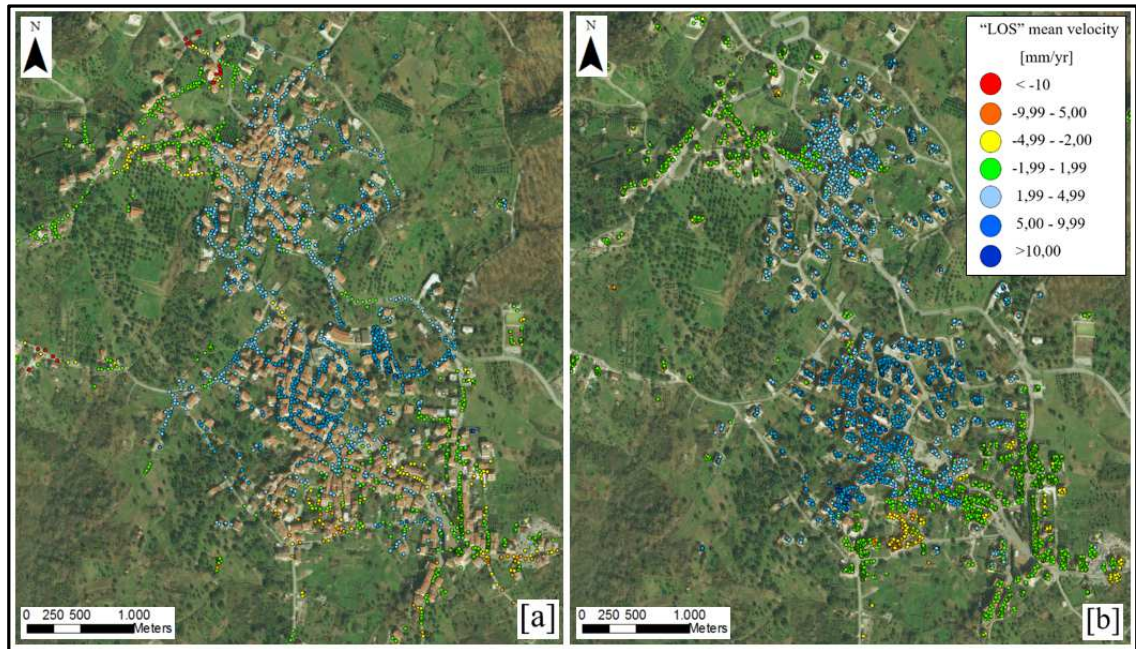


Figure 8.35 Targets identified on ground level (a) and on top of buildings (b) in ascending track.

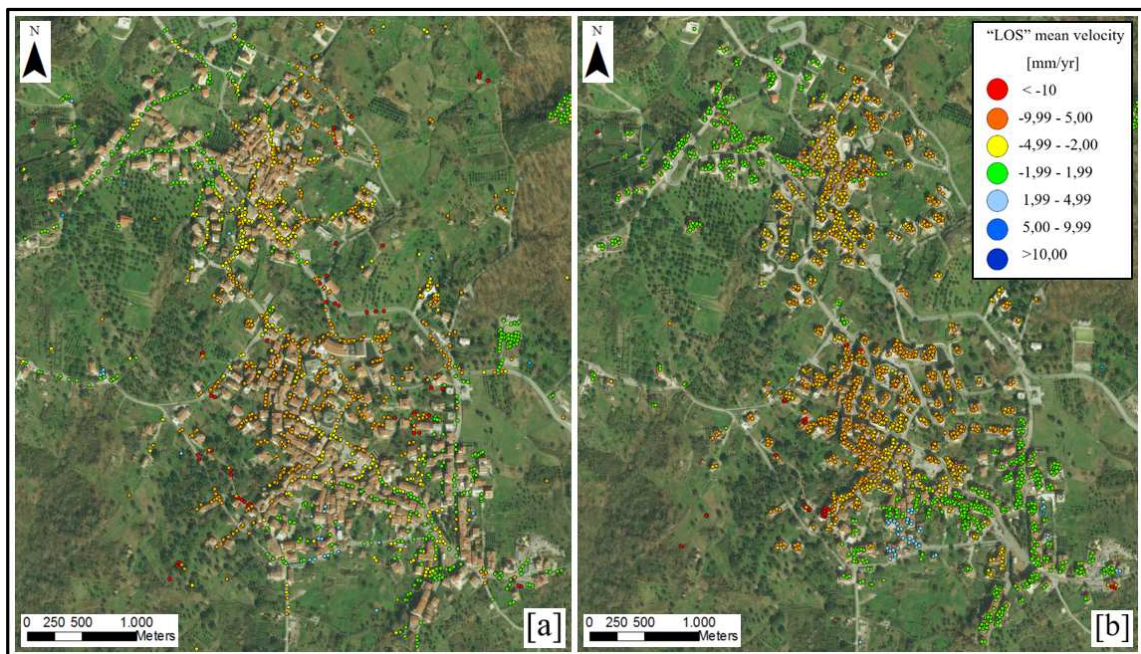


Figure 8.36 Targets identified on ground level (a) and on top of buildings (b) in descending track.

Moreover, for each building, combination of COSMO-SkyMed interferometric data acquired along “ascending” and “descending” tracks allows to identify maximum vertical and horizontal (East-West) components (Fig. 8.37) and prevalent direction of movement (Fig. 8.38).

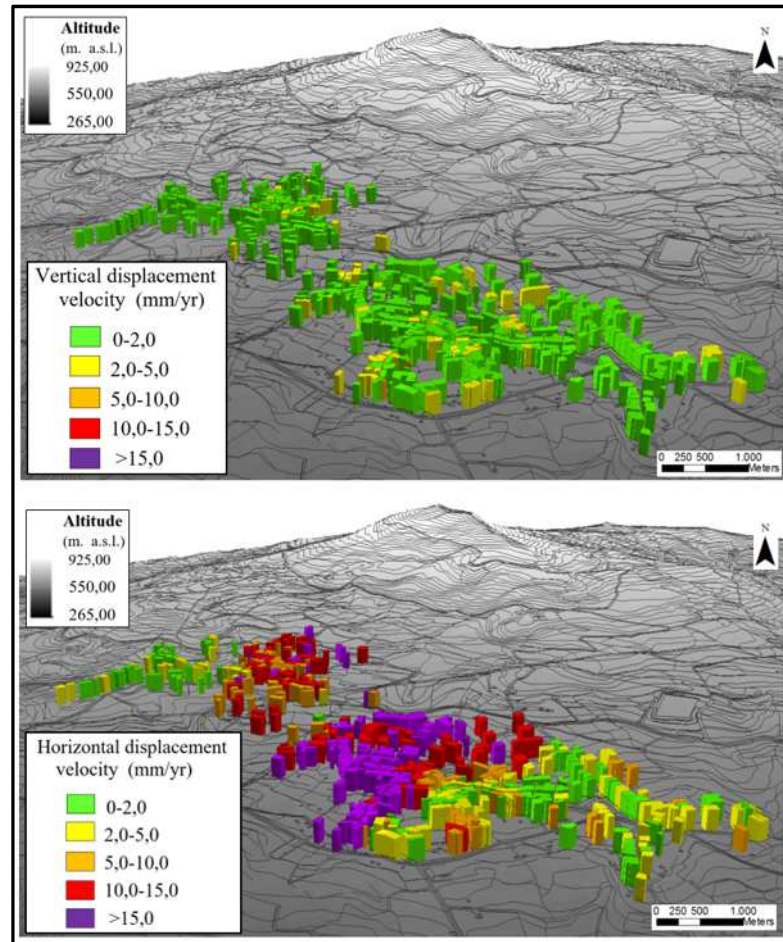


Figure 8.37 Maximum vertical and horizontal displacement rate of buildings in Moio della Civitella.

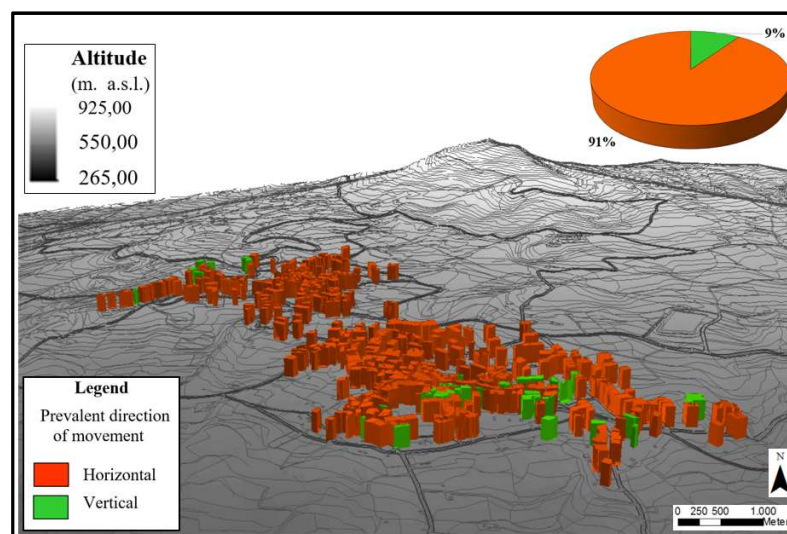


Figure 8.38 Prevalent direction of movement of buildings in Moio della Civitella urban settlement.

As it is possible to note, most buildings in Moio della Civitella urban settlement are characterized by horizontal component higher than vertical: such point is more evident in the historical urban center of Moio and Pellare, where value of ratio between horizontal and vertical components is generally greater than 5 (Fig. 8.39).

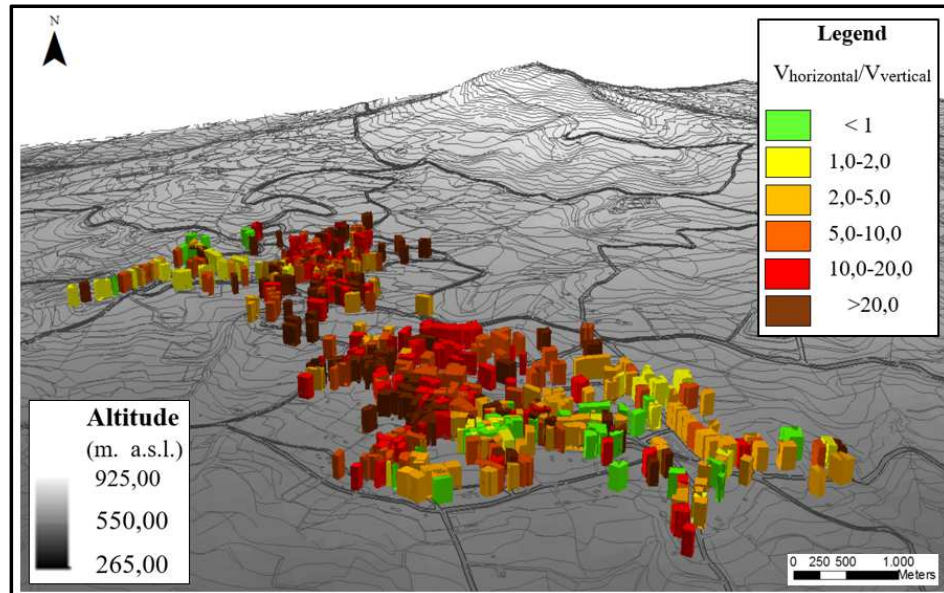


Figure 8.39 Ratio between horizontal and vertical components of movement for each building in Moio della Civitella urban settlement.

Subsequently, both for each building and surrounding area, the highest velocity of displacement among vertical and horizontal components has been compared with a threshold value of 2 mm/year, thus distinguishing buildings and areas that are “moving” from those that are “not moving” (Figs. 8.40 and 8.41).

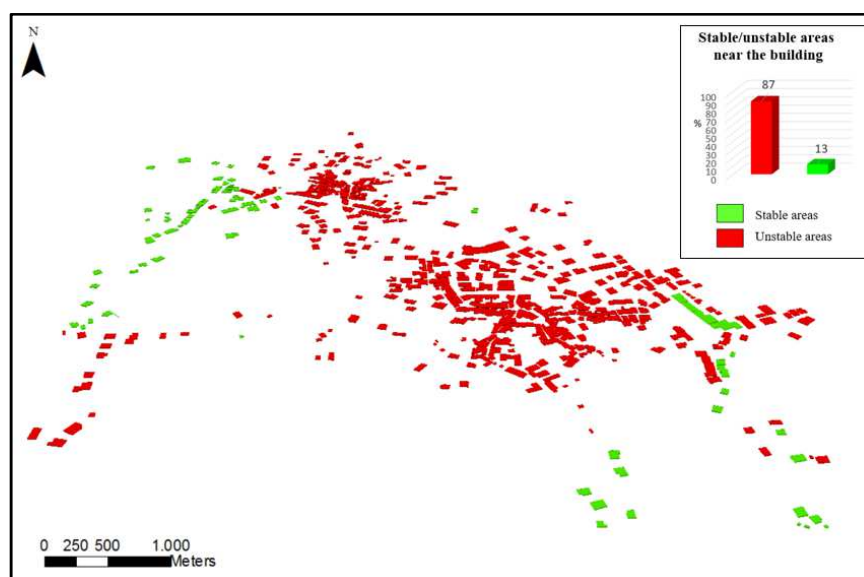


Figure 8.40 Map of stable/unstable areas surrounding the buildings at Moio della Civitella.

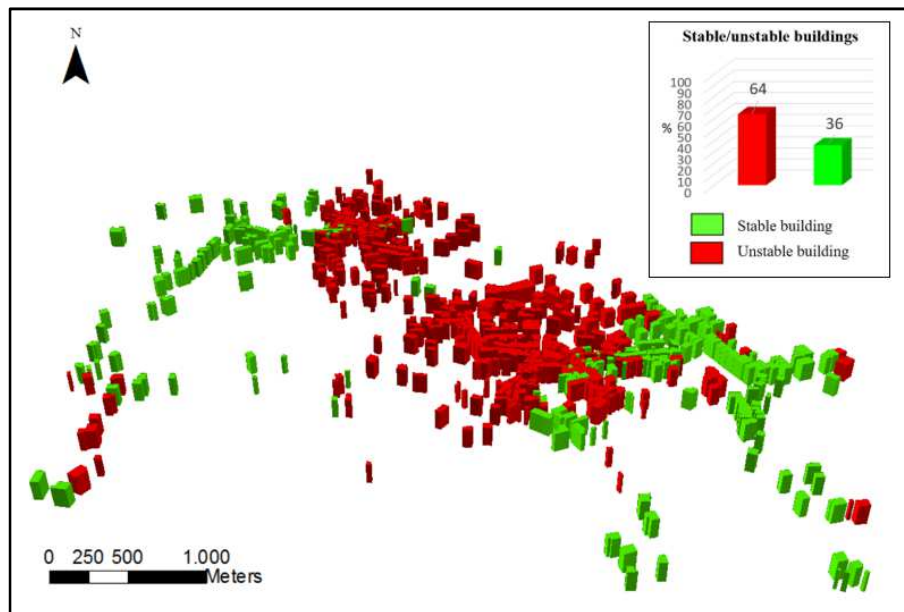


Figure 8.41 Map of stable/unstable buildings at Moio della Civitella.

It is important to highlight that 87% out of 504 buildings show in surrounding areas, at ground level, a displacement velocity higher than the threshold value of 2 mm/year, thus confirming the occurrence of ground instability and of movements under their foundations.

On the other hand, the analysis showed that 64% out of 504 buildings showed on the top of structure movement rates higher than the stability threshold and for this reason they are moving.

The above zoning of Moio della Civitella territory, showing stable/stable areas and buildings, allowed the identification of portions of the urban settlement where different problems may exist. In detail, the whole historical centers both of Moio and Pellare are affected by ground instability phenomena with maximum movement rate of about 20 mm/year along horizontal direction, higher than vertical component.

In the following, four possible scenarios of building behavior, basing on the comparison between displacement velocity of structure and of surrounding areas, were identified.

8.5.4 Assessment of possible scenarios of building behavior

Starting from the distinction between “stable/unstable” structures and areas near buildings, as indicators respectively of building response and ground movement, four possible scenarios of building behavior have been identified, as mentioned in paragraph 7.2.

Comparison of displacement velocity both of building and surrounding area at ground level, and the analysis of crack patterns exhibited by building façades, provided useful information to assess preliminary relationship between landslide-induced movements and performance of superstructures.

Below, some examples of above mentioned scenarios are shown.

- Scenario n. 1

	Occurrence of damage	Possible scenario
$V_{\text{building}} < 2 \text{ mm/yr}$ $V_{\text{ground}} < 2 \text{ mm/yr}$	NO	Building and surrounding area are stable. No damage and deformation to building

The first possible scenario (Figs. 8.42 and 8.43) is characterized by stability conditions both of building and of surrounding area. Moreover, no damage was surveyed on building façades, thus confirming that area is stable and structure does not show structural problems and deformations.

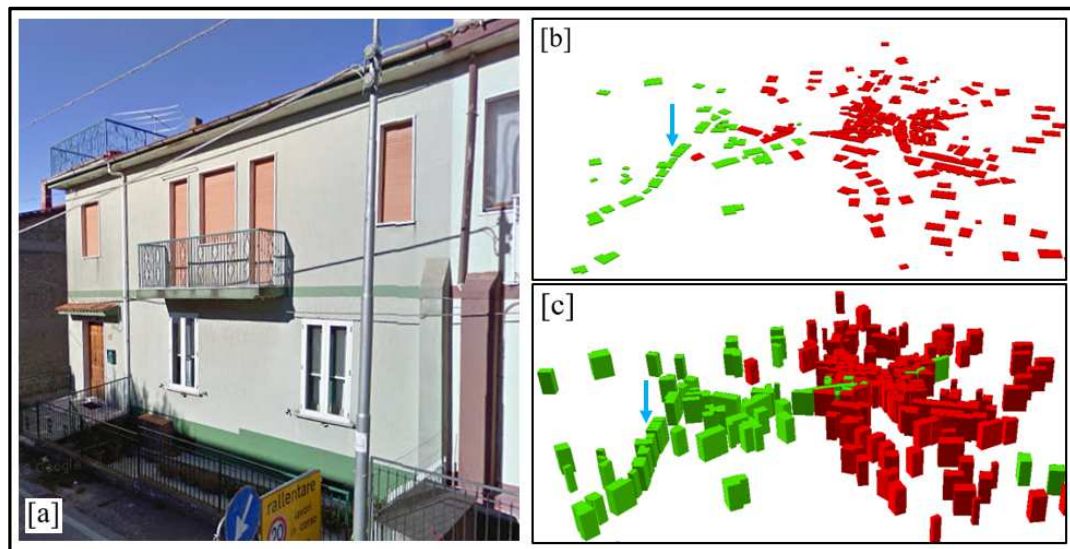


Figure 8.42 Example of buildings representative of the first possible scenario in Moio urban settlement (a): its identification in stable/unstable areas map (b) and in stable/unstable buildings map (c).

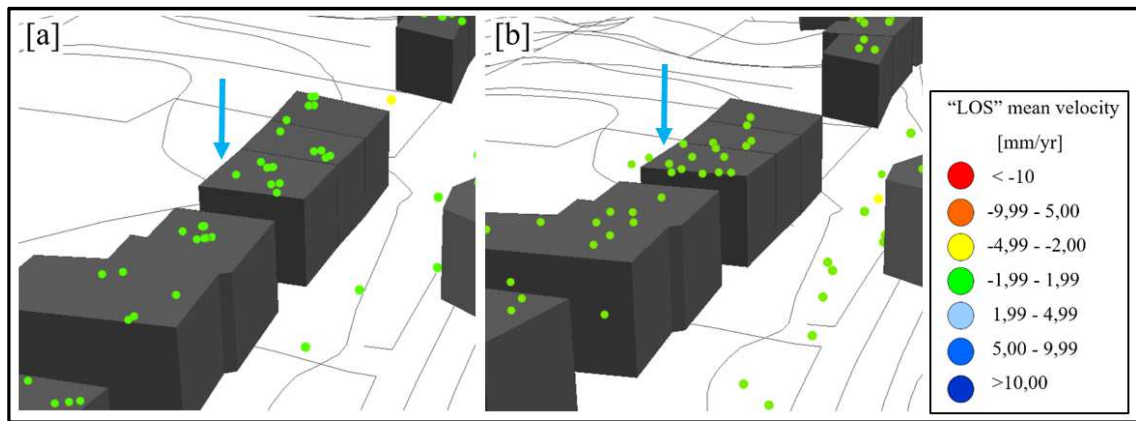


Figure 8.43 Targets identified on a building and on the surrounding area by COSMO-SkyMed products obtained by ascending (a) and descending (b) tracks.

- Scenario n. 2

	Occurrence of damage	Possible scenario
$V_{\text{building}} < 2 \text{ mm/yr}$ $V_{\text{ground}} > 2 \text{ mm/yr}$	NO	Areas near building are unstable while building does not show deformations and damage

The second possible scenario (Figs. 8.44 and 8.45) is characterized by ground instability, while the building is not moving, showing a displacement velocity under the set moving threshold.

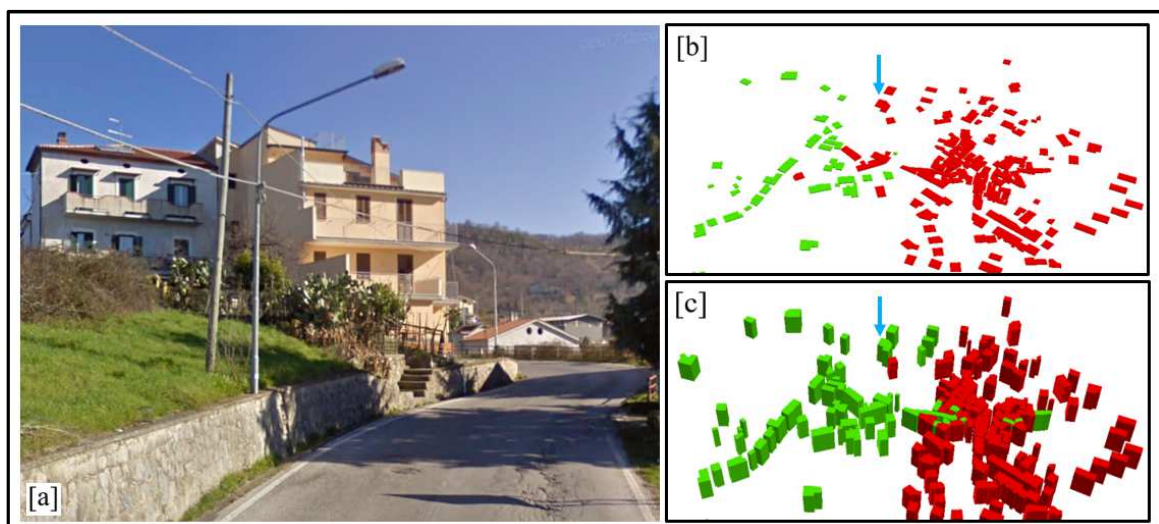


Figure 8.44 Example of buildings representative of the second possible scenario in Moio urban settlement (a): its identification in stable/unstable areas map (b) and in stable/unstable buildings map (c).

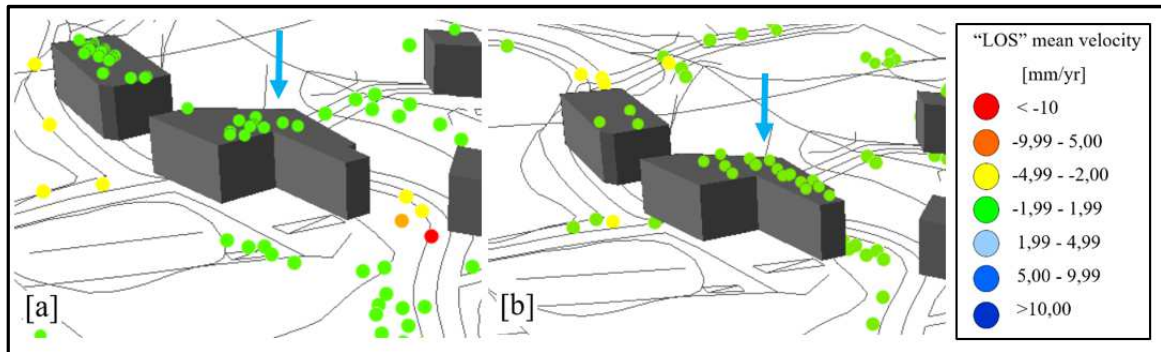


Figure 8.45 Targets identified on a building and on the surrounding area by COSMO-SkyMed products obtained by ascending (a) and descending (b) tracks.

As it is possible to note in Figure 8.44, areas near the building are not stable with damage to roads, as indicator of occurrence of a landslide event; no damage, instead, was surveyed on façades, thus confirming that building structural properties allow to decrease effects transmitted to superstructure by ground movement.

- **Scenario n. 3**

	Occurrence of damage	Possible scenario
$V_{\text{building}} > 2 \text{ mm/yr}$ $V_{\text{ground}} < 2 \text{ mm/yr}$	YES/NO	Areas near building are stable. Damage and deformation of building are due to other causes

Such case shows velocity values that are above the set movement threshold on the building and below at ground level. Building deformation and possible damage could be induced by other causes, such as structural problems due to errors during design or construction phases. In Moio della Civitella urban settlement, cases of buildings showing this scenario have not been recorded.

- **Scenario n. 4**

	Occurrence of damage	Possible scenario
$V_{\text{building}} > 2 \text{ mm/yr}$ $V_{\text{ground}} > 2 \text{ mm/yr}$	YES/NO	Building and surrounding areas are unstable. Damage could occur both on building and on the surrounding areas

In this case, both areas near the building and structure are unstable, generating damage to roads and services and probably to superstructure.

According to such condition, two further scenarios could occur, depending on building displacement velocity compared with ground movement rate:

- **Scenario n. 5**

	Occurrence of damage	Possible scenario
$V_{\text{building}} < V_{\text{ground}}$	NO	Building and surrounding areas are unstable, but constructive properties allow to decrease effects on building

Building and surrounding areas show a displacement rates that are above the movement threshold: moreover, foundations stiffness and constructive properties allow to decrease effects transmitted to superstructure (Figs. 8.46 and 8.47).

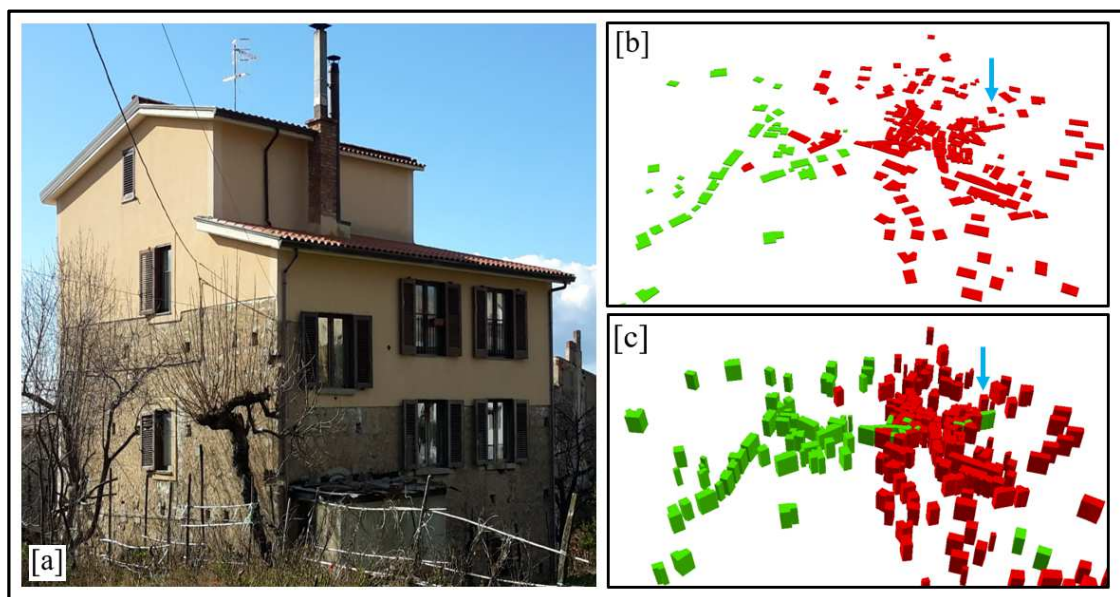


Figure 8.46 Example of buildings representative of the fifth possible scenario in Moio urban settlement (a): its identification in stable/unstable areas map (b) and in stable/unstable buildings map (c).

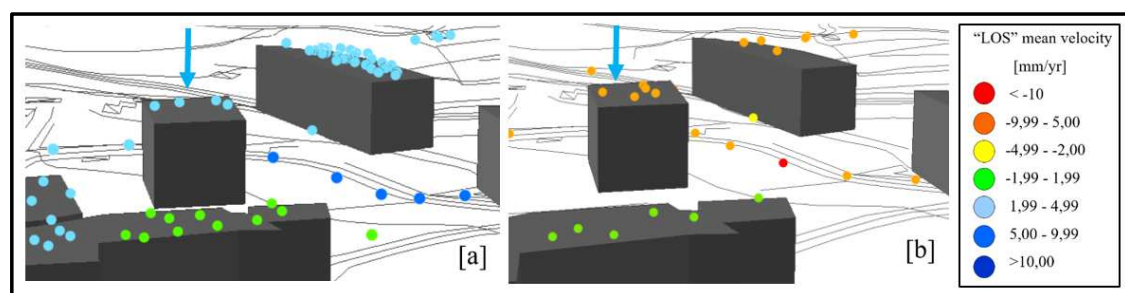


Figure 8.47 Targets identified on a building and on the surrounding area by COSMO-SkyMed products obtained by ascending (a) and descending (b) tracks.

- **Scenario n. 6**

	Occurrence of damage	Possible scenario
V_building > V_ground	YES	Building and surrounding areas are unstable, but structural problems or geological local conditions induce an increase of effects on building

Both building and the surrounding areas are unstable showing a displacement rates higher than 2 mm/yr, but structural problems and constructive properties such as different floor height of adjacent buildings, or geological conditions (e.g. local rock outcropping), can generate an increase of landslide-induced effects on superstructure (Figs. 8.48 and 8.49).

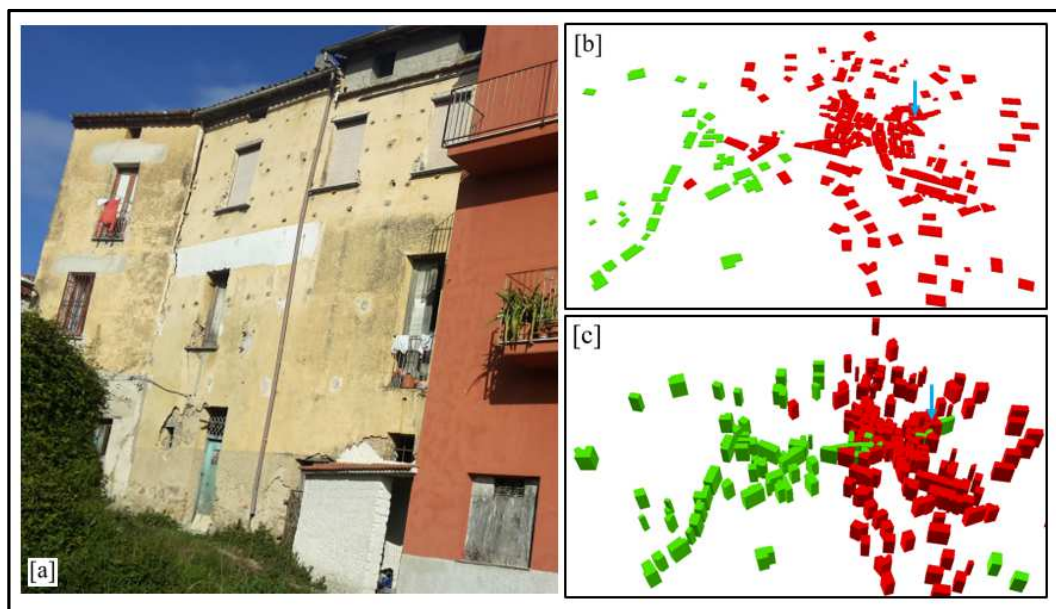


Figure 8.48 Example of buildings representative of the sixth possible scenario in Moio urban settlement (a): its identification in stable/unstable areas map (b) and in stable/unstable buildings map (c).

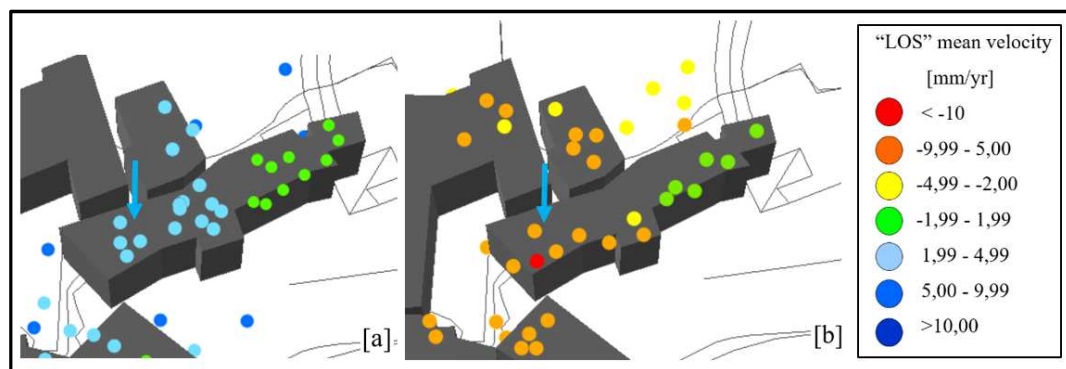


Figure 8.49 Targets identified on a building and on the surrounding area by COSMO-SkyMed products obtained by ascending (a) and descending (b) tracks.

Assessment of observed damage on buildings, characterized by occurrence of vertical cracks with increasing width from bottom to top of structure, confirms the results obtained by DInSAR data analysis. In detail, displacement rate on top of building is higher than at ground level, thus showing a rotational movement that produces the above -mentioned crack pattern.

Finally, availability of targets identified both in ascending and descending geometry for several buildings allowed to define ratio between building and surrounding area displacements, along horizontal and vertical directions of movement.

To this purpose, cumulated displacement of targets obtained by interferometric products in time span 2011-2016 has been taken into account (Figs. 8.50 and 8.51).

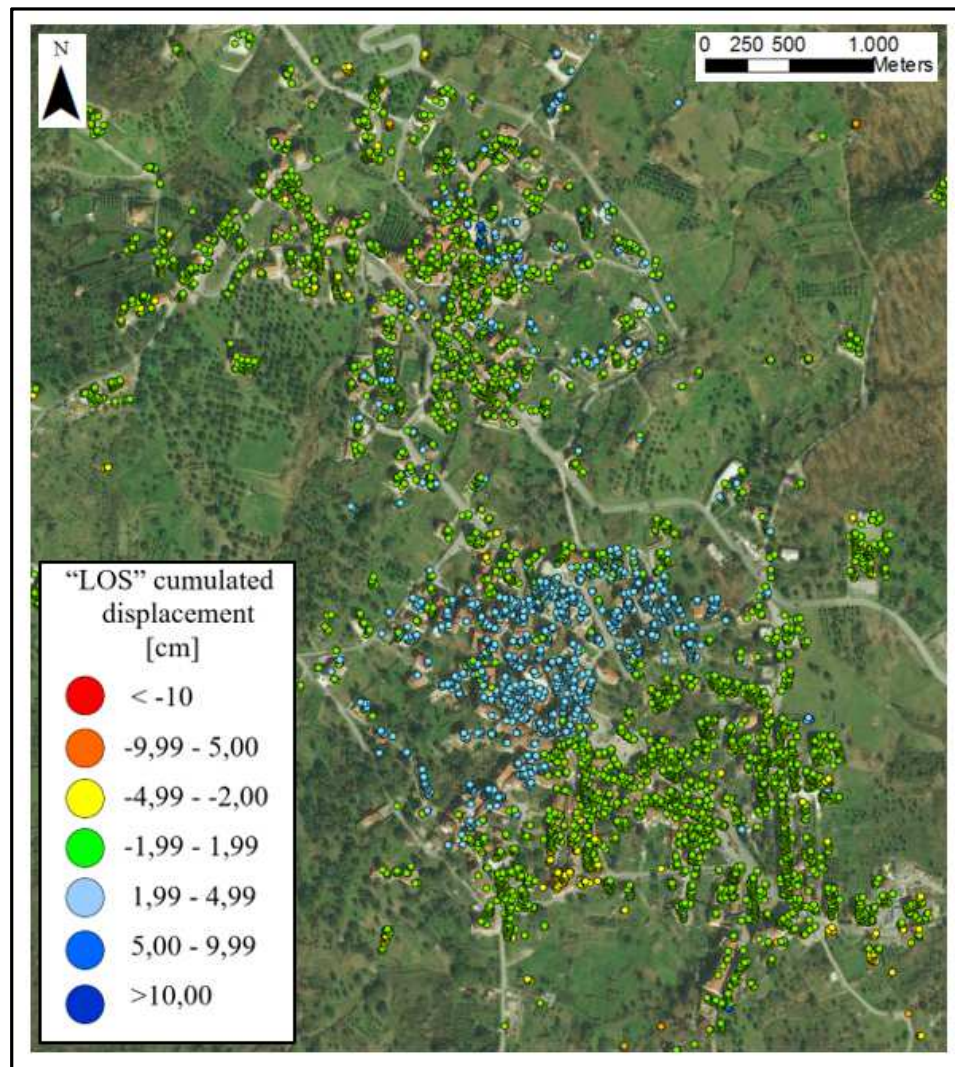


Figure 8.50 “LoS” cumulated displacement map of targets identified in Moio della Civitella urban settlement in “ascending” track in time span 2011-2016.

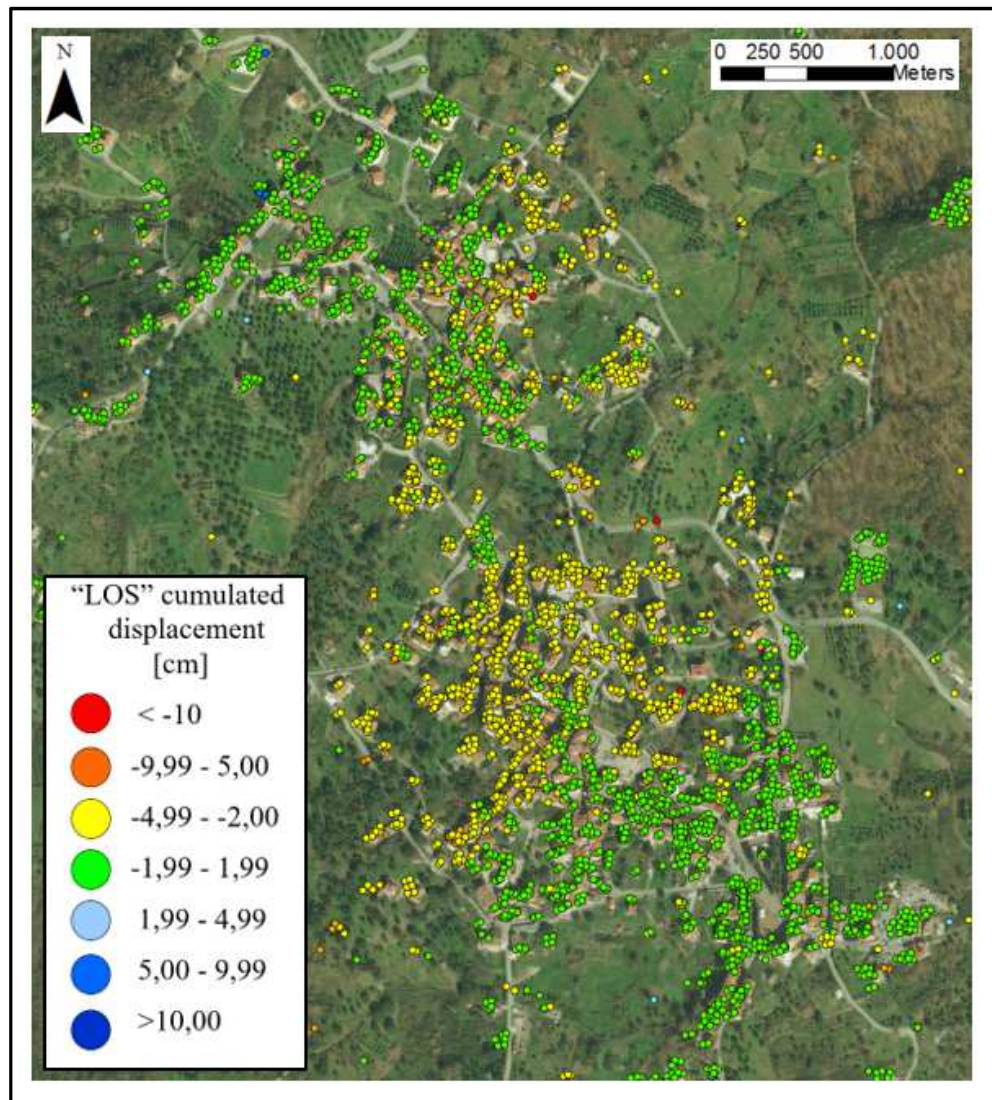


Figure 8.51 "LoS" cumulated displacement map of targets identified in Moio della Civitella urban settlement in "descending" track in time span 2011-2016.

According to different structural properties, all 504 buildings have been distinguished in terms of homogeneous constructive typology, in masonry and reinforced concrete buildings (Table 8.1).

Building ID	Constructive typology	Building Displacement		Surrounding area displacement		Dv_building / Dv_ground	Dh_building / Dh_ground
		Vertical	Horizontal	Vertical	Horizontal		
-	Masonry/ Reinforced concrete	Dv_build	Dh_build	Dv_ground	Dh_ground	[-]	[-]

Table 8.1 Scheme to evaluate ratio between displacements of building and surrounding area.

Such analysis allowed to get the following information (Fig. 8.52):

- reinforced concrete buildings showed displacements on top of structure equal or lower than those at ground level, due to high values of stiffness of reinforced concrete foundations (footings connected by beams or raft foundation) and of structure load-bearing, which allow to decrease effects transmitted by ground movements. Only 15% out of 143 reinforced concrete buildings showed values of ratio greater than 1,1.

Furthermore, such point is more evident with reference to horizontal displacement than to vertical movement, probably due to structural properties of reinforced concrete structures, in turn characterized by very high values of strength along horizontal direction, awarded during design phase to withstand an earthquake devastating effect;

- on the other hand, 46% out of 352 masonry buildings have horizontal displacement higher than in surrounding areas, showing a behavior very different from reinforced concrete buildings, while, with reference to vertical component of movement, their behavior seems to be similar. Probably, such results could be due to masonry damage susceptibility higher to horizontal deformations than to vertical distortions, depending on high values of compressive strength and very low values of tensile strength.

Furthermore, historical masonry structures are generally built in aggregates and their different construction properties, such as foundation typology, height of floors, mechanical properties of materials, could increase landslide-induced effects.

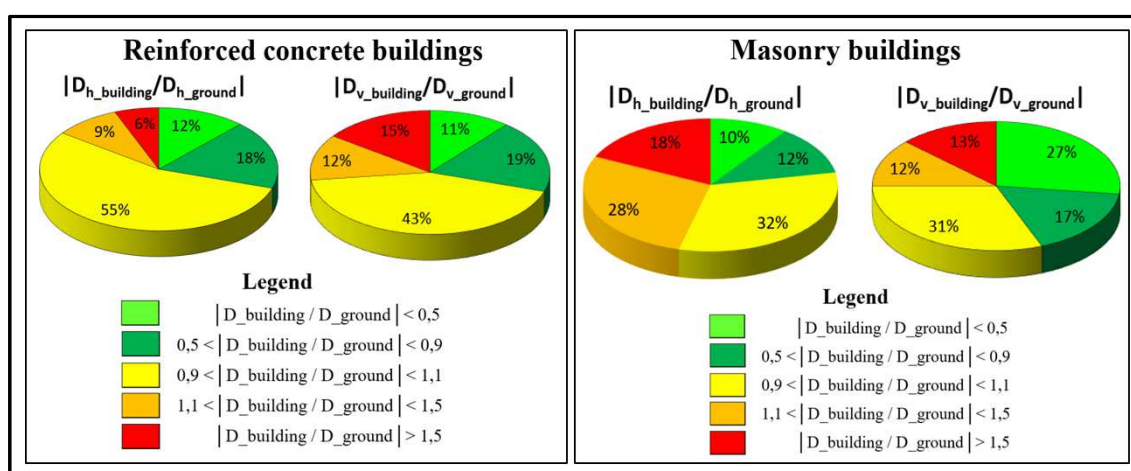


Figure 8.52 Ratio between displacement of buildings and of surrounding areas along horizontal and vertical directions of movement for reinforced concrete (on the left) and masonry (on the right) buildings.

8.5.5 Updating of available landslide inventory map

As mentioned in paragraph 7.2, integrated analysis of DInSAR data with results of damage survey to facilities, allows to update boundary and state of activity of landslide inventory maps. In detail, such analysis is reported in February 2015, according to availability of damage recorded on structures and infrastructures of the whole territory.

To this purpose, the landslide inventory map produced in 2012 by South Campania River Basin Authority has been used.

Building damage survey (Fig. 8.53) was performed in February 2015 using Iovine & Parise (2002) classification.

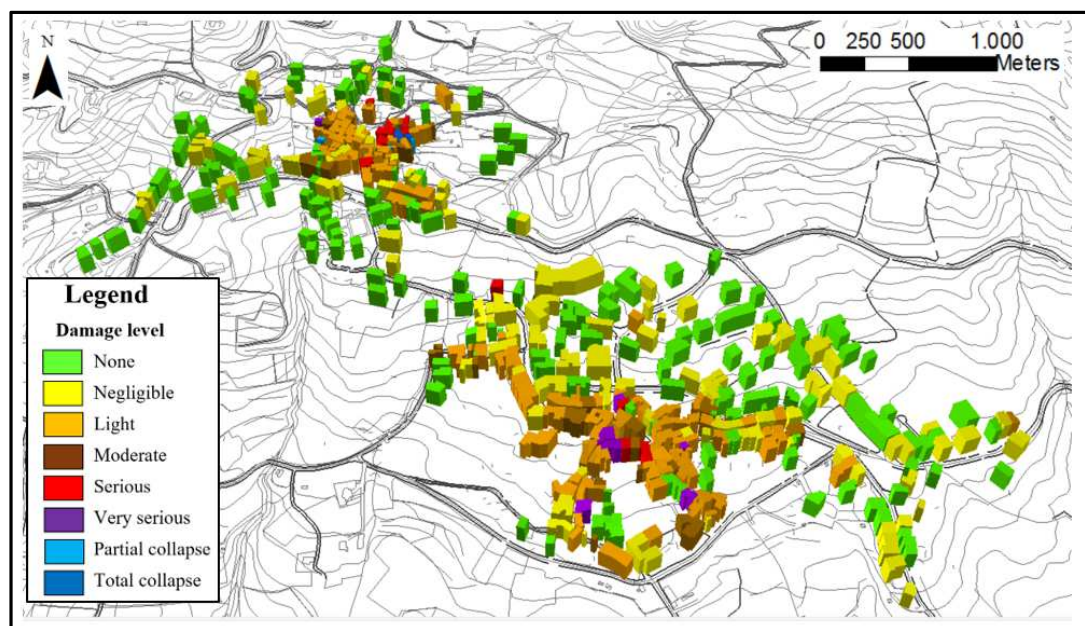


Figure 8.53 Building damage map of Moio della Civitella urban settlement in February 2015, according to Iovine & Parise classification (2002).

Moreover, to assess state of activity of landslides affecting Moio della Civitella municipality by DInSAR data, only the displacement velocity map in 2014 has been considered: movement rate of targets in the year preceding damage survey is an useful indicator of landslide intensity (Fig 8.54).

Aimed to identify moving areas, the following parameters have been assessed:

- as regards the velocity threshold, a value of ± 2 mm/yr, along the LoS, has been selected;
- at least two targets have been identified for the individuation of the anomalous area;
- homogeneity index, defined as the ratio between number of moving targets and total number of targets within a given area, was fixed equal to 0,2.

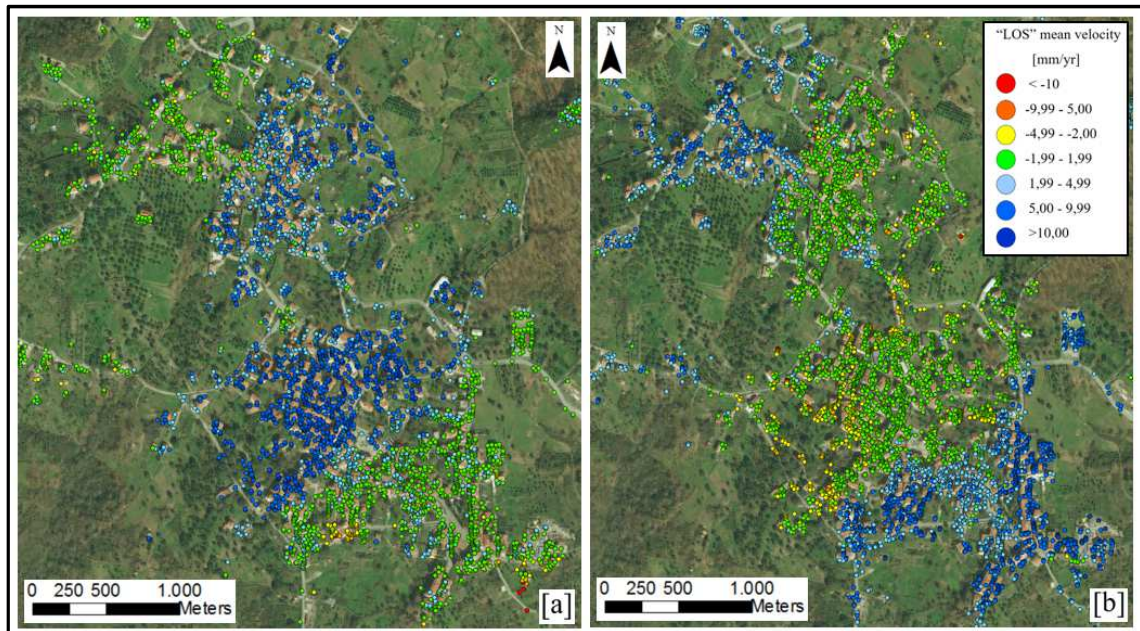


Figure 8.54 Displacement velocity maps obtained by COSMO-SkyMed images in 2014: along ascending (a) and descending (b) tracks.

Furthermore, the cross-comparison of surveyed damage and DInSAR radar-interpreted data with the existing landslide inventory map of the whole study area was performed.

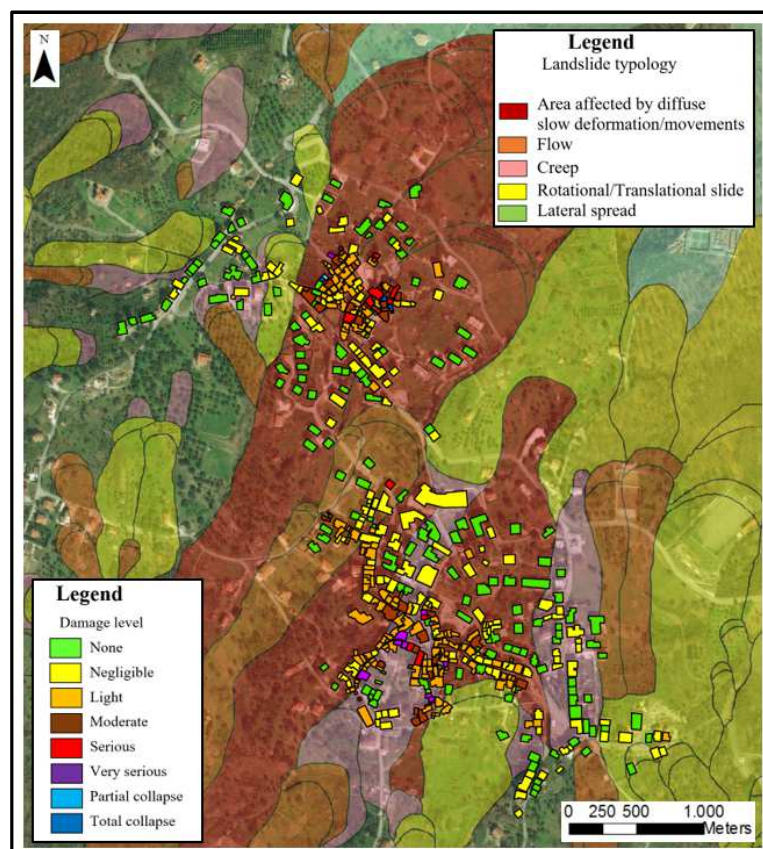


Figure 8.55 Integrated map of landslide typologies and building damage in Moio della Civitella urban settlement.

Moio della Civitella urban settlement is affected by four main landslide typologies: rotational/translational slide, creep, flow and diffuse slow deformation/movements.

Moreover, 466 of 502 buildings are located within landslide-affected areas. As is possible to note in Figure 8.56, higher damage severity levels have been surveyed within areas affected by flows, creep and diffuse slow deformations, while rotational/translation slides induce generally negligible and light damage on buildings.

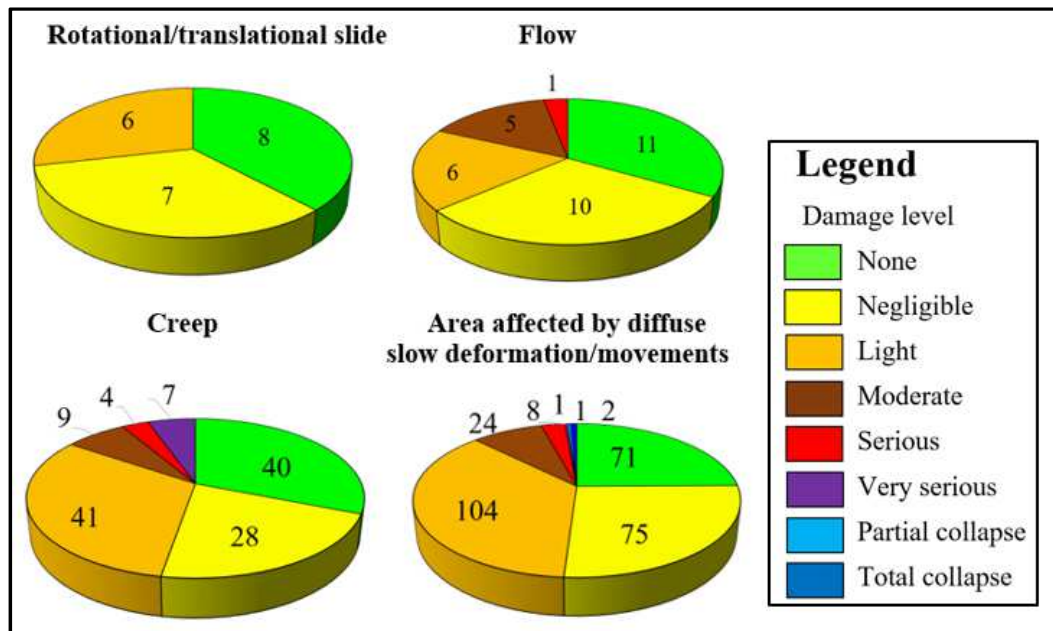


Figure 8.56 Distribution of building damage level for different landslide typologies in Moio della Civitella urban settlement.

Subsequently, anomalous areas identified through DInSAR analysis and recognized also by *in situ* survey, allowed to update the boundary of two landslides, as indicated in Figures 8.57 and 8.58.

In the first case, a landslide in the N-W sector of Moio della Civitella territory was considered: several targets recorded in the surrounding area showed in 2014 a displacement velocity along LoS direction of about 8 mm/yr and 6 mm/yr, respectively measured by ascending and descending images (Fig. 8.57 a, b), thus highlighting occurrence of ground movement. Furthermore, *in situ* survey showed evidence of cracks on roads near the considered landslide (Fig. 8.57 c, d).

According to these reasons, landslide boundary has been updated assuming a retrogressive distribution of activity, whose rupture surface is extending in the opposite direction with respect to the movement direction (Fig. 8.57e).

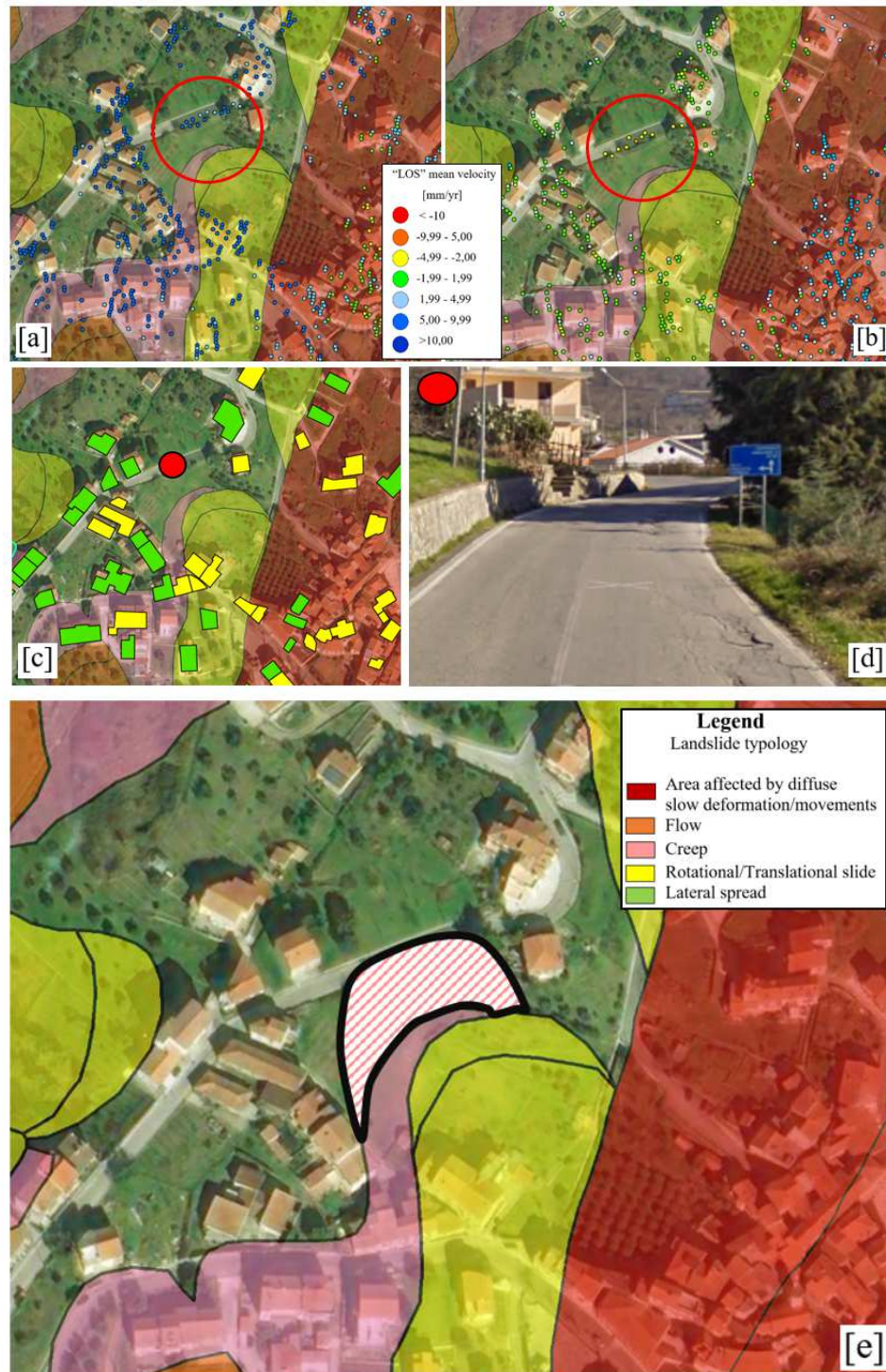


Figure 8.57 Combined use of DInSAR data (a, b) and results of *in situ* survey (c, d) for updating of landslide boundary (e).

The second landslide affects a S-E sector of the municipality territory: scatterers identified on buildings and roads showed in 2014 a displacement rate along LoS direction of about 4 mm/yr and 8 mm/yr, respectively acquired by ascending and descending images (Fig. 8.58 a,b); moreover, several damage corresponding to negligible and light degrees have been surveyed on buildings and facilities in surrounding areas (Fig. 8.58 c,d,e,f,g).

Such considerations allowed to identify a new landslide, probably a slow-moving rotational slide, as shown in Figure 8.58h.

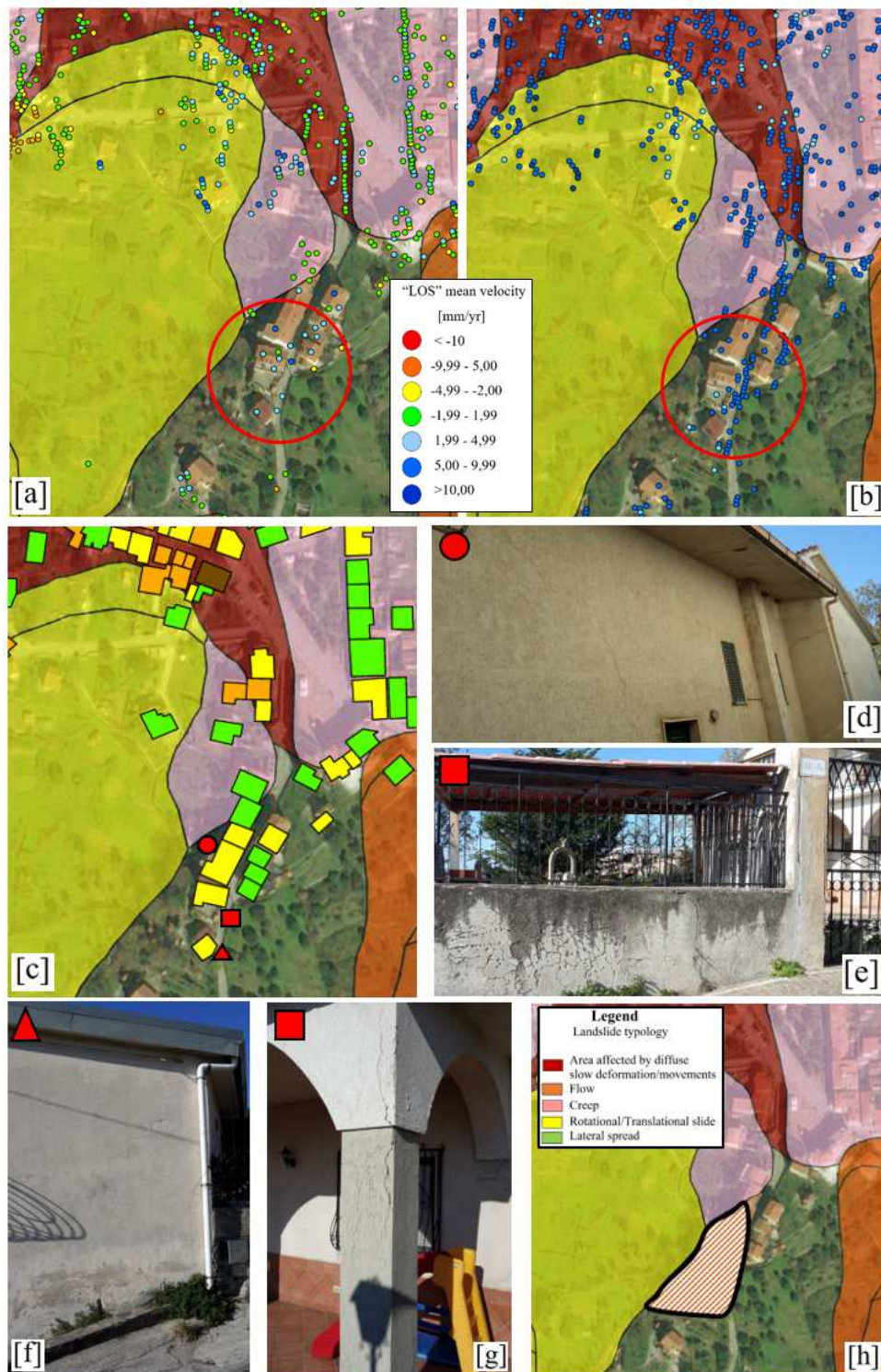


Figure 8.58 Combined use of DInSAR data (a, b) and results of *in situ* survey (c, d, e, f, g) to identify a new landslide (e).

As regards state of activity, comparison of available landslide inventory map with results of damage survey showed the occurrence of medium and high damage levels also within dormant landslide-affected areas (Figs. 8.59 and 8.60).

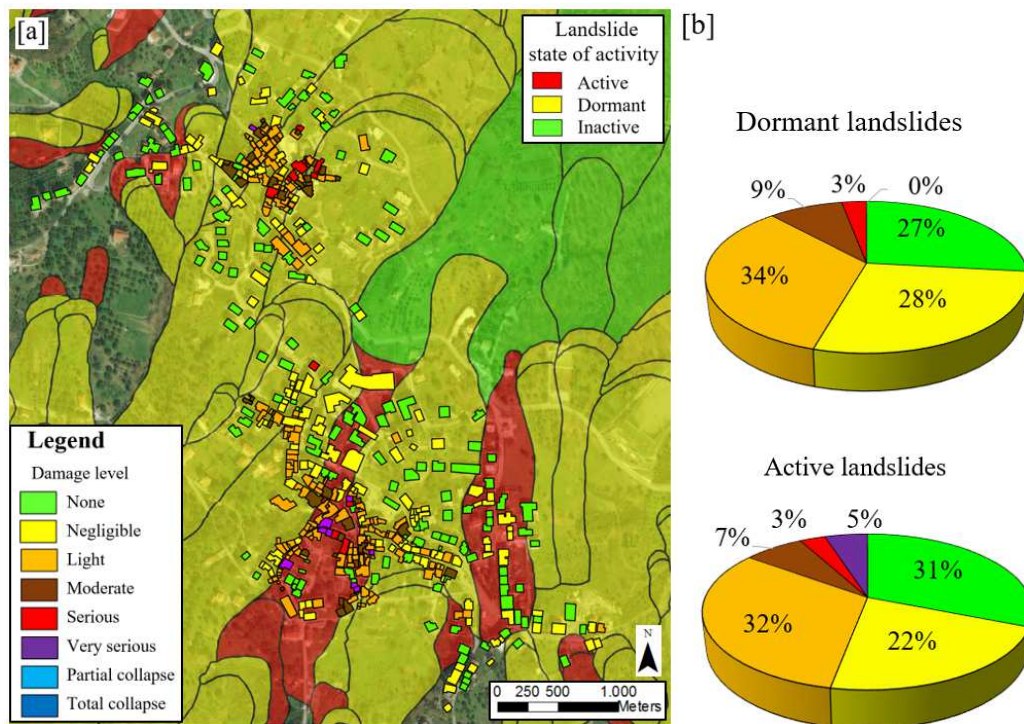


Figure 8.59 Distribution of building damage for different landslide state of activity recorded in Moio della Civitella urban settlement: map (a) and pie-chart (b).



Figure 8.60 Examples of damage occurred to buildings within dormant landslide affected areas.

In addition, the analysis of ascending and descending DInSAR data in 2014 allowed to investigate displacement rates both of buildings and surrounding ground within areas affected by landslides, showing significant velocities of targets identified (Fig. 8.61).

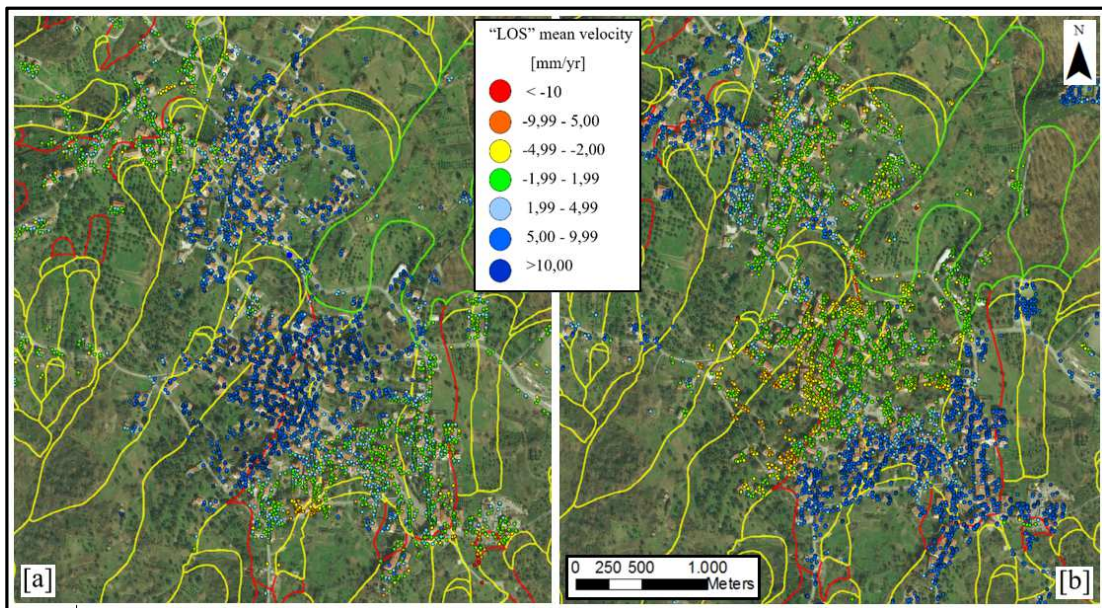


Figure 8.61 Integrated map of landslides state of activity and targets identified by ascending (a) and descending (b) SAR images in Moio della Civitella urban settlement.

Finally, according to the above mentioned results, several landslides, mapped as dormant in 2012, have been updated and re-classified as active in February 2015: they are characterized by local reactivations, probably due to intense and continuous rainfall (Fig. 8.62).

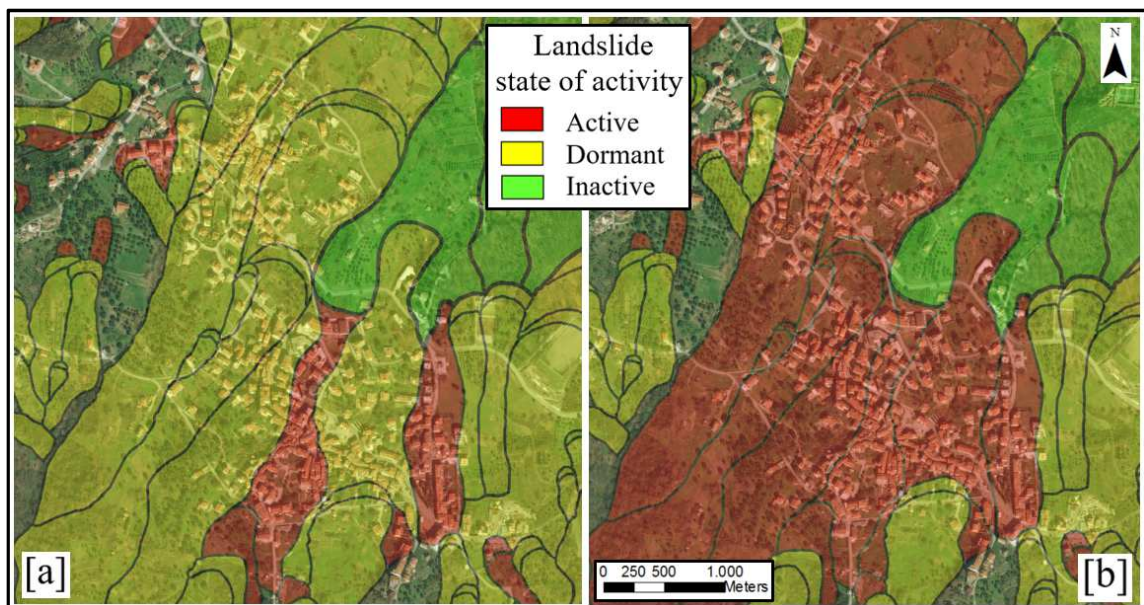


Figure 8.62 Landslide state of activity map in Moio della Civitella urban settlement: as mapped by Hydro-geomorphological Setting Plan in 2012 (a) and updated in 2015 (b).

8.5.6 Preliminary zoning of buildings vulnerability

According to the proposed approach, a qualitative matrix, combining landslide intensity and building damage degree, provides information on current instability of structures induced by ground movement.

Building damage map used in such analysis was carried out in February 2015 by *in situ* campaigns: in particular, damage assessment was performed using Iovine & Parise (2002) classification (Fig. 8.53).

As indicator of landslide intensity in time span preceding damage survey, the highest velocity of displacement among horizontal and vertical components, measured in 2014 by combining ascending and descending products near each building, has been taken into account (Fig. 8.54).

Subsequently, as discussed in paragraph 7.2, the two obtained datasets were merged in a qualitative vulnerability matrix, which, distinguishing masonry and reinforced concrete buildings, provided a preliminary zoning map of different “vulnerable areas” (Fig. 8.63).

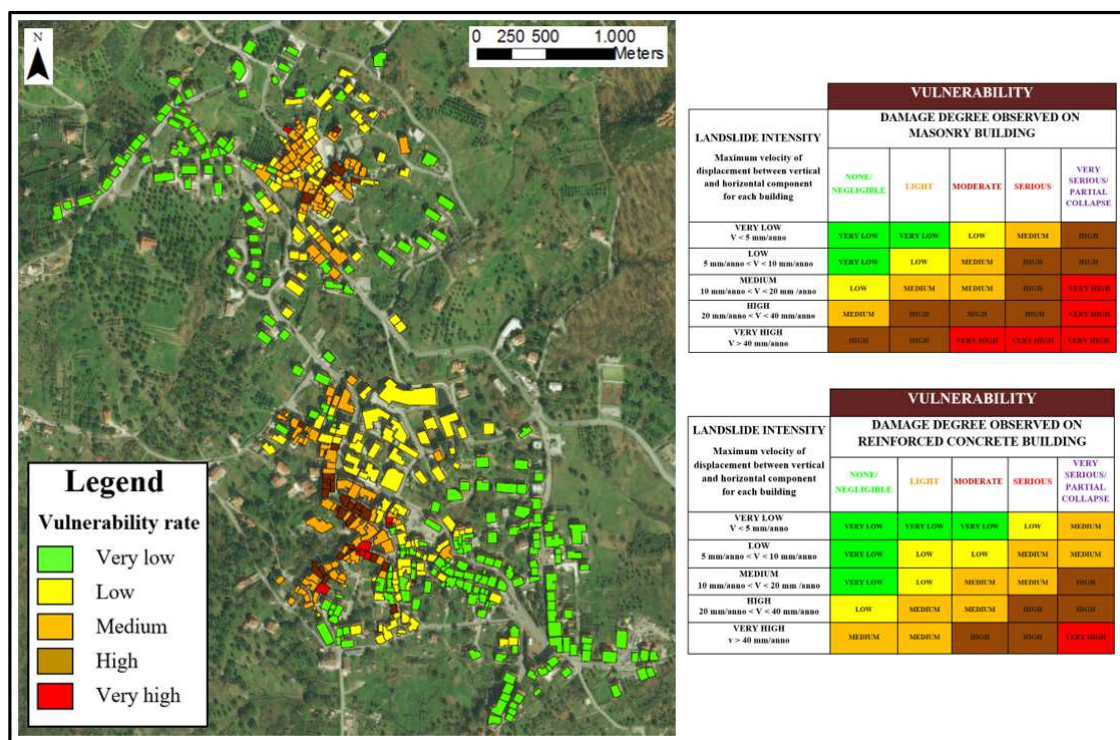


Figure 8.63 Vulnerability map of Moio della Civitella in February 2015 according to proposed matrices.

The matrix-based approach, at this scale of representation, seems a helpful tool in government and planning activities, allowing to identify, very quickly, different vulnerability rates and most critical cases in Moio della Civitella municipality.

8.6 Vulnerability assessment at medium scale

As mentioned in the paragraph 7.3, aim of medium scale analysis is to provide information on building damage future conditions, depending on spatial and temporal evolution of landslide intensity. To this aim, added to information of previous level, more detailed parameters aimed to better characterize landslides and exposed elements are required.

Furthermore, availability of additional characteristics related to building construction allowed to investigate also the vulnerability factors influencing performance of the structures affected by slow-moving landslide.

8.6.1 Detection of landslide kinematics by integrated analysis of DInSAR and conventional monitoring data

At this scale of representation, the combined use of conventional and innovative monitoring techniques allows to obtain more detailed information on slope failure mechanisms and their temporal evolution. It is important to highlight that a thorough knowledge of landslide kinematics cannot be conveniently reached without an adequate *in situ* monitoring.

To this aim, Moio della Civitella territory and, more in detail, the two urban centers of Pellare and Moio, have been thoroughly investigated by means of conventional monitoring instruments such as boreholes, topographic measure points, inclinometers, GPS network and a pluviometer station (Fig. 8.64), in order to study superficial and sub-superficial movements; furthermore, as regards piezometers, the water table was surveyed at the same boreholes used for the inclinometer measurements; they revealed groundwater levels regularly hosted by the debris cover, located very close to the ground surface (depth <5 m) without showing any significant oscillation in relation to rainfall.

More detailed results on past conventional monitoring campaigns have been discussed by Calcaterra et al. (2008), Calò (2009), Di Martire et al. (2015).

During this PhD research, displacement measurements were performed only on five out of 10 inclinometer boreholes still available, characterized by depth varying between 7,5 m and 28 m (Table 8.2), while the others resulted to be broken at different depths.

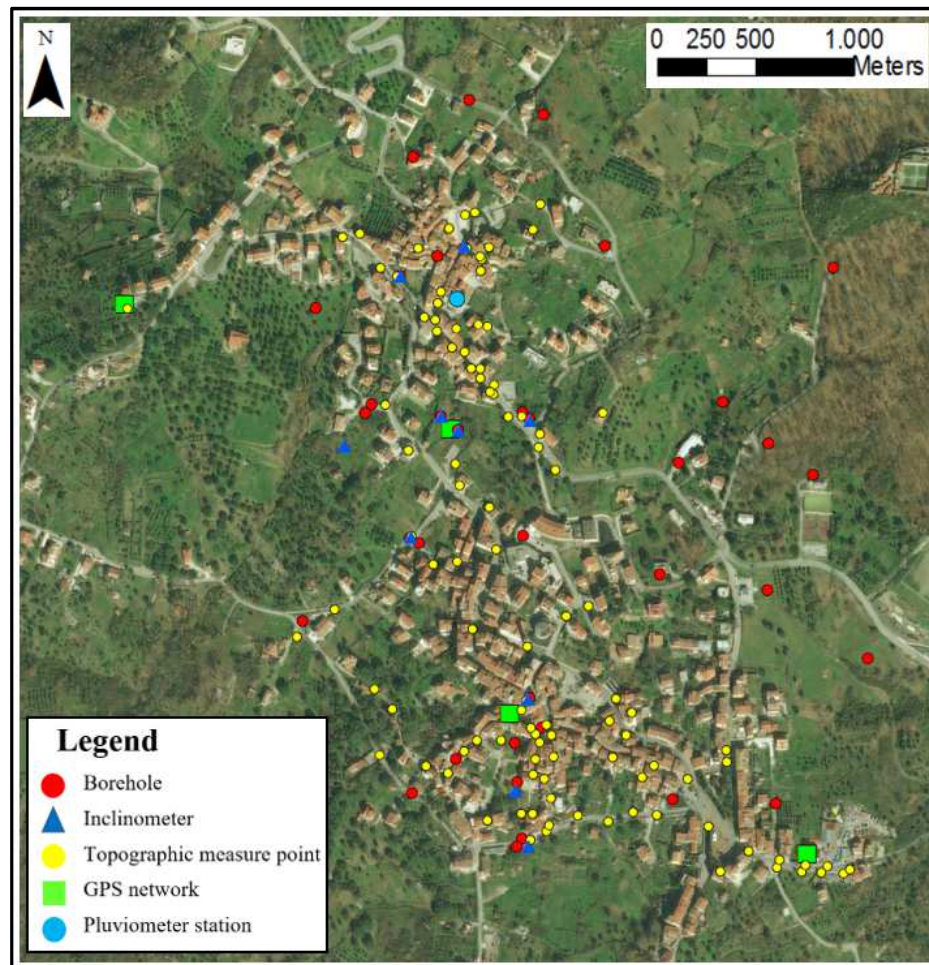


Figure 8.64 Conventional monitoring network installed at Moio della Civitella.

Inclinometer	Depth (m)	Location	Availability
I1	11,0	Moio	No (broken at 4 m)
I2	12,0	Moio	Yes
I3	12,5	Moio	Yes
I4bis	14,0	Pellare	Yes
I5	8,5	Pellare	No (broken at 3 m)
I6	10,5	Pellare	No (broken at 10 m)
I7	7,5	Pellare	No (broken at 3 m)
I8	20,5	Pellare	No (broken at 3,5 m)
I9	11,5	Pellare	Yes
I10	28,0	Pellare	Yes

Table 8.2 Summary of inclinometers features at Moio della Civitella.

Integrated analysis of stratigraphic columns and displacement measurements performed on inclinometer boreholes allowed to investigate the litho-stratigraphical features of the terrains and to localize shear surface (Fig. 8.65).

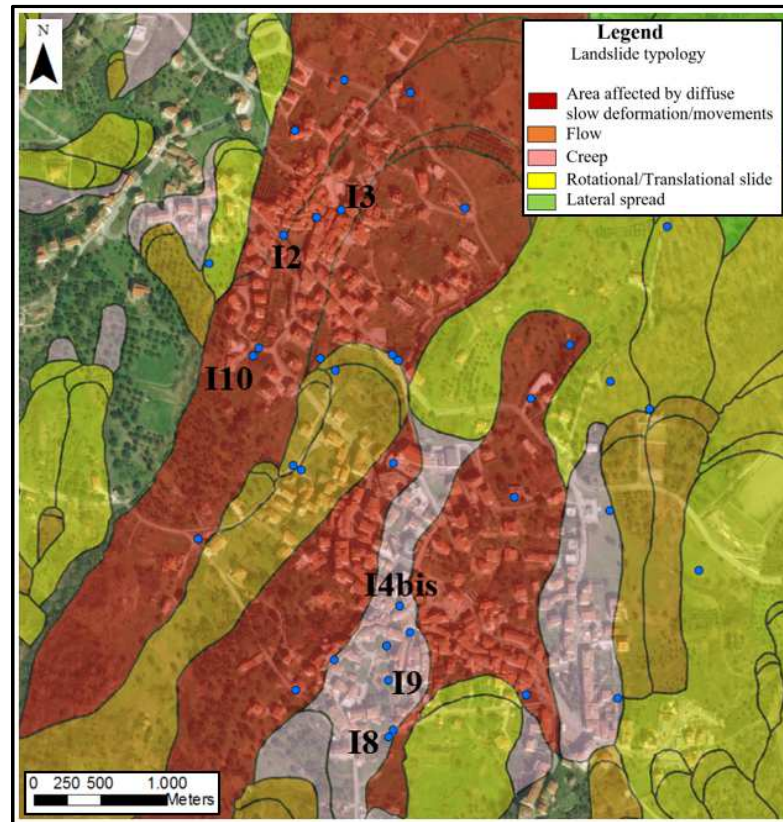


Figure 8.65 Location of boreholes at Moio della Civitella and identification of inclinometers investigated.

Inclinometer boreholes have been measured in the time span November 2015-May 2017.

Only millimetric movements have been recorded in the borehole I2; in addition, the measurements do not clearly indicate the presence of an active slip surface (Fig. 8.66).

Low rate of displacements (2 cm at ground surface) have been recorded in the borehole I3 in the considered time span; the displacements – depth graph allowed to recognize slip surface at a depth of about 7 m (Fig. 8.67).

As regards inclinometer I10, it is possible to note a clear difference of displacements at the depth of 11,50 m, where bed rock has been recognized, thus confirming the occurrence of shear surface (Fig. 8.68).

The readings related to the inclinometer I4bis showed, at ground surface, a cumulated displacement of 1,8 cm, while a slip surface was identified at a depth of about 12 m, corresponding to a level of conglomerates (Fig. 8.69).

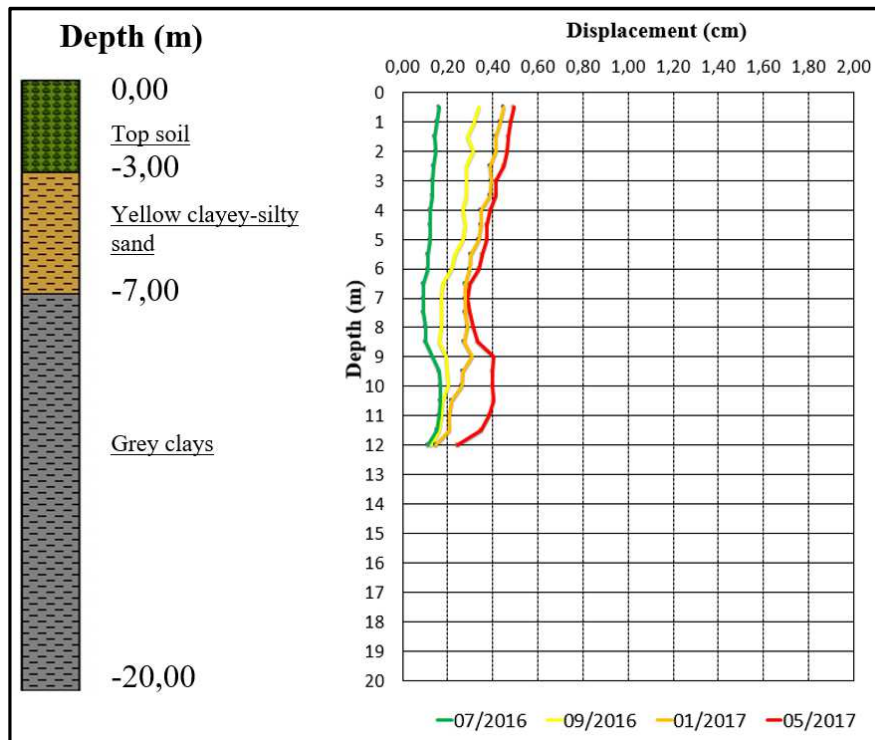


Figure 8.66 Inclinometer readings and stratigraphic column related to borehole I2.

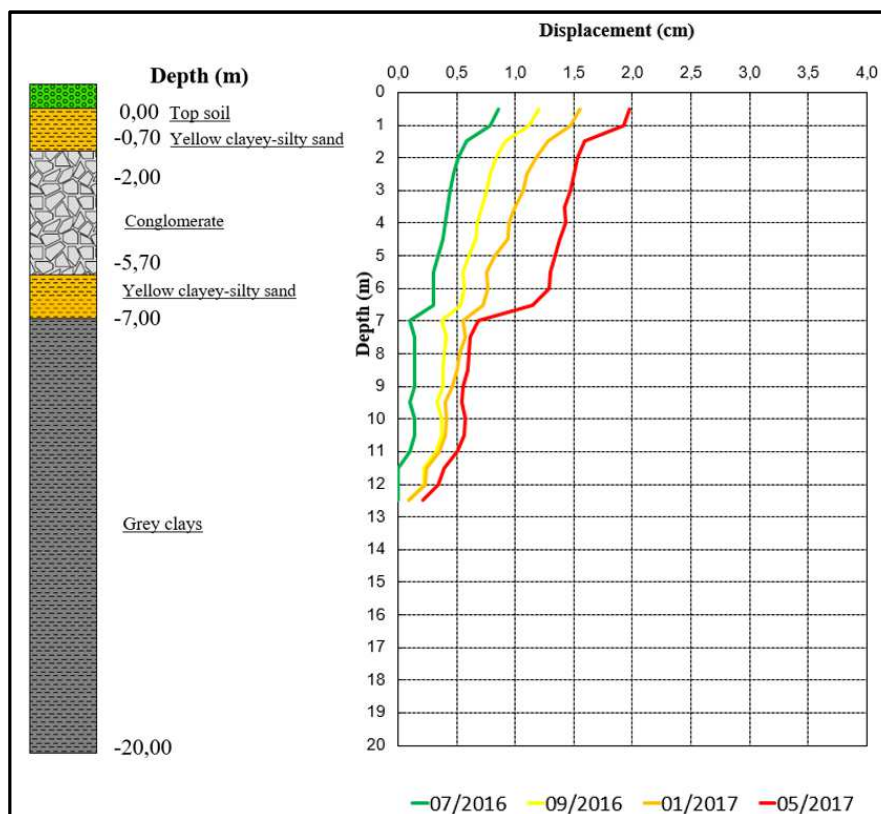


Figure 8.67 Inclinometer readings and stratigraphic column related to borehole I3.

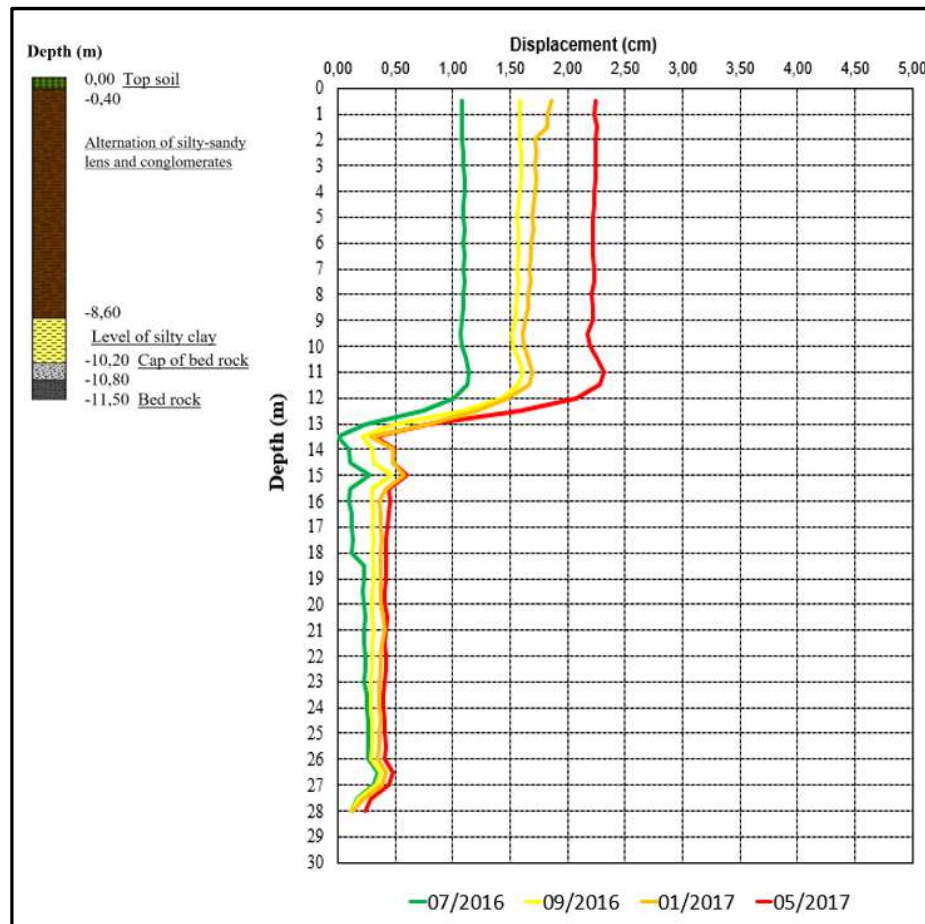


Figure 8.68 Inclinometer readings and stratigraphic column related to borehole I10.

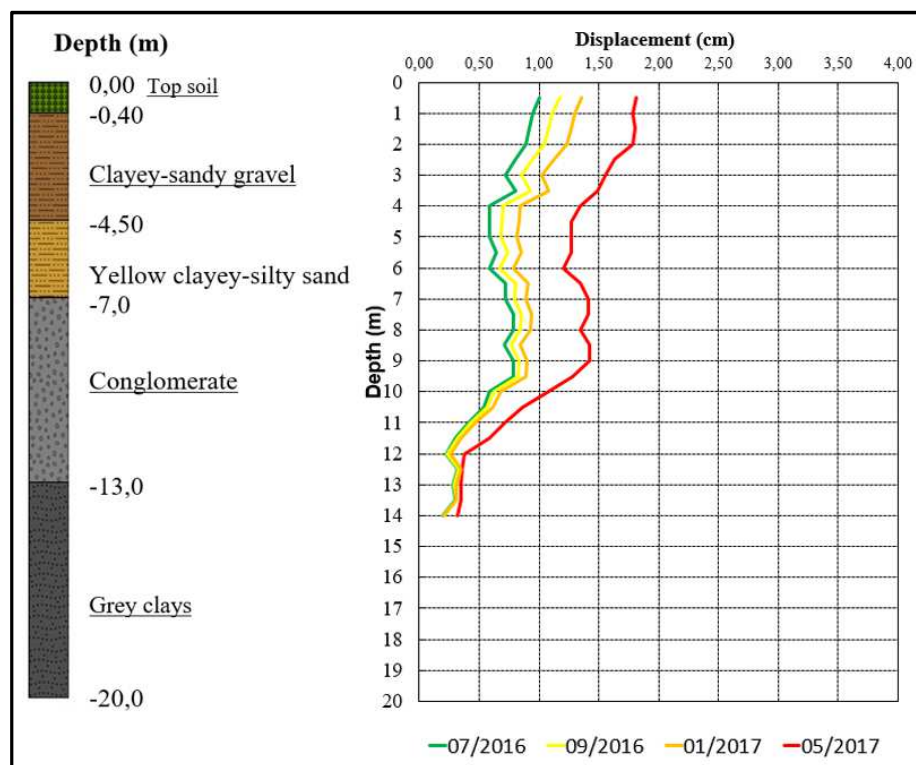


Figure 8.69 Inclinometer readings and stratigraphic column related to borehole I4bis.

Inclinometer I9 registered superficial displacements of 2,5 cm, showing an active shear surface at a depth of about 9 m (Fig. 8.70).

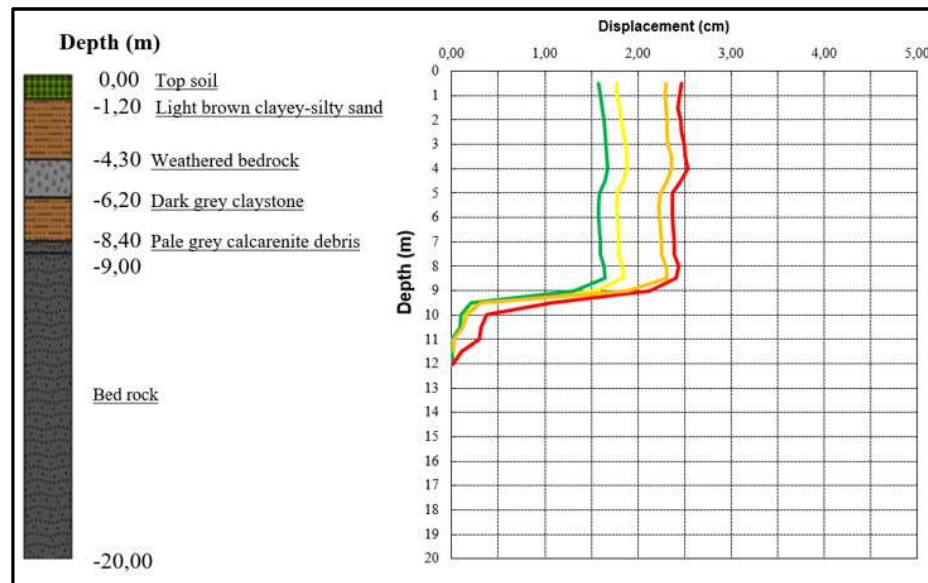


Figure 8.70 Inclinometer readings and stratigraphic column related to borehole I9.

Finally, as regards inclinometer in borehole I8, measurements were not performed in the considered time span, being broken at a depth of about 3 m. As is possible to note by previous measurements obtained in time-span October 2014- January 2015, high displacement rate (1 cm) has been recorded in 3 months and two active shear surfaces, respectively, at depths of about 3,5 and 11 m have been identified in January 2015 (Fig 8.71).

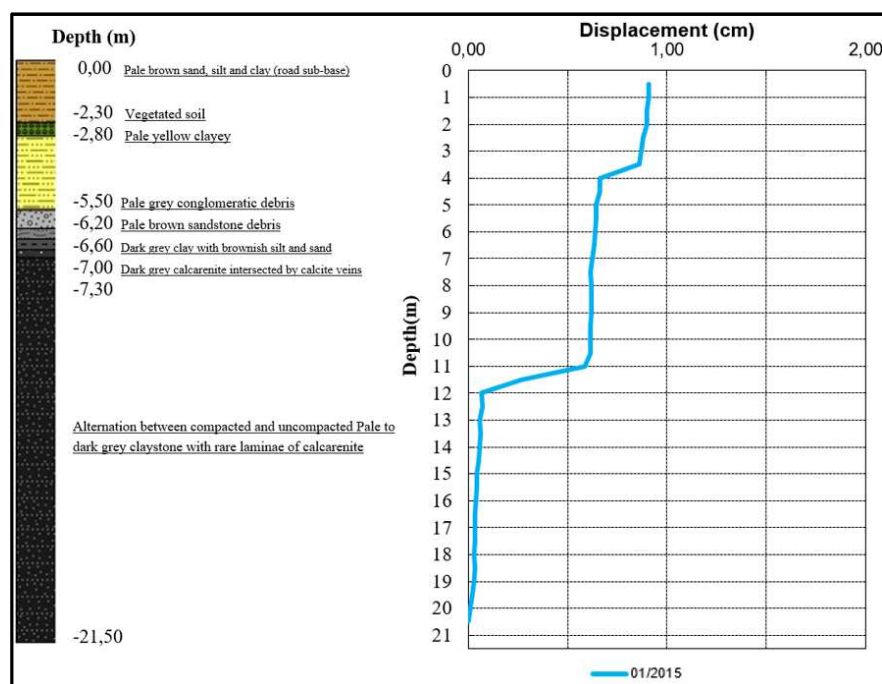


Figure 8.71 Inclinometer readings and stratigraphic column related to borehole I8.

Subsequently, conventional measurements recorded by *in situ* campaigns have been compared with results of interferometric processing, obtained by combining displacement of targets identified at ground level by ascending and descending tracks in the same period (Fig. 8.72); as mentioned, their integrated analysis allows to provide more detailed information on landslide kinematics.

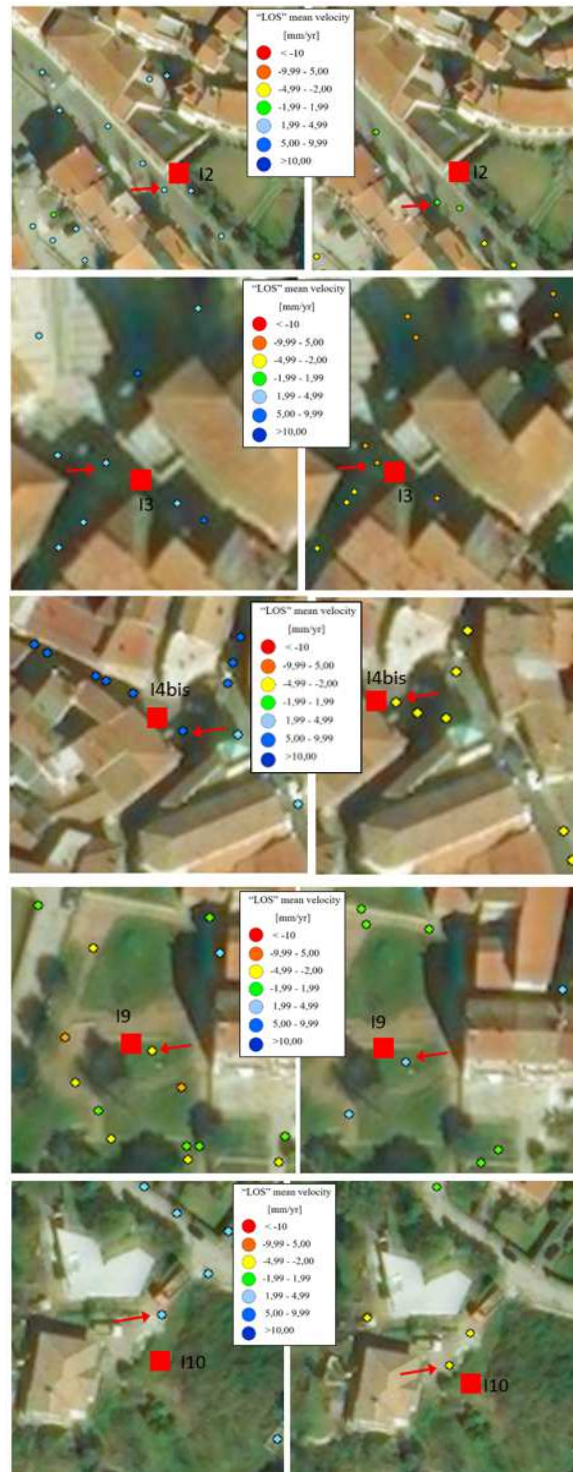


Figure 8.72 Location of targets identified for comparison with measurements of inclinometer boreholes: in ascending (on the left) and descending (on the right) tracks.

From November 2015 to September 2016, horizontal displacements obtained by combining interferometric ascending and descending products are in agreement with measures of inclinometer boreholes (Table 8.3).

Inclinometer borehole	Period of comparison	Displacement obtained by DInSAR data [cm]	Displacement at inclinometer borehole [cm]
I2	11/2015-09/2016	0,43	0,37
I3	11/2015-09/2016	1,09	1,12
I4bis	11/2015-09/2016	1,05	1,17
I9	11/2015-09/2016	1,61	1,77
I10	11/2015-09/2016	1,47	1,58

Table 8.3 Comparison between displacement obtained by DInSAR data and by inclinometer borehole.

Futhermore, at medium scale of analysis, as to define slow-moving landslide intensity parameter, differential displacements and derivable parameters (angular distortion β_w and horizontal strain β_h) induced by ground movement to building foundations, have been taken into account.

To this reason, starting from scatterer data identified at ground level, continuous displacement maps by geostatistical interpolation processing have been generated.

The Inverse Distance Weighted (IDW) method (Bedient & Huber, 1992) has been used. The IDW method is based on the principle that observations that are close to each other on the ground tend to be more alike than those further apart, thus they should receive a higher weight.

As mentioned in detail in the following paragraphs, cumulated displacements of ground and buildings in time-span 2010-2014 have been considered. To this purpose, ascending and descending discretized data have been interpolated through IDW method, thus providing continuous displacement maps (Fig. 8.73).

Subsequently, combination of continuous displacement maps acquired along the two tracks allowed to obtain vertical and horizontal displacements (Fig. 8.74).

Horizontal displacement obtained by DInSAR data is defined along E-W direction: to obtain real movement direction in the horizontal plane, measurements provided by inclinometer boreholes represented an useful tool.

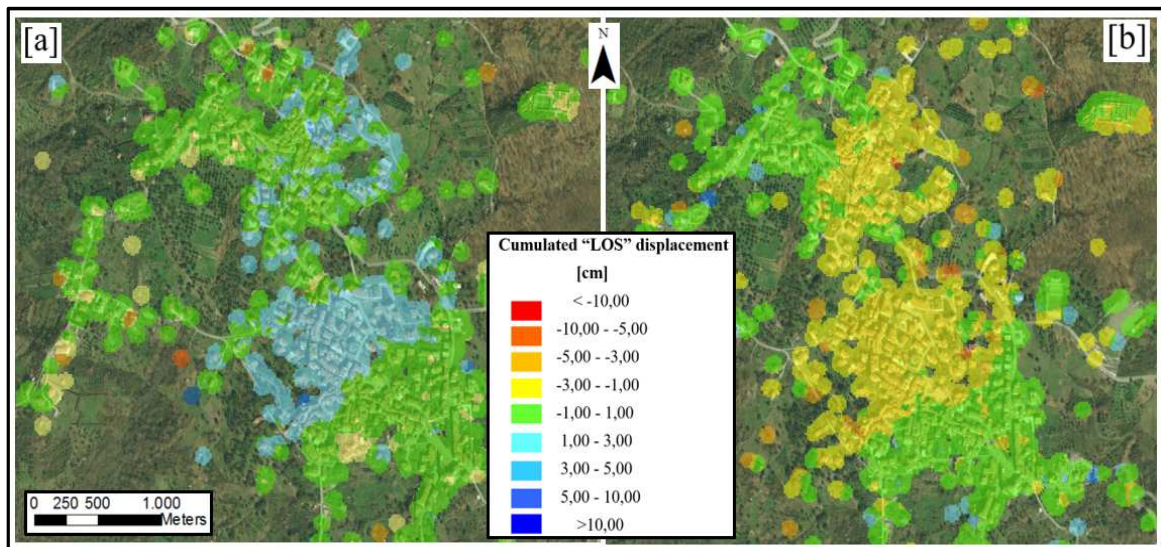


Figure 8.73 Cumulated "LoS" displacement maps in time-span 2010-2014 acquired by "ascending" (a) and "descending" images.

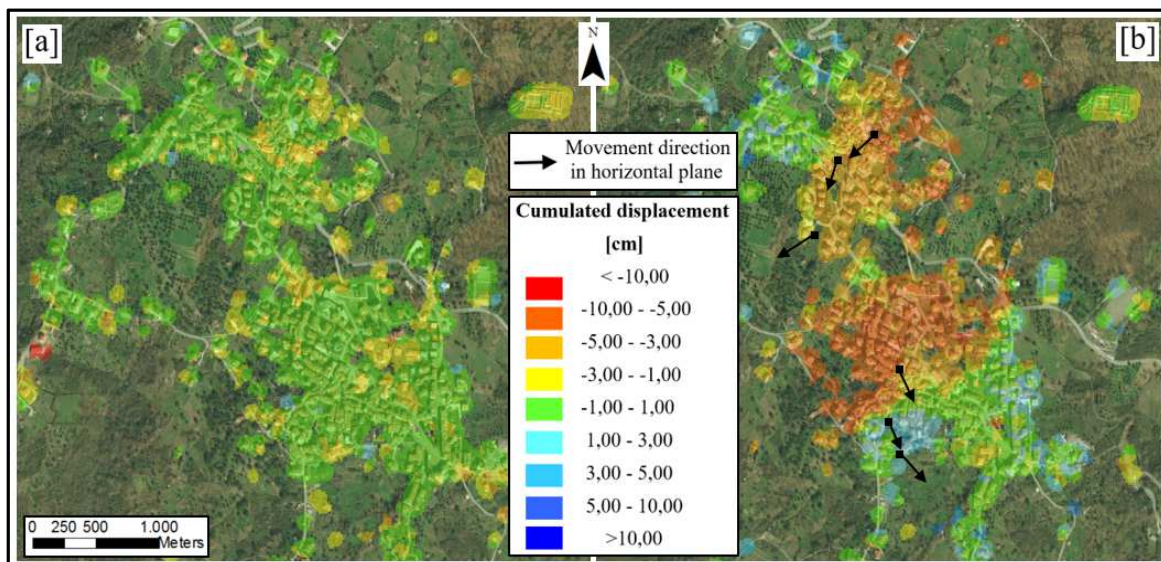


Figure 8.74 Cumulated displacement maps in time-span 2010-2014 along vertical (a) and horizontal E-W (b) directions: in the latter, also movement directions in horizontal plane recorded by inclinometers are indicated.

8.6.2 Characterization of exposed elements

As for detection of landslide kinematics, also for characterization of exposed elements the parameters considered at previous level of analysis have to be integrated. Indeed, such level of representation requires to define further characteristics of buildings, such as geometrical properties and constructive parameters.

In detail, starting from a preliminary buildings identification based on available digital topographic map, *in situ* survey allowed to define geometrical characteristics, providing information concerning metrical data, such as length of building façades and total number of storeys above the ground level (Fig.8.75).

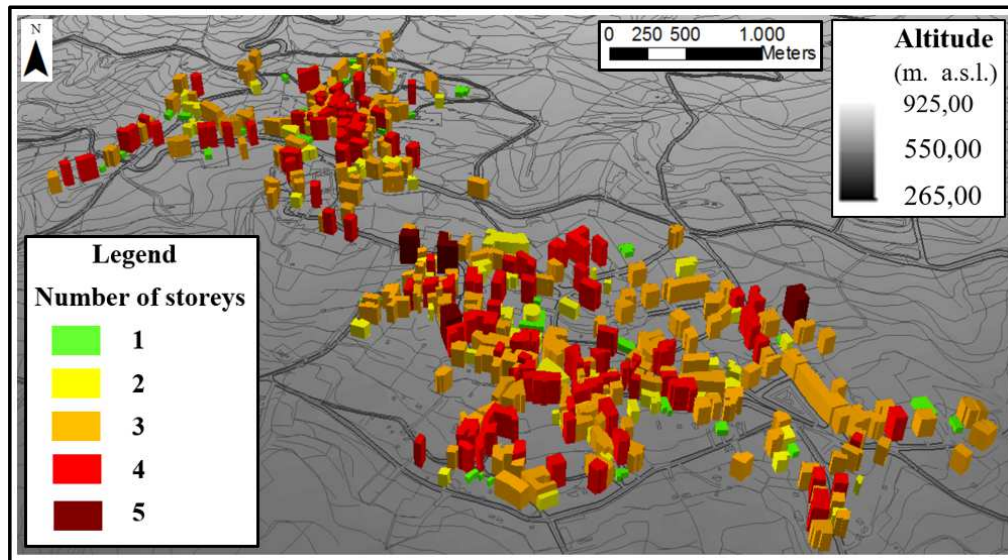


Figure 8.75 Map of number building of storeys at Moio della Civitella.

Subsequently, distinguishing structures in isolated and aggregated, four possible types of position in a building aggregate have been defined, as shown in Figure 8.76.

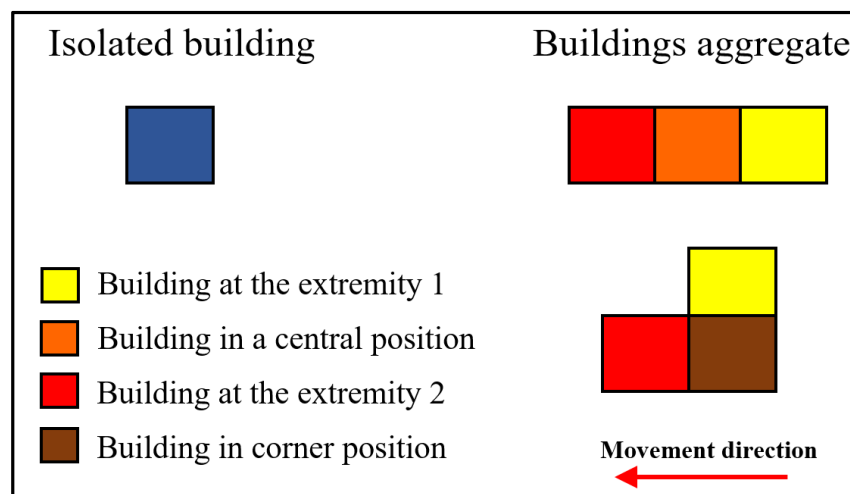


Figure 8.76 Isolated and aggregated buildings: possible configurations.

Complex configurations can increase building's vulnerability, generating concentration of stresses during landslide movement. For this reason, distinction of building position in the aggregate is necessary. In a rectangular shaped or L-shaped configuration, each building can be located according to the following cases:

- building at the extremity 1, if it is located at the beginning of an aggregate along movement direction;
- building at the extremity 2, if it is located at the end of an aggregate along movement direction;
- building in a central position, if it is adjacent to buildings on either side in a rectangular configuration;
- building in a corner position, if it is adjacent to buildings on either side in a L-shaped configuration.

Finally, according to the main goal of this level analysis, assessment of damage level in different times allows to provide information on temporal and spatial evolution of building damage degree and to detect its relationship with landslide intensity.

To this purpose, a damage survey of buildings at Moio della Civitella recorded in 2009 was available from previous studies (Calò, 2009); subsequently in February 2015, using the same classification approach (Iovine and Parise, 2002) an updating has been performed (Fig. 8.77).

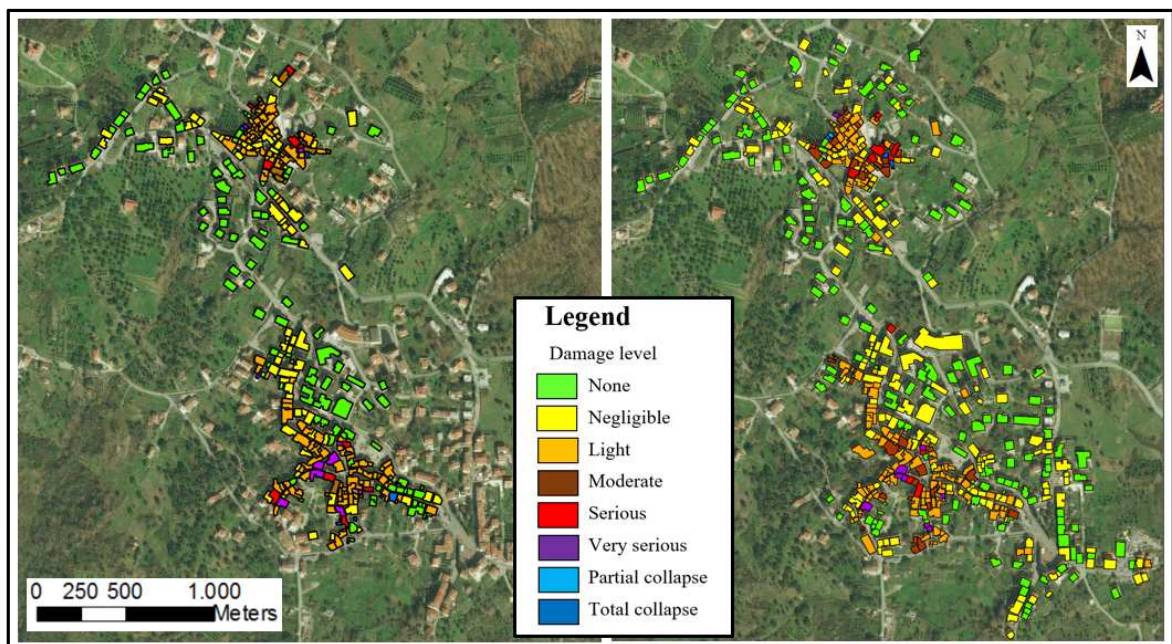


Figure 8.77 Building damage maps of Moio della Civitella, performed in 2009 (on the left) and in 2015 (on the right), according to Iovine and Parise (2002) classification.

In the following paragraphs, main goals of medium scale analysis, according to approach proposed in paragraph 7.3, are discussed.

8.6.3 Identifying areas with different degree of vulnerability at more detailed level

Such analysis, more detailed than in the previous scale of representation, provided a vulnerability zoning map, helpful to identify most critical cases in terms of buildings damage likelihood induced by ground movement.

According to the qualitative matrix proposed in paragraph 7.3, landslide intensity and current damage degree have been taken into account.

Dealing with very slow-moving landslides, in turn characterized by low distortion rates to building foundation, differential displacements and derivable parameters (angular distortion β_w and horizontal strain β_h) occurred to each building in five years preceding each damage survey have been considered.

It is important to highlight that horizontal displacements obtained by DInSAR data is measured along E-W direction: for this reason, it have to be decomposed in the two components along each building façade, by considering alignment of structure on the North direction (Fig. 8.78).

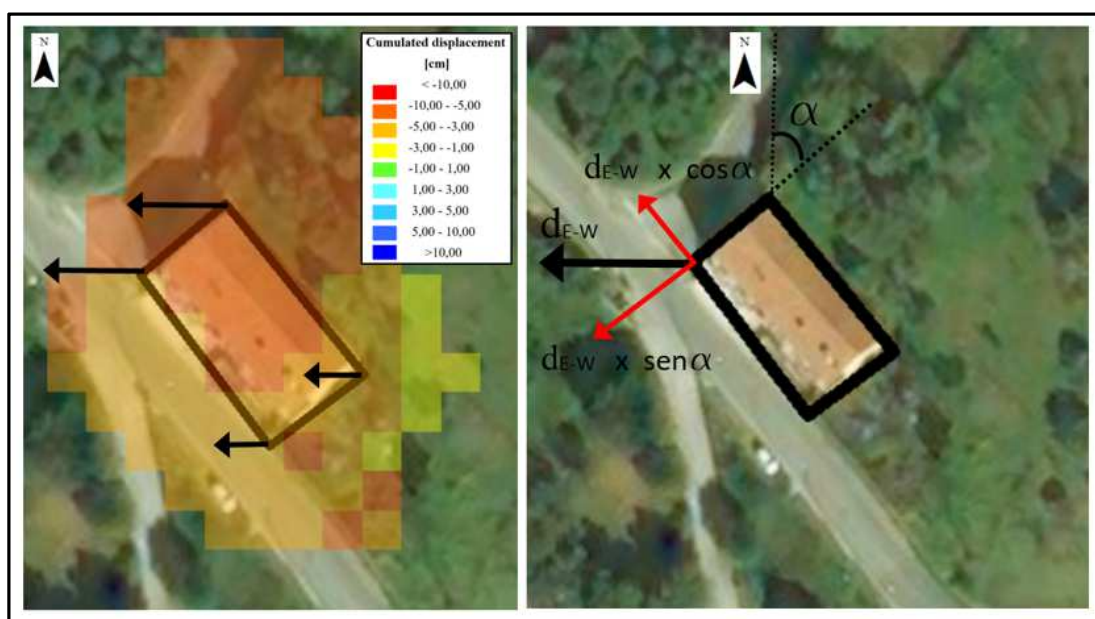


Figure 8.78 Example of decomposition of E-W horizontal displacement obtained by DInSAR data in two components along building façades.

In such case, having performed a damage survey in February 2015, maximum angular distortion β_w and horizontal strain β_h occurred along building façades in time-span 2010-2014 have been measured.

To this aim, starting from cumulated displacements in time-span 2010-2014 along vertical and horizontal E-W direction (Fig. 8.74), angular distortion β_w and horizontal strain β_h , have been evaluated according to equations 7.1 and 7.2 (Figs. 8.79 and 8.80).

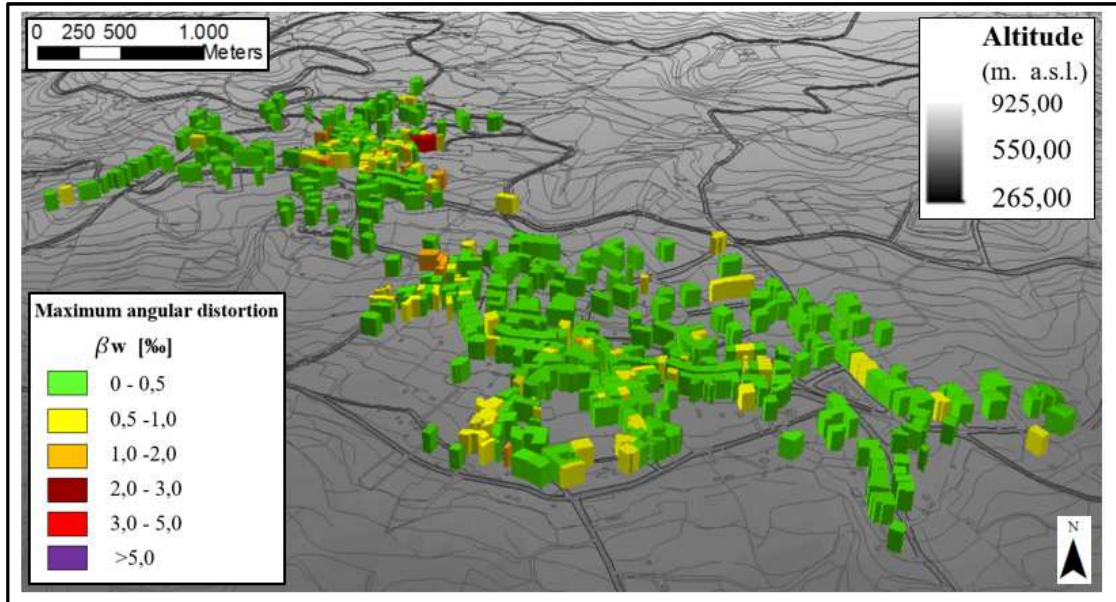


Figure 8.79 Map of maximum angular distortions measured on each building in period 2010-2014.

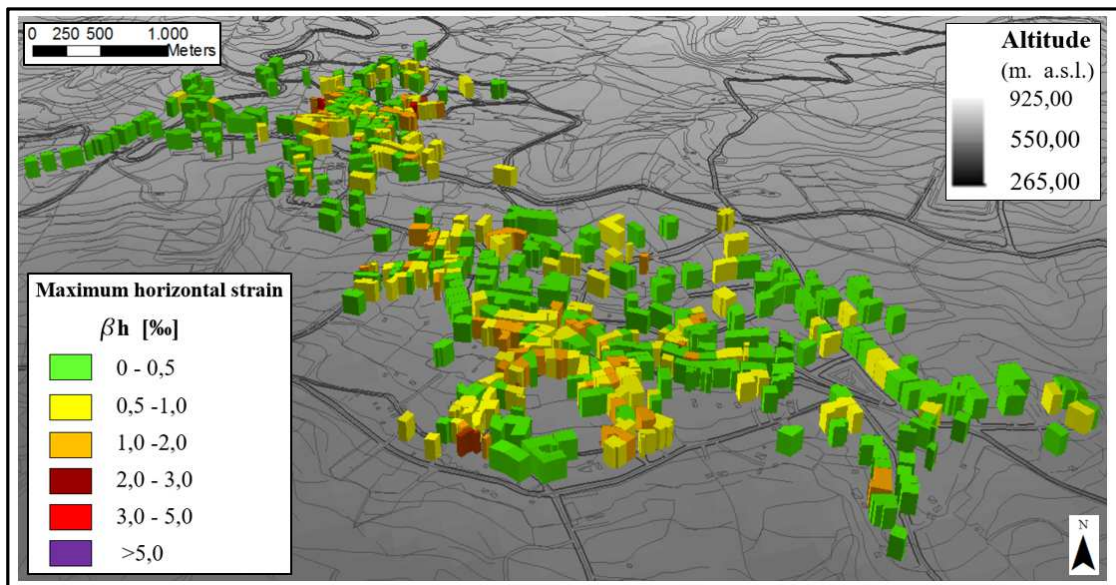


Figure 8.80 Map of maximum horizontal strains measured on each building in period 2010-2014.

As it is possible to note, most of buildings showed, in the examined period, horizontal strains higher than angular distortions.

Subsequently, by combining for each building level of damage surveyed in February 2015 (Fig. 8.53) and distortions occurred to its foundation (Figures 8.79 and 8.80), a vulnerability zoning map of Moio della Civitella has been obtained (Fig. 8.81).

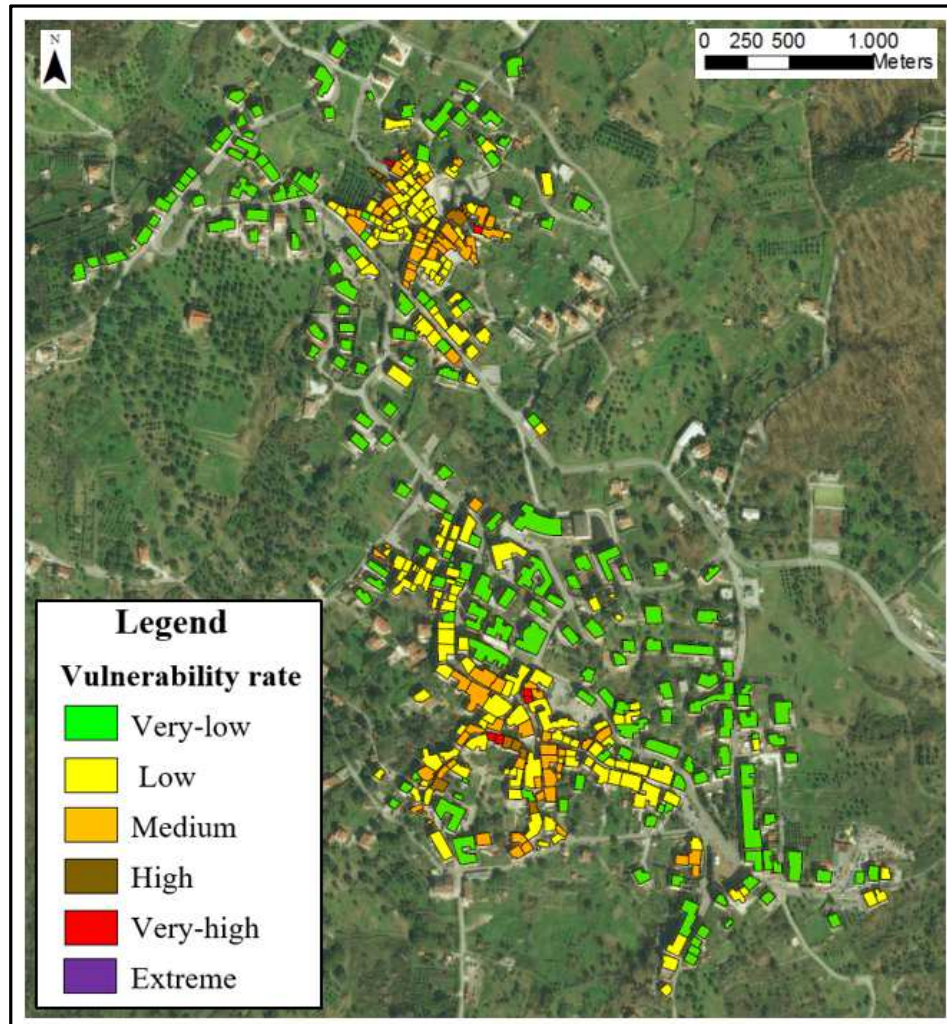


Figure 8.81 Vulnerability zoning map of buildings in Moio della Civitella.

Buildings showing low levels of vulnerability have been recorded above all in peripheral areas of Moio della Civitella municipality, while most critical cases have been identified in historical urban centers, both of Moio and Pellare: in such areas, in fact, masonry building aggregates, representing the most common construction typology, showed a damage susceptibility to landslide movement higher than isolated reinforced concrete structures, widespread in particular externally to historical center.

Examples of buildings with different vulnerability level are shown in Figure 8.82.



Figure 8.82 Buildings with different vulnerability level in Moio della Civitella urban center.

Vulnerability zoning map obtained by medium scale analysis is more detailed than that at small scale of representation. Angular and horizontal distortions occurred to building foundations are a very useful parameter to define landslide intensity, aimed to assess the real performance of a structure to ground movement.

Cracking and post-cracking behavior of structures, in fact, depend on differential displacements and derivable parameters occurred along each façade: instead, maximum velocity of displacement in areas near the building, considered to define landslide intensity in the analysis at small scale, can be used as an indicator of absolute movement and it is useful for preliminary and very quick vulnerability assessment.

8.6.4 Assessment of relationship between landslide intensity and worsening of damage level

As discussed in paragraph 7.3, damage surveys carried out in different times, allow to provide information about temporal and spatial evolution of building damage degree.

Furthermore, analysis of corresponding change of magnitude intensity parameter exhibited by each building in the time-span elapsed between two damage surveys allows to find a preliminary relationship between landslide intensity and the worsening of damage severity level.

In 2009, 259 masonry and 89 reinforced concrete structures have been surveyed, while in 2015 the level damage classification regarded to 352 masonry and 143 reinforced concrete structures: distributions of damage severity degree are shown in Figure 8.83.

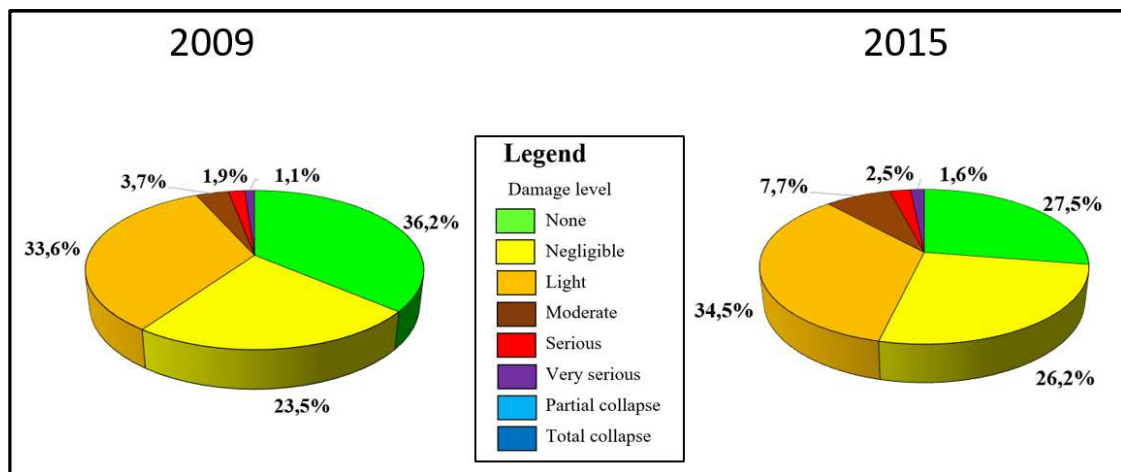


Figure 8.83 Pie-charts of distribution of damage levels surveyed in 2009 and in 2015.

Subsequently, starting from available damage maps in 2009 and in 2015 (Fig 8.77), for each building surveyed in 2009, the progressive change of damage level has been assessed.

In detail, 181 out of 348 structures do not show an increase of damage level, 147 buildings show an increase of damage of one level, 18 buildings show an increase of damage of two levels and only 2 buildings show a decrease of damage level due to restoration and maintenance works (Fig. 8.84).

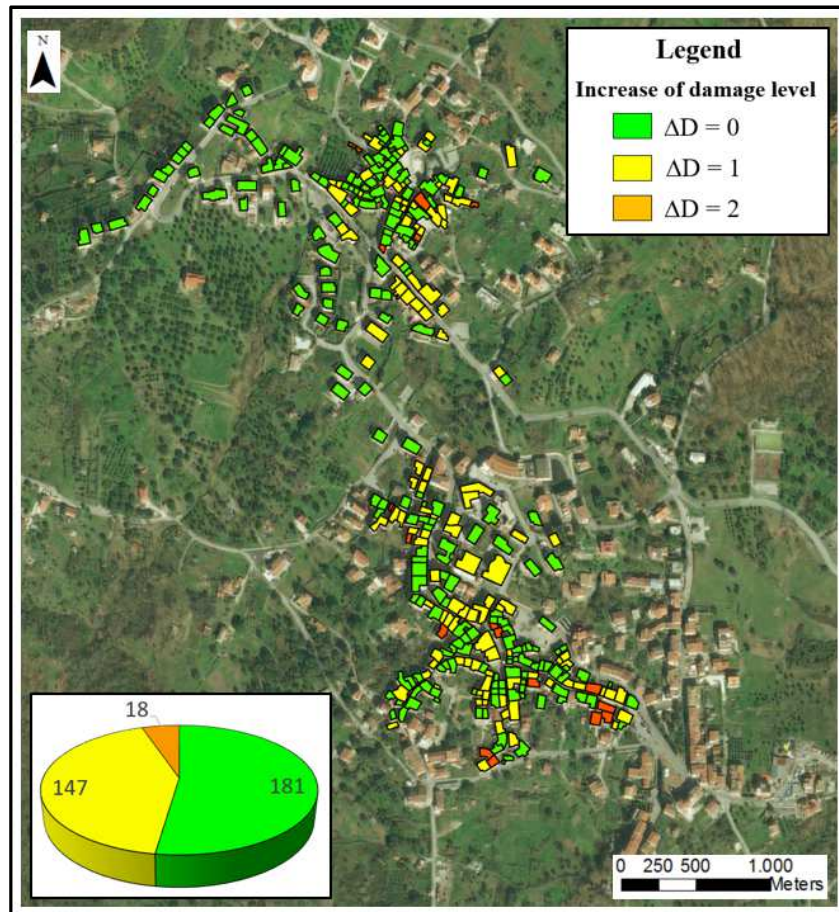


Figure 8.84 Map of increase of damage level surveyed from 2009 to 2015 in Moio della Civitella.

The availability of two surveys in different times allowed to identify buildings that showed a worsening of damage level, as it is possible to note in Figures 8.85 and 8.86: such areas are affected by the highest values of distortions in time-span 2010-2014, thus confirming a relationship between landslide intensity and the increase of damage severity degree.

Furthermore, most of buildings showing a worsening of damage are masonry structures, in turn characterized by poor-quality structural elements, bad state of maintenance, irregular geometry and very low critical tensile strength to high horizontal strain occurred to their foundations.

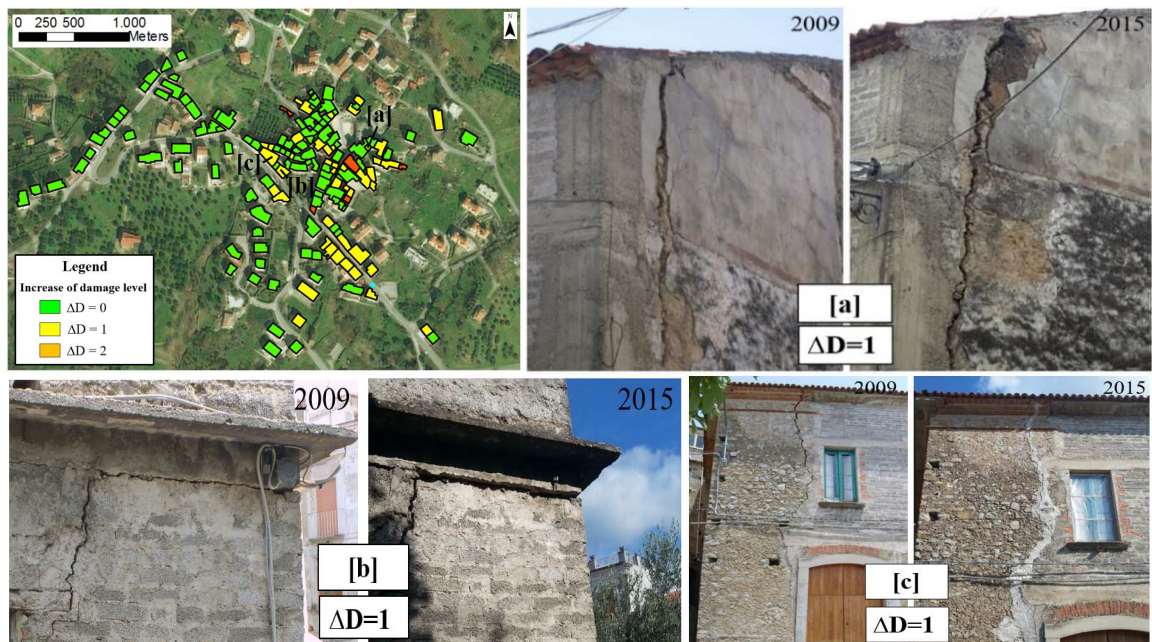


Figure 8.85 Examples of buildings that showed an increase of damage level in Moio urban center.

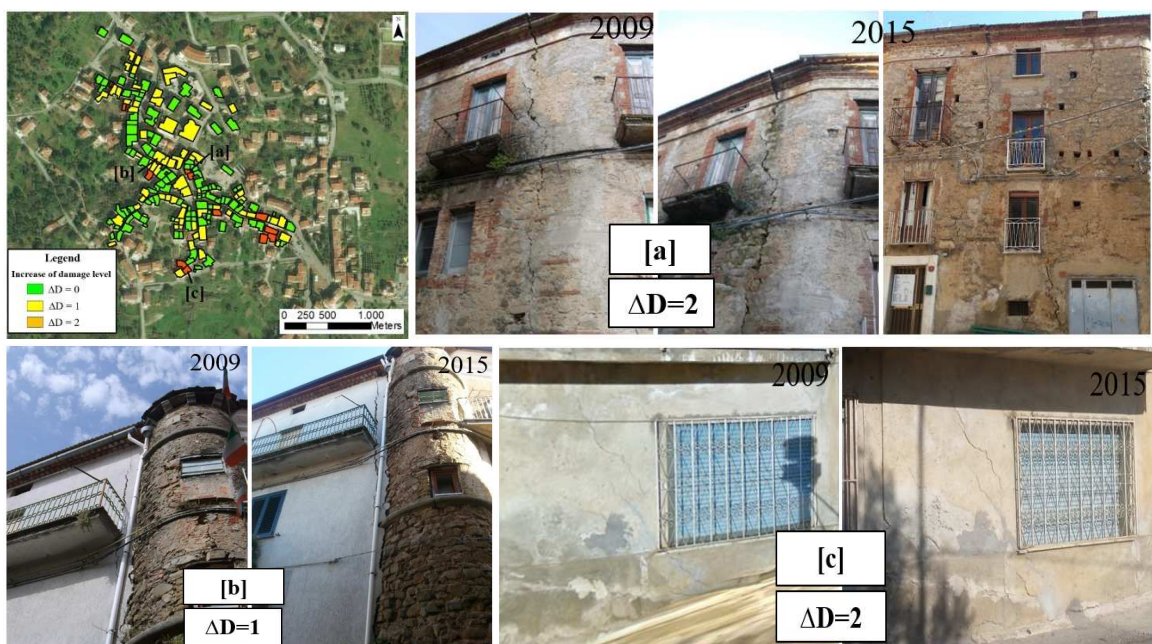


Figure 8.86 Examples of buildings that showed an increase of damage level in Pellare urban center.

Firstly, a semi-quantitative relationship between landslide intensity and building damage has been defined by means of empirical fragility curves: they are obtained by considering each building surveyed in 2009 and 2015 and corresponding maximum velocity of displacement among vertical and horizontal components registered, respectively, by DInSAR ENVISAT and COSMO-SkyMed data.

In 2009, on 348 structures surveyed, 157 masonry and 49 reinforced concrete buildings have been identified by targets in ENVISAT both ascending and descending images and only for them it was possible to define vertical and horizontal displacement rates. Relationship between maximum displacement velocity and damage surveyed is shown in Figure 8.87.

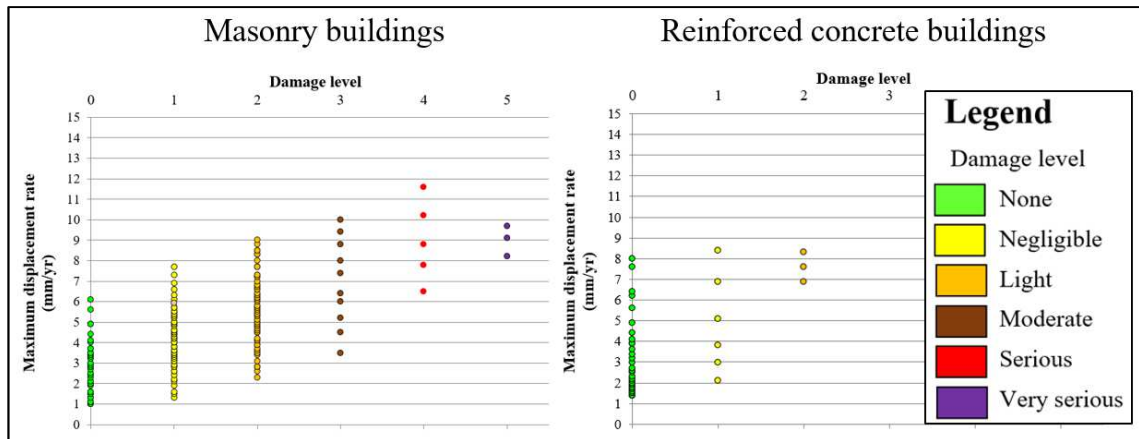


Figure 8.87 Displacement velocity-damage level relationship for buildings surveyed in 2009.

In 2015, relationship between maximum displacement velocity and damage surveyed for 352 masonry and 143 reinforced concrete buildings is shown in Figure 8.88.

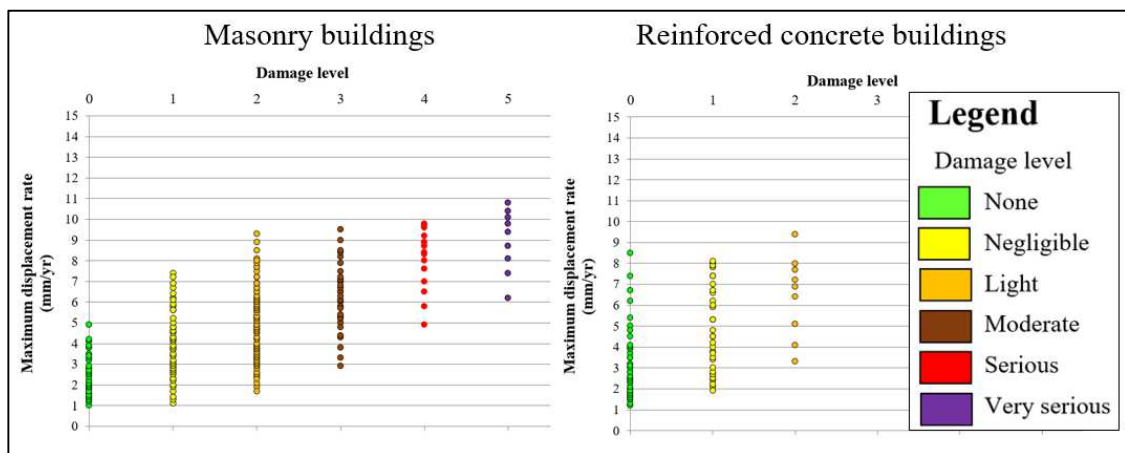


Figure 8.88 Displacement velocity-damage level relationship for buildings surveyed in 2015.

According to the approach proposed in paragraph 7.3, fragility curves have been derived using a cumulative log-normal distribution function, depending on the median value of maximum velocity V_i at which the building reaches each damage level D_i and on the standard deviation of the natural logarithm of V_i for each D_i .

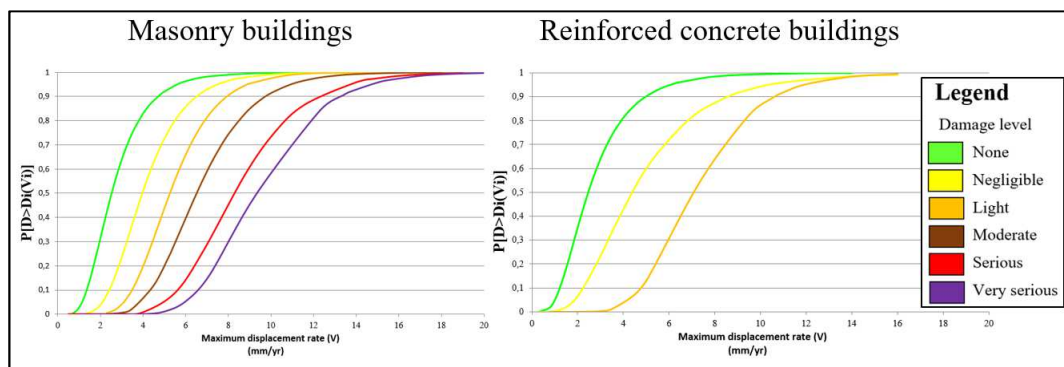


Figure 8.89 Empirical fragility curves for masonry and reinforced concrete buildings in 2009.

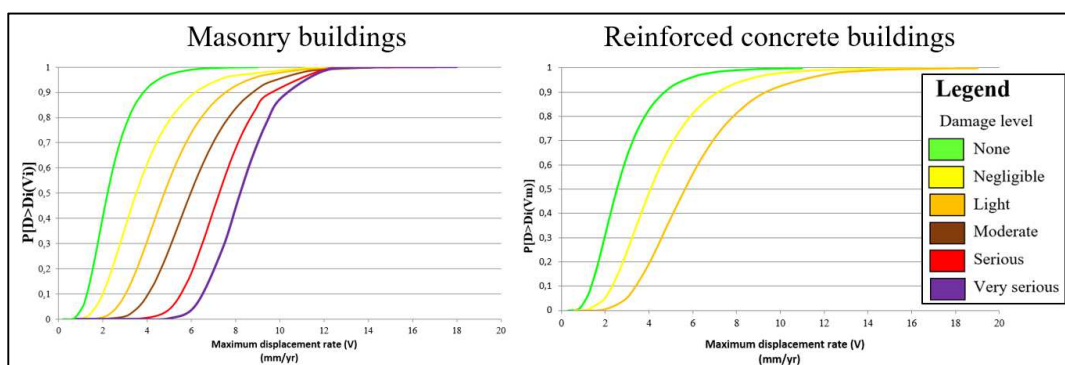


Figure 8.90 Empirical fragility curves for masonry and reinforced concrete buildings in 2015.

As it is possible to note, for reinforced concrete buildings only the probability of reaching light damage degree was assessed; indeed, no structure with higher level has been identified in Moio dell Civitella.

Moreover, the comparison of derived fragility curves for masonry and reinforced concrete buildings provides critical information on their structural behavior within landslides affected area (Fig. 8.91). Such analysis showed, both in 2009 and in 2015, a probability of reaching or exceeding a particular damage level higher in masonry buildings than in reinforced concrete buildings.

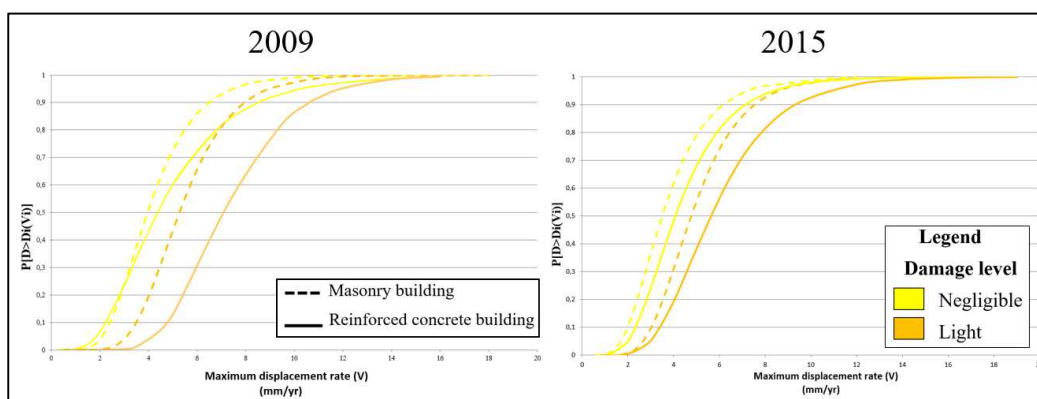


Figure 8.91 Comparison of fragility curves of masonry and reinforced concrete buildings in 2009 and in 2015.

Furthermore, from 2009 to 2015, a low increase of probability of reaching a damage level for a fixed value of displacement rate was observed, both on masonry and on reinforced concrete buildings (Fig. 8.92). Such behavior, probably due to progressive worsening of state of maintenance of buildings in the time-span considered, highlights that fragility curves approach is not a static concept, but it is characterized by a temporal evolution. Empirical fragility curves of buildings within landslide-affected area have to be periodically updated, as indicator of changing of structures performance during the years.

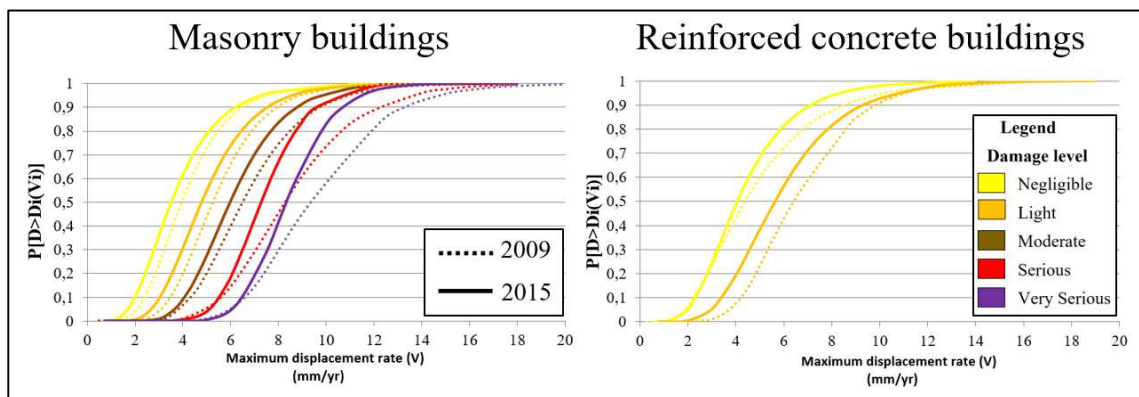


Figure 8.92 Comparison of fragility curves in 2009 and in 2015, for masonry (on the left) and reinforced concrete (on the right) buildings.

Subsequently, as regards the analysis of relationship between change of landslide intensity and worsening of damage severity level, it was possible to define an increase of displacement velocity from 2009 to 2015, for the following buildings:

- 114 on 181 structures that do not show a worsening of damage level;
- 82 on 147 structures that show an increase of damage of one level;
- 10 on 18 structures that show an increase of damage of two levels.

Figures 8.93 and 8.94 show increase of displacement velocity-increase of damage level graph and corresponding fragility curves, for masonry and reinforced concrete building.

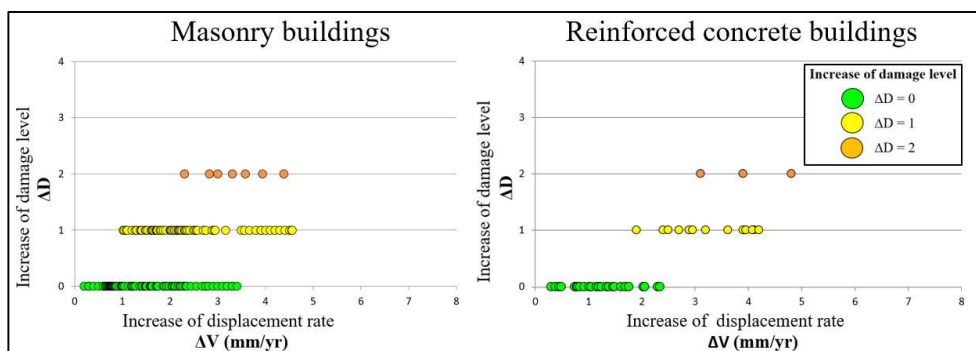


Figure 8.93 Increase of displacement velocity ΔV and related increase of damage level for masonry and reinforced concrete buildings.

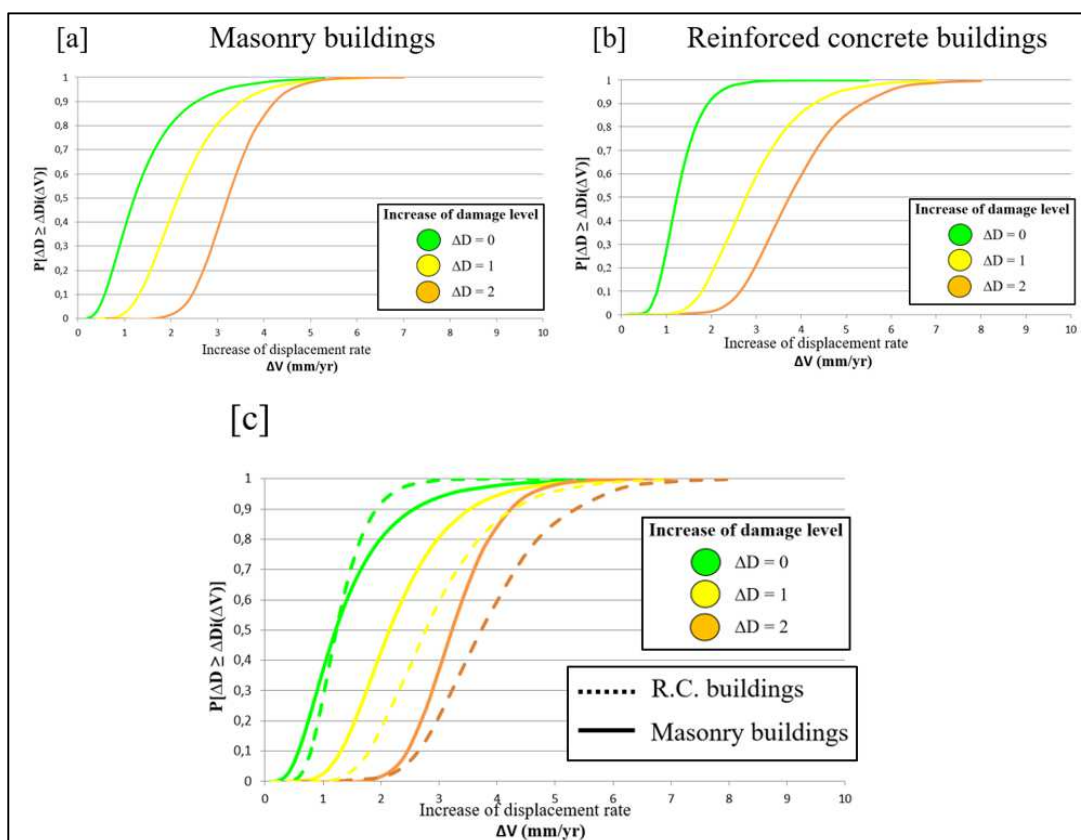


Figure 8.94 Empirical fragility curves for masonry (a) and reinforced concrete (b) buildings, and their comparison (c).

Comparison of derived empirical fragility curves showed a higher probability of reaching an increase of damage severity level on masonry buildings than on reinforced concrete structures, thus confirming poorer structural properties of the former ones.

Subsequently, aimed to a detailed detection of relationship between landslide intensity and building damage evolution, the analysis above discussed was repeated, by considering maximum angular distortion βw and horizontal strain βh occurred along building façades in time-span considered instead that maximum velocity of displacement recorded on each building.

Distinguishing buildings in terms of structural typology, empirical fragility curves have been obtained by taking into account the increase of damage level of each building from 2009 to 2015, and corresponding maximum angular and horizontal distortions occurred in time-span 2010-2014.

Firstly, effects of angular distortions and horizontal strains have been considered separately, and subsequently combined to take into account that they can occur together under building foundation.

Furthermore, in order to investigate the different performance of structures, isolated or in aggregate, they have been separated according to the classification proposed in Figure 8.76.

Finally, buildings work differently pre- and post-cracking: to take into account a different elastic or plastic behavior and existing damage level due to ground movement occurred in the past, they have been classified by considering the initial state of damage in 2009.

In the following, empirical fragility curves obtained for the above mentioned building typologies are discussed.

▪ **Isolated buildings**

According to Iovine & Parise classification, in 2009 isolated reinforced concrete buildings showed a damage degree equal to 0 (none) or to 1 (negligible).

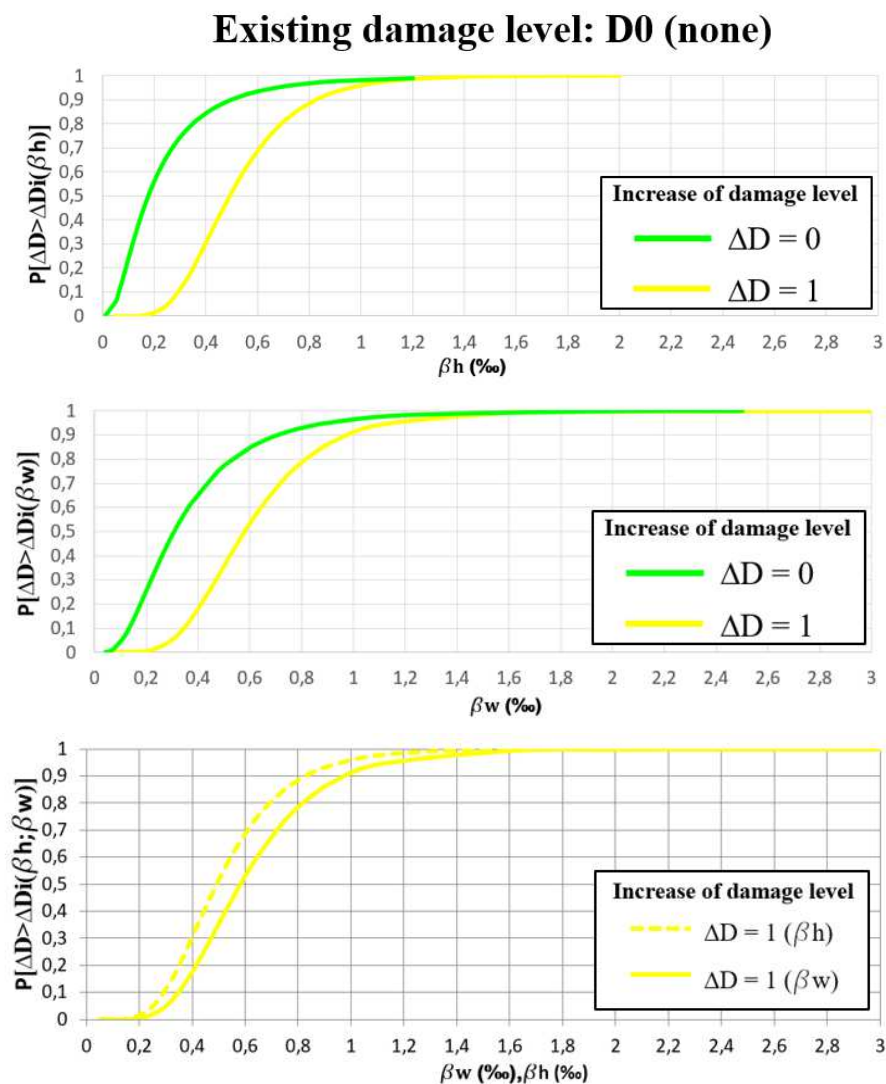


Figure 8.95 Empirical fragility curves for isolated reinforced concrete buildings with none existing damage level (D0).

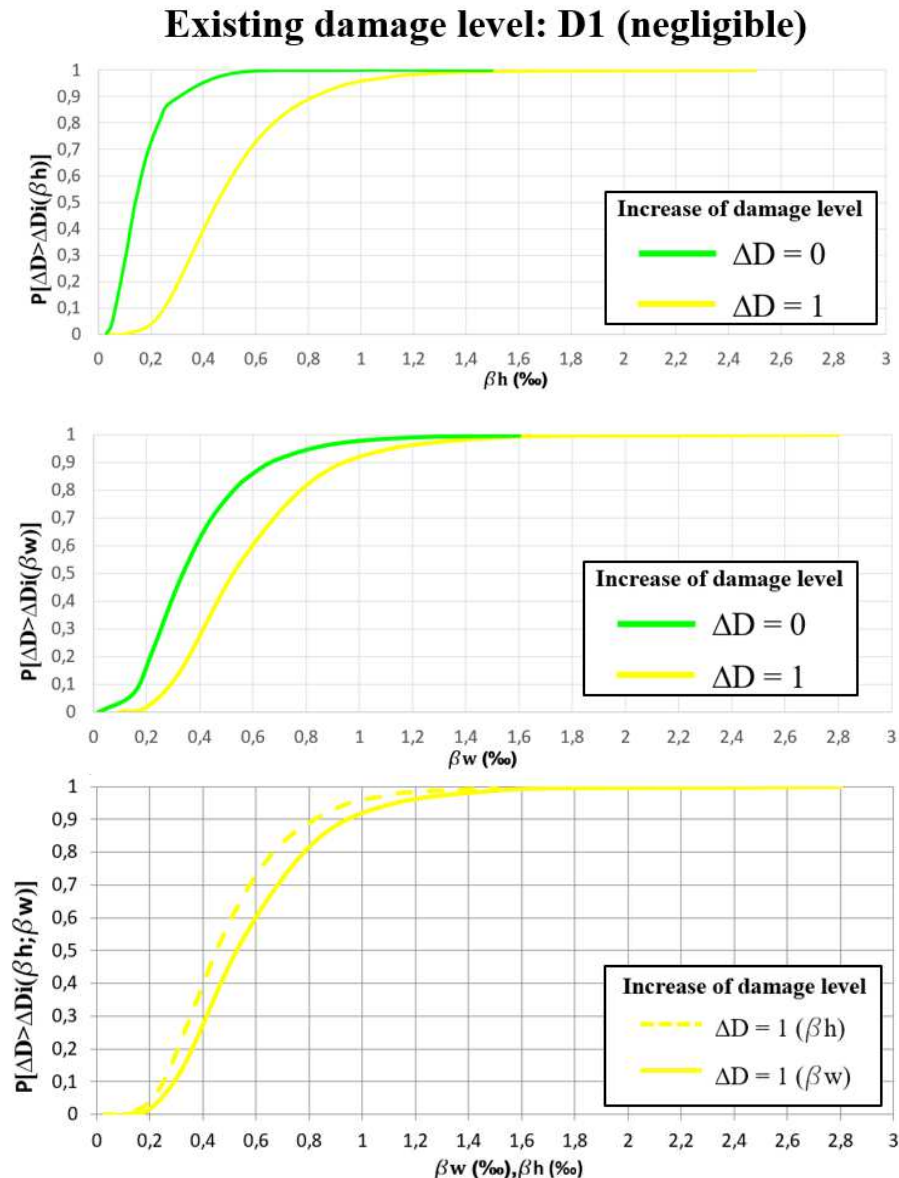


Figure 8.96 Empirical fragility curves for isolated reinforced concrete buildings with negligible existing damage level (D1).

As it is possible to note in Figures 8.95 and 8.96, isolated reinforced concrete buildings show a similar probability of reaching an increase of damage severity level, applying angular or horizontal distortions. Dealing with very low deformation rates, reinforced concrete foundations (footings connected by beams or raft foundation), in fact, provide to structures a similar stiffness and uniform behavior along vertical and horizontal directions to landslide-induced movements.

Moreover, comparison of fragility curves corresponding to different initial states of damage highlighted a similar performance of buildings with none or negligible damage (Fig. 8.97), corresponding to an elastic structural behavior.

The low difference is probably due to greater susceptibility to worsen damage degree in already damaged structures than in intact buildings.

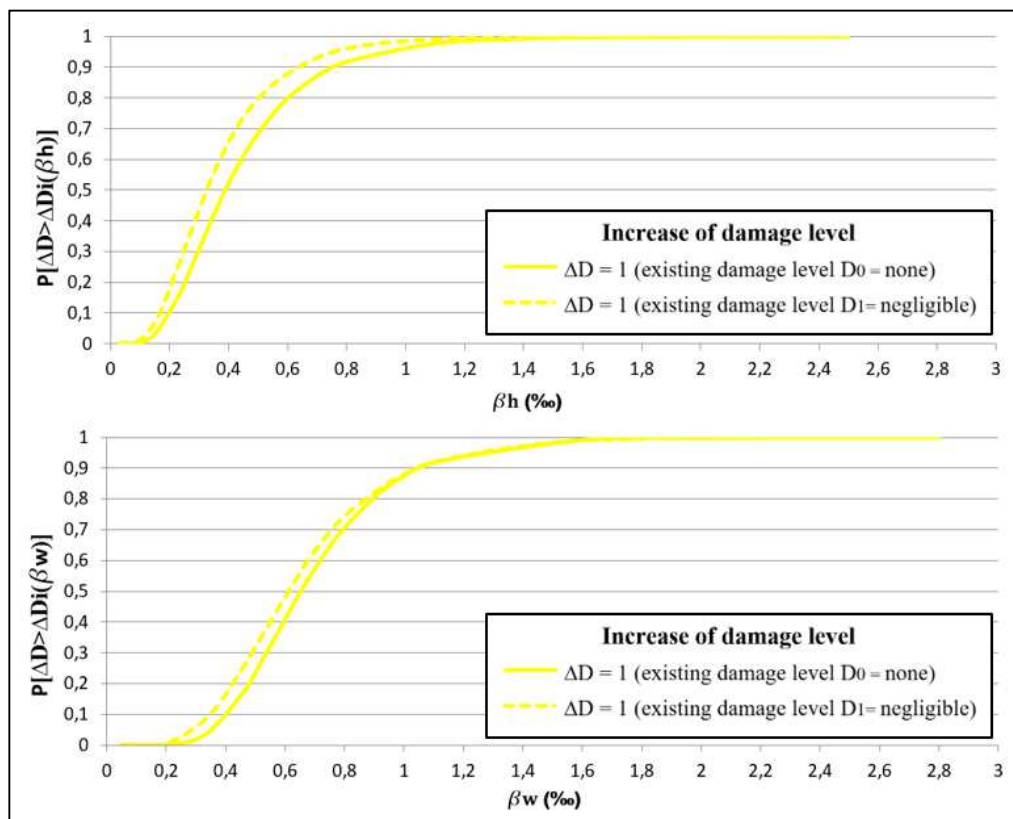


Figure 8.97 Comparison of empirical fragility curves of isolated reinforced concrete buildings with different initial damage level.

The same analysis has been repeated for isolated masonry buildings. Also in this case, in 2009, isolated masonry buildings showed a damage degree equal to 0 (none) or to 1 (negligible).

Figures 8.98 and 8.99 show that, contrary to reinforced concrete buildings, masonry structures are characterized by different behavior to landslide-induced angular and horizontal distortions. In detail, such analysis showed a higher probability of increasing damage level due to horizontal strains than to vertical deformations.

Unreinforced masonry buildings, in fact, have a strip footings foundation, such as an extension of load-bearing masonry wall, in turn characterized by high values of vertical compression strength and very low values of horizontal critical strength.

Furthermore, also in this case, comparison of fragility curves corresponding to a different initial state of damage showed a similar performance of buildings without existing damage or with negligible damage (Fig. 8.100).

The low difference, more evident with reference to horizontal distortions, confirms high susceptibility of masonry buildings to horizontal tensile strains, above all in post-cracking phase.

Finally, to summarize results above discussed, Figure 8.101 highlights that masonry buildings have a higher probability of increasing damage level than reinforced concrete buildings, in particular when horizontal strains occur, depending on a low critical strength of masonry structures. Instead, their performance to angular distortions is very similar.

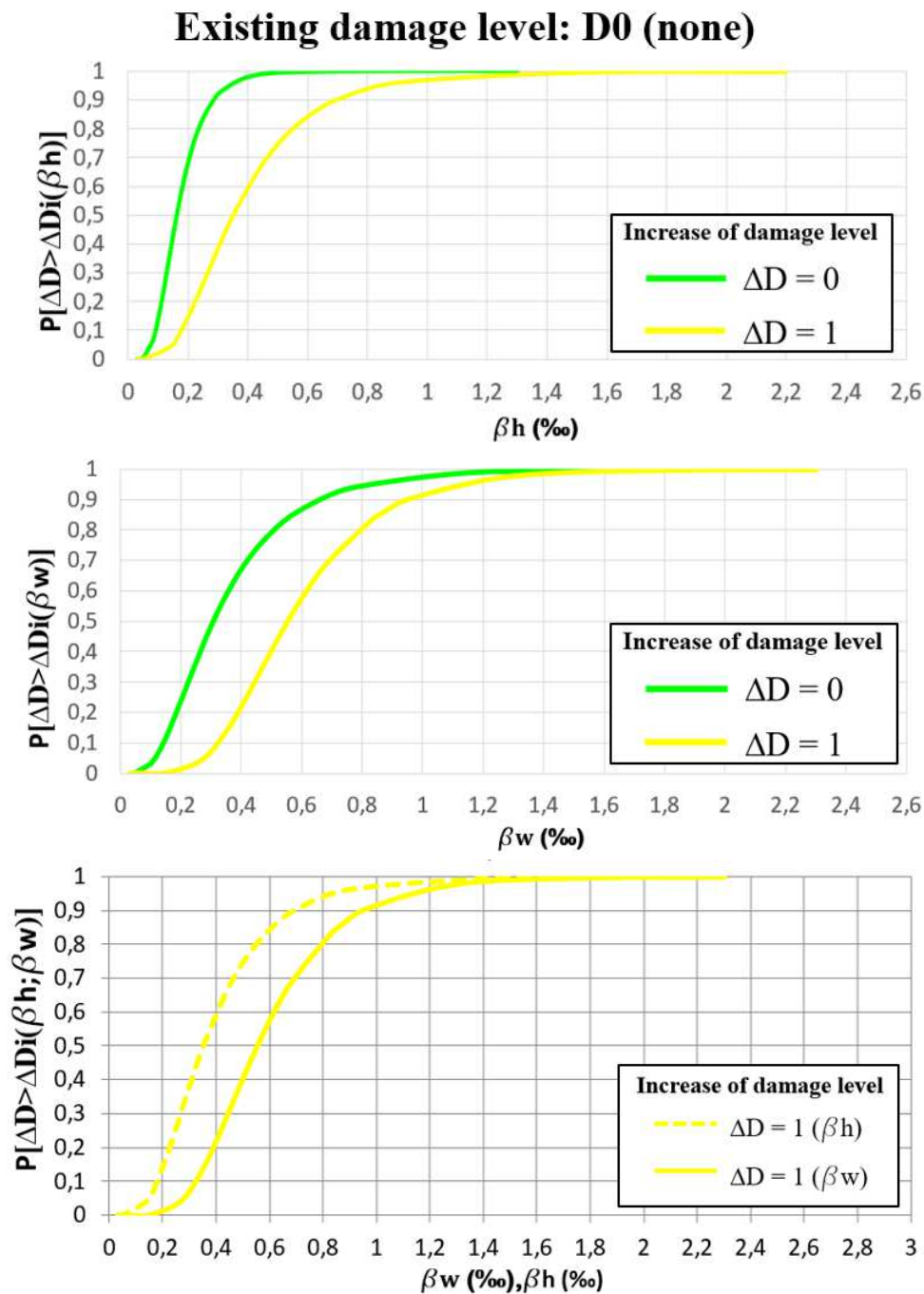


Figure 8.98 Empirical fragility curves for masonry buildings with none existing damage level (D0).

Existing damage level: D1 (negligible)

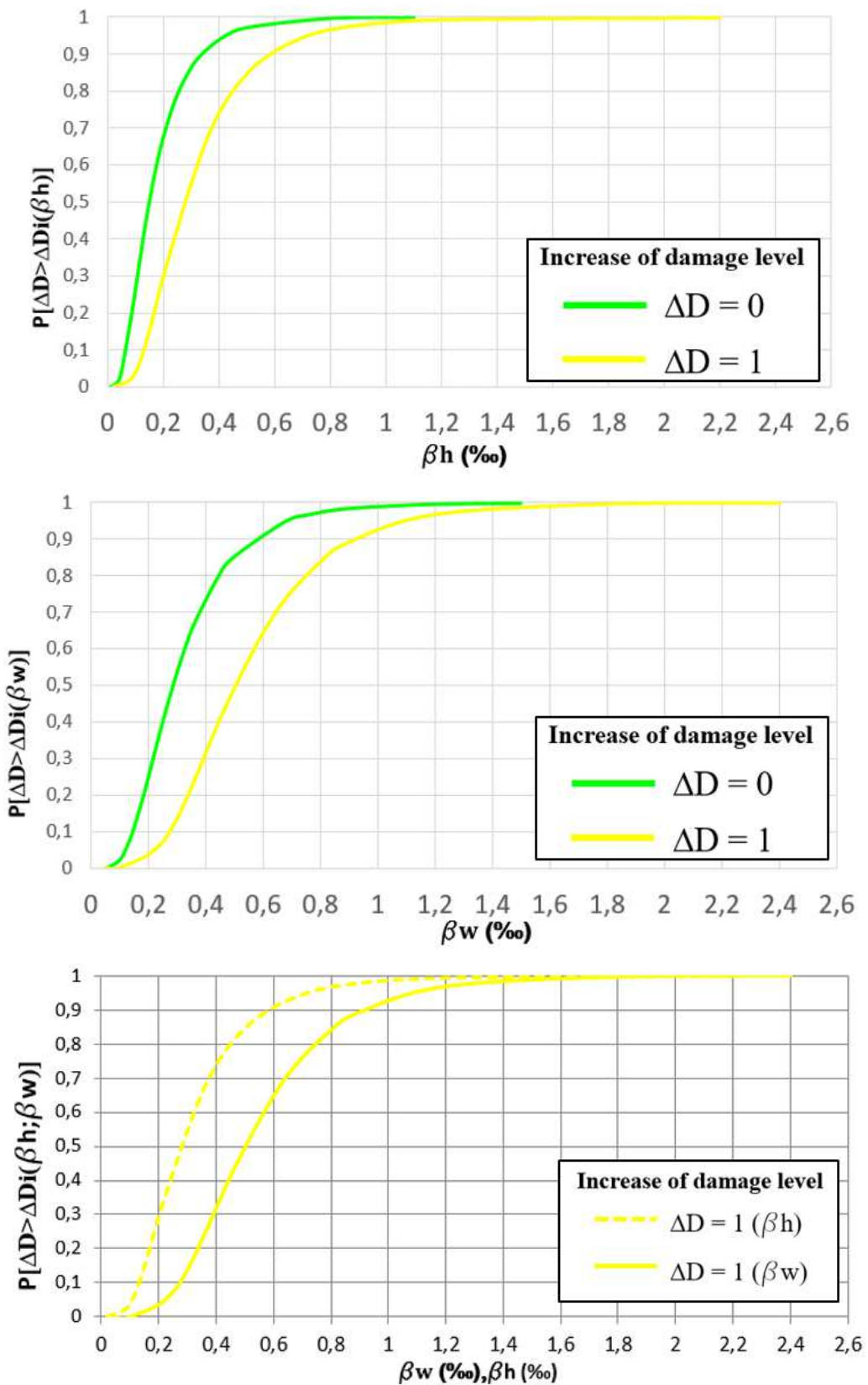


Figure 8.99 Empirical fragility curves for masonry buildings with negligible existing damage level (D1).

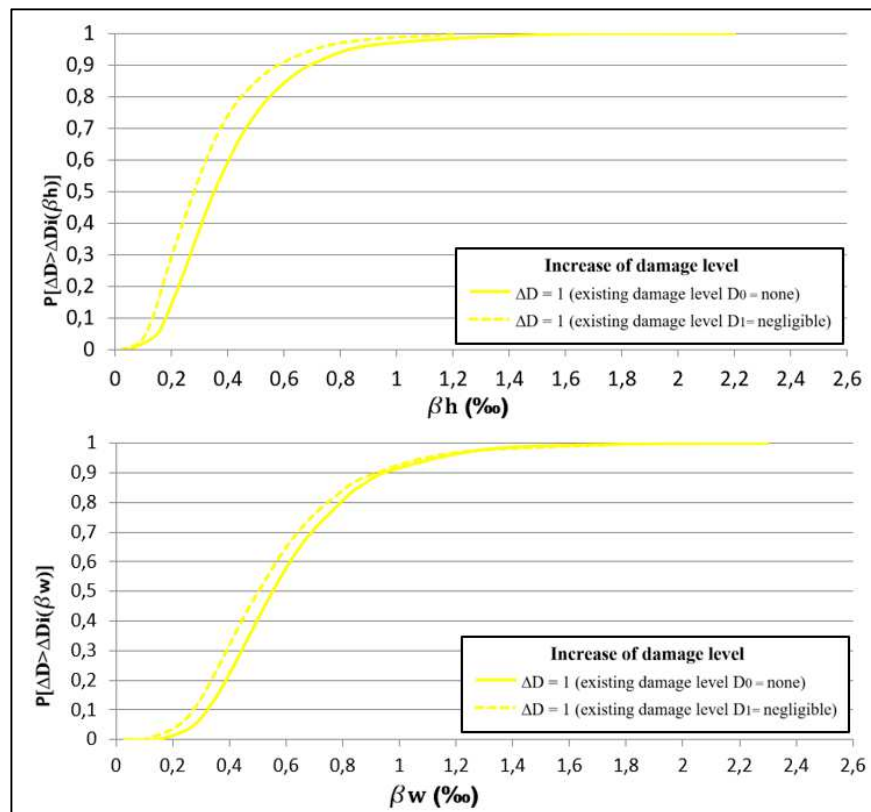


Figure 8.100 Comparison of empirical fragility curves of isolated masonry buildings with different initial damage level.

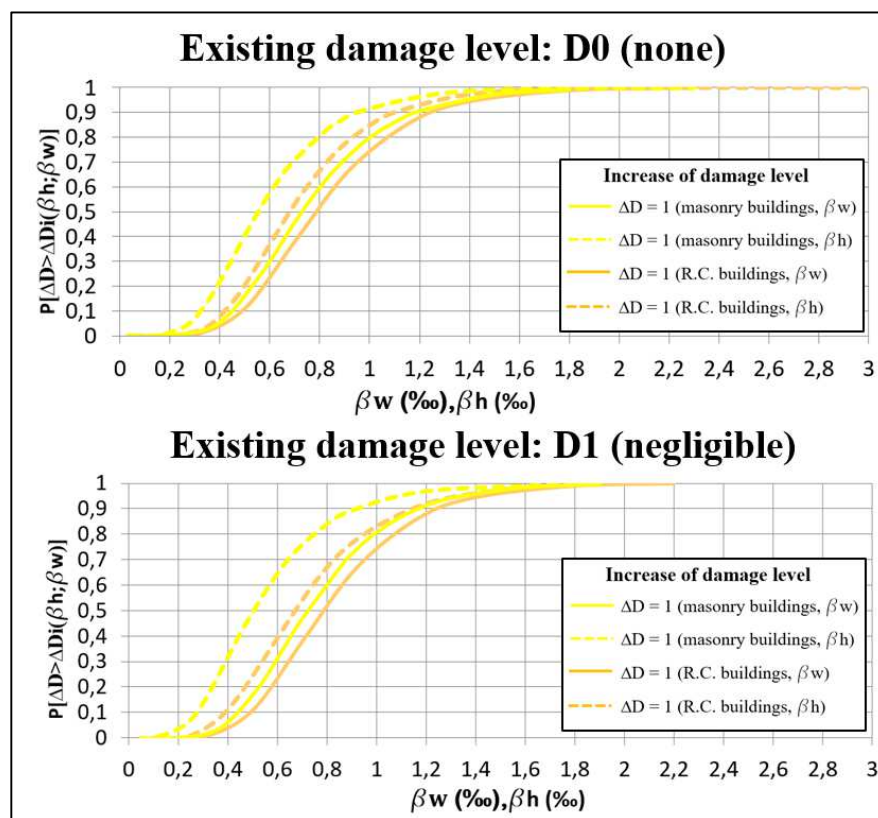


Figure 8.101 Comparison of empirical fragility curves of masonry and reinforced concrete buildings.

▪ **Buildings in aggregate**

According to the classification proposed in Figure 8.76, reinforced concrete (R.C.) structures in a building aggregate have been identified at the extremity 1, at the extremity 2 and in a central position: all these buildings are characterized by none existing damage. As discussed for isolated R.C. buildings, also structures in aggregates showed a similar probability of reaching an increase of damage severity level, under induced angular or horizontal distortions (Figures 8.102, 8.103, 8.104).

Existing damage level: D0 (none)

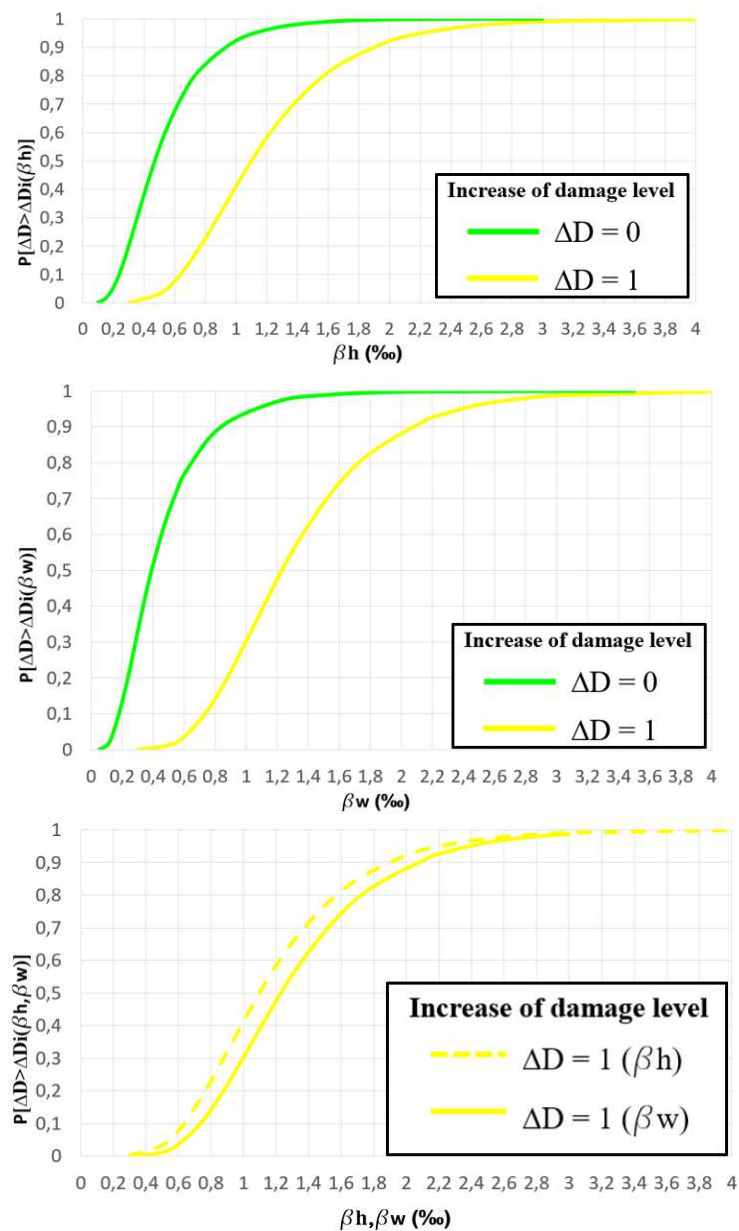


Figure 8.102 Empirical fragility curves for reinforced concrete buildings in a position of “extremity 1” of the aggregate with none existing damage level (D0).

Existing damage level: D0 (none)

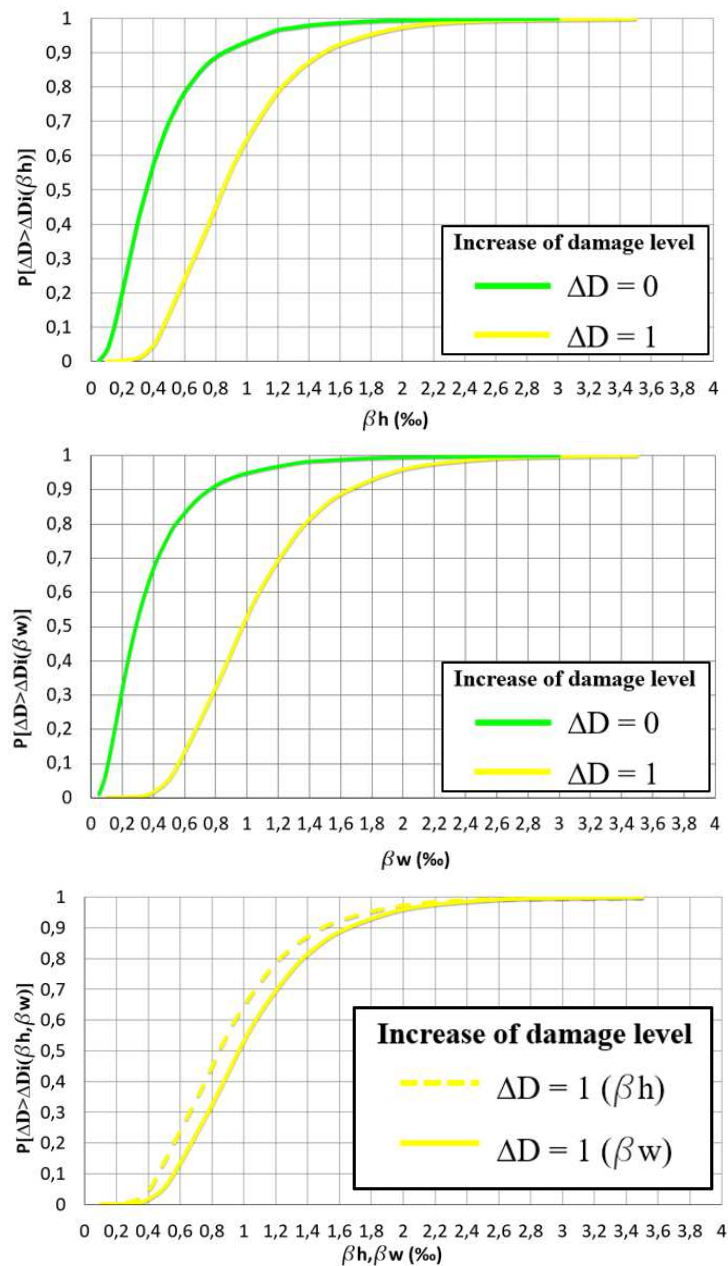


Figure 8.103 Empirical fragility curves for reinforced concrete buildings in a position of “extremity 2” of the aggregate with none existing damage level (D0).

Figure 8.105 shows a comparison of fragility curves corresponding to different positions in a building aggregate. As it is possible to note, a building located at the end of an aggregate is characterized by the highest probability of increasing damage level. Such behavior is due, probably, to progressive transferring and redistribution of stresses between adjacent buildings along movement direction. Differently, buildings located in a central position of an aggregate showed a good performance to applied distortions, depending on lateral containment of lateral structures.

Existing damage level: D0 (none)

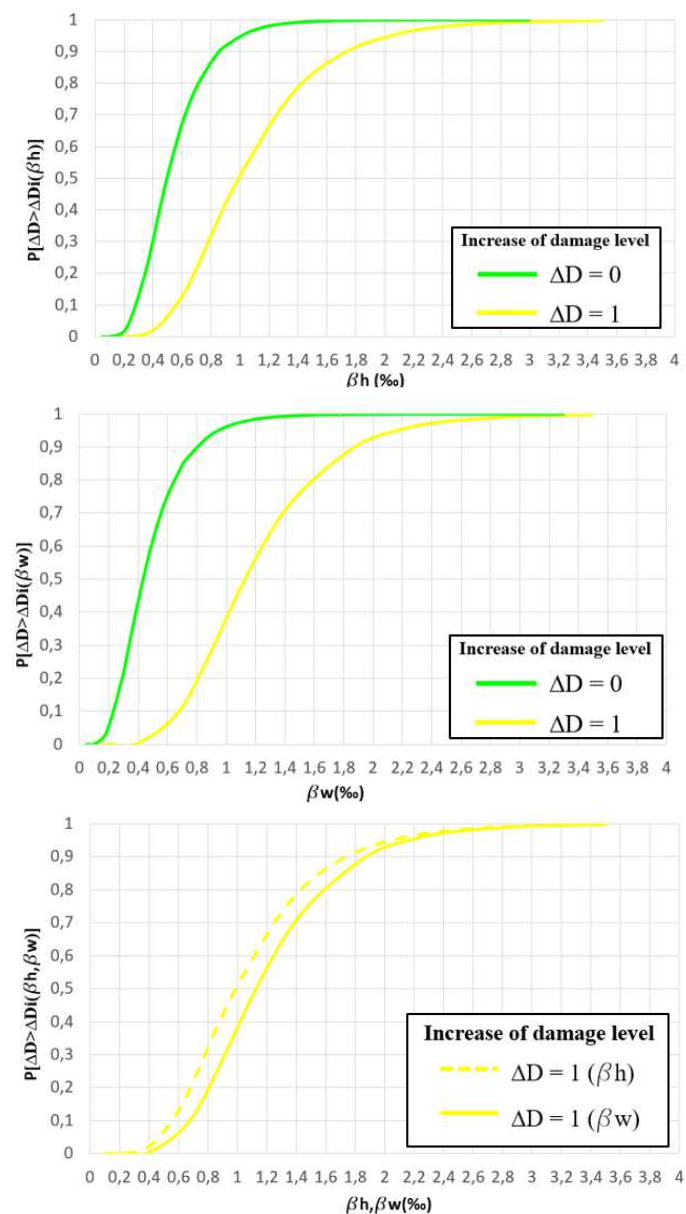


Figure 8.104 Empirical fragility curves for reinforced concrete buildings in a central position of the aggregate with none existing damage level (D0).

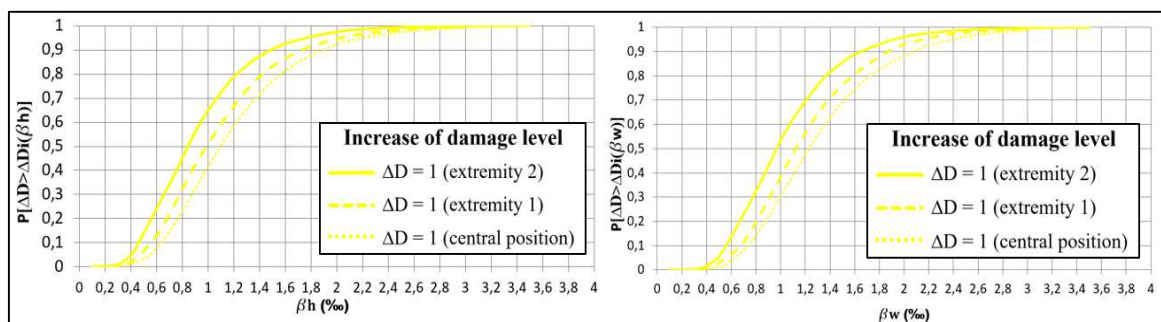


Figure 8.105 Comparison of empirical fragility curves for reinforced concrete buildings in different positions of the aggregate.

Subsequently, the same analysis has been developed for masonry buildings. In detail, the following fragility curves have been obtained.

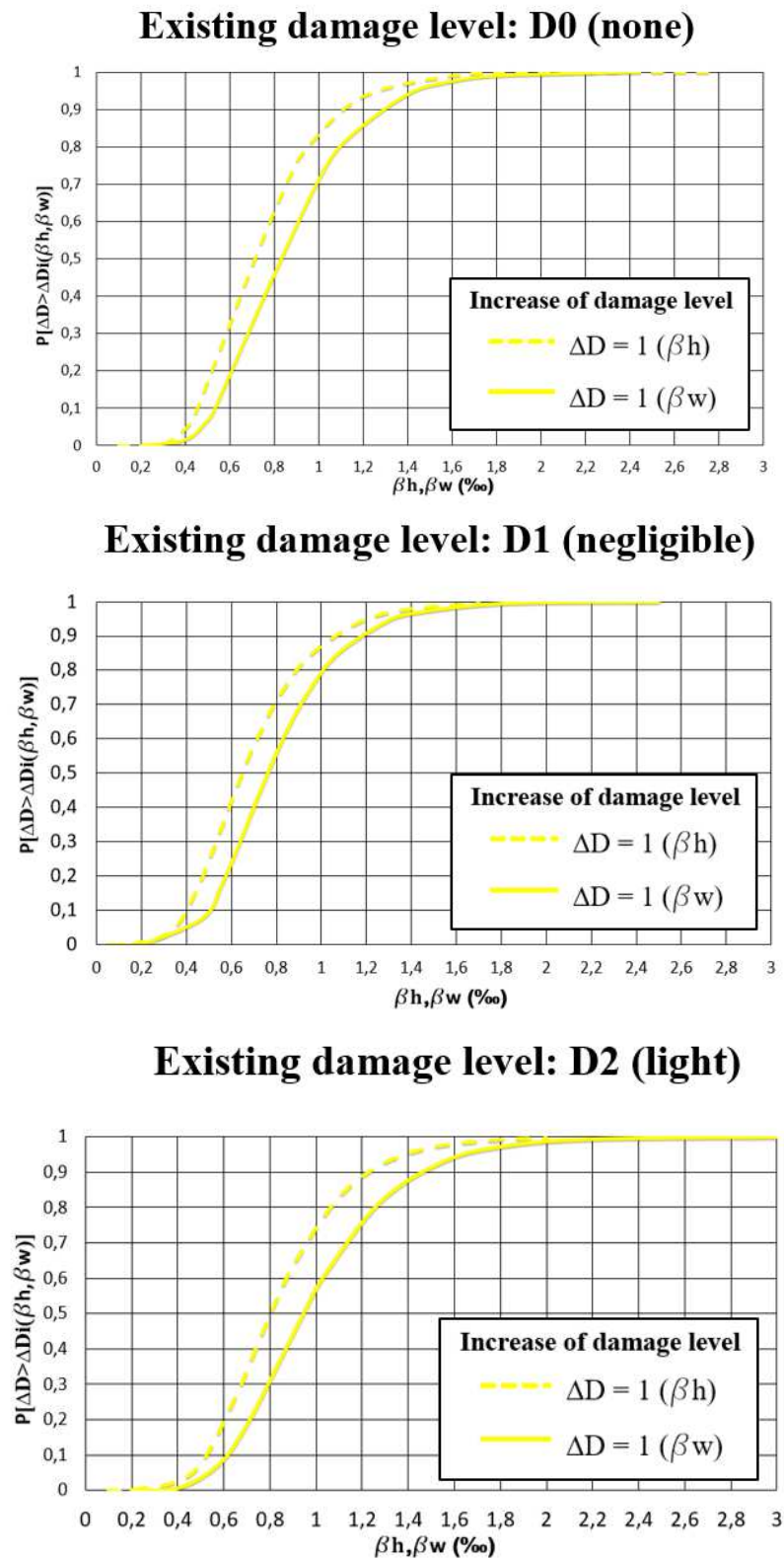


Figure 8.106 Empirical fragility curves for masonry buildings at “extremity 1” of the aggregate with different existing damage levels.

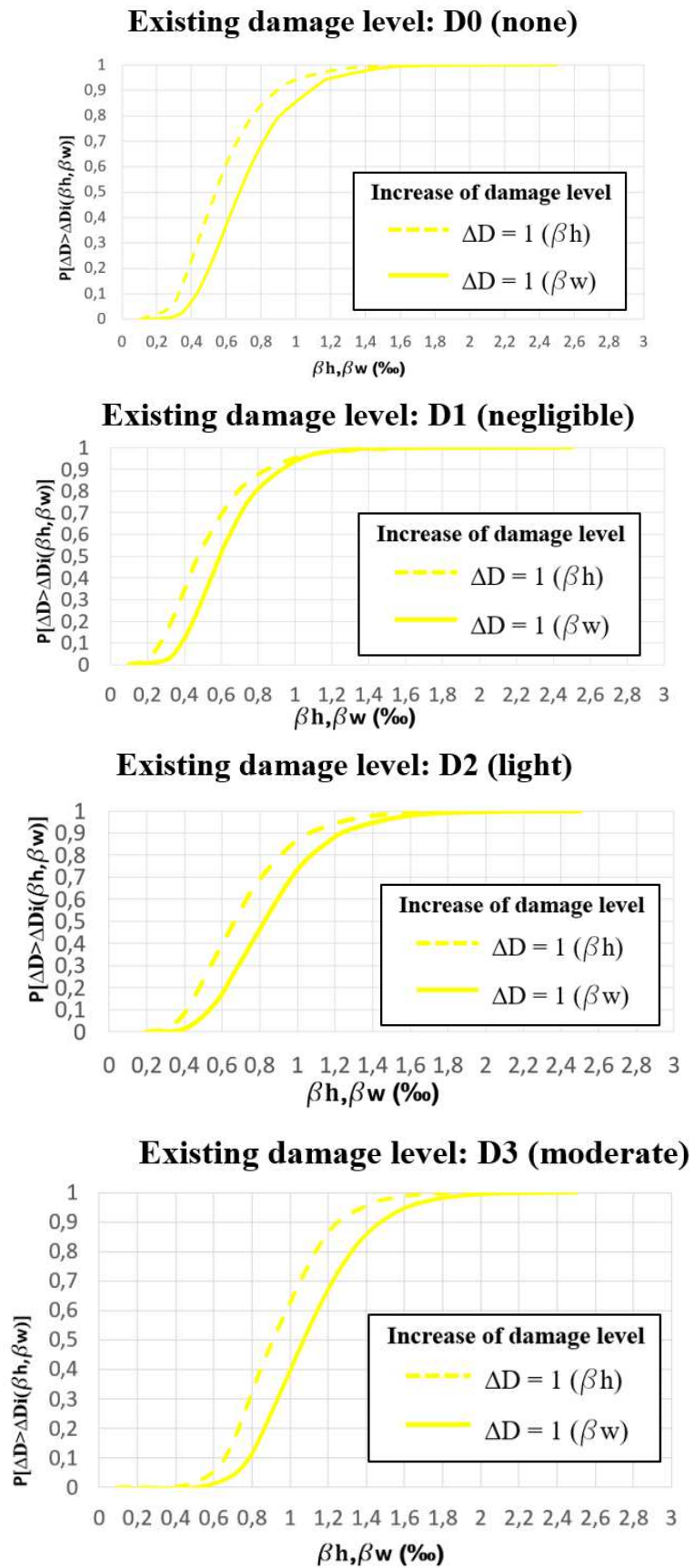


Figure 8.107 Empirical fragility curves for masonry buildings at “extremity 2” of the aggregate with different existing damage levels.

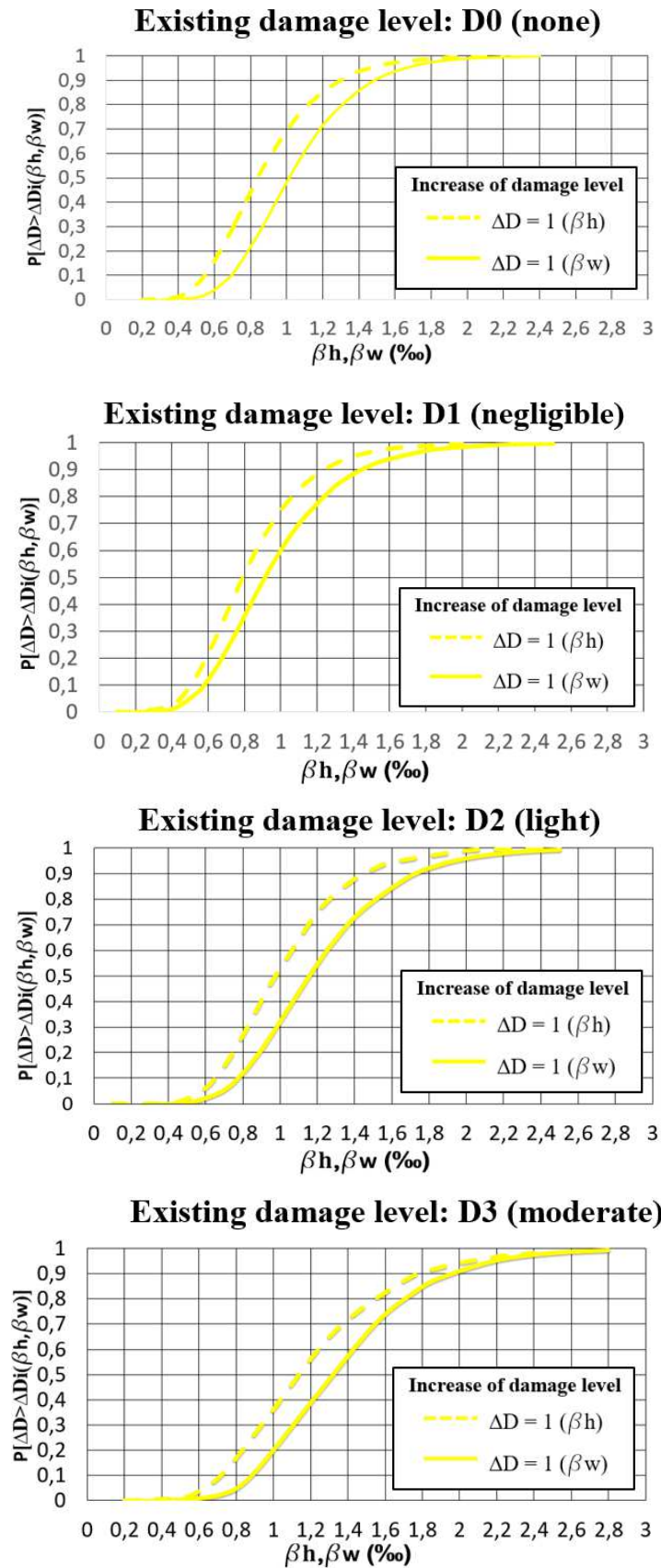


Figure 8.108 Empirical fragility curves for masonry buildings in a central position of the aggregate with different existing damage levels.

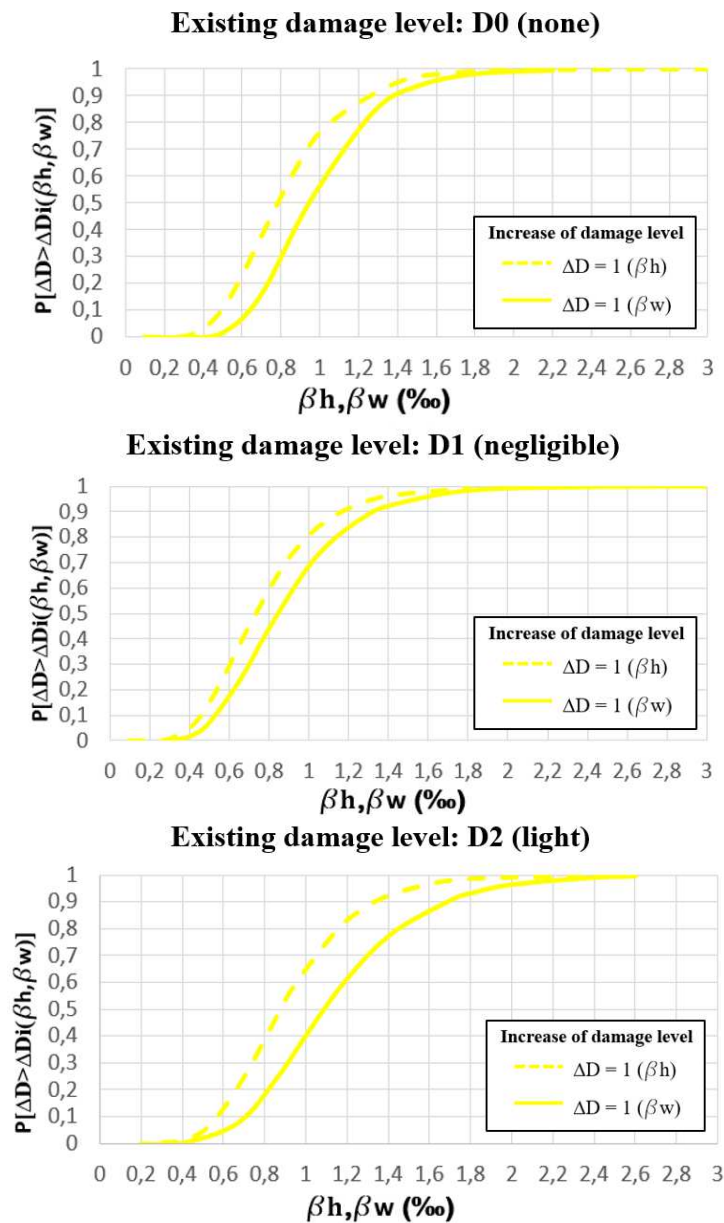


Figure 8.109 Empirical fragility curves for masonry buildings in a corner position of the aggregate with different existing damage levels.

As it is possible to note in the Figures above, masonry buildings show a higher susceptibility to worsening of damage level than reinforced concrete buildings, in particular under horizontal strains: such point, moreover, is more evident when building is characterized by existing damage degree. In detail, difference of performance to angular and horizontal distortions is more evident starting from none to higher existing damage levels.

In the following paragraph, influence of some vulnerability factors on building performance has been discussed.

8.6.5 Analysis of influence of vulnerability factors on building performance

As above mentioned, analysis of fragility curves classified for different buildings typologies and with different structural characteristics, provides critical information on structural behavior of structures.

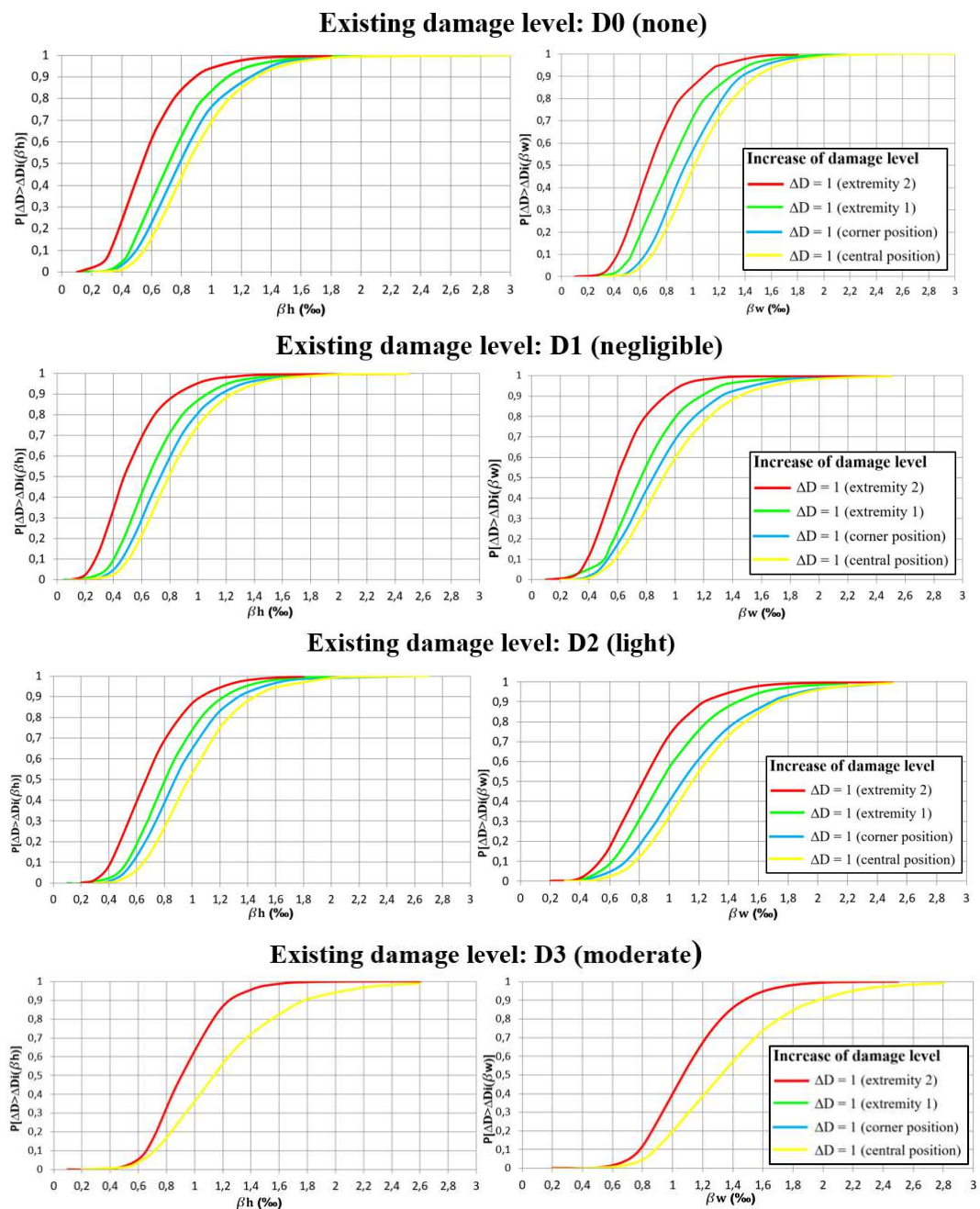


Figure 8.110 Comparison of empirical fragility curves for masonry buildings in different positions of the aggregate with different existing damage levels.

In particular, by considering the position of each structure in a building aggregate, it was possible to note that buildings located at the “extremity 2” show the highest probability to worsen their damage level: progressive redistribution of stresses between adjacent buildings along movement direction, in fact, increases strains at the end of aggregate. Buildings in a central or in a corner position, instead, showed a similar good performance (Fig. 8.110).

Furthermore, in order to investigate influence of existing damage level on building performance, fragility curves corresponding to each initial damage degree have been compared (Fig. 8.111).

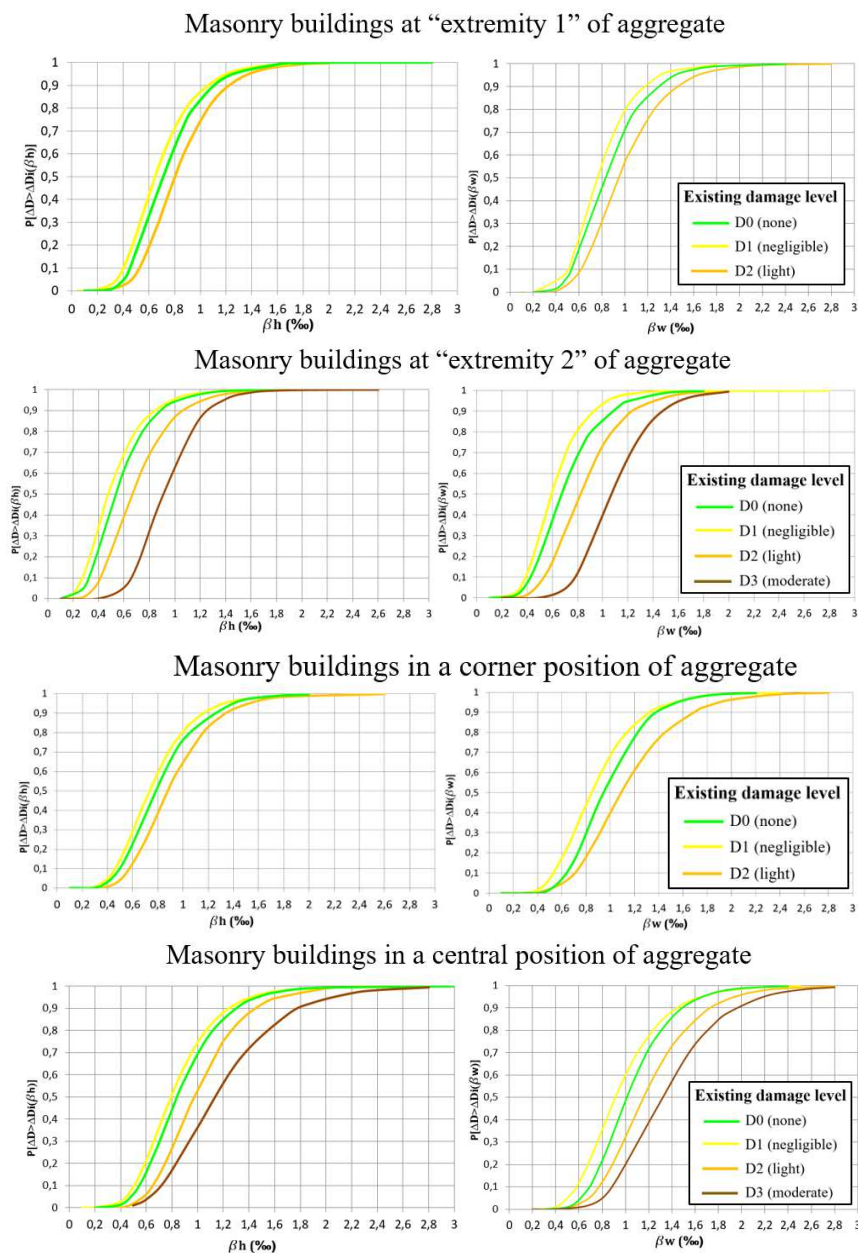


Figure 8.111 Comparison of fragility curves of buildings with different existing damage levels.

Figure 8.111 seems to show that buildings with none or negligible existing damage have a similar probability of increasing of damage level. Differently, buildings with initial light or moderate damage have a different performance: the latter, have a lower probability to worsen damage level than buildings without initial damage, probably due to plastic behavior of masonry structures.

A building characterized by initial none or negligible damage has an elastic behavior and requires low deformations to reduce capacity of masonry element, while in a moderate initial damage condition, it shows a plastic global behavior and requires greater distortions to worsen its damage level.

Number of stories also influences the degree of loss of buildings affected by ground movement. To this purpose, distinguishing buildings in terms of structural typology, empirical fragility curves for different number of stories have been provided (Figures 8.112 and 8.113)

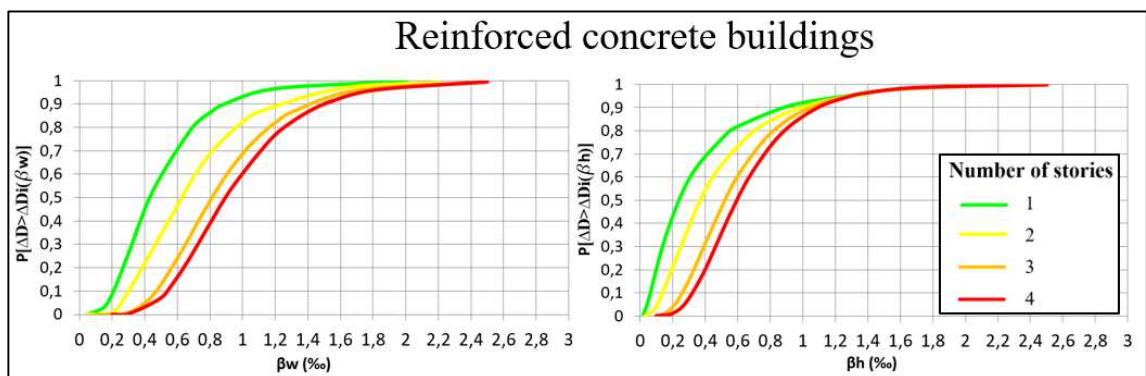


Figure 8.112 Empirical fragility curves for reinforced concrete buildings with different number of stories.

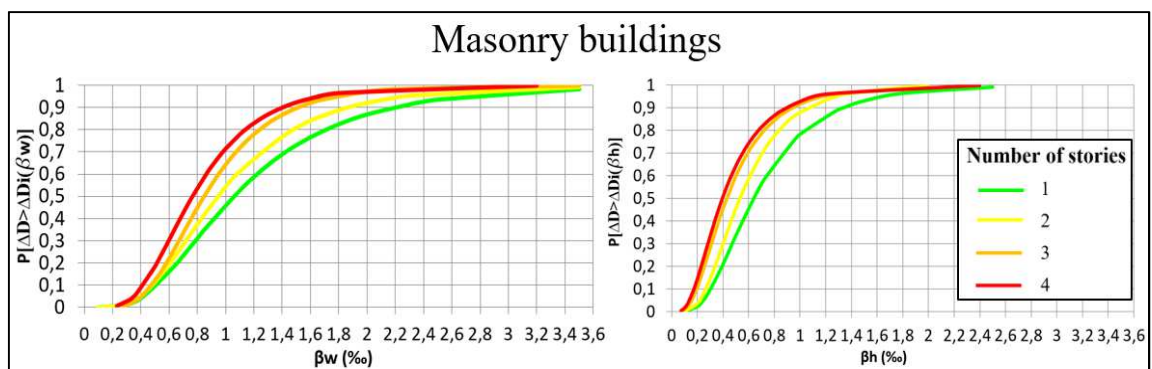


Figure 8.113 Empirical fragility curves for masonry buildings with different number of stories.

According to Figures 8.112 and 8.113, reinforced concrete and masonry buildings have a different performance: in reinforced concrete structures, the probability to worsen damage level decreases when the number of stories increases. Such behavior is due to high strength and stiffness of reinforced concrete foundations. Generally, in reinforced concrete buildings, damage occurs in fact only on story at ground level: structural properties of such buildings allow to decrease effects of ground movement to superstructure.

Differently, masonry buildings with 3 or 4 stories are more susceptible than structures with lower height. In several aggregates of structures, in fact, occurred cracks show a width increasing from bottom to up along building façade, due to rotational settlements, angular distortions or horizontal strains: for this reason, masonry buildings with more floors can be affected by high damage levels. Displacements occurred to masonry foundations induce a state of stress on story at ground level, and subsequently on upper floors, depending by progressive transferring of strain along masonry panels.

Anyway, it is important to highlight that several cracks occur generally on the connection of walls of adjacent buildings with different floor height, thus confirming that vertical irregularities can cause important damage (Fig. 8.114).

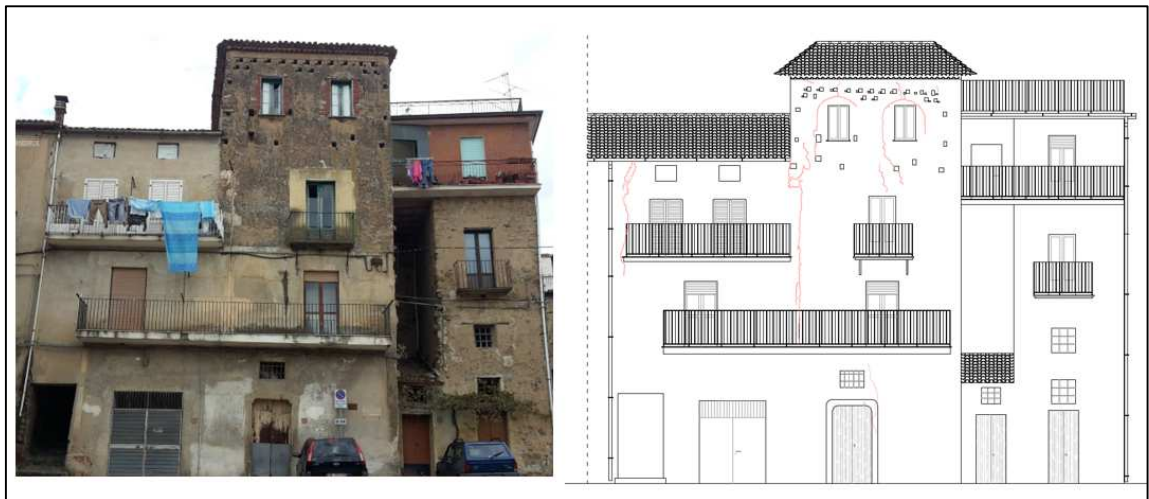


Figure 8.114 Example of damage occurred in adjacent buildings with different height of stories.

Furthermore, in order to detect the influence of building geometry on vulnerability, L/B ratio between geometric dimensions of building has been compared with:

- ratio between displacement of building and displacement of surrounding area;
- building damage level.

Distinguishing buildings in term of structural typology, such analysis highlighted that the vulnerability increases for increasing L/B ratio.

In particular, most buildings with L/B ratio equal to 1 showed a displacement lower or equal than to the surrounding area, while most buildings with rectangular shape have a displacement higher than surrounding ground level (Figure 8.115).

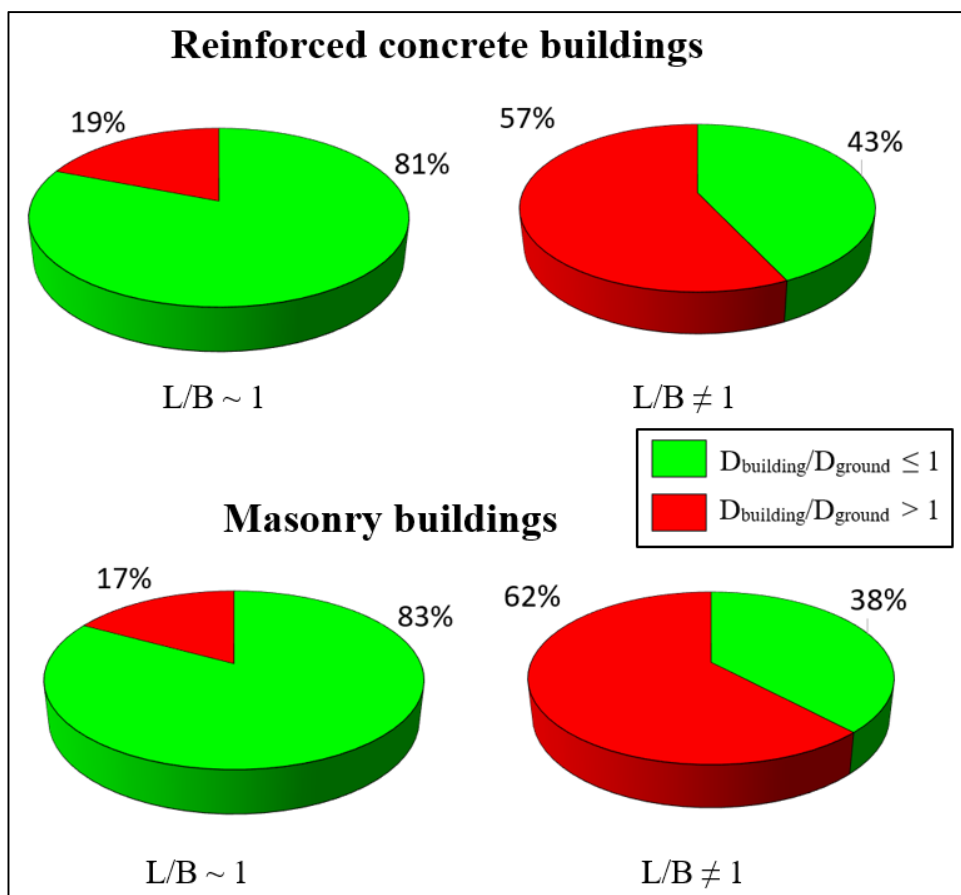


Figure 8.115 Ratio between displacement of building and displacement of the surrounding area for structures with $L/B = 1$ and $L/B \neq 1$.

Moreover, as to regards distribution of damage levels, it was observed that both masonry and reinforced concrete buildings with rectangular shape show higher damage degrees than structures with L/B equal to 1 (Fig. 8.116): such point, more evident in masonry buildings, could be due, probably, to greater distortions induced on building façades with different length and to different stiffness of masonry walls along the two directions of structure, that generate an excessive concentration of stresses during the movement.

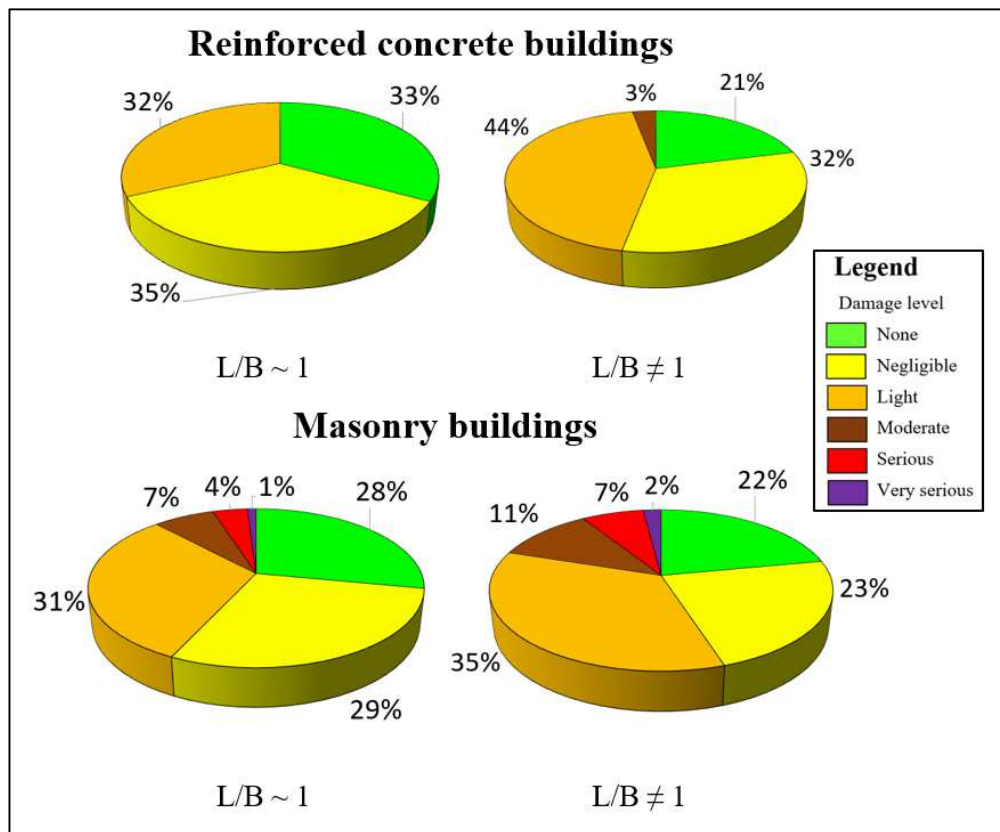


Figure 8.116 Distribution of damage levels occurred to reinforced concrete and masonry buildings with $L/B = 1$ and $L/B \neq 1$.

Finally, to investigate influence of building orientation in comparison to landslide direction, three possible configurations have been defined (Fig. 8.117).

- buildings with the long axis parallel to the landslide direction (a);
- buildings that show a varying orientation relative to movement direction (b);
- buildings with the long axis perpendicular to the landslide direction (c).

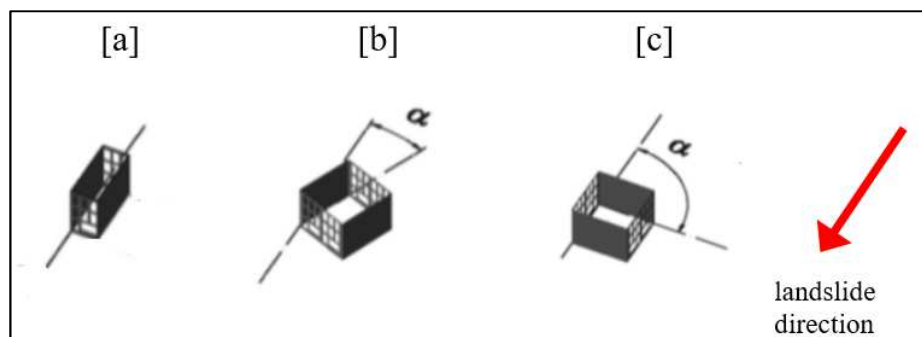


Figure 8.117 Building alignment in comparison with landslide direction.

Distinguishing buildings in term of structural typology, Figures 8.118 and 8.119 highlight that buildings with the long axis parallel to landslide direction show a lower displacement than surrounding areas and low damage levels; buildings characterized by varying angle with movement direction, instead, show high displacement and damage severity degree, in particular when $\alpha=45^\circ$. Probably, such behavior depends on greater distortions occurred to perpendicular façades and on progressive redistribution of stresses, in particular in masonry buildings.

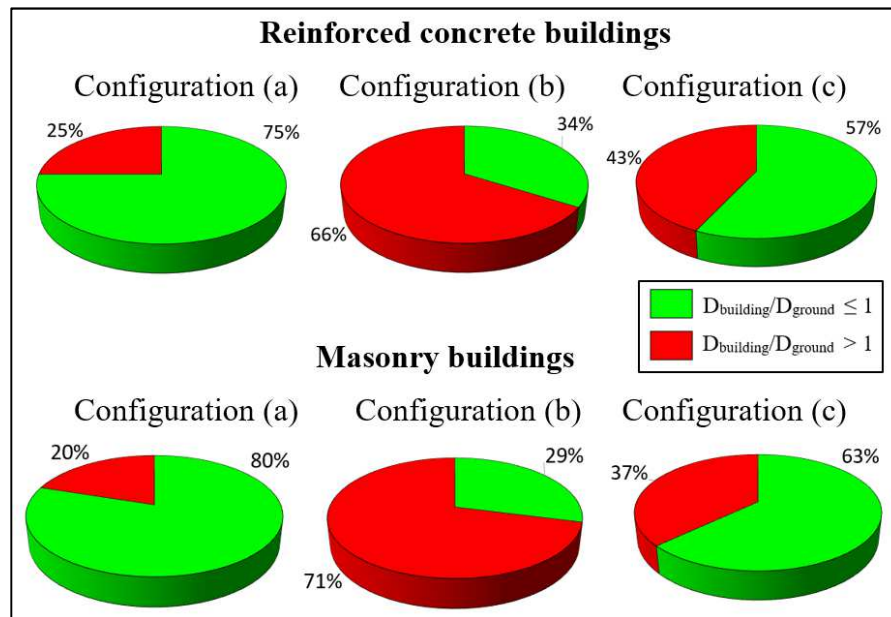


Figure 8.118 Ratio between displacement of building and displacement of surrounding area for buildings with different orientation.

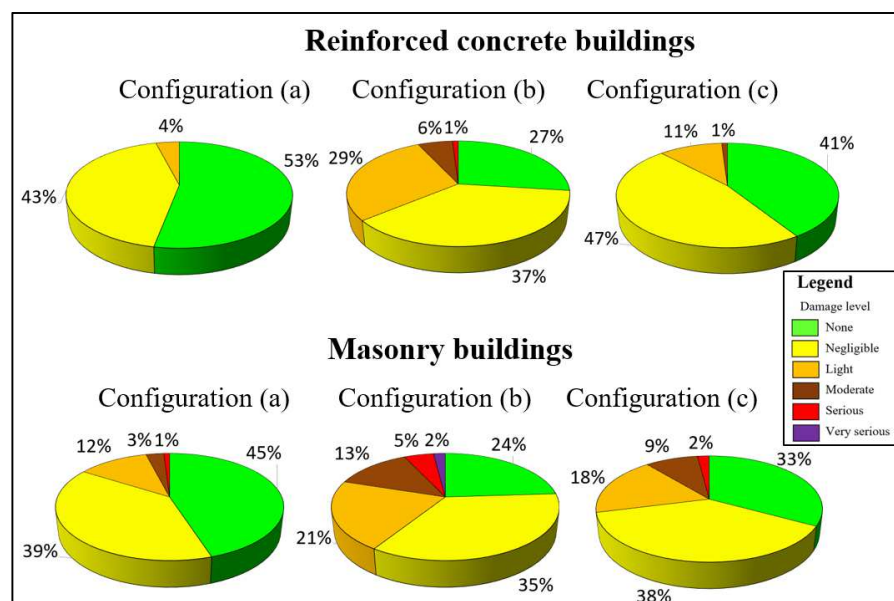


Figure 8.119 Distribution of damage levels occurred to reinforced concrete and masonry buildings with different orientation.

8.6.6 Forecasting of future damage conditions of whole urban settlement

At medium scale of analysis, the above discussed empirical fragility curves can be useful to forecast spatial and temporal evolution of buildings damage with reference to the whole territory of study area.

Under the assumption that building distortions are the representative landslide intensity parameter causing damage to single buildings, angular distortion and horizontal strain effects, assessed separately on each building, have been combined according to theoretical elements of Probability Theory, as mentioned in paragraph 7.3, in order to take into account that vertical and horizontal distortions are concurrent under building foundations.

Dealing with very slow and slow-moving landslides, in turn characterized by low and almost constant values of annual distortion rate, it is possible to assess future buildings deformation rates induced by ground instability.

In detail, two different future scenarios have been forecasted. In a first scenario, in the period 2015-2019, annual distortion rates induced by landslide movement have been considered equal to those registered in time-span 2010-2014. As to regards the second scenario, in the period 2015-2019, distortion rates have been increased of 50% of value measured in time-span 2010-2014.

For each building, empirical fragility curves, obtained in paragraph 8.6.4 for different structural typologies, provide the probability to obtain, in 2020, an increase of one damage level compared with the degree registered at the beginning of 2015 (Figs. 8.120 and 8.121).

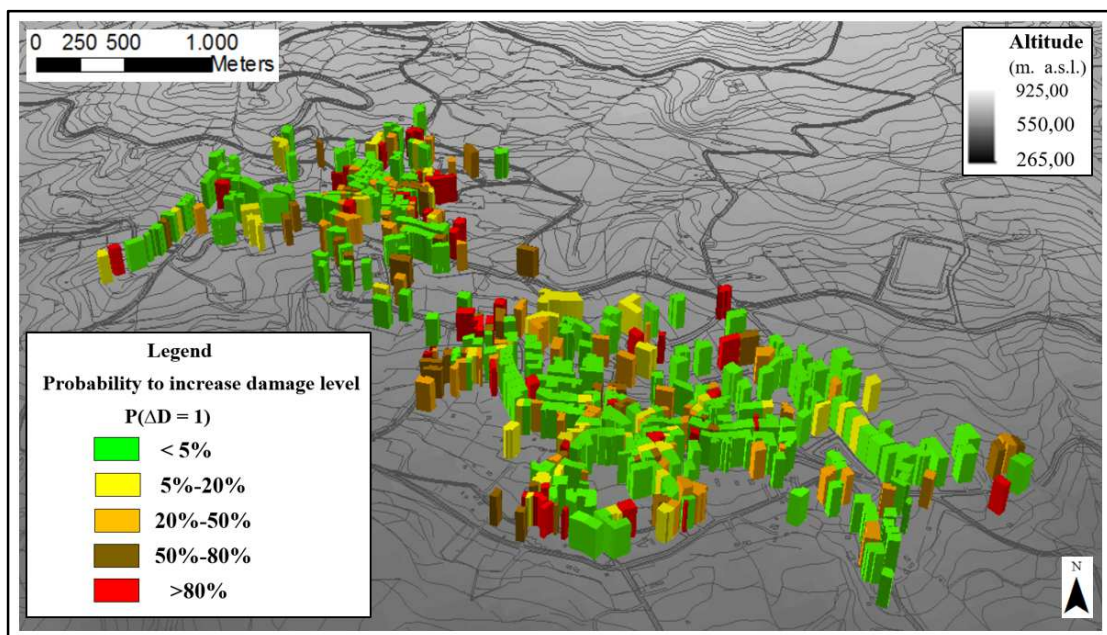


Figure 8.120 Map of probability to obtain an increase of one damage level in 2020 according to first scenario.

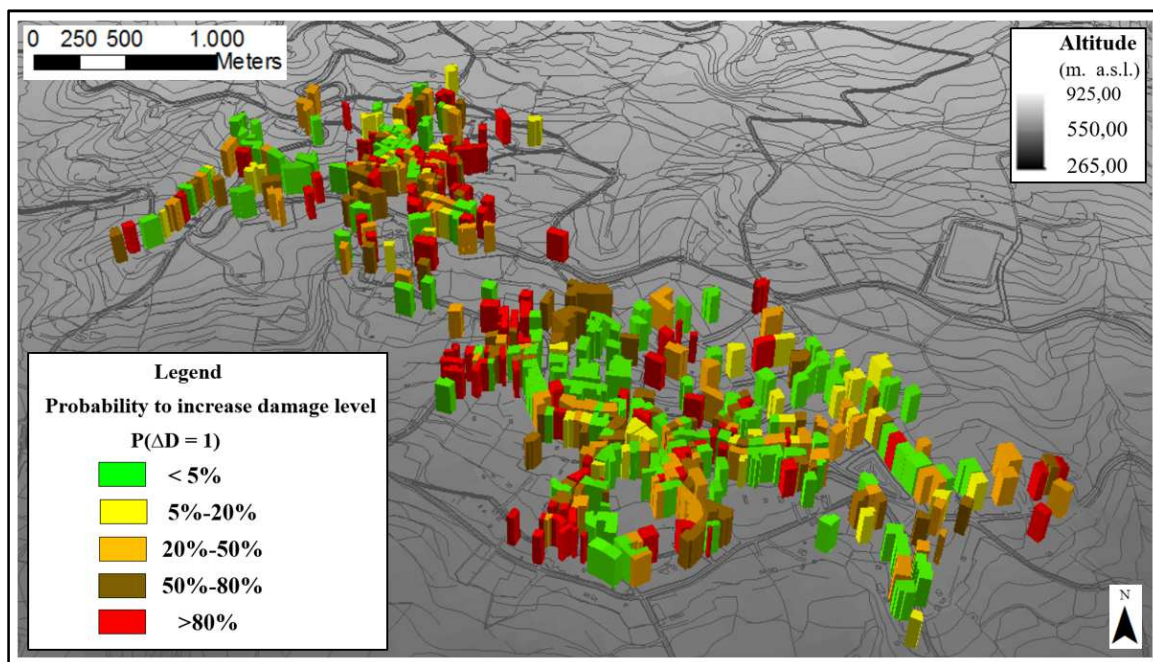


Figure 8.121 Map of probability to obtain an increase of one damage level in 2020 according to second scenario.

As it is possible to note in the above figures, such analysis allowed to evaluate different possible scenarios of exposed elements future conditions, thus identifying most critical areas where mitigation activities have to be focused. For this reason, the proposed approach can be helpful for authorities responsible of land management and government.

8.7 Vulnerability assessment at a detailed scale

As mentioned in paragraph 7.1, aim of such analysis level is to define, for each building, by analytical or numerical approaches, the relationship between landslide intensity and expected damage degree.

Analyses performed to medium scale of representation do not take into account structural properties of buildings, such as type of material and its mechanical parameters, typology of foundations, position of openings and soil geotechnical properties.

For this reason, information used in a medium scale analysis have to be integrated, aimed to fully characterize landslide kinematics and the exposed building.

In the following, input data helpful to detect building vulnerability at level of single building have been discussed.

8.7.1 Characterization of landslide kinematics affecting each building

A complete characterization of landslide requires, along with information of previous level, the assessment of lithological stratigraphy, of geotechnical parameters and mechanical properties of soils under each considered building.

Furthermore, availability of historical DInSAR data, integrated with results of conventional *in situ* measurements, allows to assess temporal evolution of landslide intensity and distortions occurred to building foundations.

To this aim, cumulated vertical and horizontal E-W displacements at the end of each year in period 2011-2015 have been obtained by means of IDW interpolation of DInSAR data.

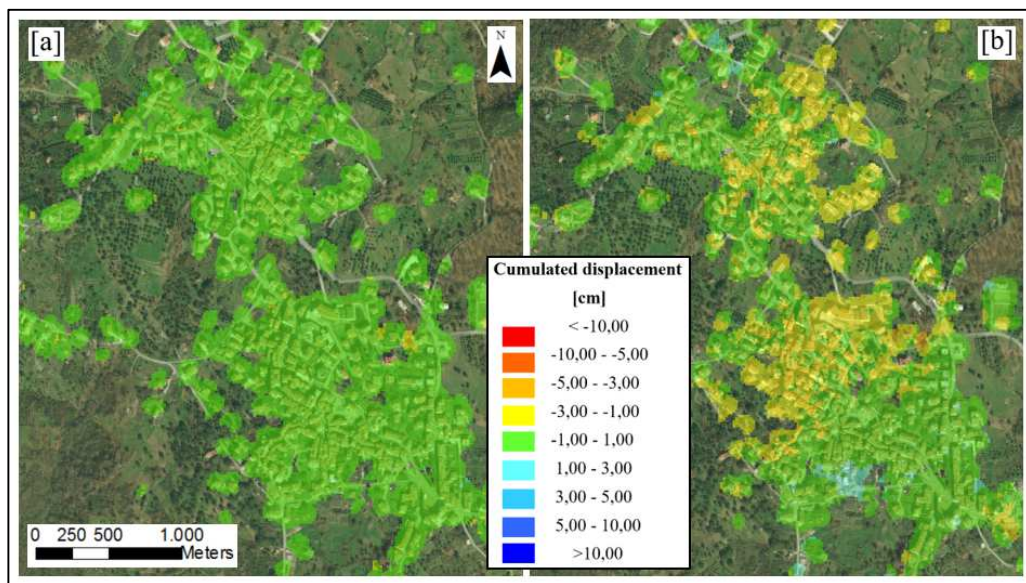


Figure 8.122 Cumulated displacement maps in 2011 along vertical (a) and horizontal E-W (b) directions.

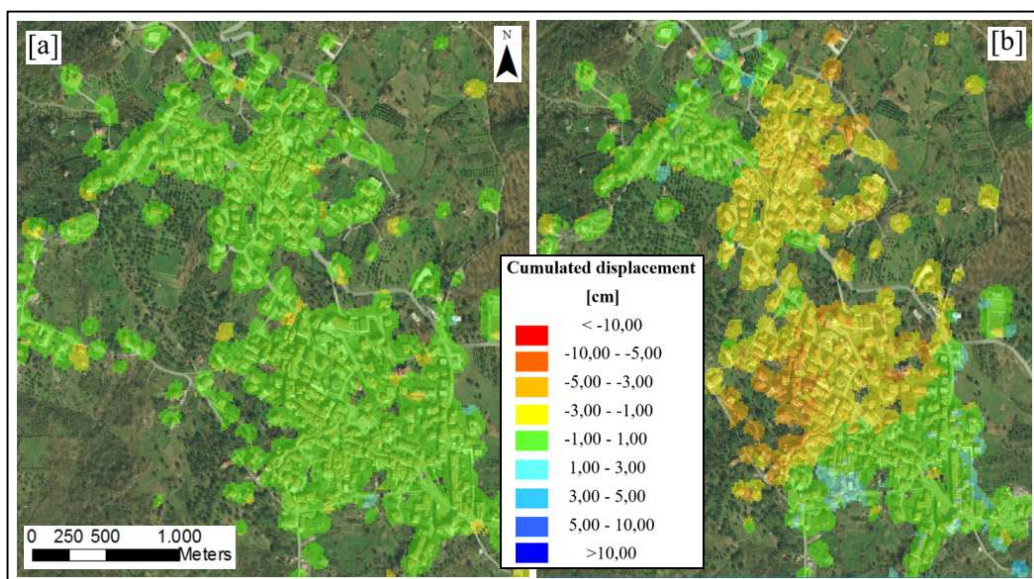


Figure 8.123 Cumulated displacement maps in period 2011-2012 along vertical (a) and horizontal E-W (b) directions.

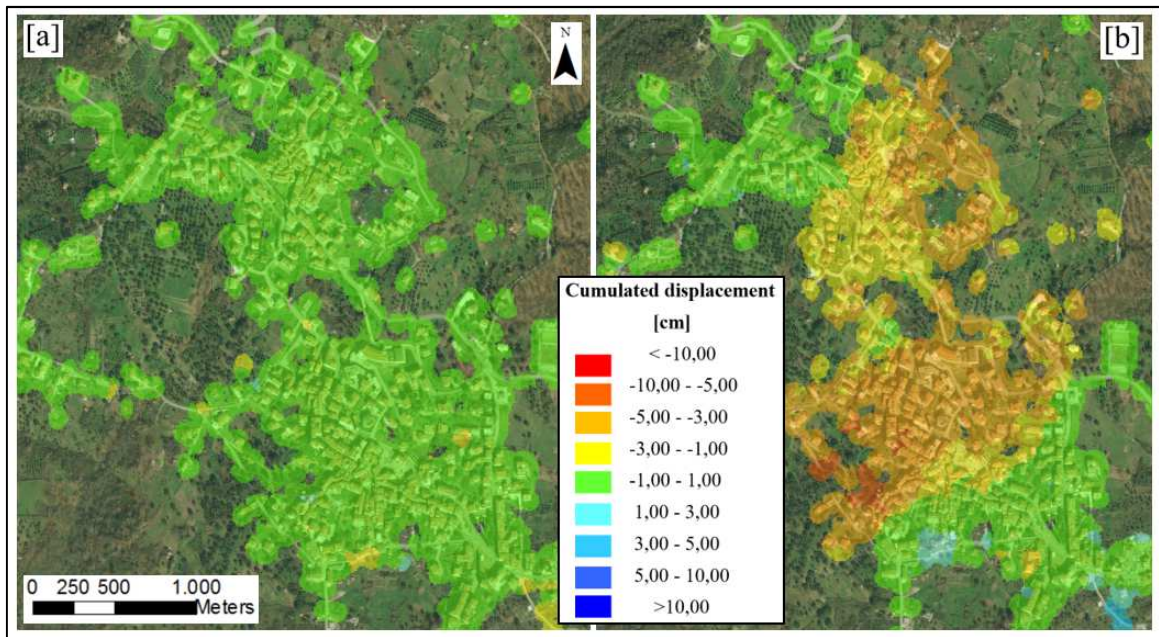


Figure 8.124 Cumulated displacement maps in period 2011- 2013 along vertical (a) and horizontal E-W (b) directions.

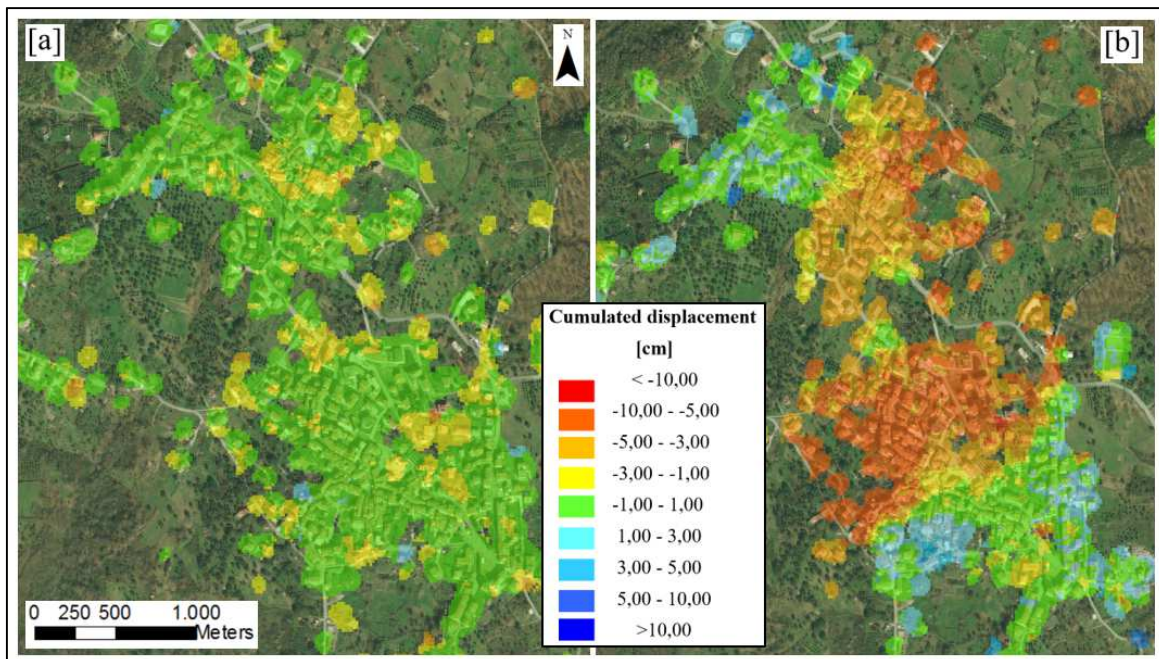


Figure 8.125 Cumulated displacement maps in period 2011- 2014 along vertical (a) and horizontal E-W (b) directions.

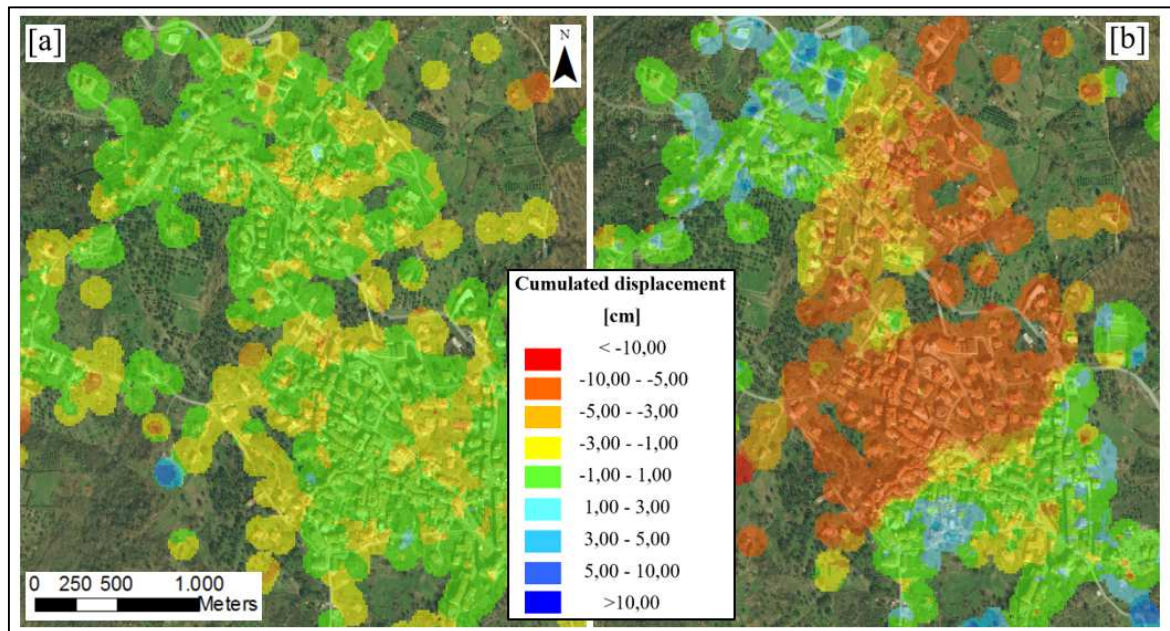


Figure 8.126 Cumulated displacement maps in period 2011- 2015 along vertical (a) and horizontal E-W (b) directions.

Assessment of annual distortions rate induced on each building foundations by landslides is a difficult task and it is possible only at a detailed scale of analysis. It requires to define, firstly, DInSAR displacements profile measured on areas surrounding building boundary and, subsequently, to evaluate differential displacements and derived parameters occurred under structure façades.

Furthermore, analysis of historical distortions induced by ground instability allows to forecast their temporal and spatial evolution, representing a useful tool to investigate future conditions of building damage and local failures.

In the following, integrated analysis of kinematic and geometrical characteristics, stratigraphic and geotechnical parameters of local soils where available, of landslide involved each studied building, have been developed.

8.7.2 Detailed survey of exposed elements

As mentioned in Chapter 7, analytical and numerical approaches to assess building damage future conditions require information more detailed than previous level of representation. To implement building computational model in a numerical software, in particular, geometrical data, types and materials of structures, typology of foundation, mechanical properties of structural materials, have to be assessed through *in situ* survey.

For this reason, the scheme provided by the Italian Department of Civil Protection (DPC) represents a useful tool to obtain an objective procedure of building survey.

In the following, an example of building detailed survey, performed according to DPC scheme, is shown.



Figure 8.127 Example of building surveyed according to the scheme proposed by Italian “DPC”.

SEZIONE 1 Identificazione edificio		SALERNO		IDENTIFICATIVO SOPRALLUOGO		giorno mese anno		
Provincia:		Moio della Civitella		Squadra		Data		
Comune:		Moio		IDENTIFICATIVO EDIFICIO		Istat Reg. Istat Prov. Istat Comune N° aggregato N° edificio		
Frazione/Località: (denominazione Istat)		Moio		Cod. di Località Istat		Tipo carta		
1 <input checked="" type="checkbox"/> via		D G a l z e r a n o		Sez. di consimento Istat		N° carta		
2 <input type="checkbox"/> corso		Num. Civico		Dati Catastali		Foglio 9 Allegato A		
3 <input type="checkbox"/> vicolo				Particelle		2 1 1		
4 <input type="checkbox"/> piazza				Posizione edificio		<input checked="" type="checkbox"/> Isolato <input type="checkbox"/> Interno <input type="checkbox"/> D'estremità <input type="checkbox"/> D'angolo		
5 <input type="checkbox"/> altro (Indicare: contrada, località, traversa, salita, etc.)		Coordinate geografiche (E 22-32) UTM fuso N		Denominazione edificio o proprietario		Codice Uso S		
<p>Fotocopia dell'aggregato strutturale con identificazione dell'edificio</p>								
SEZIONE 2 Descrizione edificio								
Dati metrici			Età	Uso - esposizione				
N° Piani totali con interrati	Altezza media di piano [m]	Superficie media di piano [m²]	Costruzione e ristrutturaz. [max 2]	Uso	N° unità d'uso	Utilizzazione	Occupanti	
<input type="checkbox"/> 1 <input type="checkbox"/> 9	1 <input type="checkbox"/> ≤ 2.50	A <input type="checkbox"/> ≤ 50 I <input type="checkbox"/> 400 + 500	1 <input type="checkbox"/> ≤ 1919	A <input checked="" type="checkbox"/> Abitativo	<input type="checkbox"/> 1 <input type="checkbox"/> 5	A <input checked="" type="checkbox"/> > 65%	100 10 1	
<input type="checkbox"/> 2 <input type="checkbox"/> 10	2 <input checked="" type="checkbox"/> 2.50 + 3.50	B <input type="checkbox"/> 50 + 70 L <input type="checkbox"/> 500 + 650	2 <input checked="" type="checkbox"/> 19 + 45	B <input type="checkbox"/> Produttivo	<input type="checkbox"/>	B <input type="checkbox"/> 30-65%	0 0 0	
<input type="checkbox"/> 3 <input type="checkbox"/> 11	3 <input type="checkbox"/> 3.50 + 5.0	C <input type="checkbox"/> 70 + 100 M <input type="checkbox"/> 650 + 900	3 <input type="checkbox"/> 46 + 61	C <input type="checkbox"/> Commercio	<input type="checkbox"/>	C <input type="checkbox"/> < 30%	1 1 1	
<input type="checkbox"/> 4 <input type="checkbox"/> 12	4 <input type="checkbox"/> > 5.0	D <input checked="" type="checkbox"/> 100 + 130 N <input type="checkbox"/> 900 + 1200	4 <input type="checkbox"/> 62 + 71	D <input type="checkbox"/> Uffici	<input type="checkbox"/>	D <input type="checkbox"/> Non utilizz.	2 2 2	
<input checked="" type="checkbox"/> 5 <input type="checkbox"/> > 12		E <input type="checkbox"/> 130 + 170 O <input type="checkbox"/> 1200 + 1600	5 <input type="checkbox"/> 72 + 81	E <input type="checkbox"/> Serv. Pub.	<input type="checkbox"/>	E <input type="checkbox"/> In costruz.	3 3 3	
<input type="checkbox"/> 6		F <input type="checkbox"/> 170 + 230 P <input type="checkbox"/> 1600 + 2200	6 <input type="checkbox"/> 82 + 91	F <input type="checkbox"/> Deposito	<input type="checkbox"/>	F <input type="checkbox"/> Non finito	4 4 4	
<input type="checkbox"/> 7	Piani interrati	G <input type="checkbox"/> 230 + 300 Q <input type="checkbox"/> 2200 + 3000	7 <input type="checkbox"/> 92 + 01	G <input type="checkbox"/> Strategico	<input type="checkbox"/>	G <input type="checkbox"/> Abbandon.	5 5 5	
<input type="checkbox"/> 8	A <input type="checkbox"/> 0 C <input type="checkbox"/> 2	H <input type="checkbox"/> 300 + 400 R <input type="checkbox"/> > 3000	8 <input checked="" type="checkbox"/> ≥ 2002	H <input type="checkbox"/> Turis-ricel.	<input type="checkbox"/>		6 6 6	
	B <input checked="" type="checkbox"/> 1 D <input type="checkbox"/> ≥ 3						7 7 7	
							8 8 8	
							9 9 9	
						Proprietà	A <input type="checkbox"/> Pubblica B <input checked="" type="checkbox"/> Privata	

Figure 8.128 Sections 1 and 2 of DPC classification scheme for considered building.

SEZIONE 3 Tipologia (multiscelta; per gli edifici in muratura indicare al massimo 2 tipi di combinazioni strutture verticali-solai)

Strutture verticali / Strutture orizzontali		Strutture in muratura								Altre strutture				
		Non identificate		A tessitura irregolare e di cattiva qualità (Pietrame non squadrato, ciottoli,...)				A tessitura regolare e di buona qualità (Blocchi; mattoni; pietra squadrata,...)		Piastrati isolati	Mista	Rinforzata	Telai in c.a.	
		Senza catene o cordoli	Con catene o cordoli	Senza catene o cordoli	Con catene o cordoli	A	B	Telai in c. a.						
A	B	C	D	E	F	G	H	REGOLARITA'	Non regolare	Regolare				
1	Non identificate	<input type="radio"/>	<input type="checkbox"/>	<input type="checkbox"/>	<input type="checkbox"/>	<input type="checkbox"/>	<input type="checkbox"/>	<input type="checkbox"/>	SI	<input type="checkbox"/>	<input type="checkbox"/>	<input type="checkbox"/>	<input type="checkbox"/>	
2	Volte senza catene	<input type="checkbox"/>	<input type="checkbox"/>	<input type="checkbox"/>	<input type="checkbox"/>	<input type="checkbox"/>	<input type="checkbox"/>	<input type="checkbox"/>	<input type="checkbox"/>	G1	H1	<input type="checkbox"/>	<input type="checkbox"/>	
3	Volte con catene	<input type="checkbox"/>	<input type="checkbox"/>	<input type="checkbox"/>	<input type="checkbox"/>	<input type="checkbox"/>	<input type="checkbox"/>	<input type="checkbox"/>	<input type="checkbox"/>	<input type="checkbox"/>	<input type="checkbox"/>	<input type="checkbox"/>	<input type="checkbox"/>	
4	Travi con soletta deformabile (travi in legno con semplice tavolato, travi e voltine,...)	<input type="checkbox"/>	<input type="checkbox"/>	<input type="checkbox"/>	<input type="checkbox"/>	<input type="checkbox"/>	<input type="checkbox"/>	<input type="checkbox"/>	NO	G2	H2	<input type="checkbox"/>	<input type="checkbox"/>	
5	Travi con soletta semirigida (travi in legno con doppio tavolato, travi e tavoloni,...)	<input type="checkbox"/>	<input type="checkbox"/>	<input checked="" type="checkbox"/>	<input type="checkbox"/>	<input type="checkbox"/>	<input type="checkbox"/>	<input type="checkbox"/>	<input type="checkbox"/>	<input type="checkbox"/>	<input type="checkbox"/>	<input type="checkbox"/>	<input type="checkbox"/>	
6	Travi con soletta rigida (solai di c.a., travi ben collegate a solette di c.a,...)	<input type="checkbox"/>	<input type="checkbox"/>	<input type="checkbox"/>	<input type="checkbox"/>	<input type="checkbox"/>	<input type="checkbox"/>	<input type="checkbox"/>	<input type="checkbox"/>	G3	H3	<input type="checkbox"/>	<input type="checkbox"/>	

REGOLARITA'

	Non regolare		Regolare
	A	B	
1 Forma pianta ed elevazione	<input type="radio"/>	<input checked="" type="checkbox"/>	<input checked="" type="checkbox"/>
2 Disposizione tamponature	<input type="radio"/>	<input type="checkbox"/>	<input checked="" type="checkbox"/>

Copertura

1 <input checked="" type="checkbox"/> Spingente pesante
2 <input type="radio"/> Non spingente pesante
3 <input type="radio"/> Spingente leggera
4 <input type="radio"/> Non spingente leggera

SEZIONE 4 Danni ad ELEMENTI STRUTTURALI e provvedimenti di pronto intervento (P.I.) eseguiti

Livello - estensione / Componente strutturale - Danno preesistente	DANNO ⁽¹⁾									PROVEDIMENTI DI P.I. ESEGUITI						
	D4-D5 Gravissimo			D2-D3 Medio grave			D1 Leggero			Nullo	Nessuno	Demolizioni	Cercature eoltranti	Riparazione	Puntelli	Trasenne e protezione passaggi
	> 2/3	1/3 - 2/3	< 1/3	> 2/3	1/3 - 2/3	< 1/3	> 2/3	1/3 - 2/3	< 1/3							
A	B	C	D	E	F	G	H	I	L	A	B	C	D	E	F	
1 Strutture verticali	<input type="checkbox"/>	<input type="checkbox"/>	<input type="checkbox"/>	<input type="checkbox"/>	<input checked="" type="checkbox"/>	<input type="checkbox"/>	<input type="checkbox"/>	<input type="checkbox"/>	<input checked="" type="checkbox"/>	<input type="checkbox"/>	<input checked="" type="checkbox"/>	<input type="checkbox"/>	<input type="checkbox"/>	<input type="checkbox"/>	<input type="checkbox"/>	<input type="checkbox"/>
2 Solai	<input type="checkbox"/>	<input type="checkbox"/>	<input type="checkbox"/>	<input type="checkbox"/>	<input type="checkbox"/>	<input type="checkbox"/>	<input type="checkbox"/>	<input type="checkbox"/>	<input checked="" type="checkbox"/>	<input type="checkbox"/>	<input checked="" type="checkbox"/>	<input type="checkbox"/>	<input type="checkbox"/>	<input type="checkbox"/>	<input type="checkbox"/>	<input type="checkbox"/>
3 Scale	<input type="checkbox"/>	<input type="checkbox"/>	<input type="checkbox"/>	<input type="checkbox"/>	<input type="checkbox"/>	<input type="checkbox"/>	<input type="checkbox"/>	<input type="checkbox"/>	<input checked="" type="checkbox"/>	<input type="checkbox"/>	<input checked="" type="checkbox"/>	<input type="checkbox"/>	<input type="checkbox"/>	<input type="checkbox"/>	<input type="checkbox"/>	<input type="checkbox"/>
4 Copertura	<input type="checkbox"/>	<input type="checkbox"/>	<input type="checkbox"/>	<input type="checkbox"/>	<input type="checkbox"/>	<input type="checkbox"/>	<input type="checkbox"/>	<input type="checkbox"/>	<input checked="" type="checkbox"/>	<input type="checkbox"/>	<input checked="" type="checkbox"/>	<input type="checkbox"/>	<input type="checkbox"/>	<input type="checkbox"/>	<input type="checkbox"/>	<input type="checkbox"/>
5 Tamponature-tramezzi	<input type="checkbox"/>	<input type="checkbox"/>	<input type="checkbox"/>	<input type="checkbox"/>	<input checked="" type="checkbox"/>	<input type="checkbox"/>	<input type="checkbox"/>	<input type="checkbox"/>	<input checked="" type="checkbox"/>	<input type="checkbox"/>	<input checked="" type="checkbox"/>	<input type="checkbox"/>	<input type="checkbox"/>	<input type="checkbox"/>	<input type="checkbox"/>	<input type="checkbox"/>
6 Danno preesistente	<input type="checkbox"/>	<input type="checkbox"/>	<input type="checkbox"/>	<input type="checkbox"/>	<input type="checkbox"/>	<input type="checkbox"/>	<input type="checkbox"/>	<input type="checkbox"/>	<input type="checkbox"/>	<input type="checkbox"/>	<input type="checkbox"/>	<input type="checkbox"/>	<input type="checkbox"/>	<input type="checkbox"/>	<input type="checkbox"/>	<input type="checkbox"/>

(1) - Di ogni livello di danno indicare l'estensione solo se esso è presente. Se l'oggetto indicato nella riga non è danneggiato campire **Nullo**.

SEZIONE 5 Danni ad ELEMENTI NON STRUTTURALI e provvedimenti di pronto intervento eseguiti

Tipo di danno	PRESENZA DANNO	PROVEDIMENTI DI P.I. ESEGUITI					
		Nessuno	Rimozione	Puntelli	Riparazione	Divieto di accesso	Trasenne e protezione passaggi
	A	B	C	D	E	F	G
1 Distacco intonaci, rivestimenti, controsoffitti...	<input type="radio"/>	<input type="checkbox"/>	<input type="checkbox"/>	<input type="checkbox"/>	<input type="checkbox"/>	<input type="checkbox"/>	<input type="checkbox"/>
2 Caduta tegole, cornicioni...	<input type="radio"/>	<input type="checkbox"/>	<input type="checkbox"/>	<input type="checkbox"/>	<input type="checkbox"/>	<input type="checkbox"/>	<input type="checkbox"/>
3 Caduta cornicioni, parapetti...	<input type="radio"/>	<input type="checkbox"/>	<input type="checkbox"/>	<input type="checkbox"/>	<input type="checkbox"/>	<input type="checkbox"/>	<input type="checkbox"/>
4 Caduta altri oggetti interni o esterni	<input type="radio"/>	<input type="checkbox"/>	<input type="checkbox"/>	<input type="checkbox"/>	<input type="checkbox"/>	<input type="checkbox"/>	<input type="checkbox"/>
5 Danno alla rete idrica, fognaria o termoidraulica	<input type="radio"/>	<input type="checkbox"/>	<input type="checkbox"/>	<input type="checkbox"/>	<input type="checkbox"/>	<input type="checkbox"/>	<input type="checkbox"/>
6 Danno alla rete elettrica o del gas	<input type="radio"/>	<input type="checkbox"/>	<input type="checkbox"/>	<input type="checkbox"/>	<input type="checkbox"/>	<input type="checkbox"/>	<input type="checkbox"/>

SEZIONE 6 Pericolo ESTERNO indotto da altre costruzioni e provvedimenti di p.i. eseguiti

Causa potenziali	PERICOLO SU			PROVEDIM. DI P.I. ESEGUITI	
	Edificio	Via d'accesso	Vie interne	Divieto di accesso	Trasenne e protez. passaggi
	A	B	C	D	E
1 Crolli o cadute da altre costruzioni	<input type="checkbox"/>	<input checked="" type="checkbox"/>	<input type="checkbox"/>	<input type="checkbox"/>	<input type="checkbox"/>
2 Rottura di reti di distribuzione	<input type="checkbox"/>	<input type="checkbox"/>	<input type="checkbox"/>	<input type="checkbox"/>	<input type="checkbox"/>

SEZIONE 7 Terreno e fondazioni

MORFOLOGIA DEL SITO				DISSESTI (in atto o temibili):			
1	2	3	4	A	B	C	D
<input type="radio"/> Cresta	<input type="radio"/> Pendio forte	<input checked="" type="checkbox"/> Pendio leggero	<input type="radio"/> Pianura	<input type="checkbox"/> Assenti	<input type="checkbox"/> Generati dal sisma	<input type="checkbox"/> Acuiti dal sisma	<input checked="" type="checkbox"/> Terreno di fondazione

Figure 8.129 Sections 3,4,5,6,7 of DPC classification scheme for considered building.

SEZIONE 8 Giudizio di agibilità					
<i>Valutazione del rischio</i>				<i>Esito di agibilità</i>	
RISCHIO	STRUTTURALE (Sezz. 3 e 4)	NON STRUTTURALE (Sezz. 5)	ESTERNO (Sezz. 6)	GEOTECNICO (Sezz. 7)	
BASSO	<input type="radio"/>	<input checked="" type="radio"/>	<input type="radio"/>	<input type="radio"/>	A Edificio AGIBILE <input checked="" type="checkbox"/>
BASSO CON PROVVEDIMENTI	<input checked="" type="radio"/>	<input type="radio"/>	<input checked="" type="radio"/>	<input checked="" type="radio"/>	B Edificio TEMPORANEAMENTE INAGIBILE (tutto o parte) ma AGIBILE con provvedimenti di pronto intervento (1) <input type="checkbox"/>
ALTO	<input type="radio"/>	<input type="radio"/>	<input type="radio"/>	<input type="radio"/>	C Edificio PARZIALMENTE INAGIBILE (1) <input type="checkbox"/>
					D Edificio TEMPORANEAMENTE INAGIBILE da rivedere con approfondimento <input type="checkbox"/>
					E Edificio INAGIBILE <input type="checkbox"/>
					F Edificio INAGIBILE per rischio esterno (1) <input type="checkbox"/>
(1) riportare nella colonna argomento della Sez. 9 l'esito e nelle annotazioni le parti di edificio inagibili (esiti B, C) e le cause di rischio esterno (esito F)					
Sull'accuratezza della visita		1 <input type="radio"/> Solo dall'esterno 4 <input type="radio"/> Non eseguito per: a <input type="radio"/> Sopralluogo rifiutato (SR) b <input type="radio"/> Rudere (RU) c <input type="radio"/> Demolito (DM) 2 <input checked="" type="radio"/> Parziale d <input type="radio"/> Proprietario non trovato (NT) e <input type="radio"/> Altro (AL) 3 <input type="radio"/> Completa (> 2/3)			
Provvedimenti di pronto intervento di rapida realizzazione, limitati (*) o estesi (**)					
* <input type="checkbox"/>	**	PROVVEDIMENTI DI P.I. SUGGERITI	* <input type="checkbox"/>	**	PROVVEDIMENTI DI P.I. SUGGERITI
1 <input type="checkbox"/>	<input type="checkbox"/>	Messa in opera di cerchiate o tiranti	7 <input type="checkbox"/>	<input type="checkbox"/>	Rimozione di cornicioni, parapetti, oggetti
2 <input checked="" type="checkbox"/>	<input type="checkbox"/>	Riparazione danni leggeri alle tamponature e tramezzi	8 <input type="checkbox"/>	<input type="checkbox"/>	Rimozione di altri oggetti interni o esterni
3 <input type="checkbox"/>	<input type="checkbox"/>	Riparazione copertura	9 <input type="checkbox"/>	<input type="checkbox"/>	Trasennature e protezione passaggi
4 <input type="checkbox"/>	<input type="checkbox"/>	Puntellatura di scale	10 <input type="checkbox"/>	<input type="checkbox"/>	Riparazioni delle reti degli impianti
5 <input type="checkbox"/>	<input type="checkbox"/>	Rimozione di intonaci, rivestimenti, controsoffittature	11 <input type="checkbox"/>	<input type="checkbox"/>	
6 <input type="checkbox"/>	<input type="checkbox"/>	Rimozione di tegole, cornignoli, parapetti	12 <input type="checkbox"/>	<input type="checkbox"/>	
Unità immobiliari inagibili, famiglie e persone evacuate					
Unità immobiliari inagibili <input type="text"/>		Nuclei familiari evacuati <input type="text"/>		N° persone evacuate <input type="text"/>	
SEZIONE 9 Altre osservazioni					
Sul danno, sui provvedimenti di pronto intervento, l'agibilità o altro					
Argomento	Annotazioni			Foto d'insieme dell'edificio	spilla
	Width of cracks: 1-2 cm, generally vertical or with inclination to the vertical of 45°-60° almost				
	Restoration and maintenance works in reinforced concrete surveyed to roof				
	Damage occurred to facilities in surrounding areas				
Il compilatore (in stampatello)		Firma			

Figure 8.130 Sections 8 and 9 of DPC classification scheme for considered building.

In the following paragraphs, the proposed approach has been applied to assess vulnerability at a detailed scale of single building and building aggregate.

8.7.3 Analytical approach: equivalent beam model and building 3D fragility curves

An example of building vulnerability assessed by means of equivalent beam model is discussed in the following. The structure, the same shown in Figure 8.127, is located in the historical center of Moio.

According to the landslide inventory map provided by Hydro-geomorphological Setting Plan of South Campania River Basin Authority in 2012, the surrounding area is affected by diffuse slow deformation/movements. Integrated analysis of a stratigraphic column and displacement measurements performed on inclinometer borehole near the building allowed to localize an active shear surface at a depth of about 7 m (Fig. 8.131).

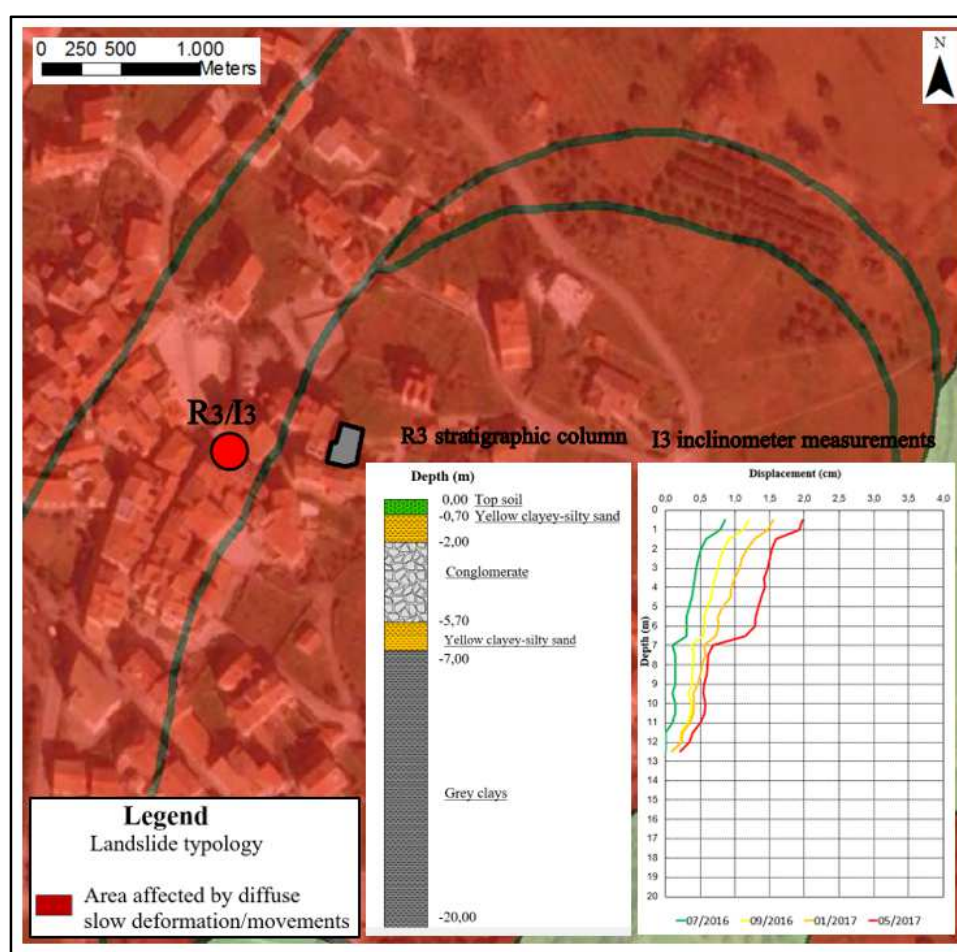


Figure 8.131 Location of considered building and results of inclinometer measurements in the period November 2015-May 2017 in I3 borehole.

Furthermore, availability of displacement maps obtained by DInSAR data in time span 2011-2015 (Figs. 8.122, 8.123, 8.124, 8.125, 8.126), allowed to define profiles of cumulated vertical and horizontal displacements occurred to building foundations (Figs. 8.132 and 8.133).

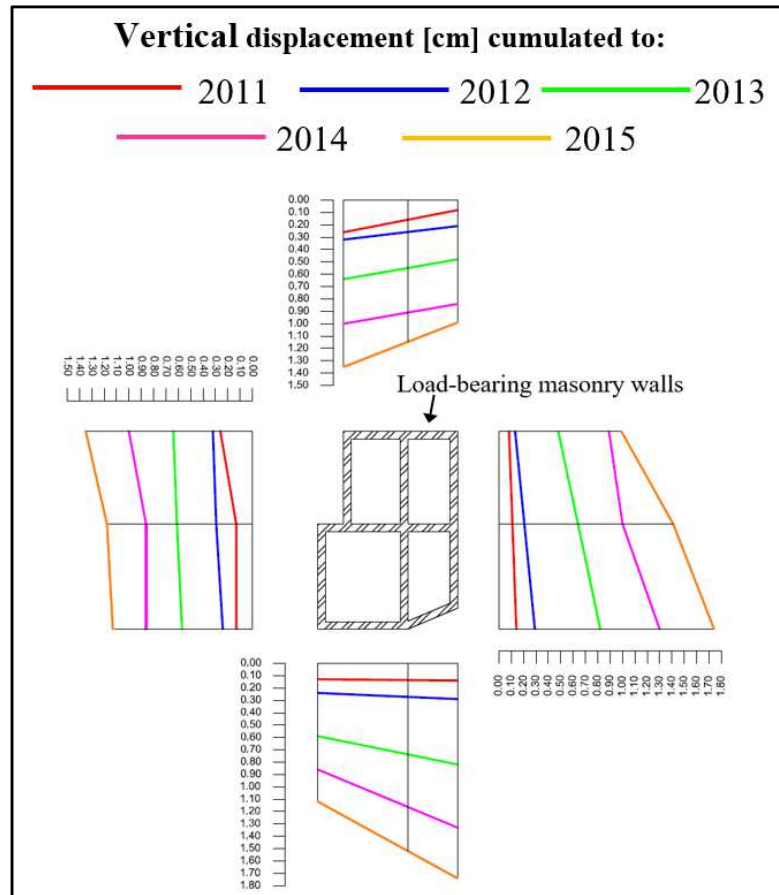


Figure 8.132 Vertical displacement profiles measured along building façades in period 2011-2015.

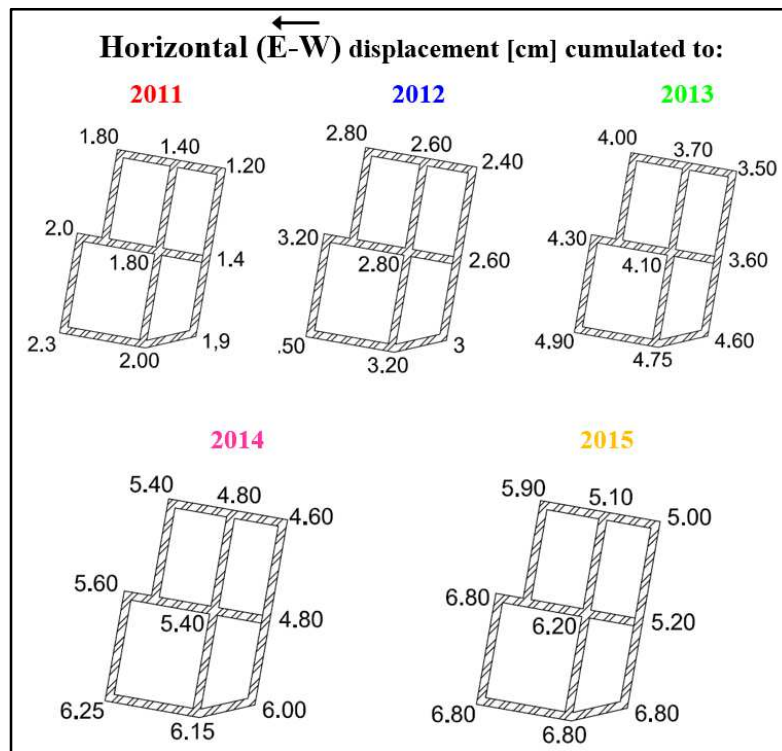


Figure 8.133 Horizontal displacement (E-W) profiles measured along building façades in period 2011-2015.

Analysis of interferometric products provided information on landslide intensity in the surrounding area: in detail, instability phenomena show a displacement rate of about 0.3 mm/yr in vertical direction and 1.2 mm/yr along horizontal E-W direction.

Subsequently, building has been modelled as an equivalent laminated beam, as to simplify structure by considering only its major features and adequately representing the response to ground movements (Fig. 8.134).

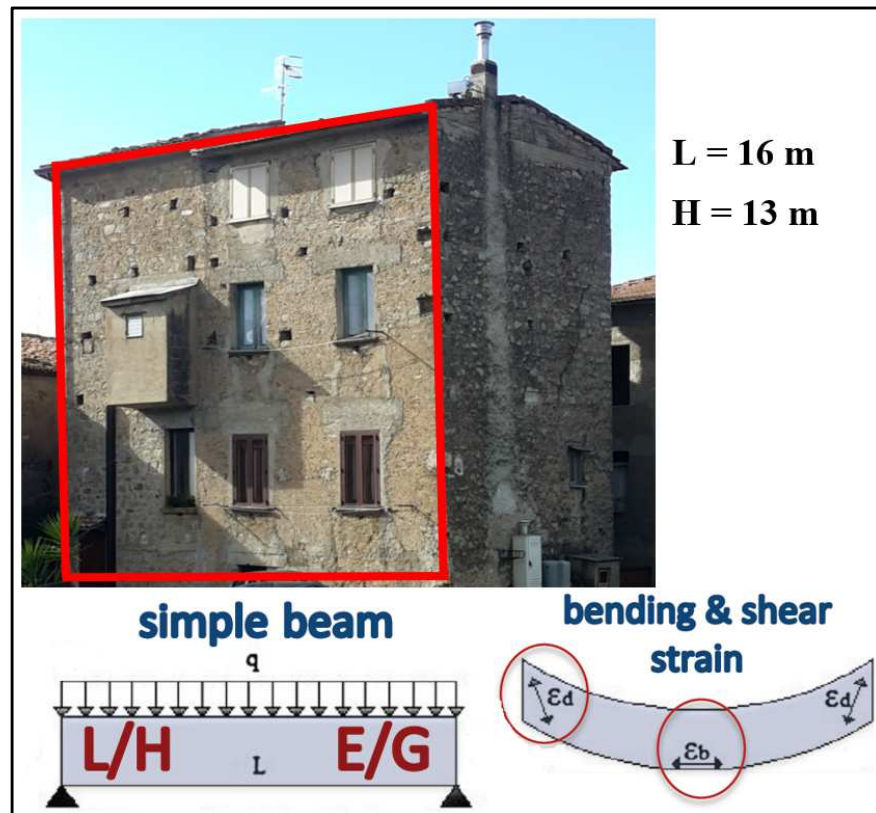


Figure 8.134 Equivalent laminated beam model of considered building.

According to Timoshenko theory (1955) and Boscardin & Cording (1989) approach, the maximum tensile strain in a building can be obtained as the maximum of the values ε_{dr} and ε_{br} provided by Equations 8.1 and 8.2:

$$\varepsilon_{br} = \varepsilon_{b\max} + \varepsilon_h \quad (\text{eq. 8.1})$$

$$\varepsilon_{dr} = \frac{1-\nu}{2} \varepsilon_h + \sqrt{\varepsilon_h^2 \left(\frac{1+\nu}{2}\right)^2 + \varepsilon_{d\max}^2} \quad (\text{eq. 8.2})$$

where the maximum bending strain $\varepsilon_{b\max}$ and the maximum shear strain $\varepsilon_{d\max}$ are provided by Equations 8.3 and 8.4:

$$\frac{\Delta}{L} = \left(\frac{L}{12h} + \frac{3I}{2hLH} \frac{E}{G} \right) \varepsilon_{b,max} \quad (\text{eq. 8.3})$$

$$\frac{\Delta}{L} = \left(1 + \frac{HL^2}{18I} \frac{G}{E} \right) \varepsilon_{d,max} \quad (\text{eq. 8.4})$$

In such case of sagging deformation, the distance h to the neutral axis from the edge of the beam in tension is chosen usually as $h = H/2$ (neutral axis in the middle), while the second moment of inertia of a rectangular beam with respect to an extreme fiber is equal to $I = H^3/12$. Moreover, as mentioned in Chapter 7, application of this approach requires to assess constitutive properties of building, such as the length L , height H , Young's modulus E , shear modulus G and Poisson's ratio ν of constructive material.

Since data of materials mechanical parameters performed by *in situ* measurements on masonry walls were not available, they have been obtained by considering guidelines of Italian "Norme tecniche per le costruzioni" (NTC, 2008). In detail, dealing with irregular layout or bad quality masonry, built with rubble stones and pebbles, an average of minimum and maximum values of E and G have been taken into account (Table 8.4); Poisson's ratio ν has been evaluated according to Equation 8.5.

$$E = 2 \cdot G(1 + \nu) \quad (\text{eq. 8.5})$$

Typology of masonry	E (N/mm ²)		G (N/mm ²)		ν
	min	max	min	max	
Irregular layout or bad quality masonry (rubble stones and pebbles)	690	1050	230	350	0,5
	Average		Average		
	870 N/mm ²		290 N/mm ²		

Table 8.4 Mechanical parameters E , G and ν of masonry material considered in the analysis.

Subsequently, starting from displacement profiles recorded in time span 2011-2015, deflection ratio Δ/L and horizontal strain occurred during each year along considered façade have been assessed.

Furthermore, dealing with slow moving landslides, in turn characterized by low and almost constant values of distortions induced to building foundations, evolution of damage conditions has been forecasted under the assumption that such deformations will occur in the future with same rate than in the past. To this aim, firstly, an average value of occurred annual distortions have been estimated (Table 8.5); after it has been used to forecast future possible deformations (Table 8.6).

Year	Δ/L (annual)	Average	ε_h (annual)	Average
2011	0,00012	0,000102	0,00033	0,00026
2012	0,00008		0,00018	
2013	0,00009		0,00028	
2014	0,00009		0,00027	
2015	0,00013		0,0003	

Table 8.5 Annual distortions and corresponding average values measured in period 2011-2015.

Year	Δ/L (cumulated)	ε_h (cumulated)
2011	0,00012	0,00033
2012	0,00020	0,00051
2013	0,00029	0,00079
2014	0,00038	0,00106
2015	0,00051	0,00131
2016	0,000612	0,00163
2017	0,000714	0,00191
2018	0,000816	0,00217
2019	0,000918	0,00245
2020	0,00102	0,00272
2021	0,001122	0,00299
2022	0,001224	0,00327
2023	0,001326	0,00354
2024	0,001428	0,00381
2025	0,00153	0,00408

Table 8.6 Cumulated angular and horizontal distortions projected from 2011 to 2025.

Equations 8.1, 8.2, 8.3 and 8.4 allow to assess maximum between ε_{dr} and ε_{br} .

It is important to highlight that in 2011 building was previously damaged: in detail, in 2009 a negligible damage level had been surveyed, while in 2015 it turned out into a moderate degree (Fig. 8.135).

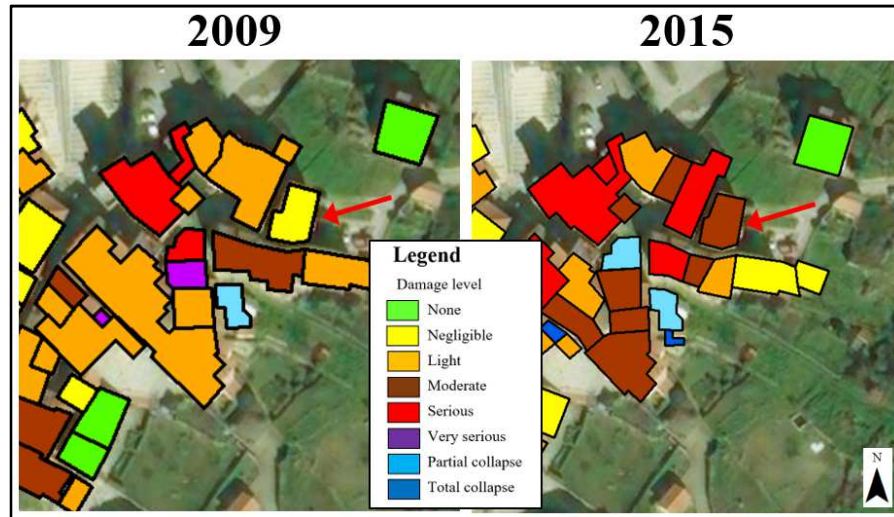


Figure 8.135 Building damage level surveyed in 2009 and in 2015.

To take into account existing damage level in 2011, a value of limiting tensile strain equal to 0,0005, corresponding to negligible severity degree (Table 7.1), was added to maximum between ε_{br} and ε_{dr} obtained each year, thus providing maximum tensile strain.

Year	Δ/L (cumulated)	ε_h (cumulated)	ε_{bmax}	ε_{dmax}	ε_{br}	ε_{dr}	ε_{max}
2011	0,00012	0,00033	0,000171	0,000132	0,00070	0,000556	0,00120
2012	0,00020	0,00051	0,000235	0,000182	0,00088	0,000746	0,00138
2013	0,00029	0,00079	0,000288	0,000223	0,00096	0,000933	0,00146
2014	0,00038	0,00106	0,000352	0,000273	0,00151	0,001209	0,00201
2015	0,00051	0,00131	0,000544	0,000422	0,00190	0,001457	0,00240
2016	0,000612	0,00163	0,000653	0,000506	0,00229	0,001748	0,00279
2017	0,000714	0,00191	0,000761	0,000591	0,00267	0,002039	0,00298
2018	0,000816	0,00217	0,00087	0,000675	0,00305	0,00233	0,00355
2019	0,000918	0,00245	0,000979	0,00076	0,00343	0,002622	0,00393
2020	0,00102	0,00272	0,001088	0,000844	0,00381	0,002913	0,00431
2021	0,001122	0,00299	0,001197	0,000928	0,00419	0,003204	0,00469
2022	0,001224	0,00327	0,001305	0,001013	0,00457	0,003496	0,00507
2023	0,001326	0,00354	0,001414	0,001097	0,00495	0,003787	0,00545
2024	0,001428	0,00381	0,001523	0,001182	0,00533	0,004078	0,00583
2025	0,00153	0,00408	0,001632	0,001266	0,00571	0,00437	0,00621

Table 8.7 Maximum tensile strain obtained by equivalent beam model in period 2011-2025.

Comparison of obtained maximum tensile strain with values of limiting tensile strain (Table 7.1) allowed to identify level of damage reached every year (Table 8.8).

Year	ε_{\max} (cumulated)	Damage level
2011	0,00120	Slight
2012	0,00138	Slight
2013	0,00146	Slight
2014	0,00201	Moderate
2015	0,00240	Moderate
2016	0,00279	Moderate
2017	0,00298	Moderate
2018	0,00355	Severe
2019	0,00393	Severe
2020	0,00431	Severe
2021	0,00469	Severe
2022	0,00507	Severe
2023	0,00545	Severe
2024	0,00583	Severe
2025	0,00621	Very severe

Table 8.8 Damage level corresponding to maximum tensile strain reached every year.

As it is possible to note, in 2015, equivalent beam approach gave back a moderate damage level, such as that recorded on building by *in situ* survey, thus confirming goodness of model: moreover, according to this and under the assumption that in the future distortions to building foundations will occur with the same rate of previous years, severe damage level will be reached probably in 2018 or 2019.

Subsequently, correlation between maximum tensile strain, deflection ratio Δ/L and horizontal strain ε_h (Fig. 8.136) can be defined by fragility functions that describe the probability of exceeding a certain limit states, given a value of ground deformations.

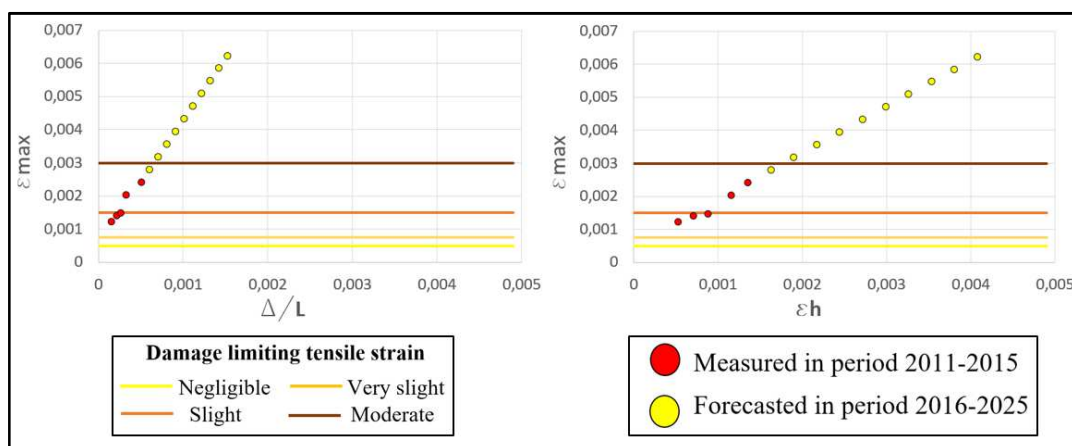


Figure 8.136 Relationship between maximum tensile strain and distortions to building foundations (deflection ratio Δ/L and horizontal strain ε_h).

Finally, interpolation in a MATLAB numerical model of pairs of distortions corresponding to each damage severity level, allowed to define 3D fragility curves: they provide the probability of exceeding a damage level as function of deflection ratio and horizontal strain (Figs. 8.137, 8.138, 8.139).

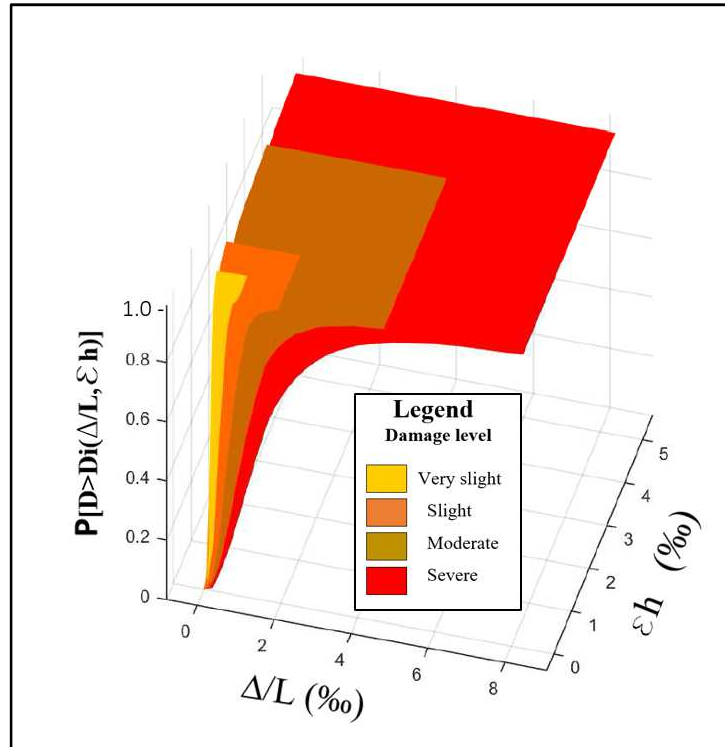


Figure 8.137 3D fragility curves obtained by equivalent beam model: axonometric views n. 1.

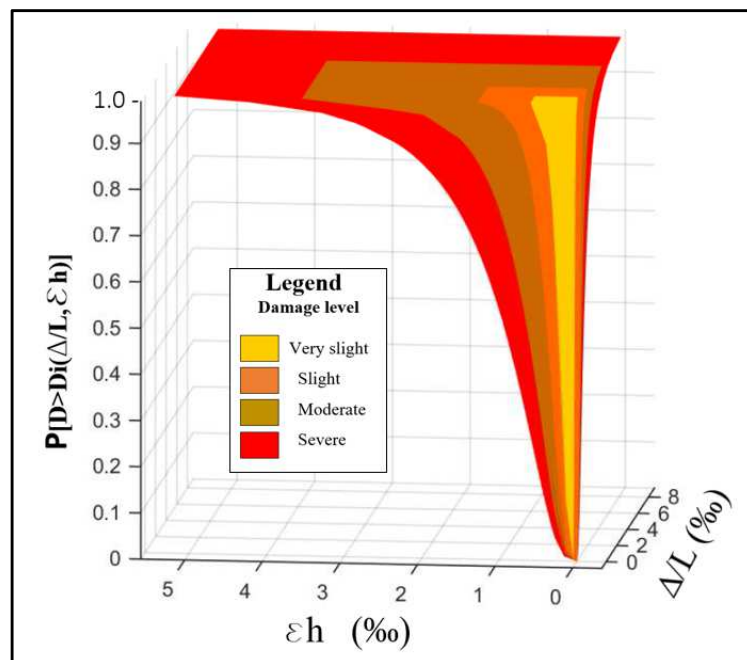


Figure 8.138 3D fragility curves obtained by equivalent beam model: axonometric views n. 2.

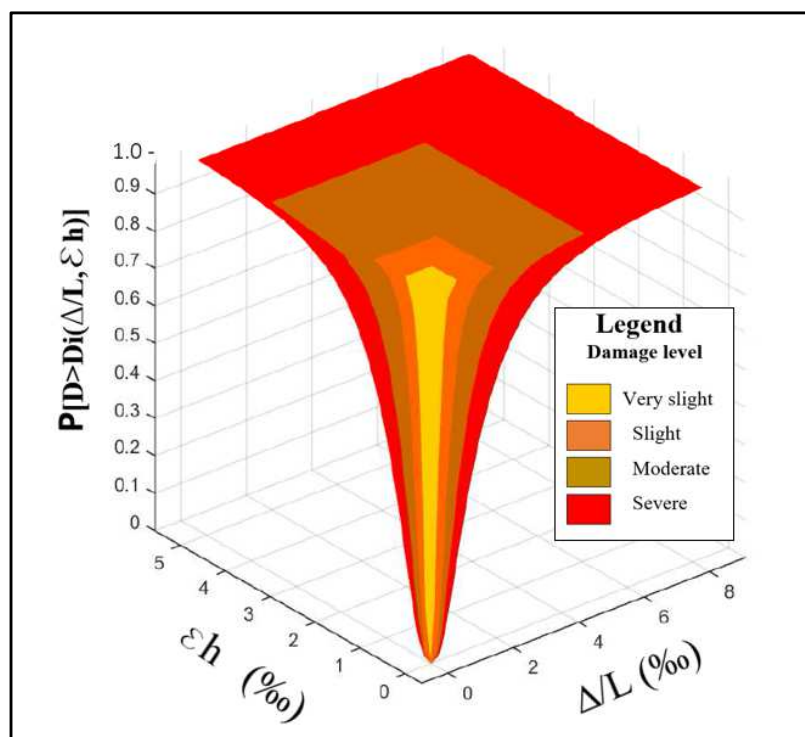


Figure 8.139 3D fragility curves obtained by equivalent beam model: axonometric views n. 3.

8.7.4 Numerical approach: 3D computational model and building vulnerability domains

Building schematized as a linear beam along a single façade, does not take into account three-dimensional behavior of structures. For this reason, occurrence and location of cracks and local failures cannot be investigated.

To overcome these constraints, a 3D building model has been created using a numerical software and subsequently structural analysis on computational model has been performed.

In detail, computer code 3DMacro (Gruppo Sismica, 2014), developed to assess non-linear behaviour of masonry buildings, has been used.

The different behaviour of masonry structures, compared to ordinary concrete and steel buildings, requires *ad hoc* algorithms capable of reproducing the non-linear behaviour of masonry and providing reliable numerical simulations.

An original modelling approach for the simulation of the non-linear behaviour of masonry structures under static and seismic loadings is considered.

The proposed approach is based on the concept of macro-element discretization and has been conceived with the aim of capturing the non-linear behaviour of an entire building by means of an assemblage of several discrete elements, which, in turn, can be characterized by different levels of complexity according to the role of the element in the global model.

The proposed model is based on a discrete element to model masonry panels (Caliò et al., 2012): such element is characterized by a simple mechanical scheme, constituted by an articulated quadrangle with rigid edges connected by four hinges and two nonlinear diagonal springs (Fig. 8.140).

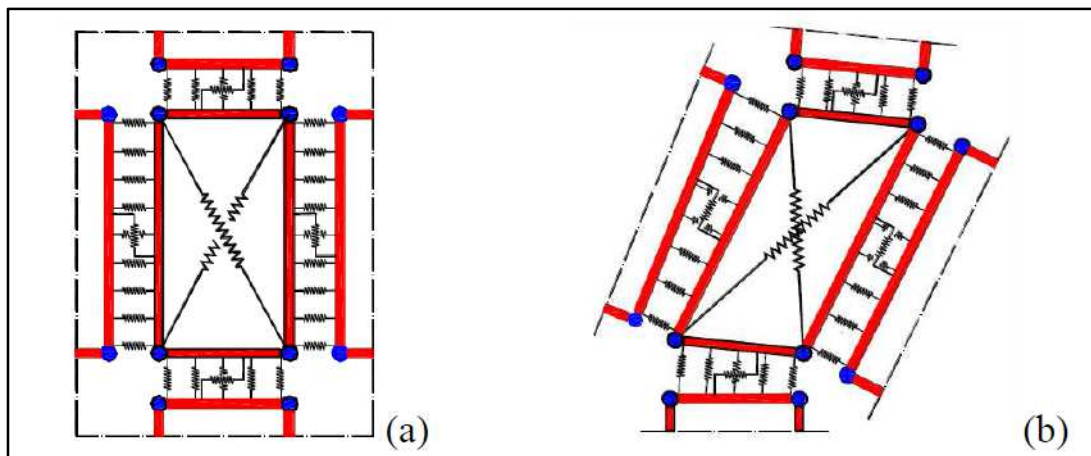


Figure 8.140 The basic macro-element for masonry: (a) un-deformed configuration; (b) deformed configuration (from Caliò et al., 2012).

Each side of the quadrangle can interact with other elements or supports by means of a discrete distribution of the non-linear springs, denoted as interface. Each interface is constituted by n non-linear orthogonal springs, perpendicular to the panel side, and an additional longitudinal spring, parallel to the panel edge (Fig. 8.141).

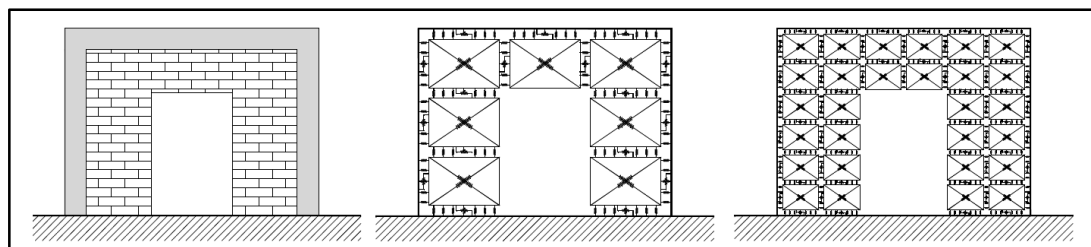


Figure 8.141 Modelling of infilled frame with central door opening. (a) geometrical layout; (b) model corresponding to the basic mesh; (c) model corresponding to a more refined mesh resolution (from Caliò et al., 2014).

In spite of its great simplicity, such basic mechanical scheme is able to simulate the main in plane failures of a portion of masonry wall subjected to horizontal and vertical loads. Each element exhibits three degrees-of-freedom, associated to the in-plane rigid body motion, plus a further degree-of-freedom needed to describe the in-plane deformability.

Subsequently, according to the above mentioned assumptions, the three-dimensional global model of building considered in the previous paragraph has been implemented in 3DMacro code (Fig. 8.142).

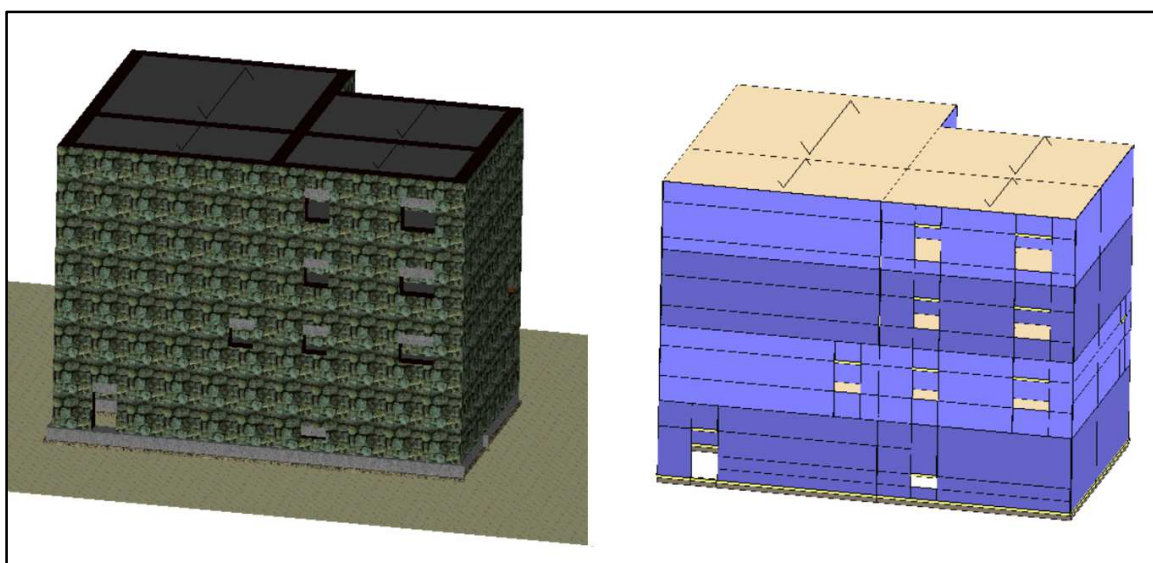


Figure 8.142 Three-dimensional finite-macro-element global model: axonometric views.

Because *in situ* tests on masonry walls have been not performed, mechanical properties of material have been derived by Italian NTC (2008), with reference to irregular layout or bad quality type of masonry (Table 8.9).

Young's Modulus E [Mpa]	Shear Modulus G [MPa]	Compressive strength σ_c [MPa]	Tensile strength σ_t [MPa]	Shear strength τ_0 [MPa]	Unit weighth W [KN/m ³]
870	290	1,4	0,1	0,03	19

Table 8.9 Mechanical characteristics of the masonry.

Angular distortions and horizontal strains, progressively increasing according to displacement profiles measured in period 2011-2015 (Figs. 8.132 and 8.133) have been applied to computational model (Fig. 8.143) and only non-linear static analyses have been performed.

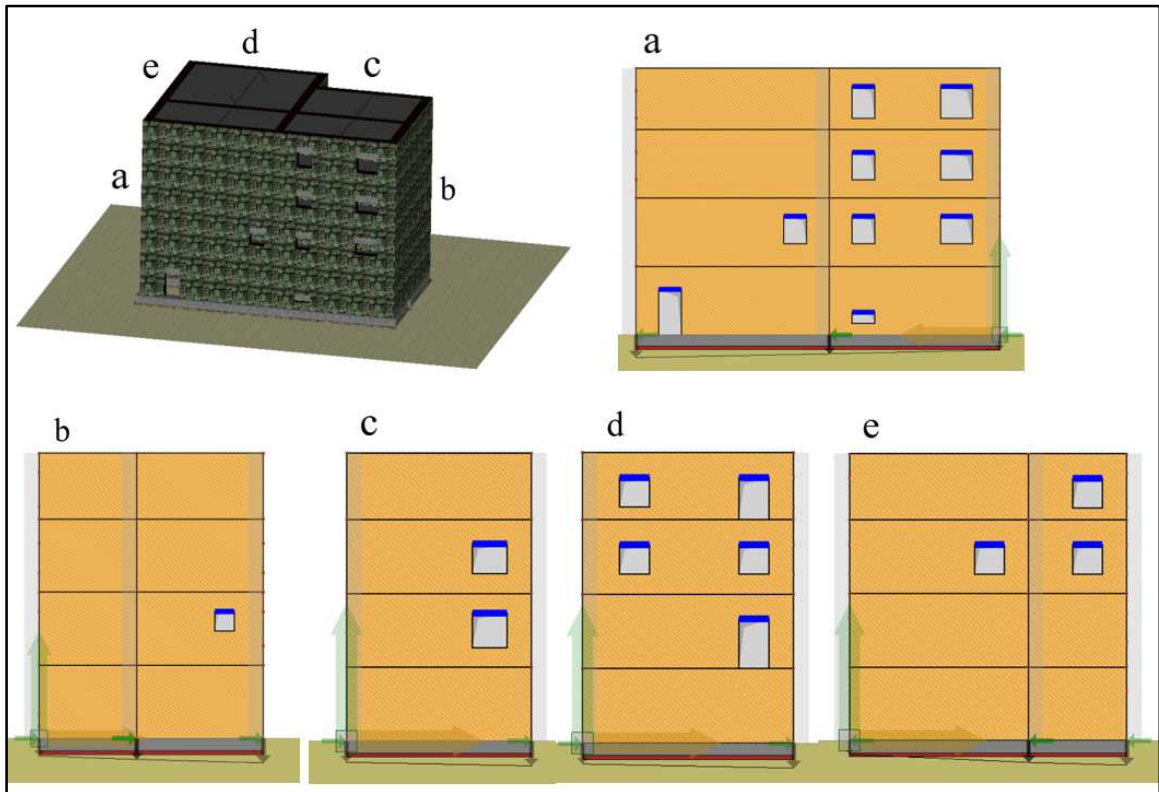


Figure 8.143 Example of displacement profiles applied to building foundations along each façade according to DInSAR data recorded in period 2011-2015.

In detail, based on DInSAR recorded data, displacement profiles under structure foundations have been increased in subsequent steps with the same rate on entire building. Moreover, according to the procedure proposed in Chapter 7 (Tables 7.4 and 7.5), damage degree, obtained by non-linear analysis correspondent to each pair of applied distortions β_w and β_h , has been assessed.

Figure 8.144 shows damage distribution on masonry façades correspondent to displacement profiles defined in Figure 8.143. It is important to highlight that the proposed discrete-element approach allows to investigate tensional state of each panel and to identify portion of masonry wall where the main collapse mechanisms occur.

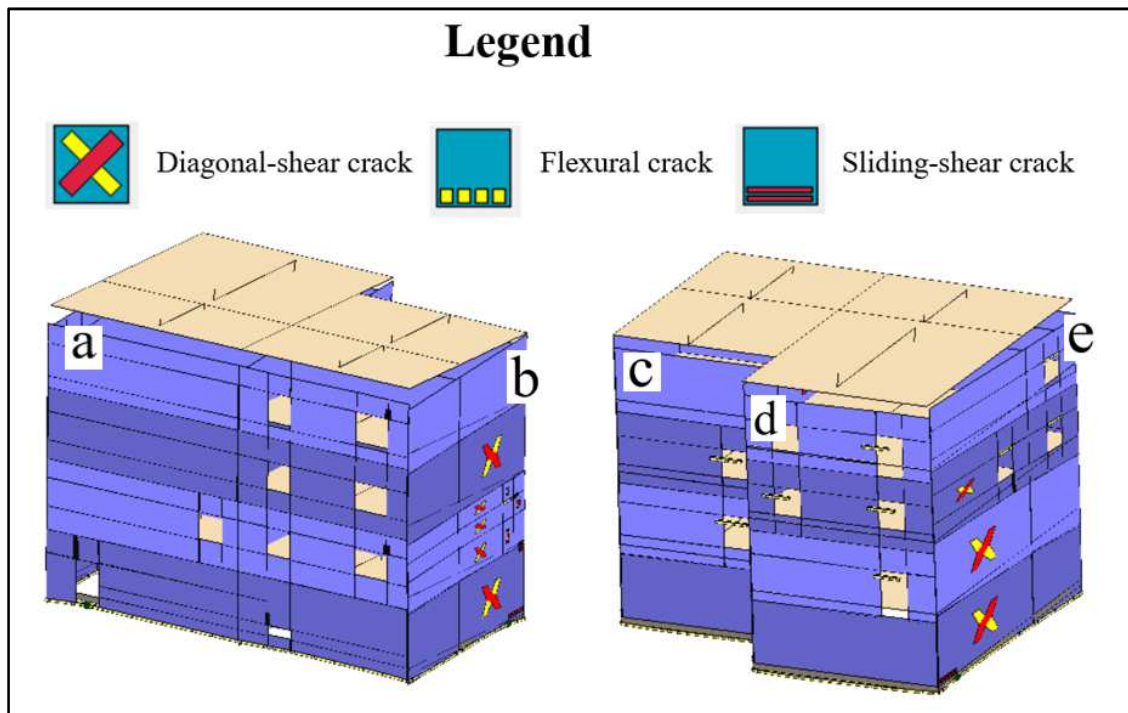


Figure 8.144 Damage distribution on masonry walls induced by displacement profiles shown in Figure 8.143.

As it is possible to note in Figure 8.145, a good correspondence among distribution of damage provided by numerical analysis on computational model and real damage observed by *in situ* survey has been observed.

In particular, on masonry façades, named as “b” and “e”, diagonal shear cracks have been identified: they are associated to the loss of the bearing capacity of masonry panel due to excessive shear and the consequent formation of inclined diagonal cracks along the direction of principal stresses.

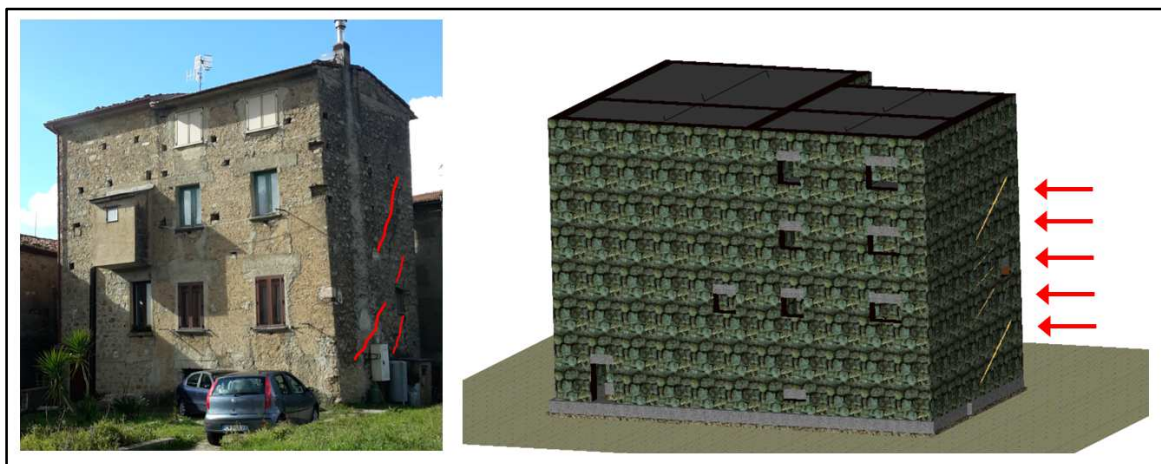


Figure 8.145 Comparison between damage surveyed by *in situ* campaign (on the left) and provided by analysis on computational model (on the right) on building façade named “b”.

Relationship between angular and horizontal distortions affecting building foundations and damage level obtained on computational model, has been provided by means of “vulnerability domains”. They were generated as a function of the angular distortion and of horizontal strain, interpolating the point derived from the analysis and characterized by the same damage degree (Figs. 8.146 and 8.147).

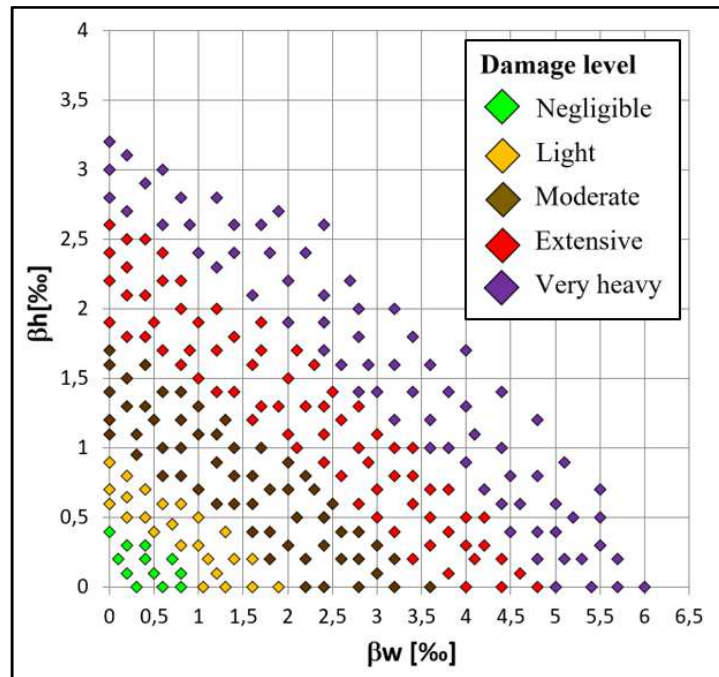


Figure 8.146 Distribution of damage levels obtained on computational model for each pair of distortions applied to building foundations.

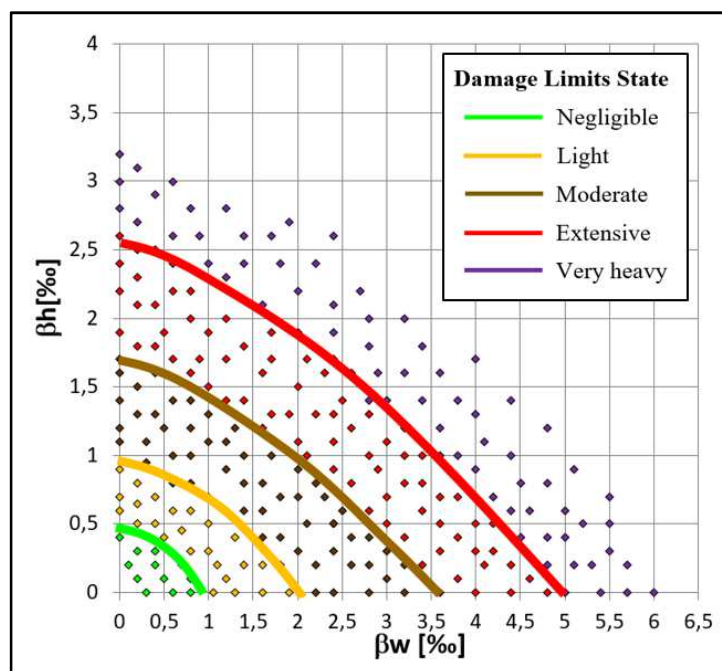


Figure 8.147 Vulnerability domains obtained by interpolating points with same damage level.

Vulnerability domains define performance of single structures to landslide induced movements. The overcoming of these domains entails a progressive worsening of damage degree. As it is possible to note, to obtain a same damage level, angular distortions higher than horizontal strains are required. Such point is due to high susceptibility of masonry buildings to deformations occurred along horizontal direction, depending on very low critical tensile strength of masonry material.

Moreover, the comparison between domains here gained and the empirical ones found in literature (Boscardin & Cording, 1989) showed some inconsistencies, related to the threshold values, mostly because the empirical methods, based on functional connection phenomenon intensity – damage degree, do not take into account any structural and architectonic building characteristic, nor the mechanical properties of the soil. The analysis accomplished, instead, even if detailed, is characterized by simplified assumptions, concerning building modeling and adopted criterion for damage assessment correspondent to every pair of distortions applied to the numerical model, different from that used by Boscardin & Cording (Fig. 8.148).

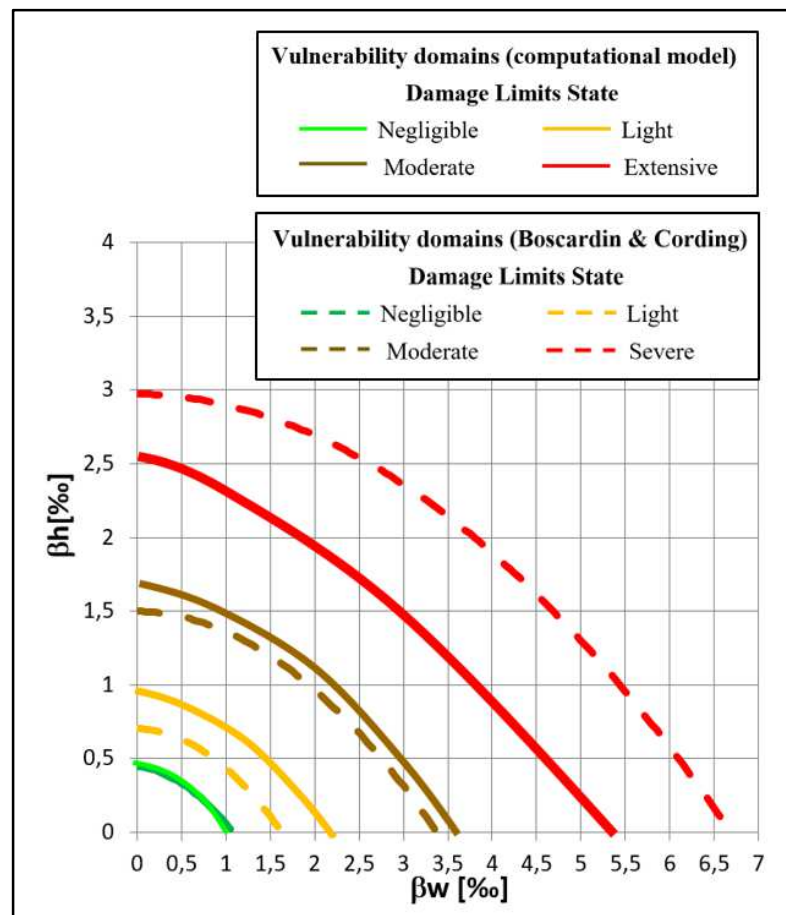


Figure 8.148 Comparison between vulnerability domains obtained by numerical analysis on computational model and empirical domains provided by Boscardin & Cording (1989).

The empirical vulnerability domains suffer from the major drawback of being used directly by risk assessment practitioners without having to repeat the analysis for each building, given the expected range of landslide intensity and for similar building typologies and ranges of structural characteristics. Consequently, not taking into account uncertainties which may relate to the landslide attributes, to the inherent characteristics of the buildings or to their interaction with the landslide, the same ground displacement can generate a similar damage degree in structures which are really different from each other.

8.7.5 Assessment of building behavior through DInSAR and structural analysis

Vulnerability analysis at a detailed scale of representation allows to investigate structural performance of single building affected by ground movements. In detail, behavior of a masonry building aggregate and efficacy of restoration works have been assessed through integrated assessment of DInSAR time-series pre- and post-repair intervention, and structural analysis performed with numerical code.

Building aggregate analyzed is located near to the structure examined in previous paragraph, thus it is affected by diffuse slow deformations/movements (Fig. 8.149).

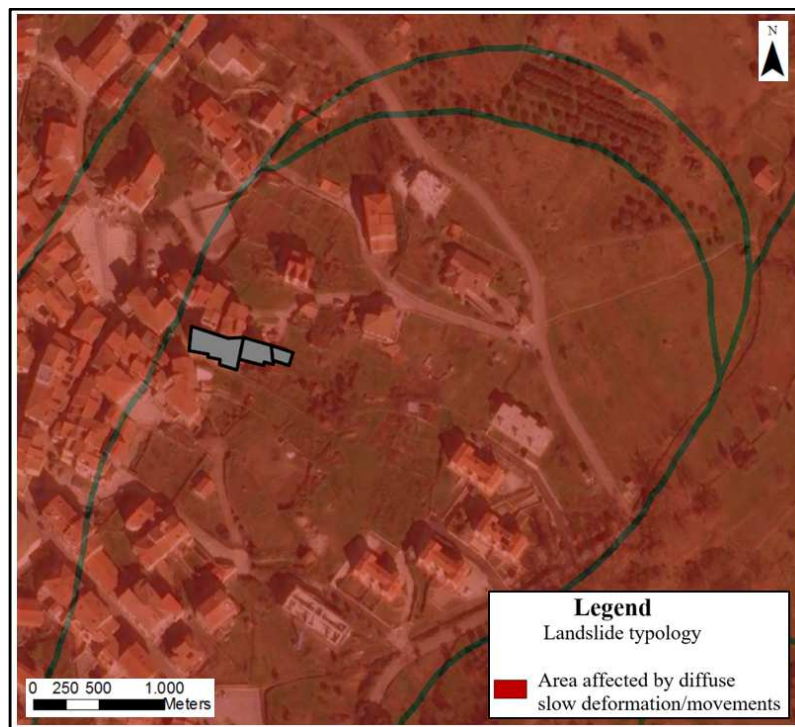


Figure 8.149 Location of building aggregate within an area affected by slow deformation/movements.

The investigated area is overlain by a continuous, heterogeneous debris cover, consisting of arenaceous and conglomeratic blocks of various dimensions, in a silty – clayey matrix. The above mentioned building aggregate has been built, in several points, on such basement rocky outcrops, as shown in Figure 8.150.

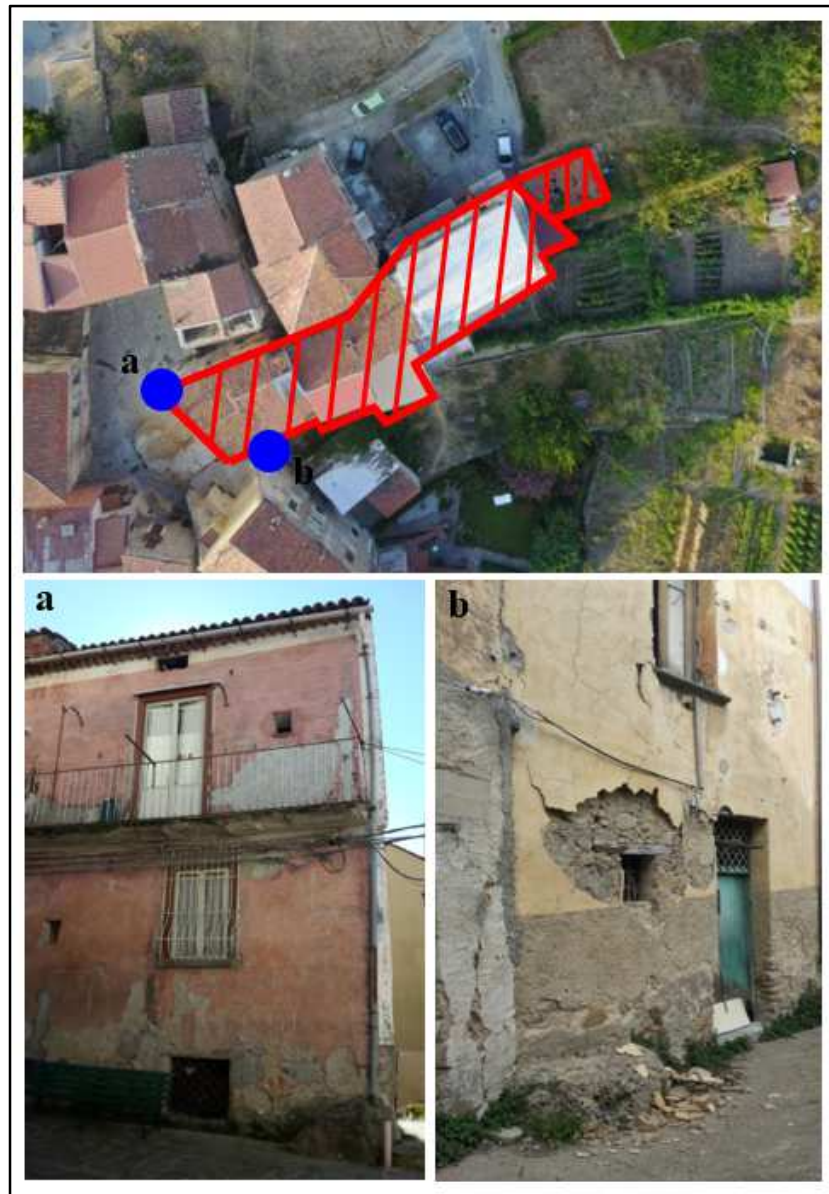


Figure 8.150 Arenaceous and conglomeratic blocks outcrops on which building has been founded.

In the aggregate, four adjacent buildings have been identified. For each of them, “DPC” classification scheme has been compiled. Detailed *in situ* survey allowed to define geometrical and structural properties of involved buildings. They are 3-stories edifices and are irregular in plan and in elevation.

Structures, built in different periods at the beginning of 20th century, show vertical irregularities depending on different floor height of adjacent buildings.

Masonry walls, with thickness of 60 cm, were built with natural stones of different type: a part of aggregate is characterized by elements without any regular shape with different size, while another part shows elements more regular but not perfectly rectangular dressed.

In the original configuration, foundations were long masonry stripes that support the weight of an entire wall; for what concerns flat structures (floors), they showed beams with semi-rigid slab (wooden beams with a double layer of wooden planks, beams and hollow flat blocks). Subsequently, in 2010, a building of aggregate was interested by restoration works: reinforced concrete beams as foundations and beams well connected to rigid reinforced concrete slab as floors were made (Fig. 8.151).

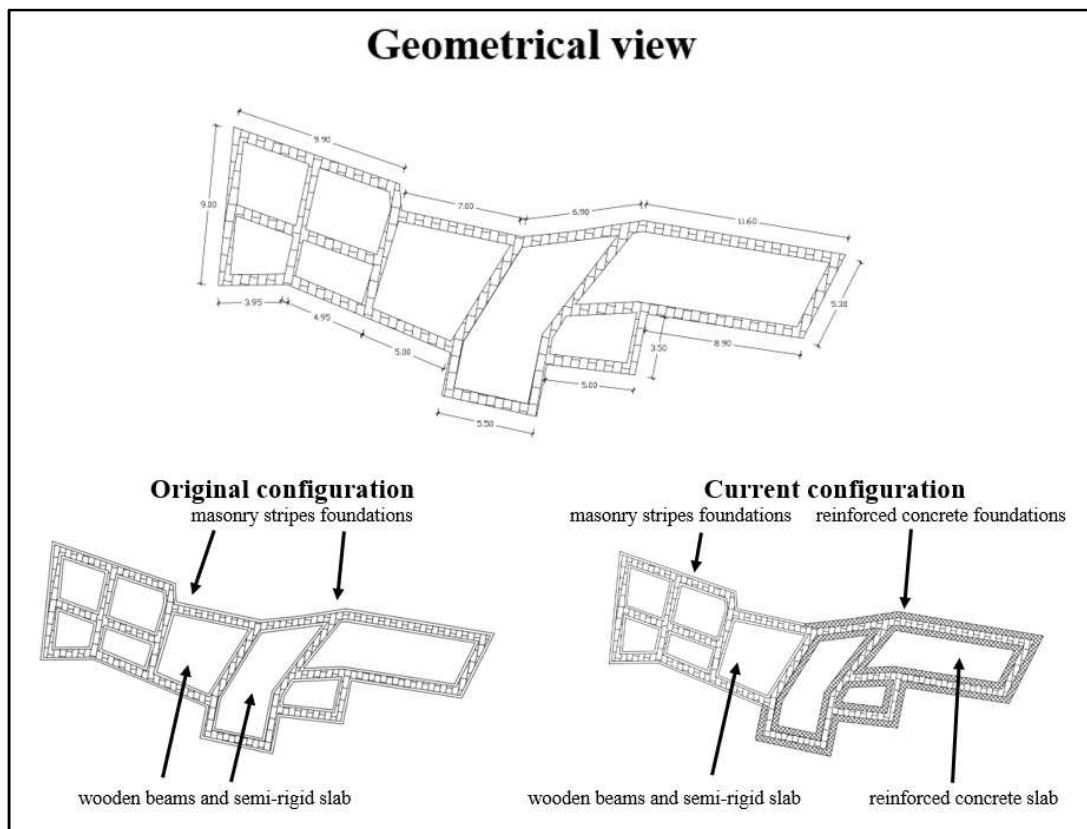


Figure 8.151 Schematic geometrical view of building aggregate plan in original (pre-intervention) and current (post-intervention) configurations.

In such case, performance of building to ground movements and efficacy of restoration works has been assessed following two ways, as below discussed:

- analysis of Differential Synthetic Aperture Radar Interferometry (DInSAR) time-series pre- and post-repair intervention;

- structural analyses performed in a numerical code (3DMacro) of computational models corresponding to original and current configurations.

As to regards the analysis of displacement time series before and after the intervention, only ascending ENVISAT and COSMO-SkyMed data have been taken into account.

In detail, ENVISAT displacement rate data in time span 2002-2010 and COSMO-SkyMed displacement rate data in time span 2011-2016 have been used (Fig. 8.152).

Indeed, no target has been identified on building aggregate in descending ENVISAT products, thus vertical and horizontal displacements occurred in time-span 2002-2010 cannot be evaluated.

ENVISAT data allowed to define displacement time series of building aggregate corresponding to configuration before restoration works, while COSMO-SkyMed products identify movements in post-intervention configuration.

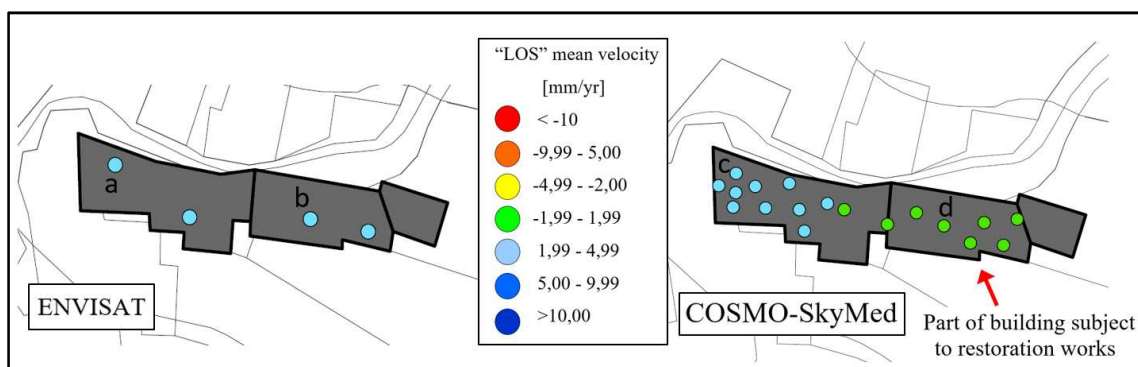


Figure 8.152 “LoS” displacement velocity map of targets identified on building aggregate by ascending ENVISAT and COSMO-SkyMed data.

The analysis of displacement time series before and after the intervention (Fig. 8.153) showed:

- an increase of displacement rate on part of the aggregate not subject to restoration work; in detail, on this building, a mean displacement velocity equal to 3,5 mm/yr was observed in period 2002-2010, while a velocity of 4,8 mm/yr has been recorded in period 2011-2016;
- a significant decrease of the mean velocity after the completion of the works on the repaired part; starting from 2011, a mean displacement rate equal to 0 mm/yr has been surveyed, thus confirming the efficacy of interventions.

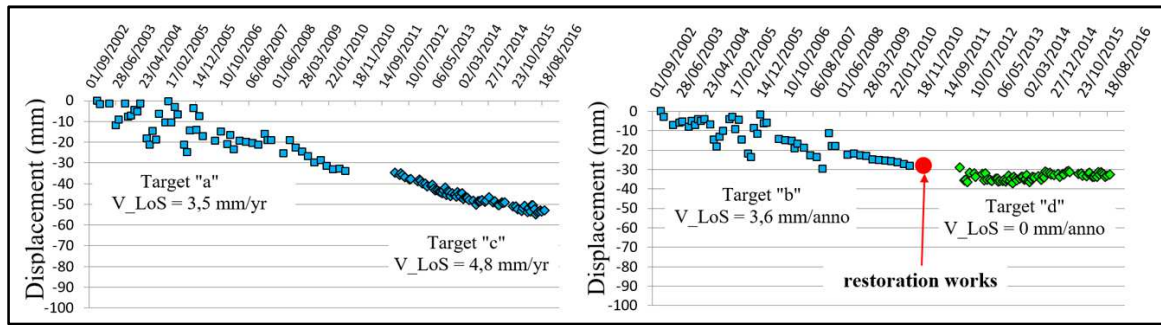


Figure 8.153 “LoS” displacement time series measured on part of aggregate not subject to restoration works (on the left) and on the repaired part (on the right).

Subsequently, such results have been confirmed by structural analyses performed in a numerical software. Computational models of building aggregate corresponding to configurations pre- and post-intervention respectively, have been implemented in numerical code (Fig. 8.154).



Figure 8.154 Computational models of building aggregate corresponding to configurations pre- (a) and post- (b) restoration works: axonometric views.

As it is possible to note in Figure 8.154 (b), in current configuration consolidation works, such as reinforced concrete beams in foundations and rigid reinforced concrete slab as floors, have been implemented.

Further, *in situ* tests on structural elements are not available, therefore mechanical properties of material have been derived by Italian NTC (2008), by considering typologies of masonry surveyed on building aggregate (Tables 8.10 and 8.11).

With reference to parts of aggregate characterized by elements without any regular shape and with different size (rubble stones, pebbles), the following values have been fixed:

Young's Modulus E [Mpa]	Shear Modulus G [MPa]	Compressive strength σ_c [MPa]	Tensile strength σ_t [MPa]	Shear strength τ_0 [MPa]	Unit weight W [KN/m ³]
1050	350	1,8	0,1	0,032	19

Table 8.10 Mechanical characteristics of irregular masonry elements.

On the other hand, with reference to parts of aggregate characterized by masonry elements only roughly worked, not perfectly rectangular dressed, following values have been fixed:

Young's Modulus E [Mpa]	Shear Modulus G [MPa]	Compressive strength σ_c [MPa]	Tensile strength σ_t [MPa]	Shear strength τ_0 [MPa]	Unit weight W [KN/m ³]
1500	500	2,6	0,2	0,056	21

Table 8.11 Mechanical characteristics of masonry elements roughly worked.

As regards rigid reinforced concrete slab as floors, and reinforced concrete beams as foundations, a concrete of strength class 25/30 and B450C steel bars have been used.

Reinforced concrete beams as foundations, in particular, have a rectangular shape with width 100 cm and height 50 cm, connected to existing masonry foundations.

Subsequently, displacement profiles measured at ground level along building façades in period 2011-2015 have been progressively applied to both models, corresponding to configurations pre- and post-restoration works (Figs. 8.155 and 8.156).

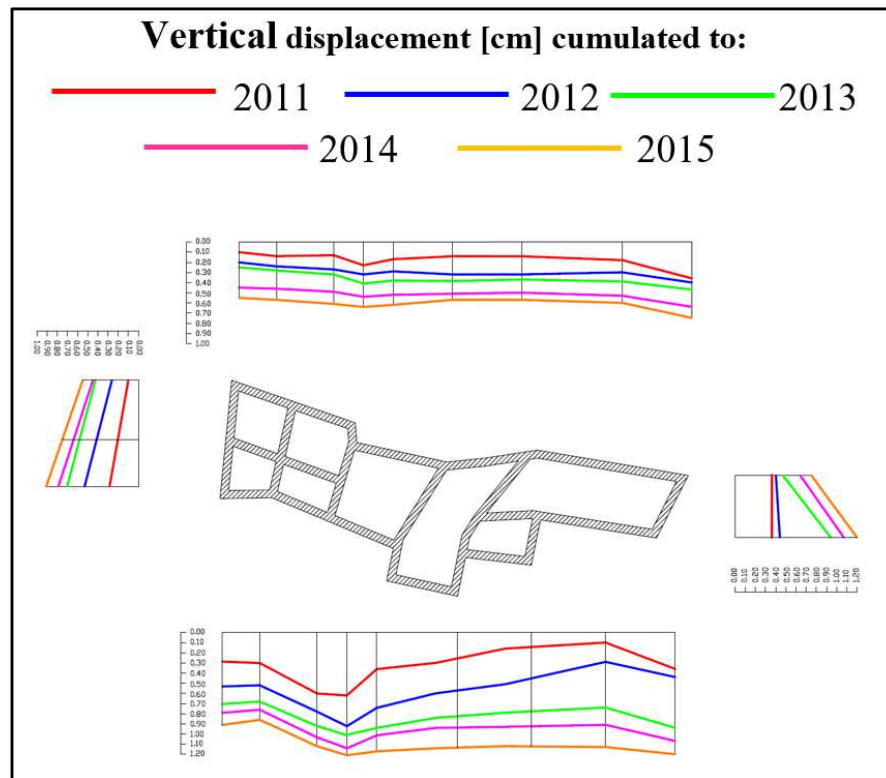


Figure 8.155 Vertical displacement profiles measured along building façades in period 2011-2015.

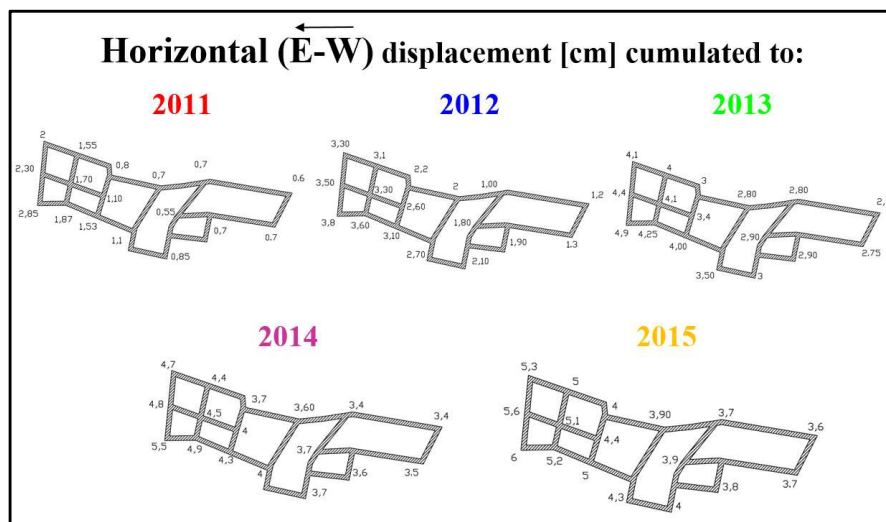


Figure 8.156 Horizontal displacement profiles measured along building façades in period 2011-2015.

It is important to highlight that such displacement profiles have been measured in areas surrounding building aggregate, therefore they have been applied to foundations as indicator of landslide induced movements. Non-linear analyses performed on computational model corresponding to current configuration showed a good correspondence between distribution of cracks on numerical model and real damage surveyed on building façades.

In particular, considering cumulated displacements in period 2011-2015, several cracks occur on parts of aggregate not subject to restoration works.

As it is possible to note in Figures 8.157 and 8.158, diagonal-shear cracks and a vertical sliding-shear crack have been identified in particular on façade along South direction. These cracks have been induced by differential displacements occurred on building foundations due to local geological conditions: in detail, a basement rocky outcrop, on which building has been locally founded, generates vertical and horizontal differential movements on masonry foundations and a rotational settlement on a part of masonry wall.

Such latter effect has been confirmed by analyzing vertical crack surveyed on masonry wall near rock outcrop, whose width increases from bottom to top along façade, thus confirming occurrence of a rotational settlement on a part of load-bearing wall.

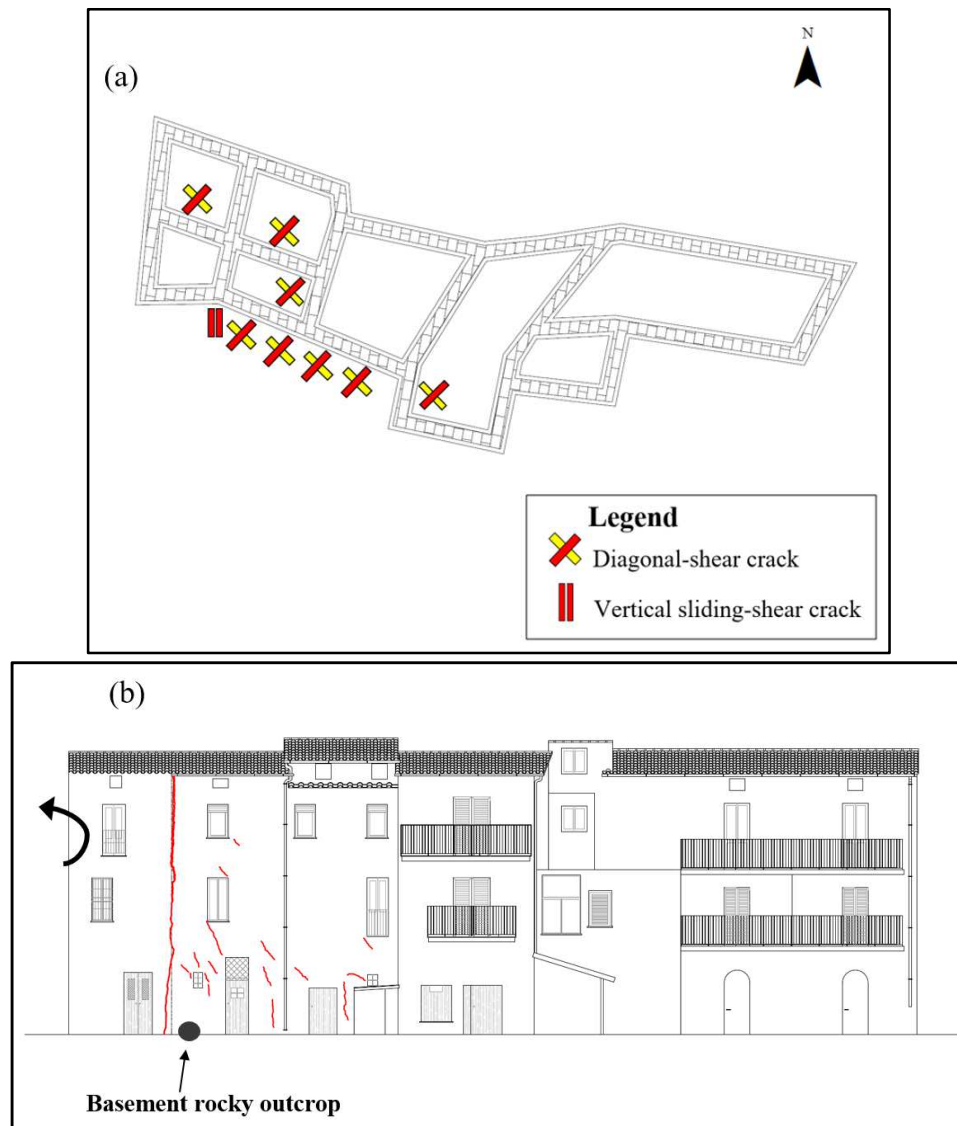


Figure 8.157 Distribution of cracks surveyed on building aggregate (a) and on façade along South direction (b).

On parts of the aggregate repaired with restoration works, only aesthetic cracks have been surveyed: reinforced concrete beams as foundations and reinforced concrete slab as floors allowed to increase global stiffness of structure, thus reducing effects induced by ground movements on superstructure.



Figure 8.158 Comparison between damage distribution obtained by computational model (on the top) and surveyed by *in situ* campaign in February 2015 (on the bottom) on building façade more damaged.

Furthermore, comparison of results obtained by numerical analyses on models corresponding to pre- and post-restoration works highlighted a difference of behavior among the two configurations.

Aimed to assess global performance of building aggregate to induced displacement profiles, number of masonry panels with elastic behavior, number of elements reaching a plasticity and breaking conditions have been evaluated.

As it is possible to note in Figure 8.159, starting from pre- to post-intervention configurations, an increase of masonry macro-elements characterized by elastic behavior and a decrease of number of panels that reach plasticity and breaking conditions occur under each applied displacement profiles.

Such point is more evident on parts of aggregate directly interested by restoration works than on part not subject to remedial interventions, thus confirming their efficacy to improve performance of building within landslide-affected areas.

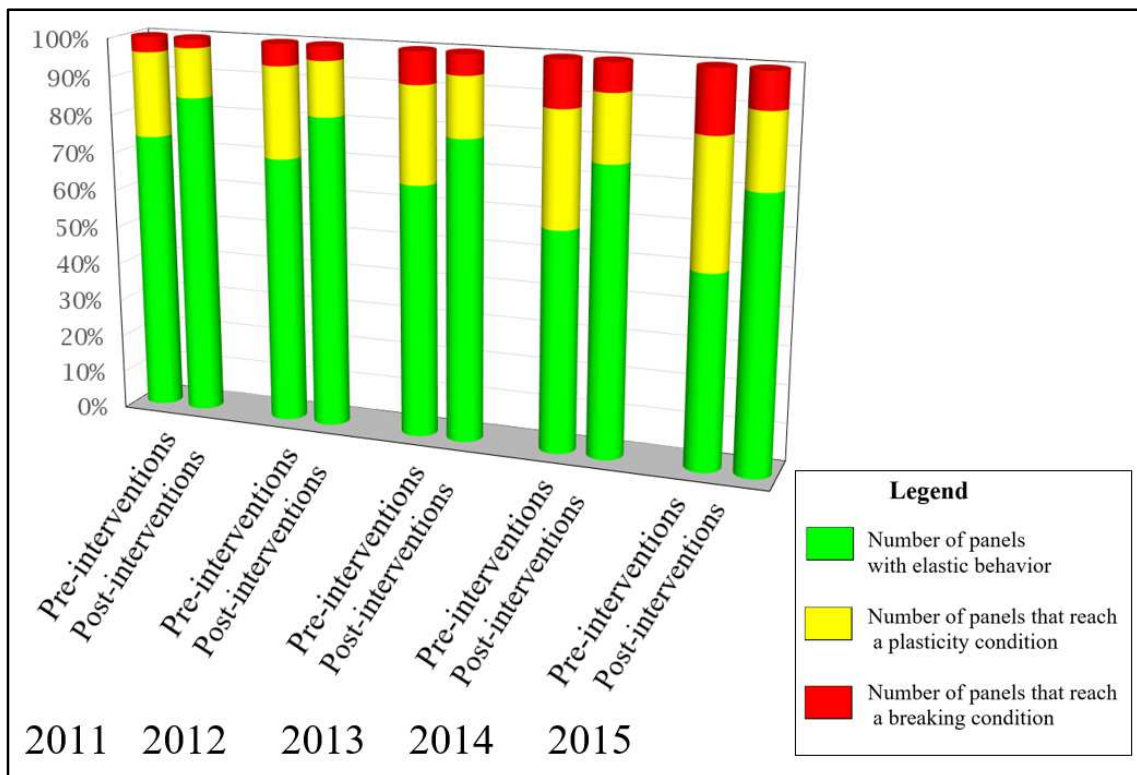


Figure 8.159 Comparison of results obtained by numerical analyses performed on computational models corresponding to pre- and post-restoration works.

Finally, from 2011 to 2015, an increase of displacements applied to building foundations induces a progressive worsening of damage level, increasing the number of panels that reach a plasticity or breaking conditions, being such phenomenon more evident in pre-interventions configuration than in post-restoration works.

CHAPTER 9

CONCLUSIONS

Prevention and mitigation of ground instability phenomena require effective technologies to reduce the vulnerability of existing facilities. In fact, ground failures, and landslides in particular, are globally widespread phenomena caused by natural geological and climatic processes or induced by anthropogenic sources. Slow-moving and intermittent landslides determine a significant number of losses, as well as physical damage and extensive economic losses to private and public properties.

The physical vulnerability of buildings to landslides is a term used to describe their potential for physical loss when they are affected by movements induced by unstable terrains. Therefore, monitoring plays a key-role in natural hazard management and it assumes a paramount task for providing cost-effective solutions in order to mitigate or minimize physical and economic losses.

In the last decades, *Remote Sensing DInSAR techniques* have demonstrated to be powerful investigation tools for their high spatial and multi-temporal coverage, fast data acquisition, and overall reasonable costs.

Widely used for the monitoring and the analysis of the deformational phenomena occurring on the Earth surface, in this work remote sensing techniques have been used to investigate also the structural behavior of buildings affected by slow-moving landslides.

The main objective of the present thesis project has been to provide a general methodology which can be used to forecast spatial and temporal evolution of building physical vulnerability in urban areas affected by slow-moving and intermittent landslides.

Multi-level and integrated analysis of conventional and innovative monitoring techniques with structural analysis methods for damage assessment allows to estimate, at different levels of accuracy, future conditions of damage and local failures of single buildings and building aggregates. The proposed approach is based on a logical structure which takes into account vulnerability key factors, landslide kinematics and structural characterization of the exposed elements.

At different scales of representation and at different levels of accuracy, the two above mentioned datasets have been separately analyzed and subsequently merged in order to detect landslide-induced damage to buildings.

Generally, from low-resolution analysis to medium and to detailed scale, parameters useful for the landslide intensity definition and for the exposed elements characterization change.

To this aim, one test site has been chosen: Moio della Civitella urban settlement, in Salerno Province (Italy), whose territory is affected by several landslides, identified as flows, rotational/translational landslides and areas affected by diffuse slow movements.

Preliminarily, it is important to highlight that a thorough knowledge of landslide kinematics cannot be conveniently reached without an adequate *in situ* monitoring.

The combined use of conventional and innovative monitoring techniques allows to obtain more detailed information on slope failures mechanisms and their temporal evolution. To this aim, Moio della Civitella territory has been thoroughly investigated by means of conventional monitoring techniques such as boreholes, topographic measure points, inclinometers, GPS network and pluviometer station.

In the following, aims and results of vulnerability assessment at different levels of detail in Moio della Civitella urban settlement are discussed.

Aim of **small scale** analysis is to assess preliminary cause-effect relationship between landslide kinematics and building damage susceptibility. In order to characterize landslide kinematics, starting from available landslide inventory map, DInSAR data, acquired by ENVISAT and COSMO-SkyMed satellites, allowed to estimate vertical and horizontal components of movement for considered landslides phenomena, highlighting that horizontal displacements rate are higher than vertical.

Further, by distinguishing targets identified at ground level and on top of buildings, maps of stable/unstable buildings and of stable/unstable areas near structures have been obtained: 87% out of 504 buildings showed in surrounding areas a ground instability, while 64% out of 504 buildings showed on the top of structure movement rates higher than the stability threshold.

Comparison of displacement rates both of buildings and surrounding areas at ground level provided useful information to assess preliminary relationship between landslide-induced movements and performance of superstructures. Four different scenarios have been defined. In particular, most common cases identified in Moio della Civitella are:

- area near the building is unstable, as indicator of occurrence of landslides, while structure is stable, thus confirming that building structural properties allow to decrease effects transmitted to superstructure by ground movement;

- both building and the surrounding area are unstable, but structural problems, constructive properties or geological conditions can generate an increase of landslide induced effects on superstructure.

Distinguishing buildings in terms of homogeneous structural type, analysis of ratio between displacements of building and surrounding area, along horizontal and vertical direction of movement, showed that reinforced concrete buildings have displacements on top of structure equal or lower than those at ground level, due to high values of stiffness of reinforced concrete foundations.

Masonry buildings, instead, have horizontal displacements higher than on surrounding areas, showing a behavior very different from reinforced concrete buildings, while with reference to vertical component of movement, their behavior seems to be similar. Such results are due to masonry damage susceptibility higher to horizontal deformations than to vertical distortions, depending on high values of compressive strength and very low values of tensile strength. Furthermore, historical masonry structures are generally built in aggregate and their different construction properties, such as foundation typology, height of floors, mechanical properties of materials, could increase landslide-induced effects.

At this scale of representation, integrated analysis of DInSAR data with results of *in situ* damage survey to facilities allowed to update boundary and state of activity of available landslide inventory map. In particular, as regards state of activity, building damage map showed the occurrence of medium and high damage levels also within landslide-affected areas classified as dormant, while through interferometric products significant displacement rates have been identified. For this reason, several landslides, mapped as dormant in 2012, have been re-classified as active in February 2015: they are characterized by local reactivations, probably due to intense and continuous rainfall.

At last, a qualitative vulnerability matrix provided a preliminary vulnerability zoning map that allowed to identify different vulnerability rates and most critical cases in Moio della Civitella municipality.

Medium scale analysis provided a vulnerability zoning map more detailed than in the previous scale of representation, by using differential displacements and derivable parameters occurred to building foundations instead of absolute displacement rates.

Such analysis identified high levels of vulnerability in historical urban centers, both in Moio and Pellare, where masonry building aggregates, representing the most common

construction typology, showed a damage susceptibility to landslide movement higher than isolated reinforced concrete structures, widespread in particular in peripheral areas.

Moreover, empirical fragility curves provided the relationship among evolution of landslides intensity and building damage future conditions. They confirm that probability of reaching or exceeding a particular damage level is higher in masonry buildings than in reinforced concrete buildings.

Such analysis, repeated in different periods from 2009 to 2015, showed a low increase of probability of reaching a damage level for a fixed value of displacement rate, both on masonry and on reinforced concrete buildings. This behavior, due probably to progressive worsening of state of maintenance of buildings in the time-span considered, highlights that fragility curves approach is not a static concept, but it is characterized by a temporal evolution. Empirical fragility curves of buildings within landslide-affected area have to be periodically updated, as indicator of changing of structures performance during the years.

Subsequently, influence of vulnerability factors on performance of structures to slow-moving landslide-induced movements has been investigated.

Isolated reinforced concrete buildings show a similar behavior to applied angular or horizontal distortions. Reinforced concrete foundations (footings connected by beams or raft foundation), in fact, provide to structure a similar stiffness along vertical and horizontal directions to landslide-induced movements.

Isolated masonry structures, instead, are characterized by different behavior to angular and horizontal distortions. In detail, such analysis showed a higher probability of increasing damage level due to horizontal strains than to vertical deformations.

As regards performance of building aggregates, it was possible to note that buildings located at the end of aggregate show the highest probability to worsen their damage level: progressive redistribution of stresses between adjacent buildings along movement direction, in fact, increases strains at the end of aggregate. Buildings in a central or in a corner position, instead, showed a similar good performance, depending on lateral containment provided by lateral structures.

Moreover, different behavior of buildings in pre- and post-cracking phases have been assessed: structures with initial damage have a lower probability to worsen damage degree than buildings without initial damage, probably due to their plastic behavior, which requires greater distortions to worsen damage level when initial cracks just occurred.

Subsequently, influence of building height has been investigated. To this respect, reinforced concrete and masonry buildings have a different performance: in reinforced concrete structures, probability of worsening damage level decreases as the number of storeys increases, and cracks generally occurred only on elements at first floor. Masonry buildings with three or four storeys, instead, are more vulnerable than structures with low height, and cracks usually show an increasing width from bottom to top along building façade.

As regards the influence of building geometry on vulnerability, it was observed that most structures with L/B ratio equal to 1 showed a displacement lower or equal to the surrounding area; on the other hand, most buildings with rectangular shape have a displacement higher than surrounding ground level and showed higher damage degrees than structures with L/B equal to 1: such behavior is probably due to different stiffness of masonry walls along the two directions of a rectangular structure, that generate an excessive concentration of stresses under landslide-induced movements.

Also building orientation compared to landslide direction can modify vulnerability of structures: in detail, buildings characterized by a varying orientation relative to movement direction showed the highest damage susceptibility.

Finally, the above mentioned empirical fragility curves allowed to forecast different possible scenarios of future damage conditions to exposed elements, thus identifying most critical areas where mitigation activities have to be focused. They provided a thematic map showing, for each building, the probability to obtain an increase of damage level in 2020.

At last, aim of a **detailed scale** analysis is to fully characterize structural behavior of single buildings to landslide movement.

Equivalent beam model, based on an analytical method, provided 3D fragility curves: they define the probability of exceeding a damage level as function of vertical and horizontal strains. Such quantitative approach takes into account mechanical properties of materials and distortions occurred to considered buildings, recorded by DInSAR data, but does not consider three-dimensional behavior of structures. For this reason, occurrence and location of cracks and local failures cannot be exactly investigated.

3D computational model, based on a numerical approach, overcomes these constraints. In particular, temporal evolution of displacements under building foundations can be forecasted, by considering historical displacements registered by satellite data.

Subsequently, non-linear analyses performed by means of a building computational model, applying increasing vertical and horizontal distortions, allow to identify structural and non-structural elements on which cracks could occur in the future. Moreover, derived vulnerability domains define performance of single structures to landslide-induced movements. The overcoming of these domains entails a progressive worsening of damage level thus they allow to define distortions for which each damage degree occur.

Finally, such approach represents a useful tool also to assess efficacy of restoration works built on a single building, through a combined use of DInSAR time-series pre- and post-repair intervention and structural analyses performed with a numerical code on computational models corresponding to original and current configurations.

This PhD thesis introduced a general framework and scale-specific procedures tailored for the use of DInSAR data in the study of landslides affecting urban areas. Thanks to a validation process based on *in-situ* observations, results of the analyses showed the capability of the proposed approach to pursue goals commensurate with the scale of analysis (varying from small to detailed). Widely used in several analyses as tool capable to provide a help for monitoring of ground instability phenomena, such work has demonstrated its helpful support in vulnerability assessment activities, aimed to investigate consequences to exposed facilities. High spatial and temporal resolution of SAR images allow, nowadays, to develop a quasi-real time monitoring, investigating deformations and structural behavior of single part of building.

9.1 Future perspectives

Dealing with slow-moving and intermittent landslides in Moio della Civitella urban settlement, whose re-activations are induced by rainfall phenomena, future development of research will regard the investigation of relationship between rainfall data, provided by pluviometer station installed in 2015, and ground displacements recorded by SAR images. Such analysis will provide a detailed model to forecast, based on historical data, temporal and spatial evolution of ground instability phenomena and of building damage when rainfall events occur.

Furthermore, the proposed approach will be applied in other small urban settlements affected by slow-moving landslides. In particular, fragility curves' approach need to be further calibrated and validated before being used for forecasting purposes over similar areas where input data are not sufficient.

References

- AGS, (2000). "Landslide risk management concepts and guidelines". Australian Geomechanics Society, Sub-committee on landslide risk management.
- Alexander D. (1986). "Landslide damage to buildings". *Environmental Geology and Water Sciences* 8: 147-151.
- Alexander D. (1989). "Urban landslides". *Progress in Physical Geography*, 13, 157-191.
- Alexander D. (2002). *Principles of emergency planning and management*, 340, Oxford University.
- Alexander D. (2005). "Vulnerability to landslides". *Landslide Hazard and Risk*, 175-198.
- Almagià R. (1910). "Studi geografici sulle frane in Italia". *Memorie della Società Geografica Italiana*, XIV, Roma. (In Italian).
- Amatruda G., Bonnard C., Castelli M., Forlati F., Giacomelli M., Morelli M., Paro L., Piana F., Pirulli M., Polino R., Prat P., Ramasco M., Scavia C., Bellardone G., Campus S., Durville J.L., Poisel R., Preh A., Roth W., Tentschert E.H. (2004). "A key approach: the IMIRILAND project method". *Identification and mitigation of large landslide risks in Europe—advances in risk assessment*". European Commission Fifth Framework Program. Rotterdam, 13–44.
- Angeli M. G., Pasuto A., Silvano S. (2000). "A critical review of landslide monitoring experiences". *Engineering Geology*, 55(3), 133-147.
- Anzani A., Binda L., Cantini L., Cardani G., Condoleo P., Saisi A. E. (2008). "L'insegnamento nei corsi di Diagnostica e Consolidamento". In "Conservazione e riuso del costruito esistente", 83-106.
- Aronica G. T., Brigandì G., Morey N. (2012). "Flash floods and debris flow in the city area of Messina, north-east part of Sicily, Italy in October 2009: the case of the Giampileri catchment". *Natural Hazards Earth Systems Science*, 12, 1295-1309.
- ASPRS, American Society for Photogrammetry and Remote Sensing (2009).
- Baggio C., Bernardini A., Colozza R. and Corazza L., (2009). "Manuale per la compilazione della scheda di 1 livello di rilevamento danno, pronto intervento e agibilità per edifici ordinari nell'emergenza post-sismica". Editrice Italiani nel Mondo - Roma.
- Bamler R. & Hartl P. (1998). "Synthetic aperture radar interferometry". *Inverse problems*, 14(4), R1.
- Barbat A. H. (2003). "Vulnerability and holistic risk indices from engineering perspective and holistic approach to consider hard and soft variables at urban level", IADB/IDEA Program of Indicators for Disaster Risk Management.
- Barbieri M. & Lichtenegger J. (2005). "Introduction to SAR for geology. Spaceborne radar applications in Geology".
- Bardi F., Frodella W., Ciampalini A., Bianchini S., Del Ventisette C., Gigli G., Fanti R., Moretti S., Basile G., Casagli, N. (2014). "Integration between ground based and satellite SAR data in landslide mapping: The San Fratello case study". *Geomorphology*, 223, 45-60.

- Barrett E.C. & Curtis L. F. (1976). "Introduction to Environmental Remote Sensing". Chapman and Hall Ltd.
- Bedient P. B. and Huber W. C. (2008). "Hydrology and Floodplain Analysis", 4th Ed. Prentice-Hall Publishing Co., Upper Saddle River, NJ, 795 pp.
- Bell R. & Glade T. (2004). "Quantitative risk analysis for landslides - Examples from Bıldudalur, NW-Iceland". *Natural Hazard and Earth System Science*, 4, 1-15.
- Bennett G. J., Ask R. E., Warren T. E., Russel K. B., Miller O. M., William C., Tewinkel G. C., Druhot G. S., Sanders R. G., Committee on Nomenclature of the American Society of Photogrammetry. (2009). "Definitions of terms used in photogrammetric surveying and mapping". Preliminary Report.
- Berardino P., Fornaro G., Lanari R., Sansosti E. (2002). "A new Algorithm for Surface Deformation Monitoring based on Small Baseline Differential SAR Interferograms". *IEEE Transactions on Geoscience and Remote Sensing*, 40(11), 2375-2383.
- Bianchini S., Tapete D., Ciampalini A., Di Traglia F., Del Ventisette C, Moretti S. and Casagli N. (2014). "Multi-temporal evaluation of landslide-induced movements and damage assessment in san Fratello (Italy) by means of C-and X-band PSI data. *Mathematics of Planet Earth, Springer*, 257-261
- Bianchini S., Pratesi F., Nolesini T. and Casagli N. (2015). "Building deformation assessment by means of persistent scatterer interferometry analysis on a landslide-affected area: The Volterra (Italy) case study". *Remote Sensing* 7, 4678-4701.
- Blahut J., van Westen C.J. and Sterlacchini S. (2010). "Analysis of landslide inventories for accurate prediction of debris - flow source areas". *Geomorphology: an international journal of pure and applied geomorphology*, 119, 36-51.
- Bonnard C., Fell R., Corominas J., Cascini L., Leroi E., Savage W. (2008). "Guidelines for landslide susceptibility, hazard and risk zoning for land use planning". *Engineering Geology*, 102, 85-98.
- Borgatti L., Corsini A., Barbieri M., Sartini G., Truffelli G., Caputo G., Puglisi C. (2006). "Active large-scale slow moving landslides in weak rock masses: a remarkable example from the Northern Apennines (Italy), *Landslides*, (3)2, 115-124.
- Boscardin M.D. and Cording E.J. (1989). "Building response to excavation-induced settlement". *Journal of Geotechnical Engineering*, 115, 1-21.
- Boschi E., Guidoboni E., Ferrari G., Valensise G., Gasperini P. (1997). "Catalogo dei forti terremoti in Italia dal 461 a.C. al 1990". ING-SGA, Bologna 2, 1-644.
- Botts M.E. (1998). "Effects of slaking on the strength of clay shales: A critical state approach". *The Geotechnics of Hard Soils-Soft Rocks*, Evangelista & Picarelli eds, Rotterdam, 447-458.
- Bozzano F., Martino S., Naso G., Prestininzi A., Romeo R.W., Scarascia Mugnozza G. (2004). "The large Salcito landslide triggered by the 31st October 2002, Molise earthquake". *Earthquake Spectra*, 20 (2), 1-11.
- Bressani L., Pinheiro R., Bica A., Eisenberger C. and Soares J. (2008). "Movements of a large urban slope in the town of Santa Cruz do Sul (rgs), Brazil. CHEN, Z; ZHANG, J; LI, Z: 293-298.

- Bru G., Herrera G., Tomás R., Duro J., De la Vega R. and Mulas J. (2013). "Control of deformation of buildings affected by subsidence using persistent scatterer interferometry". *Structure and infrastructure engineering*, 9: 188-200.
- Burland J.B. & Wroth C.P. (1974). "Settlement of buildings and associated damage". SOA Review. *Settlement of Structures*, Cambridge, London, 611- 654.
- Burland J.B. (1977). "Behavior of foundations and structures on soft ground". *Proceedings of the 9th International Conference on Soil Mechanics and Foundation Engineering*; Tokyo, Japan, vol. 2, 495-546.
- Burland J.B. (1995). "Assessment of risk of damage to buildings due to tunneling and excavations". Invited special lecture. *Proceedings of 1st Int. Conf. Earthquake Geotechnical Engineering*, 1189-1201.
- Burland J.B. (1997). "Assessment of risk of damage to buildings due to tunnelling and excavation". *Earthquake and Geotechnical Engineering*, Balkema, 1189 – 1201.
- Caine N. (1980). "The rainfall intensity: duration control of shallow landslides and debris flows". *Geografiska Annaler. Series A. Physical Geography*, 23-27.
- Calcaterra D., Parise M., Palma B., Pelella L. (2000). "Multiple debris-flows in volcanoclastic materials mantling carbonate slopes", *Proc. 2nd Int. Conf. On Debris-flow Hazards Mitigation*, Taipei, 99-107.
- Calcaterra D., De Riso R. and Santo A. (2003). "Landslide hazard and risk mapping: experiences from Campania, Italy". In: Picarelli L. (ed.), *Proc. Int. Conf. "Fast slope movements prediction and prevention for risk mitigation"*, 63-70.
- Caliò I., Marletta M., Pantò B. (2012). "A new discrete element model for the evaluation of the seismic behaviour of unreinforced masonry buildings". *Engineering Structures*, 40, 327-338.
- Caliò I., Cannizzaro F., De Falco A., Andreini M., Giresini L., Pantò B., Sassu M. (2014). "Seismic assessment of the historical mixed masonry reinforced concrete government palace in La Spezia". *SAHC2014 – 9th International Conference on Structural Analysis of Historical Constructions*, Mexico.
- Calò F., Calcaterra D., Iodice A., Parise M., Ramondini M. (2012). "Assessing the activity of a large landslide in southern Italy by ground-monitoring and SAR interferometric techniques". *International Journal of Remote Sensing*, 33(11), 3512-3530.
- Cannon S.H. and Ellen S.D. (1985) "Rainfall conditions for abundant debris avalanches in the San Francisco Bay region, California". *California Geology*, 38(12), 267- 272.
- Capecchi F. and Focardi P. (1988). "Rainfall and landslides: research into a critical precipitation coefficient in an area of Italy". *Proceedings of the 4th Internationale Symposium on Landslides*, Vol. 2, 1031-1136.
- Cardinali M., Reichenbach P., Guzzetti F., Ardizzone F., Antonini G., Galli M., Cacciano M., Castellani M. and Salvati P. (2002). "A geomorphological approach to the estimation of landslide hazards and risks in Umbria, Central Italy". *Natural Hazards Earth System Sciences*, 2, 57–72.

- Cascini L., Bonnard Ch., Corominas J., Jibson R. and MonteroOlarte J. (2005). "Landslide hazard and risk zoning for urban planning and development – State of the Art report". Proceedings of the International Conference on Landslide Risk Management, 199–235.
- Cascini L., Fornaro G., Peduto D. (2010). "Advanced low- and full-resolution DInSAR map generation for slow-moving landslide analysis at different scales". Engineering Geology, 112, 29-42.
- Cascini L., Peduto D., Reale D., Arena L., Ferlisi S., Verde S. and Fornaro G. (2013). "Detection and monitoring of facilities exposed to subsidence phenomena via past and current generation SAR sensors". Journal of Geophysics and Engineering, 10(6), 064001.
- Castellanos Abella E. A. (2008). "Multi-scale landslide risk assessment in Cuba". Doctoral thesis, Utrecht University.
- Casu F., Manconi A., Pepe A., Lanari R. (2011). "Deformation time-series generation in areas characterized by large displacement dynamics: the SAR amplitude pixel-offset SBAS technique". Geoscience and Remote Sensing, IEEE Transactions on, 49(7), 2752-2763.
- Cevasco A., Pepe G., Brandolini P. (2013). "Geotechnical and stratigraphic aspects of shallow landslides at Cinque Terre (Liguria, Italy)". Rendiconti Online Società Geologica Italiana, 24, 52-54.
- Chakraborty S. (2008). "Spatio-temporal landslide hazard analysis along a road corridor based on historical information: case study from Uttarakhand India. Thesis.
- Chandler R. J., Pellegrini M., Tosatti G. (1995). "Le cause del disastro". Stava perché. Curcu & Genovese, Trento, 221-230. (In Italian).
- Chiocchio C., Iovine G. and Parise M. (1997). "A proposal for surveying and classifying landslide damage to buildings in urban areas". Engineering Geology and the Environment: 553-558.
- Ciampalini A., Bardi F., Bianchini S., Frodella W., Del Ventisette C., Moretti S. and Casagli N. (2014). "Analysis of building deformation in landslide area using multisensor PSInSAR™ technique". International Journal of Applied Earth Observation and Geoinformation 33: 166-180.
- Colesanti C., Ferretti A., Prati C., Rocca F. (2003). "Monitoring landslides and tectonic motion with the Permanent Scatterers technique". Engineering Geology, 68(1-2), 3-14.
- Colesanti C. & Wasowski J. (2006). "Investigating landslides with space-borne Synthetic Aperture Radar (SAR) interferometry". Engineering Geology, 88, 173-199.
- Coltorti M., Dramis F., Gentili B., Pambianchi G., Crescenti U., Sorriso Valvo M. (1985). "The December 1982 Ancona landslide. A case of deep-seated gravitational slope deformation evolving at unsteady rate". Zeitschrift fur geomorphologie, 29(3), 335-345.
- Cooper A.H., (2008). "The classification, recording, databasing and use of information about building damage caused by subsidence and landslides". Quarterly Journal of Engineering Geology and Hydrogeology 41: 409-424.

- Costantini M. (1998). "A novel phase unwrapping method based on network programming". *Geoscience and Remote Sensing, IEEE Transactions on*, 36(3), 813-821.
- Costantini M., Iodice A., Magnapane L., Pietranera L. (2000). "Monitoring terrain movements by means of sparse SAR differential interferometric measurements". In *Geoscience and Remote Sensing Symposium. Proceedings. IGARSS 2000. IEEE 2000 International*, 7, 3225-3227.
- Cotecchia V. (1978). "Systematic reconnaissance mapping and registration of slope movements". *Bulletin of the International Association of Engineering Geology-Bulletin de l'Association Internationale de Géologie de l'Ingénieur*, 17(1), 5-37.
- Cotecchia V. (2006). "The second Hans Cloos lecture. Experience drawn from the great Ancona landslide of 1982". *Bulletin of Engineering Geology and the Environment*, 65(1), 1-41.
- Corominas J., van Westen C., Frattini P., Cascini L., Malet J.-P., Fotopoulou S., Catani F., Van Den Eeckhaut M., Mavrouli O., Agliardi F., Pitilakis K., Winter M.G., Pastor, M. Ferlisi S., Tofani V., Hervás J., Smith, J.T. (2014). Recommendations for the quantitative analysis of landslide risk". *Bull. Eng. Geol. Environ.* 73 (2), 209–263.
- Crescenzi E., Iovine G. and Parise M. (1994). "Analysis of landslide damage in a village in southern Italy: A preliminary report. Incontro Internazionale dei Giovani Ricercatori in Geologia Applicata, Lausanne Suisse: 68-72.
- Crosetto M., Tscherning C. C., Crippa B., Castillo M. (2002). "Subsidence monitoring using SAR interferometry: Reduction of the atmospheric effects using stochastic filtering". *Geophysical Research Letters*, 29(9).
- Crosetto M., Biescas E., Duro J., Closa J., Arnaud A. (2008). "Generation of advanced ERS and Envisat Interferometric SAR Products using the Stable Point Network Technique". *Photogrammetric Engineering and Remote Sensing*, 74(4), 443-451.
- Crosta G.B. (2003). "Distributed modelling of shallow landslides triggered by intense rainfall". *Natural Hazards and Earth System Sciences*, 3, 81-93.
- Crozier M.J. (1986). "Landslides: causes, consequences & environment". Croom Helm Pub., London and Dover.
- Crozier M.J. (1999). "Prediction of rainfall-triggered landslide: a test of antecedent water status model". *Earth surface processes and landforms*, 24, 825-833.
- Crozier M.J. and Glade T. (2005). "Landslide Hazard and Risk: Issues, Concepts and Approach". *Landslide Hazard and Risk*, England, 1-40.
- Cruden D.M. (1991). "A simple definition of a landslide". *Bulletin International Association of Engineering Geology*, 43, 27-29.
- Cruden D.M. and Varnes D.J. (1996). "Landslide types and processes". *Landslides, Investigation and Mitigation. Transportation Research Board Special Report*, 247, 36-75.
- Cruden D.M. and Fell R. (1997) "Landslide risk assessment". *Proc. Int. Workshop on Landslide Risk Assessment*, Honolulu, Balkema Pub., Rotterdam, 371 pp.

- Cutter S.L. (1996). "Vulnerability to environmental hazards". *Progress in Human Geography* 20, 529-539.
- Cutter S.L., Barnes L., Berry M., Burton C., Evans E., Tate E. & Webb J. (2008). "A place-based model for understanding community resilience to natural disasters", *Global Environmental Change*, vol.18, 598–606.
- Dai F.C. and Lee C.F. (2001). "Frequency-volume relation and prediction of rainfall-induced Landslides". *Engineering Geology*, 59, 253–266.
- Dai F.C., Lee C.F. and Ngai Y.Y. (2002). "Landslide risk assessment and management: an overview". *Engineering Geology*, 64 (1), 65-87.
- DeBano L.F. (2000). "The role of fire and soil heating on water repellency in wildland environments: a review". *J- Hydrol*, 231–232, 195–206
- Del Prete M. (1993). "Rainfall induced landslides: general historical review of landslides/climate in Basilicata". Report to CEC EPOCH PL-890112, Università degli studi della Basilicata, 237 pp.
- Del Prete M., Guadagno F. M., Hawkins A. B. (1998). "Preliminary report on the landslides of 5 May 1998, Campania, southern Italy". *Bulletin of Engineering Geology and the Environment*, 57(2), 113-129.
- Del Soldato M., Di Martire D., Tomàs R., (2016). "Comparison of different approaches for landslide-induced damage assessment: the case study of Agnone (southern Italy)". *Rendiconti Online Societa Geologica Italiana*, 41:139–142.
- Del Soldato M., Bianchini S., Calcaterra D., De Vita P., Di Martire D., Tomàs R., Casagli N., (2017). "A new approach for landslide-induced damage assessment". *Geomatics, Natural Hazards and Risk*, 1-14.
- De Luca D.L. (2014). "Analysis and modelling of rainfall fields at different resolutions in southern Italy". *Hydrological Sciences Journal*, 56(8), 1536-1558.
- Del Ventisette C, Intrieri E., Luzi G., Casagli N., Fanti R. and Leva D., (2011). "Using ground based radar interferometry during emergency: the case of the A3 motorway (Calabria Region, Italy) threatened by a landslide", *Nat. Hazards Earth. Sys.*, vol. 11, no. 9, 2483–2495.
- De Zan F., & Guarnieri A. M. (2006). "TOPSAR: Terrain observation by progressive scans". *Geoscience and Remote Sensing, IEEE Transactions on*, 44(9), 2352-2360.
- Di Martire D., (2013). "Application of DInSAR data for slow-moving landslides monitoring", PhD thesis.
- Di Martire D., Iglesias R., Monells D., Centolanza G., Sica S., Pagano L., Mallorquì J.J., Calcaterra D. (2014). "Comparison between Differential SAR interferometry and ground measurements data in the displacement monitoring of the earth-dam of Conza della Campania (Italy)". *Remote Sensing of Environment*, 148, 58-69.
- Di Martire D., Tessitore S., Brancato D., Ciminelli M. G., Costabile S., Costantini M., Graziano G. V., Minati F., Ramondini M., Calcaterra D. (2016). "Landslide detection integrated system (LaDIS) based on in-situ and satellite SAR interferometry measurements". *Catena*, 137, 406-421.

- Dikau R., Brundsen D., Schrott L., Ibsen M.L. (1996). "Landslide Recognition: Identification, Movement and Causes". Wiley, Chichester.
- Doerry A.W. (2008). "Reflectors for SAR Performance Testing". SANDIA REPORT SAND 2008-0396.
- Douglas J., and Ransom W. H. (2007). "Understanding Building Failures", 3rd edn. New York: Routledge. 326 pp.
- Du J., Yin K., Nadim F., and Lacasse S. (2013). "Quantitative vulnerability estimation for individual landslides" 18th International Conference on Soil Mechanics and Geotechnical Engineering, Paris, 2181–2184.
- Einstein H.H. (1997). "Landslide Risk - Systematic approaches to assessment and management". In "Landslide Risk Assessment", Rotterdam, 25-50.
- Fatland D. R. & Lingle C. S. (1998). "Analysis of the 1993-95 Bering Glacier (Alaska) surge using differential SAR interferometry". *Journal of Glaciology*, 44(148), 532-546.
- Faure R.M. (2004). "Data-bases and the management of landslides". Solem Expertises S.A.
- Fell R. (1994). "Landslide risk assessment and acceptable risk". *Canadian Geotechnical Journal*, 31, 2, 261–272.
- Fell R., Ho K.K.S., Lacasse S. and Leroi, E. (2005). "A framework for landslide risk assessment and management". *Landslide Risk Management*, London, 533-541.
- Fell R., Corominas J., Bonnard C., Cascini L., Leroi E., Savage W. (2008). "Guidelines for landslide susceptibility, hazard and risk zoning for land use planning". *Engineering Geology*, 102, 85-98.
- Ferlisi S., Peduto D., Gulla G., Nicodemo G., Borrelli L., Fornaro, G. (2015). "The use of DInSAR data for the analysis of building damage induced by slow-moving landslides". *Engineering Geology for Society and Territory*, Vol. 2., Springer International Publishing Switzerland, 1835–1839.
- Ferretti A., Prati C., Rocca F. (2000). "Non-linear subsidence rate estimation using permanent scatterers in differential SAR interferometry". *IEEE Transactions on Geoscience and Remote Sensing*, 38 (5), 2202-2212.
- Ferretti A., Prati C., Rocca F. (2001). "Permanent scatterers in SAR interferometry". *IEEE Transactions on Geoscience and Remote Sensing* 39(1), 8-20.
- Ferretti A., Savio G., Barzaghi R., Borghi A., Musazzi S., Novali F., Prati C. and Rocca F. (2007). "Submillimeter Accuracy of InSAR Time Series: Experimental Validation". *IEEE Transactions On Geoscience And Remote Sensing*, 45, 5.
- Fiaschi S., Di Martire D., Tessitore S., Achilli V., Ahmed A., Borgstrom S., Calcaterra D., Fabris M., Ramondini M., Serpelloni E., Siniscalchi V., Floris M. (2015). "Monitoring of land subsidence in Ravenna Municipality using two different DInSAR techniques: comparison and discussion of the results". *Ecology*, 23(1), 38-50.
- Franceschetti G. & Lanari, R. (1999). "Synthetic Aperture Radar Processing", CRC Press, Boca Raton (FL), ISBN 8493-7899.

- Freeman T.J., Littlejohn G.S. and Driscoll R.M. (1994). "Has your house got cracks? A guide to subsidence and heave of buildings on clay". Thomas Telford.
- Fried D. L. (1977). "Least-square fitting a wave-front distortion estimate to an array of phase-difference measurements". *JOSA*, 67(3), 370-375.
- Frost V. S., Stiles J. A., Shanmugan K. S., Holtzman J. C. (1982). "A model for radar images and its application to adaptive digital filtering of multiplicative noise". *Pattern Analysis and Machine Intelligence, IEEE Transactions on*, (2), 157-166.
- Fruneau B., Achache J., Delacourt C. (1996). "Observation and modelling of the Saint-Etienne de Tinee landslide using SAR interferometry", *Tectonophysics*, 265 (3-4), 181- 190.
- Fuchs S., Heiss K., and Hubl J. (2007). "Towards an empirical vulnerability function for use in debris flow risk assessment". *Natural Hazards and Earth System Sciences*, 495–506.
- Fuchs S. (2009). "Susceptibility versus resilience to mountain hazards in Austria. Paradigms of vulnerability revisited", *Natural Hazards and Earth System Sciences* 9(2): 337-352.
- Gabriel A. K., Goldstein R. M., Zebker H. A. (1989). "Mapping small elevation changes over large areas: Differential interferometry", *Journal Geophysical Research*, 94, 9183-9191.
- Galli M. and Guzzetti F. (2007). "Landslide Vulnerability Criteria: A Case Study from Umbria, Central Italy". *Environmental Management*, 40:6, 49-664.
- Galloway D.L., Hudnut K.W., Ingebritsen S.E., Phillips S.P., Peltzer G., Rogez F., Rosen, P.A. (1998). "Detection of aquifer synthetic aperture radar, Antelope Valley, Mojave Desert, California". *Water Resources Research*, 34 (10), 2573-2585.
- Gattinoni P., Scesi L., Arieni L., Canavesi M. (2012). "The February 2010 large landslide at Maierato, Vibo Valentia, Southern Italy". *Landslides*, 9(2), 255-261.
- Giordan D., Allasia P., Manconi A., Baldo M., Santangelo M., Cardinali M., Corazza A., Albanese V., Lollino G., Guzzetti F. (2013). Morphological and kinematic evolution of a large earthflow: The Montaguto landslide, southern Italy. *Geomorphology*, 187, 61-79.
- Glade T. (2004). "Vulnerability assessment in landslide risk analysis". *Die Erde*, 121–138.
- Glade T., Anderson M.G., Crozier, M.J. (2005). "Landslide hazard and risk". Wiley, Chichester, 803 pp.
- Goldstein R. M., Engelhardt H., Kamb B., Frolich R. M. (1993). "Satellite radar interferometry for monitoring ice sheet motion: application to an Antarctic ice stream". *Science*, 262 (5139), 1525-1530.
- Goldstein R. M. & Werner C. L. (1998). "Radar interferogram filtering for geophysical applications". *Geophysical Research Letters*, 25(21), 4035-4038.
- Gonçalves C., Zêzere J.L., Pereira S., Garcia R.A.C. (2016). "Assessment of physical vulnerability of buildings and analysis of landslide risk at the municipal scale –

- application to the Loures municipality, Portugal”. *Natural Hazards and Earth System Sciences*, 16, 311–331.
- Gonzalez A.J. (1989). “Metodologia y criterios de clasificacion para inventario de movimientos”. I Simposio sudamericano de deslizamientos. Sociedad Colombiana de Geotecnia, 677-698.
- Grünthal G., (1998). “European Macroseismic Scale 1998 (EMS-98)”. European Seismological Commission, subcommission on Engineering Seismology, working Group Macroseismic Scales.
- Gruppo Sismica (2014). “3DMacro. Il software per le murature (3D computer program for the seismic assessment of masonry buildings)”. Catania, Italy, www.3dmacro.it
- Guillaumont P. (2009). “An economic vulnerability index: its design and use for international development policy”. *Oxford Development Studies*, vol. 37, 3, 193-228.
- Guerriero L., Revellino P., Coe J., Focareta M., Grelle G., Albanese V., Corazza A. Guadagno F.M. (2013). “Multi-temporal Maps of the Montaguto Earth Flow in Southern Italy from 1954 to 2010”. *Journal of Maps*, 9(1), 135-145.
- Guragain R., Pandey B.H., Shrestha S.N. (2004). “Guidelines for seismic vulnerability assessment of hospitals”. National Society for Earthquake Technology-Nepal
- Guzzetti F., Carrara A., Cardinali M., Reichenbach P. (1999). “Landslide hazard evaluation: a review of current techniques and their application in a multi-scale study, Central Italy”. *Geomorphology*, 31, 181-216.
- Guzzetti F. (2000). “Landslide fatalities and the evolution of landslide risk in Italy”. *Engineering Geology*, 58 (2), 89-107.
- Guzzetti F., Malamud B.D., Turcotte D.L. and Reichenbach P. (2002). “Power-law correlations of landslide areas in Central Italy”. *Earth and Planetary Science Letters*, 195: 169-183.
- Guzzetti F. and Tonelli G. (2004). “SICI: an information system on historical landslides and floods in Italy”. *Natural Hazards and Earth System Sciences*, 4:2, 213-232.
- Guzzetti F., Peruccacci S., Rossi M. and Stark, C. P. (2007). “Rainfall thresholds for the initiation of landslides in central and southern Europe”. *Meteorol. Atmos. Phys.*, 98, 239–267.
- Hanssen R. (2001). “Radar interferometry”. Kluwer Academic Publishers, Dordrecht (The Netherlands).
- Herrera G., Notti D., García-Davalillo J.C., Mora O., Cooksley G., Sánchez M., Arnaud A., Crosetto M. (2011). “Analysis with C- and X-band satellite SAR data of the Portalet landslide area”. *Landslides*, 8, 195-206.
- Hooper A., (2008). “A multi-temporal InSAR method incorporating both persistent scatterer and small baseline approaches”, *Geophysical Research*, 35, 16302.
- Hu K.H., Cui P. and Zhan, J.Q. (2012). “Characteristics of damage to buildings by debris flows on 7 August 2010 in Zhouqu, Western China”, *Natural Hazards and Earth System Sciences*, 12, 2209–2217.

- Hungr O., Evans S. G., Bovis M. J., Hutchinson J. N. (2001). "A review of the classification of landslides of the flow type". *Environmental & Engineering Geoscience*, 7, 221-238.
- Hutchinson J.N. (1988). "General report: morphological and geotechnical parameters of landslides in relation to geology and hydrology". 5th International Symposium on Landslides, Lausanne, 1, 3-35.
- IADB, (2005). "Indicators of disaster risk and risk management". Summary report for WCDR, Inter-American Development Bank, Colombia.
- ICG, (2003). "Risk assessment. Basic terms for landslides". International Centre for Geohazards.
- Iglesias R., Mallorqui J.J., Monells D., López-Martíne C., Fabregas X., Aguasca A., Gili J.A., Corominas J. (2015). "PSI Deformation Map Retrieval by Means of Temporal Sublook Coherence on Reduced Sets of SAR Images". *Remote Sensing*, 7, 530-563.
- Infante D., Confuorto P., Di Martire D., Ramondini M., Calcaterra D. (2016). "Use of DInSAR data for multi-level vulnerability assessment of urban settings affected by slow-moving and intermittent landslides". *Procedia Engineering*, 158, 470– 475.
- Infante D., Confuorto P., Di Martire D., Ramondini M., Calcaterra D. (2016). "Integrated analysis of DInSAR and buildings damage data for preliminary vulnerability assessment of urban settlements affected by slow-moving landslides". *Atto di Convegno, 88° Congresso della Società Geologica Italiana*. Napoli.
- Iovine G. and Parise M., (2002). "Schema illustrato per la classificazione ed il rilievo dei danni da frana in aree urbane". *Memorie Società Geologica Italiana* 57: 595-603.
- IUGS, Working Group on Landslides, Committee on Risk Assessment, (1997). "Quantitative risk assessment for slopes and landslide - The state of the art". *Landslide risk assessment*, Rotterdam, 3-12.
- Iverson R. M., Reid M. E., LaHusen R. G. (1997). "Debris-flow mobilization from landslides". *Annual Review of Earth and Planetary Sciences*, 25(1), 85-138.
- Jaiswal P. and van Westen C. J. (2009). "Estimating temporal probability for landslide along transportation routes based on rainfall threshold". *Journal Elsevier, Geomorphology*, 112, 96-105.
- Jaiswal P., van Westen C. J., & Jetten V. (2010). "Quantitative landslide hazard assessment along a transportation corridor in southern India". *Engineering Geology*, 116, 236-250
- Jakob, M. and Weatherly, H. (2003) A hydroclimatic threshold for landslide initiation on the North Shore Mountains of Vancouver, British Columbia. *Geomorphology*, 54,137-156.
- Jennings J. and Kerrich J. (1962). "The heaving of buildings and the associated economic consequences with particular reference to the orange free state goldfields". *Civil Engineer in South Africa, Transactions of the South African Institute of Civil Engineering* 4: 221-248.
- Johnson R.B. and DeGraff J.V. (1988). "Principles of Engineering Geology". John Wiley & Sons, New York, 497 pp.

- Kampes, B. M. (2006). "Radar interferometry". Springer.
- Klinger Y., Michel R., Avouac J. P. (2000). "Co-seismic deformation during the Mw7. 3 Aqaba Earthquake (1995) from ERS-SAR interferometry". *Geophysical research letters*, 27(22), 3651-3654.
- Kwok R., Fahnestock M.A. (1996). "Ice sheet motion and topography from radar interferometry". *IEEE Transactions on Geoscience and Remote Sensing*, 34, 189-200.
- Lanari R., Lundgren P., Sansosti E. (1998). "Dynamic deformation of Etna volcano observed by satellite radar interferometry". *Geophysical Research Letters*, 25(10), 1541-1544.
- Larsen MC. (2008). "Rainfall-triggered landslides, anthropogenic hazards, and mitigation strategies". *Advances in Geosciences* 14, 147-153.
- Larsen MC. and Torres-Sánchez A.J. (1998). "The frequency and distribution of recent landslides in three montane tropical regions of Puerto Rico". *Geomorphology*, 309-331.
- Lee E. and Moore R. (1991). "Coastal landslip potential assessment: Isle of wight undercliff". Technical Report prepared by Geomorphological Services Ltd for the Department of the Environment, research contract PECD 7/1/272.
- Lee J. S., Jurkevich L., Dewaele P., Wambacq P., Oosterlinck A. (1994). "Speckle filtering of synthetic aperture radar images: A review". *Remote Sensing Reviews*, 8(4), 313-340.
- Leroi E. (1996). "Landslide hazard-risk maps at different scales: Objectives, tools and developments". *Landslides*, Rotterdam, 35-51.
- Li F. & Goldstein R. (1987). "Studies of multi-baseline spaceborne interferometric synthetic aperture radars". In *IGARSS'87-International Geoscience and Remote Sensing Symposium*, 1, 1545-1550.
- Li Z., Nadim F., Huang H., Uzielli M., and Lacasse S. (2010). "Quantitative vulnerability estimation for scenario-based landslide hazards". *Landslides*, 7, 125–134.
- Liu J.K., Wong C.C., Huang J.J., Yang M.J. (2002). "Landslide enhancement images for the study of torrential rainfall landslides". *Proceedings of 23rd Asian Conference on Remote Sensing*, Kathmandu, 193–198.
- Lopes A., Nezry E., Touzi R., Laur, H. (1993). "Structure detection and statistical adaptive speckle filtering in SAR images". *International Journal of Remote Sensing*, 14(9), 1735-1758.
- Lu Z., Mann D., Freymueller J.T., Meyer D.J. (2000). "Synthetic aperture radar interferometry of Okmok volcano, Alaska: Radar observations". *Journal of Geophysical Research*, 105, 10791-10806.
- Lundgren P., Berardino P., Coltelli M., Fornaro G., Lanari R., Puglisi G., Sansosti E., Tesauro M. (2003). "Coupled magma chamber inflation and sector collapse slip observed with synthetic aperture radar interferometry on Mt. Etna volcano". *Journal of Geophysical Research: Solid Earth*, 108 (B5).

- MacLeod I.A. and Littlejohn G.S. (1974). "Discussion on Session 5. Conf. Settlement of Structures, Cambridge, Pentech Press, London, 792-795.
- Malamud B.D., Turcotte D.L., Guzzetti F. and Reichenbach P. (2004). "Landslide inventories and their statistical properties". *Earth Surface Processes and Landforms*, 29:6, 687-711.
- Mansour M.F., Morgenstern N.R. and Martin C.D., (2011). "Expected damage from displacement of slow-moving slides". *Landslides* 8: 117-131.
- Massonnet D., Thatcher W., Vadon H. (1996). "Detection of post-seismic fault zone collapse following the Landers earthquake". *Nature*, 382, 489-497.
- Massonnet D. and Feigl K.L. (1998). "Radar interferometry and its application to changes in the Earth's surface". *Reviews of Geophysics*, 36(4), 441-500.
- Mavrouli O., Fotopoulou S., Pitilakis K., Zuccaro G., Corominas J., Santo A., Cacace F., De Gregorio D., Di Crescenzo G., Foerster E., Ulrich T. (2014). "Vulnerability assessment for reinforced concrete buildings exposed to landslides". *Bulletin of Engineering Geology and the Environment*. 73, 265–289.
- Mazzorana B., Hübl J., and Fuchs S. (2009). "Improving risk assessment by defining consistent and reliable system scenarios", *Natural Hazards and Earth System Sciences*, 9, 145–159.
- McGuffey V.C., Modeer V.A., Turner A.K. (1996). "Subsurface exploration". *Landslides. Investigation and mitigation. Transp. Res. Board Spec. Rep. 247, Nat. Res. Council, Washington, D.C., 231-277.*
- Medvedev S.V. (1965). "Engineering seismology", book, 260 pp.
- Meusburger K., Alewell C. (2008). "Impacts of anthropogenic and environmental factors on the occurrence of shallow landslides in an alpine catchment (Urseren Valley, Switzerland)". *Natural Hazards and Earth System Sciences* 8, 509–520.
- Meisina C., Zucca F., Notti D., Colombo A., Cucchi A., Savio G., Giannico C., Bianchi M. (2008). "Geological interpretation of PSInSAR data at regional scale". *Sensors*, 8, 7469-7492.
- Milillo P., Cigna F., Masini N., Lasaponara R., Tapete D. (2014). "Persistent Scatterer Interferometry Processing of COSMO-SkyMed StripMap HIMAGE Time Series to Depict Deformation of the Historic Centre of Rome, Italy". *Remote Sensing*, 6, 12593-12618.
- Milillo P., Bürgmann R., Lundgren P., Salzer J., Perissin D., Fielding E., Biondi F., Milillo G. (2016). "Space geodetic monitoring of engineered structures: The ongoing destabilization of the Mosul dam, Iraq". *Scientific Reports* 6, pp. 7.
Francesca Cigna 1,2, Rosa Lasaponara 2
- Milillo P., Perissin D., Salzer J., Lundgren P., Lacava G., Milillo G., Serio C. (2016). "Monitoring dam structural health from space: Insights from novel InSAR techniques and multi-parametric modeling applied to the Pertusillo dam Basilicata, Italy". *International Journal of Applied Earth Observation and Geoinformation*, 52:221-229.
- Menditto G. (2010). "Fessurazioni nelle strutture. Rilievo, lettura, diagnosi: una visione degli eventi degradanti alla luce delle nuove NTC" – (Flaccovio Editore).

- Mora O., Mallorquí J. J., Duro J., Broquetas A. (2001). “Long-term subsidence monitoring of urban areas using differential interferometric SAR techniques”. In *Geoscience and Remote Sensing Symposium, IEEE 2001 International*, 3, 1104-1106.
- Mora O., Mallorquí J.J., Broquetas A. (2003). “Linear and nonlinear terrain deformation maps from a reduced set of interferometric SAR images”. *IEEE Transactions on Geoscience and Remote Sensing*, 41, 2243-2253.
- Mora O. (2004). “Advanced differential SAR techniques for detection of terrain and building displacements”. Tesis doctoral, Universidad Politécnica de Barcelona, 182 pp.
- Mulas J., Aragón R., Clemente A.A., (2010). “La subsidencia del terreno en la ciudad y área metropolitana de Murcia: Modelización, seguimiento y control”, (coord. Madrid: Instituto Geológico y Minero de España y Consejería de Obras Públicas y Ordenación del Territorio de la Comunidad Autónoma de la Región de Murcia).
- Nadim F., Kjekstad O., Domaas U., Rafat R. and Peduzzi P. (2006). “Global landslide risk case study”. *Natural disaster hotspots. Case Studies*, 204.
- Nawy E.G. (1968). “Crack control in reinforced concrete structures”. *Journal Proceedings*, 825-836.
- Negulescu C., Foerster E. (2010). “Parametric studies and quantitative assessment of the vulnerability of a RC frame building exposed to differential settlements”. *Natural Hazards and Earth System Sciences*, 10: 1781–1792.
- Negulescu C., Ulrich T., Baills A., Seyedi D. M. (2014). “Fragility curves for masonry structures submitted to permanent ground displacements and earthquakes”. *Natural Hazards*, 74, 1461–1474.
- Nicodemo G., Ferlisi S., Peduto D., Cascini L., Gullà G., Borrelli L., Fornaro G. (2014). “Analisi di livello preliminare delle conseguenze indotte agli edifici da frane a cinematica lenta”. *IARG 2014, Incontro annuale dei ricercatori di geotecnica*, 6 pp.
- Nolesini T., Di Traglia F., Del Ventisette C., Moretti S. and N. Casagli. (2013). “Deformations and slope instability on Stromboli volcano: Integration of GBInSAR data and analog modelling”, *Geomorphology*, vol. 180-181, 242-254.
- Notti D., Garcia-Davallilo J.C., Herrera G., Mora, O. (2010). “Assessment of the performance of X-band satellite radar data for landslide mapping and monitoring: Upper Tena valley case study”. *Natural Hazards and Earth System Sciences*, 10, 1865-1875.
- Notti D., Herrera G., Bianchini S., Meisina C., García-Davalillo J.C., Zucca F. (2014). “A methodology for improving landslide PSI data analysis”. *International Journal of Remote Sensing*, 35, (6), 2186-2214.
- Novellino A., De Agostini A., Di Martire D., Ramondini M., Floris M., Calcaterra D. (2015). “Using Data from Multiple SAR Sensors in Landslide Characterization: Case Studies from Different Geomorphological Contexts in Italy”. In *Engineering Geology for Society and Territory*, 2, 395-398.

- Peduto D., Pisciotta G., Nicodemo G., Arena L., Ferlisi S., Gulla G., Borrelli L., Fornaro G., Reale D. (2016). "A procedure for the analysis of building vulnerability to slow-moving landslides". Proceedings of the 1st IMEKO TC4 International Workshop on Metrology for Geotechnics, 248–254.
- Peduto D., Ferlisi S., Nicodemo G., Real D., Pisciotta G., Gullà G., (2017). "Empirical fragility and vulnerability curves for buildings exposed to slow-moving landslides at medium and large scales". Landslides, 1-15.
- Peltzer G., Rosen, P.A. (1995). "Surface displacement of the 17 Eureka valley, California, earthquake observed by SAR interferometry". Science, 268, 1333-1336,
- Peltzer G., Rosen P., Rogez F., Hudnut K. (1996). "Post seismic rebound in fault stepovers caused by pore fluid flow". Science, 273, 1202-1204.
- Peltzer G., Crampé F., Hensley S., Rosen R. (2001). "Transient strain accumulation and fault interaction in the eastern California shear zone". Geology, 29, 975-978.
- Petley D. (2012). "Global patterns of loss of life from landslides". Geology, 40, 927-930.
- Perissin D., Prati C., Rocca F. (2009). "PSInSAR Analysis over the Three Gorges Dam and urban areas in China". Urban Remote Sensing Joint Event, 1-5.
- Picarelli L. & Olivares L. (2006). "Modelling of flowslides behavior for risk mitigation". Physical Modelling in Geotechnics, 6th ICPMG '06, Hong Kong, 1, 99-112.
- Picarelli L. & Urciuoli G. (2008). "Interaction between landslides and man-made works". Landslides and Engineered Slopes, 1301-1307.
- Pierson T. C. & Costa J. E. (1987). "A rheologic classification of subaerial sediment-water flows". Reviews in Engineering Geology, 7, 1-12.
- Pisciotta G. (2008). "Physical vulnerability of elements at risk in landslide prone areas". PhD thesis, University of Salerno.
- Pitilakis K.D., Fotopoulou S.D. (2013). "Fragility curves for reinforced concrete buildings to seismically triggered slow-moving slides". Soil Dynamics and Earthquake Engineering, 143–161.
- Plank S., Singer J., Thuro K. (2013). "Assessment of number and distribution of persistent scatterers prior to radar acquisition using open access land cover and topographical data". ISPRS Journal of Photogrammetry and Remote Sensing, 85, 132-147.
- Pratesi F., Nolesini T., Bianchini S., Leva D., Lombardi L., Fanti R., Casagli N., (2014). "Integrated TLS and GBInSAR System for Monitoring Structural Instabilities over Urbanized Areas: the Case of Volterra (Tuscany, Italy)". DVW-Seminar Terrestrisches Laserscanning. Proc. 139.
- Prati C., Rocca F., Guarnieri A. M. (1989). "Effects of speckle and additive noise on the altimetric resolution of interferometric SAR (ISAR) surveys". Geoscience and Remote Sensing Symposium. IGARSS'89. 12th Canadian Symposium on Remote Sensing, 2469-2472

- Ragozin A. L. and Tikhvinsky I. O. (2000). "Landslide hazard, vulnerability and risk assessment in Landslides in research, theory and practice". Proceedings of the 8th ISL, Cardiff, Vol. 3. Thomas Telford, London, 1257–1262.
- Revellino P., Guerriero L., Grelle G., Hungr O., Fiorillo F., Esposito L., Guadagno F. M. (2013). "Initiation and propagation of the 2005 debris avalanche at Nocera Inferiore (Southern Italy)". Italian Journal of Geosciences, 132(3), 366-379.
- Rockaway J. D. (1976). "The influence of map scale on engineering geologic mapping". Bulletin of the International Association of Engineering Geology-Bulletin de l'Association Internationale de Géologie de l'Ingénieur, 13(1), 119-122.
- Roberds W. (2005). "Estimating temporal and spatial variability and vulnerability". Landslide Risk Management. Balkema Publishers, 129-157.
- Rosen P. A., Hensley S., Zebker H. A., Webb F. H., Fielding E. J. (1996). "Surface deformation and coherence measurements of Kilauea Volcano, Hawaii, from SIR-C radar interferometry". Journal of Geophysical Research: Planets, 101(E10), 23109-23125.
- Rosen P.A., Hensley S., Joughin I.R., Li F.K., Madsen S.N., Rodriguez E., Goldstein R. (2000). "Synthetic aperture radar interferometry", IEEE Proceedings, 88, 333- 376.
- Sammarco O. (2004). "A tragic disaster caused by the failure of tailings dams leads to the formation of the Stava 1985 Foundation". Mine Water and the Environment, 23, 91-95.
- Sarabandi K. and Chiu T. C. (1995). "An optimum corner reflector for calibration of imaging radars". IEEE Trans. Antennas Propagation.
- Schuster R.L. (1996). "Socioeconomic significance of landslides". Landslides, Investigation and Mitigation. Transportation Research Board Special Report, 247, 12-35.
- Schuster R. L. and Kockelman W. J. (1996). "Principles of landslide hazard reduction". Landslides Investigation and Mitigation, National Academy Press, 91-105,
- Seymour M.S., Cumming I.G., 1994. "Maximum Likelihood Estimator for SAR Interferometry". Geoscience Remote Sensing Symposium. Pasadena, USA, 2272-2275.
- Shinozuka M., Feng M.Q., Lee J., Naganuma T. (2000). "Statistical analysis of fragility curves. Journal of Engineering Mechanics ASCE, 126(12):1224–1231.
- Skempton A.W. and MacDonald D. (1956). "Allowable settlement of buildings". Proc. Institution of Civil Engineers, 3, 5, 727-768.
- Soeters R. and van Westen C.J. (1996). "Slope instability recognition, analysis, and zonation". In "Landslide. Investigation and mitigation", 12-35.

- Sousa J. J., & Bastos L. (2013). "Multi-temporal SAR interferometry reveals acceleration of bridge sinking before collapse". *Natural Hazards and Earth System Science*, 13(3), 659-667.
- Sowers G.F. and Royster D.L. (1978). "Field investigations". In Special Report 176: Landslides: Analysis and Control, TRB, National Research Council, Washington, D.C., Chap. 4, 1-111.
- Squarzonzi C., Delacourt C., Allemand P. (2003). "Nine years of spatial and temporal evolution of the La Valette landslide observed by SAR interferometry". *Engineering Geology*, 68(1), 53-66.
- Srivastava A. (2016). "Review of Causes of Foundation Failures and Their Possible Preventive and Remedial Measures". Department of Civil & Environmental Engineering The NorthCap University.
- Stabile T. A., Giocoli A., Perrone A., Palombo A., Pascucci S., Pignatti S. (2012). "A new joint application of non-invasive remote sensing techniques for structural health monitoring" *Journal of Geophysics and Engineering*, 9, 53.
- Stramondo S., Tesauro M., Briole P., Sansosti E., Salvi S., Lanari R., Anzidei M., Baldi P., Fornaro G., Avallone A., Buongiorno M. F., Franceschetti G., Boschi E. (1999). "The September 26, 1997 Colfiorito, Italy, earthquakes: modeled coseismic surface displacement from SAR interferometry and GPS". *Geophysical Research Letters*, 26(7), 883-886.
- Strozzi T., Wegmüller U., Tosi L., Bitelli G., and Spreckels V. (2001). "Land Subsidence Monitoring with Differential SAR Interferometry". *Photogrammetric Engineering and Remote Sensing*, 67(11), 1261-1270.
- Strozzi T., Luckman A., Murray T., Wegmüller U., Werner C. L. (2002). "Glacier motion estimation using SAR offset-tracking procedures". *IEEE Transaction on Geoscience Remote*, 40(11), 2384-2391.
- Strozzi T., Farina P., Corsini A., Ambrosi C., Thüring M., Zilger J., Wiessman A., Wegmüller U., Werner C. (2005). "Survey and monitoring of landslide displacements by means of L-band satellite SAR interferometry". *Landslides*, 2(3), 193-201.
- Tan K., Razak H.A., Suhatri M., Lu D. (2014). "Fragility Curves of a RC Frame Building Subjected to Seismic Ground Motions". *Journal of Civil Engineering Research*, 4(3A): 159-163.
- Tapete D., Casagli N., Fanti R., Del Ventisette C., Cecchi R., Petrangeli P. (2011). "Satellite and ground-based radar interferometry for detection and monitoring of structural instability in archaeological sites". In *Geophysical research abstracts* (Vol. 13).
- Tapete D. & Cigna F. (2012). "Site-Specific Analysis of Deformation Patterns on Archaeological Heritage by Satellite Radar Interferometry". *MRS Proceedings*, 1374, 283-295, Cambridge University Press.

- Tarbotton C., Dall’Osso F., Dominey-Howes D. and Goff J. (2015). “The use of empirical vulnerability functions to assess the response of buildings to tsunami impact: comparative review and summary of best practice”, *Earth-Science Review*, 142, 120–134.
- Tarchi D., Casagli N., Fanti R., Leva D., Luzi G., Pasuto A., Pieraccini M., Silvano S. (2003). “Landslide monitoring by using ground-based SAR interferometry: An example of application to the Tessina landslide in Italy”. *Engineering Geology*, 68 (1-2), 15-30.
- Terzaghi K. (1935). “The actual factor of safety in foundations”. In “*Structure Engineering*”, 13, 126.
- Tessari G., Cerchiello V., Velterop E., Riccardi P., De Filippi M., Pasquali P. (2016). “Risk of building damage by modelling interferometric time series”. *IGARSS 2016*, 7334-7337.
- Tessitore S., (2014). “Application of DInSAR techniques to the monitoring of ground deformations”, PhD thesis.
- Tessitore S., Fernández-Merodo J. A., Herrera G., Tomás R., Ramondini M., Sanabria M., Duro J., Mulas J., Calcaterra D. (2016). “Comparison of water-level, extensometric, DInSAR and simulation data for quantification of subsidence in Murcia City (SE Spain)”, *Hydrogeology Journal*, 24, 3, 727-747.
- Thywissen K., (2006). “Core terminology of disaster risk reduction: A comparative glossary”. In: *Measuring Vulnerability to Natural Hazards*. Tokyo, Japan, 448-496.
- Tobita M., Fujiwara S., Ozawa S., Rosen P. A., Fielding E. J., Werner C. L., Murakami M., Nakagawa H., Nitta K., Murakami M. (1998). “Deformation of the 1995 North Sakhalin earthquake detected by JERS-1/SAR interferometry”. *Earth, planets and space*, 50(4), 313-325.
- Tomàs R. (2009). “Estudio de la subsidencia de la ciudad de Murcia mediante interferometría SAR diferencial avanzada”, PhD thesis.
- Tomás R., Herrera G., Delgado J., Lopez-Sanchez J.M., Mallorquí J.J., Mulas, J., (2010). “A ground subsidence study based on DInSAR data: Calibration of soil parameters and subsidence prediction in Murcia City (Spain)”. *Engineering Geology* 111, 19-30.
- Tomas R., Herrera G., Cooksley G., Mulas J., (2011). “Persistent Scatterer Interferometry subsidence data exploitation using spatial tools: The Vega Media of the Segura River Basin case study”. *Journal of Hydrology*, Volume 400, Issues 3–4, 411-428.
- Tomás R., García-Barba J., Cano M., Sanabria M. P., Ivorra S., Duro J., Herrera G. (2012). “Subsidence damage assessment of a Gothic church using differential interferometry and field data”. *Structural Health Monitoring*, 751-762.
- Tomás R., Romero R., Mulas J., Marturia J., Mallorquí J., Lopez-Sanchez J.M., Herrera G., Gutierrez J.; González P.J., Fernandez J., Duque S., Concha-Dimas A., Cocksley G., Castaneda C., Carrasco D. and Blanco. P. (2013). “Radar interferometry techniques for the study of ground subsidence phenomena: a review of practical issues through cases in Spain”. *Environmental Earth Sciences*, 71, 163-181.

- UNDRO, (1991). "Mitigation Natural Disasters. Phenomena, Effects and Options. A manual for policy makers and planners". United Nations Disaster Relief Co-ordinator, 164 pp.
- UNISDR (2009). "Terminology on disaster risk reduction, Published by United Nations UNISDR, Geneva, Switzerland.
- United Nations (2005). "Report of the World Conference on Disaster Reduction". Kobe, Hyogo, Japan.
- Van Rooy J. (1989). "A new proposed classification system for dolomitic areas south of Pretoria". Contributions to engineering geology, 1: 57-65.
- Van Westen C.J. (1993). "Application of Geographical Information System to landslide hazard zonation". ITC Publication n. 15, ITC, 245 pp.
- Van Westen C.J. (2004). "Geo-information tools for landslide risk assessment: an overview of recent developments. Landslides: evaluation and stabilization. Vol. 1: 39- 56.
- Van Westen C.J. (2009). "Distance Education course on the use of spatial information in multi-hazard risk assessment". <http://www.itc.nl/Pub/study/Courses/C11-AES-DE-01>.
- Varnes D.J. (1978). "Slope movement types and processes". Landslides: Analysis and control. National Research Council, Washington, D.C., 11-33.
- Varnes D. J., IAEG (1984). "Landslide Hazard Zonation - a review of principles and practice". Commission on Landslides. Paris, UNESCO, 60 pp.
- Viscardi A., (2009). "Gli effetti indotti sul costruito da frane a cinematica lenta". PhD thesis, University of Salerno.
- Wasowski J. and Mazzeo (1998). "Some results of topographic monitoring of the Acquara-Vadoncello landslide, Italy". Proc. 8th Int. IAEG Congress, Rotterdam, 1705-1712.
- Wegmuller U., Werner C., Strozzi T. (1998). "SAR interferometric and differential interferometric processing chain". International geoscience and remote sensing symposium. Vol. 2. Institute of electrical & electronics engineers, Inc (IEE).
- Westgate K.N. and O'Keefe (1976). "Some definitions of disaster". Disaster Research Unit. University of Bradford.
- Wieczorek G.F. (1996). "Landslide triggering mechanism". Landslides-investigation and mitigation. Chapter 4. Transportation Research Board Special Report, 247, 76-90.
- Wong H.N. (2005). "Landslide risk assessment for individual facilities. State of the Art Report". Proceedings of the International Conference on "Landslide Risk Management", Vancouver (Canada), 237-296.
- Wood H.O. and Neumann F. (1931). "Modified Mercalli intensity scale of 1931". Seismological Society of America.

- WP/WLI (1993). International Geotechnical Societies' UNESCO Working Party on World Landslide Inventory. "A suggested method for describing the activity of a landslide". International Association Engineering Geology, Bulletin 47, 53-57.
- Wright T., Parsons B., Fielding E. (2001). "Measurement of interseismic strain accumulation across the North Anatolian Fault by satellite radar interferometry". *Geophysical Research Letters*, 28 (10), 2117-2120.
- Xia Y., Kaufmann H., and Guo X.F. (2004). "Landslide monitoring in the Three Georges Area using DInSAR and corner reflectors". *Photogrammetric Engineering and Remote Sensing*, 70/10, 1167-1172.
- Xu W. & Cumming, I. (1999). "A region-growing algorithm for InSAR phase unwrapping". *Geoscience and Remote Sensing, IEEE Transactions on*, 37(1), 124-134.
- Zahran S., Brody S.D., Peacock W.G., Vedlitz A. & Grover H. (2008). "Social vulnerability and the natural and built environment: a model of flood casualties in Texas". *Disasters*, vol.32, 537– 560.
- Zanchetta G., Sulpizio R., Pareschi M. T., Leoni F. M., Santacroce R. (2004). "Characteristics of May 5-6, 1998 volcanoclastic debris flows in the Sarno area (Campania, southern Italy): relationships to structural damage and hazard zonation". *Journal of volcanology and geothermal research*, 133(1), 377-393.
- Zebker H. A. & Goldstein R. M. (1986). "Topographic mapping from interferometric synthetic aperture radar observations". *Journal of Geophysical Research: Solid Earth*, 91(B5), 4993-4999.
- Zebker H. A. & Rosen P. (1994). "On the derivation of co-seismic displacement fields using differential RADAR interferometry: the Launderers earthquake". *International Geoscience and Remote Sensing Symposium (IGARSS)*, Pasadena, California, USA, v. 85, 286-288.
- Zhou X., Chang N. B., Li, S. (2009). "Applications of SAR interferometry in earth and environmental science research". *Sensors*, 9(3), 1876-1912.
- Zuccaro G., Mavrouli O., Fotopoulou S., Pitilakis K., Corominas J., Santo A., Cacace F., De Gregorio D., Di Crescenzo G., Foerster E., Ulrich T. (2014). "Vulnerability assessment for reinforced concrete buildings exposed to landslides". *Bulletin of Engineering Geology and the Environment*. 73, 265–289.

Acknowledgements

I am deeply grateful to all people which have given their support to my PhD research.

First, I have to thank my Advisor, **Prof. Domenico Calcaterra**, who believed in me despite he didn't know me: his remarks and his objective criticism have provided me a great opportunity of professional and personal growth.

Then, I have to say thank to my co-Advisor, **Prof. Massimo Ramondini**: he has been my reference point, starting from thesis of master degree and during these three years of PhD project. His ideas and encouragements were the main engine for the development of the thesis.

I would to express my gratitude to **Dr. Ing. Diego Di Martire** for the great help in the SAR technique learning: he has been a constant support in every moment and at every hour both of night and day. Without its time, its patience and above all its friendship, I would not like the “SAR Interferometry” world.

I hope that such experience represents just the beginning of future professional and scientific partnerships with them.

I feel obligated to say thank to **Prof. Roberto Tomás**, for welcoming me in University of Alicante (Spain) and for its important suggestions to the work improvement. Collaborating with him has been an honor.

Thanks are due to the PhD coordinator, **Prof. Maurizio Fedi**, who encouraged me to enrich my studies with an international experience.

I am very grateful to **Dr. Carmine Galzerano** for the know-how regarding the geological and hydrogeological settings of Moio della Civitella and for the data feedback.

An important thanksgiving has to be made to my colleagues of the University of Naples: **Dr. Pierluigi Confuorto, Dr. Ing. Serena Tessitore, Dr. Anna Claudia Angrisani, Dr. Alessandro Novellino, Dr. Gianfranco Finicelli**, whose encouragements towards my studies represented a special support to my scientific experience.

At last, the greatest thank goes to my family, for unconditional support ever.

I will be grateful for life to you.